Bandwidth Extension Techniques for High-Efficiency Power Amplifiers

Albert Garcia i Tormo

Thesis' supervisors
Dr. Alberto Poveda López
Dr. Eduard Alarcón Cot

Full report of Albert Garcia i Tormo's PhD thesis
to apply for the degree of Doctor in Electronic Engineering

October 2006 – March 2011
PhD programme "Electronic Engineering"
Electronic Engineering Department (DEE)
Technical University of Catalunya (UPC)

Every single little action matters;
save energy, save the world.

Acknowledgments

First of all, I would like to thank my supervisors and all people in the group for these years working together, especially to whom we have worked closely together. Some of the results herein presented are the culmination of the work of many years by different people in the group; without them, this thesis would not have been possible.

I would like to thank my family, my friends and the other PhD students in the Electronic Engineering Department, some of them already doctors, for their help and company, which made these years less tough. I would like to especially thank Susanne Pech, who kindly and gently answered all my weird questions, Dr. Daniel Fernández, who did a great job finishing the integrated circuit before the summer run, Dr. Lázaro Marco, who suggested me the max decimation algorithm indispensable to include more than two hundred plots in this document and with high quality, Dr. Xavier Garcia i Tormo, whose thesis inspired me to undertake this adventure, and also to Mr. Joan Garcia i Tormo, for his constant push for notation accuracy.

Partial funding by projects TEC2004-05608-C02-01, TEC2007-67988-C02-01 and TEC2010-15765 from the Spanish MCYT and EU FEDER funds and by grant RUE CSD2009-00046, Consolider-Ingenio 2010 Programme, Spanish Ministry of Science and Innovation. With the support of the Commissioner for Universities and Research of the Department of Innovation, Universities and Companies (AGAUR) of the Catalan Government (Generalitat de Catalunya) and the European Social Fund.

Contents

List of Figures

List of Tables

Chapter 1

Introduction

This chapter expounds the thesis subject matter and contextualises it by describing the application framework and the challenges which have motivated this research. A brief review of power-processing electronic devices is included to aid in identifying the issues and challenges to address; based on this identification, the problem is stated generally and the main objectives are defined. Finally, this initial chapter compiles the level of development of state-of-the-art high-efficiency power amplifiers, including some techniques used in state-of-the-art switching regulators.

1.1 Context

This work is about high-efficiency power amplification of time-varying signals; more precisely, it is about efficient power conversion, i.e. with minimum losses, of DC constant voltages into non-constant voltage signals.

This kind of power conversion is quite common in power-management circuits and electronics in general. It is present in most everyday use electronic devices, including mobile phones, portable audio players and routers, as well as in high-power devices such as audio amplifiers and wireless base stations. In fact, all devices directly interacting with the real world must deliver time-varying analogue outputs, since the world is analogue and can only be interacted with analogue signals.

In most electronic devices, whether portable or not, the energy is available as DC constant voltage (typically from a battery or a power supply). According to the information to transmit, this energy must be processed or transformed into a time-varying analogue signal so that, for instance, it can be directly converted into audio by a speaker or radiated by an antenna.

The power-modulation process must be efficient, since only the delivered power (sometimes only part of it) is to be interpreted by the receiver. Despite the current miniaturisation and power saving trends in electronic devices, human-scale powers must be handled in order to interact with the real-world environment. Therefore, efficient power amplifiers are necessary in state-of-the-art technology and are going to be necessary in the future as well.

1.1.1 Thesis' Quick Summary

This document is arranged in nine chapters and five appendices. This section compiles the summaries of the different chapters and appendices, aiming a quick description of their content.

The present chapter expounds the thesis subject matter and contextualises it by describing the application framework and the challenges which have motivated this research. A brief review of power-processing electronic devices is included to aid in identifying the issues and challenges to address; based on this identification, the problem is stated generally and the main objectives are defined. Finally, this initial chapter compiles the level of development of state-of-the-art high-efficiency power amplifiers, including some techniques used in state-of-the-art switching regulators.

Chapter 2 presents a new perspective on switching amplifiers, aiming to characterise their behaviour when operating at relatively low switching frequencies (non-conventional operating conditions), thereby allowing to explore their suitability as high-efficiency power amplifiers. According to the new perspective, chapter 2 restates the problem and defines the figures of merit and the comparison metrics used throughout this work.

Based on the encoding-reconstruction interpretation of switching amplifiers, chapter 3 explores the fundamental bandwidth limits in two-level time encoding, by analysing the tracking capabilities of two-level switching signals. With this aim, chapter 3 synthesises two-level switching signals by obtaining the distribution of switching events providing both minimum average switching frequency and inband-error-free encoding when tracking a generic bandlimited signal, targeting switching losses minimisation in the context of switching amplifiers.

Chapter 4 characterises and compares two-level switching modulations for switching amplifiers (modulations which can be feasibly implemented) from the encoding-reconstruction standpoint of switching amplifiers and revisits them under the fundamental limit perspective derived in chapter 3. The scope is to analyse and characterise these common modulations under non-conventional operating conditions.

Chapter 5 extends PWM, AΣΔM and AAΣΔM to multi-level modulations, targeting to reduce the remaining error signal's power by reducing the outband power of the switching signal, in the context of multi-level switching amplifiers. Chapter 5 also identifies the new blocks and subsystems due to multi-level operation in switching amplifiers, thereby providing an extended model of multi-level switching power amplifiers.

Chapter 6 analyses the decoding process in switching amplifiers, i.e. the process of recovering a continuous-time continuous-amplitude signal from a switching signal. This process typically consists in filtering the baseband content of the power switching signal; different techniques to improve this process are analysed, including high-order filtering, cutoff frequency optimisation and pre-equalisation. Nevertheless, in accordance with the extended modelling of multi-level converters presented chapter 5, the decoding process in switching amplifiers also consists in translating the switching signal (i.e. the modulator's output signal) into a set of switch-driving signals; chapter 6 also explores the feasibility of improving the amplifier's decoding process by enhancing the logic translation of the switching signal.

The previous chapters, by in-depth analysing the power-amplification pro-

cess performed by switching amplifiers and splitting it into sub-processes (encoding, translating, power amplifying and decoding), have presented different techniques to improve the performance of each individual sub-process. Chapter 7 explores the advantages of combining these techniques in a single amplifier, targeting to extend the relative bandwidth of switching amplifiers when tracking a general f_0-bandlimited reference signal.

Chapter 8 briefly describes an integrated circuit implementation of a 2-level AΣΔM / AAΣΔM switching amplifier for low-OSwR signal tracking applications; this amplifier has been used to experimentally validate the analyses and the results obtained in the previous chapters.

The appendices provide supplementary information related to the thesis and this topic in general. In particular, appendix A lists the acronyms and abbreviations used in this work. Appendix B defines the most relevant parameters and figures of merit used throughout this work, as well as the signals' amplitude and the power normalisation. Appendix C derives the expression of the Fourier series decomposition of a generic two-level switching signal, as well as it discusses the frequency normalisation herein used and in chapter 3. Appendix D briefly describes the hardware and the programs used to compute the simulations presented in this work, as well as it provides specific information about the parameters used in each simulation (simulated data, points per cycle, etc.). Appendix E provides general information about this document and the list of thesis-derived publications and patents; the list of other author's publications, not directly related to this thesis, is also included at the end of this appendix.

1.2 Motivation and Applications

Electronic devices have grown very popular during the twentieth century, especially late in the century with the popularisation of handheld consumer electronic devices such as radios, cameras, game consoles, audio players, mobile phones and, more recently, multipurpose communication devices (enhanced mobile phones). Furthermore, electronic devices are also present in many other devices and machines, such as cars or televisions; even in refrigerators and washing machines, depending on the brand.

Amongst all everyday use electronic devices, mobile phones have probably become the most common ones. Certainly, by the end of 2009, the density of mobile phone lines in Spain had already risen beyond 112 lines per 100 inhabitants [1]. Besides the user terminals, a large infrastructure is required to provide the mobile phone service with proper coverage. The infrastructure comprises wireless base stations (depending on the orography and the users density, a single antenna might provide radio coverage up to a few km far from it) and broadband wired transceivers to communicate with the call centers.

Despite the popularisation of electronic devices and their usage in many different application fields, any electronic signal processing results in an electrical signal, which usually needs to be converted into another kind of signal to be properly interpreted by the receiver. Indeed human beings, for instance, can easily interpret acoustic waves and light belonging to a certain wavelength range, whereas communication antennas are sensitive to electromagnetic waves of a specific wavelength range.

All electronic devices delivering outputs to the real world therefore include

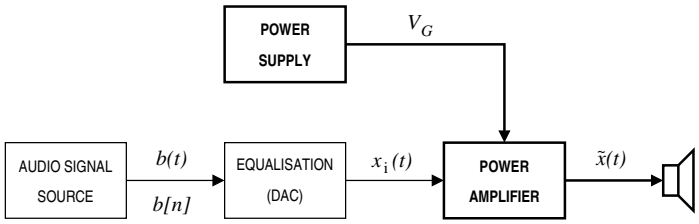

Figure 1.1: Identification of the power amplifier in a simplified audio amplifier (the power path is highlighted in bold). Regardless of the audio signal's form, either analogue $b(t)$ or digital $b[n]$, the power amplifier's input signal is an analogue signal $x_\mathrm{i}(t)$.

transducers, to convert the output electrical signals into signals of another nature. There exist several kinds of transducers, yet the most common ones in communications and consumer electronics are those which convert electrical signals into electromagnetic waves (antennas), acoustic waves (loudspeakers and earphones) or light (mostly Light Emission Diodes—LEDs, Light Amplification by Stimulated Emission of Radiation—LASERs and Cold Cathode Fluorescent Lamps—CCFLs).

Nonetheless, transducers convert one type of energy into another without control: all the energy supplied at their input is automatically converted and delivered to the output. Whilst some energy forms can be afterwards processed (such as light, which can be processed with optical devices), some other ones cannot (such as acoustic waves or electromagnetic waves). In such cases, the only way to control waveform and power of the converted signal is to control the input signal of the transducer, i.e. waveform and power of the electrical signal.

Besides acoustic (audio) and electromagnetic (wireless) applications, some other applications also require modulated electrical signals. For instance, Digital Subscriber Lines (xDSL) and Power Line Communications (PLC), two wired broadband data communication technologies, transmit modulated electrical signals in order to maximise the information transfer rate.

1.2.1 Portable and High-Power Audio Applications

Audio power amplifiers are one of the most common applications for power amplifiers. As discussed above, in electronic audio power amplifiers, audio signals have to be power amplified before being delivered to the speaker and thus converted into acoustic waves (i.e. played, see figure 1.1).

Targeting high audio-quality power amplifiers, low-distortion has historically been the keynote in audio applications. Low-distortion audio power amplifiers are based on low-efficiency power-processing devices, which allow power-amplifying audio signals with very low distortion rates, but at the cost of consuming high power (low efficiency).

Nowadays, audio power amplifiers are also used in applications in which other features such as size, weight or efficiency, predominate over audio quality (moderate audio distortion is tolerated). As a result, in these applications, high-efficiency designs are preferred over low-distortion ones. For instance, in battery-powered applications (portable and handheld devices, including mobile phones), high-efficiency audio amplifiers not only aid in maximising the terminal

autonomy but also in reducing size and weight of the overall terminal, as high-efficiency amplifiers require smaller and lighter heatsinks than low-efficiency ones. In high-power applications, high-efficiency amplifiers are also preferred over low-efficiency ones because of reliability and size and weight (and thus cost) of the heatsink.

Whilst the efficiency of low-distortion power-processing devices cannot be improved as it is intrinsically limited by its principle of operation (see section 1.3.3), the distortion of high-efficiency power-processing devices has been improved in recent years. As a result, in most mass market applications, high-efficiency audio power amplifiers are superseding low-distortion ones [2]. Even if targeting low-distortion, high-efficiency power-processing devices are used in combination with low-distortion power-processing devices, to improve the global efficiency (linear-assisted amplifiers, see section 1.5.4). Nevertheless, low-distortion amplifiers are still being used in some specific applications, since their audio quality is higher.

Therefore, for most audio applications, it is desirable to explore techniques to reduce the distortion (or, equivalently, extend the bandwidth) of high-efficiency power-processing devices, which may result in higher audio quality or further efficiency improvements.

1.2.2 Wireless and Broadband Communication Devices

All communication devices, either wired or wireless, need a power amplifier to transmit the information through the communication channel (i.e. to supply the output transducer). Since communication channels are often shared, thereby hosting several users and/or services at the same time, channel multiple access methods are used. A common multiple access technique is Frequency-Division Multiplexing[1] (FDM). FDM splits the communication channel into slots or sub-channels (frequency ranges); each user or service is assigned a specific sub-channel and it should only transmit power within the specified sub-channel.

The communication standards determine the form through which the transmission must be performed (modulation, sub-channels' bandwidth and central frequency, power levels, tolerances, etc.), as well as the maximum power allowed out of the user sub-channel. The physical layer specifications generally include a transmit spectrum mask (as in figure 1.2), which must be strictly complied to avoid interfering with the adjacent sub-channels. Pursuing a workaround, unlike in audio for portable and high-power applications, low-distortion is always a compulsory feature in power amplifiers for communication devices.

Current and Upcoming Communication Standards

Global System for Mobile communications (GSM), the second generation mobile phone system and still the most popular standard for mobile telephony, was the first communication standard to concern Radio Frequency (RF) power management. The GSM standard was developed taking precedence of ergonomics over performance, since, at the time it was deployed, the then current mobile phone system was analogue. The scope was to provide a mobile phone system whose

[1] FDM is the generic name of assigning non-overlapping frequency ranges to different signals (generally different services). When FDM is used by a specific service to allow multiple users to share a communication channel, it is called Frequency-Division Multiple Access (FDMA).

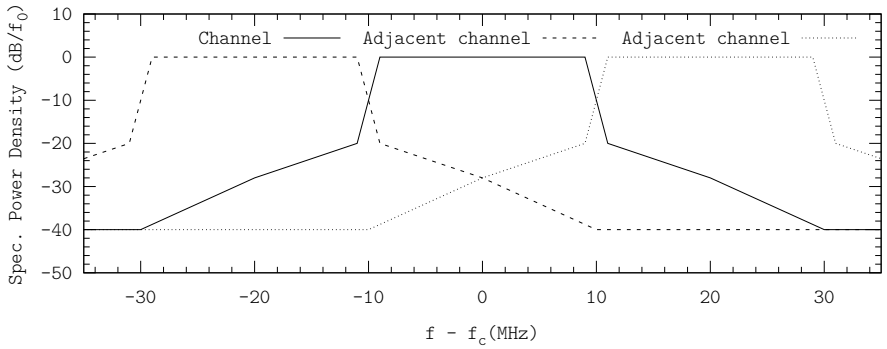

Figure 1.2: Communication mask for IEEE 802.11 (20 MHz channel spacing).

terminals could be smaller, lighter and with longer autonomy than the analogue ones, without compromising the service quality (phone calls only).

Achieving both high-efficiency and low-distortion in power-processing RF devices was (and it still is) an open challenge. Because of this reason, GSM was developed to transmit the binary data stream using Gaussian Minimum Shift Keying (GMSK), a constant-envelope modulation (only the zero crossings convey information). Whilst this constraint simplifies the design of the Radio Frequency Power Amplifiers (RFPAs), it also limits the bit transfer rate, although the standard was designed to cope with it and handle real-time conversations.

As a result of the commercial success of GSM, and also of the evolution of the Complementary Metal Oxide Semiconductor (CMOS) technology, the standard was revised to also support data transfers. The first revision (General Packet Radio Service—GPRS, a 2,5G service), still using the same GMSK modulation, uses all eight time slots in a GSM frame to provide data transfers. Further revisions and newer standards use multibit modulations, more efficient in terms of transmitted information per bandwidth unit but whose envelopes are not constant. Besides, to achieve higher data transfer rates, these new standards transmit over sub-channels of wider bandwidth. For instance, Universal Mobile Telecommunications System (UMTS, a 3G service) uses Quadrature Phase Shift Keying (QPSK, with pulse-shaping) and sub-channels up to 5 MHz-wide.

Whilst these mobile phone system standards were being deployed, wireless and broadband communication devices for consumer electronics were becoming popular as well. Technologies such as Wireless-Fidelity (WiFi, IEEE 802.11), Worldwide Interoperability for Microwave Access (WiMAX, IEEE 802.16) or Digital Subscriber Lines (xDSL), which are exclusively intended for data transfer, also transmit non-constant envelope signals within MHz-wide sub-channels. E.g. the IEEE 802.11 [3] defines sub-channel bandwidths from 5 MHz up to 40 MHz (maximum expected bandwidth in the upcoming standard variant n), using modulations from Binary Phase Shift Keying (BPSK, one per symbol) up to 64-Quadrature Amplitude Modulation (64-QAM, six bits per symbol); the sub-channel center frequency is in the range of GHz (generally 2,4 GHz or 5 GHz, depending on the standard variant).

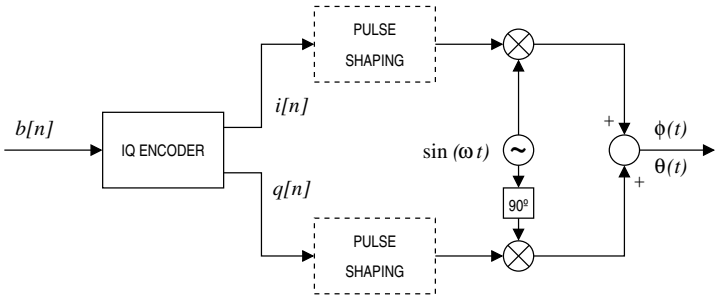

Figure 1.3: Block diagram of an IQ modulator (with pulse-shaping). $b[n]$ stands for the input bitstream (the digital data generated in the baseband processing); $\theta(t)$ stands for the raw output (without pulse-shaping) and $\phi(t)$ stands for the pulse-shaped output.

Multibit Modulations in Wireless and Broadband Communications

All multibit modulations used in communications can be implemented using the I-Q modulator (see figure 1.3). This modulator relies on the orthogonality of the sine and the cosine functions to transmit two independent components [4]. The information bits $b[n]$ (data stream) are grouped in symbols, which are decomposed into its I and Q components ($i[n]$ and $q[n]$ respectively) according to the constellation diagram. These components are then modulated in quadrature and mixed, thus generating the modulated output signal $\theta(t)$, which must be subsequently power amplified and transmitted.

Each modulation uses a specific constellation diagram, i.e. a specific number of symbols and layout. Figure 1.4 shows the constellation diagram of two modulations: QPSK (two bits per symbol) and 64-QAM (six bits per symbol). The corresponding time waveforms and power spectra are included in figures 1.5 and 1.6 respectively. Since the power spectrum of both modulated signals spreads, which is not suitable for sharing communication channels, a pulse-shaping filter is applied during the modulation process (see figure 1.3). The pulse-shaped modulated signal $\phi(t)$ conveys the same amount of information than the raw signal $\theta(t)$, although it concentrates most of its power within a band narrower than twice the chip rate (symbols per time unit); the pulse-shaped signal $\phi(t)$ can therefore be transmitted and properly received using this reduced bandwidth, at the cost of increasing the complexity of the time waveforms (see figures 1.5 and 1.6).

The time waveforms and the power spectra of different multibit modulations operating at the same chip rate are very similar (compare figures 1.5 and 1.6, which correspond to QPSK and 64-QAM respectively). However, as more information is transmitted within the same bandwidth, better Signal-to-Noise Ratio (SNR) is required for proper demodulation. Some communication standards change the modulation (e.g. from 64-QAM to 16-QAM) depending on the channel's quality.

Therefore, in wireless and broadband communications, the signal to be power amplified and transmitted is the pulse-shaped modulated signal $\phi(t)$: a MHz-wide bandpass signal centered at f_{m}, modulated in both amplitude and phase. E.g. in Universal Mobile Telecommunications System (UMTS), the QPSK modulation is used, with pulse-shaping, at modulation frequencies in the range of GHz with chip rates of 3,84 Mcps, yielding a channel bandwidth of 5 MHz.

Figure 1.4: Constellation bit encoding, as specified in the IEEE 802.11 standard [3], of QPSK (2 bits per symbol, left) and 64-QAM (6 bits per symbol, right). Encoded values are displayed in decimal base.

Designing Radio Frequency Power Amplifiers (RFPAs) capable of power-amplifying these kind of RF signals whilst fulfilling both distortion and efficiency requirements is challenging indeed. As discussed above, low-distortion is a mandatory feature in these applications, to comply with communication masks. This constraint suggests using low-efficiency power-processing devices, although the efficiency of the RFPAs would be very low. On the other hand, high or moderate efficiency is a desirable feature (yet not mandatory) as well, since most battery-powered applications include broadband services. Furthermore, efficiency is also desirable in non-portable high-power applications such as wireless base stations, mainly because of reliability and size and cost of the heatsink. Unfortunately, due to distortion requirements, using high-efficiency power-processing devices as RFPAs is inadvisable.

With the scope of improving the efficiency of RFPAs for broadband communications (based on low-efficiency power-processing devices), specific RFPA architectures have been proposed. These architectures simplify the design specifications by addressing the power amplification in multiple stages (adaptive supply for RFPAs), without using special active devices.

Adaptive Supply for Radio Frequency Power Amplifiers

There exist several variants of adaptive supply for RFPAs, although, essentially, they all consist in supplying the RF power modulator with variable voltage, according to the instantaneous amplitude of the RF signal's envelope (see figure 1.7).

The original adaptive supply voltage architecture is Kahn's Envelope Elimination and Restoration (EER) technique [5]. In EER, the RF signal is split into two signals, envelope (baseband signal) and phase (constant-envelope modulated signal). These two signals are independently power-amplified and subsequently joined in the output modulated stage, wherein the power-amplified envelope

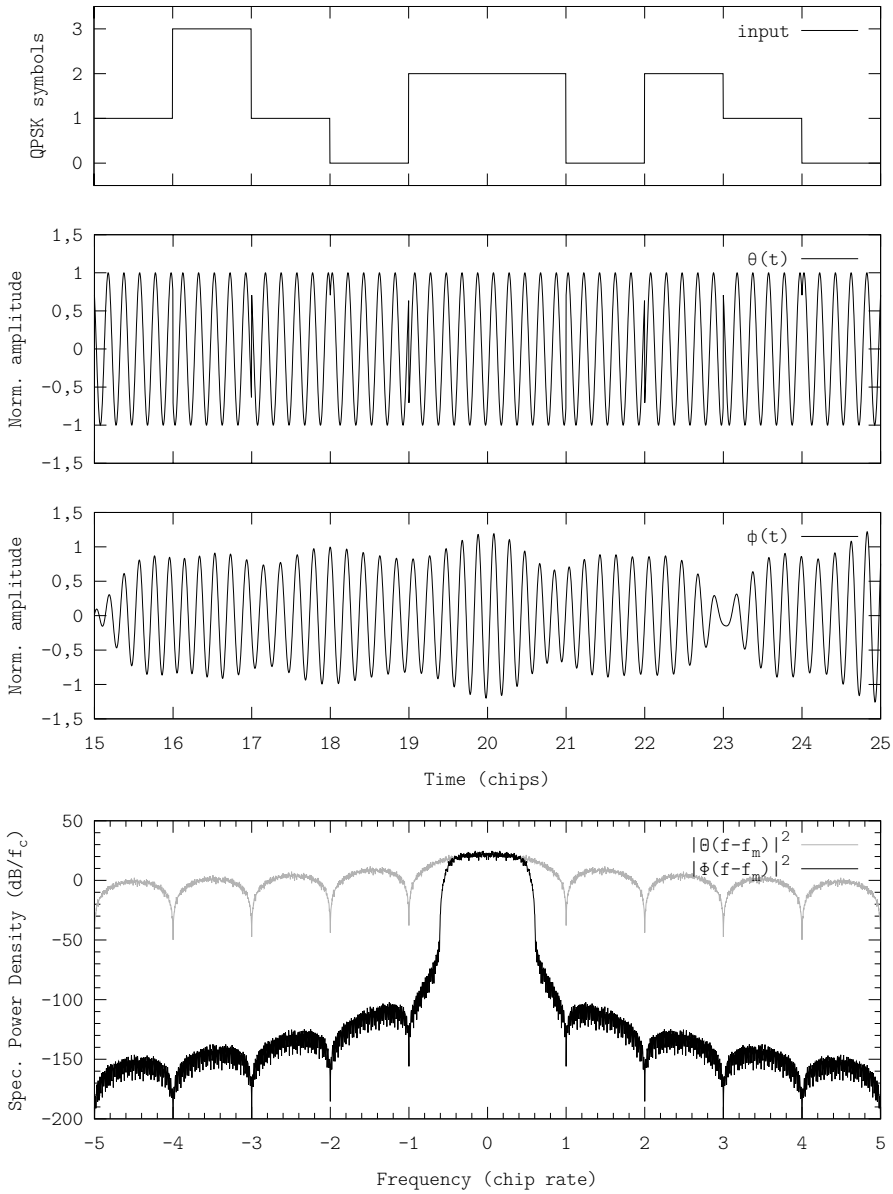

Figure 1.5: QPSK time waveforms and power spectra, raw $\theta(t)$, $\Theta(f - f_{\mathrm{m}})$ and pulse-shaped $\phi(t)$, $\Phi(t - f_{\mathrm{m}})$. The signal has been modulated at five times the chip rate $f_{\mathrm{m}} = 5f_{\mathrm{chip}}$. Simulation performed using the configuration D.4.1.

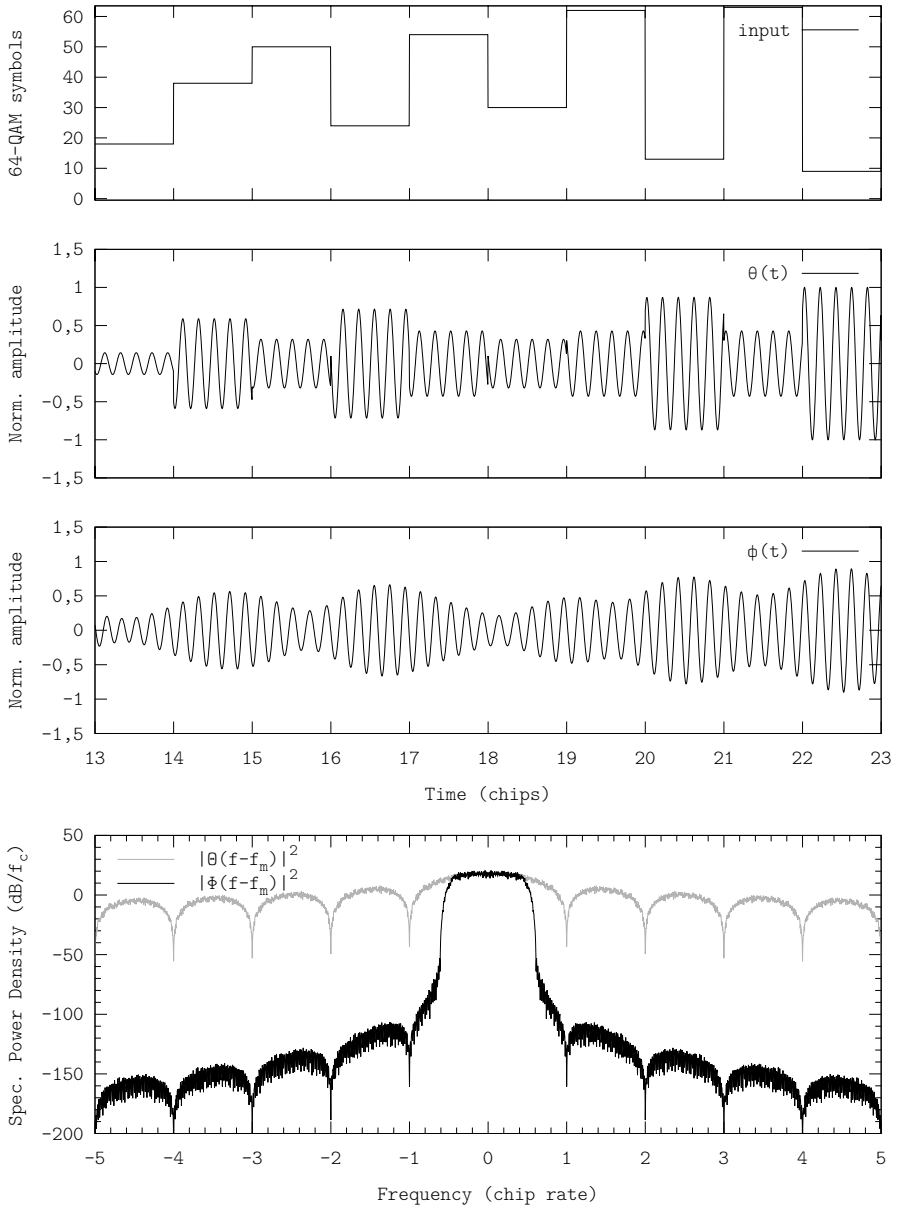

Figure 1.6: 64-QAM time waveforms and power spectra, raw $\theta(t)$, $\Theta(f - f_{\mathrm{m}})$ and pulse-shaped $\phi(t)$, $\Phi(t - f_{\mathrm{m}})$. The signal has been modulated at five times the chip rate $f_{\mathrm{m}} = 5f_{\mathrm{chip}}$. Simulation performed using the configuration D.4.1.

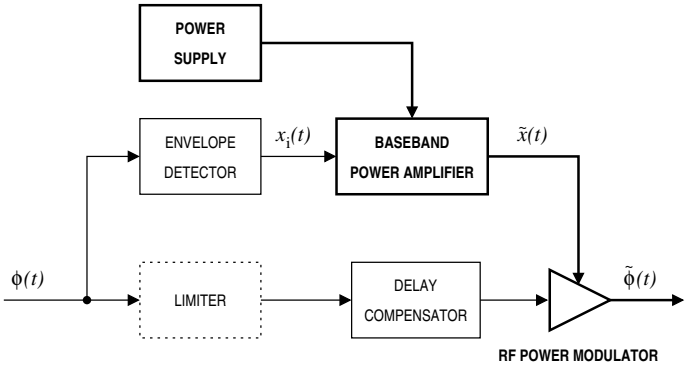

Figure 1.7: Block diagram of a power amplifier with adaptive supply voltage. In EER, a limiter is used in the phase path. The power path is highlighted in bold.

signal modulates the phase-modulated power signal. The original RF signal is then recovered.

The main advantage of this technique is that it allows combining simpler power amplifiers (with regard to linearity specifications) to generate a complex power signal. In the original paper, the envelope amplifier was referred as "Audio-Frequency Amplifier", due to the similarity between envelope and audio signals (in terms of time waveforms and specifications). Unfortunately, the current and upcoming communication standards define multibit modulations whose envelope signals are not bandlimited (see section 1.4.2) and hence the specifications for the envelope amplifier are still challenging (yet it is feasible to design envelope amplifiers with acceptable efficiency by combining high-efficiency and low-efficiency power-processing devices, see section 1.5.4).

Based on EER, Envelope Tracking (ET) techniques have been proposed [6], [7]. In ET, the envelope signal is approximated by a simpler signal (e.g. a bandlimited or a discrete-amplitude signal), which can easier be power-amplified. The amplitude of the approximated envelope signal must be always higher than the original envelope signal's, so that a power-amplified version of the original envelope signal can be generated from the approximated signal by simply trimming the voltage excess. The RF amplifier therefore modulates both amplitude trimming and phase, thus generating the desired power RF signal.

Both EER and ET are similar; the main difference between them is the RF power modulator. Whilst in EER it is only a phase-modulator, thus the amplitude modulation is exclusively up to the envelope amplifier, in ET it is a full RFPA, as it modulates both amplitude and phase.

Challenges in Adaptive Supply

Adaptive supply techniques are very common in state-of-the-art RFPAs. One of the main challenges in these techniques is properly compensating the delay of the envelope amplifier. The performance of both EER and ET is very sensitive to different delays in the envelope and the phase paths.

The other main challenge, relevant to this thesis, is designing the envelope amplifier which, in order to adaptively supply the RF power modulator, must power-amplify the envelope signal (or an approximation to it) with low distor-

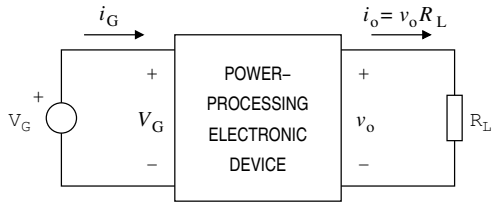

Figure 1.8: Block diagram of a generic power-processing electronic device. Example showing a power-processing device draining power from a constant-voltage source V_G and delivering a voltage v_o to a load R_L.

tion and high efficiency. Although in ET the envelope signals and the envelope amplifier's specifications are simpler than in EER, the efficiency of ET-based RFPAs is not necessarily higher than that of EER-based RFPAs. Indeed the simpler the envelope signal, the lower the RFPA's efficiency (the RF modulating stage must trim more power).

Therefore, either EER or ET, in order to improve the efficiency of RFPAs, it is desirable to explore techniques to reduce the distortion (or extend the bandwidth) of high-efficiency power-processing devices.

1.3 Power-Processing Electronic Devices

Power-processing electronic devices are electronic components, consisting of one or more power electronic devices, capable of draining power $P_G = v_G i_G$ from a source in a certain form (either the voltage v_G is determined by the source and the current i_G is determined by amount of drained power or vice versa) and delivering it to a load R_L in another form $P_o = v_o i_o$ whilst controlling the output power (generally the magnitude of either the voltage v_o or the current i_o is independent of the load R_L). Figure 1.8 illustrates a generic power-processing electronic device, draining power from a constant-voltage source V_G and delivering a voltage v_o to a resistive load R_L.

Strictly speaking, all electronic devices are power devices, since, by definition, all electrical signals convey power. Nevertheless, what distinguishes a power electronic device from a regular electronic device is the capability of handling high power (e.g. power diodes and regular diodes are essentially the same kind of devices, although the formers are intended and designed to handle higher currents and/or voltages than the latters).

In general, in power-processing electronic devices, both the input and output voltages and currents may not be constant; however, the explicit time dependency has been omitted in all expressions and figures because of notation simplicity.

1.3.1 Power Electronic Devices

There are two main kind of power electronic devices: active devices and passive devices. In active devices, the source-to-load power-flow can be externally controlled, whereas in passive devices it is mostly determined by the source and load conditions (i.e. circuit conditions).

The most common electronic active devices for power processing are power transistors, such as Metal Oxide Semiconductor Field-Effect Transistors (MOSFETs) or Bipolar Junction Transistors (BJTs)[2]. Power transistors are based on semiconductors, although not all semiconductor-based power devices can be controlled (such as diodes, non-controllable passive devices which are very common in signal tracking power applications).

Either active or passive, in all semiconductor-based power devices the power-flow is limited (i.e. opposition to the passage of current) by the device's electrical resistance R (device's conductivity). The electrical resistance R is defined as the ratio of the device's voltage V to the current I across it, in accordance to Ohm's law $R = V/I$, and it is determined by the density of free charge carriers and the properties of the semiconductor.

The electrical resistance R depends upon the device's temperature in almost all electronic devices, although, in some devices, it also depends upon other factors. For instance, in active devices, the free charge carriers can be rearranged by driving their control input end u, thus resulting in a different or variable electrical resistance $R(u)$; in passive devices, a specific structure of the semiconductor can result in different electrical resistances depending on the polarity of the current flow. Note that, if the device's temperature remain constant and other effects such as skin or proximity are not significant, the electrical resistance R does not depend upon the amount of power-flow nor the frequency (in alternating electrical signals).

On the other hand, in reactive devices (a particular kind of passive devices), the opposition to the passage of electrical current is determined by electric or magnetic fields (capacitors or inductors respectively), the so-called electrical reactance X, instead of by the semiconductors' conductivity.

The electrical resistance of reactive devices is very low, as they are made of high-conductivity materials, and hence they dissipate almost no power (lossless devices).

$$v_{\mathrm{C}}(t) = \frac{1}{C}\int_{\Delta t} i_{\mathrm{C}}(t)\,\mathrm{d}t \qquad i_{\mathrm{L}}(t) = \frac{1}{L}\int_{\Delta t} v_{\mathrm{L}}(t)\,\mathrm{d}t \tag{1.1}$$

Essentially, reactive devices store energy within an electric or a magnetic field, as the integral ratio between voltage and current expresses (because of this energy-storing properties, these components sometimes referred as "energy-storage devices" in the literature). Since the capacity of these devices is limited, the magnitude of this field increases as the amount of stored energy increases; the accumulated charge results in a frequency-dependent non-resistive opposition to the passage of current (electrical reactance X).

$$X_{\mathrm{L}}(\omega) = L\omega \quad X_{\mathrm{C}}(\omega) = \frac{1}{C\omega} \qquad \omega \in \mathbb{R},\ \omega \geq 0 \tag{1.2}$$

Besides the frequency dependency, the main difference between electrical resistance R and electrical reactance X concerns the amount of dissipated power due to the opposition to the passage of current (i.e. efficiency), a key feature in power-processing devices (especially if targeting battery-powered and embedded applications).

[2]Thyristors are also power electronic active devices, although they are mostly used in very high-power applications such as High-Voltage Direct Current (HDVC) and not in signal tracking, the framework of this thesis.

1.3.2 Efficiency and Losses in Power Processing

Ideally, power-processing electronic devices should be lossless, i.e. all power drained from the source P_{G} should be delivered to the load P_{o}.

$$P_{\mathrm{o}} = P_{\mathrm{G}} \tag{1.3}$$

Unfortunately, lossless power processing is unfeasible with actual power devices, since the conductivity of common materials (such as copper—Cu and aluminum—Al) is finite. This results in built-in stray resistances (Equivalent Series Resistors—ESRs) which dissipate power; the delivered power is therefore always lower than the drained power.

$$P_{\mathrm{o}} < P_{\mathrm{G}} \tag{1.4}$$

This constraint suggests quantifying the efficiency η of power-processing devices, defined as the ratio of the delivered power to the drained power.

$$\eta := \frac{P_{\mathrm{o}}}{P_{\mathrm{G}}} < 1 \tag{1.5}$$

This figure of merit expresses the power required by a power-processing device to deliver a specified power to a load in a certain form. The power required to perform the power conversion (i.e. the power drained from the source but not delivered to the load, including the power to supply auxiliary elements if any), is called power-loss or simply losses P_{L}.

$$P_{\mathrm{L}} = P_{\mathrm{G}} - P_{\mathrm{o}} \tag{1.6}$$

This power is dissipated as heat in the power device(s). In low-efficiency processes, the high power dissipation generally requires a heatsink to avoid overheating and damaging the power devices.

Power-processing electronic devices can comprise energy-storage elements (inductors and capacitors). Even in an ideal lossless case, the instantaneous drained and delivered powers may not be equal due to the energy storing-releasing cycles

$$\exists\, t_0,\ t_0 \in \mathbb{R} \mid P_{\mathrm{G}}(t_0) \neq P_{\mathrm{o}}(t_0) \tag{1.7}$$

In such cases, the power should be evaluated in average, over an appropriate time interval Δt[3] (averaged drained power and averaged delivered power). The efficiency η is then defined and evaluated as

$$\eta := \frac{\displaystyle\int_{\Delta t} P_{\mathrm{o}}(u)\,\mathrm{d}u}{\displaystyle\int_{\Delta t} P_{\mathrm{G}}(u)\,\mathrm{d}u} < 1 \tag{1.8}$$

note that this definition is also valid for power-processing devices not comprising energy-storage elements. This also applies to losses, which can be evaluated either instantaneously or in average.

From the efficiency standpoint, power-processing electronic can be classified as either low-efficiency or high-efficiency ones.

[3] The time interval Δt depends upon each specific power-processing electronic device and the operating conditions.

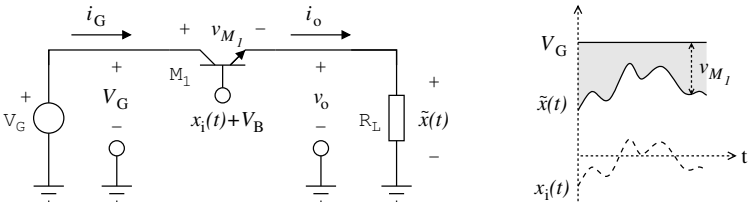

Figure 1.9: General scheme of a linear power-processing device using a bipolar transistor and representative time waveforms. Highlighted in grey, the power dissipated in the power transistor.

1.3.3 Low-Efficiency Power-Processing Devices

Historically, electrical power has been processed by low-efficiency electronic devices[4] (namely linear power-processing devices), mainly because of their simplicity and for the lack of necessity of high efficiency.

Linear power-processing devices essentially consist of a single active device (power transistor), biased so that it operates (quasi)linearly. In this operating conditions, the resistivity of the active device is modulated according to the signal $x_\mathrm{i}(t)$ applied at the control input end (input signal). As a result, the active device behaves as a variable resistor, so that the load is directly supplied with a voltage signal v_o whose magnitude $\tilde{x}(t)$ accurately tracks the waveform of the resistivity-modulating signal $x_\mathrm{i}(t)$ and whose current (i.e. power, as the voltage is already set) is determined by the load and the voltage $i_\mathrm{o} = v_\mathrm{o}/R_\mathrm{L}$ (assuming no saturation).

Figure 1.9 shows an example of a linear power-processing device based on a bipolar power transistor[5]. The collector is connected to the power supply, the emitter (output end) is connected to the load and the base is the resistivity-modulating input. An input signal $x_\mathrm{i}(t)$ is applied to the transistor's base, together with a constant bias voltage V_B, so that the emitter voltage (output signal) tracks the base voltage (input signal), if not exceeding the dynamic range. The transistor can deliver high current, therefore the input signal is power-amplified.

The active device drains constant voltage V_G and supplies a lower voltage v_o by trimming the voltage excess (see figure 1.9); because of the series connection, the load current i_o and the supply current i_G are the same. The active device therefore drains more power than it delivers; the undelivered power is dissipated as heat (losses) in the active device. The amount of dissipated power (i.e. the efficiency of a linear power-processing device) depends upon the difference between the supply voltage V_G and the output voltage v_o.

Another drawback of these power-processing devices is the output signal's polarity. By using a single active device, only unipolar voltages can be supplied, which can be an issue in some applications. It can be addressed by using another active device in parallel, supplied from a negative supply voltage, although it

[4] The exception is electric power distribution, which uses transformers to efficiently power-process the power electrical signals. Transformers can only process Alternate Current (AC) signals; because of this reason, the electric power has traditionally been distributed in AC. In all other applications, low-efficiency power-processing devices were used.

[5] Although there exist several variants of linear power-processing devices, they are all based on the same principle of operation as the one depicted in figure 1.9.

requires further power resources and the efficiency would still be low.

Note that this power conversion is performed through resistive paths and hence it is not frequency-dependent. The AC performance of linear power-processing devices is only limited by the AC characteristics of the active device. This feature is especially important in signal tracking applications (power amplifiers, see section 1.3.5). Linear power-processing devices can also be used to deliver constant-voltage or constant-current signals (regulation).

Even if using state-of-the-art technology, it is not possible to achieve high-efficiency power processing with only a single active device, as the efficiency of linear power-processing devices is intrinsically limited by their principle of operation. Due to this unbridgeable constraint, the popularisation of portable battery-powered devices (including mobile phones) late in the twentieth century triggered the development of alternative power-processing electronic devices, targeting high-efficiency power processing.

High-efficiency power processing yields a twofold benefit in portable battery-powered applications: besides extending the terminal autonomy, it enhances their ergonomics, as terminals can be smaller and lighter (mainly due to the smaller heatsink).

1.3.4 High-Efficiency Power-Processing Devices

High-efficiency power-processing devices are electronic circuits which combine both active and passive devices, including reactive components, to achieve high-efficiency power processing.

Both low-efficiency and high-efficiency power-processing devices include active devices, although they are driven in different ways: whilst in the formers they are driven as variable resistors (and hence they perform power processing), in the latters they are driven as switches (either fully ON –very low resistance– or fully OFF –very high resistance–). Switches allow to control the power processing performed by passive devices, instead of performing power processing by themselves. The different way of driving active devices is indeed what distinguishes both power-processing devices, from a functional standpoint.

Historically, high-efficiency power-processing devices were developed to efficiently convert a source of Direct Current (DC) from one voltage level to another one (high-efficiency DC-to-DC converters). Nonetheless, as discussed in section 1.3.5, in general neither the input nor the output voltages need to be constant; even in some converters the output voltage can be bipolar.

General Structure and Principle of Operation

In high-efficiency DC-to-DC converters, the power processing essentially consists in storing a certain amount of energy (drained from the source) within energy-storage devices (reactive components) and subsequently delivering it to the load. The energy-storing and energy-delivering processes are controlled by switches, which allow to externally change the circuit conditions by settling different low-resistance paths. Indeed switches can drive the converter either to accumulate energy into its energy-storage devices (ON-state) or to release energy from its energy-storage devices (OFF-state).

Power is therefore processed by reactive components (passive devices) and hence the source-to-load power-flow is determined by electrical reactances X.

Since the electrical reactance is frequency-dependent, the power must flow in AC form in order to control it (i.e. in order to perform power processing).

By periodically repeating the energy storing-releasing cycle (i.e. by periodically switching between the ON-state and the OFF-state), the reactive components deal with AC signals and hence the source-to-load power-flow can be controlled. As a result, the converter operates at a certain switching frequency $f_s = 1/T_s$. Due to this switched-mode operation, these kind of converters are often referred as "switching power converters" in the literature.

Within each switching cycle, the ratio of the converter ON time T_{ON} to the switching period T_s (defined as the converter ON time T_{ON} plus the converter OFF time T_{OFF}) is defined as the duty cycle d

$$d(t) := \frac{T_{ON}(t)}{T_s(t)} = \frac{T_{ON}(t)}{T_{ON}(t) + T_{OFF}(t)} \tag{1.9}$$

The time-dependency has been explicitly added to emphasise that none of these magnitudes need to be constant, despite switching converters are generally driven at a constant switching frequency. For the sake of notation simplicity, constant switching frequency $f_s = 1/T_s$ is assumed in the following analyses. If the switching frequency were not constant, the analyses would still apply, but everything would also depend upon the instantaneous switching frequency.

In regular converters, the range of the duty cycle $d(t)$ extends from 0 (the converter is in the OFF-state all the time) to 1 (the converter is in the ON-state all the time).

Transient-State and Steady-State Analysis

Right after turning the converter ON, the energy-storage elements (reactive components) are depleted; during the first switching periods, these elements accumulate energy. During these initial periods, the value of the state variables (inductors' current and capacitors' voltage) at the end of a switching period is to be different than their value at the beginning, e.g. $i_L(0) \neq i_L(T_s)$, see figure 1.10.

The amount of energy stored within the reactive components determines how the energy is delivered to the load: the higher the energy is stored, the faster the energy is delivered (i.e. the higher the output power). Consistently, the converter will keep accumulating energy until it reaches an equilibrium point, in which the converter drains the same amount of energy than it delivers (within one switching period). At this point, the converter operates in steady-state and, if the operating conditions do not change, it is going to remain in this operating state.

Similarly, if at a certain time instant the energy stored in the converter is too high, the converter delivers more energy than it drains until it reaches the steady-state again. In these transient situations in which the converter needs to accumulate or release energy, the converter is in transient-state (see figure 1.10).

Converter Modelling

The state variables are suitable to describe the converter, since they are integral variables (initial conditions can be included) and the other variables of the

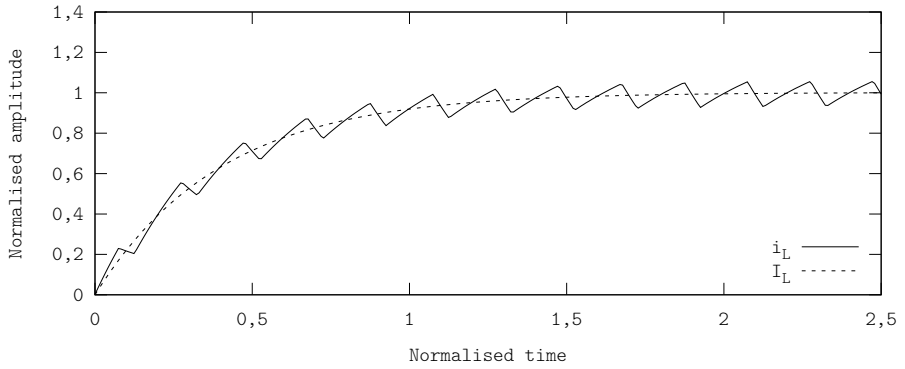

Figure 1.10: Inductor current waveform (solid line) and averaged value (dashed line) of a second-order buck converter. Displayed waveforms show the turn-on transient (up to normalised time 1) and steady-state operation (from normalised time 1 onwards).

circuit can be derived from the state ones. Because of these reasons, the state variables are generally expressed together, using the state vector $\underline{x}$[6]. In converter modelling, the state vector's first derivative, which models the converter's dynamics, is often used as well. In a converter using n reactive elements, the state vector $\underline{x}$ and its derivative $\dot{\underline{x}}$ are defined as

$$\underline{x} := \begin{pmatrix} i_{\mathrm{L}_1} \\ v_{\mathrm{C}_2} \\ i_{\mathrm{L}_3} \\ \vdots \\ v_{\mathrm{C}_n} \end{pmatrix} \qquad \dot{\underline{x}} := \frac{\mathrm{d}}{\mathrm{d}t}\underline{x} = \begin{pmatrix} \dot{i}_{\mathrm{L}_1} \\ \dot{v}_{\mathrm{C}_2} \\ \dot{i}_{\mathrm{L}_3} \\ \vdots \\ \dot{v}_{\mathrm{C}_n} \end{pmatrix} \tag{1.10}$$

The dynamics of any switching power converter can be described in the state-space, with an expression of the form $\dot{\underline{x}} = f(\underline{x}, z)$, where z is the control variable (matrix notation). Unfortunately, because of the switched-mode operation, the converter dynamics is non-linear and it cannot be linearised due to derivative discontinuities. Certainly, consider a simple switching power converter with two states, ON ($z = 1$) and OFF ($z = 0$); its dynamics is given by

$$\dot{\underline{x}} = f_1(\underline{x})z + f_0(\underline{x})(1 - z) \tag{1.11}$$

therefore it is a discontinuous function (instantaneous time-domain bilinear model). This behaviour is generally modelled by approximating the instantaneous value of the state variables by their averaged value. The average value of the state variables is usually expressed using capital letters. In what follows, state variables expressed with capital letters stand for their averaged steady-state value. This also applies to the duty cycle $D :=< d(t) >$.

$$\underline{X} :=< \underline{x} >:= \frac{1}{T_\mathrm{s}} \int_{<T_\mathrm{s}>} \underline{x}(t + \tau)\, \mathrm{d}\tau \neq f(t) \tag{1.12}$$

[6]The state vector is time-dependent $\underline{x}(t)$ as so are the state variables; to avoid confusion with the reference signal $x(t)$, the explicit time-dependency will be omitted in the state vector unless a specific time instant is to be emphasised.

Whilst the averaged model allows subsequent linearisation of the converter equations, the approximation is only valid in a low frequency range with respect to the switching frequency (quasi-static approximation) [8]. Furthermore, the switching frequency must be constant to apply the averaged model.

The average value of the state variables is constant in steady-state (1.13), whereas during transients it is not constant (1.14).

$$\underline{x}(t) = \underline{x}(t + T_\mathrm{s}) \Rightarrow \dot{\underline{x}} = \underline{0} \qquad \forall t \in \mathbb{R} \tag{1.13}$$

$$\underline{x}(t) \neq \underline{x}(t + T_\mathrm{s}) \Rightarrow \dot{\underline{x}} \neq \underline{0} \qquad \forall t \in \mathbb{R} \tag{1.14}$$

Switching Converter Topologies

The specific layout and the interconnections between the active and the reactive components of a switching converter is defined as converter topology; the number of reactive components or energy-storage elements (i.e. inductors and capacitors) included in a certain topology defines its order.

The converter topology determines the forms through which the converter drains and delivers power. The most common converter topologies are those suited to a voltage input whilst supplying an output voltage, especially second-order ones because they are simpler to control, including the buck, the full-bridge, the boost and the buck-boost topologies (none of these comprise a transformer). There also exist higher order topologies, such as SEPIC and Ćuk, although they are not widely used because of their high-order dynamics.

Next, the most common second-order topologies are described. These descriptions include the ratio between the output voltage V_o and the supply voltage V_G in steady-state. These ratios can be calculated by applying the steady-state condition (1.13) to the inductor in each converter.

Buck Topology In this topology, switches S_1 and S_2 connect the input of an LC filter to either the supply voltage V_G (ON-state) or ground GND (OFF-state); the output of this filter is directly connected to the load (see figure 1.11). In steady-state, the ratio of the output voltage V_o to the supply voltage V_G is directly determined by the duty cycle D (linear control-to-output ratio).

$$\frac{V_\mathrm{o}}{V_\mathrm{G}} = D \qquad D \in [0, 1] \tag{1.15}$$

Note that, in this topology operating in steady-state, the output voltage cannot be higher than the supply voltage. The load is grounded and the polarity of the output voltage is the same than that of the supply voltage. Because of its linear control-to-output ratio, this is the most common topology in high-efficiency power amplifiers for unipolar applications.

Full-Bridge Topology The full-bridge topology is the differential version of the buck topology. Whereas in the buck topology the load and the output filter are grounded, in the full-bridge topology the load floats (both the positive and the negative terminals are connected to a live voltage, see figure 1.12). The output filter can be grounded (common-mode filter) or floating as well (differential-mode filter). The floating output allows doubling the output dynamic range by

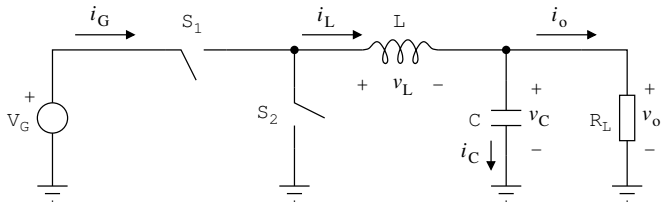

Figure 1.11: 2nd order buck converter. With the displayed polarities, the output voltage V_o is positive if so is the supply voltage V_G.

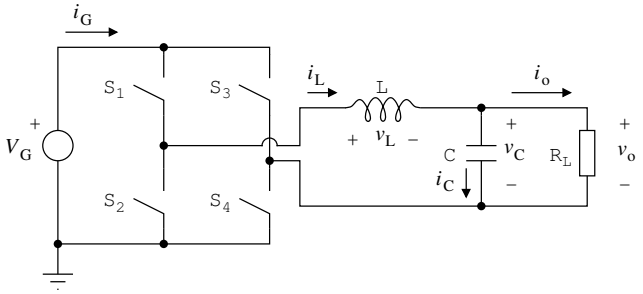

Figure 1.12: 2nd order full-bridge converter with differential-mode filter. The floating output voltage is bipolar $v_o(t) \in [-V_G, V_G]$.

reversing the output polarity. Note that it is possible to apply negative (differential) voltages across the load with a single positive supply. This converter is capable of generating three levels: $\pm V_G$ and GND (by applying the same voltage to both ends of the filter). See sections 6.2 and 7.5 for a further analysis of the multi-level operation of this topology. Formally, the bipolar output voltage can be expressed by extending the duty cycle D to negative values as well (negative values of D correspond to negative output voltages), yielding

$$\frac{V_o}{V_G} = D \qquad D \in [-1, 1] \tag{1.16}$$

Similarly to the buck topology, in steady-state, the ratio of the output voltage V_o to the supply voltage V_G is directly determined by the duty cycle D (linear control-to-output ratio), and the magnitude of the differential output voltage V_o cannot be higher than the magnitude of the supply voltage V_G. Because of the linear control-to-output ratio, this is the most common topology in high-efficiency power amplifiers for bipolar applications.

Boost Topology In this topology (depicted in figure 1.13), switches S_1 and S_2 select either charging the inductor (ON-state, S_1 ON and S_2 OFF) or discharging it to the load (OFF-state, S_1 OFF and S_2 ON). In the OFF-state, even if the inductor is completely depleted ($i_L = 0$), the power supply may charge the output capacitor up to V_G; on the other hand, if the inductor is charged ($i_L > 0$), it will further charge the output capacitor thus increasing the output voltage beyond V_G. Therefore, unlike in the buck and the full-bridge topologies, in the boost topology the output voltage V_o is higher or equal than the supply

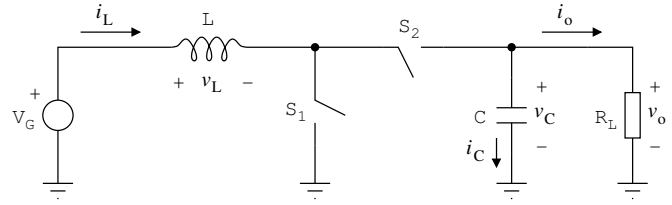

Figure 1.13: 2nd order boost converter. The output voltage v_o is always higher or equal than the supply voltage V_G.

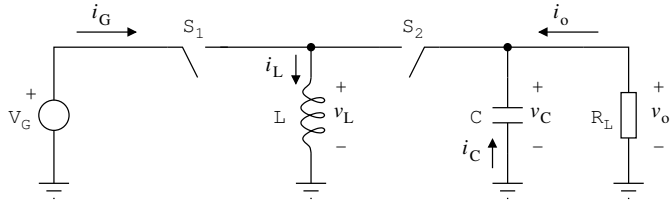

Figure 1.14: 2nd order buck-boost converter. The output voltage v_o is negative and its magnitude can be equal, higher or lower than the supply voltage V_G.

voltage V_G (in steady-state).

$$\frac{V_o}{V_G} = \frac{1}{1-D} \qquad D \in [0,1] \tag{1.17}$$

This topology is unipolar and the output voltage's polarity is the same than that of the supply voltage. The load is also grounded in this topology. Boost converters are widely used in power supplies performing Power Factor Correction (PFC), since one inductor's end is permanently connected to the power supply (continuous input current).

Buck-Boost Topology This topology is similar to the boost topology, but the switch S_1 and the inductor are swapped (see figure 1.14). In the ON-state (S_1 ON and S_2 OFF) the inductor is charged like in the boost converter; in the OFF-state (S_1 OFF and S_2 ON) the power supply is disconnected from the inductor (discontinuous input current) and its current is steered to the output capacitor, which is charged with negative voltage. If the converter remains in the OFF-state, the load will consume power until both the inductor and the capacitor are completely depleted, i.e. until the output voltage drops to 0. The buck-boost topology can therefore deliver output voltages V_o whose magnitude is higher or lower than that of the supply voltage V_G, and whose polarity is opposite to that of the supply voltage.

$$\frac{V_o}{V_G} = -\frac{D}{1-D} \qquad D \in [0,1] \tag{1.18}$$

Allowed Converter States

Not all the possible converter states are allowed in switching converters. Voltage sources and capacitors should never be short-circuited and current sources and

inductors should never be in open-circuit; otherwise it would cause very high currents or voltages.

Because of this reason, despite a converter may comprise several different states, only a few of them can be used. In common converter topologies, switches are used in twos and complementary driven, i.e. they behave as a two-way power-multiplexer or current-steering commutator switch (these kind of commutator switches are often referred as "Single-Pole Double-Throw" (SPDT) in the literature). In converters consisting of two switches, such as the buck or the boost converters, this constraint usually involves complementary driving the switches (only two of the four possible states are allowed).

Simplified Switch Synthesis When synthesising a regular two-way commutator switch, consisting of two switches complementary driven, only one active device (active switch) is required to synthesise it. The complementary switch (passive switch) can be synthesised with a diode; the circuit conditions determined by the active switch complementary drive the diode as well. This synthesis strategy simplifies the control of the converter (only one switch-driving signal is required), but it degrades the commutator switch performance (especially in low-voltage applications). Figure 1.15 includes an example of this synthesis strategy, in the case of a buck converter; note that only one switch-driving signal is required to control this converter.

Output Ripple

Because of the switched-mode operation of switching converters, the converter's output stage (a capacitor in voltage-output converters) is periodically charged and subsequently discharged through the load. As a result, the output voltage v_o continuously either increases or decreases its value, but it does not remain constant. Switching power converters, instead of delivering a constant-voltage signal, deliver a signal consisting of a constant-voltage signal plus a ripple AC signal, whose frequency is f_s.

For instance, consider a buck converter which must deliver a constant output voltage of value V_R (the example shown in figure 1.15). If the switching converter is properly designed, the averaged output voltage V_o may be equal to desired voltage V_R, although the instantaneous difference between both signals $v_\mathrm{o}(t) - V_\mathrm{R}$ is, in general, not zero.

This constraint is inherent in switching converters. Even if using ideal devices, the capacity of the reactive components is limited, therefore all voltages and currents continuously either increase or decrease. By increasing the switching frequency (or, equivalently, by increasing the value of the reactive components) the output ripple can be reduced, but it cannot be completely avoided.

There exist a few techniques to reduce the output ripple in switching power converters without increasing the switching frequency or using larger inductors and capacitors (i.e. slowering down the converter dynamics). These techniques are mostly based in parallel-connecting different converters and driving them in a specific way (interleaving, see section 1.5.3 for further details).

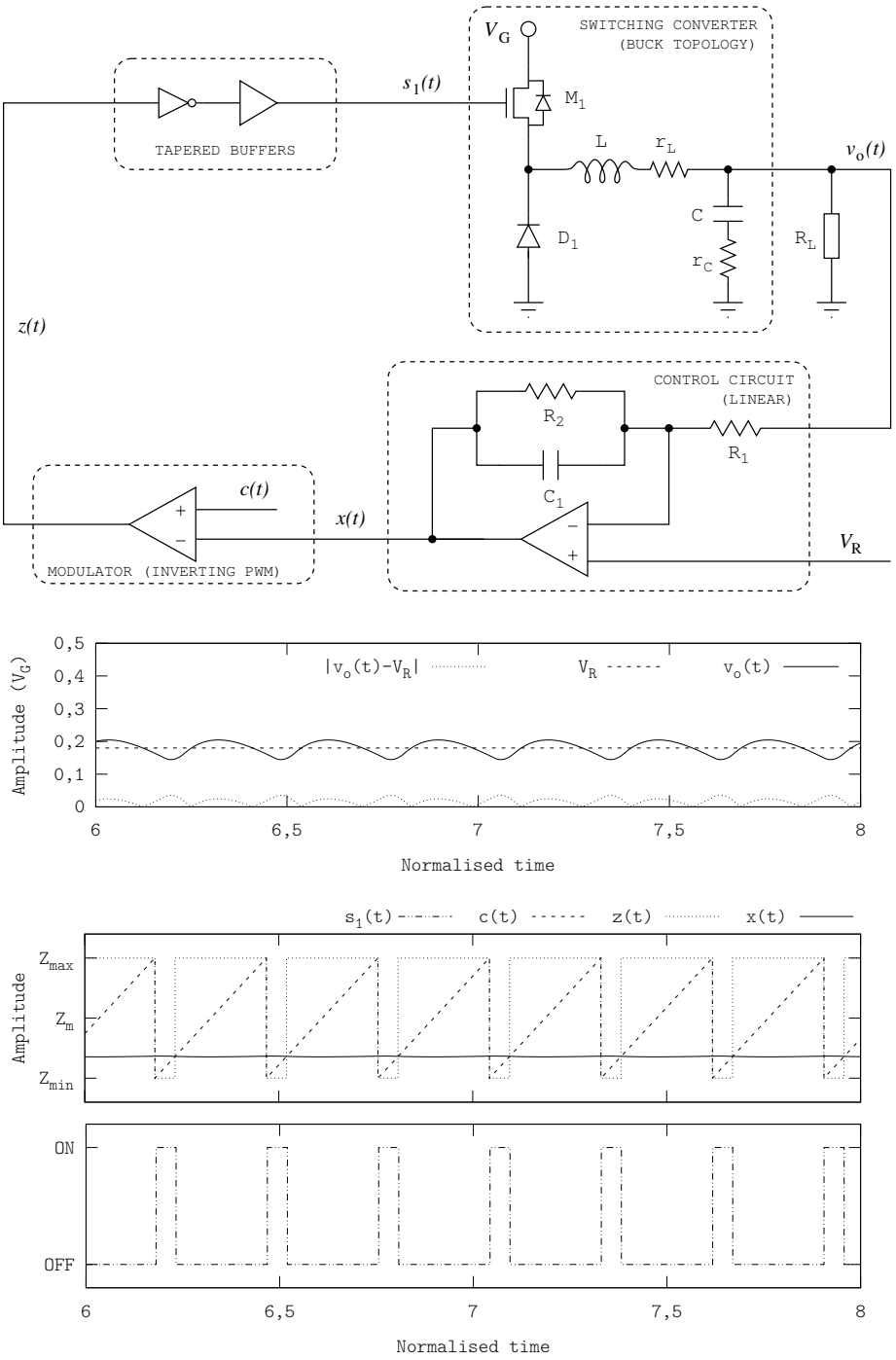

Figure 1.15: Example of a high-efficiency voltage regulator (based on a buck converter) and representative time waveforms. The power reactive components include the ESRs. The modulator is a sawtooth PWM and the control circuit is linear.

Tapered Buffers

Each power switch synthesised with an active device must be driven by a switch-driving signal $s_i(t)$, a binary switching signal whose amplitude and current must be suitable to turn the power switch ON and OFF. The power requirements of the switch-driving signals $s_i(t)$ often make advisable to drive the power switches through a chain of tapered buffers, in order to ensure proper driving. Figure 1.15 includes an example of tapered buffers in a buck converter driven as voltage regulator.

Tapered buffers (and hence the switch-driving signals) are specific for each switch technology and operating conditions (a common technique consists in power-amplifying the switch-driving signals up to the supply voltage). Regarding the time waveforms of the switch-driving signals $s_i(t)$, the ON-OFF and OFF-ON transitions must be fast (sharp edges, high slew-rate) to avoid the linear operation of switches as much as possible; otherwise the power-loss during transitions would be high. Because of this reason, tapered buffers are included in almost all designs including a switching power converter.

At system level, the operation of tapered buffers is transparent. In what follows, unless otherwise stated, tapered buffers are considered part of the switching power converter, i.e. switching converters can be directly driven by low-power binary switching signals.

Complementary Circuitry for Output Regulation

Even though switching power converters are devices capable of high-efficiency power processing, they must be properly driven so that they behave as, for instance, high-efficiency voltage regulators. It is therefore necessary to generate a proper set of binary switching signals $s_i(t)$ so that, when the switching converter is driven by these signals, the value of the averaged output voltage (or current, depending on the topology) is the desired one.

Modulator The electronic circuit which generates the binary switching signal is the modulator. The modulator processes an analogue reference signal $x(t)$ and provides a two-level switching signal $z(t)$. This signal $z(t)$, and hence the modulator, therefore determines the converter state at any time instant; furthermore, the modulator determines the switching frequency f_s of the switching power converter.

The most common modulator in switching power converters is Pulse Width Modulator (PWM[7], as in the example included in figure 1.15). This modulator is analysed in section 4.1. The reference signal $x(t)$ processed by the modulator can simply be the reference signal V_R (the converter operates without sensing any state variable, open-loop operation). However, the output voltage (or current) in actual switching power converters is usually affected by load variations,

[7] The abbreviation PWM may also stand for Pulse Width Modulation. Although the terms modulator and modulation are often used without distinction, formally they express different concepts. Whereas the term modulation denotes a process (a mathematical operation), the term modulator denotes an electronic circuit (a physical device) which implements a modulation. Modulation, the mathematical operation, is the process through which a signal with a certain waveform is shaped into another waveform. This process can be either lossy or lossless, and it can be off-line or real-time (the process delay is not significant) performed. Both abbreviations are used in this work. From the context, it should be clear which one is being used, either the electronic circuit (modulator) or the mathematical process (modulation).

disturbances caused by ElectroMagnetic Interferences (EMI) or non-idealities in general. As a result, the average value of the converter's output signal deviates from the desired value V_{R}.

Control Circuit The most common and effective technique to compensate these effects is feedback. This technique consists in comparing the reference signal V_{R} with the converter's actual output signal (closed-loop operation); according to the difference between both signals, a new reference signal $x(t)$ is generated. The circuit which generates the reference signal $x(t)$ is the control circuit.

In general, not only the converter's output signal but all state variables can be sensed. Besides, the comparison is generally performed through a frequency-dependent transfer function (compensation), to guarantee the stability of the closed-loop amplifier.

Traditionally, control circuits have been based on linear control techniques, although sliding mode control has become quite popular in recent years. Both techniques are analysed in section 1.5.3. Figure 1.15 shows an example of a DC-to-DC switching converter driven as voltage regulator, based on a linear control circuit with output voltage feedback.

Power Rate Note that neither the modulator nor the control circuit process power signals (in the example of figure 1.15, it could be expressed as $R_{\mathrm{L}} \ll R_1, R_2$). Their input and output dynamics ranges are independent of the switching power converter's (e.g. a switching power converter could supply 10 V but internally operate at 5 V); the modulator and/or the control circuit can even be implemented digitally. The only constraint regarding the implementation and the dynamic range of the modulator and the control circuit is that they must be suitable to deal between themselves and with the converter's tapered buffers. In figure 1.15 this independence is explicit, as the dynamic range of $x(t)$ and $z(t)$ extends from $Z_{\min}$ to $Z_{\max}$ whereas the dynamic range of the output signal $v_{\mathrm{o}}(t)$ extends from GND to V_{G}.

Efficiency and Losses in High-Efficiency Power-Processing Devices

Ideally, the efficiency of switching converters should be 100 %, i.e. all power drained from the source should be delivered to the load $P_{\mathrm{o}} = P_{\mathrm{G}}$. Certainly, as can be seen in figures 1.11 to 1.14, a switching power converter exclusively consists of lossless devices (non-resistive source-to-load power path). Unfortunately, due to the limitations of actual devices and materials, the delivered power is always lower than the drained power $P_{\mathrm{o}} < P_{\mathrm{G}}$. Nonetheless, it is feasible to achieve efficiencies beyond 90 %, depending on the technology and the specifications.

Coils and actual capacitors are not pure reactive components. Instead, due to the built-in ESRs, their impedance Z consists of a resistive part (which is modelled as a real resistance) and a reactive part (which is modelled as an imaginary pure reactance, see the example included in figure 1.15).

$$Z_{\mathrm{L}}(\omega) = r_{\mathrm{L}} + \jmath X_{\mathrm{L}}(\omega) \qquad Z_{\mathrm{C}}(\omega) = r_{\mathrm{C}} + \jmath X_{\mathrm{C}}(\omega) \tag{1.19}$$

Switches (active devices) are made of semiconductor materials. When an active device is fully ON, the free charge carriers are rearranged thereby min-

imising the electrical resistance R (minimum losses at maximum power-flow); analogously, when an active device is fully OFF, the free charge carriers are rearranged thereby maximising the resistance R (minimum power-flow). By only using these two states, the amount of power dissipated in the active devices (power-loss) is minimised, but it is not completely avoided. Indeed, neither the switches' ON-resistance is 0 nor their OFF-resistance is infinite, although the power-loss due to the OFF-resistance can be usually neglected compared to the power-loss due to the ON-resistance (minimum power-flow yields minimum losses).

Besides the ON-resistance, another source of losses in switches are the ON-OFF and OFF-ON transitions. These transitions are not ideal (i.e. not instantaneous, not even with ideal switch-driving signals), which also result in losses.

Losses in switching converters are usually split into switching losses and conduction losses. The power consumed by the complementary circuitry (control circuit, modulator, etc.) can also be considered (quiescent) losses, although these losses can be usually neglected when compared to switching and conduction losses (the power consumed by the buffers is generally considered part of the switching losses).

Depending on the application and the actual design, one kind of losses may prevail over the other one; in high-power designs pursuing high-efficiency, switching and conduction losses are usually balanced. An in-depth analysis of losses in switching power converters can be found at [9].

Conduction Losses Conduction losses stand for the amount of power dissipated in the converter statically, when the converter operates in steady-state in a certain operating state. These kind of losses are mainly due to the parasitic resistances in the active and the reactive components.

The amount of power-loss depends upon the output power (the current flowing through the parasitic resistances), the converter state (the elements through which the current is flowing) and the active and the reactive components themselves. Despite these dependencies, conduction losses are usually not split state-by-state but measured in average, at a certain output power.

Conduction losses can be reduced by redesigning the switching converter, i.e. by replacing the active and/or reactive components by other ones whose ESRs are lower or by using a different architecture and/or topology.

Switching Losses Switching losses stand for to the amount of energy required to switch the converter from one state to another one, typically the ON-OFF transitions and vice versa. These losses are mainly due to the physical structure and non-idealities in the switches (synthesised with either active or passive devices). These effects result in non-instantaneous transitions, wherein switches operate in the linear region (their resistance is comparable to the load R_{L}) for a short period of time. Besides, the reverse recovery time or overlapped switch-driving signals may result in low-impedance battery-to-ground paths during the transitions.

The amount of energy-loss in each switching event mostly depends upon the switch itself and the voltage to withstand in when it is OFF and the current across the switch when it is ON.

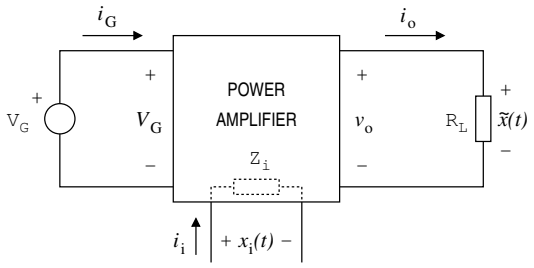

Figure 1.16: Block diagram of a generic voltage-controlled power amplifier, supplied from a DC constant-voltage source V_G and supplying a resistive load R_L with variable voltage v_o and current i_o.

Switching losses are usually expressed as power, i.e. directly related to the switching frequency, and therefore they are generally measured at a certain operating frequency. Besides reducing the switching frequency and replacing the switches by other ones, switching losses can be reduced by using soft-switching techniques, although these techniques lead to smooth edges and wider transitions.

1.3.5 Power Amplifiers

The application field of power-processing devices, either low-efficiency or high-efficiency, is not limited to regulation (supplying constant-voltage or constant-current signals). They can also be used in signal tracking applications, as power amplifiers[8], i.e. to supply a load R_L with an analogue signal $\tilde{x}(t)$, whose magnitude (either voltage v_o or current i_o) tracks the waveform of an input signal $x_i(t)$ and whose power is independent of the input signal's (see figure 1.16).

Power amplifiers can be based on low-efficiency power-processing devices (linear or class-A power amplifiers) or on high-efficiency power-processing devices (switching power amplifiers). Either linear or switching, a power amplifier should dissipate almost no power ($P_G \approx P_o$) and it should deliver a power signal $\tilde{x}(t)$ as similar as possible to the input signal $x_i(t)$ (formally, with almost neither distortion nor delay).

$$\tilde{x}(t) \approx x_i(t) \tag{1.20}$$

Furthermore, the sensing circuit may consume almost no power, to avoid loading the input signal source (e.g. $i_i \approx 0$ if voltage sensing, as in figure 1.16).

The generalisation from constant reference signals V_R to time-varying signals $x(t)$ unfolds a new range of specifications, involving linearity, distortion and frequency-dependency. Regardless of how the power-amplification is performed (in voltage, in current or in both), the amplification should be constant not only within the whole input dynamic range (linear DC input-output transfer characteristic), but also within the frequency-range of interest (i.e. the amplifier's tracking bandwidth).

[8] Power amplifiers are usually supplied from a DC (generally constant-voltage) power source but they deliver non-constant or time-varying signals, either unipolar or bipolar. Because of this reason, this kind of amplifiers are often referred as "inverters" in the literature, in contrast to "regulators" which deliver constant-voltage signals.

According to the principle of operation of power-processing devices and to these additional constraints, low-efficiency power-processing devices are more suitable to be driven as power amplifiers than high-efficiency ones (although, again, at the cost of low-efficiency). Both linear amplifiers and switching amplifiers are briefly introduced next. They are not in-depth analysed, only the most significant features for signal tracking are highlighted. A detailed analysis of both kind of amplifiers, as well as further information about switching power converters in general, can be found at [10] and [11].

Voltage-tracking (the magnitude of the output voltage v_o tracks the reference signal $x_\mathrm{i}(t)$) is more common than current-tracking in power amplifiers. Hereafter, voltage-tracking is assumed. All analyses and conclusions drawn for voltage-tracking can be extrapolated to the analogous case of current-tracking.

1.3.6 Linear or Class-A Power Amplifiers

A linear power-processing device is already capable of signal tracking itself. As long as the active device operates in the linear region, the magnitude of the output signal $\tilde{x}(t)$ precisely tracks the waveform of the input signal $x_\mathrm{i}(t)$ (i.e. low distortion). The tracking capability (or linearity) of linear power-processing devices is only limited by the AC characteristics of the active device and the parasitic capacitances and inductances (ideally, perfect signal tracking may be possible). The example shown in figure 1.9 already included the representative time waveforms in signal tracking.

Linear amplifiers achieve the the low-distortion feature at the cost of dissipating a significant amount of power in the active device. Certainly, typical efficiencies of regular linear amplifiers tracking non-constant signals are not higher than 20 %, which is generally too low for power applications such as battery-powered or portable. Besides, efficiencies as low as these ones usually require large heatsinks in the active device to avoid overheating, thus increasing the amplifier's overall size and cost.

Another constraint of linear amplifiers is that the delivered voltage v_o cannot be higher than the supply voltage V_G. Note that the power amplification can still be performed in current, amplitude or both, as the active device's input dynamic range is not set by V_G.

The linearity achieved by linear amplifiers cannot be achieved with any other power-processing electronic device. Because of their simplicity and their good tracking features, linear power amplifiers have been traditionally used in almost all application fields and are still being used in state-of-the-art power amplifiers, despite their low efficiency. However, in efficiency-sensitive applications, linear amplifiers are generally improved with adaptive voltage supply or assisting another amplifier (see section 1.3.8).

Efficiency specifications have grown in importance in recent years, mainly due to the popularisation of battery-powered devices but also because of reliability, size and weight, cost of the heatsink (especially in high-power applications) or simply to save energy. In order to satisfy the demands of all these applications, and since the efficiency of linear amplifiers is intrinsically limited by their operating principle, high-efficiency power amplifiers were developed.

1.3.7 Switching or Class-D Power Amplifiers

Switching (or class-D) power amplifiers are essentially switching DC-to-DC regulators in which the constant reference signal V_{R} is replaced by a time-varying signal $x_{\mathrm{i}}(t)$, see figure 1.17. Using this design strategy, switching regulators behave as amplifiers only in a low frequency range with respect to the switching frequency f_{s}, typically up to one tenth of f_{s} (quasi-static approximation).

If the quasi-static approximation holds, the input signal $x_{\mathrm{i}}(t)$ behaves as a slow-varying signal and hence all the theory and analyses developed for DC-to-DC switching converters can be applied to switching amplifiers. Yet there exist a few differences between the specifications and the designs of switching converters targeting signal tracking and regulation.

Besides linearity, distortion and frequency-dependent specifications, switching amplifiers generally do not require high load regulation, since the load is usually time-invariant $R_{\mathrm{L}} \neq f(t)$ and the output power is controlled by controlling the amplitude of the output signal $\tilde{x}(t)$. Instead, in regulators, the output signal is constant and the power consumption is determined by the value of the (time-variant) load $R_{\mathrm{L}}(t)$. Similarly, the transient step response of switching amplifiers does not need to be very fast either (bandlimited signal tracking).

The differences in the specifications lead to different designs. Switching amplifiers are usually driven by a triangle PWM, instead of by a sawtooth PWM (which is more common in switching regulators). The converter topologies used in switching amplifiers are the buck (for unipolar applications) and the full-bridge (for bipolar applications), because of their linear control-to-output ratio (which simplifies controlling and driving the converter as an amplifier). Commutator switches are usually synthesised with two active switches (synchronous switches) in switching amplifiers, because of the full-bridge topology and, recently in low-voltage unipolar applications, because of efficiency.

Distortion in Switching Amplifiers

Switching amplifiers are designed according to the quasi-static approach, i.e. the switching frequency f_{s} is much higher than the reference signal's bandwidth f_0. Under these operating conditions, two main sources of distortion dominate: dead time (mainly due to synchronous commutator switches) and output ripple (inherent in switching power converters).

There is a third distortion source in switching amplifiers: non-idealities and external factors (such as ESRs or EMI). These effects result in undesired behaviours (e.g. in a buck converter, the output voltage also depends upon the output power), usually causing distortion in the output signal $\tilde{x}(t)$. Nevertheless, these effects can be often mitigated by using feedback techniques (see below).

Dead Time Synchronous switches must be driven by non-overlapping switch-driving signals to avoid simultaneous conduction (which would lead to a low-resistance source-to-ground path through the switches, i.e. very high switching losses). Non-overlapping switch-driving signals are usually generated by adding a dead time between the transitions of both switches in a commutator switch, a short time interval in which both switches are OFF. No current should flow through the any of the switches in a commutator switch during dead time (dis-

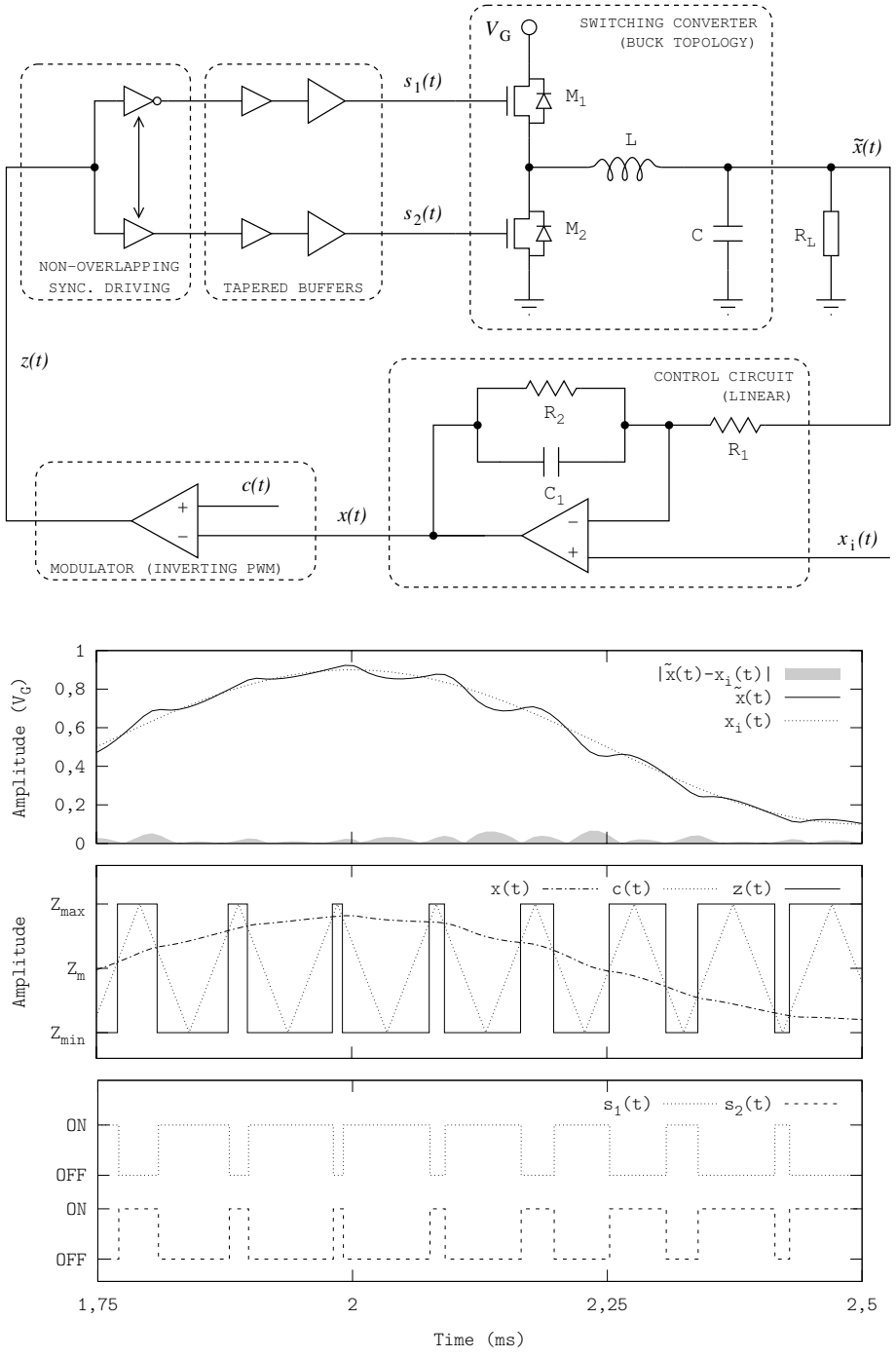

Figure 1.17: Example of a closed-loop switching amplifier and representative time waveforms. This example is based on a buck converter, compensated with a linear controller and driven by a PWM.

continuous output current). The inductor, however, which is connected in series with the load, forces the output current to be continuous thus steering it through the switches' body-diodes[9] during dead time. Under these circumstances, dead time modifies the duty cycle, which causes error in the output voltage (1.15), (1.16).

If a switching event occurs when the output current is small, the inductor current may reverse its polarity during dead time. Nevertheless, the inductor current will becomes zero and remain zero until an active switch is turned ON (discontinuous conduction mode) [12].

Either resulting in a duty cycle error or in discontinuous conduction mode, dead time degrades the tracking fidelity and therefore it results in distortion in switching amplifiers. Note that in both buck and full-bridge topologies, at least one inductor (first-order converters) in the output stage is mandatory to deliver continuous signals to the load.

Output Ripple Due to the switched-mode operation of switching converters, the output signal $\tilde{x}(t)$ chatters around the input signal $x_{\mathrm{i}}(t)$. The effects of the output ripple or chattering upon the output signal can be seen in figures 1.17 and 1.18, as the output signal continuously either increases its value beyond the input signal or decreases its value below the input signal.

If the quasi-static approximation holds and the amplifier is properly designed, the averaged output signal $\tilde{X}(t)$ tracks the input signal $x_{\mathrm{i}}(t)$, i.e. the output signal $\tilde{x}(t)$ consists in the input signal $x_{\mathrm{i}}(t)$ plus a sine-like ripple signal, whose frequency is f_{s} (the amplifier's switching frequency).

Therefore, distortion due to output ripple is mostly at high frequency $f_{\mathrm{s}} \gg f_0$. Depending on whether the application tolerates high-frequency distortion or not, it could be an issue (e.g. in EMI-sensitive applications it can be a severe drawback).

Efficiency-Distortion Trade-Off

Distortion is the main drawback of switching amplifiers. Despite it is feasible to mitigate the effects of dead time [13], the output ripple cannot be avoided (interleaving can also be applied to switching amplifiers, as discussed in section 1.5.3, although it requires additional converters, further constraints the amplifier's tracking bandwidth and it can only be applied to a particular modulation).

The output ripple can be reduced by simply increasing the switching frequency, although switching losses are increased as well (efficiency degradation). There is a trade-off involving distortion and efficiency in switching amplifiers, i.e. in designing the switching frequency. On the one hand, the switching frequency should be very high to minimise the output ripple (low distortion); on the other hand, it should also be low to minimise the switching losses (high-efficiency). If a switching amplifier is not properly designed, its efficiency could even be lower than the efficiency of a linear amplifier.

The efficiency-distortion trade-off of switching amplifiers is determined by the performance of the subsystem made up of the modulator and the switch-

[9] Active switches are usually synthesised with power MOSFETs, whose implementation results in a built-in body-diode. If active switches are synthesised with a different technology or process, which gets rid of the built-in body-diode, an external diode should be included. Otherwise the discontinuous inductor current may cause very high voltage peaks.

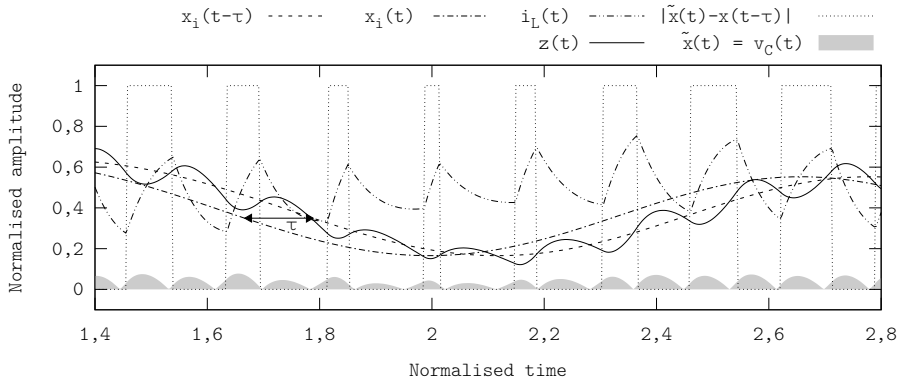

Figure 1.18: Output delay and output ripple in an open-loop switching amplifier. Example showing a second order buck converter.

ing power converter (open-loop performance), since this subsystem processes a low-power analogue signal $x(t)$ and delivers a power analogue signal $\tilde{x}(t)$. The complementary circuitry (mostly the control loop) ensures proper average tracking $\tilde{X}(t) = x(t)$, but it does not affect the output ripple.

Closed-Loop Control Techniques for Switching Amplifiers

Switching amplifiers are based on switching power converters and hence they suffer from ESRs, EMI and non-idealities in general as well. All these effects, which have an adverse impact upon the output signal $\tilde{x}(t)$, depend upon external factors and thus they cannot be beforehand predicted nor pre-compensated. Like in switching regulators, the most effective technique to address these issues is by sensing the actual output signal $\tilde{x}(t)$, comparing it with the input signal $x_{\mathrm{i}}(t)$ and accordingly compensating (feedback). In switching amplifiers, however, the control circuit must compensate these effects whilst providing constant gain within the amplifier's tracking bandwidth.

Therefore, the control circuit must provide a reference signal $x(t)$ so that, after being modulated by the modulator and subsequently processed by the switching power converter, the amplifier's output signal $\tilde{x}(t)$ approximately tracks the amplifier's input signal $x_{\mathrm{i}}(t)$, regardless of the external disturbances and non-idealities. The control circuit usually senses and feeds back the output signal $\tilde{x}(t)$, although, in general, it could sense and feed back any converter's state variable.

Like the modulator, the control circuit does not process power; it can be implemented with either analogue or digital circuitry. The compensation algorithm must be designed for each specific amplifier, since the control circuit could destabilise the amplifier if not properly tuned. The control circuit can also operate in open-loop, without sensing any state variable. In such a case, the processing performed by the control circuit can be considered pre-emphasising the input signal.

Converter's Output Delay Because of the power processing performed by reactive components (either a voltage is converted into current by an inductor

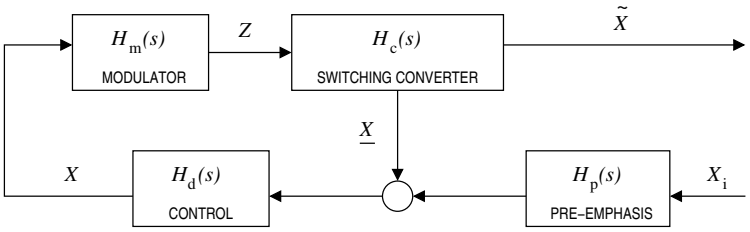

Figure 1.19: Classical control scheme for a switching amplifier.

or a current is converted into voltage by a capacitor), the output signal $\tilde{x}(t)$ is delayed with respect to the switching signal $z(t)$ (the signal which drives the converter and controls the energy-draining process). Certainly, each integration has an intrinsic time-delay associated, yielding a final delay τ in the total energy processing (in average modelling, the converter is modelled as a transfer function and thus the output delay). If the switching signal $z(t)$ is the result of instantaneously modulating a reference signal $x(t)$, i.e. $x(t_0)$ is modulated within $z(t_0)$, and distortion is not significant, then

$$\tilde{x}(t) \approx x(t - \tau) \tag{1.21}$$

Figure 1.18 shows a representative example of the previous situation, a switching amplifier operating in open-loop, based on a second-order buck converter. The waveform of the inductor current i_L is synchronised with the control signal $z(t)$, whereas the waveform of the capacitor voltage (i.e. the output signal $\tilde{x}(t)$) is delayed.

Classical Linear Control (PID) Classical control schemes rely on the averaged model to linearise all non-linear subsystems in a switching amplifier (the switching power converter and the modulation, the decoding logic is implicitly linearised when linearising the switching converter); the non-linear problem is then simplified to a classical linear control one.

Assuming that the switching frequency is much higher than the amplifier's tracking bandwidth (and that input signals are bandlimited to the amplifier's tracking bandwidth), the converter dynamics is much faster than the input signal's. When tracking a slow-varying signal, the converter locally behaves as in steady-state (its operation can be approximated by a succession of slightly different steady-states, quasi-static approximation). The linearised converter can be then modelled as a transfer function $H_c(s)$. The modulator must be modelled as a transfer function as well $H_m(s)$. Once these non-linear subsystems have been linearised and modelled as transfer functions, the control loop can be designed using classical control techniques (e.g. PID controllers, see figure 1.19).

This control scheme can only be used if the switching frequency is constant and much higher than the input signal's bandwidth (usually a ratio upwards of ten). This constraint limits the application field of classical control to kHz-bandwidth applications such as audio and grid-interactive inverters. In wider bandwidth applications, this strategy would lead to designs operating at very high switching frequencies, unfeasible in terms of switching losses (using state-of-the-art technology).

Note that the addition of the control circuit does not address the efficiency-distortion trade-off of switching amplifiers, although the control circuit mitigates the distortion caused by non-idealities and external factors.

1.3.8 Linear-Assisted Power Amplifiers

Broadly speaking, linear amplifiers are energetically inefficient but linear, whereas switching amplifiers are efficient but distorting. Certainly their respective principles of operation intrinsically limit the efficiency in the formers and the tracking fidelity in the latters. The linear-assisted technique combines both kind of amplifiers, pursuing power amplifiers with balanced efficiency and distortion.

A linear-assisted power amplifier consists in parallel-connecting an open-loop switching amplifier (modulator and switching power converter) and a linear amplifier, both tracking the same input signal $x_{\mathrm{i}}(t)$ (see figure 1.20). If properly designed, the switching amplifier provides a distorted power-amplified signal which conveys most of the output power, whereas the linear amplifier tunes the output waveform either by trimming the voltage excess or by providing additional voltage (thus handling low power). The combined operation may lead to a power-amplified low-distortion output signal, performed with moderate efficiency.

The dissociation is more clear in the frequency-domain, as each amplifier should operate in a different range. The switching amplifier should properly track the lowband content of the input signal $x_i(t)$, which could be even the DC component solely. The linear amplifier should track highband content of the input signal $x_{\mathrm{i}}(t)$ as well as eliminate the output ripple generated by the switching amplifier (mostly at high frequency).

When parallel-connecting a linear amplifier and a switching amplifier, it is difficult to guarantee the proper band separation, i.e. that the low-band power is supplied by the switching amplifier and not by the linear amplifier. Furthermore it is necessary to properly compensate time-delay τ in the switching path; otherwise each stage would try to supply the load with a different voltage, thus degrading the efficiency.

Consistently with the scope of high-efficiency, the switching amplifier generally operates at switching frequencies comparable to the input signal's bandwidth, even though the actual switching frequency has to be optimised in each specific design [14]. In this way, it is feasible to track wideband input signals (in the range of hundreds of kilohertz and upwards) in applications requiring low distortion and moderate efficiency.

Note that this technique does not address the efficiency-distortion trade-off of switching amplifiers. Indeed all the power associated to the high-frequency distortion of the switching amplifier is dissipated in the linear amplifier; the distortion is reduced, but at the cost of degrading the efficiency.

1.4 Problem Identification and Challenges

The previous sections have identified the two main applications which require high-efficiency power amplifiers (portable and high-power audio and adaptive supply for RFPAs) and have reviewed the different kinds of available power

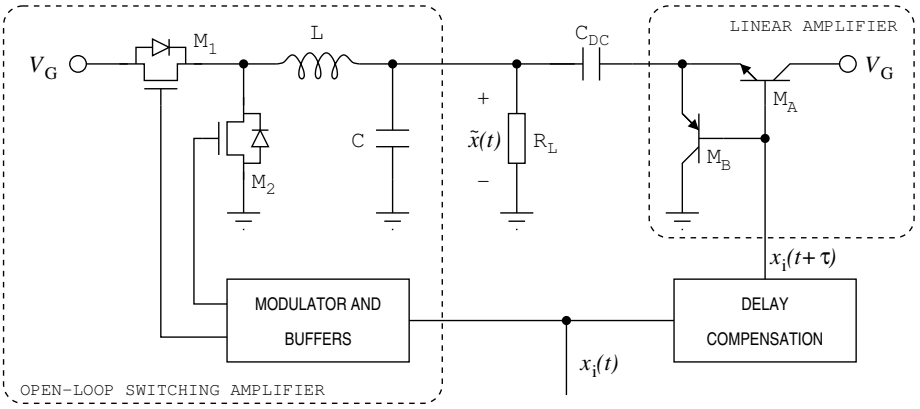

Figure 1.20: Example of a linear-assisted power amplifier. The switching amplifier is based on a buck converter and the linear amplifier is decoupled with a series capacitor.

amplifiers. As discussed above, high-efficiency power amplification can only be achieved with switching amplifiers (including linear-assisted amplifiers).

This research explores alternative techniques to reduce the distortion caused by switching amplifiers and extend their bandwidth, i.e. techniques to address the efficiency-distortion trade-off of switching amplifiers, mainly targeting (but not limited to) adaptive supply for RFPAs and portable and high-power audio. In order to properly state the problem, it is necessary to analyse the specifications and characterise the statistics and the properties of the signals involved in these applications: audio signals and envelope signals of pulse-shaped multibit modulations.

1.4.1 Audio Signals

There exists controversy in defining the audible frequency range. Whilst young people can sense high-pitch sounds close to 20 kHz, most adults and especially elderly are unable to sense sounds beyond 16 kHz. Despite the controversy, the frequency range defined by High-Fidelity (HiFi) digital audio, from 20 Hz up to 20 kHz, is widely accepted as standard audio frequency range. Consistently, audio in Compact Disc Digital Audio system (CD-DA) is sampled at 44 100 Hz; besides, each sample is quantised with 16 bits (96 dB of dynamic range) and encoded using Pulse-Code Modulation (PCM), a lossless format. CD-DA comprises two channels (stereo).

Audio signals are therefore bipolar (zero average). The amplitude histogram of pure audio signals is gaussian; the shape of the power spectrum of pure audio signals is approximately gaussian as well. However, the parameters of these two distributions, as well as other parameters such as the amplitude peak-to-RMS ratio, strongly depend upon each specific audio sample. Furthermore, if the audio signal is clipped (a common technique in audio power amplifiers to increase the output power without increasing the output peak voltage), all parameters and distributions change.

Most of the power conveyed by audio signals concentrates at low frequencies, around 1 kHz. Nevertheless, high-fidelity audio power amplifiers must guarantee low distortion within the whole audio range (up to 20 kHz), since low-power

distortion even at frequencies upwards of 10 kHz is still audible (otherwise the definition of audible range would be narrower). The power distribution of audio signals is only significant for power amplifiers processing specific audio subbands.

Figure 1.21 shows the power spectrum, the cumulative-power frequency distribution and the amplitude histogram of two different audio signals: classical music[10] and industrial metal music[11].

Besides the intrinsic differences for being different kinds of music, there is a significant difference between these two audio samples: clipping. Despite both samples have been directly extracted from their respective original CDs, the industrial metal sample clips (clipping time is less than 1 %). The other sample, classical music, does not clip because it was recorded at a lower volume. Indeed, if normalising the available dynamic range to ± 1 V, the RMS value would be 48 mV in the classical sample (peak-to-RMS ratio of 6,0), whereas in the metal industrial sample would it be 379 mV (peak-to-RMS ratio of 2,6). In both signals, 90 % of the audio power concentrates below 2 kHz.

The higher volume of the metal industrial sample can be seen in the he power spectrum (higher power values) and in the amplitude histogram (higher probability of higher values). The clipping effect can be seen in the amplitude histogram, as is not continuous (hence not gaussian); the probability of the maximum and minimum values is higher than that of any other value.

1.4.2 Envelope Signals of Pulse-Shaped Multibit Modulations

The envelope signals of pulse-shaped multibit modulations are unipolar, baseband, continuous-time and with DC component. Different modulations yield different envelope signals, although the differences are not significant. Two representative examples, the envelope signals of QPSK and 64-QAM, are included in figure 1.22, which shows their time waveforms, power spectra and the cumulative-power frequency distribution.

The envelope signals of pulse-shaped multibit modulations are not bandlimited [15]. Yet more than 85 % of the power is conveyed at DC; furthermore, more than 98 % of power is conveyed within the first modulation's chip rate (including DC). Unfortunately, the current and upcoming communication standards define wide chip rates, in the range of several MHz; e.g. in UMTS the chip rate is 3,84 Mcps, the envelope signal's 98 %-bandwidth is hence 3,84 MHz.

Regarding the time waveform of the envelope signals, the amplitude peak-to-RMS ratio is 2,3 in envelope of 64-QAM, whereas it is 1,9 in envelope of QPSK. The amplitude histogram is approximately gaussian in both cases, although the parameters (mean and variance) depend upon the modulation (see figure1.23).

[10] Sample extracted from Wolfgang Amadeus Mozart's Hornkonzert Nr.3 Es-dur, KV 447 - Allegro, from the album Hornkonzerte Nr. 1-4; the sample comprises 35 seconds of music (60 s − 95 s). Data directly extracted from the original CD.

[11] Sample extracted from Rammstein's Rosenrot, from the album Rosenrot; the sample comprises 33 seconds of music (93 s − 126 s). Data directly extracted from the original CD.

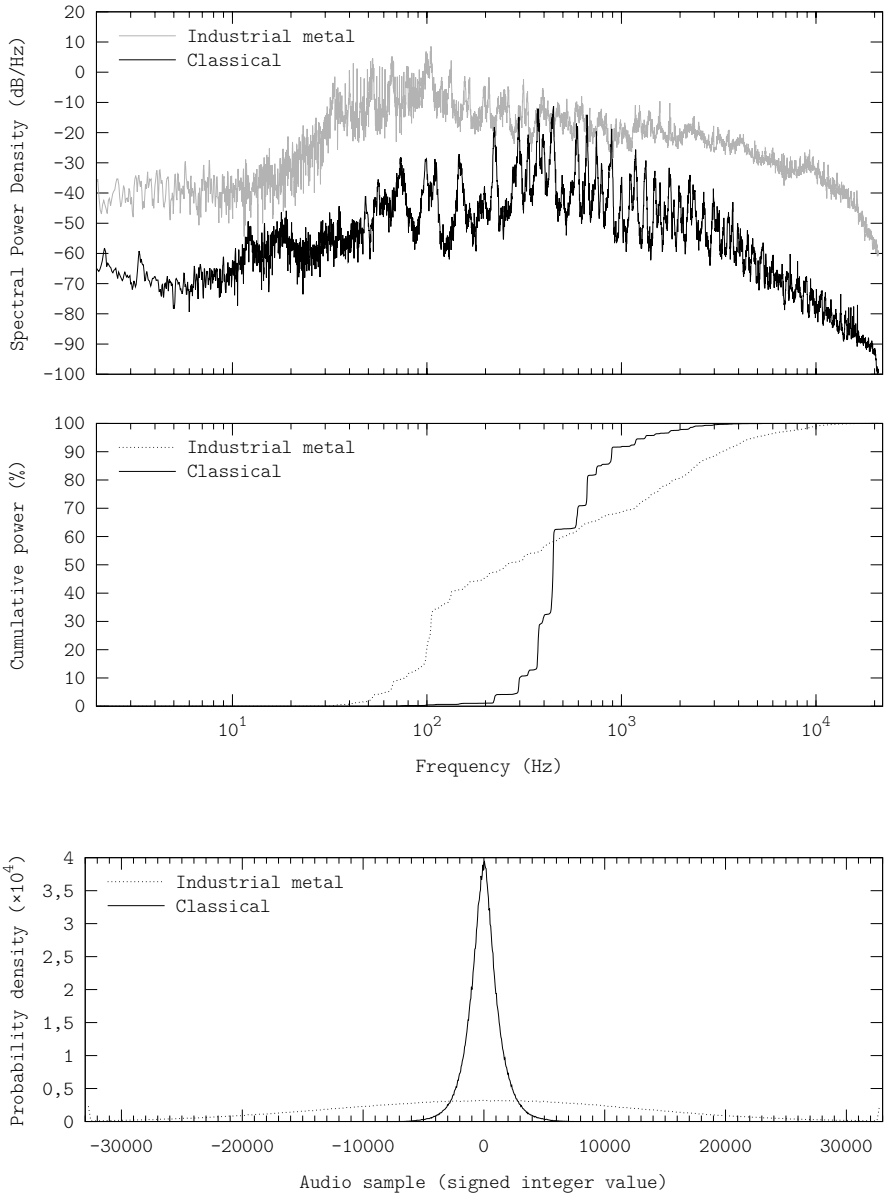

Figure 1.21: Power spectrum (upper plot), cumulative-power frequency distribution (middle plot) and amplitude histogram (lower plot) of two audio signals. Simulation performed using the configuration D.4.2.

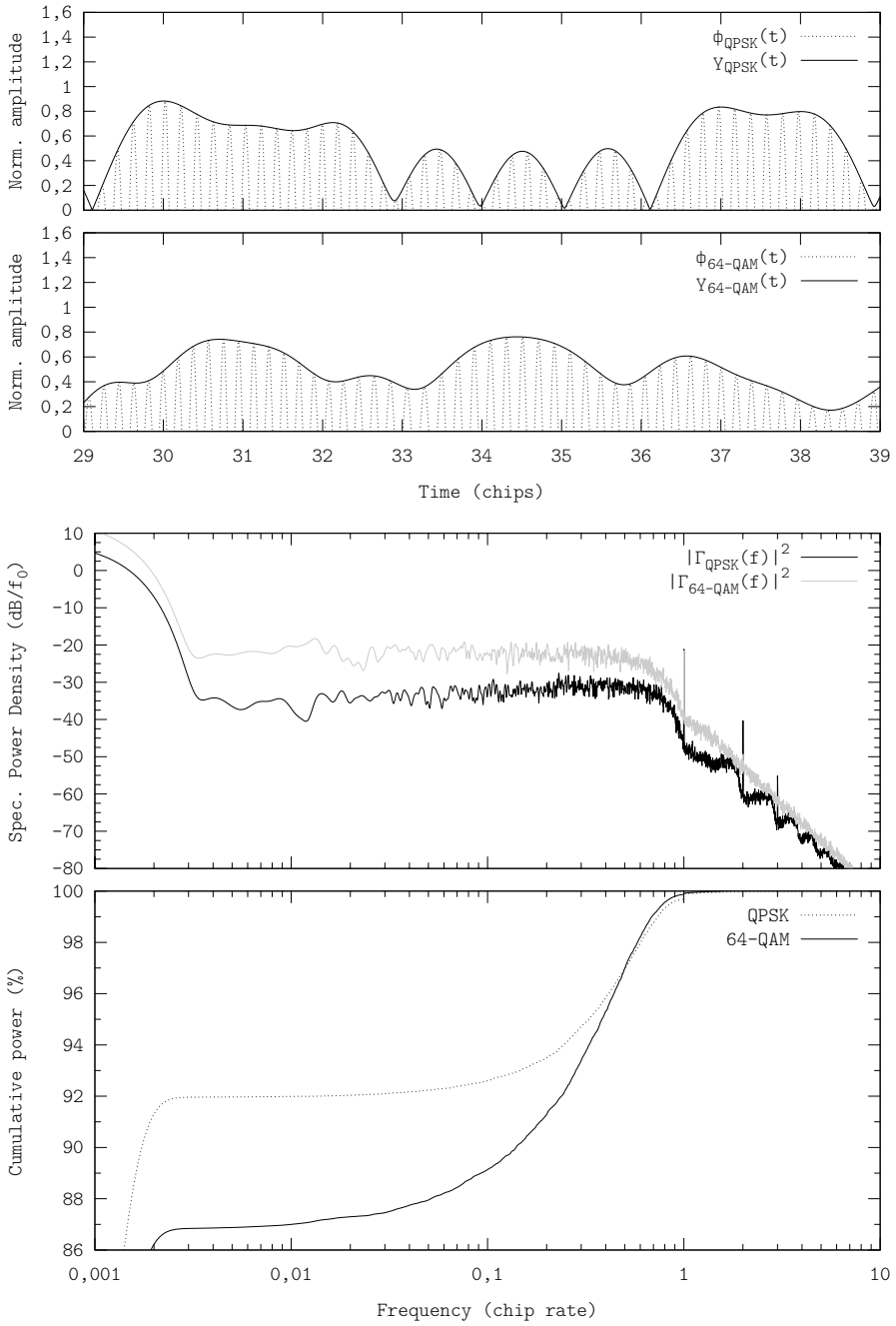

Figure 1.22: Envelope signals of QPSK and 64-QAM. $\gamma(t)$ and $\Gamma(f)$ stand for the envelope signal's time waveform and power spectrum respectively. Displayed waveforms show the time waveforms (time-domain plots), the power spectrum (upper frequency-domain plot) and the cumulative-power frequency distribution (lower frequency-domain plot). Simulations performed using the configuration D.4.1.

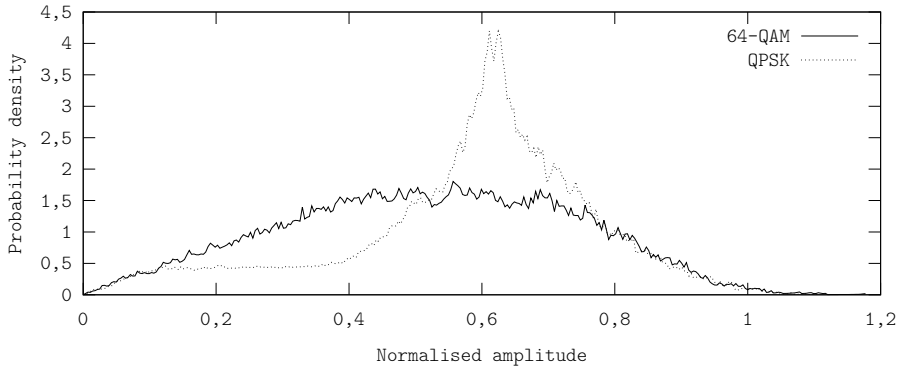

Figure 1.23: Amplitude distribution of the envelope signals of pulse-shaped QPSK and 64-QAM.

1.4.3 General Problem Statement and Main Objectives

Despite the heterogeneous nature of audio and envelope signals, the power-amplification challenge can be stated in a similar way for both audio (including portable and high-power applications) and envelope tracking applications. Certainly, as discussed above, audio signals effectively behave as bipolar 20 kHz-bandlimited signals (yet strictly speaking, they are bandpass signals). On the other hand, envelope signals either are bandlimited as well (ET) or can be approximated by bandlimited signals (EER), typically in the range of MHz.

Therefore, in both cases, a bandlimited signal must be power amplified with maximum efficiency, i.e. with a switching amplifier. Due to the efficiency-distortion trade-off of switching amplifiers, the challenge is to reduce the amplifier's switching frequency whilst still achieving satisfactory tracking (e.g. a switching audio amplifier in which switching losses must be reduced to use a smaller and lighter heatsink) or, alternatively, to properly track faster signals at a specified switching frequency (e.g. a linear-assisted envelope amplifier operating at the maximum switching frequency bearable by the technology, the wider the switching amplifier's tracking bandwidth, the lower the power supplied by the linear amplifier).

In either scenario, with the goal of addressing the efficiency-distortion trade-off of switching amplifiers, this research explores system-level techniques to reduce the distortion generated by switching amplifiers when power-amplifying a bandlimited signal (without increasing the switching frequency), i.e. to reduce the ratio of the amplifier's average switching frequency to the amplifier's tracking bandwidth required for satisfactory tracking. Despite the different architectures for high-efficiency power amplifiers (closed-loop and linear-assisted), this general statement is valid in both cases, since the performance of all power amplifiers including a switching amplifier is limited by the efficiency-distortion trade-off of switching amplifiers.

This research has been carried out at system level because, in recent years, most performance and efficiency improvements have been achieved at transistor or layout level, by minimising the energy loss in each switching event [13]. Whilst these improvements allow operating at higher switching frequencies and hence tracking faster signals, it is possible to further extend the amplifier's tracking

bandwidth at system level, by using alternative modulations and/or topologies. This alternative strategies may allow reducing the ratio of the amplifier's average switching frequency to the amplifier's tracking bandwidth required for satisfactory tracking.

For analyses at system level, bandlimited flat-spectrum signals properly model the actual reference signals. Besides, defined in this way, the problem is not stated for any specific application; it is about analysing structure and the operating principle of high-efficiency power amplifiers. The results can be afterwards particularised to a specific application considering its specific details, if necessary.

1.5 State of the Art

State-of-the-art high-efficiency power amplifiers (and regulators) are mostly closed-loop. Particularly in applications such as audio (especially portable and battery-powered), DC-to-DC regulation (including power supplies for portable devices such as mobile phones) and utility grid feeding (power injection through grid-interactive inverters), amplifiers based on closed-loop switching converters are quite consolidated and corner the market, well ahead of any other kind of amplifier.

Most research in state-of-the-art switching amplifiers is focused in optimising their performance by fine-tuning the design (transistor or layout-level improvements). As a representative example [16], the research in switching audio amplifiers for mobile applications is focused in minimising implementation-induced effects such as of dead time, digital modulators or settling time.

The efficiency-distortion trade-off of switching amplifiers is often addressed using design techniques which where originally intended to improve the performance of switching regulators. Pursuing to explore alternative techniques for switching amplifiers, some system-level techniques specifically developed to improve the performance of switching regulators are also analysed next.

1.5.1 Closed-Loop Switching Power Amplifiers

The most common design strategy of closed-loop switching amplifiers is the classical fixed-frequency PWM compensated by linear control techniques. This strategy has been successfully applied to both regulators and amplifiers and, nowadays, its use is widespread. For instance, most audio switching amplifiers for portable battery-powered applications are based on a second-order full-bridge converter, driven by a triangle PWM operating at switching frequencies in the range of hundreds of kHz [16].

The key of the success of closed-loop amplifiers in these applications (audio, grid-interactive inverters and regulators) is the low bandwidth of the signals to track. Indeed audio signals, the widest signals in these three applications, are bandlimited to 20 kHz. When tracking these kind of signals, it is feasible to mitigate the audible distortion (due to output ripple) by increasing the switching frequency, as state-of-the-art switching converters can operate at switching frequencies in the range of hundreds of kilohertz, even at a few megahertz, with reasonable high efficiency [17].

Furthermore, outband audio specifications are not very strict (signals in the range of hundreds of kilohertz are not audible) and thus the high-frequency distortion due to output ripple is not a significant drawback.

Since audio signals are bipolar (the DC component is not audible), audio switching amplifiers are based on a full-bridge converter. This topology is capable of generating a multi-level output (specifically, three levels: $\pm V_{\mathrm{G}}$ and GND); this feature is often used in switching audio amplifiers.

3-Level Audio Switching Amplifiers

Full-bridge converters for audio applications can be driven as two independent buck converters, one tracking the input signal $x_{\mathrm{i}}(t)$ and the other one tracking the inverted input signal $-x_{\mathrm{i}}(t)$, see figure 1.24.

If properly designed, a power-amplified input signal is applied at the load's positive end $v_{\mathrm{o}}^{+} \approx x_{\mathrm{i}}(t)$, whereas a power-amplified inverted input signal is applied at the load's negative end $v_{\mathrm{o}}^{-} \approx -x_{\mathrm{i}}(t)$. The load is therefore subdued to a (differential-mode) voltage signal

$$\tilde{x}(t) = v_{\mathrm{o}}^{+} - v_{\mathrm{o}}^{-} \approx 2x_{\mathrm{i}}(t) \tag{1.22}$$

hence this scheme not only properly tracks the input signal but also doubles the supply voltage dynamic range V_{G}.

Even though by driving a full-bridge converter with this modulation strategy a 3-level switching signal $\tilde{z}(t)$ is generated (defined as the voltage difference between the full-bridge converter's ends, i.e. before the inductors),

$$\tilde{z}(t) = \tilde{z}_{\mathrm{p}}(t) - \tilde{z}_{\mathrm{n}}(t) \tag{1.23}$$

this modulation strategy is not a multi-level modulation. Indeed the modulation is a regular 2-level PWM. The combination performed by the full-bridge converter (floating output) results in three different differential-mode voltages (applied before the inductors). The generation of multiple levels is therefore due to the full-bridge topology and not due to the modulation. Note that this strategy of independently driving each buck converter is not limited to PWM; it can be applied with any two-level modulation.

The 3-level switching signal $\tilde{z}(t)$ only aids in modelling and analysing the amplifier's performance, as the performance achieved by this driving strategy is equivalent to the performance achieved by a 3-level buck converter (this analogy is further discussed in section 5.3).

Figure 1.24 shows an example of an audio switching amplifier based on a full-bridge converter, operating in open-loop, driven as two independent buck converters. The modulation used is PWM, but this driving strategy can be used with any modulation. Actual amplifiers are designed to operate in closed-loop (each buck converter has its own control circuit) and the negative modulator would probably use an inverted carrier $c'(t) = c(t - t_{\mathrm{d}})$ (because of the delay added by the inversion block when generating the inverted reference signal), but the operating principle is the same.

This driving strategy is simple to implement and yields some of the benefits of multi-level operation, although the intermediate level in the 3-level switching signal $z(t)$ is generated by driving both buck converters either ON or OFF (high common-mode voltage). Multi-level modulations and common-mode and differential mode voltages are further analysed in chapters 5 and 7.

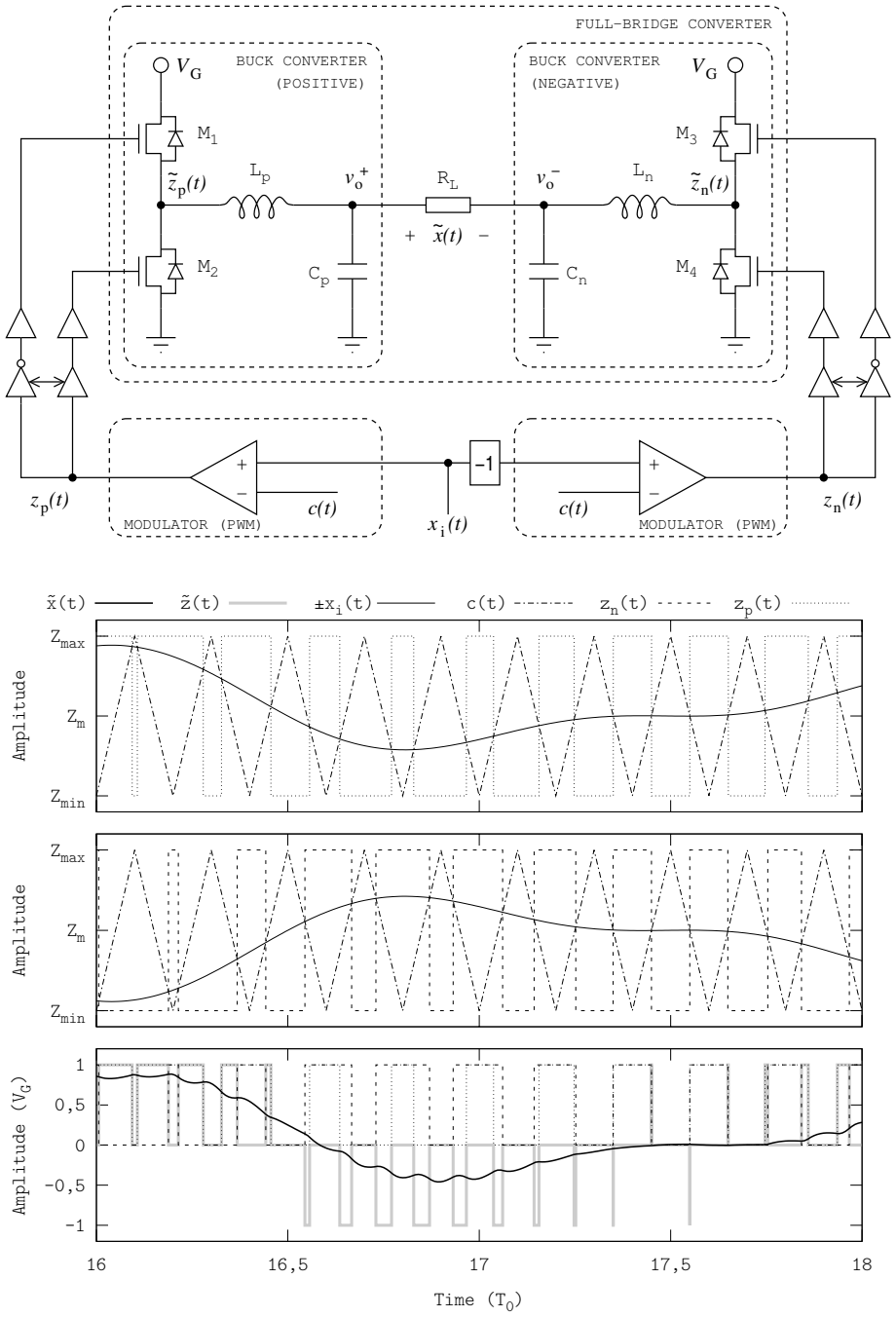

Figure 1.24: Example of a 3-level open-loop audio switching amplifier. The full-bridge converter is driven as two independent buck converters, tracking the input and the inverted input signals ($z_p(t)$ and $z_n(t)$ have been scaled in the lower plot to be properly displayed).

1.5.2 System-Level Enhancements for Switching Amplifiers

Despite the popularity of closed-loop switching amplifiers and their good performance, some system-level enhancements have been explored to improve their performance. These enhancements have not had commercial success, but they indeed provide insights about how to address the efficiency-distortion trade-off of switching amplifiers. The most promising and relevant techniques are described next.

Self-Oscillating Amplifiers

In closed-loop switching amplifiers, it is possible to improve the tracking bandwidth by using unstable control loops. Even if no reference signal is applied to the amplifier, it keeps oscillating (self-oscillating amplifiers).

In self-oscillating amplifiers, the control loop is designed to deliberately destabilise the amplifier (e.g. by adding a time delay or a phase-shift) [18], thus converting it in an oscillator. Note that the standalone modulator is stable, such as a fixed-frequency PWM.

In phase-shift self-oscillating amplifiers, the control loop is designed so that the transfer function has unity gain at 180° (the loop is unstable and hence the amplifier oscillates). This technique has been applied to audio amplifiers [19] and it significantly improves the THD+N performance, yet it is very sensitive to EMI (in multichannel applications such as stereo, it results in crosstalk).

Asynchronous ΣΔ Modulator

Asynchronous ΣΔ Modulator (AΣΔM) is a continuous-time modulator [20], which generates an analogue two-level switching signal $z(t)$ by integrating the difference between the discrete-amplitude signal $z(t)$ and the reference signal $x(t)$, see figure 1.25 [21]. The principle of operation and the performance of this modulator is further analysed and described in section 4.2.

Despite AΣΔM is well-known [20], different names have been used to refer to it. Regardless of the name, this modulator (consisting of an integrator and a hysteresis comparator) has been used to achieve very low THD values in audio applications [22], [23]. The switching signal $z(t)$ is generally sensed after the power switches and the switching frequency is experimentally tuned by adjusting the integrator gain and/or the hysteresis width.

Different techniques to achieve constant switching frequency have been proposed [24]. Despite AΣΔM has a built-in fast feedback loop (there is no filtering or compensation in the feedback loop), it can be applied to both open-loop and closed-loop designs.

Note that the switching frequency of switching amplifiers based on asynchronous modulations (e.g. AΣΔM) is not set by an external oscillator; instead, the system locks to a certain frequency depending on the modulator and the reference signal. Because of this adaptive principle of operation, switching amplifiers based on asynchronous modulations are often referred as "self-oscillating" in the literature. Nevertheless this work distinguishes between switching amplifiers based on asynchronous modulations, in which the modulator itself is an oscillator, and self-oscillating amplifiers, in which the oscillation is caused by

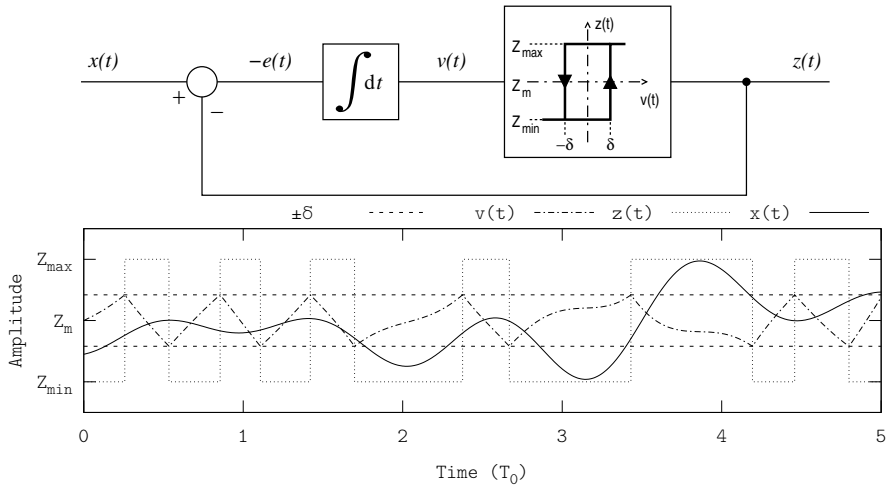

Figure 1.25: Asynchronous ΣΔ modulator and representative time waveforms. Displayed waveforms show the reference signal $x(t)$ (solid line), the switching signal $z(t)$ (dotted line) and the integrator's output signal $v(t)$ (dashed line).

the control loop and not to the modulation (e.g. in open-loop they do not oscillate). For instance, a standalone AΣΔM is already asynchronous and hence a closed-loop amplifier based on an AΣΔM is asynchronous as well.

Click Modulation

This modulation was presented in 1984 [25] pursuing signal prefect recovery in high-distortion conditions, in the context of analogue signal processing. Despite this modulation was not originally intended for switching systems, it can also be applied to switching amplifiers. The peculiarity and unique feature of this modulation is that, if using an appropriate filter, the information conveyed by the reference signal $x(t)$ can be perfectly recovered from the click modulated two-level switching signal $z(t)$, i.e. the original information is preserved (neither PWM nor AΣΔM allow perfect recovery by low-pass or bandpass filtering, see chapter 4 for further details).

Given that zero-crossings are more robust against distortion than amplitude, click modulation encodes the information conveyed by the reference signal $x(t)$ within the zero-crossings of a bandlimited signal $s(t)$, suitable for transmission over highly distorting channels. The bandlimited signal $s(t)$ can be afterwards clipped, leading to a two-level switching signal $z(t)$ which preserves the original information.

The encoding process described by this modulation is more complex than that of conventional switching modulations. Click modulation describes a sort of pulse-position modulation leading to a sequence of equal-intensity impulses or clicks $g(t)$

$$g(t) = \pi \sum_{k=-\infty}^{\infty} \delta(t - t_k) \tag{1.24}$$

where $\delta(t)$ stands for the Dirac delta function, so that a desired bandpass signal

$\dot{x}(t)$ may be obtained by filtering the clicks, i.e.

$$\dot{x}(t) = g(t) * h(t) = \pi \sum_{k=-\infty}^{\infty} h(t - t_k) \tag{1.25}$$

where $h(t)$ is the impulse response of a suitable band-pass filter. If $x(t)$, the bandpass reference signal[12] whose derivative is $\dot{x}(t)$, is sufficiently small, $x(t)$ can be obtained as

$$x(t) = \int_{-\infty}^{\infty} z(\tau)h(t - \tau)\,\mathrm{d}\tau \tag{1.26}$$

where $z(t)$ is a two-level switching signal simply related to $g(t)$, the impulse train.

The time instants t_k, which indeed convey the reference signal's information, are found as zeros of the bandlimited signal $s(t)$. Referring to figure 1.26, the signal $s(t)$ is generated through the reference signal $\dot{x}(t)$, its Hilbert transform $\hat{\dot{x}}(t)$ and an analytic exponential modulator, which furnishes the outputs

$$W(t) = e^{\hat{\dot{x}}(t)} \cos\left(x(t)\right) \tag{1.27}$$

$$Y(t) = -e^{\hat{\dot{x}}(t)} \sin\left(x(t)\right) \tag{1.28}$$

These two signals $W(t)$ and $Y(t)$ are low-pass filtered, yielding the signals $w(t)$ and $y(t)$ respectively. The bandlimited signal $s(t)$ can be the generated by combining both low-pass filtered signals

$$s(t) = w(t)\cos(\omega_1 t + \varphi) + y(t)\sin(\omega_1 t + \varphi) \tag{1.29}$$

where ω_1, the carrier frequency, is constrained by the bandpass and the stopband of the low-pass filter.

The properties of this modulation [26] make it a candidate of interest for switching amplifiers. Compared to PWM, since the original information is preserved, it may be possible to reduce the switching frequency and still properly track the reference signal (i.e. reduce the amplifier's switching frequency without reducing the amplifier's tracking bandwidth).

Click modulation has been successfully implemented and applied to audio applications [27], [28], [29]. Even though analogue circuitry was suggested to implement the analytic exponential modulator [25], click modulation has only been implemented digitally, with Digital Signal Processors (DSPs).

Nevertheless, this modulation is not used in commercial designs because the tracking fidelity improvements achieved by this modulation are challenged by its implementation hardness (especially in the upcoming MHz-bandwidth applications). Furthermore, a reduction of the switching frequency does not necessarily involve an efficiency improvement, especially in low-frequency (e.g. audio) applications.

Indeed, the power-loss saved due to the reduction of the switching frequency could be lower than the additional power consumed by the click modulator and

[12] The constraint of the reference signal $x(t)$ being bandpass instead of low-pass, only involves that, with regard to the modulator's dynamic range, the average of the reference signal $x(t)$ must be Z_m (midpoint of the modulator's input dynamic range). Any low-pass signal with no DC component can be modulated with click modulation.

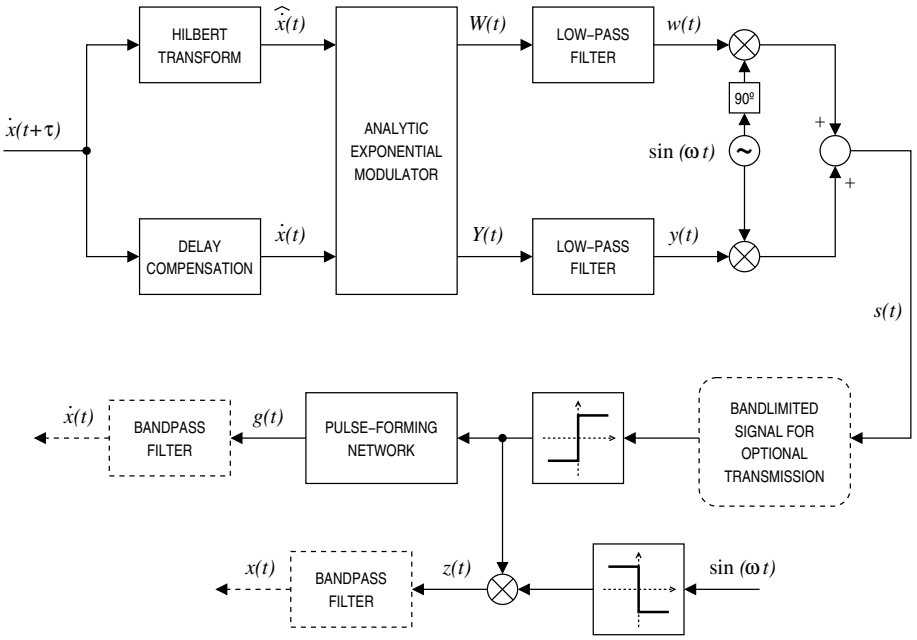

Figure 1.26: A click modulation system. Only the delay of the Hilbert transform block τ is explicit, since this delay must be properly compensated.

the higher output ripple. Note that a reactive filter attenuates the output ripple but it does not consume power (high-efficiency power-processing), whereas if the output ripple is supplied to the speaker, it is played (i.e. it consumes power), despite not belonging to the human audible frequency range.

Compared to conventional PWM-based audio switching amplifiers, the improvements in terms of tracking error are not significant, since other distortion sources such as dead time or EMI limit the amplifier's performance thus masking the distortion-less feature of click modulation.

Like AΣΔM, click modulation has also been referred as "Zero-Position-Coding with Separated Baseband" (SB-ZePoC) in the literature, although the modulation algorithm is the same.

Optimum-Time Control and Minimum-Time Control

The computation capabilities of state-of-the-art digital controllers and modulators, allow to perform real-time operations to optimise each switching event. In particular, it is feasible to, based on the evaluation of the system trajectories, evaluate the optimum time instants so that the power converter reaches the desired state with only two transitions [30].

This technique has been successfully applied to different applications, including servomechanisms to position the head of hard-drives [31], [32], [33]. Nevertheless, the application field of these techniques (i.e. the bandwidth of the signals to track) is strongly constrained to the computation capacity and the circuit (or mechanism) to control.

1.5.3 State-of-the-Art Switching Regulators

The classical linear closed-loop design strategy has been successfully applied to switching regulators. Regardless of its good performance, alternative techniques have also been explored targeting additional features such as enhanced robustness against load variations.

The specifications for switching regulators are different than the specifications of switching amplifiers. For instance, typical specifications for switching regulators often require fast transient responses to handle sudden and wide load variations or accepting a wide range of supply voltages.

Recent research has been focused in exploring asynchronous modulations (mostly sliding mode control) and multi-level operation. Non-linear switching converter topologies have also been explored.

Sliding Mode Control

Sliding mode control [34] is a control technique for switching power converters, originally intended for regulators, which does not rely on the averaged model. Instead, it defines an error vector $\underline{e_{\mathrm{v}}}$ (1.30), through which the converter can be modelled.

Although this control strategy was originally intended for regulators, it can also be applied to switching amplifiers. The ratio of the switching frequency to the amplifier's tracking bandwidth is lower than in classical linear controllers, since sliding mode control does not rely on the quasi-static approximation (still a similar approximation is necessary to approximate the input signal $x_{\mathrm{i}}(t)$ by a slow-varying signal, although this constraint is less severe). However, this control technique is not as popular as classical control techniques in switching amplifiers because its implementation generally results in non-constant switching frequency.

Analysing sliding mode control in more detail, the error vector $\underline{e_{\mathrm{v}}}$ is defined as

$$\underline{e_{\mathrm{v}}} := \left[(v - V^*) \quad \cdots \quad \frac{\mathrm{d}^{N-1}\,(v - V^*)}{\mathrm{d}t^{N-1}} \right] \tag{1.30}$$

where v stands for the variable to control (typically the output voltage) and V^* stands for the reference signal. The converter can be modelled and expressed in terms of the error vector

$$\dot{\underline{e_{\mathrm{v}}}} = f_0(\underline{e_{\mathrm{v}}}) + f_1(\underline{e_{\mathrm{v}}})z(t) \tag{1.31}$$

The sliding mode controller imposes a specific dynamics to the system (error dynamics). By defining the proper gain vector $\underline{G} := [g_0 \ \cdots \ g_{N-1}]$, the differential equation $\underline{G} \cdot \underline{e_{\mathrm{v}}}^{\mathrm{T}} = 0$ expresses the dynamics which converges to the desired value (i.e. $v \to V^*$ when $t \to \infty$, see figure 1.27). The differential equation is usually written as a switching surface $\sigma(v,t)$

$$\sigma(v,t) := \underline{G} \cdot \underline{e_{\mathrm{v}}}^{T} = \sum_{i=0}^{N-1} g_i \frac{\mathrm{d}^i (v - V^*)}{\mathrm{d}t^i} \tag{1.32}$$

The main feature of this control technique is robustness, since the controller always leads the system to the switching surface, and keeps it there once it is

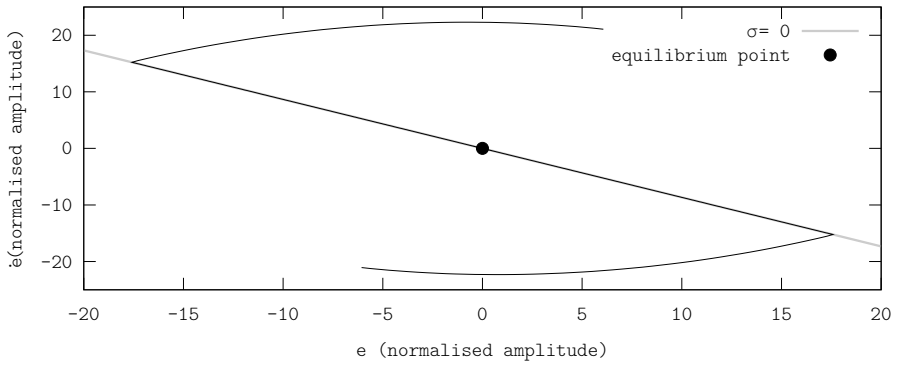

Figure 1.27: System trajectories in the phase plane in a sliding mode control, using the surface $\sigma(t) = \lambda\dot{e}(t) + e(t)$.

reached. Formally, the value of the control variable is chosen so that

$$\sigma(v,t)\,\dot{\sigma}(v,t) < 0 \tag{1.33}$$

The control law is designed using the equivalent control (the control value when the system is on the switching surface, z_{eq}). Switching converters generally comprise two states, which can be modelled as $z_{\min}$ and $z_{\max}$. If the controller is properly designed $z_{\min} < z_{\text{eq}} < z_{\max}$, therefore the control law is given by the sign of $\sigma(v,t)$

$$\begin{cases} \sigma < 0 \Rightarrow z > z_{\text{eq}} \Rightarrow z = z_{\max} \\ \sigma > 0 \Rightarrow z < z_{\text{eq}} \Rightarrow z = z_{\min} \end{cases} \tag{1.34}$$

Note that this control technique already provides the control signal $z(t)$, i.e. the modulator is built-in the controller. As the previous expression shows, the switching frequency is not set by any external signal and hence this modulator is asynchronous. Nonetheless, sliding mode control applied to switching systems leads to unbounded (infinite) switching frequencies. Indeed the equivalent control $z_{\text{eq}} \in (z_{\min}, z_{\max})$, but $z \in \{z_{\min}, z_{\max}\}$ and hence the controller drives the system to continuously switch (there exist techniques to bound the switching frequency, see below). Figure 1.28 summarises sliding mode control in a block diagram.

Pseudo-Sliding Mode Control

The robustness against load variations and fluctuations in the supply voltage and the enhanced transient response makes sliding mode control a candidate of strong interest for regulators, especially for Voltage Regulator Modules (VRMs) for microprocessor supply.

Unfortunately, pure sliding mode control is not feasible in switching systems, as the desired dynamics can only be achieved operating at infinite switching frequency. There exist several approaches to implement sliding mode control at bounded switching frequencies, although the dynamics and the performance is an approximation to the sliding case (pseudo-sliding mode control).

In pseudo-sliding mode, since the switching frequency is finite, the system is not able to reach the switching surface. Instead it keeps chattering around it

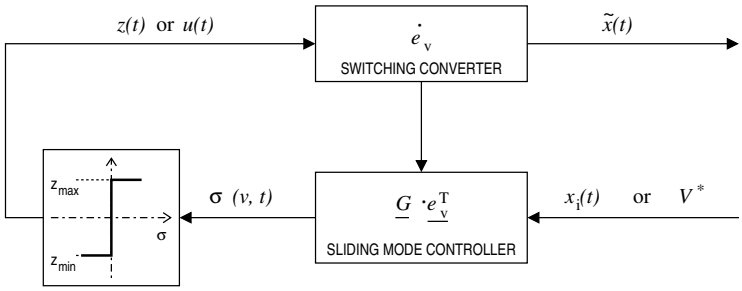

Figure 1.28: Block diagram of sliding mode control. The control signal is denoted as $z(t)$, consistently with the notation used throughout this work, yet it is often denoted as $u(t)$ in the literature.

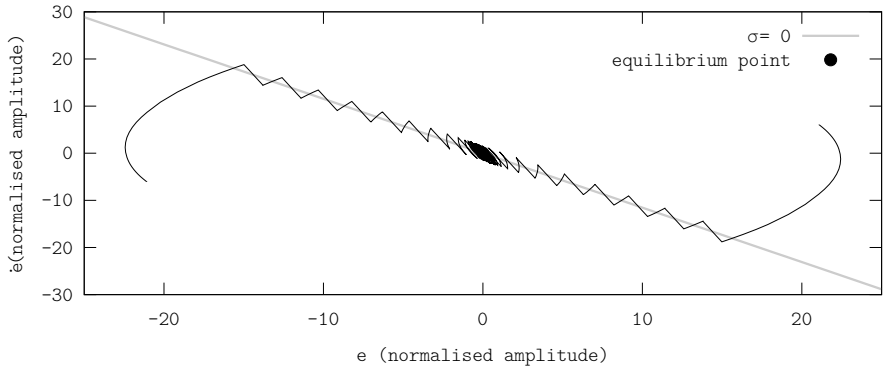

Figure 1.29: System trajectories in the phase plane in a pseudo-sliding mode control, using the surface $\sigma(t) = \lambda\dot{e}(t) + e(t)$.

(see figure 1.29), according to the switching frequency. The different approaches of pseudo-sliding mode control are aimed at reducing or bounding chattering, as well as achieving additional features such as constant switching frequency.

Zero Order Hold The first approach consists in simply adding a zero order hold after the comparator, operating at a switching frequency f_z much higher than the amplifier's switching frequency f_s. This sampled approach is simple to implement, but it yields a variable switching frequency which is highly dependent upon the sampling frequency and the converter's parameters.

Hysteresis Bandwidth This technique consists in adding hysteresis (of constant width δ) to the comparator [35]. This approach is also very simple to implement (a hysteresis comparator can be implemented with analogue circuitry).

The performance in terms of system dynamics and voltage error are similar to pure sliding mode control. The switching frequency is variable, although its value is given by

$$f_s = \frac{\partial\sigma}{\partial X}\frac{g(x)}{2\delta}\left(\frac{(z_{\min} - z_{eq})(z_{eq} - z_{\max})}{z_{\min} - z_{\max}}\right) \tag{1.35}$$

where X denotes the state vector and $g(x)$ is defined as $\mathrm{d}X/\mathrm{d}t = f(x) + g(x)z$ (often, in practical designs, the hysteresis width is experimentally tuned).

Note the similarity between the hysteresis bandwidth quasi-sliding approach and AΣΔMs. Indeed, by defining the switching surface

$$\sigma(t) = \int_{-\infty}^{t} (z(\tau) - x_{\mathrm{i}}(\tau))\ \mathrm{d}\tau \tag{1.36}$$

then both systems are the same. AΣΔMs can be therefore analysed using the theory of sliding mode control.

However, sliding mode control has been developed to track constant input signals, not bandlimited signals. The generalisation of the sliding theory to bandlimited signals is still to be addressed [36]; sliding mode control is only applied to signal tracking under quasi-static conditions.

Adaptive Hysteresis As expression (1.35) shows, the switching frequency in hysteresis bandwidth pseudo-sliding mode control depends upon the hysteresis bandwidth δ. This dependency can be used to tune the switching frequency [37]. Using a proper adaptive hysteresis law, the switching frequency may be constant [38], [39], although, depending on the implementation, the required hysteresis width could depend upon the converter's parameters.

External Synchronisation Signal It is also feasible to lock the switching frequency using an external synchronisation (reset) signal, an alternate impulse train, added at the comparator's input [40]. This signal forces the system to switch at a certain rate f_{s}, and the duty cycle within each switching period is determined by the circuit conditions. Whilst this scheme locks the switching frequency, it also modifies the system dynamics, thus resulting in a system whose dynamics, compared to pure sliding mode control, is significantly degraded.

Hybrid Controllers (PWM-Sliding Mode Control)

The theory of sliding mode control can be used to enhance the performance of conventional modulators, specifically, to generate the reference signal $x(t)$ (see figure 1.30). This hybrid approach has been applied to fixed-frequency PWM.

Equivalent Control A possible approach consist in computing the equivalent control z_{eq} and use this value as reference signal $x(t)$, with an optional zero-order hold to keep the reference signal $x(t)$ constant within each switching period (equivalent control [41]). However, even if controlling a buck converter with a simple surface such as

$$\sigma(t) = \lambda \frac{\mathrm{d}e(t)}{\mathrm{d}t} + e(t) \tag{1.37}$$

the equivalent control depends upon the system parameters $z_{\mathrm{eq}} = f(L, C, R_{\mathrm{L}})$, which results in a degradation of the robustness against load variations and input voltage fluctuations. This degradation challenges its tracking error performance, which is better than in any other quasi-sliding or hybrid approach. Because of this reason, this technique is seldom used in actual designs.

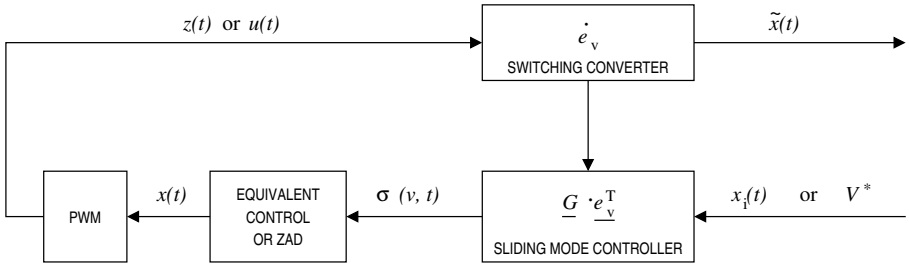

Figure 1.30: Hybrid PWM-sliding mode controller showing two different approaches, equivalent control and zero average dynamics.

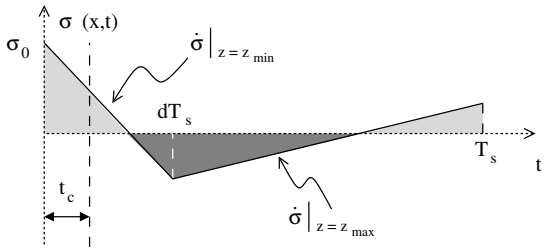

Figure 1.31: Duty cycle in ZAD pseudo-sliding mode control: the area highlighted in light grey equals the area highlighted in dark grey.

Zero Averaged Dynamics A more complex approach is Zero Averaged Dynamics (ZAD) [42]. In ZAD the reference signal $x(t)$ is generated so that the average of the switching surface is zero within each switching period (hence the ZAD name, see figure 1.31)

$$\langle \sigma(x,t) \rangle := \frac{1}{T_\mathrm{s}} \int_{kT_\mathrm{s}}^{(k+1)T_\mathrm{s}} \sigma(x,\tau)\,\mathrm{d}\tau = 0 \qquad \forall k \in \mathbb{Z} \tag{1.38}$$

The duty cycle d fulfilling (1.38) is a non-linear function of the initial condition σ_0 (the value of the surface at the beginning of the switching period) and it requires estimating the derivatives of the switching surface.

$$d = 1 - \sqrt{\frac{\dot{\sigma}|_{z=z_\mathrm{max}} - 2\dfrac{\sigma_0}{T_\mathrm{s}}}{\dot{\sigma}|_{z=z_\mathrm{max}} + \dot{\sigma}|_{z=z_\mathrm{min}}}} \tag{1.39}$$

The implementation of ZAD must therefore be digital. In digital implementations, the minimum duty cycle is set by the modulator's computation time t_c. This value limits the minimum duty cycle which, effectively, limits the amplifier's tracking bandwidth. t_c can be reduced by increasing the modulator's computation capabilities, which generally involves increasing its power consumption. Using state-of-the-art technology, it is feasible to implement ZAD for grid-interactive inverters.

Despite the finite switching frequency and the PWM, ZAD exhibits similar properties than sliding mode control. Compared to a PWM based on linear control techniques, ZAD improves the trade-off between steady-state error and

transient recovery time (yet the equivalent control technique exhibits better performance than ZAD).

End of Point Prediction

Regulators are also used in ET applications (adaptive supply for RFPAs) in which the envelope signal is approximated by a discrete-amplitude signal [43]. For these applications, targeting to improve the converter's transient response, the End of Point Prediction (EPP) technique was proposed [44]. EPP consists in feedforwarding the reference voltage to the output of the controller circuit, thereby anticipating the controller compensation. Whilst this technique improves the transient response, its application is limited to fixed-frequency PWM regulators, delivering a discrete-amplitude voltage.

Parallel-Connected Converters

In some applications such as VRMs for microprocessors, the inductor current and/or the output current are very high; dealing with very high currents is challenging. A common technique to address this issue consists in parallel-connecting several identical converters (a parallel-connected converter consisting of N identical subconverters, see the example in figure 1.32).

By using this parallel-connected configuration, the output current of all subconverters are added at the output stage and hence each subconverter only handles a fraction (precisely I_o/N) of the output current I_o. If all subconverters are driven by the same two-level switching signal $z(t)$, the parallel-connected converter behaves as a high-power regular converter.

Note that the output capacitors of all subconverters are parallel-connected and hence they can be added in a single capacitor. The output capacitor is shared in any voltage-output subconverter topology.

Also note that, since the output current of all subconverters are added, so are the output ripples of each subconverter. If these output ripples are not the same (i.e. their time waveforms do not coincide), their addition may partially cancel them out, yielding a low-ripple output current $i_\mathrm{o}(t)$.

Multi-Phase Converters Parallel-connected converters can be upgraded by driving the subconverters with different switching signals $z(t)$. This technique is generally implemented by driving all subconverters with a PWM operating at the same switching frequency f_s, but using different phases in the carrier signal $c_i(t)$ of each subconverter [45] (multi-phase converters). Using the proper phase-shifts, the ripples in each subconverter or phase may partially cancel out, thus minimising the output ripple of the multi-phase converter.

Let us consider a simple case, a two-phase buck converter (consisting of two triangle PWM-based buck subconverters). A phase-shift can be added to one carrier signal, e.g. $180\,^\mathrm{o}$ or π rad

$$c_1(\omega_\mathrm{s} t) = c_0(\omega_\mathrm{s} t + \pi) \qquad \forall t \in \mathbb{R} \tag{1.40}$$

so that the steady-state inductor currents in both phases are phase-shifted as well. When adding the current of both phases, the ripple signals partially cancel out, thus minimising the output ripple of the 2-phase buck converter. This example is illustrated in figure 1.32; compared to the case with-

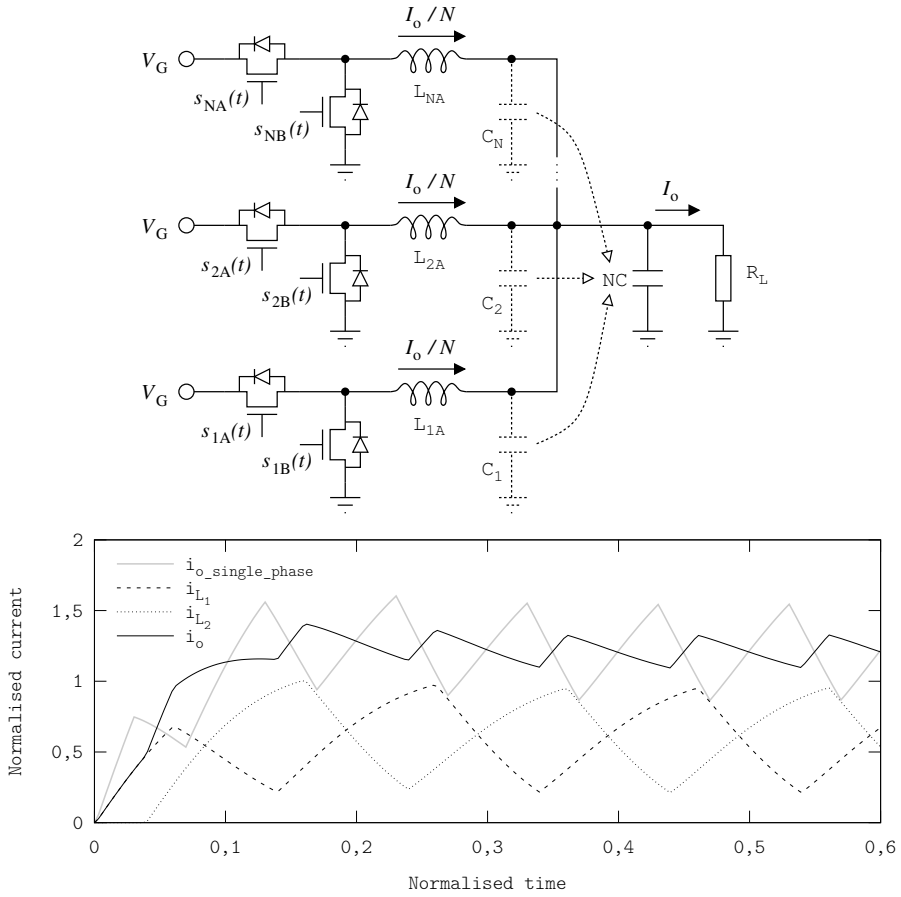

Figure 1.32: Buck parallel-connected converter. Example showing a buck converter consisting of N buck subconverters. Displayed waveforms correspond to $N = 2$, showing the output current without interleaving (grey), the output current with interleaving (solid black) and the current through each inductor (with interleaving, dashed and dotted lines).

out phase-shift (i.e. $c_0(t) = c_1(t)$ in grey), the peak-to-peak output ripple is $\Delta i_o = 0{,}34 \Delta i_{o\_single\_phase}$.

Actual parallel-connected converters use several phases, to further reduce the output ripple. The phases are generally regularly separated, although due to practical limitations, there exists an optimum number of phases (depending on the technology and the application) beyond which, more phases do not yield further performance improvements [9]. The phase-shifts are generally given by

$$c_i(\omega_s t) = c_0 \left(\omega_s t + \frac{2\pi}{N-1} i \right) \qquad \forall t \in \mathbb{R},\ i = \{0, \ldots, N-1\} \tag{1.41}$$

where n is the number of phases.

Because of the output ripple reduction, with multi-phase converters it is feasible to fulfil the specifications with smaller reactive components (high ripple in each phase, but low output ripple). Smaller reactive components lead to faster

system dynamics, i.e. enhanced transient responses. This technique is widely used in state-of-the-art Voltage Regulator Modules (VRMs) for microprocessor supply, because it allows both providing a voltage with low ripple and handling sudden and wide load variations (fast transient responses).

Note that with this technique, the output ripple is not eliminated (as in linear-assisted amplifiers); instead it is partially cancelled out or not generated. The ripple is reduced without compromising the converter's efficiency: even though the number of switches increases, the power involved in every single switching event (which mainly determines the power-loss in each switching event) is only a fraction of that in a hypothetical equivalent single-phase converter, i.e. switching losses are not significantly increased.

Although this technique was originally proposed for regulators, to improve the transient response and reduce the output ripple, the ripple-reduction features of this technique makes it a candidate of interest for switching amplifiers. The multi-phase technique has been generalised and applied to audio switching amplifiers, to address the efficiency-distortion trade-off (multi-phase full-bridge converters consisting of n full-bridge subconverters connected in parallel, each of them driven by a fixed-frequency PWM with a different phase, Parallel Phase Shifted Carrier Pulse Width Modulation).

Parallel Phased Shifted Carrier Pulse Width Modulation Parallel Phased Shifted Carrier Pulse Width Modulation (PSCPWM) is the application of multi-phase techniques to signal tracking. The converter's structure is the same than in multi-phase converters: several identical buck subconverters connected in parallel and sharing the output capacitor; all subconverters are supplied from the same supply voltage and driven with different phases. The structure can be applied to unipolar signals (all subconverters are connected in parallel and the load is grounded) or to bipolar signals (the load floats and each of its ends is driven by half of the subconverters, see figure 1.33).

Each buck subconverter generates a 2-level PWM voltage signal (the levels are GND and the supply voltage V_{G}), which is subsequently converted into current by an inductor; the output current of all subconverters are then added, yielding harmonic cancellation if driving the subconverters with the proper phases.

The analysis of the output ripple reveals that, due to harmonic cancellation, PSCPWM achieves the same performance in terms of distortion (spectral content of the output ripple) than multi-level PWM (multi-level PWM is described in the next subsection and in section 5.3). It is therefore possible to establish an analogy between PSCPWM and multi-level PWM.

It is important to note that regardless of harmonic cancellation, N-PSCPWM is not a multi-level switching modulation; it is a combination of two-level modulations instead. Similarly to multi-phase converters, no multi-level switching voltage signal is generated with this configuration.

PSCPWM was originally proposed for audio applications, i.e. bipolar configuration, with each subconverter driven by constant-frequency PWM [46], [47]. The scope was to reduce the output ripple across the load R_{L} by taking advantage of harmonic cancellation. Several variants were proposed, including carriers with other waveforms (leading edge and trailing edge sawtooth PWMs) and a topology or switching power stage for multi-level PWM synthesis.

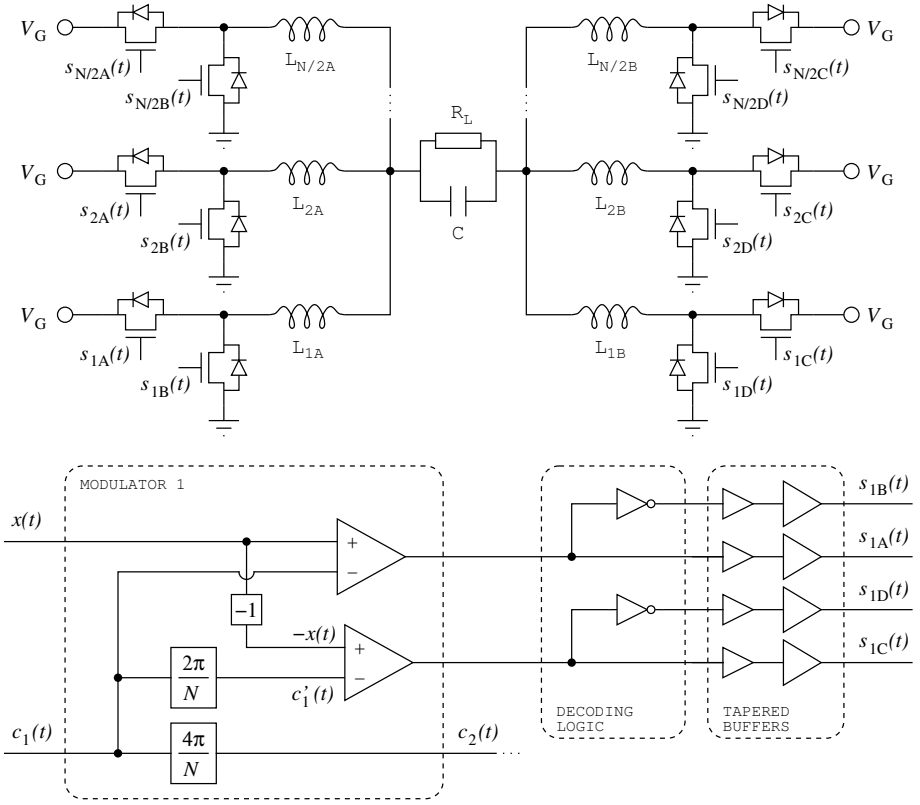

Figure 1.33: Parallel phase shifted carrier pulse width modulation. Example showing a bipolar converter (full-bridge topology) and the modulator for the first full-bridge sub-converter.

Implementation details may vary depending on the variant, but they are all based on the same operating principle. Let us consider a unipolar converter consisting in N buck subconverters. Each buck subconverter tracks the input signal $x(t)$ and is driven by a different carrier $c_i(t)$. The carriers are phase-shifted so that they are regularly distributed (see figure 1.34). In this case, the load would be supplied with $N+1$ effective different levels.

$$c_i(t) = c_1\left(t + \frac{2\pi}{N}(i-1)\right) \qquad \forall t \in \mathbb{R},\ i = \{1,\ldots,N\} \tag{1.42}$$

In bipolar configurations, the load is driven by two sets of subconverters; let us upgrade the previous example to a bipolar converter by connecting $N/2$ of the buck subconverters to the load's negative end (still N buck subconverters in total, as figure 1.33 shows). The buck subconverters connected at the load's positive end track the input signal $x(t)$ and are driven by carriers $c_i(t)$ (with $i = 1,\ldots,N/2$, $i \in \mathbb{N}$), whereas the buck subconverters connected to the load's negative end track the inverted reference signal $-x(t)$ and are driven by carriers $c'_i(t)$ (with $i = 1,\ldots,N/2$, $i \in \mathbb{N}$). Three different phase strategies were proposed, each one with its own advantages and drawbacks (analysed in [47]); in type I, all phase-shifts are different but all phases are equally distributed (as

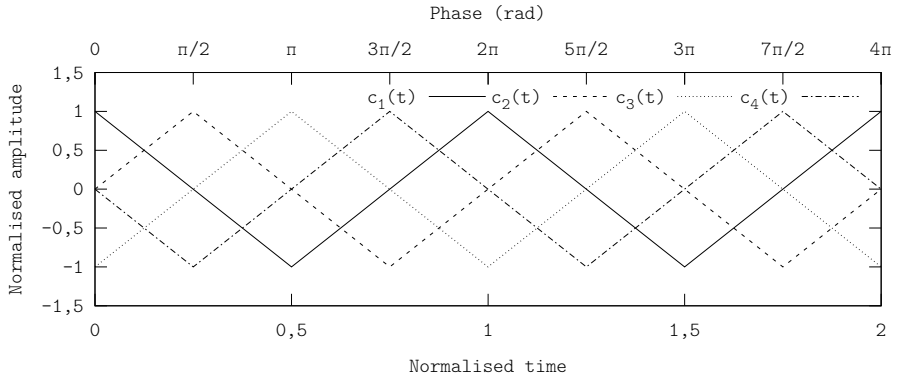

Figure 1.34: Phase-shifted carriers for unipolar phase shifted carrier pulse width modulation. Example showing four different phases ($N = 4$).

in multi-phage regulators, see figure 1.34).

$$\begin{aligned} c'_i(t) &= c_i\left(t + \frac{2\pi}{N}\right) \\ c_i(t) &= c_1\left(t + \frac{4\pi}{N}(i-1)\right), \quad i = 1, \ldots, N/2 \end{aligned} \tag{1.43}$$

In type II the phases are the same for each symmetrical buck subconverter, but they are not equally distributed.

$$\begin{aligned} c'_i(t) &= c_i\,(t) \\ c_i(t) &= c_1\left(t + \frac{2\pi}{N}(i-1)\right), \quad i = 1, \ldots, N/2 \end{aligned} \tag{1.44}$$

Type III is like type II, but the phases in each set of subconverters are equally distributed.

$$\begin{aligned} c'_i(t) &= c_i\,(t) \\ c_i(t) &= c_1\left(t + \frac{4\pi}{N}(i-1)\right), \quad i = 1, \ldots, N/2 \end{aligned} \tag{1.45}$$

There exists controversy in defining the switching frequency in multi-phase systems; it can be defined according to the number of switching events or according to the carriers' frequency. This controversy is discussed in section B.3.

Multi-Level Switching Regulators

Another technique to reduce the output ripple in switching converters, without increasing the switching frequency, consists in supplying the converter with several different supply voltages (multi-level converters). Multi-level converters, instead of generating a two-level switching signal (whose value can only be either V_{G} or GND), can generate a multi-level switching signal (whose value can be GND or any supply voltage V_i, with $i > 0$ and $i \in \mathbb{N} - 1$ if using $N - 1$ supply voltages and GND).

The extension to multiple levels is one of the most effective and promising techniques to address the efficiency-distortion trade-off of switching power processing. Multi-level switching power amplifiers consist of a multi-level modulation and a multi-level switching power converter. The operating principle is the same than that of regular (2-level) switching power amplifiers, although the discrete-amplitude signal $z(t)$ in multi-level amplifiers comprises N levels instead of two ($N > 2$, $N \in \mathbb{N}$). Both the reference signal $x(t)$ and the recovered signal $\tilde{x}(t)$ are analogue (i.e. continuous-time).

Multi-level amplifiers have been mainly used in audio, targeting filterless power amplifiers, although they have also been used in ET (approximating the envelope by a discrete-amplitude signal) [48].

Multi-Level Modulations The most common multi-level modulation in switching regulators and inverters is multi-level PWM. The natural extension of 2-level PWM to multiple levels is by using a carrier between each pair of adjacent levels ($N - 1$ amplitude-shifted carriers). Within each carrier (or encoding slot), the switching signal is generated as in a regular 2-level PWM. Even though this modulation has already been used in different applications, especially in inverters, many different variants have been reported in the literature [49], including different phases in each amplitude-shifted carrier [50] or even different frequencies [51] to adapt the encoding dynamics to the dynamics of the signal to track. The performance of multi-level pulse width modulation, including different variants, is in-depth characterised in section 5.3.

Other multi-level modulations have been reported in the literature, targeting switching amplifiers. These designs are based on a high-order $\Sigma\Delta$ modulator (generally mixing both continuous-time and discrete-time implementations), which generates a high-frequency 1-bit datastream. By upgrading the quantiser to multiple levels, multi-level amplification is achieved [52]. In order to control (reduce, in this case) the switching frequency, the hysteresis width of the quantiser is dynamically adapted using a slow control loop (the dynamics of this loop and hence the dynamics of the hysteresis width are much slower than the reference signal's dynamics), so that the average switching frequency is the desired one [53].

Multi-Level Switching Converter Topologies Different multi-level switching converter topologies have been presented in the literature, mainly targeting multi-level switching inverters. The most conventional multi-level converter topology is full-bridge, driven as a 3-level converter [16].

In multi-level inverters, conventional full-bridge converters are upgraded with multiple supply voltages [54], to generate more output voltage levels. Further description and the characteristics of multi-level full-bridge converters can be found in chapters 6 and 7.

Besides inversion, the idea of using multiple supply voltages to generate a multi-level output signal has been recently applied to envelope amplifiers [48], to supply a linear amplifier with variable voltage (yet discrete voltage values).

These topologies rely on different supply voltages to generate different voltage levels. There exist other topologies which, by using flying capacitors, are able to generate intermediate voltage levels [55], see figure 1.35. In this topology, the capacitors are charged to a fraction of the supply voltage V_{G}, thereby pro-

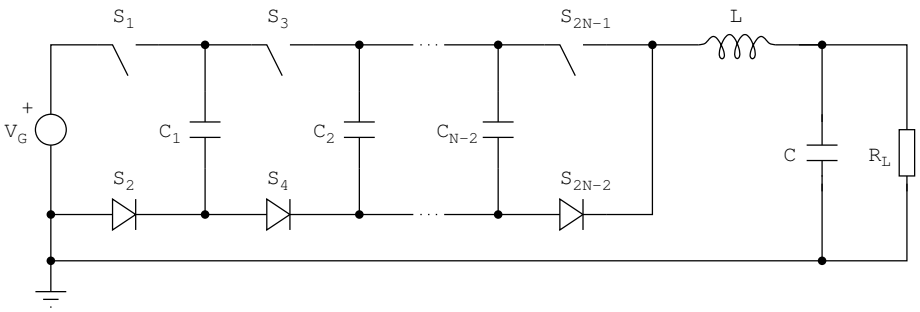

Figure 1.35: Single supply N-level buck converter (flying capacitor topology)

.

viding additional supply voltages. This topology has been tested for envelope tracking applications [56].

Non-Linear Converter Topologies

Apart from the linear converter topologies (buck and full-bridge), using non-linear converter topologies in switching amplifiers has also been explored. These topologies are more difficult to control, but they yield enhanced features such as supplying voltages beyond the supply voltage or continuous input and output currents. For instance, the boost converter is the most common topology in PFC applications, because of the continuous input current (note the inductor in series with the supply).

In the context of switching amplifiers, the suitable converter topologies are those which are able to step up and step down the supply voltage (i.e. to deliver output signals from GND to kV_{G}, being $k > 1$, $k \in \mathbb{N}$). Bipolarity can be achieved with any converter topology by differentially driving the load with two converters (floating output).

Ćuk Converter The Ćuk topology (see figure 1.36) [57], is a fourth-order converter topology whose main feature is that both the input and the output current are continuous. Similarly to the buck-boost converter topology, this topology reverses the output polarity and is able to step up and step down the supply voltage.

$$\frac{V_{\mathrm{o}}}{V_{\mathrm{G}}} = -\frac{D}{1-D} \quad D \in [0,1] \tag{1.46}$$

This converter has been used as voltage regulator [58], although because of the fourth-order dynamics, this converter is not very popular.

If this converter topology is to be used as amplifier, it is necessary to compensate the non-linear control-to-transfer function (it can be linearised by properly designing the inductors' and capacitors' ESRs [57], but this is generally unfeasible in practical designs).

Multipurpose Non-Inverting Converter By merging the buck and the boost converter topologies, a multipurpose converter is obtained (see figure 1.37). This topology can be driven as a buck (S_3 ON, S_4 OFF and S_1 and S_2 to drive

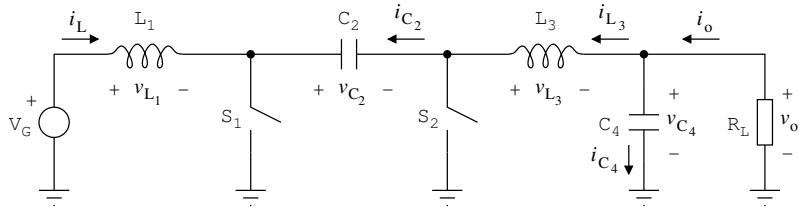

Figure 1.36: Fourth-order Ćuk converter. With displayed polarities, the output voltage v_o is negative.

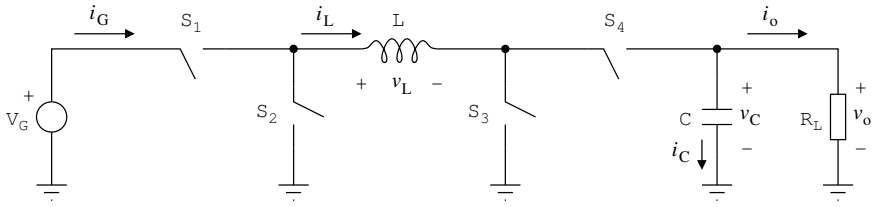

Figure 1.37: Multipurpose non-inverting second-order converter. It can be driven as a buck, as a boost or as a non-inverting buck-boost converter. An additional LC stage can be added before the load to further filter (smooth) the output signals.

the converter), as a boost (S_1 ON, S_2 OFF and S_3 and S_4 to drive the converter) or as a non-inverting buck-boost (ON-state: S_1 and S_3 ON, S_2 and S_4 OFF; OFF-state: S_1 and S_3 OFF, S_2 and S_4 ON).

This topology is able to step up and step down the supply voltage (not only as a non-inverting buck-boost, but also as a boost or a buck) and does not reverse the output polarity. The control-to-output transfer function depends upon how the converter is driven.

One of the main challenges in this topology is transitioning between the different operating modes (buck, boost or non-inverting buck-boost) without distorting the output signal.

A feasible technique to address the transition is by driving the converter as either a buck or a boost, and starting each cycle with S_1 and S_4 ON and S_2 and S_3 OFF. This state can be either the ON-state if driving the converter as a buck, or the OFF-state if driving it as a boost. By combining a leading and a trailing sawtooth PWM, the converter can be properly driven.

Using this driving technique [59], this converter has been used in ET, for adaptive supply for RFPAs. The converter operates at 1,68 MHz to track a 100 kHz signal, with an efficiency close to 90 % over a wide range of conversion ratios.

There exist other techniques to achieve smooth transition between the buck and the boost modes. The effects of pulse skipping and discontinuities during transitions upon the output ripple (distortion) have analysed and characterised [60].

This converter has also been used as a regular non-inverting buck-boost converter in ET, for adaptive supply for RFPAs [61]. Supplied from a supply voltage in the range of 2,7 V to 4,2 V, the converter is able to supply dynamically adjustable (on-the-fly) voltages in the range of 0,4 V to 4,0 V.

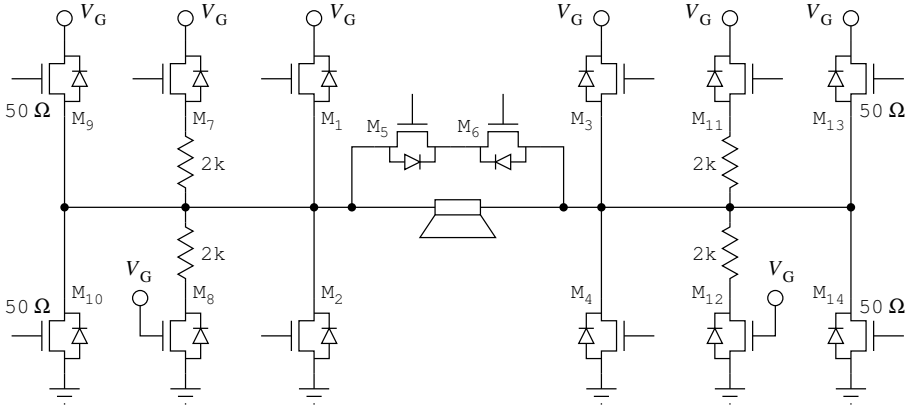

Figure 1.38: Full-bridge converter with reduced common-mode signal.

Reduced Common-Mode in 3-Level Audio Switching Amplifiers

In some applications (mostly portable) based on the 3-level audio switching amplifiers, the output filter is omitted in order to save the size, weight and cost of the reactive components (filterless amplifiers). In such a case, the output common-mode voltage signal can be an issue, especially to comply with EMI standards such as Federal Communications Commission (FCC) rules and regulations.

In regular operation of this converter, three differential-mode voltage levels are possible: positive (one side is set to the supply voltage and the other to ground, yielding a common-mode voltage of half the supply voltage), negative (the opposite operation, yielding a common-mode voltage of half the supply voltage) and zero (driving both sides to the same voltage, either ground or the supply voltage, yielding a common-mode voltage of ground or the supply voltage respectively). The common-mode voltage signal therefore switches at the amplifier's switching frequency, similarly to the differential-mode signal.

A technique to mitigate the effects of the common-mode voltage signal was recently presented [62]. This technique bases in upgrading the full-bridge converter with additional transistors (see figure 1.38), so that the zero level can be generated by driving both sides of the full-bridge converter to half the supply voltage (yielding a common-mode voltage signal of half the supply voltage).

The common-mode voltage signal is then half the supply voltage in all levels, thereby reducing its spectral power density to a DC component (ideal case). Note that additional power resources are required to generate the zero level, as well as additional circuitry is required to properly enable the additional power transistors. Mainly because of the additional power transistors and the generation of half the supply voltage, the efficiency degrades between 5 % and 10 %.

Common-Mode Signal Shaping Regarding the common-mode issue in filterless audio amplifiers, a technique to partially shape the waveform of the common-mode voltage signal was recently reported in the literature [52]. This technique consists in using a control loop to determine how the zero level is generated (either by driving both sides of the full-bridge converter to GND or to the supply voltage V_G). With this technique, it is feasible to, for instance,

to reshape and/or shift the spectral power density of the common-mode voltage signal to higher frequencies.

1.5.4 Linear-Assisted Power Amplifiers

In recent years, the popularisation of broadband communication standards, even for mobile applications, has triggered again the research upon switching regulators and amplifiers (mostly for EER and ET). Nowadays, due to the strict specifications defined by communication masks, the emerging design trend considers linear-assisted power amplifiers. Nevertheless, this design strategy is in a research stage and has not been widely applied to commercial designs yet.

Linear-assisted amplifiers are being tested in adaptive supply applications, mainly for WLAN 802.11g and CDMA2000. Adaptive supply for RFPAs is an emerging topic in power amplification; there are still several different research trends in this field. For instance, different band-separation strategies have been used in ET, including wideband tracking (sometimes referred as Wide-Bandwidth Envelope Tracking, WBET) [6], [63] and lowband tracking (sometimes referred as Average Envelope Tracking, AET) [64], [65].

Despite the different band-separation strategies, all these designs have shown a performance good enough to be considered candidates of interest. However, the efficiency of RFPAs based on adaptive supply not only depends upon the envelope amplifier, but also upon the delay equalisation and the RF modulating stage. As a result, the envelope amplifier (and the band-separation, if appropriate) must be optimised for each specific application and technology.

More recent research have been focused in optimising the output RF spectral behaviour [66] with pre-distortion techniques (signal processing) [67], [7], instead of further enhancing or optimising the envelope power amplifier. The scope is to simplify the distortion specifications of the envelope power amplifiers, so that more efficient (yet more distorting) amplifiers can be used and still comply with communication masks.

Design Techniques for Linear-Assisted Amplifiers

Either wideband or average envelope tracking, there is a common trend in the design of linear-assisted amplifiers: to reduce the ratio of the average switching frequency to the amplifier's tracking bandwidth (even below 1). As a representative example [68], a linear-assisted 20 MHz-bandwidth power amplifier (for WLAN 802.11g applications) operates at 5,3 MHz, yielding an efficiency between 50 % and 60 % (the efficiency of the standalone switching power amplifier is 75 %).

In these designs operating at switching frequencies below the reference signal's bandwidth, the switching converter is often controlled with a hysteretic current controller. The switching amplifier supplies a (rough) large slow-varying current, and the linear amplifier partially drains it or supplies further current in order to shape it into the desired waveform. The linear current (the current drained or supplied by the linear amplifier) triggers a hysteresis comparator, so that when the linear current is too low (the linear amplifier drains too much current) the switching converter switches to the OFF-state, whereas when it is too high (the linear amplifier supplies too much current) the switching switching converter switches to the ON-state.

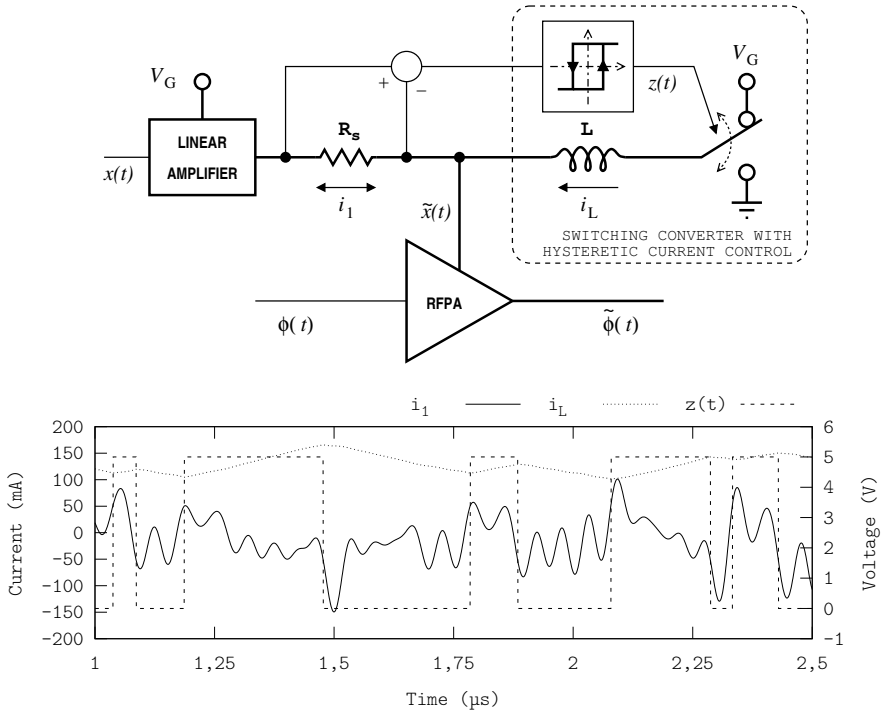

Figure 1.39: Hysteretic current controller for a linear-assisted power amplifier. In the block diagram the power path is highlighted in bold; time waveforms display the linear amplifier's output current i_1, the inductor current i_L and the switching signal $z(t)$.

Figure 1.39 shows the schematic of a hysteretic current controller and the representative time waveforms. This data has been simulated using similar values as the ones described in [68]: 20 MHz-bandwidth bandlimited reference signal, switching frequency of 3,83 MHz and $L = 12\,\mu\mathrm{H}$. The voltage supplied by the switching amplifier must be either the maximum or the minimum of the dynamic range.

Linear-assisted amplifiers have also been used in audio applications [69], to achieve high efficiency (more than 90 % delivering 10 W) and low distortion (Total Harmonic Distortion—THD of 0,1 %). In this case, the switching converter is also controlled with a hysteretic current controller, although it operates at a switching frequency around 200 kHz (so that the high-frequency distortion is not audible). There exist other architectures for linear-assisted power amplifiers [70], which are also candidates of interest for adaptive supply.

Chapter 2

A New Perspective on Switching Amplifiers

This chapter presents a new perspective on switching amplifiers, aiming to characterise their behaviour when operating at relatively low switching frequencies (non-conventional operating conditions), thereby allowing to explore their suitability as high-efficiency power amplifiers. According to the new perspective, this chapter restates the problem and defines the figures of merit and the comparison metrics used in this work.

2.1 Motivation

Switching amplifiers are generally designed like switching regulators, but replacing the constant-reference signal V_{ref} by a time-varying signal $x(t)$. In order to achieve good tracking performance relying on this design strategy, the ratio between the amplifier's switching frequency f_{s} to the amplifier's tracking bandwidth f_0 (OverSwitching Ratio—OSwR, see appendix B for the formal definition) must be high, usually upwards of ten.

Consistently with the scope of this work of extending the relative bandwidth of switching amplifiers, i.e. reducing the OSwR without compromising the amplifier's tracking fidelity, signal- and system-level techniques to satisfactorily track bandlimited signals at OSwRs below ten are explored.

Under these non-conventional operating conditions, switching amplifiers cannot be analysed with the classical theory of switching regulators. The output voltage (or current, depending on the topology) may broadly sweep the available dynamic range within a switching period. As a result, within each switching period, neither the inductors' currents can be approximated by straight currents nor the capacitors' voltages can be approximated by constant voltages.

In this context of low-OSwR operation, the performance of switching amplifiers has not been described in the literature, neither by modelling nor by characterising. The new perspective on switching amplifiers herein presented allows to in-depth characterise their performance when operating at both low and high OSwRs, thus exploring their suitability as low-OSwR power amplifiers.

All analyses described in this chapter, and also in the other chapters, refer to voltage-output amplifiers because they are the most common topologies. Yet,

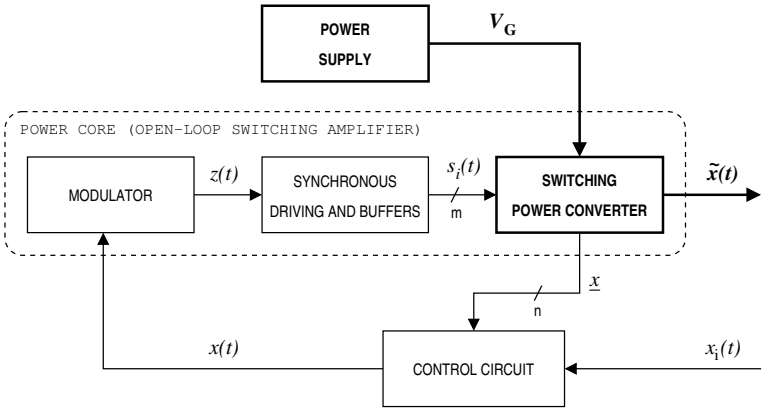

Figure 2.1: Power core identification in closed-loop switching amplifiers; the power path is highlighted in bold. $x_\mathrm{i}(t)$ denotes the closed-loop amplifier's input signal, $x(t)$ the reference signal, $z(t)$ the two-level switching signal, $s_i(t)$ the switch-driving signals, $\tilde{x}(t)$ the power-amplified output signal and V_G the supply voltage.

these analyses can be extrapolated to current-output amplifiers.

2.1.1 Open-Loop Switching Amplifiers

Switching amplifiers consist of a two-level switching modulator, a buck-based switching power converter (including the drivers to generate the set of switch-driving signals $s_i(t)$) and either a control circuit (closed-loop amplifiers) or an auxiliary linear amplifier (linear-assisted amplifiers). In both cases, the power core, the subsystem which processes an analogue signal $x(t)$ and delivers a power-amplified analogue signal $\tilde{x}(t)$, comprises the modulator and the switching power converter (see figures 2.1 and 2.2).

In power cores, the modulator processes a f_0-bandlimited reference signal $x(t)$, being f_0 the amplifier's tracking bandwidth, and delivers a switching signal $z(t)$; the switching converter, driven by the switching signal $z(t)$, delivers a power-amplified signal $\tilde{x}(t)$. The performance of the power core is independent of the auxiliary amplifier and the control circuit; none of these two subsystems modify the power core's internal operation or its performance.

In closed-loop designs, the control circuit senses the state vector $\underline{x}$ and fine-tunes the reference signal $x(t)$ so that the amplifier's output signal $\tilde{x}(t)$ tracks the amplifier's input signal $x_\mathrm{i}(t)$ regardless of non-idealities and external factors. As a result, the reference signal $x(t)$ may not be the amplifier's input signal $x_\mathrm{i}(t)$ itself, but still a f_0-bandlimited reference signal[1]. Formally, the control circuit's dynamics is much slower than the switching frequency f_s.

Similarly, in linear-assisted amplifiers, the reference signal $x(t)$ is directly the amplifier's input signal $x_\mathrm{i}(t)$, a f_0-bandlimited signal. Regarding the switching

[1]Ideally, the power core is unable of processing signals beyond its tracking bandwidth f_0 (as discussed in section 2.2.2) and thus wider reference signals do not result in a performance improvement. Nevertheless, in actual power cores, the tracking fidelity beyond f_0 gradually degrades and hence the amplifier may be able to process wider reference signals. Despite this nuance, the concept is still valid: the control circuit just provides a different reference signal $x(t)$.

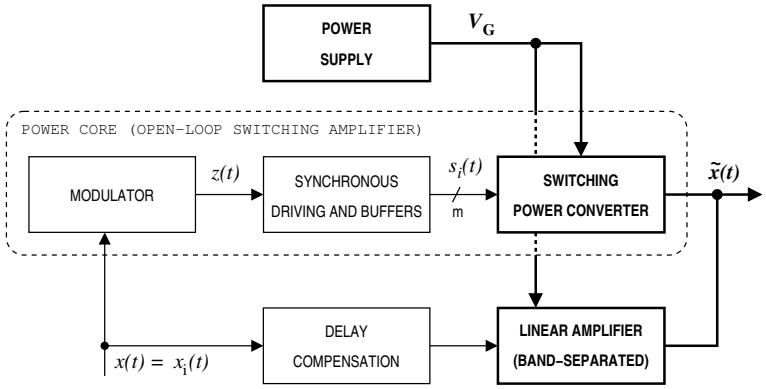

Figure 2.2: Power core identification in linear-assisted switching amplifiers. The power path is highlighted in bold. $x_{\mathrm{i}}(t)$ denotes the linear-assisted amplifier's input signal, $x(t)$ the reference signal, $z(t)$ the two-level switching signal, $s_i(t)$ the switch-driving signals, $\tilde{x}(t)$ the power-amplified output signal and V_{G} the supply voltage.

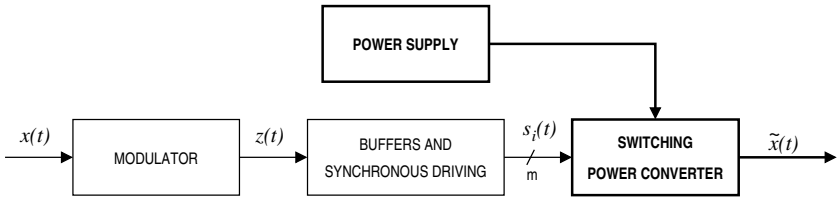

Figure 2.3: Open-loop switching amplifier, the power core of a high-efficiency power amplifier. This work is aimed at extending its relative bandwidth.

power converter, the auxiliary linear amplifier does not significantly modify its performance, since these two amplifiers operate in different frequency ranges. The inband spectral content (defined as the spectral content within the amplifier's tracking bandwidth, $|f| \leq f_0$) is provided by the switching power converter, whereas the outband spectral content (defined as the spectral content beyond the amplifier's tracking bandwidth, $|f| > f_0$) is provided by both the switching converter and the linear amplifier[2].

Therefore, in either case, the modulator tracks a low-power f_0-bandlimited reference signal $x(t)$, whether with control circuit or not, and the switching power converter, driven by the modulator, supplies the load R_{L} with a power-amplified analogue signal $\tilde{x}(t)$. Note that, in a switching amplifier (either closed-loop or linear-assisted), the power core performs the power amplification; consequently, the power core mostly determines the switching amplifier's efficiency-distortion trade-off (performance): the better the power core's performance, the better the switching amplifier's performance. Indeed, the power core is a switching amplifier itself, operating in open-loop (see figure 2.3).

[2]As discussed in the state-of-the-art revision, there exist different band-separation strategies, including inband tracking by the linear amplifier. Nevertheless, the internal operation and the performance of the switching amplifier is not affected by the band-separation strategy; the main difference is the amount of average power flowing through each power-processing device, leading to different efficiencies (this non-dependency becomes more clear with the encoding-reconstruction approach presented in section 2.2).

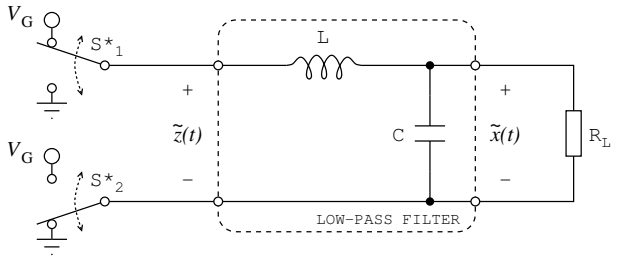

Figure 2.4: Low-pass filter interpretation of buck-based switching converters, identifying the filter's input signal $\tilde{z}(t)$ and the filter's output signal $\tilde{x}(t)$. Displayed converter shows a full-bridge topology. In the buck topology, the low-pass filter is grounded (instead of floating through the commutator switch S_2^*).

The challenge to extend the relative bandwidth of switching amplifiers is therefore addressing the efficiency-distortion trade-off of open-loop switching amplifiers operating at low OSwRs (below ten). This work is aimed at extending the relative bandwidth of switching amplifiers and hence it deals with open-loop switching amplifiers. In what follows, the term "switching amplifier" refers to open-loop switching amplifiers, unless otherwise stated.

2.2 Encoding-Reconstruction Interpretation of Switching Amplifiers

Regular switching amplifiers are based on buck-derived switching power converters, either buck or full-bridge topology. In these particular converter topologies, the reactive components are arranged in a LC ladder layout (Linear Time Invariant—LTI reactive low-pass filter). The output port of this low-pass filter is connected to the load R_L and its input port is connected to either V_G or GND (V_G or $-V_\mathrm{G}$ in the full-bridge topology) through commutator switches S_i^*, as figure 2.4 shows. It is hence feasible to define and measure the filter's input signal, namely $\tilde{z}(t)$, and the filter's output signal $\tilde{x}(t)$, which is the amplifier's output signal.

Using this interpretation and referring to figure 2.5, a switching amplifier consists of a two-level modulator and a buck-based switching power converter, which interconnects the power supply V_G and the load R_L through a set of switches and a reactive low-pass filter. The modulator processes the reference signal $x(t)$ and generates a two-level switching signal $z(t)$; this signal, properly applied through buffers, drives the switches of the switching converter so that they generate a power-amplified switching signal $\tilde{z}(t)$, which is subsequently low-pass filtered thus recovering $\tilde{x}(t)$.

In this process, the power amplification is performed by the switching power converter, specifically by its commutator switches when generating the power switching signal $\tilde{z}(t)$. Since commutator switches can only power amplify two-level switching signals (i.e. a single commutator switch can only generate either V_G or GND), the modulator must encode the information conveyed by the analogue reference signal $x(t)$ into a two-level switching signal $z(t)$, suitable to be power amplified by the switching converter (encoding process).

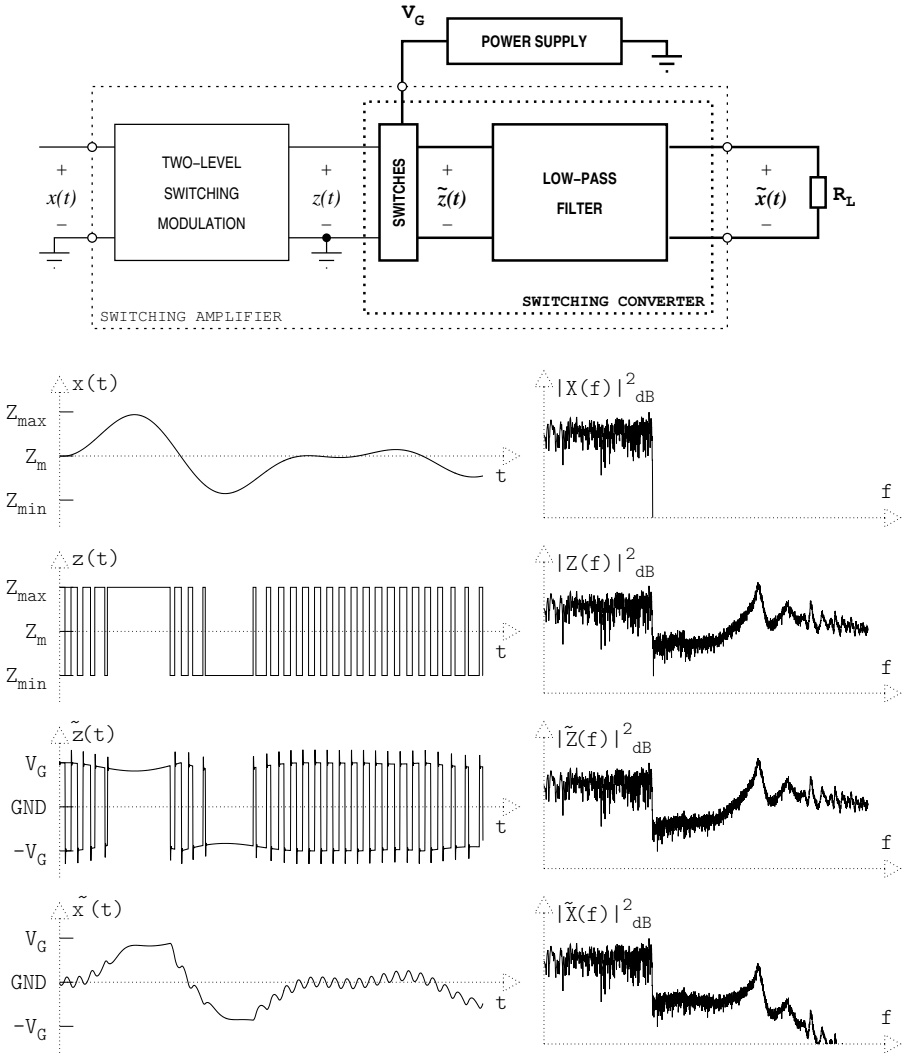

Figure 2.5: Block diagram and significant waveforms in an nth order switching power core. The power path is highlighted in bold in the block diagram and the waveforms correspond to a full-bridge topology.

Driven by the two-level switching signal $z(t)$, commutator switches generate the power-amplified two-level switching signal $\tilde{z}(t)$, which is subsequently low-pass filtered thus recovering $\tilde{x}(t)$, ideally a power-amplified distorted approximation to the reference signal $x(t)$ (decoding process).

The power-amplification process performed by switching amplifiers is therefore a twofold process: two-level time encoding (performed by the modulator) and power decoding (performed by the switching power converter). Although the information must be encoded considering how is it going to be decoded (low-pass filtering in this case), the encoding and the decoding processes can be decoupled and hence separately analysed.

The main advantage of this alternative interpretation of switching amplifiers is decoupling the encoding and the decoding processes. In this way, it is feasible to separately analyse each process, as well as optimise them by identifying the error sources involved in each process, including the effects of non-idealities. Furthermore, this interpretation also allows extending to other decoding processes (i.e. other converter topologies), including non-linear ones.

Appendix B includes a summary of the definitions of all the different signals in switching amplifiers.

2.2.1 Encoding Process: Two-Level Time Encoding

Two-level time encoding, the encoding process performed by two-level switching modulations, consists in encoding the information conveyed by an analogue reference signal $x(t)$ (continuous-time and continuous-amplitude) into a two-level switching signal $z(t)$ (continuous-time and discrete-amplitude).

Considering that the decoding process consists in band-separation (low-pass filtering), the encoding process can be modeled as the addition of an error signal $e(t)$ to the reference signal $x(t)$, in order to shape it into the two-level switching signal $z(t)$.

$$z(t) = x(t) + e(t) \tag{2.1}$$

Figure 2.6 shows a conceptual example of two-level time encoding, displaying the reference signal $x(t)$ and the switching signal $z(t)$ in the time domain and the reference signal $X(f)$, the error signal $E(f)$ and the switching signal $Z(f)$ in the frequency domain.

Provided that the encoded information is to be decoded by low-pass filtering, the error signal's inband spectral power density, $E(f)$ with $|f| \leq f_0$, should be low to avoid masking the original information. Furthermore, most of the error signal's power should concentrate at high frequency, more precisely at frequencies beyond the filter's cutoff frequency f_c, to be rejected by the low-pass filter in the decoding process.

The frequency distribution of the power of the error signal $E(f)$ is mainly determined by the switching frequency f_s (most of the error signal's power concentrates around it) and, to a lesser extent, by the modulation. Broadly speaking, the switching frequency f_s determines the frequency range wherein the error signal's power mostly concentrates, whereas the modulation shapes the spectral power density of the error signal.

In actual modulators, the switching frequency is generally constrained by switching losses and the modulation is usually constrained by a feasible implementation (implementing a real-time modulator which performs the desired

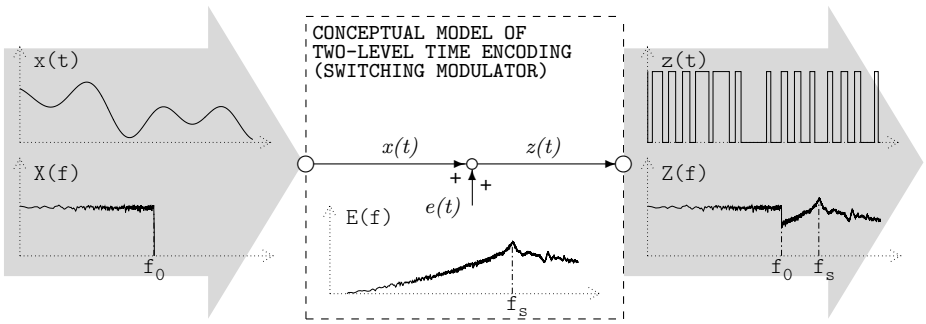

Figure 2.6: Conceptual model of two-level time encoding. Displayed waveforms show the reference signal $x(t)$ and the switching signal $z(t)$ in the time domain and the reference signal $X(f)$, the error signal $E(f)$ and the switching signal $Z(f)$ in the frequency domain.

modulation). The most common two-level switching modulation in switching amplifiers is PWM, generally operating at OSwRs upwards of 10.

Figure 2.7 shows the power spectrum and the cumulative-power frequency distribution of a PWM error signal. 70 % of error signal's power concentrates around the switching frequency $f_\mathrm{s} = 10 f_0$, whereas the error signal's inband content is very low (more than 80 dB below the reference signal, in this simulation is not visible because the simulation noise masks it).

2.2.2 Decoding Process: Power Amplification and Low-Pass Filtering

The decoding process describes the operation of the switching power converter, which performs a twofold process: power amplification and low-pass filtering.

Ideally, the time waveform of the power-amplified switching signal $\tilde{z}(t)$ is proportional to that of the switching signal $z(t)$

$$\tilde{z}(t) = G z(t), \quad \forall t \in \mathbb{R} \tag{2.2}$$

where G is the level-shifting factor (see section 2.2.3 for the formal definition).

The combination of the power supply V_G and the switches S_i, driven by the switching signal $z(t)$, behave as a controlled voltage source supplying a two-level switching voltage $\tilde{z}(t)$. According to the low-pass filter interpretation of buck-derived switching converters, this controlled voltage source supplies a low-pass filter whose output is connected to the load R_L (see figure 2.8).

Therefore, the decoding process (i.e. a buck-derived switching power converter driven at an arbitrary OSwR by a certain two-level switching signal $z(t)$) can be analysed using the classical signal processing theory of LTI systems. Indeed the switching power converter can be modeled as a gain factor G and a transfer function $H(s) = \mathcal{L}[h(t)]$, where $h(t)$ denotes the filter's impulse response, $\mathcal{L}[\,]$ the Laplace transform and $H(s)$ the filter's transfer function. In second-order topologies, the transfer function can be expressed as

$$H(s) = \frac{\dfrac{1}{LC}}{s^2 + \dfrac{1}{CR_\mathrm{L}} s + \dfrac{1}{LC}} = \frac{\omega_0}{s^2 + 2\zeta\omega_0 s + \omega_0^2} \tag{2.3}$$

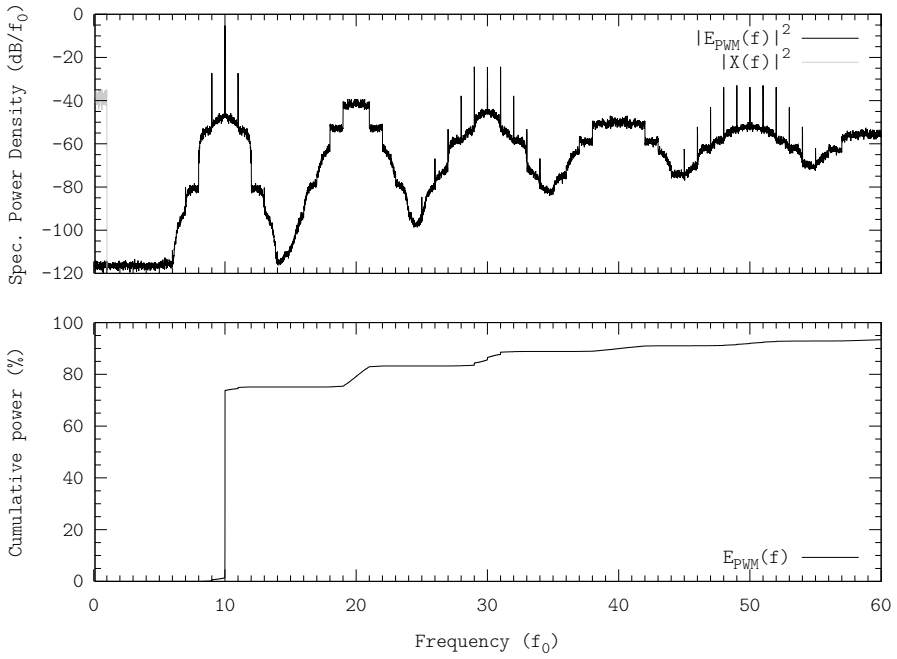

Figure 2.7: Power spectrum (upper plot) and cumulative-power frequency distribution (lower plot) of a common modulator (PWM), tracking a f_0-bandlimited reference signal at OSwR = 10. Simulation performed using the configuration D.4.1.

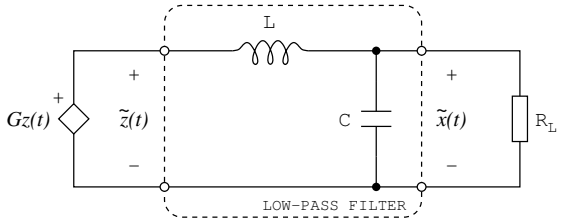

Figure 2.8: Electronic model of the decoding process performed by a switching power converter. The controlled voltage source models the power supply V_G and the switches S_i driven by the switching signal $z(t)$.

The filter's state variables correspond to the converter's state variables. The recovered signal $\tilde{x}(t)$, i.e. the amplifier's output signal, can be obtained by low-pass filtering the power switching signal $\tilde{z}(t)$. From the signal processing standpoint, the recovered signal $\tilde{x}(t)$ can be obtained by convolutioning $\tilde{z}(t)$ with the filter's impulse response $h(t)$

$$\tilde{x}(t) = \tilde{z}(t) * h(t) \tag{2.4}$$

Provided that the time waveforms of $z(t)$ and $\tilde{z}(t)$ are similar (2.2), the power switching signal $\tilde{z}(t)$ conveys the same information than the switching signal $z(t)$ and hence the power amplification itself affects neither the encoding process nor the decoding process. Therefore, applying (2.1) and (2.2) to the previous expression yields

$$\tilde{x}(t) = Gz(t) * h(t) = Gx(t) * h(t) + Ge(t) * h(t) \tag{2.5}$$

Ideally, the inband content of the error signal should be zero (inband-error-free encoding, this concept is analysed in chapter 3) and the low-pass filter should reject the content beyond f_0 and not alter the inband content (ideal low-pass filter, see section 6.1.1 for the formal definition), yielding

$$\tilde{x}(t) = Gx(t) \tag{2.6}$$

Nevertheless, switching amplifiers comprise a LTI filter. Since the stopband rejection of LTI filters is finite and their bandpass gain is not constant (not even if made with ideal reactive components, i.e. pure inductances and pure capacitances), the recovered signal $\tilde{x}(t)$ consists in a power-amplified (and delayed) approximated reference signal $\tilde{x}(t)$ and a remaining error signal $\xi(t)$ (in classical converter analysis, this remaining error signal is referred as "output ripple")

$$\tilde{x}(t+\tau) = Gx(t) + \xi(t) \tag{2.7}$$

where the remaining error signal is defined as all content present in the recovered signal $\tilde{x}(t)$ differing from the information to track and power-amplify, i.e. the (scaled) reference signal $x(t)$.

$$\xi(t) := \tilde{x}(t+\tau) - Gx(t) \tag{2.8}$$

Note that if the power-amplification process is ideal, i.e. it consists in a gain factor G, then the remaining error signal $\xi(t)$ can also be evaluated as

$$\xi(t) = Ge(t) * h(t) \tag{2.9}$$

Since LC-ladder low-pass filters are passive, the inband content of the power switching signal $\tilde{z}(t)$ is not further power amplified in the filtering process. Despite a passive filter can provide voltage gain within a narrow band, this feature is not suitable to recover bandlimited low-pass signals.

Linear-Assisted Power Decoding

Relying on the low-pass filter interpretation of buck-derived switching converters, it becomes more clear that a linear amplifier assisting a switching power

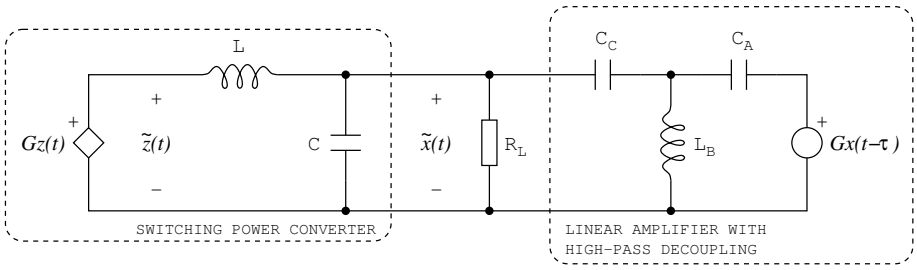

Figure 2.9: Circuit-model of a switching converter assisted by a linear amplifier (decoupled by a high-pass filter).

converter (linear-assisted power amplifiers) does not affect its operating principle; it only determines the amount of power supplied by each power-processing device.

Both the power supply V_{G} and the switches S_i operate regardless of the output voltage; consequently, the waveform power switching signal $\tilde{z}(t)$ is an approximation to the waveform of the switching signal $z(t)$ whatsoever, whether assisted by a linear amplifier or not. This combination results in the load R_{L} supplied by two different voltage sources, $Gz(t)$ and $Gx(t+\tau)$, each one decoupled by a different filter. The amount of power supplied by each source depends upon the filters' cutoff frequencies, i.e. the band-separation strategy. Figure 2.9 illustrates this situation with a circuit-model of both amplifiers.

2.2.3 Power Rate and Dynamic Ranges

In switching amplifiers, power amplification is performed by the commutator switches when generating the power switching signal $\tilde{z}(t)$ according to the switching signal $z(t)$, as discussed above. However, the switching signal $z(t)$ and the power switching signal $\tilde{z}(t)$ are energetically decoupled by the buffers. Indeed the commutator switches of the power converter, together with the buffers, generate a power switching signal $\tilde{z}(t)$ whose time waveform tracks the time waveform of the switching signal $z(t)$; given the time waveform, the power conveyed by the power switching signal $\tilde{z}(t)$ is only determined by the power supply V_{G} and the load R_{L}.

Provided that both switching signals are energetically independent, so are the encoding and the decoding processes. The encoding process (modulator) only handles low-power signals –the reference signal $x(t)$ and the switching signal $z(t)$–, whereas the decoding process (power converter) only handles power signals –the power switching signal $\tilde{z}(t)$ and the recovered signal $\tilde{x}(t)$–. Note that the encoding process can be even digitally implemented, as long as the buffers are able to generate the analogue switch-driving signals $s_i(t)$.

The instantaneous value of the two-level switching signal $z(t)$ can only be either high $Z_{\max}$ or low $Z_{\min}$.

$$z(t) \in \{Z_{\min}, Z_{\max}\}, \quad \forall t \in \mathbb{R} \tag{2.10}$$

The reference signal $x(t)$ is a continuous-time continuous-amplitude bandlimited signal bounded by $X_{\min}$ and $X_{\max}$.

$$X_{\min} \leq x(t) \leq X_{\max}, \quad \forall t \in \mathbb{R} \tag{2.11}$$

The ratio of the reference signal's amplitude sweep (or dynamic range) to the modulator's input dynamic range is defined as the modulation depth c.

$$c := \frac{X_{\max} - X_{\min}}{Z_{\max} - Z_{\min}} \tag{2.12}$$

Although, in general, the modulator's input and output dynamic ranges can belong to different ranges, they are assumed to be the same, so that the reference signal $x(t)$ and the switching signal $z(t)$ can be directly compared. In what follows and unless otherwise stated, 100 % of modulation depth c is assumed, i.e. the reference signal $x(t)$ sweeps all the modulator's input dynamic range without saturating it.

$$Z_{\min} = X_{\min} \leq x(t) \leq X_{\max} = Z_{\max}, \quad \forall t \in \mathbb{R} \tag{2.13}$$

Provided that the decoding process consists in band-separation (passive low-pass filtering), assuming the same dynamic range for the input and the output of the modulator involves no lose of generality. Certainly, from a two-level switching signal $z(t)$ bounded by $Z_{\min}$ and $Z_{\max}$, only analogue signals $x(t)$ bounded by $Z_{\min}$ and $Z_{\max}$ can be recovered by passive low-pass filtering (i.e. unitary gain) the two-level switching signal $z(t)$[3].

The levels of the two-level power switching signal $\tilde{z}(t)$ are determined by the supply voltage V_{G} and the converter topology. In a buck topology,

$$\tilde{z}(t) \in \{GND, V_{\mathrm{G}}\}, \quad \forall t \in \mathbb{R} \tag{2.14}$$

in a full-bridge topology the low-level is $-V_{\mathrm{G}}$ instead of GND.

As discussed above, by low-pass filtering the power switching signal $\tilde{z}(t)$, an analogue signal $\tilde{x}(t)$ bounded by the same levels is obtained

$$GND \leq \tilde{x}(t) \leq V_{\mathrm{G}}, \quad \forall t \in \mathbb{R} \tag{2.15}$$

in a full-bridge topology the lowerboud is $-V_{\mathrm{G}}$ instead of GND.

For the sake of notation simplicity, it is often convenient to express these signals according to the mean value Z_{m} and to the peak-to-peak Z_{pp} value of the modulator's dynamic range, defined as

$$Z_{\mathrm{m}} := \frac{Z_{\max} + Z_{\min}}{2} \tag{2.16}$$

$$Z_{\mathrm{pp}} := Z_{\max} - Z_{\min} \tag{2.17}$$

Level shifting between low-power signals and power signals, as well as power decoupling, is performed by the buffers, when generating the switch-driving signals $s_i(t)$ from the switching signal $z(t)$. In order to compare power signals and low-power signals, it is necessary to scale them by the level-shifting factor G defined as

$$G := \frac{V_{\mathrm{o}}}{Z_{\mathrm{pp}}} \tag{2.18}$$

assuming a buck-based amplifier (in full-bridge-based amplifiers $G := 2V_{\mathrm{o}}/Z_{\mathrm{pp}}$).

The different dynamic ranges of the low-power and power switching signals is explicit in figure 2.5, as low-power signals sweep from $Z_{\min}$ to $Z_{\max}$ whereas power signals sweep from $-V_{\mathrm{G}}$ to V_{G}.

[3]Under some special circumstances, it is feasible to recover signals exceeding the switching signal's dynamic range, as discussed in section 3.2.1, yet these cases are not common.

2.3 Tracking Error in Switching Amplifiers

The encoding-reconstruction interpretation of switching amplifiers points out that, even with an ideal switching converter (i.e. a switching converter consisting of ideal devices), perfect signal tracking is not possible in switching amplifiers. As expression (2.7) shows, the recovered signal $\tilde{x}(t+\tau)$ comprises the reference signal $x(t)$ and a remaining error signal $\xi(t)$, since the stopband rejection of LTI filters is finite and thus the error signal $e(t)$ cannot be completely rejected[4].

Besides the error due to the remaining error signal $\xi(t)$, tracking error can also be caused by improper time encoding (the reference signal $x(t)$ cannot be perfectly recovered from the switching signal $z(t)$ by low-pass filtering) and/or by improper power decoding (the inband content of the recovered signal is not a scaled version of the switching signal's, $\tilde{X}(f) \neq GZ(f)$, $|f| \leq f_0$).

2.3.1 Tracking Error in the Encoding Process

Two-level time encoding has been modeled as an addition (2.1): the reference signal $x(t)$ plus the error signal $e(t)$ yields the switching signal $z(t)$. The error signal $e(t)$ intrinsically models the encoding process, as it shapes the continuous-amplitude reference signal $x(t)$ into a discrete-amplitude switching signal $z(t)$. If properly encoding, the reference signal $x(t)$ can be perfectly recovered from the switching signal $z(t)$ by low-pass filtering (inband-error-free encoding) and hence the error signal $e(t)$ causes no error in the recovered signal.

Nevertheless, the error signal $e(t)$ can cause error if improperly encoding. Considering that the decoding process is low-pass filtering, the information conveyed by an arbitrary f_0-bandlimited reference signal $x(t)$ is improperly encoded into the switching signal $z(t)$ if the error signal's $E(f)$ inband spectral content is not zero

$$E(f) \neq 0, \quad |f| \leq f_0 \tag{2.19}$$

In such a case, the reference signal $x(t)$ cannot be perfectly recovered by low-pass filtering the switching signal $z(t)$, not even with an ideal low-pass filter. The recovered waveform $\tilde{X}(f)$ is therefore distorted by the remaining error signal $\Xi(f)$. If decoding with an ideal f_0-low-pass filter the recovered signal becomes

$$\tilde{X}(f) = \begin{cases} GX(f) + \Xi(f), & |f| \leq f_0 \\ 0, & |f| > f_0 \end{cases} \tag{2.20}$$

Generally, the low-pass filter is designed so that it does not significantly modify the inband spectral content of the power switching signal $\tilde{Z}(f)$, therefore the inband spectral content of the error signal $E(f)$ directly results in tracking error.

$$\Xi(f) \approx GE(f), \quad |f| \leq f_0 \tag{2.21}$$

Figure 2.10 shows an example of improper time encoding, specifically an AΣΔM tracking a f_0-bandlimited reference signal at OSwR $\approx$ 3,3; the switching signal $z(t)$ is filtered with an ideal f_0-low-pass filter (this filter has been simulated in the frequency domain, see appendix D.3.5). Despite the ideal filter, the inband spectral content of the error signal $e(t)$ cannot be rejected, thus

[4]Despite the recovered signal $\tilde{x}(t)$ is τ delayed with regard to the reference signal $x(t)$, a pure time delay (constant group delay) is generally not considered tracking error.

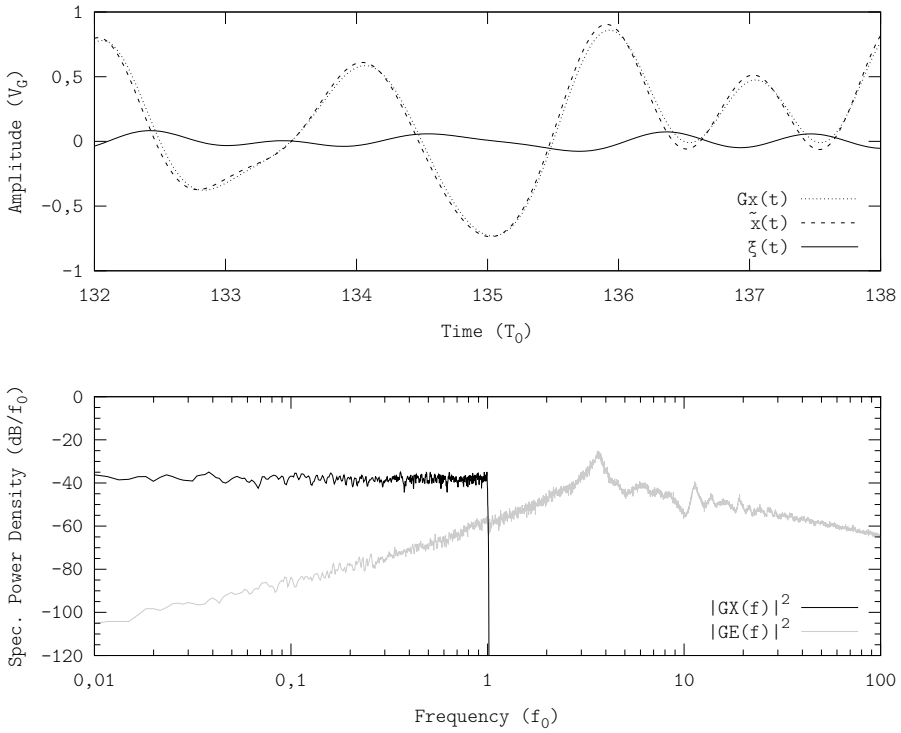

Figure 2.10: Tracking error due to improper time encoding. Example showing an AΣΔM operating at OSwR $\approx 3{,}3$ and filtering with an ideal f_0-low-pass filter. Simulation performed using the configuration D.4.1 and approximating the ideal filter in the frequency domain D.3.5.

resulting in a remaining error signal $\xi(t)$ in the recovered signal $\tilde{x}(t)$. The ratio of the remaining error signal's power $P_{\xi(t)}$ to the reference signal power $P_{x(t)}$ is approximately $-23\,\mathrm{dB}$ (0,5 %).

2.3.2 Tracking Error in the Decoding Process

The decoding process comprises power amplification and low-pass filtering, as discussed above. Ideally, the recovered signal $\tilde{x}(t)$ should be a power-amplified version of the switching signal's inband spectral content

$$\tilde{X}(f) = \begin{cases} GZ(f), & |f| \leq f_0 \\ 0, & |f| > f_0 \end{cases} \tag{2.22}$$

i.e. none of these two processes should cause error in the recovered signal.

However, due to implementation limitations, both processes degrade the tracking fidelity. As a result, referring to the recovered signal $\tilde{X}(f)$, neither its inband spectral content is a power-amplified version of the switching signal's inband spectral content $GZ(f)$, nor its outband spectral content is zero.

In the power-amplification process the error is caused by the non-idealities of the switches (mainly because of their ON-resistance and the required dead time

to avoid simultaneous conduction), which results in a power switching signal $\tilde{z}(t)$ whose time waveform differs from the switching signal's $z(t)$ and, consequently, so does its spectral content

$$\tilde{z}(t) \neq Gz(t) \Rightarrow \tilde{Z}(f) \neq GZ(f) \tag{2.23}$$

On the other hand, in the low-pass filtering process, the error is caused by the LTI filter performance (finite stopband rejection and non-constant bandpass gain). As a result, referring to the recovered signal $\tilde{X}(f)$, neither its inband content preserves the inband content of the power switching signal $\tilde{Z}(f)$, nor its outband content is zero.

$$\tilde{X}(f) \neq \begin{cases} \tilde{Z}(f), & |f| \leq f_0 \\ 0, & |f| > f_0 \end{cases} \tag{2.24}$$

Note the twofold loss of information conveyed by the switching signal $z(t)$, i.e. twofold source of inband error: some information is lost whilst power amplifying $z(t)$ and some more information is lost whilst decoding it.

The different error sources in the decoding process are described next, including simulations to illustrate the effect of each error source. All these simulations have been performed tracking a f_0-bandlimited signal with a triangle PWM operating at an OSwR of 10. The ideal performance of this modulation operating under such conditions, i.e. the error signal $e(t)$, is shown in figure 2.7. The error signal's inband spectral power density is always more than 80 dB below the reference signal's spectral power density (in figure 2.7, the actual inband spectral power density of the error signal $E(f)$ error is masked by simulation errors which, in this case, set a noise level of -120 dB, see appendix D for further information about numerical simulations and simulation parameters).

Error Due to Switches' ON-Resistance

Actual switches are made of semiconductor devices, whose ON-resistance is not zero. This ON-resistance distorts the power switching signal's time waveform $z(t)$, causing its levels not to be constant (i.e. a current-dependent supply voltage $V_{\mathrm{G}} = f(i_{\mathrm{G}})$, similarly to the effect caused by the power supply's output impedance).

Switches' ON-resistance R_{S_i}, as well as the power supply output impedance, can be incorporated to the electronic model as a resistor, connected in series with the controlled voltage source (a simple approach consists in averaging all switches' ON-resistance plus the power supply output impedance and incorporating the equivalent resistance R_{S_e}).

The effect caused upon the switching signal $\tilde{z}(t)$, which results in non-constant voltage levels, can be modeled as an additional error signal added to the power switching signal, although, for the sake of notation simplicity, this signal is not explicit. Instead this effect is expressed as

$$\tilde{z}(t) \neq Gz(t) = Gx(t) + Ge(t) \tag{2.25}$$

and hence the remaining error signal $\xi(t)$ also includes the effects due to the switches' ON-resistance and the power supply's output impedance (note that $\Xi(f) \neq 0, |f| \leq f_0$ even if inband-error-free encoding and filtering with an ideal low-pass filter).

Figure 2.11 shows a simulation of the tracking error due to switches' ON-resistance (a PWM tracking a f_0-bandlimited signal, with a full-bridge converter whose equivalent switch resistance is $R_{S_e} = 0{,}2R_L$ and decoding with an ideal f_0-low-pass filter). The difference between the power switching signal $\tilde{Z}(f)$ and the scaled switching signal $GZ(f)$ reveals that the switches' ON-resistance degrades the inband tracking fidelity, which results in an increased inband error in the recovered signal $\tilde{X}(f)$. The ratio of the remaining error power $P_{\xi(t)}$ to the reference signal power $P_{x(t)}$ is approximately $-19\,\mathrm{dB}$ (1,4 %) in this example.

Note that the RMS voltage (and hence the RMS power) of both the distorted power switching signal $\tilde{z}(t)$ and the ideal power switching signal $Gz(t)$ are similar; the high-frequency spectral content is reshaped and thus the increased error.

$$\tilde{z}(t)_{\mathrm{RMS}} \approx Gz(t)_{\mathrm{RMS}} \tag{2.26}$$

This simulation has been performed at OSwR ≈ 10, to emphasise the impact upon the inband content, although the inband content is affected regardless of the OSwR. Despite PWM shapes the power spectrum of the difference between the power switching signal $\tilde{Z}(f)$ and the switching signal $GZ(f)$ to a PWM-like spectrum, the inband error does not depend upon the modulation either. Figure 2.11 includes an additional waveform, labeled as "AΣΔM", which shows the difference between the power switching signal $\tilde{Z}(f)$ and the switching signal $GZ(f)$ in an AΣΔM signal (modulated under the same operating conditions than PWM, i.e. the same reference signal, the same equivalent switch resistance and operating at OSwR ≈ 10). The power spectra of both PWM and AΣΔM signals show similar inband error spectral power density.

Error Due to Dead Time

Finite slew-rate and non-instantaneous switch transitions have further consequences upon the power switching signal $\tilde{z}(t)$, as they require dead time to avoid cross-conduction (non-overlapping switch-driving signals). With a first-order approach (i.e. ideal switches with body-diode, but driven with dead time), dead time shifts the time edges of the switching signal $\tilde{z}(t)$ and hence

$$\tilde{z}(t) \neq Gz(t) = Gx(t) + Ge(t) \tag{2.27}$$

Whilst switches' ON-resistance distort the time waveform of the power switching signal $\tilde{z}(t)$, dead time does not distort its time waveform. Instead, dead time shifts the edges of the power switching signal $\tilde{z}(t)$ thereby causing a similar effect than improper time encoding (signal-correlated jitter).

Dead time can be modelled as a different error signal $e^*(t)$. Certainly, because of dead time, the error signal is modified in the power-amplification process $e(t) \to e^*(t)$. Even if the switching signal $z(t)$ properly tracks the reference signal $x(t)$, the resulting power switching signal $\tilde{z}(t)$ is determined by the modified error signal $e^*(t)$ thus improperly tracking the reference signal $x(t)$.

$$\tilde{z}(t) = Gx(t) + Ge^*(t) \tag{2.28}$$

Figure 2.13 shows the error due to dead time in a PWM tracking a f_0-bandlimited signal at OSwR ≈ 10 and filtering with an ideal f_0-low-pass filter (dead time has been simulated according to figure 2.12). In the frequency domain, the power-amplified error signal $GE^*(f)$ shows an increased error signal's

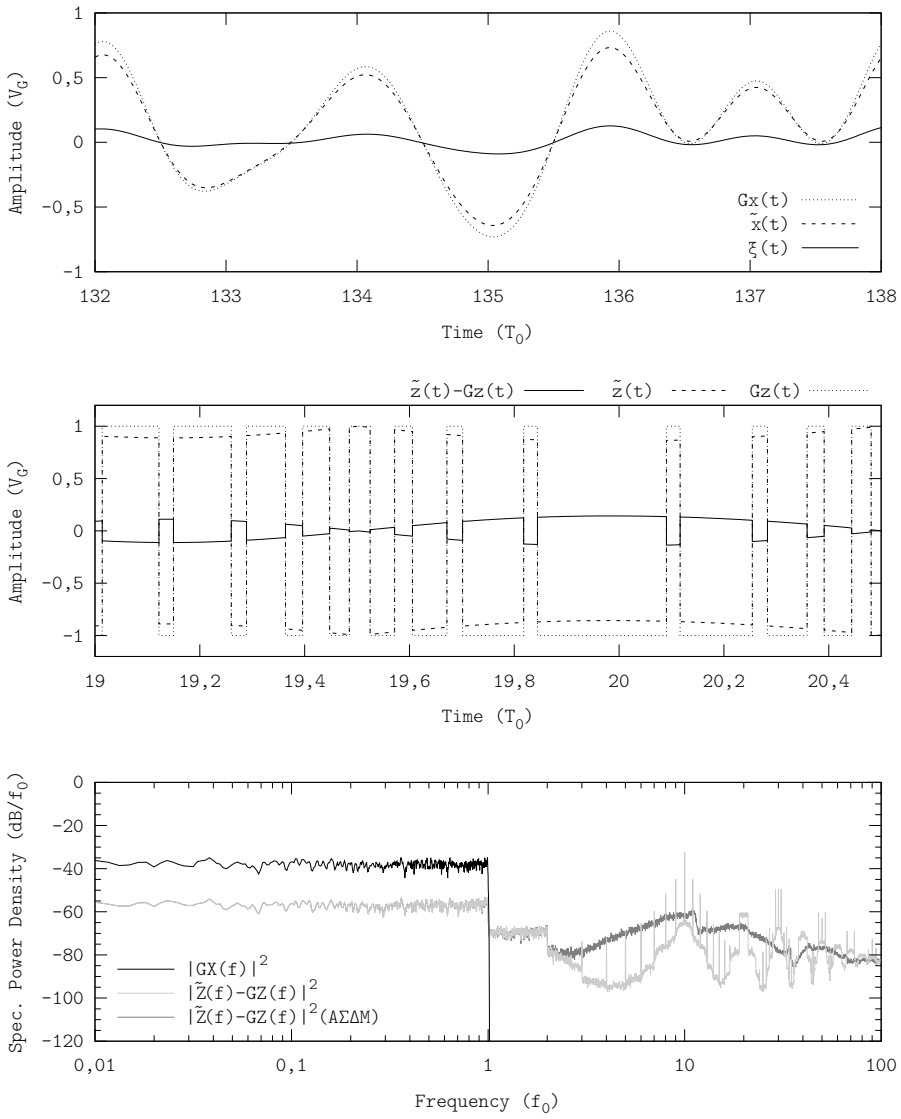

Figure 2.11: Tracking error due to switches' ON-resistance. Example showing an PWM operating at OSwR ≈ 10, with equivalent switch resistance $R_{S_e}/R_L = 0{,}2$ and filtering with an ideal f_0-low-pass filter. Simulation performed using the configuration D.4.1 and approximating the ideal filter in the frequency domain D.3.5. In the frequency domain, the waveform labeled "AΣΔM" shows $|\tilde{Z}(f) - GZ(f)|^2$ corresponding to an AΣΔM signal, modulated under the same conditions than PWM.

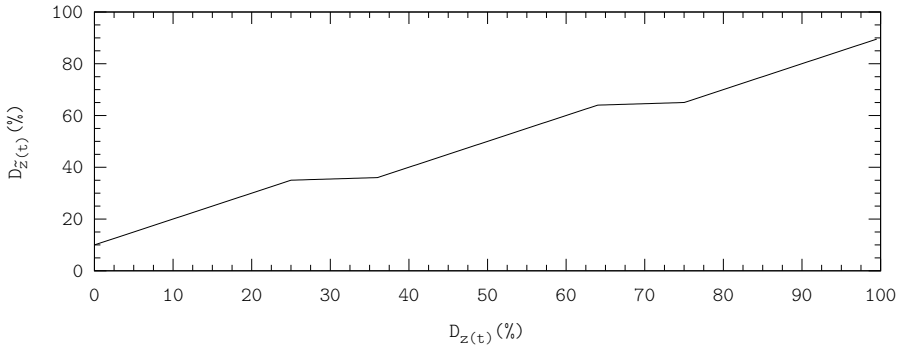

Figure 2.12: Duty cycle error due to dead time. Data extracted from [12].

inband content. The ratio of the remaining error signal's power $P_{\xi(t)}$ to the reference signal power $P_{x(t)}$ is approximately $-12\,\mathrm{dB}$ (7 %).

Similarly to switches' ON-resistance, dead time inband effects hardly depend upon the modulation. Despite the inband effect is modulation-dependent because dead time depends upon the instantaneous duty cycle, the differences are not significant. Figure 2.13 also includes the modified error signal $E^*(f)$ in an AΣΔM operating under the same conditions than PWM. The inband content of both modified error signals $E^*(f)$ is similar (in AΣΔM the inband error is lower because the pulses' width is bounded from below, see chapter 4, thus minimising the relative effect of dead time).

Dead time can be incorporated to the electronic model of switching amplifiers by driving the controlled voltage source with the modified power switching signal $\tilde{z}(t)$. Generating the power switching signal $\tilde{z}(t)$ which properly models dead-time is challenging, yet properly modelling dead-time in classical converter analysis is challenging as well.

Error Due to LTI Filters

LTI filters have finite stopband rejection and non-constant bandpass gain, with a smooth transition between bandpass and stopband. Figure 2.14 shows an example of a common transfer function of a second-order filter with cutoff frequency $f_\mathrm{c} = 2f_0$, shaped to maximally flat inband response (Butterworth filter, these kind of filters are the most common ones in switching amplifiers).

The error in the recovered signal $\tilde{x}(t)$ due to LTI low-pass filters is twofold: inband and outband. On the one hand, because of the finite stopband rejection, the outband spectral content of the power-amplified error signal $GE(f)$ cannot be completely rejected, thus resulting in a remaining outband error signal $\Xi(f)$.

$$\Xi(f) = GE(f)H(f) \neq 0, \quad |f| > f_0 \tag{2.29}$$

Given that most of the error signal's $E(f)$ outband power concentrates around the switching frequency f_s, so does most of the outband power of the remaining error signal $\Xi(f)$. At higher frequencies, the error signal's power is lower and the stopband rejection is higher and therefore the outband power of the remaining error signal $\Xi(f)$ concentrates within a narrower band than that of the error signal $E(f)$.

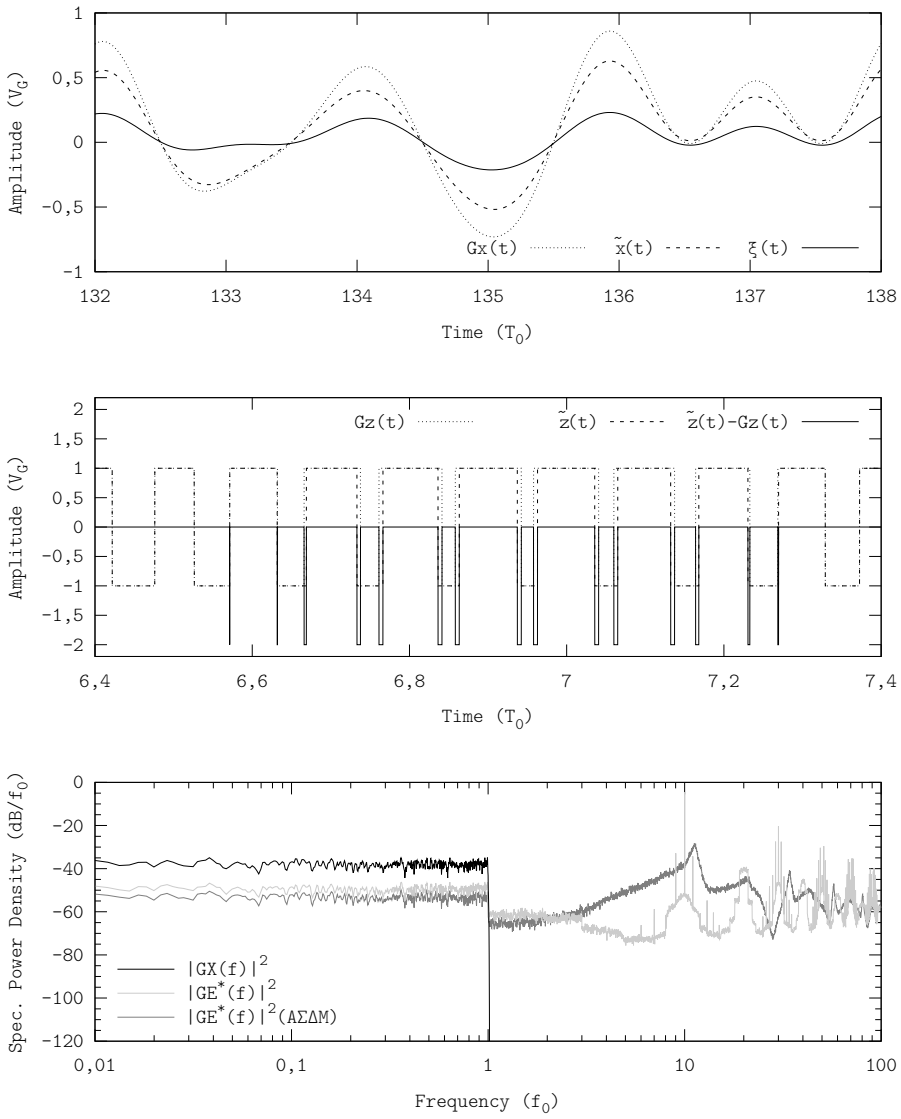

Figure 2.13: Tracking error due to dead time. Example showing a PWM operating at OSwR ≈ 10 and filtering with an ideal f_0-low-pass filter. Dead time simulated under the same conditions than in figure 2.12. Simulation performed using the configuration D.4.1 and approximating the ideal filter in the frequency domain D.3.5. In the frequency domain, the waveform labeled "AΣΔM" shows $|GE^*(f)|^2$ corresponding to an AΣΔM signal, modulated under the same conditions than PWM.

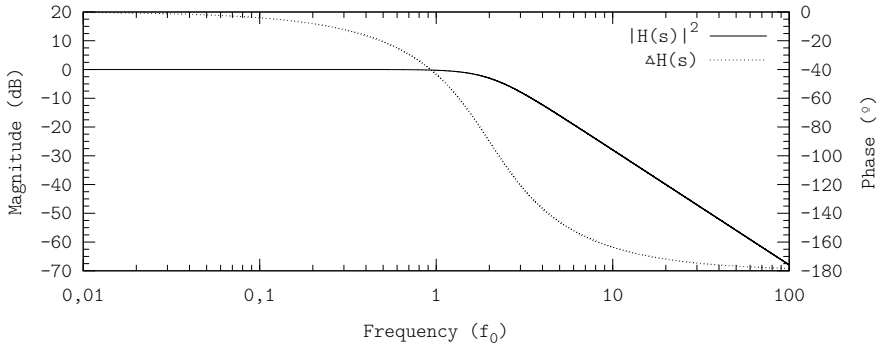

Figure 2.14: Bode plot of a second-order low-pass filter. The filter's cutoff frequency is $f_c = 2f_0$ and the transfer function has been shaped to maximally flat inband response (Butterworth filter).

On the other hand, the non-constant bandpass gain modifies the inband spectral content of the power switching signal $\tilde{Z}(f)$, yielding

$$\tilde{X}(f) = \tilde{Z}(f)H(f) \neq \tilde{Z}(f), \quad |f| \leq f_0 \tag{2.30}$$

Note that not only the amplitude is modified but also the phase, and both by frequency-dependent values, thus resulting in a certain inband error power. Indeed even if directly filtering the reference signal $x(t)$, the recovered signal would differ from the original signal

$$x(t) * h(t) \neq x(t) \tag{2.31}$$

Furthermore, the recovered signal is τ delayed with regard to the reference signal $x(t)$, i.e. the recovered signal $\tilde{x}(t)$ approximately tracks a delayed reference signal $x(t-\tau)$. However, a constant group delay is generally not considered distortion.

Figure 2.15 shows the tracking error due to an LTI filter (a second-order low-pass Butterworth filter with cutoff frequency $f_c = 1{,}25f_0$), when tracking a f_0-bandlimited signal with a triangle PWM operating at an OSwR of 10. The spectral power density of the remaining error signal $\Xi(f)$ is shaped according to the error signal $E(f)$, i.e. the modulation, and the filter transfer function $H(s)$. The ratio of the remaining error signal's power $P_{\xi(t)}$ to the reference signal's power $P_{x(t)}$ is approximately $-23\,\mathrm{dB}$ (0,5 %).

To emphasise the inband error due to the LTI filter, the recovered signal $\tilde{x}(t)$ has been filtered with an ideal f_0-low-pass filter, so that it becomes feasible to separate the inband and outband content of the remaining error signal $\xi(t)$. These time waveforms are also included in figure 2.15, in the lower time-domain plot. After applying the ideal f_0-low-pass filter, the ratio of the remaining error signal's power $P_{\xi(t)}$ (i.e. the inband power of the remaining error signal $\xi(t)$) to the reference signal's power $P_{x(t)}$ is approximately $-25\,\mathrm{dB}$ (0,3 %). Therefore, under these operating conditions, most of the remaining error signal's power $P_{\xi(T)}$ (63 %) is due to the LTI filter's non-constant inband response.

Moreover, actual LTI filters are made of actual devices which suffer from non-idealities such as ESRs, inductive and/or capacitive stray effects. These

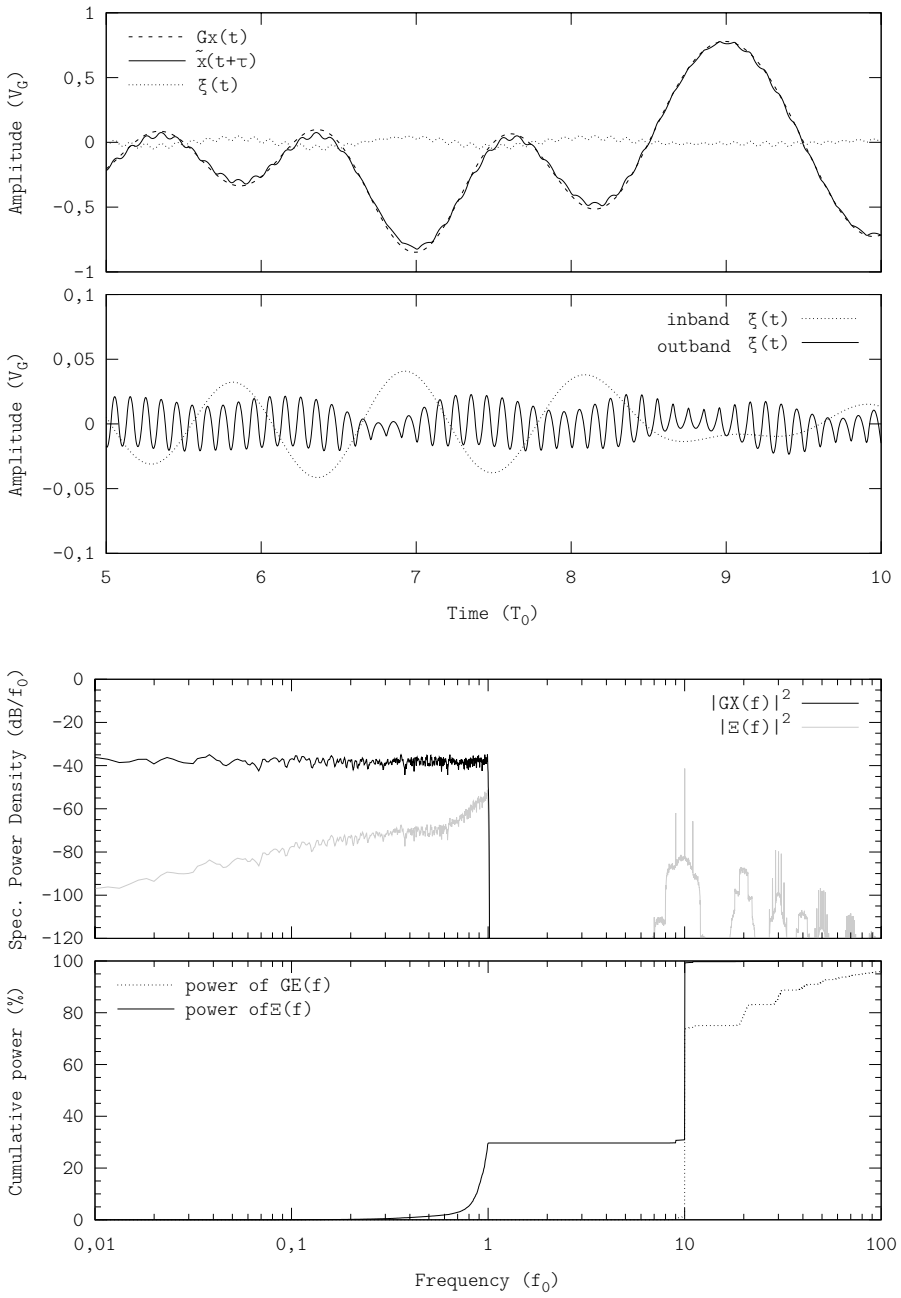

Figure 2.15: Tracking error due to LTI filters. Example showing a PWM operating at OSwR ≈ 10 and filtering with a second-order Butterworth filter with cutoff frequency $f_c = 1{,}25 f_0$. The lower time-domain plot shows, separately, the inband and the outband remaining error signals. Simulation performed using the configuration D.4.1.

non-idealities result in a more complex transfer function, but still a LTI low-pass filter in the frequency range of interest, and hence they can be incorporated to the electrical model. Nevertheless, the filter's performance is generally degraded: more resistive elements result in more conduction losses and the inband response becomes more frequency-dependent (increased inband error).

2.3.3 Required Tracking Fidelity

Actual amplifiers suffer from all tracking error sources, besides external and/or environmental factors (such as EMI) and implementation-induced effects. For instance, in actual PWMs, the non-ideal performance of actual comparators degrades the encoding process (increased error due to improper time encoding). The dominant error source depends upon each specific implementation, the operating conditions and the receiver's sensitiveness of each application.

The error due to LTI filters can be equalised by pre-emphasising the reference signal. Nevertheless, perfect pre-emphasis is not possible as it requires an improper filter $H^{-1}(s)$; whether with pre-emphasis or not, the LTI filter causes error upon the recovered signal (see section 6.1.5 for a further analysis on LTI filter pre-equalisation).

The required tracking fidelity is determined by the receiver's sensitiveness (specifications). For instance, broadband communications are very sensitive to distortion, both inband and outband, and hence a linear-assisted approach is often mandatory to comply with communication masks. On the other hand, audio applications generally tolerate outband distortion and even inband distortion.

Distortion in Audio Switching Amplifiers

Audio switching amplifiers are mostly based on triangle PWMs, operating at OSwRs upwards of 10. Under such conditions, the inband content of the error signal $E(f)$ is more than 80 dB below the reference signal's $X(f)$, see figure 2.7.

Switches' ON-resistance is generally in the range of mΩ, whereas the speaker's impedance is in the range of Ω. This leads to small tracking errors due to switches' ON-resistance. Even in area-optimised integrated audio applications, in which the switches' ON-resistance is comparable to the speaker's impedance, the OSwR is high enough so that the inband error due to switches' ON-resistance can be compensated by feedback.

The dominant error source is dead time. Indeed, as figure 2.13 shows, the inband error due to dead time can be very high (this simulation has been performed using common values in audio amplifiers [12]). This kind of inband error is only partially compensated by feedback, even if operating at high OSwRs. Dead time therefore determines the performance of PWM-based audio switching amplifiers. Nevertheless, it is feasible to mitigate its effect upon the recovered signal $\tilde{x}(t)$ by enhancing the power stage [13] (yet, the lowest THD values have been achieved with A$\Sigma\Delta$M-based audio amplifiers [22]).

Despite a typical HiFi audio filter is 25 kHz-wide ($f_c = 1{,}25 f_0$, the example shown in figure 2.15), the error due to LTI filters is generally not considered audio distortion. It is considered signal equalisation instead.

Furthermore, the speaker's inband response is not constant either and there may be echos in the transmission channel (which may lead to selective frequency cancellation). On top of that, each receiver subjectively interprets the received

audio signal (there is even more controversy in measuring and quantifying the audio quality, psycho-acoustics, than in defining audio signals). All these effects results in a very complex and unpredictable equivalent multipath channel, from the power switching signal $\tilde{z}(t)$ to the receiver (i.e. a person), and a lack of a Figure of Merit (FoM) to objectively quantify the audio quality.

Consequently, since perfect pre-equalisation is not feasible, the LTI filter's frequency response, the speaker's frequency response and the transmission channel are equalised together, tuned until the audio quality of the received audio signal is good enough for a subjective receiver. Note that the received signal could be deliberately distorted or, using the audio terminology, equalised (e.g. bass-boosting).

Harmonic Distortion Historically, audio amplifiers were linear and their performance was measured with the Total Harmonic Distortion (THD) or THD plus Noise (THD+N). These tests consist in applying one tone a the amplifier's input port $x(t) = A\sin(\omega_0 t)$ and analysing the output signal $\tilde{x}(t)$ at frequencies multiples of the tone's $\omega = k\omega_0$ with $k > 2, k \in \mathbb{N}$ (THD) or at all frequencies but ω_0 (THD+N). THD and THD+N properly characterise the performance of linear amplifiers.

Nowadays audio switching amplifiers have superseded audio linear amplifiers in many applications [2]. Nonetheless, the performance of audio switching amplifiers is still measured with THD and THD+N, mainly because of historical reasons. Note that these distortion-performance metrics only measure the amplitude errors due to improper time encoding and dead time, at frequencies different than the tone's.

For instance, consider the optimisation of the output filter of an audio switching amplifier only according to THD (or THD+N). As the filter's cutoff frequency decreases, so does the power of the harmonics thereby improving the THD, but the amplifier's tracking bandwidth also decreases. This optimisation leads to a useless solution, a cutoff frequency below the audible frequency range.

THD and THD+N only encompass a specific feature (or error source) of switching amplifiers, e.g. intermodulation effects, gain and phase errors are not encompassed by THD and THD+N. There exists other tests, such as two-tone test, to characterise other features of switching audio amplifiers. However, because of the subjectivity of the receiver, the dependency upon external factors and the lack of a unified FoM, the performance metrics used to characterise audio switching amplifiers are not appropriate to quantify, in a general way, the tracking fidelity of switching amplifiers.

Tracking Error Measurement

In broadband communications, the receiver is not subjective and is more sensitive to all kinds of distortion. The recovered signal $\tilde{x}(t)$ is used to reconstruct a more complex signal $\phi(t)$, which must both comply with communication masks and minimise the Bit Error Rate (BER). In these applications, the error is measured in the received complex signal $\phi(t)$ by using Error Vector Magnitude (EVM) [71], [72], which finally determines the BER. Unfortunately, the transformation to reconstruct the complex signal $\phi(t)$ from the recovered signal $\tilde{x}(t)$ is not linear, thus the EVM cannot be used to characterise the performance of switching amplifiers either.

All error sources described in section 2.3 cause error in the received signal. A simple FoM which encompasses them all, including phase errors, is the remaining error signal's average power $P_{\xi(t)}$. Despite this FoM considers errors up to very high frequencies, provided that filter's rejection increases with frequency;

$$\lim_{\omega\to\infty} |H(j\omega)| = 0 \tag{2.32}$$

effectively, the error mainly concentrates inband and around the switching frequency (outband).

In this work, the tracking error is quantified according to the remaining error signal's average power $P_{\xi(t)}$, normalised to the reference signal's average power $P_{x(t)}$,

$$\frac{P_{\xi(t)}}{P_{x(t)}} = \frac{\lim\limits_{T\to+\infty} \dfrac{1}{2T}\displaystyle\int_{-T}^{T} \frac{\xi^2(u)}{R_\mathrm{L}}\,\mathrm{d}u}{\lim\limits_{T\to+\infty} \dfrac{1}{2T}\displaystyle\int_{-T}^{T} \frac{x^2(u)}{R_\mathrm{L}}\,\mathrm{d}u} \approx \frac{\displaystyle\int_{\Delta t} \xi^2(u)\,\mathrm{d}u}{\displaystyle\int_{\Delta t} x^2(u)\,\mathrm{d}u} \tag{2.33}$$

where Δt is a time interval (see appendix B). Note that this definition encompasses all error sources in switching amplifiers, including phase errors.

According to Parseval's theorem, the tracking error can also be computed in the frequency domain

$$\frac{P_{\xi(t)}}{P_{x(t)}} = \frac{\displaystyle\int_{-\infty}^{\infty} |\Xi(f)|^2\,\mathrm{d}f}{\displaystyle\int_{-\infty}^{\infty} |X(f)|^2\,\mathrm{d}f} \tag{2.34}$$

In the context of switching amplifiers, both the reference signal $x(t)$ and the remaining error signal $\xi(t)$ are real, so their Fourier transforms are even. Besides, if the reference signal $x(t)$ is f_0-bandlimited, then

$$\frac{P_{\xi(t)}}{P_{x(t)}} = \frac{\displaystyle\int_{0}^{\infty} |\Xi(f)|^2\,\mathrm{d}f}{\displaystyle\int_{0}^{f_0} |X(f)|^2\,\mathrm{d}f} \tag{2.35}$$

It is often convenient to evaluate the tracking error within a specific frequency range of interest ΔB, e.g. inband plus an EMI-sensitive range. It is feasible to measure it using this FoM, by evaluating the remaining error signal's power within the frequency range of interest ΔB.

2.4 Problem Statement Under the New Perspective

According to the new perspective on switching amplifiers, the scope of this work is to explore signal- and system-level techniques for open-loop switching amplifiers to reduce the OSwR required to satisfactorily track non-periodic f_0-bandlimited flat-spectrum reference signals $x(t)$; i.e. to reduce the power of the remaining error signal $P_{\xi(t)}$ without increasing the switching frequency f_s. Figure 2.3, which has been included again here as figure 2.16, summarises the general problem statement.

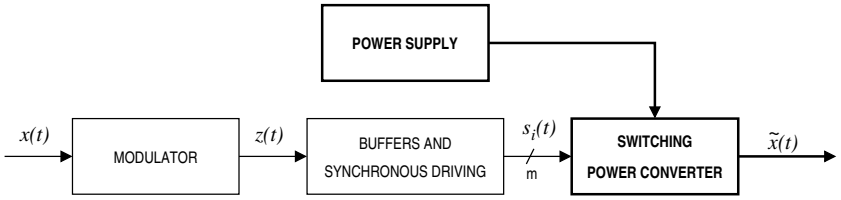

Figure 2.16: General problem statement. The scope is to reduce the power of $\tilde{x}(t) - x(t-\tau)$ without increasing the switching frequency.

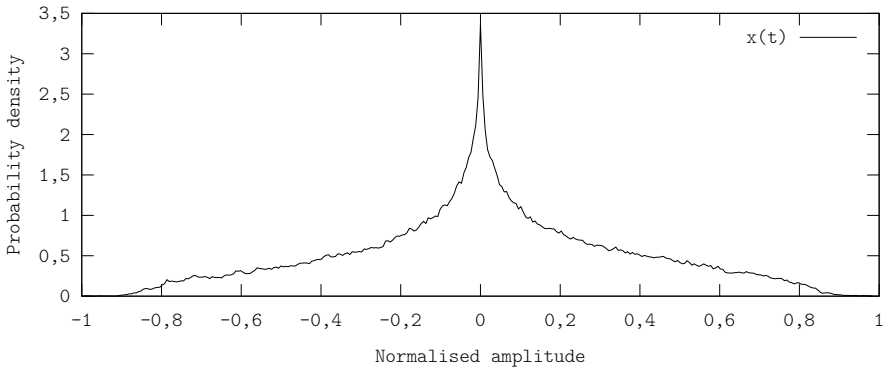

Figure 2.17: Amplitude distribution of the non-periodic f_0-bandlimited flat-spectrum reference signals, using the normalised range $Z_{\min} = -1$, $Z_{\max} = 1$.

Note that these techniques can be applied to both audio and broadband communications applications because, as discussed in section 2.1.1, the better the open-loop amplifier's performance (or power core), the better the overall switching amplifier's performance (either closed-loop or linear-assisted).

2.4.1 Non-Periodic Bandlimited Flat-Spectrum Signals

Unless otherwise stated, the reference signals used in the characterisation of switching amplifiers are non-periodic f_0-bandlimited flat-spectrum (and their amplitude is set so that they sweep all available dynamic range without saturation, i.e. 100 % of modulation depth as discussed before).

$$Z_{\min} \leq x(t) \leq Z_{\max}, \quad \forall t \in \mathbb{R} \tag{2.36}$$

Table 2.1 summarises the most relevant statistical parameters of a non-periodic f_0-bandlimited reference signal $x(t)$, obtained by processing a 2 000 T_0 periods, and figure 2.17 shows its amplitude distribution (both the table 2.1 and figure 2.17 using the normalised range $Z_{\min} = -1$, $Z_{\max} = 1$).

parameter	*value*
RMS	$3{,}493788 \cdot 10^{-1}$
mean	$1{,}376056 \cdot 10^{-2}$
peak	$9{,}947288 \cdot 10^{-1}$
peak / RMS	2,847136

Table 2.1: Statistical parameters of the non-periodic f_0-bandlimited flat-spectrum reference signals, using the normalised range $Z_{\min} = -1$, $Z_{\max} = 1$.

Chapter 3

Fundamental Bandwidth Limits in Two-Level Time Encoding

This chapter explores the fundamental bandwidth limits in two-level time encoding, by analysing the tracking capabilities of two-level switching signals. With this aim, this chapter synthesises two-level switching signals by obtaining the distribution of switching events providing both minimum average switching frequency and inband-error-free encoding when tracking a generic bandlimited signal, targeting switching losses minimisation in the context of switching amplifiers.

3.1 Motivation and Preliminaries

The new perspective of switching amplifiers presented in chapter 2, interpreting them as an encoding-decoding process, unfolds an alternative analysis method of switching amplifiers based on signal processing. Unfortunately, two-level time encoding is not described by the classical signal processing theory.

Certainly, in sampling, an analogue signal (continuous-time and continuous-amplitude) is transformed into a sampled signal (discrete-time and continuous-amplitude), instead of into a two-level switching signal (continuous-time and discrete-amplitude) as in two-level time encoding. Two-level time encoding is therefore not ruled by Nyquist's sampling criterion ($\mathrm{f_s} \geq 2f_0$). Similarly, the common analogue and digital modulations described by classical signal processing theory do not constrain the waveform of the modulated signal.

Two fundamental questions arise from this lack of mathematical characterisation of two-level time encoding: can this encoding process be lossless? If so, similarly to Nyquist's sampling criterion, what are the bandwidth limits?

In recent years different analysis techniques have been applied to describe the encoding process performed by different modulators, but generally by characterising limit cycles in a specific closed-loop modulator [73], [74]. From a more generic standpoint, approximating and digitalising bandlimited analogue signals by single-bit $\Sigma\Delta$ modulators (of arbitrary order) has also been analysed [75], although this analysis does not generically describe two-level time encoding.

In a different context, the bandwidth limits of different two-level switching modulations have been explored (this discussion is included in chapter 4). Each two-level switching modulation has its own bandwidth limits, but these are more restrictive than the bandwidth limits of generic two-level time encoding. Even though two-level switching modulations indeed perform two-level time encoding, no fundamental conclusions can be drawn from them, as these modulations are constrained by a feasible implementation whilst generic two-level time encoding is not constrained by any implementation.

Therefore, two-level time encoding has not been analysed as a generic encoding process. Relying on the encoding-reconstruction standpoint of switching amplifiers, it is feasible to analyse this encoding process and derive its fundamental bandwidth limits by analysing the tracking capabilities of two-level switching signals.

With this aim, this chapter synthesises two-level switching signals (i.e. obtaining the distribution of switching events) providing both lossless encoding and minimum average switching frequency when tracking a generic bandlimited signal. The scope is to derive the fundamental bandwidth limits in two-level time encoding, in the context of switching amplifiers. No modulator (not even a modulation) is hence presented in this chapter; a fundamental bound is derived, whose main interest is as comparison framework for practical modulators (as analysed in section 4.5).

3.1.1 Boundary Constraints

In switching amplifiers, the switching power converter constrains the decoding process to low-pass filtering. Although the analysis of the encoding process requires considering the specific decoding process (low-pass filtering in this case), the encoding and the decoding processes can be decoupled and hence separately analysed (as discussed in chapter 2). Consistently, this chapter analyses the encoding process in switching amplifiers; the decoding process is considered to be ideal (ideal low-pass filtering, see section 6.1.1 for a formal definition).

Under the previous hypotheses, the analysis of the encoding process in switching amplifiers carried out in this chapter addresses a twofold issue: on the one hand to determine the conditions that the two-level switching signal $z(t)$ must fulfil so that a f_0-bandlimited reference signal $x(t)$ can be perfectly recovered by decoding $z(t)$ with an ideal low-pass filter (inband-error-free encoding), on the other hand to determine the minimum average switching frequency of $z(t)$ in which such conditions occur.

Note that the low-pass filtering decoding constraint (i.e. the context of switching amplifiers), determines all the analysis. Using alternative decoding processes [76], [77], perfect recovery is possible even if encoding with an A$\Sigma\Delta$M [21].

3.1.2 Inband-Error-Free Encoding in Switching Amplifiers

According to the encoding-reconstruction interpretation of switching amplifiers, the process of encoding the information conveyed by an arbitrary signal can be modeled as the addition of an error signal $e(t)$ to the reference signal $x(t)$, in

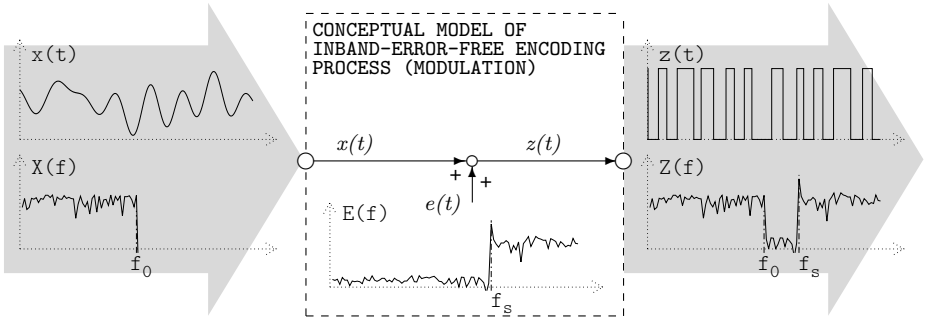

Figure 3.1: Inband-error-free tracking a f_0-bandlimited signal at f_s.

order to shape it into the two-level switching signal $z(t)$.

$$z(t) = x(t) + e(t) \tag{3.1}$$

As stated above, inband-error-free encoding in switching amplifiers implies that it must be possible to perfectly recover $x(t)$ by low-pass filtering $z(t)$ with an ideal low-pass filter. According to this constraint, $x(t)$ must be f_0-bandlimited for perfect recovery to be possible. The inband-error-free encoding condition can be then easily stated in the frequency domain: the switching signal $Z(f)$ inband-error-free tracks the reference signal $X(f)$ or the information conveyed by the reference signal $X(f)$ is inband-error-free encoded into the switching signal $Z(f)$ if the error signal $E(f)$ is f_0-high-pass (no spectral content at $|f| \leq f_0$, see the example in figure 3.1).

$$Z(f) = X(f) \Rightarrow E(f) = 0, \quad |f| \leq f_0 \tag{3.2}$$

If the reference signal is not bandlimited, perfect recovery is not possible, although the modulation can still inband-error-free track its baseband spectral content (underswitching and infinite-band signal tracking is analysed in section 3.3.1).

Figure 3.1 shows a conceptual example of inband-error-free signal tracking. The spectral content of $e(t)$ is zero below f_s; provided that $f_0 < f_s$, the inband-error-free encoding condition is satisfied.

3.2 Tracking Capabilities of Two-Level Switching Signals for Switching Amplifiers

This section analyses the tracking capabilities of two-level switching signals, aiming inband-error-free signal tracking in switching amplifiers; i.e. to determine the minimum OSwR of $z(t)$ to inband-error-free track a reference f_0-bandlimited signal $x(t)$.

This analysis is performed using periodic signals and Fourier Series because they allow stating the inband-error-free encoding condition in a convenient way; besides, it is possible to generalise the analysis to bandlimited non-periodic signals.

Hereafter, the reference signals Fourier coefficients are denoted a_k and b_k, whereas the switching signal's are denoted a_k^* and b_k^*. Only the relevant results are included next; the full expressions of a_k^* and b_k^* are listed in appendix C.

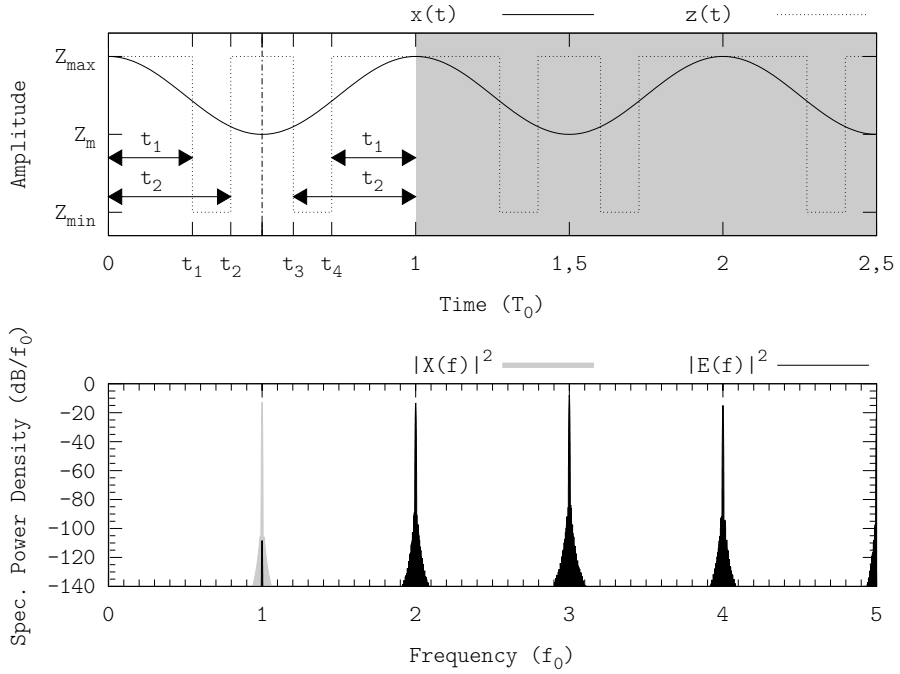

Figure 3.2: Inband-error-free tracking a single tone sinusoid at OSwR = 2. Displayed waveforms are the reference signal (solid) and the switching signal (dotted) in the time domain (upper plot), and the error signal in the frequency domain (lower plot).

3.2.1 Case Example: Single Tone Sinusoid

Let the reference signal be a single tone sinusoid with arbitrary amplitude, frequency and DC level (without exceeding the system dynamic range, see figure 3.2). It can be expressed as

$$x(t) = V_{\mathrm{DC}} + A\cos(\omega_0 t) \tag{3.3}$$

By identifying its Fourier coefficients, it only conveys information within the zeroth (a_0) and the first harmonics (a_1 and b_1), and the harmonic frequency is f_0.

$$\begin{aligned} a_0 &= 2V_{\mathrm{DC}} \\ a_1 &= A, \qquad b_1 = 0 \end{aligned} \tag{3.4}$$

According to the inband-error-free encoding condition, for the switching signal to inband-error-free track the reference signal, the baseband spectral content of both signals must be the same, i.e. the switching signal $z(t)$ must have harmonics at the same frequency and with the same amplitude than the reference signal $x(t)$.

A feasible solution to match the harmonics' frequency is to constrain the switching signal to be T_0-periodic, so that its Fourier Series decomposition yields harmonics only at frequencies kf_0, $k \in \mathbb{Z}$ (see appendix C). If $z(t)$ changes its value $2M$ times within one T_0 period ($2M$ switching events, OSwR = M), it

can be expressed as

$$z(t) = Z_{\mathrm{m}} + (-1)^{s+1}\frac{Z_{\mathrm{pp}}}{2}\left(1 + \sum_{i=1}^{2M}(-1)^{i}\mathrm{u}(t - T_0 t_i)\right) \tag{3.5}$$

where $\mathrm{u}(t)$ denotes the Heaviside function, $0 < t_i < 1$ with $i = 1, \ldots, 2M$ and s is either 1 or 0 depending on the switching signal initial value (high or low respectively).

Furthermore, by constraining the switching signal to be even symmetrical around $T_0/2$, all b_k^* are zero (note the even symmetry of the reference signal around its maxima and minima).

By imposing the inband-error-free encoding condition (both b_k and b_k^* have been omitted because they are all 0) it turns out that two switching events (t_1 and t_2) are necessary to inband-error-free track the single tone,

$$\begin{aligned} z(t) &= \frac{a_0^*}{2} + \sum_{k=1}^{+\infty} a_k^* \cos(\omega_0 k t) = \\ &= x(t) + \sum_{k=2}^{+\infty} a_k^* \cos(\omega_0 k t) = x(t) + e(t) \end{aligned} \tag{3.6}$$

where $e(t)$ is the error signal added by the encoding process.

Despite there are only two independent variables (t_1 and t_2), because of the even symmetry, there are four switching events within T_0 ($t_1, \ldots, t_4$, with $t_4 = 1 - t_1$ and $t_3 = 1 - t_2$, see figure 3.2), thus the OSwR of this encoding process is 2. Without the even symmetry, the coefficients b_k^* would not have been zero, and therefore four switching events would have been required anyway[1].

The expression (3.6) yields an equations system with two equations and two variables. By identifying the Fourier coefficients, the equations system can be written as

$$\begin{cases} a_0^*(t_1, t_2) = a_0 = 2V_{\mathrm{DC}} \\ a_1^*(t_1, t_2) = a_1 = A \end{cases} \tag{3.7}$$

These two equations can be written in a compact form using the mean value Z_{m} and the peak-to-peak value Z_{pp} of the two-level switching signal, i.e. the modulation's dynamic range (note that the coefficients t_i are dimensionless, see appendix C)

$$\begin{cases} t_1 - t_2 = \dfrac{2V_{\mathrm{DC}} - 2Z_{\mathrm{m}} - Z_{\mathrm{pp}}}{4Z_{\mathrm{pp}}} \\ \sin(2\pi t_1) - \sin(2\pi t_2) = \dfrac{\pi A}{2Z_{\mathrm{pp}}} \end{cases} \tag{3.8}$$

Even though is not possible to isolate $t_{1,2} = f(V_{\mathrm{DC}}, A)$, by numerically sweeping the design space of t_1 (from 0 to 1/2) and t_2 (from t_1 to 1/2), the outcome solutions show that it is possible to track single tones within all dynamic

[1] Although only three coefficients are to be matched (hence only three switching events may be necessary), with three switching events the switching signal would not be T_0-periodic; the Fourier Series decomposition would then yield harmonics at other frequencies than kf_0, which should be zero as well. Nevertheless, it is possible to inband-error-free track a single tone sinusoid at OSwRs lower than 2 (see section 3.2.3 for minimum switching frequency inband-error-free encoding).

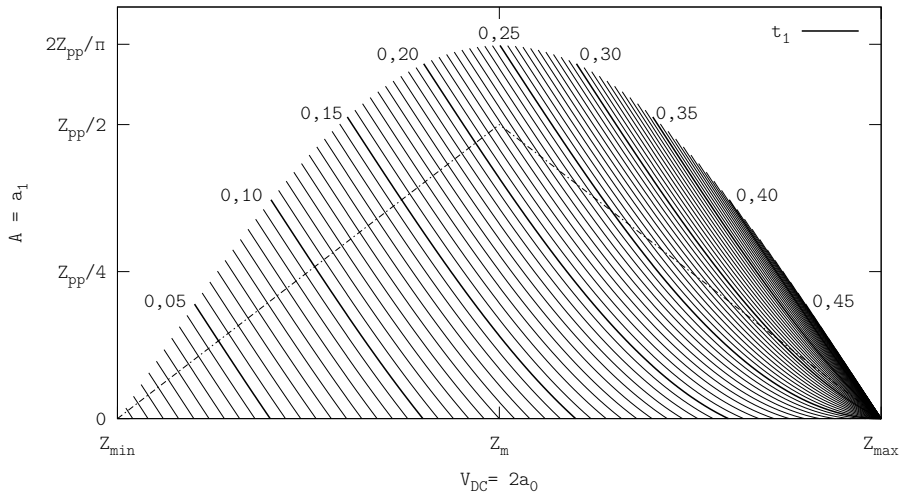

Figure 3.3: Required value for t_1 when inband-error-free tracking the reference signal $x(t) = V_{\mathrm{DC}} + A\cos(\omega_0 t)$ at OSwR = 2; the value of t_2 can be calculated from the first equation in (3.8). Above the dash-dot line, the single tone exceeds the dynamic range.

range, i.e. it is possible to reproduce the spectral content of the single tone in the switching signal. Figure 3.3 shows the results of the numerical sweep; note that it is possible to track single tones even beyond the supply levels, specifically up to $2Z_{\mathrm{pp}}/\pi$.

From expression (3.6) it is clear that the inband-error-free encoding condition holds, as the frequency of the slowest harmonic of $e(t)$ is $2f_0$. There are four switching events within T_0, thus a single tone can be inband-error-free tracked at an OSwR of 2.

3.2.2 Periodic Signals

A bandlimited periodic signal may convey information within several coefficients. Let the reference signal be a f_0-bandlimited multi-tone signal, consisting of N tones with arbitrary phase at frequencies sub-multiples of f_0 and a certain DC offset, of the form

$$x(t) = \frac{a_0}{2} + \sum_{k=1}^{N} a_k \cos\left(\frac{\omega_0 k t}{N}\right) + b_k \sin\left(\frac{\omega_0 k t}{N}\right) \tag{3.9}$$

Again, the switching signal should be constrained to the same nature than that of the reference signal to match the harmonics frequency; in this case, it should be constrained to be NT_0-periodic. In order to inband-error-free track the reference signal, both the a_k and b_k coefficients must be matched. Hence

$$z(t) = \frac{a_0^*}{2} + \sum_{k=1}^{+\infty} a_k^* \cos\left(\frac{\omega_0 k t}{N}\right) + b_k^* \sin\left(\frac{\omega_0 k t}{N}\right) =$$

$$= x(t) + \sum_{k=N+1}^{+\infty} a_k^* \cos\left(\frac{\omega_0 k t}{N}\right) + b_k^* \sin\left(\frac{\omega_0 k t}{N}\right) = \\ = x(t) + e(t) \tag{3.10}$$

which yields a system of $2N + 1$ equations.

Even though only $2N + 1$ variables are necessary to solve this system, given that the switching signal has been constrained to be NT_0-periodic, it must have an even number of switching events (see appendix C), and thus $2N+2$ switching events are required. The additional degree of freedom ($2N+2$ variables to solve $2N + 1$ equations) can be devoted to match the b_{N+1} coefficient, which is zero, although the a_{N+1}^* will not be zero and thus the full $N + 1$th harmonic will not be matched. Still, the system becomes

$$\begin{cases} a_0 = a_0^*(t_1, \ldots, t_{2N+2}) \\ a_1 = a_1^*(t_1, \ldots, t_{2N+2}) \\ \vdots \\ a_N = a_N^*(t_1, \ldots, t_{2N+2}) \\ b_1 = b_1^*(t_1, \ldots, t_{2N+2}) \\ \vdots \\ b_N = b_N^*(t_1, \ldots, t_{2N+2}) \\ \hline b_{N+1} = b_{N+1}^*(t_1, \ldots, t_{2N+2}) \end{cases} \tag{3.11}$$

These simultaneous equations can be numerically solved by properly applying a multi-dimensional root finding algorithm, such as the Newton's method. Therefore, a bandlimited NT_0-periodic signal can be inband-error-free encoded at an OSwR of $1 + 1/N$.

$$\mathrm{OSwR}_{NT_0} = \frac{2N + 2}{2N} = 1 + \frac{1}{N} \tag{3.12}$$

Figure 3.4 shows an example of a reference signal consisting of 50 tones ($N = 50$) of arbitrary amplitude and phase (yet avoiding saturation), inband-error-free encoded at an OSwR of $1 + 1/50 = 1{,}02$.

However, despite the low OSwR, the encoding process is still sub-optimum. Certainly, the additional degree of freedom has been devoted to match the b_{N+1} coefficient, whilst the a_{N+1} coefficient and thus the full $N + 1$th harmonic has not been matched. Instead, this degree of freedom could have been devoted to reduce the OSwR (see section 3.2.3) or to shape the high-frequency spectral content (see section 3.3.2).

Note that the previous analysis simplifies to well-known results in simple cases. It is consistent with the example in the previous subsection, a single tone ($N = 1$ and the OSwR is $1 + 1/1 = 2$), and, in the simplest case (a constant signal), it is even possible to analytically solve the system.

Constant Signals

A constant signal only conveys information within a_0; all the rest of Fourier coefficients are 0.

$$x(t) = V_{\mathrm{DC}} = \frac{a_0}{2} \tag{3.13}$$

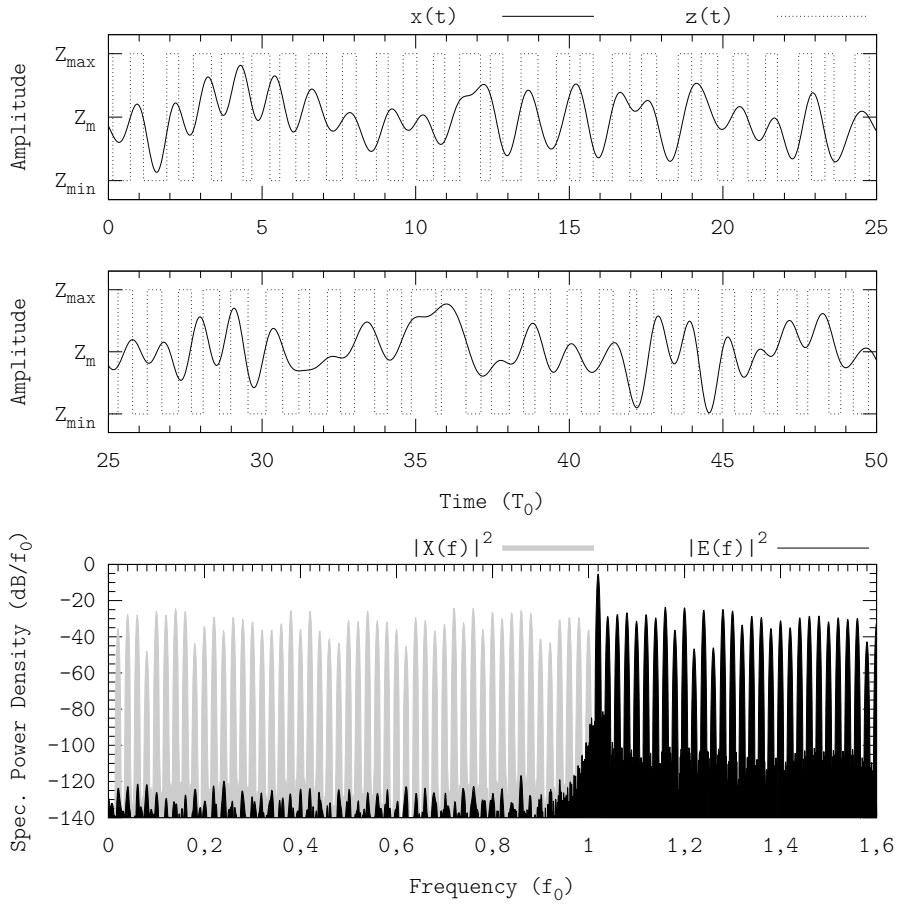

Figure 3.4: Inband-error-free tracking a 50-tone periodic signal at OSwR = 1,02. Displayed waveforms are the reference signal (solid) and the switching signal (dotted) in the time domain (upper plot), and the error signal in the frequency domain (lower plot).

The switching signal must be

$$z(t) = x(t) + \sum_{k=1}^{+\infty} a_k^* \cos(\omega_0 k t) + b_k^* \sin(\omega_0 k t) \tag{3.14}$$

which yields an equations system with one equation. The system can be solved with only one switching event, thus the switching signal $z(t)$ is not periodic. This non-periodic solution does not make sense in the context of switching amplifiers, as the switching signal must be periodic. Therefore, two switching events are required to inband-error-free track a constant signal.

A simple solution to easily match the a_0 coefficient is to impose $t_2 = 1 - t_1$ (even symmetry). If so, the condition $a_0 = a_0^*(t_1)$ yields (because of the even symmetry, the value of all the coefficients b_k^* is always 0)

$$t_1 = \frac{a_0 - 2Z_{\mathrm{m}} + Z_{\mathrm{pp}}}{4Z_{\mathrm{pp}}} \tag{3.15}$$

The switching signal is in fact a PWM signal of arbitrary frequency f_0 and duty cycle set by t_1. Note that, because of the even symmetry, $0 < t_1 < 0.5$, hence $D = 2t_1$. The previous expression can be rewritten in a more common form

$$D = \frac{V_{\mathrm{DC}} - Z_{\mathrm{min}}}{Z_{\mathrm{max}} - Z_{\mathrm{min}}} \tag{3.16}$$

3.2.3 Minimum OSwR Inband-Error-Free Signal Tracking

The result (3.12) derived in the previous subsection, an OSwR of $1 + 1/N$ to inband-error-free encode a bandlimited signal consisting of N equidistant tones with arbitrary phase and amplitude, whilst it is valid, it does not express the minimum OSwR required to inband-error-free track these kind of signals. The encoding process is indeed sub-optimum, since the switching signal matches one coefficient of the $N + 1$th harmonic but not the full harmonic.

The encoding process described in the previous subsection considers an encoding window whose length is set by the period of the reference signal, yielding a switching signal whose time period (and therefore its frequency resolution) is the same than that of the reference signal. Note that the expression (3.12) states the required OSwR as 1 (the reference signal bandwidth) plus the frequency resolution $1/N$. Consider the worst case, a single tone; its period is the smallest possible, T_0 ($N = 1$, yielding a frequency resolution of $1/N = 1$), thus the minimum OSwR required to inband-error-free track it is 2.

The encoding process can be optimised by extending the encoding window and therefore improving the frequency resolution. In order to inband-error-free encode, the switching signal must have harmonics at the same frequency than that of the reference signal, hence the original reference signal must still be periodic within the extended encoding window.

Let us consider an encoding window whose length is mNT_0, with $m \geq 1, m \in \mathbb{N}$. The period of the switching signal is mNT_0 (thereby improving the frequency resolution by a factor $1/m$) and the reference signal is periodic within each mNT_0 period, thus inband-error-free tracking is possible.

Consistently with the frequency normalisation, the Fourier Series decomposition has to be performed according to $\omega_0/(mN)$. Let us define a new reference

signal $\widehat{x}(t)$, consisting of m periods of $x(t)$. The new reference signal $\widehat{x}(t)$ conveys the same information than the original reference signal $x(t)$. Certainly

$$\widehat{a}_0 = \frac{2}{mNT_0}\int_0^{mNT_0} x(u)\mathrm{d}u = \frac{2}{NT_0}\int_0^{NT_0} x(u)\mathrm{d}u = a_0 \tag{3.17}$$

The other $\widehat{a}_k$ ($k \geq 1,\ k \in \mathbb{N}$) are given by

$$\widehat{a}_k = \frac{2}{mNT_0}\int_0^{mNT_0} x(u)\cos\left(\frac{\omega_0 k u}{mN}\right)\mathrm{d}u \tag{3.18}$$

The integral can be split into m integrals, one for each NT_0 period

$$\widehat{a}_k = \sum_{i=0}^{m+1}\frac{2}{mNT_0}\int_{NT_0 i}^{NT_0(i+1)} x(u)\cos\left(\frac{\omega_0 k u}{mN}\right)\mathrm{d}u \tag{3.19}$$

Since $x(t) = x(t + kNT_0), \forall k \in \mathbb{Z}$, by applying $\tau = t - NT_0 i$ to each integral and simplifying yields (note that each integral has a different change of variables)

$$\widehat{a}_k = \frac{2}{mNT_0}\int_0^{NT_0} x(\tau)\sum_{i=0}^{m-1}\cos\left(\frac{\omega_0 k}{mN}\tau + 2\pi k\frac{i}{m}\right)\mathrm{d}\tau \tag{3.20}$$

The summation of cosines is zero if $k \neq nm$, with $n \in \mathbb{N}$. Certainly, each cosine in the summation has a different phase. The phases will cause the summands to cancel out unless

$$k\frac{i}{m} \in \mathbb{N}, \quad i = 0, \ldots, m-1,\ i \in \mathbb{N} \tag{3.21}$$

Since $i \in \mathbb{N}$, then k/m must belong to $\mathbb{N}$. Therefore $k = nm$, with $n \geq 1$ and $n \in \mathbb{N}$, as the natural set is closed under the product. In this case, all the phases are multiples of 2π, hence all the summands can be directly added. The value of the non-zero $\widehat{a}_k$ coefficients therefore is

$$\widehat{a}_k = \frac{2}{NT_0}\int_0^{NT_0} x(u)\cos\left(\frac{\omega_0 k u}{mN}\right)\mathrm{d}u = a_{k/m} \tag{3.22}$$

which is the original reference signal Fourier coefficient a_k, but at m-multiples frequency. An analogous analysis can be performed for the $\widehat{b}_k$. Therefore (with $n \geq 1,\ n \in \mathbb{N}$)

$$\widehat{a}_k = \begin{cases} a_0, & k = 0 \\ a_{k/m}, & k = nm \\ 0, & k \neq nm \end{cases} \qquad \widehat{b}_k = \begin{cases} b_{k/m}, & k = nm \\ 0, & k \neq nm \end{cases} \tag{3.23}$$

The signal $\widehat{x}(t)$ can be inband-error-free encoded as described in the previous subsection. The switching signal must match up to the a_N and b_N coefficients (the full Nth harmonic of $x(t)$), which correspond to the $\widehat{a}_{mN}$ and the $\widehat{b}_{mN}$ coefficients respectively. This yields $2mN+1$ variables, hence $2mN+1$ switching events are required within each mNT_0 period. Again, despite the number of variables is odd, the number of switching events within each mNT_0 period must be even, thus there are $2mN + 2$ variables.

The additional variable can be devoted to match either the $\widehat{a}_{mN+1}$ or the $\widehat{b}_{mN+1}$ coefficient; nevertheless, since $mN+1$ is odd, these coefficients are 0 (they convey no information of the original reference signal). It is therefore possible to track up to the Nth harmonic of $x(t)$ with this switching signal, this is, to inband-error-free encode at OSwR $= 1 + 1/(mN)$.

Now the encoding window length (and thus the frequency resolution) also depends upon m, which can be as large as necessary. Therefore, the minimum OSwR required to inband-error-free track a f_0-bandlimited NT_0 periodic signal is 1.

$$\mathrm{OSwR}_{NT_{0\_\min}} = \lim_{m\to+\infty} 1 + \frac{1}{mN} = 1 \tag{3.24}$$

This expression (3.24) is the generalisation of expression (3.12), the particular case $m = 1$. Certainly, according to expression (3.12), the minimum OSwR to inband-error-free encode a periodic signal consisting of N tones is $1 + 1/N$, i.e. the minimum OSwR to inband-error-free encode depends upon the reference signal's complexity (e.g. a single tone $N = 1$ can be encoded at OSwR = 2, a two-tone signal $N = 2$ can be encoded at OSwR = 1,5, and so on). Expression (3.24) generalises the previous expression by considering m reference signal's periods as encoding interval. As a result, the minimum OSwR to inband-error-free encode a periodic signal consisting of N tones is 1 (m tends to infinite). Note that the minimum OSwR no longer depends upon the reference signal's complexity N.

Also note that the switching signal has m times the number of inband harmonics than that of the reference signal, as the switching signal is mNT_0-periodic (the distance between adjacent harmonics is $f_0/(mN)$, higher frequency resolution). Provided that the value of these additional harmonics is 0, the baseband spectral content of both signals is the same, i.e. the inband-error-free encoding condition is fulfilled.

Figure 3.5 shows the same single tone sinusoid than that in figure 3.2, but inband-error-free tracked at a lower OSwR ($m = 8$). The time-domain waveforms show the multiple-period encoding (wider encoding window), and the power spectrum shows the additional inband harmonics (enhanced frequency resolution).

3.2.4 Generalisation to Non-Periodic Signals

The previous analysis can be generalised to non-periodic signals by simply increasing the complexity of the reference signal (adding more tones). Certainly, if N tends to infinite, the reference signal becomes a f_0-bandlimited non-periodic signal.

Note that in the multi-tone reference signal described in (3.9), its bandwidth is independent of N, $BW_{x(t)} = f_0$, therefore its spectral content extends from DC up to f_0 regardless of the number of harmonics N. On the other hand, its period is NT_0, hence it does depend upon N.

The minimum OSwR required to error-free track a f_0-bandlimited signal is

$$\mathrm{OSwR}_{\min} = \lim_{N\to+\infty} 1 + \frac{1}{mN} = 1, \quad m \geq 1,\ m \in \mathbb{N} \tag{3.25}$$

Note that a f_0-bandlimited signal can be inband-error-free encoded at f_0, hence it could be perfectly recovered if using an ideal low-pass filter. Also

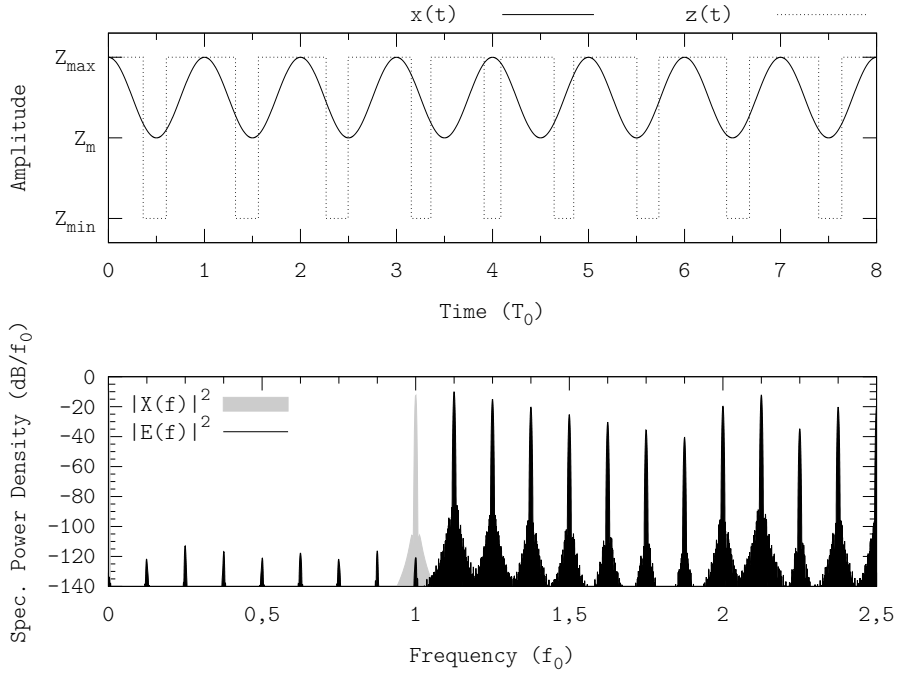

Figure 3.5: Inband-error-free tracking a single tone sinusoid at OSwR = 1,125. Displayed waveforms are the reference signal (solid) and the switching signal (dotted) in the time domain (upper plot), and the error signal in the frequency domain (lower plot).

note that widening the encoding window (increasing m) does not further reduce the minimum OSwR, as the frequency resolution set by the reference signal is already maximum.

It could seem a paradox that the more complexity the reference signal has, the lower the encoding frequency is required. Again, it is a matter of encoding window length and frequency resolution. Because of the frequency normalisation, increasing the reference signal complexity (i.e. adding more tones or increasing N) is equivalent to slowering it down, thus widening the encoding window set by the reference signal. A wider encoding window involves more resolution in the frequency domain and, in the non-periodic case, the encoding window length is already maximum.

3.3 Common Cases in Switching Amplifiers

In switching amplifiers, the decoding process is performed by a LTI low-pass filter, whose rejection in the stopband is finite. Because of this reason, even if encoding with an inband-error-free modulator, it might be necessary to encode at non-minimum OSwRs, to simplify the decoding process and thus ensure enough stopband rejection. Additionally, there are some applications wherein the reference signals are not bandlimited (such as the envelope signals of multibit modulations).

Accordingly, this section extends the minimum OSwR inband-error-free analysis to cases closer to practical situations: high-OSwR inband-error-free encoding (i.e. anticipating the effect of LTI filters, by shifting the spectral content of $E(f)$ to higher frequencies and/or reshaping it) and tracking wider or even infinite-band signals (such as the envelope signals of multibit modulations, hereafter referred as "underswitching").

3.3.1 High-OSwR and Underswitching Effects

An inband-error-free modulator operating at an average switching frequency f_s encodes regardless of the reference signal bandwidth. The generation of the switching signal $z(t)$ results in the addition of a f_s-high-pass error signal $e(t)$ to the reference signal $x(t)$.

If the input signal is bandlimited to f_0, being $f_0 < f_\mathrm{s}$ (high-OSwR inband-error-free encoding), the modulator treats it as a f_s-bandlimited signal, that is, the modulator inband-error-free tracks the reference signal up to f_s including the empty window between f_0 and f_s (padding the reference with zeros).

$$Z(f) = \begin{cases} X(f), & |f| \leq f_0 \\ 0, & f_0 < |f| \leq f_\mathrm{s} \\ E(f), & |f| > f_\mathrm{s} \end{cases} \tag{3.26}$$

On the other hand, if $f_0 > f_\mathrm{s}$ (underswitching), the lowest non-zero spectral content of $e(t)$, upwards of f_s, is mixed with the highest spectral content of $x(t)$, thus part of the information conveyed by $x(t)$ is lost (it is no longer possible to perfectly recover $x(t)$ by low-pass filtering $z(t)$, not even with an ideal filter). Note that this also applies if f_0 is infinite, such as in discontinuous reference signals.

$$Z(f) = \begin{cases} X(f), & |f| \leq f_\mathrm{s} \\ E(f), & |f| > f_s \end{cases} \tag{3.27}$$

At all effects, the modulator treats the f_0-bandlimited signal as a f_s-bandlimited signal, despite f_0 may be higher, equal or lower than f_s, and therefore the reference signal is always truncated or approximated by a f_s-bandlimited signal.

Figures 3.6 and 3.7 illustrate high-OSwR encoding and underswitching respectively, tracking the same reference signal than in figure 3.4 (50-tone signal). Note the empty window in high-OSwR, between f_0 and $f_\mathrm{s} = 2f_0$ (in the switching signal $z(t)$, there are 100 switching events within every $50T_0$ time interval).

On the other hand, in underswitching the reference signal $x(t)$ is approximated by a f_s-bandlimited reference signal $\chi(t)$, which is also depicted in figure 3.7. Note that the lowest spectral content of the error signal $E(f)$ masks the highest spectral content of the reference signal $X(f)$, hence it is not possible to perfectly recover the reference signal $x(t)$ by low-pass filtering the switching signal $z(t)$.

A case of interest of high-OSwR inband-error-free encoding is single-tone tracking, for grid-interactive inverters. By using the proper switching events, it is feasible to cancel all harmonics up to f_s. Since the reference signal is always a single-tone sinusoid, the switching events can be beforehand evaluated, and then drive the inverter (in steady-state) with a digital controller. Figure 3.8 shows a representative example of this situation: tracking a single-tone sinusoid at an OSwR of 13.

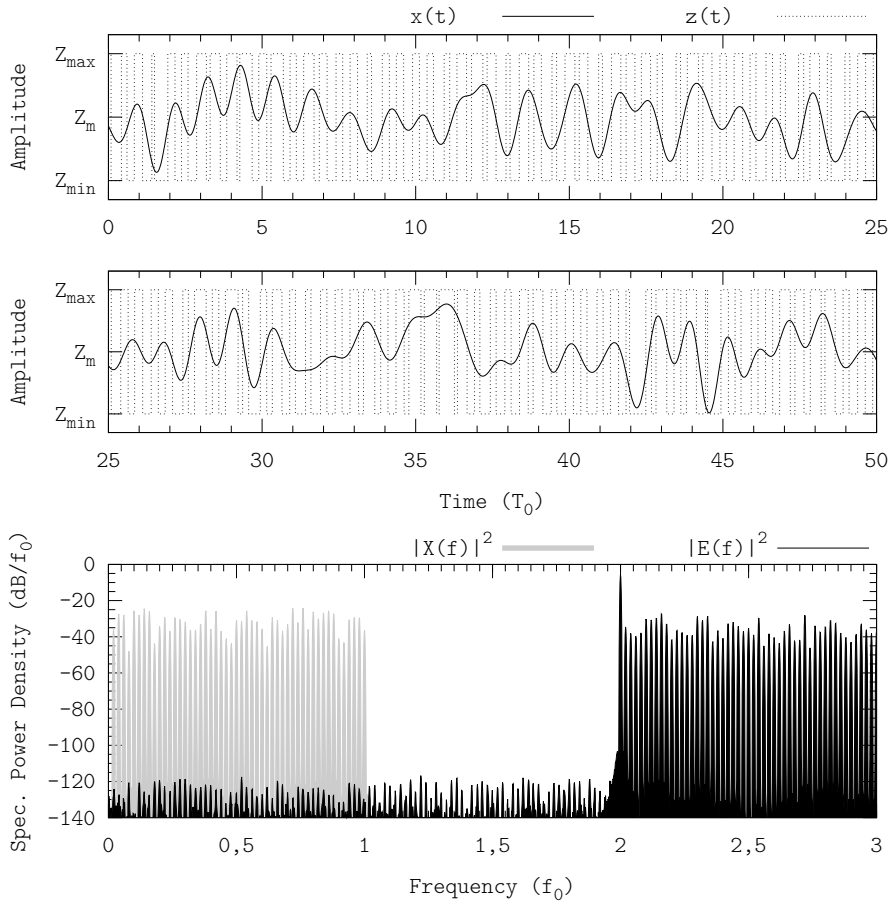

Figure 3.6: Inband-error-free tracking a 50-tone periodic signal at OSwR = 2. Displayed waveforms are the reference signal (solid) and the switching signal (dotted) in the time domain (upper plot), and the error signal in the frequency domain (lower plot).

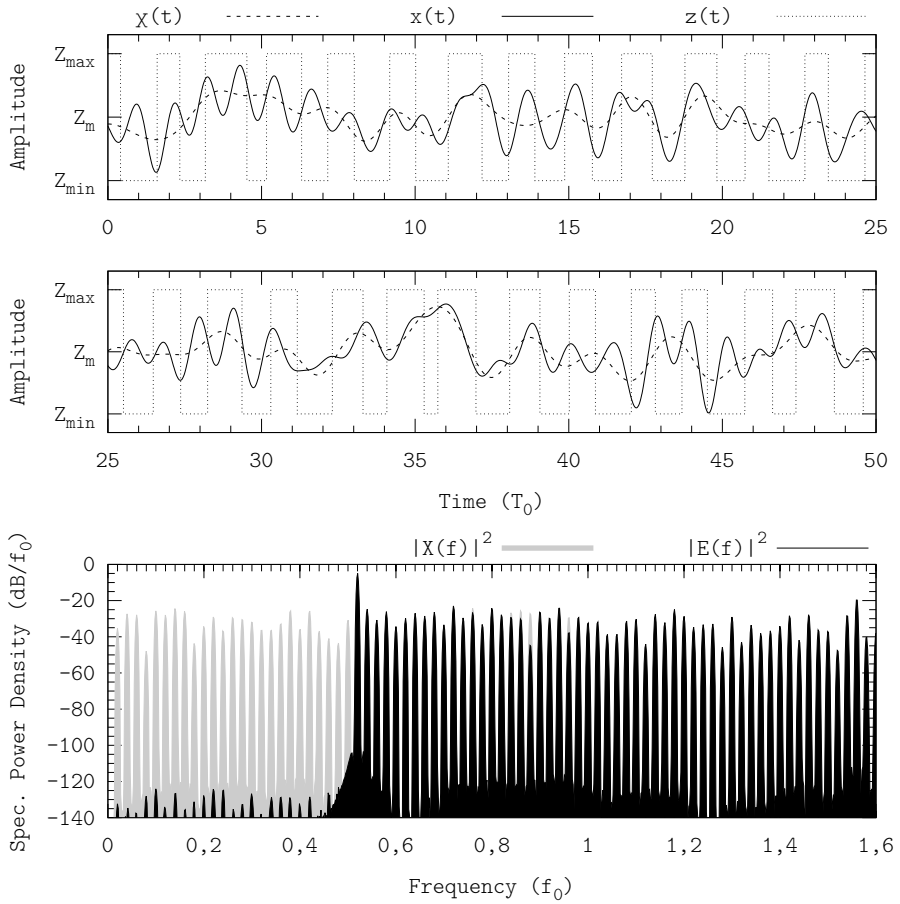

Figure 3.7: Tracking a 50-tone periodic signal at OSwR = 0,52. Displayed waveforms are the reference signal (solid), the switching signal (dotted) and the approximated reference signal in the time domain (upper plot), and the error signal in the frequency domain (lower plot).

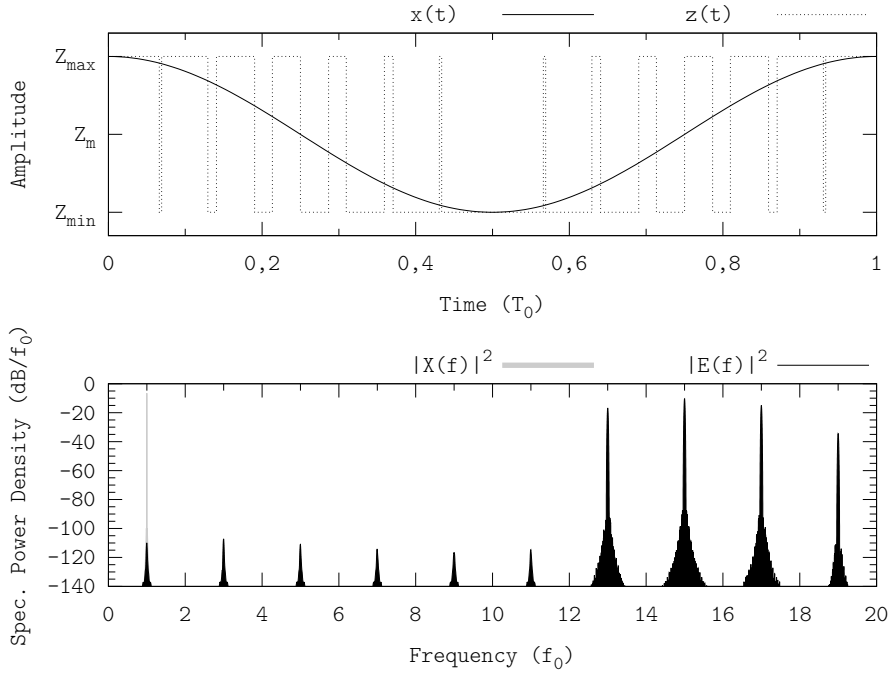

Figure 3.8: Inband-error-free tracking a single tone sinusoid at an OSwR of 13. Displayed waveforms are the reference signal (solid) and the switching signal (dotted) in the time domain (upper plot), and the error signal in the frequency domain (lower plot).

3.3.2 Multiple Inband-Error-Free Encodings at the Same OSwR

The inband-error-free encoding process described so far is not unique if encoding at OSwRs higher than 1. It is possible to find different switching signals tracking the same reference signal at the same OSwR with different time waveforms. The inband-error-free encoding condition only concerns baseband, but there is no constraint regarding the high-frequency spectral content.

In this encoding method based on Fourier Series, the switching signal is generated from a reference periodic signal; the switching events are located so that the baseband spectral content of both signals is the same. Nevertheless, this method constrains the ends of the encoding window, i.e. the ends of one full mNT_0-period of the reference signal, to be always encoded at either high or low level.

Let us consider the example in figure 3.9, a reference signal $x(t)$ consisting of four tones. The switching signal $z_1(t)$ inband-error-free tracks it at an OSwR of 1,125 ($m = 2$). In this case, the time instants $k4T_0$ are alternatively encoded at high or low level; on the other hand, the absolute minima of $x(t)$ are always encoded at low level, whereas the absolute maxima of $x(t)$ are always encoded at high level.

By applying a time delay Δt to the reference signal, it is possible to shift it so that the absolute minima of $x(t)$ are shifted to the beginning of the encoding

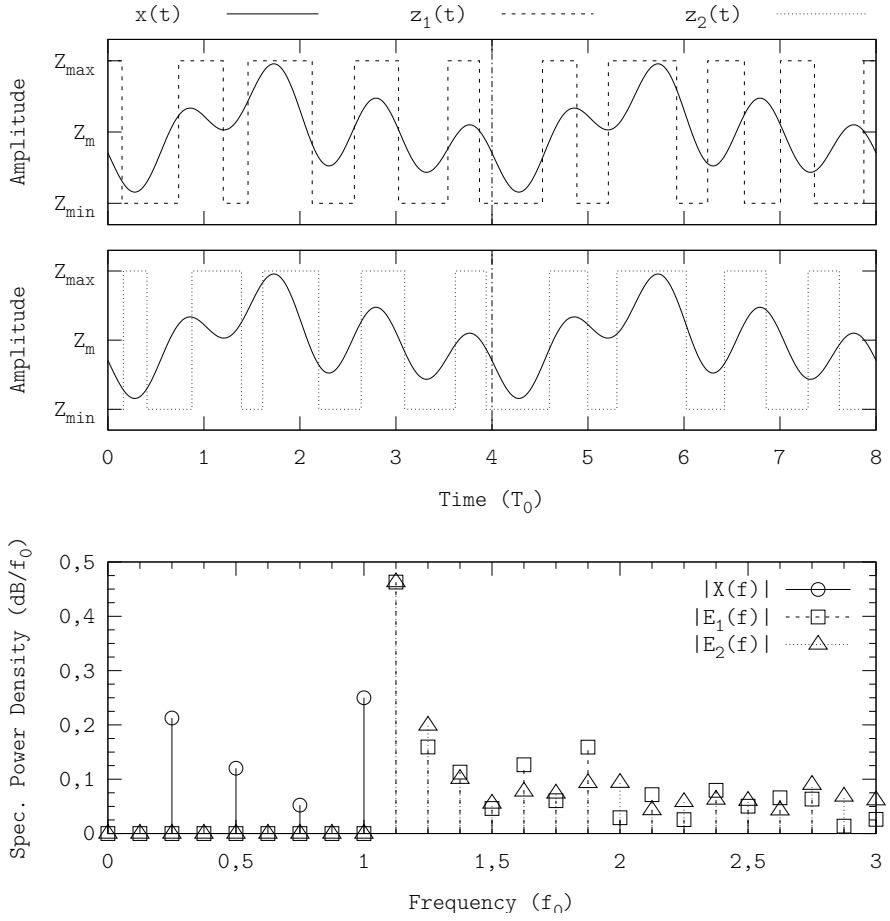

Figure 3.9: A 4-tone reference periodic signal inband-error-free tracked at OSwR = 1,125 by two different switching signals. Displayed waveforms are the reference signal (solid) and the switching signals (dashed and dotted) in the time domain (upper and middle plots), and the error signals (decimated for better readability) in the frequency domain (lower plot).

window. As the reference signal consists of single tones, the time delay involves a phase shift $\varphi_k(\Delta t)$ in each tone.

$$x_{\Delta t}(t) = x(t + \Delta t) \Rightarrow \varphi_k(\Delta t) = \frac{\omega_0 k \Delta t}{N} \tag{3.28}$$

This shifted reference signal $x_{\Delta t}(t)$ can be now encoded at the same OSwR than that of $z_1(t)$, yielding a shifted switching signal $z_{\Delta t}(t)$. Nonetheless, the absolute minima of $x(t)$ are now alternatively encoded at either high or low level (see figure 3.9).

By undoing the time delay, a switching signal $z_2(t)$ is obtained which also tracks the reference signal $x(t)$ at minimum OSwR, but with a different time waveform than that of $z_1(t)$.

$$z_2(t) = z_{\Delta t}(t - \Delta t) \tag{3.29}$$

Consistently, the power spectrum of the error signals $e_1(t)$ and $e_2(t)$ also show some differences. Note that the baseband spectral content sets the power conveyed by the switching signal, because the a_0 coefficient sets the amount of time at high level (see section 3.4.1). Since the power conveyed by the switching signal only depends upon a_0, if two different switching signals error-free track the same reference signal at the same OSwR, considering that their baseband spectral content (thus the baseband power) is the same, then their high-frequency power must be the same too. The difference between these two switching signals in the frequency domain concerns the high-frequency power distribution (figure 3.9).

It is possible to tune an inband-error-free encoding process by also considering the high-frequency power distribution, although a significant shaping needs more degrees of freedom in the encoding process.

High-Frequency Spectral Content Shaping

The high-frequency spectral content can be further shaped by adding more degrees of freedom in the encoding process. Although the encoding process is less efficient (more OSwR is required to error-free track up to the same frequency), the decoding process may be simpler (e.g. less power in the first harmonic) or it could be easier to implement an actual modulator which may perform this inband-error-free encoding process.

Consider a simple example, inband-error-free encoding a single tone at an OSwR of 5 (see figure 3.10). At each maximum of $x(t)$, the switching signal be at either low $z_1(t)$ or high $z_2(t)$ level. As figure 3.10 shows, with only this degree of freedom the difference between encoding processes is significant, namely a reduction of 50 % in the amplitude of the first harmonic.

Encoding at high OSwR does not necessarily involve adding degrees of freedom to the encoding process (e.g. adding an empty window, as described in section 3.3.1). More degrees of freedom can be added by imposing other constraints, e.g. bounding the energy of the firsts harmonics of the error signal $e(t)$ ($a_k^{*2} + b_k^{*2} \leq \alpha_k$ with $k \geq N$ if tracking a bandlimited signal consisting of N tones), but this analysis is beyond the scope of this chapter.

3.4 Interpretation of Minimum OSwR Inband-Error-Free Encoding

The result derived in section 3.2, an OSwR of 1 to inband-error-free track a f_0-bandlimited non-periodic signal (3.24), is well below the conventional design choice in switching amplifiers (OSwRs upwards of ten). The reason for this low fundamental bound is that this encoding process, based on harmonics matching, is specifically designed and intended for inband-error-free encoding, regardless of the implementation feasibility.

In order to achieve minimum OSwR inband-error-free encoding, it is necessary to know all the information of the reference signal to encode, i.e. the value of the reference signal $x(t)$ from $t = -\infty$ to $t = +\infty$ (non-causal encoding process). Note that, in periodic signals, the values within the fundamental period already provide information at any time instant. Consequently, it is

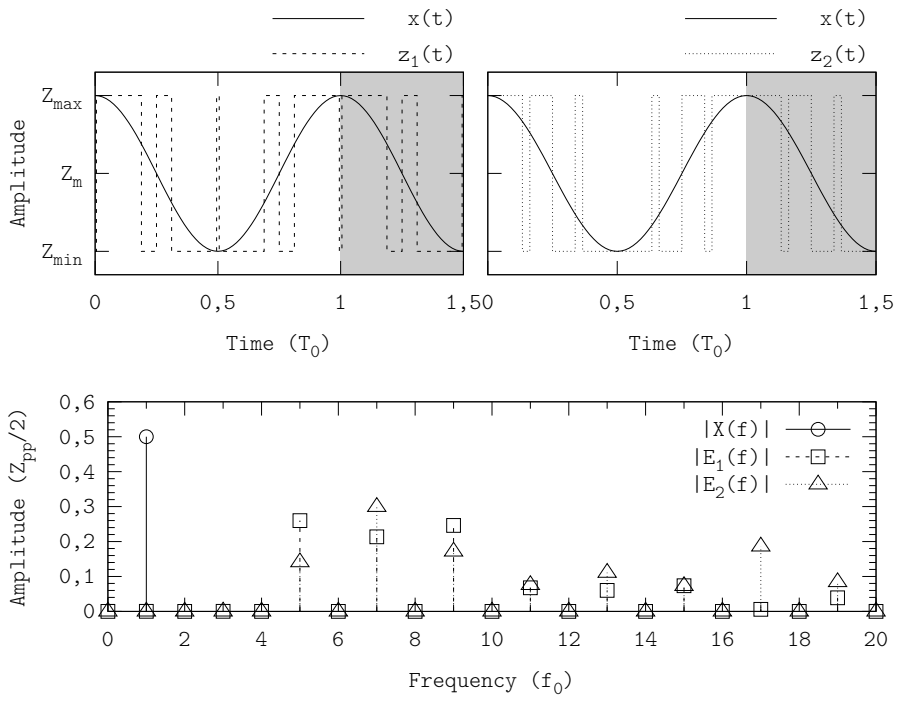

Figure 3.10: Different inband-error-free encodings at OSwR = 5. Displayed waveforms are the reference signal (solid) and the switching signals (dashed and dotted) in the time domain (upper plots), and the error signals (decimated for better readability) in the frequency domain (lower plot).

not possible to implement a real-time modulator[2] performing minimum OSwR inband-error-free encoding.

The encoding process presented in this chapter encodes by matching the harmonics' amplitude and the phase, so that the inband spectral content of the switching signal $Z(f)$ is the same than that of the reference signal $X(f)$. Due to the heterogeneous nature of these two signals in the time domain (the reference signal is a continuous-amplitude with continuous derivatives signal, whilst the switching signal is discrete-amplitude signal), both signals are moved into a domain wherein they are more homogeneous and hence they can be easily compared: the frequency domain. The signals are processed in the frequency domain; then the modulated switching signal $Z(f)$ is transformed back to the time domain $z(t)$.

If the implementation of the direct translation of the inband-error-free encoding process is to be addressed, two main challenges arise: the high computational cost (Fourier Transforms and solving non-linear equations) and the latency due

[2] Without considering implementation-induced delays, a real-time modulator is that which fulfils $z(t_0) = f\left(x(t)\right), t \leq t_0$, i.e. no information about the future behaviour of the reference signal is required. Note that a PID controller is not a real-time controller, since it requires the first derivative (computing $\dot{x}(t_0)$ requires $x(t_0 + \tau)$, being $\tau > 0$). However, the derivative can be approximated with preceding values of reference signal $x(t_0 - \tau)$; furthermore, even if using future information, the delay τ due to the computation of the derivative is usually tolerable and thus PIDs are, effectively, real-time controllers.

to the large encoding window for accurate frequency-domain representation. Nevertheless, the main interest of the quantitative bound for inband-error-free encoding presented in this chapter is as comparison framework for practical modulators, in terms of inband-error power and OSwR.

3.4.1 Switching Signal's Time Waveform Analysis

In minimum OSwR inband-error-free encoding, the switching events t_k are computed in the frequency domain so that the baseband spectral content of the switching signal $Z(f)$ matches the baseband spectral content of the reference signal $X(f)$. Unfortunately, in the time domain, the switching events t_k are irregularly distributed; moreover there is no redundancy in the switching signal $z(t)$ either (it conveys the maximum amount of information). Consequently there is no direct relation between the reference signal's time-domain waveform $x(t)$ and the distribution of switching events t_k. Despite approximating minimum OSwR inband-error-free encoding with an actual modulator may be possible, it is challenging indeed. Nevertheless, by analysing the time waveform of the switching signal $z(t)$ in inband-error-free encoding, it can be evaluated whether actual modulators can approximate inband-error-free encoding under some specific operating conditions.

Actual modulators for switching amplifiers are constrained by a feasible implementation; this constraint usually leads to implement a lossy encoding algorithm such as PWM (the encoding fidelity of common modulations is discussed in chapter 4). Given an actual modulator (e.g. triangle PWM), the only free parameter in the encoding process is the OSwR. Provided that the common modulators in switching amplifiers do not implement minimum switching frequency inband-error-free encoding (i.e. inband-error-free encoding at an OSwR of 1), they can only approximate inband-error-free encoding at high OSwRs. That is, as the OSwR increases, the encoding process performed by the modulator should tend to inband-error-free encoding to satisfy this approximation.

In inband-error-free encoding, as the OSwR increases, the switching signal $z(t)$ becomes redundant in the sense that more switching events are used to encode the same information[3]. Within each pulse of the switching signal $z(t)$, the amplitude sweep of reference signal $x(t)$ decreases. Therefore, as the OSwR increases, the reference signal $x(t)$ tends to behave as a constant-reference signal within the time interval defined by two consecutive pulses, one positive and one negative (encoding interval). Formally,

$$\lim_{\mathrm{OSwR}\to+\infty} x(t_k) - x(t_{k-1}) = 0 \tag{3.30}$$

where the time instants t_k and t_{k-1} correspond to two consecutive switching events in the switching signal $z(t)$.

Constant-reference signals can be easily inband-error-free encoded, even with actual modulators, since the only constraint to achieve inband-error-free encoding is equalling the integral (area) of the reference signal $x(t)$ and the integral

[3]Strictly speaking, the term "redundant" means that the encoding process is not unique. As discussed in sections 3.2.3 and 3.3.1, high-OSwR inband-error-free encoding does not necessarily add redundancy in the switching signal $z(t)$. Nevertheless, here the term "redundant" is used to emphasise the non-minimum OSwR in the inband-error-free encoding process.

(area) of the switching signal $z(t)$ (area-equalling encoding). Certainly, because of tracking the a_0 coefficient, the switching signal $z(t)$ fulfils

$$a_0 = a_0^* \Rightarrow \int_0^{mNT_0} x(u)\,\mathrm{d}u = \int_0^{mNT_0} z(u)\,\mathrm{d}u \tag{3.31}$$

and provided that all the information is conveyed within the a_0 coefficient, fulfilling this condition is sufficient to achieve inband-error-free encoding. Formally, area-equalling encoding can be stated as

$$\int_{t_{2k}}^{t_{2k+2}} x(u)\,\mathrm{d}u = \int_{t_{2k}}^{t_{2k+2}} z(u)\,\mathrm{d}u, \quad \forall k \in \mathbb{Z} \tag{3.32}$$

where t_k stands for the time instants of the switching events of the switching signal $z(t)$.

When tracking non-constant reference signals, tracking the a_0 coefficient becomes a necessary but not sufficient condition to inband-error-free encode (fulfilling it does not guarantee a good approximation to inband-error-free encoding). However, if the reference signal $x(t)$ can be time-locally approximated by a constant-reference signal (high OSwR encoding, i.e. the amplitude variation of the reference signal $x(t)$ within each encoding interval is small, as discussed above), the inband-error-free encoding algorithm can be approximated by area-equalling encoding with small error. That is, within each encoding interval, the integral of the switching signal $z(t)$ approximately equals the integral of the reference signal $x(t)$.

This approximation can be illustrated with a simple example, inband-error-free tracking single tone at high OSwRs.

$$x(t) = \cos\left(2\pi f_0 t\right), \quad \forall t \in \mathbb{R} \tag{3.33}$$

Let $\lambda(t)$ be the area-error signal, defined as a piecewise linear function whose value is the integral of the error signal $e(t)$ within each encoding interval (or pulse pair).

$$\lambda(t) := \int_{t_{2k}}^{t_{2k+2}} e(u)\,\mathrm{d}u, \quad t \in [t_{2k}, t_{2k+2}],\ \forall k \in \mathbb{Z} \tag{3.34}$$

Given an arbitrary reference signal $x(t)$ and a two-level switching signal $z(t)$ tracking it, the instantaneous magnitude of the area-error signal $\lambda(t)$ quantifies, within each encoding interval, the deviation of the switching signal $z(t)$ from area-equalling encoding. In the case of inband-error-free encoding, this signal can used to evaluate how good is the area-equalling encoding approximation.

Figure 3.11 shows the time waveforms of the area-error signal $\lambda(t)$ together with the reference $x(t)$ and the switching $z(t)$ signals at an OSwR of 9, as well as the time waveform of the area-error signal $\lambda(t)$ at different OSwRs. The amplitude of the area-error signal $\lambda(t)$ decreases as the OSwR increases, which points out that inband-error-free encoding tends to area-equalling encoding as the OSwR increases. The suitability of this approximation can be quantified by evaluating the RMS value of the area-error signal, $\lambda(t)_{\mathrm{RMS}}$, at different OSwRs (see figure 3.12). The RMS value tends to monotonically decrease, which reflects that, as the OSwR increases, inband-error-free encoding tends to area-equalling encoding.

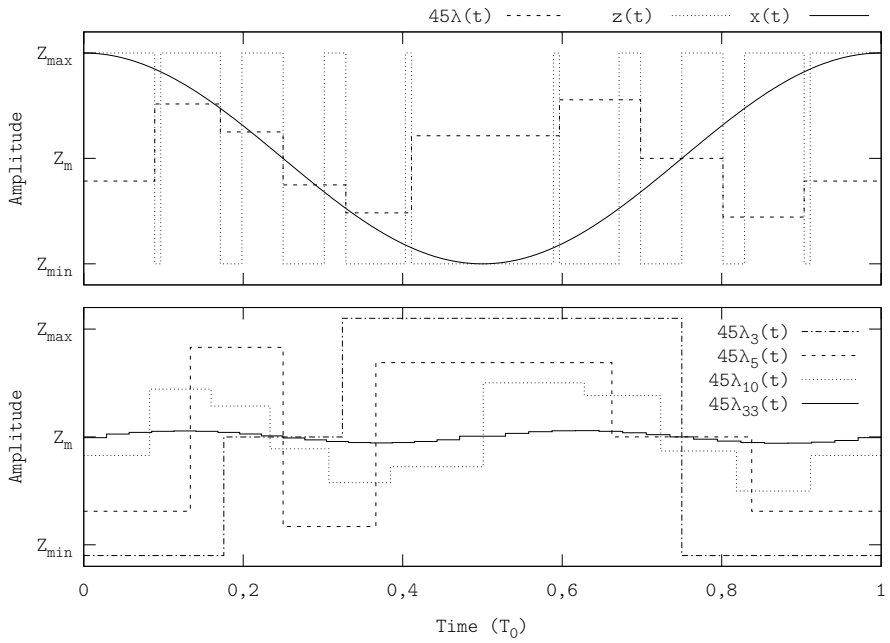

Figure 3.11: Area-error signal in inband-error-free tracking a single tone at different OSwRs. Displayed waveforms show the reference signal $x(t)$, the switching signal $z(t)$ and the (scaled) area-error signal $\lambda(t)$ in the upper plot (OSwR = 9) and the (scaled) area-error signals $\lambda_i(t)$ at different OSwRs in the lower plot (the subscript i stands for the OSwR).

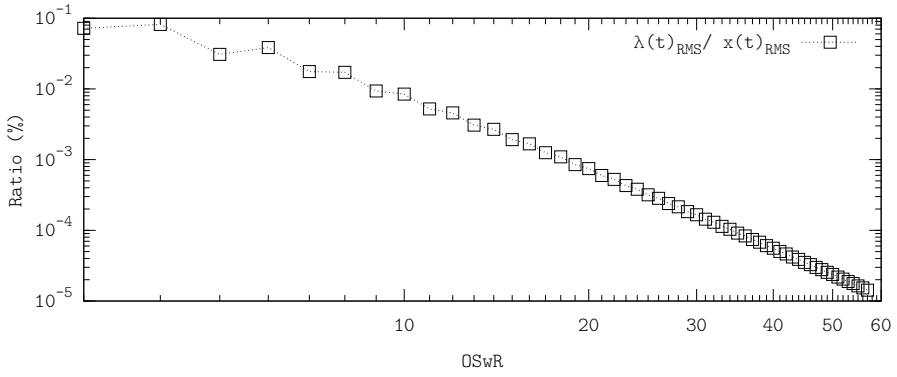

Figure 3.12: Approximating inband-error-free encoding by area-equalling encoding, showing the ratio of the RMS value of the area-error signal $\lambda(t)_{\mathrm{RMS}}$ to the RMS value of the reference signal $x(t)_{\mathrm{RMS}}$ at different OSwRs.

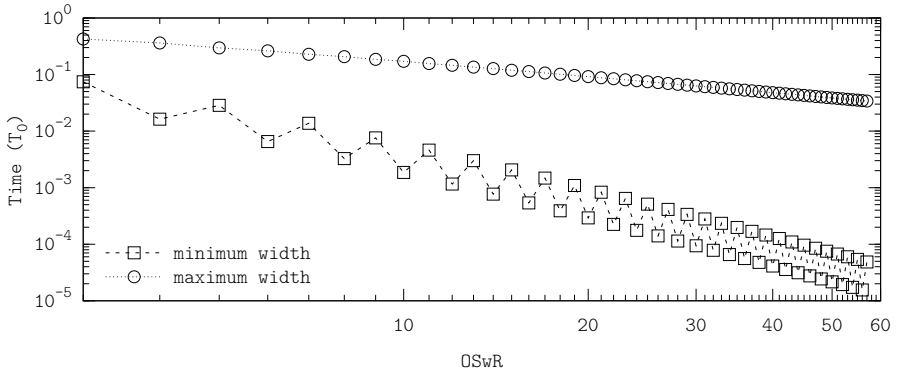

Figure 3.13: Time distribution of switching events in inband-error-free encoding (tracking a single tone sinusoid). Displayed waveforms show the maximum and minimum widths of the pulses within one period of the single tone sinusoid.

This property of inband-error-free encoding establishes a suitability constraint for modulations for switching amplifiers: the encoding process must tend to area-equalling encoding as the OSwR increases; consequently, the modulator must inband-error-free track constant-reference signals. This feature guaranties that the error due to improper encoding can be reduced by increasing the OSwR (in conventional switching amplifiers under regular operating conditions, OSwRs upwards of ten, improper encoding is usually not the dominant inband error source). Note, however, that area-equalling encoding is just an approximation to inband-error-free encoding, only valid if the OSwR is high, but not necessarily the best approximation.

The single-tone tracking characterisation can also be used to analyse the time distribution of the switching events t_k (see figure 3.13). As the OSwR increases, the distribution of switching events tends to a regular distribution, i.e. constant switching frequency (in figure 3.13, the maximum pulse width tends to decrease at a rate of 1/OSwR as the OSwR increases).

Chapter 4

Two-Level Modulations for Switching Amplifiers

This chapter characterises and compares two-level switching modulations for switching amplifiers (modulations which can be feasibly implemented) from the encoding-reconstruction standpoint of switching amplifiers presented in chapter 2, and revisits them under the fundamental limit perspective derived in chapter 3. The scope is to analyse and characterise these common modulations under non-conventional operating conditions (OSwRs below ten).

4.1 Pulse Width Modulation

Pulse Width Modulation (PWM) is the most common 2-level switching modulation in switching amplifiers. The encoding process consists in comparing the reference signal $x(t)$ with a carrier $c(t)$, thereby generating the two-level switching signal $z(t)$. PWM can be simply implemented with a comparator, as figure 4.1 shows.

By analysing the encoding process of PWM from the encoding-reconstruction standpoint of switching amplifiers, PWM turns out to be an encoding algorithm suitable to inband-error-free track constant-reference signals; it is even possible to encode constant-reference signals with non-linear gains (non-linear input-output DC voltage ratios).

4.1.1 Constant-Reference Signal Tracking

The carrier $c(t)$ continuously sweeps all the modulator dynamic range (from $Z_{\min}$ to $Z_{\max}$ or vice versa), thereby defining or splitting into encoding intervals

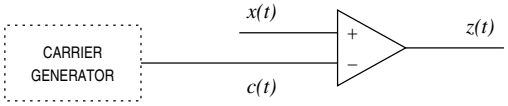

Figure 4.1: Generic non-inverting pulse width modulator. The carrier $c(t)$ is externally generated.

$T^k_{\mathrm{PMW}} = t_{\mathrm{c}}^{k+1} - t_{\mathrm{c}}^k$, $k \in \mathbb{Z}$, where $c(t_{\mathrm{c}}^k) = Z_{\min}$ if k is even and $c(t_{\mathrm{c}}^k) = Z_{\max}$ if k is odd. Provided that the constant-reference signal $x(t)$ does not saturate the modulator $Z_{\min} \leq x(t) \leq Z_{\max}$, within each encoding interval, the reference signal unavoidably intersects the carrier thus generating a pair of pulses, one negative and one positive. The combined area of both pulses equals the area of the constant-reference signal $x(t)$, corrected by the modulation's input-output DC characteristic.

If the input-output DC characteristic is linear (linear PWM), the combined area of the pulse pair equals the area of the constant-reference signal and hence PWM inband-error-free tracks the constant-reference signal $x(t)$, $a_0^* = a_0$. Consequently, the encoded information can be perfectly recovered by low-pass filtering the switching signal $z(t)$.

Provided that the carrier $c(t)$ monotonously sweeps the dynamic range within each encoding interval, the carrier determines how often the switching events are generated. The switching frequency f_{s} of the switching signal $z(t)$ is therefore determined by the carrier's frequency f_{c}.

Note that the carrier frequency, and hence the frequency of the PWM switching signal, does not necessarily need to be constant. The only constraint regarding the time waveform of the carrier is that, within each encoding interval, it must monotonously sweep all the dynamic range (from $Z_{\min}$ to $Z_{\max}$ or vice versa). Regardless, constant-frequency carriers are the most common; unless otherwise stated, constant-frequency carriers are hereafter assumed.

Variable-frequency PWM are mostly used in regulators, to reduce the switching losses in light load conditions. There exist different implementations of this variant, including pulse skipping and Pulse Frequency Modulation (PFM).

4.1.2 Modulation Variants

The modulation's input-output DC characteristic is determined by the carrier's waveform $c(t)$ within each encoding interval. Despite non-linear input-output DC characteristics lead to distorting encoding processes (in this case, $a_0^* \neq a_0$), it is possible to take advantage of this feature in non-linear decoders (non-buck-derived switching converters), so that the combination of the DC-non-linear switching modulation and the non-linear decoder results in a linear system. Nevertheless this variant is not common and it is seldom used in actual applications. Figure 4.2 includes an example of non-linear PWM, based on a discontinuous sinusoidal carrier.

A linear input-output DC characteristic (in order to inband-error-free encode the information conveyed by the constant-reference signal $x(t)$), can be achieved by linearly sweeping from $Z_{\min}$ to $Z_{\max}$, e.g. with a sawtooth carrier.

In sawtooth PWMs, one of the most common variants of PWM, the carrier is discontinuous. For instance, in the trailing-edge variant (the example included in figure 4.2), all encoding intervals yield a negative pulse followed by a positive pulse (all encoding intervals start at low level $Z_{\min}$ and end at high level $Z_{\max}$). Transitioning between two consecutive encoding intervals therefore requires an additional switching event in the switching signal $z(t)$, from high level $Z_{\max}$ to low level $Z_{\min}$.

These additional switching events, namely dummy edges, are a consequence of the modulation itself and hence they do not convey information of the constant-reference signal $x(t)$. Dummy edges degrade the encoding efficiency: higher

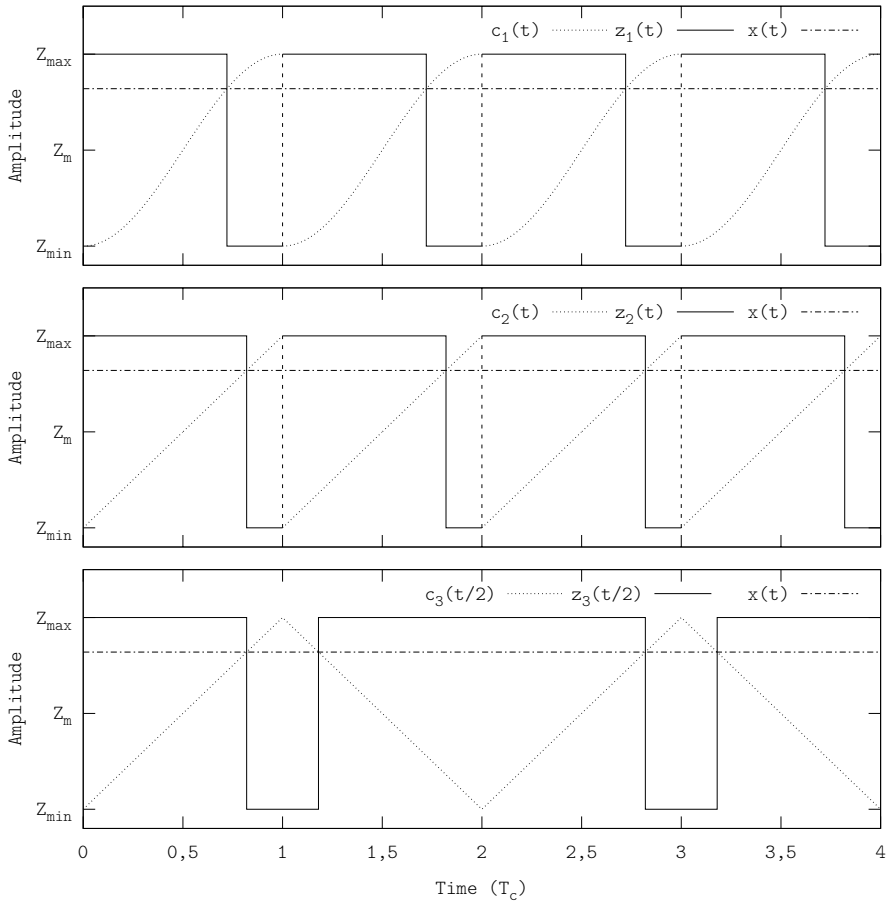

Figure 4.2: Different kinds of constant-frequency PWMs: non-linear (upper graph), linear with discontinuous carrier (trailing sawtooth carrier, middle graph) and linear with continuous carrier (triangle carrier, lower graph). The edges displayed with dashed lines convey no information of the constant-reference signal $x(t)$.

switching frequency to convey the same amount of information. Note that the width of the odd encoding intervals is zero $T_{\mathrm{PWM}}^{2k+1} = 0$, $\forall k \in \mathbb{Z}$, thus no information can be conveyed by them. This issue is common in all discontinuous carriers, including non-linear ones, such as the non-linear carrier included in figure 4.2.

The dummy edges issue can be addressed by alternatively reversing the switching signal's $z(t)$ pulses order, so that a negative-positive pulse pair is followed by a positive-negative pulse pair and vice versa. In this way, the starting level of an encoding interval is the same than the ending level of the previous encoding interval, thus skipping the dummy edges. This behaviour can be achieved by alternatively reversing the carrier's time waveform $c(t)$, e.g. a trailing-edge interval followed by a leading-edge interval and vice versa (the sawtooth carrier then becomes a symmetrical continuous triangle carrier, see figure 4.2).

The carrier's frequency $f_{\mathrm{c}} = 1/T_{\mathrm{c}}$ is generally defined so that

$$c(t) = c(t + T_{\mathrm{c}}), \quad \forall t \in \mathbb{R} \tag{4.1}$$

and hence the switching frequency f_{s} of the switching signal $z(t)$ is $f_{\mathrm{s}} = f_{\mathrm{c}}$. Note that this is valid for both discontinuous and continuous carriers. Certainly, according to expression (4.1), when converting a discontinuous carrier of frequency f_1 into continuous, the frequency of the continuous carrier is $f_2 = f_1/2$ (equivalently, $T_2 = 2T_1$). However, because of dummy edges skipping, the number of switching events N_{sw2} yielded by a PWM driven by the continuous carrier $c_2(t)$ is also half of that N_{sw1} yielded by a PWM driven by the discontinuous carrier $c_1(t)$, i.e. $N_{\mathrm{sw2}} = N_{\mathrm{sw1}}/2$. The switching frequency of both switching signals is therefore the same than that of their respective carriers.

Generalising, symmetrical continuous carriers yield switching signals with no dummy edges, thereby improving the efficiency of the encoding process when compared to discontinuous carriers.

4.1.3 Generalisation to Non-Constant Signal Tracking

Although inband-error-free encoding non-constant reference signals is not possible with PWM, provided that PWM inband-error-free tracks constant-reference signals and relying on the area-equalling approximation of inband-error-free encoding (see section 3.4.1), PWM can also be used to track non-constant reference signals $x(t)$ with a bounded error. The higher the OSwR, the lower the tracking error.

The natural extension of PWM to non-constant signal tracking consists in replacing the constant-reference signal by a time-varying reference signal. A switching event is generated whenever the reference signal $x(t)$ intersects the carrier $c(t)$, as figure 4.3 shows (natural-sampling PWM).

Nevertheless, in some applications, the analogue reference signal $x(t)$ is not explicitly available; instead only (uniformly spaced) sampled values $x[n] = x(t_i)$ of it are available. In such cases, to avoid reconstructing the analogue signal $x(t)$ by interpolating its sampled values $x[n]$, the analogue signal $x(t)$ is approximated by a piecewise constant signal $x^*(t)$ whose value, within each encoding interval, is constant and equal to the analogue signal's value at the beginning of the encoding interval (which generally coincides with a sample $x[n]$, uniform-sampling PWM).

$$x^*(t) = x(t_i), \quad \forall t \in [t_i, t_{i+1}) \tag{4.2}$$

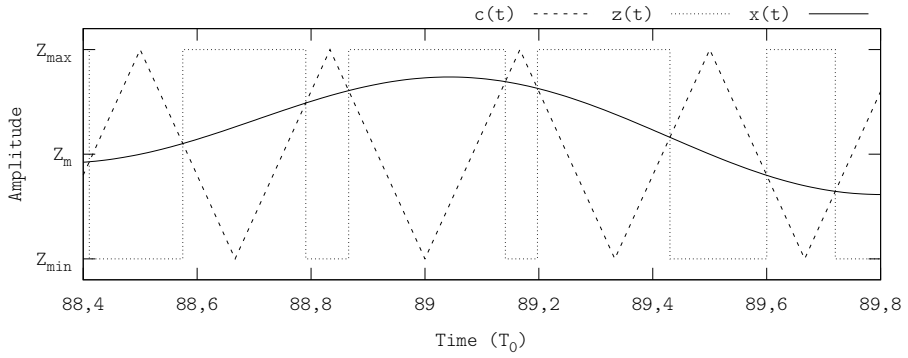

Figure 4.3: Triangle PWM tracking a f_0-bandlimited signal at OSwR = 3. Displayed waveforms show the carrier (dashed line), the switching signal (dotted line) and the reference signal (solid line).

The performance in terms of distortion and tracking error of natural-sampling PWM is better than that of uniform-sampling PWM [78]. The only advantage of uniform-sampling over natural-sampling is the actual implementation, especially in digital modulators. Because of these reasons, uniform-sampling PWM is not considered in this work.

Note that even natural-sampling PWM implicitly samples the reference signal $x(t)$. When tracking non-constant reference signals $x(t)$, only the information conveyed by the reference signal $x(t)$ at the intersections with the carrier, i.e. $x(t_k)$, is encoded; the information conveyed at all other time instants is lost. On the other hand, in constant-reference signals, the information is the same at all time instants and hence no information is lost due to this implicit sampling (inband-error-free encoding). Because of this reason, from the encoding-reconstruction standpoint, PWM is a modulation suitable to track constant-reference signals.

4.1.4 Switching Signal's Time Waveform Analysis

Within each encoding interval T^k_{PWM}, the instantaneous duty cycle d_k

$$d_k := \frac{1}{T^k_{\mathrm{PWM}}} \int_{t_{\mathrm{c}}^k}^{t_{\mathrm{c}}^{k+1}} \frac{z(u) - Z_{\mathrm{m}}}{Z_{\max} - Z_{\min}} \,\mathrm{d}u, \quad \forall k \in \mathbb{Z} \tag{4.3}$$

is determined by the intersection of the reference signal $x(t)$ and the carrier $c(t)$. When tracking a non-constant reference signal $x(t)$, the intersection may occur at any amplitude level; in particular, if the value of the reference signal $x(t)$ is close to either $Z_{\min}$ or $Z_{\max}$, its bound values, the instantaneous duty cycle d_k yielded within these encoding intervals may be very low or very high respectively.

In either case, this results in very narrow pulses in the switching signal $z(t)$. Certainly, let T_k be the width (time length) of the kth pulse

$$T_k := t_{k+1} - t_k \tag{4.4}$$

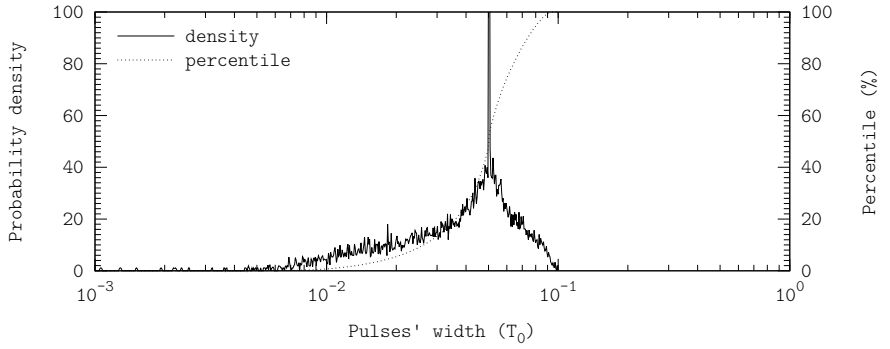

Figure 4.4: Histogram of pulses' width of triangle PWM tracking a f_0-bandlimited signal at an OSwR of 10. Simulation performed using the configuration D.4.5.

where t_k are the time edges of the switching signal $z(t)$. Formally, the pulses' width in sawtooth and triangle PWMs is not bounded from below (in fact it is bounded by 0, but the width of a pulse cannot be negative).

On the other hand, provided that the carrier $c(t)$ sweeps all the modulator's dynamic range within each encoding interval and that $Z_{\min} \leq x(t) \leq Z_{\max}$, the reference signal $x(t)$ unavoidably intersects the carrier $c(t)$ within each encoding interval. As a result, there is one switching event within each single encoding interval; the worst case (i.e. widest pulse) is bounded from above by switching at the beginning of an encoding interval and switching again at the end of the subsequent encoding interval (the carrier's period $T_\mathrm{c} = 1/f_\mathrm{c}$, which fulfils $f_\mathrm{c} = f_\mathrm{s} = \mathrm{OSwR} f_0$). Therefore,

$$0 < \frac{T_k}{T_0} < \frac{1}{\mathrm{OSwR}} \tag{4.5}$$

Note that these bounds are independent of the reference signal's waveform $x(t)$, even in discontinuous reference signals, as long as the reference signal $x(t)$ does not saturate the modulator.

The actual distribution depends upon the amplitude distribution of the signal to track $x(t)$; PWM maps the reference signal's amplitude distribution (extending from $Z_{\max}$ to $Z_{\min}$) to a time-domain pulse width distribution, which extends from 1/OSwR to 0

$$x(t) \in [Z_{\min}, Z_{\max}] \rightarrow T_k \in \left[0, \frac{1}{\mathrm{OSwR}}\right] \tag{4.6}$$

Figure 4.4 includes the histogram of the pulses' width of triangle PWM tracking a f_0-bandlimited signal at an OSwR of 10 (the amplitude distribution of the reference signal $x(t)$ is included in figure 2.17). As this figure illustrates, the pulses' width is bounded from above by $10^{-1}T_0$ and is not bounded from below, although the probability density below $10^{-2}T_0$ is very small, which corroborates expressions (4.5) and (4.6).

4.1.5 Power Spectrum Analysis

The power spectrum of PWM signals is determined by the carrier's waveform $c(t)$ and the reference signal $x(t)$. When tracking f_0-bandlimited signals with a constant-frequency triangle PWM, the power spectrum of the PWM signal is defined by a series of replicas of the reference signal $X(f)$ and modulation harmonics; each of these series is centered at a frequency multiple of the switching frequency kf_s, $k \geq 1$, $k \in \mathbb{N}$ and scaled by Bessel-shaped coefficients, which are centered at the same frequency [78].

The power spectrum of sawtooth PWM (also constant-frequency and tracking a f_0-bandlimted signal) is similar, but with more harmonics and different Bessel coefficients [78]. The increased number of harmonics is due to dummy edges.

Figure 4.5 shows the power spectra of the error signals $E(f)$ when tracking a f_0-bandlimited signal with a sawtooth PWM and with a triangle PWM, both of them operating at an OSwR of 10. The replicas of the f_0-bandlimited flat-spectrum reference signal $X(f)$ and the modulation harmonics, both scaled by Bessel coefficients, can be easily identified.

The cumulative-power frequency distribution reveals that more than 75 % of error signal's power accumulates around the switching frequency $f_\mathrm{s} = \mathrm{OSwR} f_0$ (fundamental harmonic).

4.2 Asynchronous ΣΔ Modulation

Asynchronous ΣΔ Modulation (AΣΔM) is a two-level switching modulation which has also been used in switching amplifiers. Although it is not as popular as PWM, by analysing the encoding process of AΣΔM from the encoding-reconstruction standpoint of switching amplifiers, AΣΔM turns out to be more suitable to track non-constant signals than PWM, especially at low OSwRs.

An AΣΔM consists of an integrator, an adder and an hysteresis comparator. Figure 4.6 shows a block diagram of a normalised AΣΔM (the only free parameter is the hysteresis bandwidth δ, yet considering normalised AΣΔMs does not detract generality to the analyses, as described in [21]). The operation of AΣΔM is well-known and has been in-depth analysed, in both time [21] and frequency domains [79].

4.2.1 Encoding Process

AΣΔM encodes by computing the integral of the error signal $e(t)$, i.e. the integral of the difference between the switching signal $z(t)$ and the reference signal $x(t)$. Whenever the integrator's output signal $v(t)$ reaches one of the comparator's thresholds $\pm\delta$ (the accumulated or integrated error is too large), the comparator is triggered thus generating a switching event t_k (see the time waveforms in figure 4.6).

Unlike PWM, no external signal is used in this modulation (asynchronous modulation). Instead, an AΣΔM is an astable oscillator itself, which, when no reference signal is applied $x(t) = Z_\mathrm{m}$, supplies a square switching signal (two-level switching signal with constant frequency and duty cycle $D = 50\,\%$) whose frequency is determined by δ. In general, if the reference signal is constant

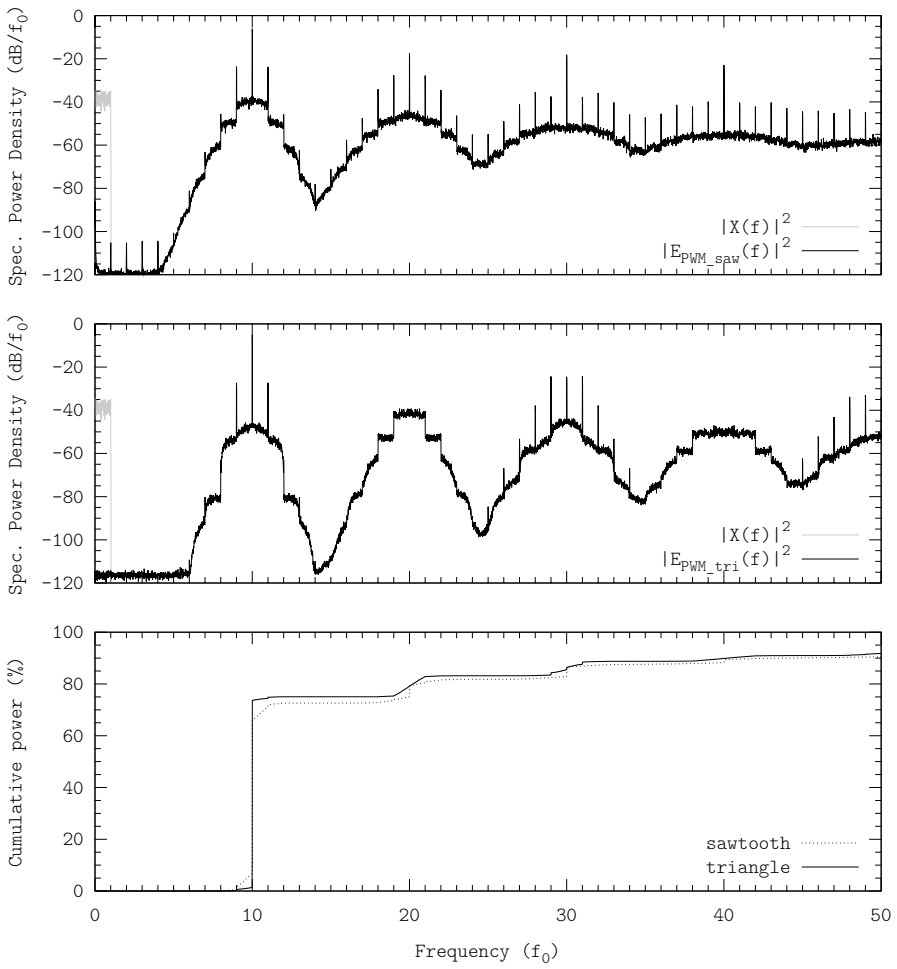

Figure 4.5: Power spectra of trailing sawtooth PWM (upper graph), triangle PWM (lower graph) and cumulative-power frequency distribution of both error signals (lower graph) tracking a f_0-bandlimited signal at an OSwR of 10. Simulation performed using the configuration D.4.1.

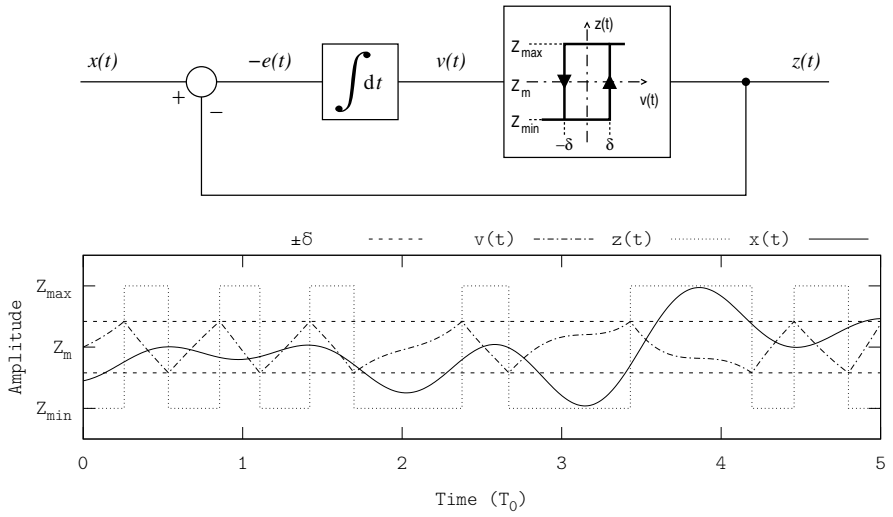

Figure 4.6: Asynchronous ΣΔ Modulator and representative time waveforms when tracking a f_0-bandlimited reference signal. The integrator output signal $v(t)$ has been scaled for better readability.

$x(t) = k$, $k \in (Z_{\min}, Z_{\max}), k \in \mathbb{R}$, AΣΔM supplies a switching signal whose frequency[1] is given by

$$f_{\mathrm{s}} = \frac{1}{T_{\mathrm{s}}} = \frac{1}{2\delta}\left(\frac{1}{Z_{\max} - k} - \frac{1}{Z_{\min} - k}\right)^{-1} \tag{4.7}$$

and whose duty cycle D is

$$D = \frac{k - Z_{\min}}{Z_{\max} - Z_{\min}} \tag{4.8}$$

Hence AΣΔM also inband-error-free tracks constant-reference signals. Note that, when tracking a constant-reference signal at a certain OSwR, both PWM and AΣΔM yield the same switching signal $z(t)$, which inband-error-free tracks the reference signal $x(t)$.

When the reference signal is not constant, the instantaneous pulses' width T_k is continuously adjusted so that, within each encoding interval $T^k_{\mathrm{A\Sigma\Delta M}}$ defined by two consecutive rising or falling switching events t_k of the switching signal $z(t)$ (i.e. either a positive-negative or a negative-positive pulse pair), the area of the switching signal $z(t)$ equals the area of the reference signal $x(t)$.

Indeed, if the comparator was triggered at $v(t_k) = -\delta$, the next switching event is triggered when the integrator's output signal reaches the upper threshold $v(t_{k+1}) = \delta$; the comparator is then triggered again when the integrator's output signal reaches the lower threshold again $v(t_{k+2}) = -\delta$. Hence, within the encoding interval $T^k_{\mathrm{A\Sigma\Delta M}} = t_{k+2} - t_k$, $\forall k \in \mathbb{Z}$, i.e. whichever two consecutive

[1] Units are not inconsistent in this expression; because of the normalisation, some parameters are not explicit in this expression [21].

pulses,

$$\int_{t_k}^{t_{k+2}} -e(u)\,\mathrm{d}u = \int_{t_k}^{t_{k+2}} \left(x(u) - z(u)\right)\,\mathrm{d}u = v(t_{k+2}) - v(t_k) = 0 \tag{4.9}$$

which leads to

$$\int_{t_k}^{t_{k+2}} x(u)\,\mathrm{d}u = \int_{t_k}^{t_{k+2}} z(u)\,\mathrm{d}u \tag{4.10}$$

equal areal of both signals within this encoding interval.

Area-equalling is therefore achieved regardless of the reference signal's waveform $x(t)$, even if underswitching (the reference signal is not bandlimited or its fastest non-zero component is faster than the switching frequency f_s), as long as it does not exceeds the modulator's dynamic range $Z_\mathrm{min} \leq x(t) \leq Z_\mathrm{max}$. Moreover, area-equalling is independent of the encoding interval; it is valid for both positive-negative and negative-positive pulse pairs.

Note that since there is no external carrier nor synchronisation signal, both the instantaneous duty cycle d_k and the encoding intervals' length $T^k_{\mathrm{A\Sigma\Delta M}}$ (instantaneous switching frequency) are continuously adjusted according to the reference signal $x(t)$. Furthermore, the encoding intervals are delimited by switching events t_k, instead of by an external signal like in PWM.

Unlike PWM, AΣΔM encodes using all the information conveyed by the reference signal $x(t)$, which is captured in the integrator's output signal $v(t)$. No approximation nor implicit sampling is performed in this encoding process. Therefore, AΣΔM is suitable to track non-constant reference signals, even if underswitching or operating at low OSwRs.

4.2.2 Switching Signal's Time Waveform Analysis

AΣΔM is an asynchronous modulator (astable oscillator) which continuously adapts the pulses' width according to the reference signal $x(t)$, as discussed above. If the reference signal $x(t)$ does not saturate the modulator (yet it sweeps all the available dynamic range), the pulses' width T_k is bounded by [21]

$$\frac{2\delta}{Z_\mathrm{max} - Z_\mathrm{min}} \leq T_k < +\infty \tag{4.11}$$

The lower and upperbounds are achieved for a constant-reference signal $x(t) = k$; $z(t) = Z_\mathrm{max}$ and $k = Z_\mathrm{max}$ (and also $z(t) = Z_\mathrm{min}$ and $k = Z_\mathrm{min}$) lead to the upperbound width (plus infinite i.e. AΣΔM stops switching, formally T_k is unbounded instead of bounded by plus infinite), whereas $z(t) = Z_\mathrm{max}$ and $k = Z_\mathrm{min}$ (and vice versa) lead to the lowerbound width (maximum instantaneous switching frequency). AΣΔM may stop switching because, whenever the value of the reference signal $x(t)$ is similar to the switching signal's $z(t)$ value, the error signal $e(t)$ is very small, causing the integrator's output signal $v(t)$ to remain almost constant.

According to (4.11), AΣΔM maps the reference signal's amplitude distribution (extending from Z_max to Z_min) to a time-domain pulse width distribution, which extends from $4\delta/Z_\mathrm{pp}$ to $+\infty$.

$$x(t) \in [Z_\mathrm{min}, Z_\mathrm{max}] \rightarrow T_k \in \left[\frac{4\delta}{Z_\mathrm{pp}}, +\infty\right) \tag{4.12}$$

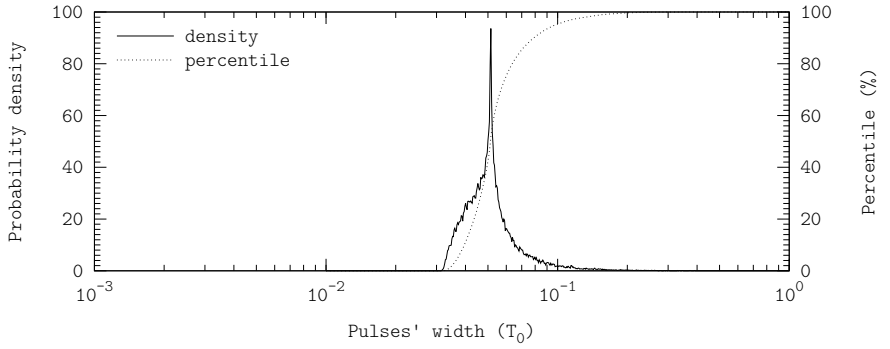

Figure 4.7: Histogram of pulses' width of AΣΔM tracking a f_0-bandlimited signal at an OSwR of 10. Simulation performed using the configuration D.4.5.

Note that the amplitude-time mappings of AΣΔM and PWM are complementary: in the former the mapped time is bounded from below and unbounded from above, whereas in the latter it is unbounded from below and bounded from above.

The actual distribution of pulses' width T_k depends upon the amplitude distribution of the reference signal $x(t)$, like in PWM. Nevertheless, when tracking bandlimited signals with an AΣΔM, provided that this kind of signals do not remain constant for a long time period, the pulses' width is effectively bounded from above as well (see figure 4.7).

4.2.3 Power Spectrum

According to the analytic expression [79], the power spectrum of an AΣΔM signal consists in a series of harmonic bands. Similarly to PWM, the zeroth-order harmonic band (baseband) equals the reference signal $x(t)$ without distortion; the subsequent bands (higher-order bands) contain spectral components around a central frequency, although they extend to all frequencies.

However, unlike in PWM, the addition of all higher-order bands does not necessarily result in a main harmonic in AΣΔM. For instance, when tracking non-periodic signals, the power spectrum spreads yielding a distribution with no harmonics (see figure 4.8). The harmonic bands are visible in simpler signals such as single tones, as illustrated in figure 4.9.

The inband content of the error signal is significant in AΣΔM. It logarithmically increases from very low values at DC, up to a maximum value around the average switching frequency. Under the operating conditions of figure 4.8 (tracking a f_0-bandlimited signal at an OSwR of 10), the inband content of the error signal $E(f)$ logarithmically grows up to 40 dB below the reference signal's level; in this case, the ratio of the error signal's inband power $P^{\mathrm{i}}_{e(t)}$ to the reference signal's power $P_{x(t)}$ is approximately -46 dB.

4.2.4 Encoding Limitations

AΣΔM encodes according to the area-equalling criterion which, as described in section 3.4.1, leads to inband-error-free encoding if the reference signal $x(t)$

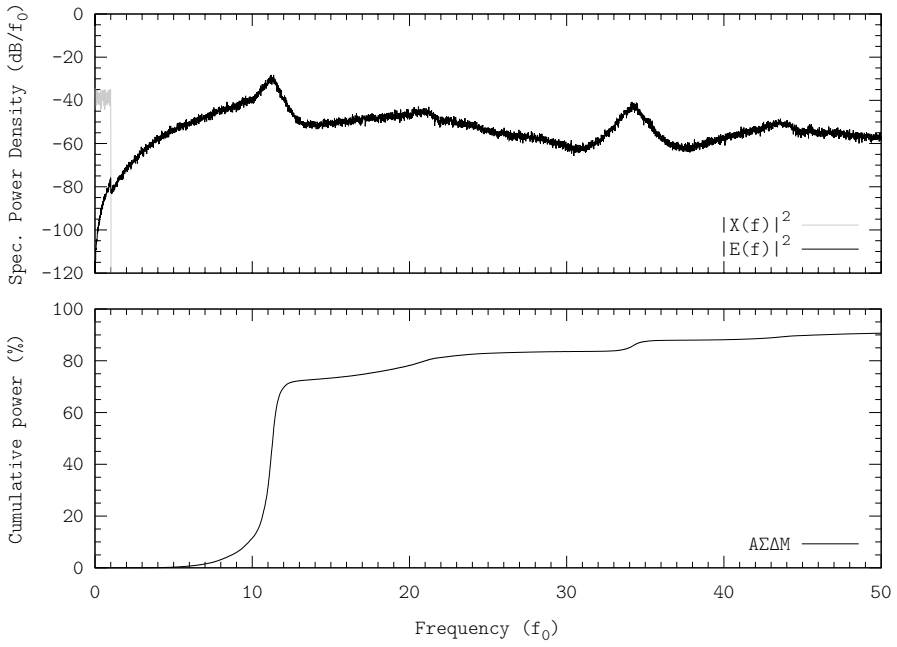

Figure 4.8: Power spectrum of AΣΔM tracking a f_0-bandlimited signal at an OSwR of 10. Simulation performed using the configuration D.4.1.

is constant. If the reference signal is not constant, this criterion results in a certain inband error depending on the the encoding intervals' length (i.e. the instantaneous switching frequency): the narrower the encoding intervals, the better the tracking fidelity.

When tracking non-constant reference signals, AΣΔM adjusts the encoding intervals' length according to the area-equalling criterion; more precisely, the length of every single pulse is adjusted so that the integrated error within that pulse is $\pm 2\delta$. This is illustrated in figure 4.6: the integrator's output signal either increases from $-\delta$ to δ ($\Delta v = 2\delta$) or decreases from δ to $-\delta$ ($\Delta v = -2\delta$) within each pulse. Formally, the time interval comprised between the time edges t_k and t_{k+1} fulfils

$$\int_{t_k}^{t_{k+1}} v(u)\,\mathrm{d}u = \pm 2\delta \tag{4.13}$$

where the sign depends upon the pulse's polarity, either negative or positive.

If the rate of change of the integrator output's signal $v(t)$ is small, sweeping 2δ results in a wide pulse (low switching frequency), whereas if the rate of change is high, sweeping 2δ results in a narrow pulse (high switching frequency). Given a certain hysteresis width δ, the length of each encoding interval is therefore determined by the rate of change (i.e. the derivative) of the integrator output signal, the error signal $e(t)$; provided that $e(t) = z(t) - x(t)$, the length of each encoding interval (i.e. the instantaneous switching frequency) is finally determined by the instantaneous value of the reference signal $x(t)$.

Let us consider a simple example, an AΣΔM with hysteresis width δ tracking a constant-reference signal $x(t) = k$. According to expressions (4.7) and (4.8),

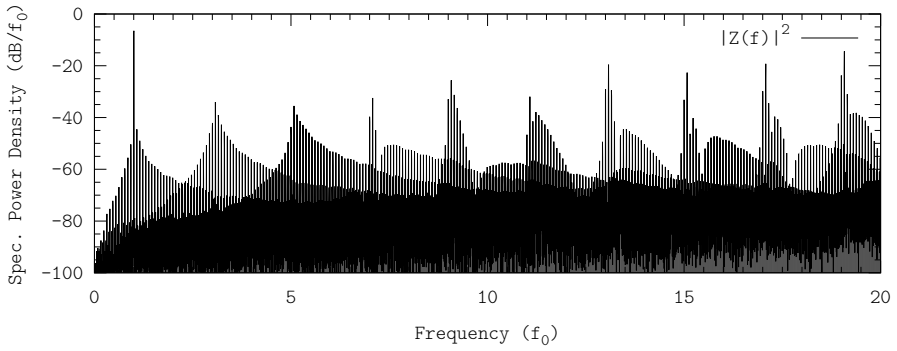

Figure 4.9: Power spectrum of an AΣΔM switching signal tracking a single-tone sinusoid of frequency f_0; the harmonic bands can be identified. Simulation performed using the configuration D.4.1.

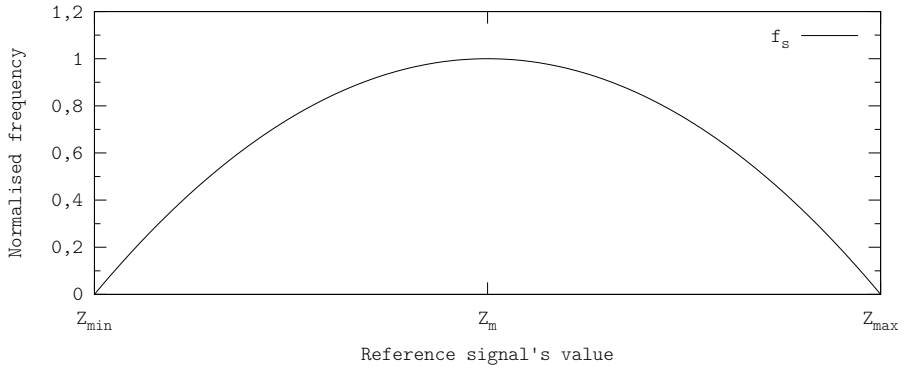

Figure 4.10: Switching frequency dependency in AΣΔM when tracking a constant-reference signal $x(t) = k$, $k \in (Z_{\min}, Z_{\max})$.

if $k = Z_{\mathrm{m}}$ the switching frequency is maximum and the duty cycle is 50 %. As k either increases or decreases, so does the duty cycle; however, since the minimum pulse width is bounded in AΣΔM, high and low duty cycles are achieved by reducing the switching frequency. As a result, the switching frequency depends upon the reference signal's value k (see figure 4.10).

When tracking a non-constant reference signal, this dependency constrains the tracking fidelity. Whenever the reference signal approaches to the switching signal's value $x(t_0) \approx z(t_0)$, the switching frequency reduces and hence the tracking fidelity degrades. Figure 4.11 illustrates this effect on an AΣΔM tracking a non-constant reference signal at an (average) OSwR of 20, The length of the widest pulse is 0,19; together with an adjacent pulse (either the previous or the subsequent, the difference is not significant) the encoding interval is approximately 0,20, yielding an instantaneous OSwR of 5,1, quarter of the average OSwR. This issue is known and has been partially characterised in the literature, when tracking single tones [80].

The local reduction of the switching frequency can be an issue in the decoding process. Actual decoders are LTI (invariant response); decoding switching

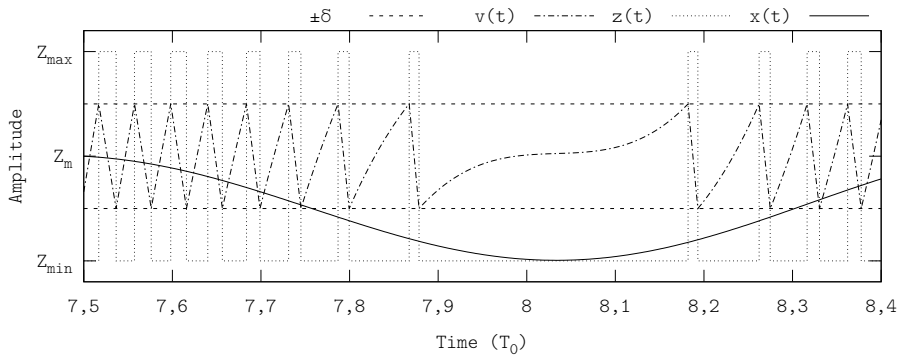

Figure 4.11: AΣΔM tracking a non-constant reference signal at an OSwR of 20. The integrator's output signal $v(t)$ and the hysteresis width δ have been scaled for better readability.

signals whose instantaneous switching frequency widely varies may result in locally high remaining error signals $\xi(t)$, especially if the switching frequency is not bounded from below (the instantaneous switching frequency could locally be lower than the filter's cutoff frequency).

AΣΔM can be upgraded so that the encoding intervals' length is independent of the reference signal's instantaneous value, thereby simplifying the decoding process with LTI low-pass filters.

4.3 Adaptive Asynchronous ΣΔ Modulation

The dependency of the encoding intervals' length upon the reference signal's instantaneous value can be removed by adding the proper reference signal feedforward to the comparator's hysteresis width (Adaptive Asynchronous ΣΔ Modulator—AAΣΔM). The required feedforward law to achieve this behaviour can be derived by inverting the expression (4.7), yielding[2]

$$\delta(t) = \frac{1}{2\alpha} \frac{1}{\dfrac{1}{Z_{\max} - x(t)} - \dfrac{1}{Z_{\min} - x(t)}} \tag{4.14}$$

where α is a free parameter to set the average switching frequency; the comparator's thresholds are symmetrical $\pm\delta(t)$.

This hysteresis law achieves the desired behaviour by reducing the hysteresis width according to the reference signal; for instance, when tracking a constant-reference signal $x(t) = k$, with $k \in (Z_{\min}, Z_{\max})$, the switching frequency

$$f_{\mathrm{s}} = \alpha \neq f\left(x(t)\right) \tag{4.15}$$

Figure 4.12 shows a block diagram of AAΣΔM and the representative time waveforms when tracking a f_0-bandlimited signal. As this figure illustrates, the hysteresis width $\delta(t)$ is continuously adjusted according to the reference signal $x(t)$.

[2]Strictly, the hysteresis-width function depends upon the reference signal $\delta\left(x(t)\right)$, although, for the sake of notation simplicity, it is denoted as a time-dependent function $\delta(x(t)) \to \delta(t)$.

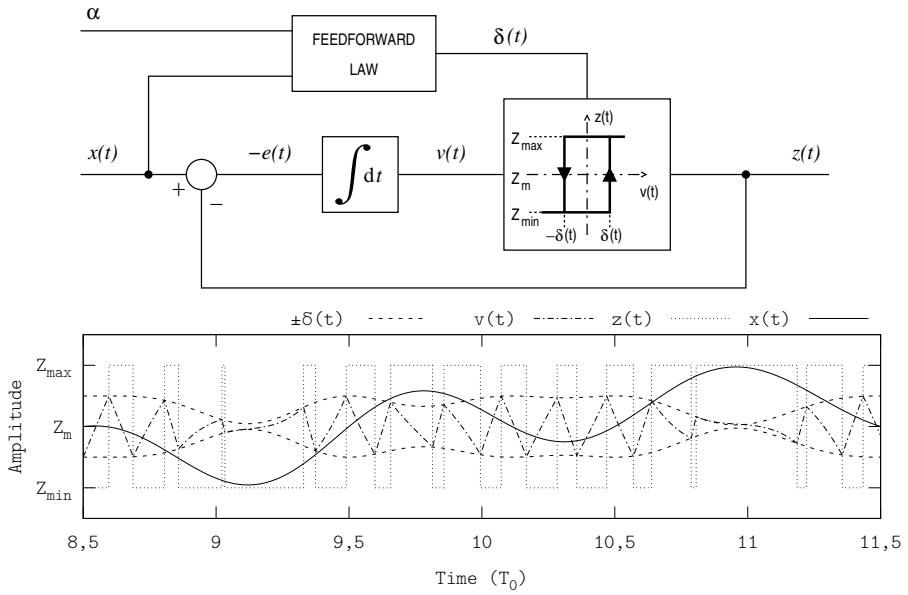

Figure 4.12: Adaptive Asynchronous ΣΔ Modulator and representative time waveforms when tracking a f_0-bandlimited reference signal. The integrator output signal $v(t)$ and the hysteresis-width function $\delta(t)$ have been scaled for better readability.

Unlike AΣΔM, AAΣΔM does not encode according to the area-equalling criterion. Certainly, the hysteresis-width function $\delta(t)$ continuously varies; since this function determines the amount of integrated error within each pulse, in general, two consecutive pulses may involve different integrated error. Let t_k be the time instant of a switching event and let t_{k+1} and t_{k+2} be the time instants of the two subsequent switching events; provided that

$$\delta(t_{k+1}) - \delta(t_k) \neq \delta(t_{k+2}) - \delta(t_{k+1}) \tag{4.16}$$

the integrated error within each pulse is different. Consequently $\Delta v = v(t_{k+2}) - v(t_k) \neq 0$ and hence

$$\int_{t_k}^{t_{k+2}} x(u)\,\mathrm{d}u \neq \int_{t_k}^{t_{k+2}} z(u)\,\mathrm{d}u \tag{4.17}$$

Regardless, the errors in the different encoding intervals compensate, so that switching signal $z(t)$ still tracks the reference signal $x(t)$. Note that if the reference signal is constant $x(t) = k$ with $k \in (Z_{\min}, Z_{\max})$, the hysteresis-width function remains constant as well $\delta(t) = \delta_k$, $\forall t \in \mathbb{R}$. In this case, AAΣΔM encodes according to equalling-area criterion, thus resulting in inband-error-free encoding.

4.3.1 Conditions for Astable Operation

Like AΣΔM, AAΣΔM operates as an astable oscillator for all reference signals not saturating the modulator $Z_{\min} < x(t) < Z_{\max}$, i.e. the integrator's output signal $v(t)$ fulfils $|v(t)| \leq \delta(t)$, $\forall t \in \mathbb{R}$.

The hysteresis-width function $\delta(t)$ is positive and bounded for all values of $x(t)$ not saturating the modulator

$$Z_{\min} < x(t) < Z_{\max} \rightarrow 0 < \delta(t) \leq \frac{Z_{\text{pp}}}{2\alpha}, \quad \forall t \in \mathbb{R} \tag{4.18}$$

The upperbound is achieved by $x(t) = Z_{\text{m}}$, which fulfils $Z_{\max} - x(t) = x(t) - Z_{\min} = Z_{\text{pp}}/2$ and the lowerbound is achieved if $x(t) = Z_{\max}$ or $x(t) = Z_{\min}$.

Despite the feedforward law, the integrator's output signal $v(t)$ monotonically increases (decreases) until it reaches the value $\delta(t)$ ($-\delta(t)$ if decreasing) whenever the switching signal $z(t)$ is $Z_{\min}$ ($Z_{\max}$). Therefore, the modulator operates as an astable oscillator and the strictly increasing sequence (t_k), $k \in \mathbb{Z}$ defined by the recursive equation

$$\int_{t_k}^{t_{k+1}} x(u)\,\mathrm{d}u = (-1)^k \left(\delta(t_{k+1}) + \delta(t_k)\right) + z[k]\,(t_{k+1} - t_k) \tag{4.19}$$

where $z[k] = Z_{\min}$ if k is odd and $z[k] = Z_{\max}$ if k is even, uniquely describes the switching signal $z(t)$, $\forall t \in \mathbb{R}$.

If the reference signal $x(t)$ becomes either $Z_{\max}$ or $Z_{\min}$, the hysteresis-width function $\delta(t)$ and the derivative of the integrator's output signal, the error signal $e(t)$, become zero; regardless, if evaluating the limit for $x(t) \rightarrow Z_{\min}, Z_{\max}$, the pulses' width T_k fulfils $0 \leq T_k \leq 1/\alpha$. Therefore, the amplitude-time mapping performed by AAΣΔM is similar to that of PWM

$$x(t) \in [Z_{\min}, Z_{\max}] \rightarrow T_k \in \left[0, \frac{4}{\alpha}\right] \tag{4.20}$$

Considering eventual implementations, zero-width hysteresis may result in unexpected or unpredictable behaviour. In order to make feasible implementing this modulator, the hysteresis width should be limited to a very small value $\delta_{\min} > 0$, $\delta_{\min} \in \mathbb{R}^+$ so that the AAΣΔM locally behaves as an AΣΔM operating at very high frequency. In such a case, provided that the actual distribution depends upon the reference signal's amplitude distribution, both the maximum and the minimum pulses' width are bounded and the bounds can be set by design parameters.

4.3.2 Switching Signal's Time Waveform Analysis

The main motivation for the adaptive-hysteresis approach is to provide a switching signal $z(t)$ whose dynamics better adapts to the natural dynamics of the LTI low-pass filter, i.e. to simplify the decoding process especially when the reference signal locally approaches to the switching signal's actual value (the issue illustrated in figure 4.11).

As figure 4.13 shows, AAΣΔM overcomes this issue by generating narrow pulses instead of widening the encoding interval (the time interval comprised between three consecutive switching events). The instantaneous switching frequency remains more constant than in AΣΔM.

Figure 4.14 shows the histogram of pulses' width T_k in AAΣΔM tracking a f_0-bandlimited reference signal at an OSwR of 10. The pulses' width is bounded from above by $10^{-1}T_0$ and not bounded from below, similarly to PWM, although

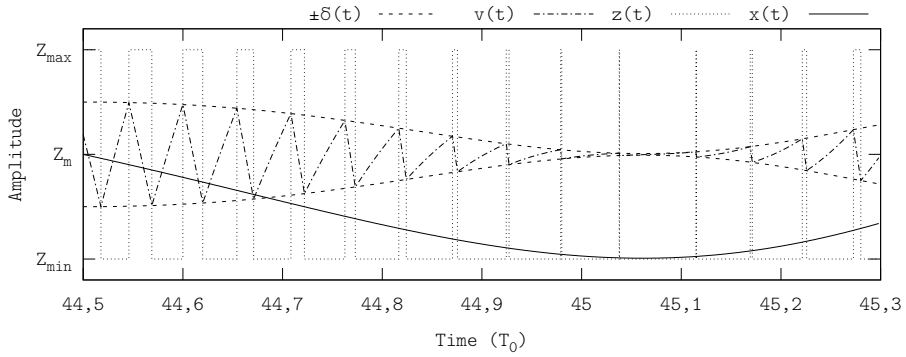

Figure 4.13: AAΣΔM tracking a non-constant reference signal at an OSwR of 20. The integrator's output signal $v(t)$ and the hysteresis-width function $\delta(t)$ have been scaled for better readability.

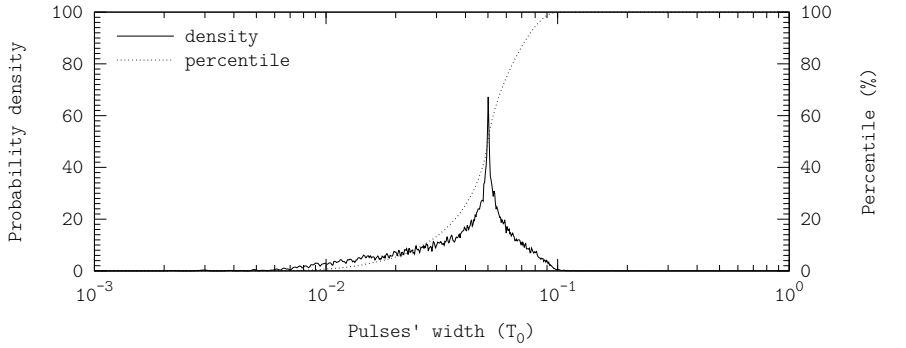

Figure 4.14: Histogram of pulses' width of AAΣΔM tracking a f_0-bandlimited signal at an OSwR of 10. Simulation performed using the configuration D.4.5.

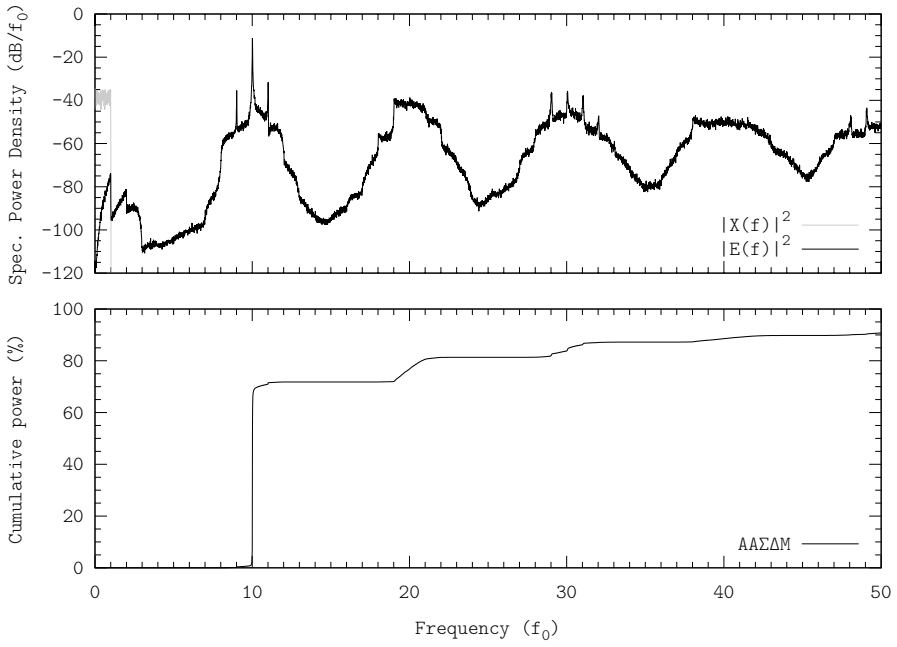

Figure 4.15: Power spectrum of AAΣΔM tracking a f_0-bandlimited signal at an OSwR of 10 and cumulative-power frequency distribution. Simulation performed using the configuration D.4.1.

the pulses' width is more variable than in PWM (note the lower peak of probability density around 2/OSwR, half the average switching period).

Despite the adaptive hysteresis, AAΣΔM is still an asynchronous modulator; there is no external carrier nor synchronisation signal and hence an AAΣΔM is an astable oscillator itself as well (the encoding intervals' length and the duty cycle are adjusted according to a different criterion than in regular AΣΔMs).

4.3.3 Power Spectrum

The power spectrum of AAΣΔM has not been analytically derived, but it can be characterised. This characterisation has been carried out tracking a f_0-bandlimited signal, to compare the AAΣΔM power spectrum with that of AΣΔM and PWM.

Despite the adaptive hysteresis, AAΣΔM's inband performance is similar to AΣΔM's. It is determined by the integrator: the error signal's inband content $E(f)$ logarithmically grows up to 40 dB below the reference signal's level, when operating at an OSwR of 10 (see figure 4.15). However, the outband spectral content is more similar to PWM: it comprises a main harmonic (yet its amplitude is lower than that of PWM) and the power accumulates in bands around frequencies multiples of the switching frequency $f = k\text{OSwR}f_0$, with $k \in \mathbb{N}$.

The full characterisation reveals that, as the OSwR decreases, the power spectrum is shaped to an AΣΔM-like spectrum (see the example in figure 4.16).

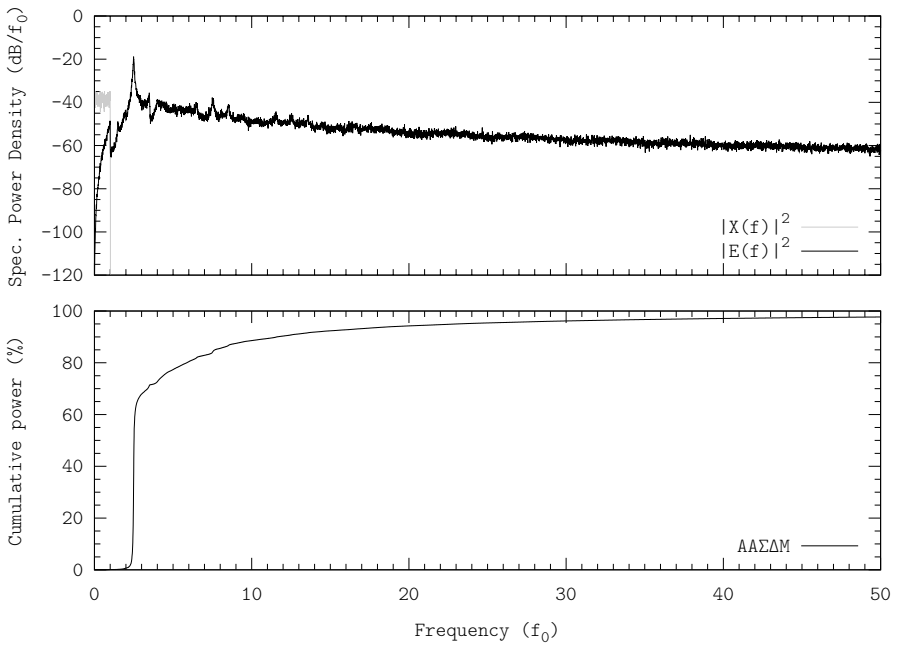

Figure 4.16: Power spectrum of AAΣΔM tracking a f_0-bandlimited signal at an OSwR of 2,5 and cumulative-power frequency distribution. Simulation performed using the configuration D.4.1.

4.4 Other Modulations

Modulations such as click or minimum time require a significant amount of signal processing. It is not feasible to real-time implement them with analogue circuitry. Instead, they are digitally implemented, e.g. with DSPs or Field Programmable Gate Arrays (FPGAs), therefore computing the switching time instants t_k of the switching signal $z(t)$ instead of directly generating the switching signal $z(t)$.

Using state-of-the-art technology, it is not feasible to implement real-time modulators performing these modulations targeting signal tracking and operating at the required switching frequencies, especially for broadband communications. Because of this reason, these modulations are not analysed in this work.

4.5 Modulations Performance

The performance of triangle PWM, AΣΔM and AAΣΔM tracking a f_0-bandlimited reference signal have been characterised and compared. In the description of these modulations, high OSwRs ratios have been used to emphasise the differences between them. However, consistently with the scope of this work of extending the relative bandwidth of switching amplifiers, the compare characterisation has been carried out at OSwRs below 10.

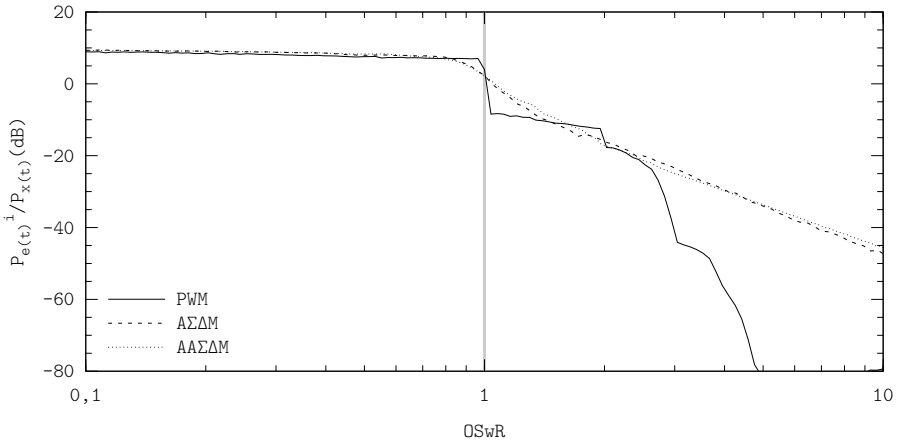

Figure 4.17: Inband error power of two-level switching modulations. Displayed waveforms are normalised to the reference signal's power $P_{x(t)}$. Simulation performed using the configuration D.4.4 (values below $-80\,\mathrm{dB}$ are not shown because they are masked by simulation errors).

4.5.1 Analysis Under the Fundamental Limit Perspective

The fundamental bound derived in chapter 3 provides a comparison framework to characterise the inband performance and the deviation from such limit in common modulations. According to this fundamental bandwidth limit, it is possible to inband-error-free track a f_0-bandlimited signal at OSwRs upwards of 1. However, the inband performance characterisation of these modulations reveals that none of them achieve the ideal performance (see figure 4.17).

At high OSwRs (upwards of 10, conventional operating conditions), area-equalling encoding approximates inband-error-free encoding with small error. Provided that these three modulations inband-error-free encode a constant-reference signal, the inband error signal's power $P^{\mathrm{i}}_{e(t)}$ tends to zero as the OSwR tends to infinite (consistently with the discussion in section 3.4).

Note that, when tracking bandlimited signals at a finite OSwR, area-equalling encoding is not the best approximation to inband-error-free encoding. Certainly, the approximation performed by PWM is better than AΣΔM (which encodes according to the area-equalling criterion), especially at OSwRs upwards of 3.

As the OSwR decreases, the difference between the approximation (area-equalling encoding) and inband-error-free encoding becomes significant. The performance characterisation of AΣΔM illustrates this difference, as AΣΔM performs area-equalling encoding regardless of the OSwR. It is consistent with the single-tone characterisation shown in figure 3.12. Despite AAΣΔM does not perform area-equalling encoding, the error compensation in different encoding intervals leads to a similar inband performance than that of AΣΔM (area-equalling encoding).

Performance Comparison

According to figure 4.17, when tracking bandlimited non-periodic signals, the error signal's inband power $P^{\mathrm{i}}_{e(t)}$ of PWM is lower than that of AΣΔM and

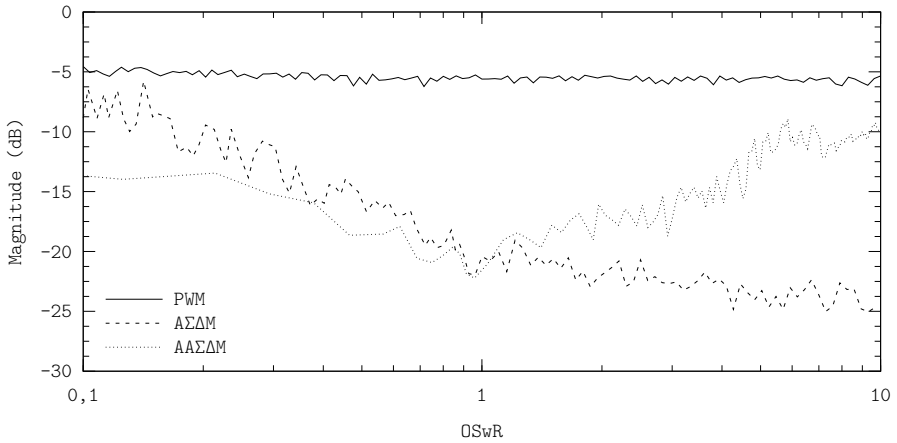

Figure 4.18: Upperbound of the spectral power density of the error signal in two-level switching modulations. Simulation performed using the configuration D.4.4.

AAΣΔM. Regardless, no conclusions can be directly drawn from this characterisation, since it only concerns inband. In actual applications both inband and outband contents are significant and there may be non-idealities and external factors which also affect the final performance. For instance, AΣΔM-based amplifiers can be very robust against non-idealities and interferences; furthermore, when considering and optimising the output filter, the performance of AAΣΔM-based amplifiers is better than that of AΣΔM-based ones, whose performance is already better than that of PWM-based ones (this is discussed in chapter 7).

Still, by comparing the power spectra and the time waveforms of these different modulations, some differences arise. PWM has the best inband behaviour, at almost any OSwR. This feature is achieved at the cost of generating very narrow pulses (see figure 4.4), although the probability of generating pulses narrower than one tenth of the average switching period is very small. Indeed, the time histograms of figures 4.4, 4.7 and 4.14 reveal that, despite the complementary bounds of the amplitude-time mappings, the width of 99 % of pulses of these three modulations belongs to the range $[10^{-2}T_0, 10^{-1}T_0]$ (OSwR of 10).

These differences become more significant in the frequency domain, especially when comparing the outband power spectra. Provided that the power spectrum of AΣΔM has no main harmonic, the upperbound of the AΣΔM spectral power density is lower than that of PWM; specifically, in the examples tracking a f_0-bandlimted signal at an OSwR of 10, the difference is approximately 23 dB.

This different behaviour of PWM and AΣΔM also applies to lower OSwRs, as figure 4.18 shows. On the other hand, the behaviour of AAΣΔM is similar to AΣΔM at low OSwRs (no main harmonic) but, as the OSwR increases, its behaviour tends to PWM (a peak at the average switching frequency emerges).

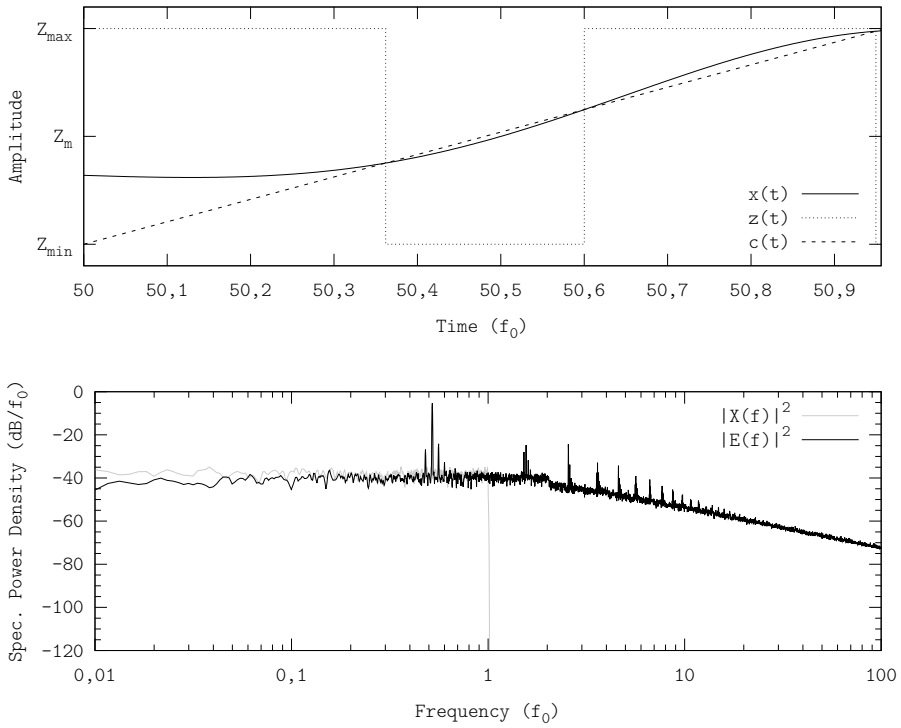

Figure 4.19: Extra switching in PWM. Example showing a triangle PWM tracking a f_0-bandlimited signal (the carrier frequency is $0{,}52f_0$). Displayed waveforms show an encoding interval in which the reference signal $x(t)$ crosses the carrier $c(t)$ trice, in the time domain, and the power spectra of the reference signal $X(f)$ and the error signal $E(f)$ in the frequency domain. Simulation performed using the configuration D.4.1.

4.5.2 Underswitching and Minimum OSwR

In the context of linear-assisted power amplifiers, the reference signals may not be bandlimited or the switching amplifier may operate at a switching frequency lower than the reference signal's bandwidth (OSwRs below 1, underswitching). Targeting this kind of applications, the inband performance of these three modulations has also been characterised at OSwRs below 1. As discussed in section 3.3.1, when underswitching, the modulation should track the reference signal $X(f)$ up to the operating switching frequency $f_\mathrm{s} = \mathrm{OSwR} f_0$ with small error (i.e. low content of the error signal $e(t)$ up to f_s), so that the reference signal can be partially recovered (specifically, its lowest spectral content).

Pulse Width Modulation

As the OSwR decreases, so does the magnitude of the slope of the carrier; if the OSwR is small enough, the reference signal $x(t)$ may cross the carrier more than once within a single encoding interval. The frequency f_s of the resulting switching signal $z(t)$ would be higher than the carrier's frequency f_c (extra switching, see figure 4.19).

Extra switching is generally undesirable, as it degrades the inband tracking fidelity even at frequencies much lower than the average switching frequency (constant inband error content, see figure 4.19). Not even a f_s-bandlimited approximation to reference signal $x(t)$ can be recovered from the switching signal $z(t)$.

This issue is usually addressed with a latch, which locks the comparator once it has been triggered; the latch is reset at the beginning of each encoding interval. Whilst in regular operation the latch does not affect the PWM encoding process, it prevents extra switching, although at the cost of further degrading the encoding quality. Nevertheless, latches are usually included to avoid multiple triggering due to noise and EMI, which would both degrade the tracking fidelity and increase switching losses.

When tracking bandlimited reference signals, extra switching may occur if the slope of the reference signal is higher than the slope of the carrier frequency. In non-periodic reference signals, the slew rate continuously varies; consequently, extra switching may eventually occur without significantly degrading the PWM encoding performance (averaging the performance over a long time interval Δt). Regardless, the analysis of extra switching upon single tones provides a good approximation to estimate when extra switching may start being significant in bandlimited signal tracking.

Let the reference signal be a single tone of frequency f_0 and amplitude $cZ_{\mathrm{pp}}/2$ and arbitrary phase φ

$$x(t) = Z_{\mathrm{m}} + c\frac{Z_{\mathrm{pp}}}{2}\sin\left(2\pi f_0 + \varphi\right) \tag{4.21}$$

The maximum slew rate of this signal is

$$\dot{x}(t)_{\max} = Z_{\mathrm{pp}} c\pi f_0 \tag{4.22}$$

Similarly, the maximum slew rate of a sawtooth carrier $c(t)$, whose frequency is $f_{\mathrm{c}} = \mathrm{OSwR} f_0$, is

$$\dot{c}(t)_{\max} = \frac{Z_{\mathrm{pp}}}{T_{\mathrm{c}}} = Z_{\mathrm{pp}}\mathrm{OSwR} f_0 \tag{4.23}$$

The switching signal $z(t)$ is free of extra switching if

$$\dot{c}(t)_{\max} > \dot{x}(t)_{\max} \tag{4.24}$$

which, by applying (4.21) and (4.23), leads to the condition

$$\mathrm{OSwR}_{\mathrm{saw}} > \pi c \approx 3c \tag{4.25}$$

In triangle carriers, the slew rate is twice the sawtooth's, yielding

$$\mathrm{OSwR}_{\mathrm{tri}} > \frac{\pi}{2} c \approx 1{,}6c \tag{4.26}$$

Therefore, in triangle PWM tracking a f_0-bandlimited signal sweeping all dynamic range ($c = 1$), extra switching may occur when operating at OSwRs below 1,6. This value sets a threshold from which the performance of PWM quickly degrades. However, in triangle PWM, this threshold is low enough so that the inband error due to extra switching is masked by the PWM inband error itself (error due to improper encoding, see figure 4.17). Figure 4.17 has been simulated with a PWM including a latch.

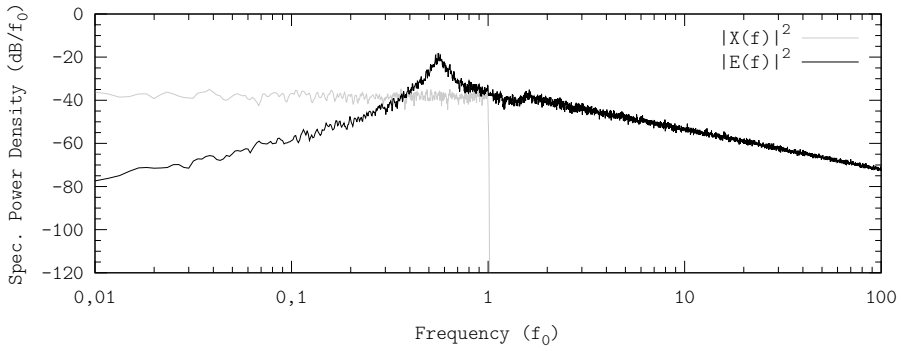

Figure 4.20: Underswitching in AΣΔM. Example showing the power spectrum of an AΣΔM tracking a f_0-bandlimited signal at an OSwR of 0,55. Simulation performed using the configuration D.4.1.

Asynchronous ΣΔ Modulations

Neither AΣΔM nor AAΣΔM suffer from extra switching or minimum OSwRs. For instance, when tracking a f_0-bandlimited signal with an AΣΔM operating at an OSwR of 0,55, the inband content of the error signal $E(f)$ still logarithmically increases up to the switching frequency (see figure 4.20). AΣΔM tracks the lowest frequency spectral content of the reference signal $X(f)$ regardless of the OSwR. By low-pass filtering the switching signal $z(t)$, a f_s-bandlimited approximation of the reference signal can be recovered.

This performance is not visible in the characterisation included in figure 4.17 because in the evaluation of the error signal's inband power $P^{\mathrm{i}}_{e(t}$ the content between $f_s = \mathrm{OSwR} f_0$ and f_0 masks the rest of the inband content. Once the main harmonic is shifted inband, the inband power of the error signal $P^{\mathrm{i}}_{e(t)}$ is almost independent of the reference signal and the tracking fidelity (see the cumulative-power frequency distribution included in figures 4.5, 4.8 and 4.15). Note that the error signal $E(f)$ conveys no information, it only shapes the reference signal $X(f)$ into the two-level switching signal $Z(t)$.

4.5.3 Outband Power in Two-Level Switching Signals

If the modulations track the reference signal $x(t)$ with small inband error, the error signal's outband power $P^{\mathrm{o}}_{\mathrm{e(t}}$ is independent of the modulation. Certainly, let $z_1(t)$ and $z_2(t)$ be two two-level switching signals, both tracking a certain f_0-bandlimited reference signal $x(t)$ with small inband error (for instance, $z_1(t)$ could be generated with a triangle PWM and $z_2(t)$ with an AΣΔM).

$$E_1(f), E_2(f) \ll X(f), \quad |f| \leq f_0 \tag{4.27}$$

Given that $Z(f) = X(f) + E(f)$, the inband content of both switching signals is approximately the reference signal's. Hence

$$Z_1(f) \approx Z_2(f), \quad |f| \leq f_0 \tag{4.28}$$

leading to

$$P^{\mathrm{i}}_{z_1(t)} \approx P^{\mathrm{i}}_{z_2(t)} \tag{4.29}$$

equal inband power of both switching signals.

A consequence of (4.27) is that both modulations track the DC component of the reference signal $x(t)$, i.e. its a_0 coefficient.

$$\lim_{m\to+\infty} \frac{2}{mNT_0} \int_0^{mNT_0} z_1(u)\,\mathrm{d}u \approx a_0 \tag{4.30}$$

$$\lim_{m\to+\infty} \frac{2}{mNT_0} \int_0^{mNT_0} z_2(u)\,\mathrm{d}u \approx a_0 \tag{4.31}$$

Provided that the area of both switching signals is the same and that there are only two possible values, $Z_{\min}$ and $Z_{\max}$, it follows that the power of both switching signals is the same.

$$P_{z_1(t)} \approx P_{z_2(t)} \tag{4.32}$$

Since the inband power of both switching signals is the same (4.29), the outband power of both switching signals must be the same as well.

$$P^{\mathrm{o}}_{z_1(t)} \approx P^{\mathrm{o}}_{z_2(t)} \tag{4.33}$$

The outband power in two-level time encoding is independent of the modulation and the OSwR, as long as (4.27) holds; it cannot be reduced by improving or changing the two-level time-encoding process (i.e. the two-level switching modulation). By using alternative modulations (operating at the same OSwR), the outband power can only be reshaped (e.g. to a wider and/or higher frequency range). Unfortunately, as figures 4.5, 4.8 and 4.15 show, even in asynchronous modulations more than 70 % of switching signal's power concentrates around the switching frequency, hence the performance of two-level switching amplifiers in terms of remaining error signal's power $P_{\xi(t)}$ cannot be significantly improved by only using alternative modulations.

Chapter 5

Extension to Multi-Level Modulations

This chapter extends PWM, AΣΔM and AAΣΔM to multi-level modulations, targeting to reduce the remaining error signal's power by reducing the outband power of the switching signal, in the context of multi-level switching amplifiers. This chapter also identifies the new blocks and subsystems due to multi-level operation in switching amplifiers, thereby providing an extended model of multi-level switching power amplifiers.

5.1 Motivation for Multi-Level Amplifiers

As discussed in chapter 4, when encoding the information conveyed by a bandlimited signal $x(t)$ into a two-level switching signal $z(t)$, the power of the switching signal $P_{z(t)}$ is independent of the modulation, as long as the reference signal's DC component is properly tracked. Furthermore, if the whole reference signal is properly tracked $P^{\mathrm{i}}_{e(t)} \ll P_{x(t)}$, the switching signal's outband power $P^{\mathrm{o}}_{z(t)}$ is independent of the two-level modulation as well. In conventional designs, the outband content of the switching signal is usually responsible of more than 60 % of the remaining error signal's power (even more if the filter's inband effects are not considered error, as in audio applications).

The switching signal's outband power $P^{\mathrm{o}}_{z(t)}$, and hence the remaining error signal's power $P_{\xi(t)}$, can be reduced by simply increasing the OSwR, but at the cost of increasing the switching losses as well. In order to reduce the switching signal's outband power $P^{\mathrm{o}}_{z(t)}$ without increasing the OSwR, which is the main issue addressed in this thesis, alternative topologies and structures of switching amplifiers must be used.

The switching signal's outband power $P^{\mathrm{o}}_{z(t)}$ is related to the amount of power required to shape the continuous-time continuous-amplitude reference signal $x(t)$ into the continuous-time two-level switching signal $z(t)$, i.e. the power required to fill the reference signal $x(t)$ up to the discrete values $Z_{\min}$ and $Z_{\max}$. The amplitude of the reference signal $x(t)$ continuously varies (time-dependent function); whenever it approaches to a discrete value, $Z_{\min}$ or $Z_{\max}$, shaping the reference signal $x(t)$ to that value may require low power, although shaping it to the other value may require high power.

If more discrete values (or output voltage[1] levels L_i, $i = 0, \ldots, N-1$, $i \in \mathbb{N}$ if N levels are used) are available, the reference signal $x(t)$ may be closer to two discrete values than in two-level time encoding, thus lower outband power may be required to shape the reference signal $x(t)$ into the multi-level switching signal $z(t)$ (multi-level encoding).

Multi-level modulations, pursuing multi-level switching amplifiers, are hence candidates of interest to extend the relative bandwidth of switching amplifiers, i.e. to reduce the power of the remaining error signal $\xi(t)$ without increasing the OSwR or, conversely, reduce the OSwR required to achieve a certain tracking error. Compared to two-level switching amplifiers, multi-level switching amplifiers require a multi-level modulator and a multi-level switching power converter, besides some additional circuitry to generate and/or properly handle the additional levels.

In what follows, multi-level (or N-level, if the number of levels is to be explicit) stands for more than two levels $N \geq 3$, $N \in \mathbb{N}$.

5.1.1 Extended Modelling of Switching Amplifiers

State-of-the-art switching amplifiers for audio applications already use a 3-level power stage (the so-called 3-level audio amplifier, as described in section 1.5.1), although these amplifiers are still designed using conventional design criteria. Certainly, consider a state-of-the-art 3-level switching amplifier for audio applications. It is designed and driven as two independent 2-level buck-based switching regulators operating at OSwR upwards of 10 and supplying a floating load R_L (each regulator or 2-level amplifier with its own drivers, 2-level PWM and control circuit, as the example depicted in figure 1.24). Whilst the power switching signal $\tilde{z}(t)$ is indeed a 3-level signal, it is generated like 2-level switching signals thus some capabilities of multi-level power amplification might be missed. As the present chapter is going to show, the generalisation to multiple levels unfolds additional subsystems of switching amplifiers which are not visible in two-level amplifiers; in order to take full advantage of a multi-level switching power amplifier, the whole device should be designed as a multi-level amplifier, considering all the specificness and characteristics of multi-level amplification.

A multi-level switching amplifier operating with N levels (N-level switching amplifier) comprises an N-level modulation, a decoding logic and an N-level power converter (see figure 5.1). The multi-level modulation encodes the information conveyed by the reference signal $x(t)$ into an N-level switching signal $z(t)$. By processing the magnitude of the multi-level switching signal $z(t)$, the decoding logic generates a set of m switch-driving signals $s_i(t)$, one for each power switch of the switching converter, suitable to drive the multi-level power converter. Driven by these signals, the converter generates an N-level power switching signal $\tilde{z}(t)$, ideally a power-amplified version of the multi-level switching signal $z(t)$. The power switching signal is is finally filtered by the low-pass filter thus recovering $\tilde{x}(t)$, a power-amplified approximation to the reference signal $x(t)$.

Note that a multi-level power converter can generate a multi-level switching signal $\tilde{z}(t)$ by combining several supply voltages (coming from a power-

[1] The magnitude of the switching signal $z(t)$ and/or the power switching signal $\tilde{z}(t)$ can either be a voltage or a current. All this chapter is referred to voltage signals because they are more common, but all the analysis is valid for current signals as well.

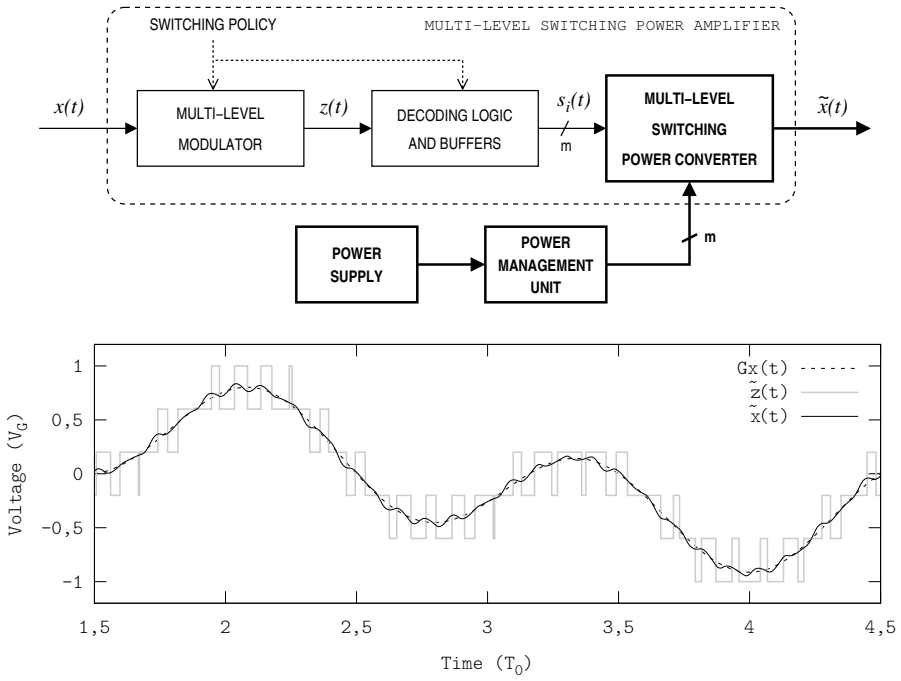

Figure 5.1: Extended modelling of multi-level switching amplifiers and time waveforms example (6-level example). In the block diagram, the power path is highlighted in bold.

management unit), by generating additional voltages (e.g. with charge pumps or flying capacitors) or by both. In either case, switching between levels (i.e. converter states) may be constrained by a switching policy, e.g. switching between two specific levels may not be allowed.

5.1.2 Decoding Logic

Multi-level switching amplifiers, compared to 2-level switching amplifiers, require an additional element, the decoding logic. This logic translates the magnitude of the multi-level switching signal $z(t)$, typically an analogue voltage level which determines the converter state at any time instant, into a set of m binary control signals $s_i(t)$ suitable to drive the switching converter (one binary control signal $s_i(t)$ for each switch of the multi-level switching power converter). The buffers are either merged with the power converter or with the decoding logic; in either case, the output of the decoding logic (the binary control signals) drive the converter and therefore they are the switch-driving signals $s_i(t)$ themselves.

The implementation of the decoding logic depends upon each specific design and technology. In integrated implementations, the decoding logic can be merged with the modulator, so that the switching signal $z(t)$ may not explicit. In a general scheme with an explicit voltage switching signal $z(t)$, the decoding logic may consist in comparators (to identify the magnitude of the multi-level switching signal) and digital logic, not necessarily synchronous, to generate the set of switch-driving signals $s_i(t)$.

In synchronous 2-level converters, such as the one included in figure 1.17, the decoding logic is very simple: just an inverter and a buffer to compensate the delay (asynchronous logic). Yet, in multi-level switching converters, the decoding logic is usually more complex.

5.1.3 Switching Policy

A switching policy is a set of rules which constrain the multi-level power-amplification process, e.g. limiting the maximum time at a specific level or banning switching between certain levels. The actual constraints are determined by the multi-level converter topology and the specifications.

Depending on the converter topology, a switching policy may be necessary to guarantee the proper amplifier's operation, although a switching policy can be devoted to provide additional features such as maximisation of the number of distinct output voltage levels (see section 6.2 for examples of switching policies).

The switching policy can constrain the multi-level encoding process and/or the operation of the decoding logic (i.e. the process of translating the multi-level switching signal $z(t)$ into a set of switch-driving signals $s_i(t)$).

Switching Policy in Multi-Level Encoding (Modulator)

Some converter topologies, such as flying-capacitor ones, generate voltage levels from intermediate voltages (the filter is supplied from a flying capacitor instead of from a voltage source when generating certain levels). In such cases, the intermediate voltages may drop if the converter remains in that state for a long time period or if the capacitor is not properly recharged (which generally involves not using that state whilst recharging).

In other multi-level converter topologies, switching between certain levels may not be possible or may be very inefficient in terms of switching losses. Furthermore, in embedded and/or low-power systems, some supply voltages could be temporarily unavailable (e.g. a portable device could be set to a low-power state, which partially disables the power management unit and hence only the battery voltage is available).

In either case, the generation of the multi-level switching signal $z(t)$, i.e. the multi-level encoding process, can be (temporarily or permanently) constrained to use (or to not use) a specific set of voltage levels. The multi-level modulation should be able to adapt to the available levels at any time and generate a multi-level switching signal $z(t)$ which tracks the reference signal $x(t)$, as long as it does not saturates the available levels.

Switching Policy in Multi-Level Power Decoding (Decoding Logic)

In multi-level power converters, different converter's operating states can yield the same voltage level in the multi-level power switching signal $\tilde{z}(t)$. In such cases, the translation of the switching signal $z(t)$ into the set of switch-driving signals $s_i(t)$ is not unique; there is more than one set of switch-driving signals $s_i(t)$ which yield a multi-level power switching signal $\tilde{z}(t)$ tracking the multi-level switching signal $z(t)$. In order to resolve this ambiguity, the translation must be constrained by a switching policy in the decoding logic.

For instance, in a regular full-bridge converter, the level GND can be generated by setting both commutator switches (i.e. both ends of the low-pass filter's input port) to the same voltage level, either GND or V_{G}. With an appropriate policy, this redundancy can be used to shape the common-mode voltage to high frequency [52] (this is further analysed in section 6.2).

5.2 General Features of Multi-Level Encoding

Multi-level time encoding is the generalisation of 2-level time encoding described in chapters 2 and 3 to N levels. The information conveyed by a continuous-time continuous-amplitude reference signal $x(t)$ is now encoded within a continuous-time N-level switching signal $z(t)$.

2-level time encoding is a subset, a particular case of multi-level time encoding (N levels). The additive model used to describe 2-level time encoding can be generalised to N levels. Consequently, considering that the decoding process consists in band-separation (low-pass filtering), multi-level time encoding can also be modelled as the addition of an error signal $e(t)$ to the reference signal $x(t)$, in order to shape it into the N-level switching signal $z(t)$.

$$z(t) = x(t) + e(t) \tag{5.1}$$

From the frequency-domain standpoint, the main difference (and advantage) between multi-level time encoding and 2-level time encoding is the power of the error signal $P_{e(t)}$, which mostly determines the outband power of the switching signal $P^{\mathrm{o}}_{z(t)}$ in conventional designs. The discussion about the error signal's power distribution $E(f)$ regarding 2-level time encoding also applies to N-level time encoding. Therefore, in multi-level time encoding, the error signal's inband spectral content $E(f)$, $|f| \leq f_0$ should be very low to avoid masking the reference signal $X(f)$ whereas the error signal's outband spectral content $E(f)$, $|f| > f_0$ should concentrate at frequencies beyond the filter's cutoff frequency (i.e. an arbitrary frequency set at design stage).

Like in the 2-level case, the reference signal $X(f)$ is properly tracked if the error signal's inband spectral content $E(f)$ is much lower than that of the reference signal $X(f)$.

$$|E(f)| \ll |X(f)|, \qquad |f| \leq f_0 \tag{5.2}$$

In such a case, the power of the error signal $P_{e(t)}$ is almost independent of the modulation and the OSwR (even in multi-level time encoding), although the power of the error signal $P_{e(t)}$ depends indeed upon the number of levels N (as long as the OSwR is high enough to use all N levels).

Certainly, using a similar analysis than for 2-level modulators, if the reference signal $x(t)$ is properly tracked then the a_0 coefficient is matched, hence

$$a_0 = \frac{2}{NT_0} \int_0^{NT_0} z(u)\,\mathrm{d}u \tag{5.3}$$

Because of the periodicity, this equality applies to the whole N-level switching signal $z(t) = z(t + NT_0)$, $\forall t \in \mathbb{R}$. The power of the N-level switching signal $P_{z(t)}$ is therefore determined by the a_0 coefficient and, if the reference signal is

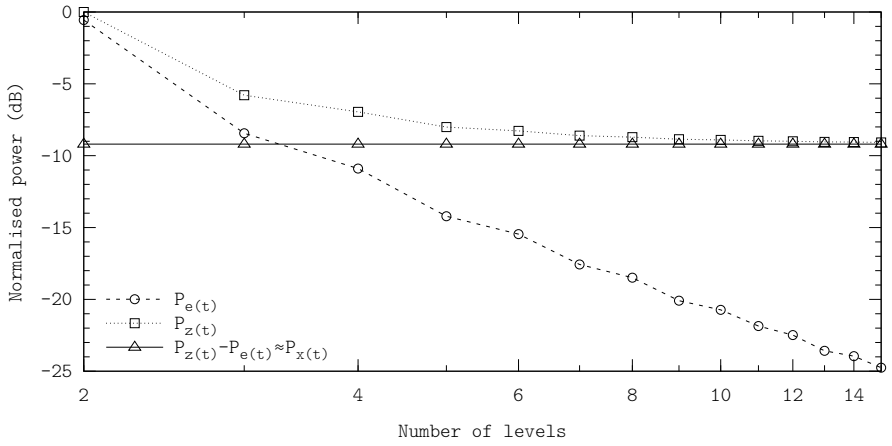

Figure 5.2: Error signal's power and switching signal's power in multi-level encoding. Example showing N-PWM operating at an OSwR of 20. Simulation performed using the configuration D.4.4.

properly tracked (5.2) then $P_{z(t)} - P_{e(t)} \approx P_{x(t)}$. As a result, the power of the error signal $P_{e(t)}$ is only determined by the reference signal $x(t)$ and the number of levels N of the switching signal $z(t)$.

Intuitively, it can be seen that the more levels N are available, the lower the error signal $e(t)$ is required for this shaping. Therefore,

$$\lim_{N\to\infty} P_{e(t)} \to 0 \Rightarrow P_{z(t)} \to P_{x(t)} \tag{5.4}$$

Figure 5.2 shows the power of the switching signal $P_{z(t)}$, the power of the error signal $P_{e(t)}$ and their difference when tracking a f_0-bandlimited signal with a multi-level modulation, using different number of levels N, at high OSwR (to properly track the reference signal $X(f)$ and hence emphasise the effects of multi-level time encoding). The error signal's power $P_{e(t)}$ decreases according to a power law; consistently, the switching signal's power $P_{z(t)}$ asymptotically tends to the reference signal's power $P_{x(t)}$.

In general, the N levels in a multi-level time encoding process do not need to be regularly distributed. From the encoding process standpoint, using non-regularly distributed levels only simplifies or improves the encoding process if the amplitude distribution of the reference signal $x(t)$ matches the output level's L_i distribution. In what follows, regularly distributed levels are assumed unless otherwise stated.

Regardless of the number of levels N, a multi-level modulator cannot track reference signals beyond its lowest and highest levels, $Z_{\min}$ and $Z_{\max}$ respectively. These two boundary levels define the modulator's dynamic range; the additional (intermediate) levels aid in encoding the information.

$$Z_{\min} =: L_0 < L_1 < \cdots < L_{N-1} := Z_{\max} \tag{5.5}$$

When extending 2-level modulations to N levels, the differences between modulations become more noticeable. Indeed, the three 2-level modulations analysed in chapter 4 (PWM, AΣΔM and AAΣΔM), inband-error-free track

constant reference signals, i.e. they yield the same 2-level switching signal $z(t)$. Therefore, for low modulation depths, the differences between modulations are hardly visible. As the modulation depth increases, each modulation generates its own switching signal $z(t)$ and hence the difference between modulations becomes more noticeable. However, the no-saturation condition combined with non-periodic bandlimited signals, limit the amplitude sweep of the reference signal, resulting in low probabilities of values of the reference signal close to $Z_{\min}$ or $Z_{\max}$, where the differences between modulations may be more visible. As a result, the behaviour in the time domain of all 2-level modulations is similar (see the time histograms of pulses' width shown in figures 4.4, 4.7 and 4.14, 99 % of pulses of the three modulations belong to the range $[10^{-2}T_0, 10^{-1}T_0]$).

In multi-level encoding, the reference signal $x(t)$ crosses over the intermediate levels. In terms of modulator's time-domain performance, approaching to an intermediate level is equivalent to approaching to a boundary level. Therefore, in multi-level encoding, the performance difference between modulations is more visible than in 2-level encoding, even with low modulation depths.

5.2.1 Bandwidth Limits in Multi-Level Time Encoding

In N-level time encoding, the information conveyed by a continuous-time continuous-amplitude reference signal $x(t)$ is encoded within an N-level switching signal $z(t)$. However, depending on the OSwR, not all the available levels should be used. Let us assume that infinite levels are available $N = +\infty$ or, more pragmatically, that the number of levels N is higher than the OSwR, $N >$ OSwR. Multi-level time encoding adds another degree of freedom in the encoding process, the switching signal's $z(t)$ amplitude (the level to switch to in a switching event).

This additional degree of freedom modifies the encoding process and, eventually, the fundamental bandwidth limit of 2-level time encoding derived in chapter 3. A priory, the bandwidth limits of multi-level time encoding (minimum OSwR to achieve inband-error-free encoding) could be different than that in 2-level time encoding (OSwR of 1). Unfortunately, including this variable in the fundamental limit derivation is challenging indeed.

Still, it is feasible to analyse simple cases which provide insights about the bandwidth limits of multi-level encoding. Let us consider a single tone sinusoid sweeping all the available dynamic range (100 % of modulation depth)

$$x(t) = Z_{\mathrm{m}} + \frac{Z_{\mathrm{pp}}}{2}\cos(\omega_0 t) \tag{5.6}$$

The modulator comprises N regularly-distributed levels,

$$L_i = Z_{\min} + \frac{Z_{pp}}{2(N-1)}i, \quad i \in \mathbb{N},\ i = 0, \ldots, N-1 \tag{5.7}$$

being

$$L_0 = Z_{\min} \qquad L_{N-1} = Z_{\max} \tag{5.8}$$

the modulator's dynamic range.

In order to simplify the analysis, let us constrain the modulator to operate at OSwR $= N - 1$ and to generate a multi-level switching signal $z(t)$ with even symmetry, as figure 5.3 shows (example with $N = 6$). That is, between

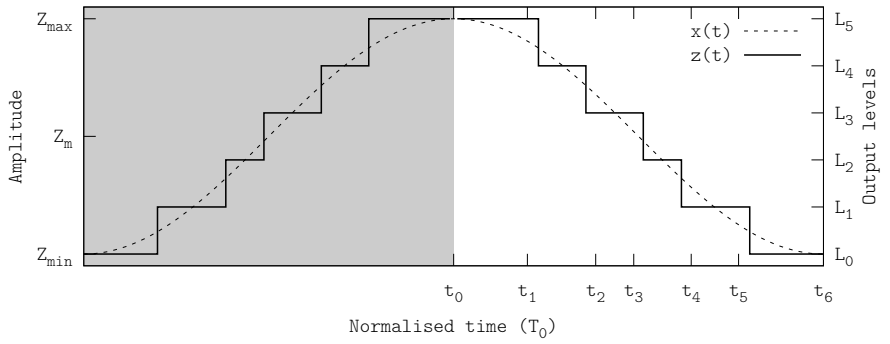

Figure 5.3: Multi-level encoding a single tone with 6 levels at an OSwR of 5.

a maximum and a minimum of the reference signal $x(t)$, all levels are used in order and only once (and vice versa).

Let us label, in order, the switching events using the normalised times t_i,

$$0 =: t_0 < t_1 < \cdots < t_{N-1} < t_N := 1/2 \tag{5.9}$$

where two additional time instants have been defined, t_0 and t_N, for the sake of notation simplicity. Within one switching period, the switching events occur at time instants $T_0 t_i$.

Provided that the reference signal is T_0-periodic and that OSwR $\in \mathbb{N}$, the switching signal $z(t)$ is T_0-periodic as well. Furthermore, given that the switching signal $z(t)$ has even symmetry, all b_k^* coefficients are 0. The a_k^* are given by

$$a_k^* = \frac{4}{T_0} \sum_{i=0}^{N-1} \int_{t_i T}^{t_{i+1} T} L_i \cos\left(k\omega_0 u\right) \, \mathrm{d}u \tag{5.10}$$

By applying (5.7) to (5.10) and operating, it follows that

$$a_k^* = \frac{2Z_{\mathrm{pp}}}{k\pi(N-1)} \sum_{i=1}^{N-1} \sin\left(2k\pi t_i\right) \tag{5.11}$$

The value of the a_k^* coefficients is set by the switching events t_i; the multi-level time encoding process itself (the N levels) reduces the amplitude of the harmonics by a factor $N-1$. Note that because of (5.9), all summands in the a_1^* coefficient are positive ($2\pi t_i > 0$, $i = 1, \ldots, N-1$, $i \in \mathbb{N}$). Therefore, as N increases (more levels and more switching events or higher OSwR), the main harmonic can still sweep up to $Z_{\mathrm{pp}}/2$ (again, the maximum according to the expression may exceed the modulator dynamic range, i.e. a modulation depth higher than 100 %) whilst the amplitude of the other harmonics reduces.

According to the previous result and considering that the decoding process consists in averaging (low-pass filtering), it can be conjectured that multi-level time encoding, compared to 2-level time encoding, reduces the power of the error signal $e(t)$ but it does not provide further tracking capabilities. Each switching event allows tracking one harmonic of the reference signal and therefore the minimum OSwR to inband-error-free track a non-periodic f_0-bandlimited reference signal is still 1.

The switching events t_i determine the number and the frequency of the harmonics of the multi-level switching signal $z(t)$, including the inband harmonics, whereas the number of levels N (precisely, the distance between the reference signal $x(t)$ and the switching signal $z(t)$, i.e. the error signal $e(t)$) determines the power of the outband harmonics.

Broadly speaking, by increasing the number or levels N, the power spectrum of the error signal $E(f)$ is shifted down in power, whereas by increasing the OSwR it is shifted to higher frequencies (thereby widening the inband-error-free encoding frequency range).

In order to ensure proper tracking fidelity (i.e. the inband harmonics of the switching signal $Z(f)$ match the harmonics of the reference signal $X(f)$, regardless of the number of levels N), each time edge t_i of the switching signal $z(t)$ must intersect the reference signal $x(t)$. If the OSwR is low (or, equivalently, more levels than OSwR are available), the levels should be chosen according to a specific criterion, e.g. to minimise the power of the error signal $P_{e(t)}$.

5.3 Multi-Level Pulse Width Modulation

Multi-level Pulse Width Modulation (N-PWM) is the extension of 2-level PWM (2-PWM) to N levels. If properly extended, N-PWM keeps the encoding properties of 2-PWM, including constant frequency. Even though many variants of N-PWM have been reported in the literature, there are still aspects of this multi-level modulation that remain unexplored. Most of the analyses reported in the literature mainly describe the performance of an implementation or pursuing a specific application; the performance due to the modulation itself (i.e. the error due to improper encoding) is masked by other error sources. These analyses provide an important background, but they are not comprehensive enough to characterise the modulation tracking non-periodic signals at low OSwRs.

Regardless of the variant, N-PWM still encodes by comparing the reference signal $x(t)$ with a set of carriers $c_i(t)$, thereby generating a multi-level switching signal $z(t)$. The difference between the N-PWM variants are the set of carrier signals $c_i(t)$: their alignment, their frequencies or even the layout (amplitude-shifted or phase-shifted carriers).

5.3.1 Alignment of Multiple Carriers

The natural extension of 2-PWM to multiple levels is by using a carrier between each pair of adjacent levels ($N-1$ amplitude-shifted carriers). Within each carrier (or encoding slot), the switching signal is generated as in a regular 2-PWM, as figure 5.4 shows.

Similarly to 2-PWM, each carrier splits into encoding intervals. The constraint regarding the carrier waveform in 2-PWM (continuity of the encoding intervals to avoid dummy edges) also applies to N-PWM. However, in the multi-level case, this constraint becomes more restrictive, since the encoding intervals must be continuous in both time and amplitude (between different encoding slots).

Therefore, assuming triangle carriers (which guarantees time continuity), the encoding intervals defined by whichever two adjacent carriers must be aligned and their time length must be the same to achieve amplitude continuity. In

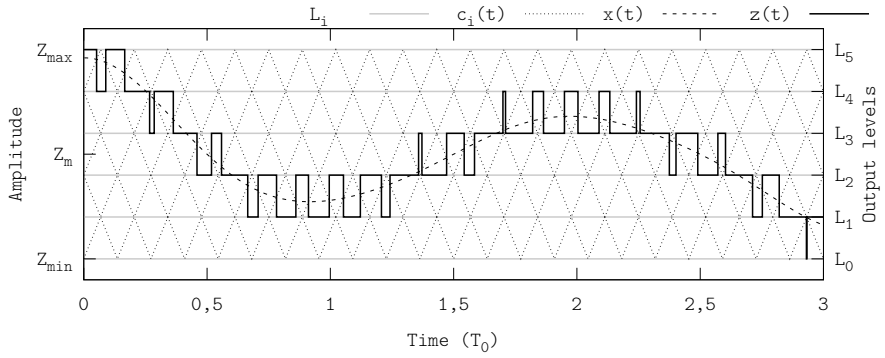

Figure 5.4: Multi-level pulse width modulation. Example with six levels (6-PWM, waveforms L_i) and using aligned triangle carriers $c_i(t)$.

such a case, the ending time instant of an encoding interval coincides with the starting time instant of the subsequent encoding interval of the adjacent slot. Since this applies to whichever two adjacent encoding slots, by extension, this applies to all encoding slots and hence the encoding intervals of defined by all carriers are aligned. From a geometrical standpoint, the maxima (minima) of all amplitude-shifted carriers must coincide with the minima (maxima) of the superadjacent (subadjacent) carrier, except in the absolute bounds.

If the encoding intervals are aligned (aligned carriers or aligned N-PWM), when sweeping the modulator's dynamic range with a constant-reference signal from $Z_{\min}$ to $Z_{\max}$ or vice versa, the pulse pairs generated by each carrier are continuous in amplitude as well. For instance, in a 3-PWM, the switching signals $z_1(t)$ and $z_2(t)$ resulting of encoding $x_1(t) = Z_{\mathrm{m}} + \varepsilon$ and $x_2(t) = Z_{\mathrm{m}} - \varepsilon$ with $0 < \varepsilon < Z_{\mathrm{pp}}/2$ must be symmetrical. Figure 5.5 illustrates this issue with an example: tracking two symmetrical constant-reference signals with a misaligned 3-PWM and with an aligned 3-PWM. In the aligned 3-PWM, the maxima of the lower carrier coincide with the minima of the upper carrier (geometrical interpretation), which leads to symmetrical PWM signals.

Whilst the alignment does not affect the performance of N-PWM tracking constant-reference signals, when tracking non-constant reference signals $x(t)$, the misalignment results in a non-constant encoding frequency. Indeed, whenever the reference signal changes the encoding slot, it may avoid the carriers thus skipping some pulses or intersect the carriers at a rate up to twice as fast than the carrier's frequency. Figure 5.6 illustrates these effects with an example: tracking non-periodic f_0-bandlimited signal with a misaligned 3-PWM and with an aligned 3-PWM. The OSwR is approximately 5 in both cases. Note the irregular distribution of switching events in the misaligned 3-PWM.

Similarly to dummy edges, discontinuities or irregularities in the carriers degrade the quality of the encoding process (increased error due to improper encoding). Still with the example of figure 5.6, figure 5.7 shows the waveforms of the recovered signals $\tilde{x}(t)$ and the remaining error signals $\xi_1(t)$ and $\xi_2(t)$ corresponding filtering with an ideal filter both switching signals $z_1(t)$ and $z_2(t)$, generated with the misaligned 3-PWM and with the aligned 3-PWM respectively. The peak-to-peak amplitude of the remaining error signal $\xi(t)$ decreases

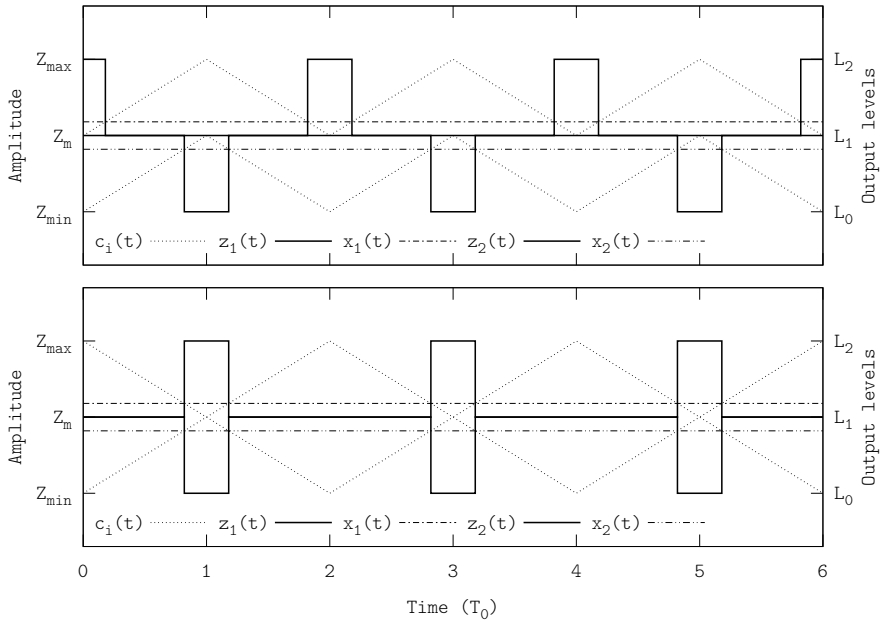

Figure 5.5: 3-PWMs tracking two symmetrical constant-reference signals to emphasise the amplitude continuity; misaligned 3-PWM (upper plot) and aligned 3-PWM (lower plot).

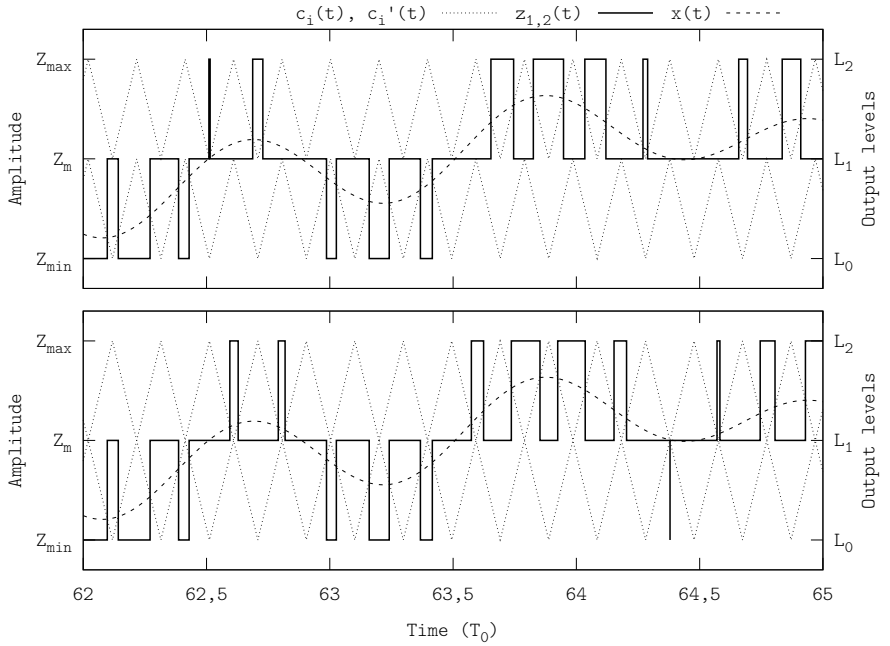

Figure 5.6: Example of tracking a non-constant reference signal with a misaligned triangle 3-PWM (upper plot) and with an aligned 3-PWM (lower plot), both operating at an OSwR of 5.

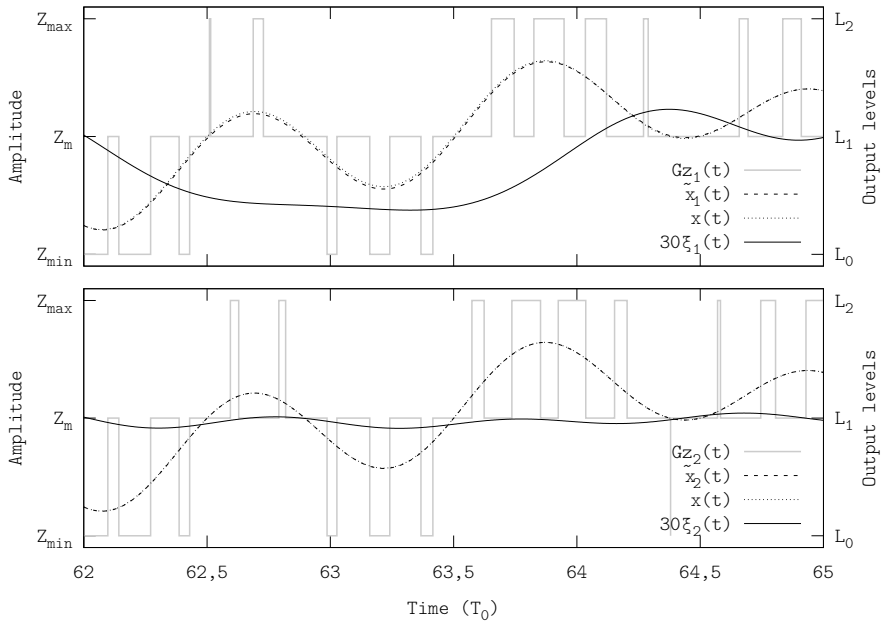

Figure 5.7: Example of tracking a non-constant reference signal with a misaligned triangle 3-PWM (upper plot) and with an aligned 3-PWM (lower plot); filtering with an ideal filter (approximated in the frequency domain D.3.5).

from $2{,}5 \cdot 10^{-2} Z_{\text{pp}}$ (misaligned 3-PWM) to $4 \cdot 10^{-3} Z_{\text{pp}}$ (aligned 3-PWM), a reduction of 84 %. These differences can also be seen in the frequency domain, since the error signal's inband content $E(f)$, $|f| \leq f_0$ is higher in the misaligned 3-PWM than in the aligned 3-PWM.

Despite the better tracking performance of aligned N-PWM over misaligned N-PWM, both approaches have been used in the literature [50]. Multi-level PWM, using more than three levels, has been mainly implemented at very high OSwRs (grid-tie inverters, wherein f_0 is typically 50 Hz or 60 Hz) and in audio applications. In these applications, the operating OSwR is high enough so that, despite the increased inband error due to misalignment or other irregularities in the carriers, improper encoding is still not the dominant inband source in the remaining error signal $\xi(t)$.

On the other hand, additional features can be achieved with misaligned N-PWMs, e.g. in grid-tie inverters, using carriers of different frequencies, the switching frequency can be adapted to the reference signal's dynamics [51]. Since in this work aims to reduce the OSwR of switching amplifiers without increasing the tracking error, only aligned N-PWM will be considered. In what follows, N-PWM stands for aligned triangle N-PWM unless otherwise stated.

5.3.2 Switching Signal's Time Waveform Analysis

The aligned triangle N-PWM variant keeps the encoding properties of 2-PWM. Certainly, if the reference signal is bandlimited and the OSwR is high enough to avoid extra switching (extra switching in N-PWM is analysed in section 5.3.3),

the pulses' width can be analysed in a similar way than in the 2-level case, but using the local levels $z_{\min}$ and $z_{\max}$ (i.e. the two levels surrounding the reference signal, $z_{\min} < x(t_0) < z_{\max}$) instead of the boundary levels $Z_{\min}$ and $Z_{\max}$. Therefore,

$$0 < \frac{T_k}{T_0} < \frac{1}{\text{OSwR}} \tag{5.12}$$

where the inverse of the carrier's period fulfils $T_c^{-1} = f_c = \text{OSwR} f_0$ and T_k is the width (time length) of the kth pulse, defined as the time interval between two consecutive switching events t_k

$$T_k := t_{k+1} - t_k \tag{5.13}$$

Like in 2-PWM, the pulses' width is bounded from above by the carrier's frequency and not bounded from below. Note that, due to the alignment of the carriers, these bounds are independent of the reference signal's time waveform $x(t)$, i.e. the pulses' width is bounded by these values even if the reference signal changes the encoding slot, as long as the slew rate limit is not exceeded (see subsection 5.3.3).

As section 5.2 already begun to emerge, when tracking a non-periodic signal, the intermediate levels are crossed over often, even in small-amplitude reference signals. As a result, the probability of generating very narrow pulses (i.e. intersecting the carrier at a value close to an encoding level, where the carrier changes its slope and it is quickly intersected again, thereby generating a very narrow pulse) is as high as the probability of generating pulses of any other possible width.

Figure 5.8 shows the histograms and the percentile of pulses' width T_k for different N-PWMs, all of them tracking a f_0-bandlimited non-periodic signal at an OSwR of 10. As this figure shows, once an intermediate level is added ($N \geq 3$), the probability distribution is shaped to an approximately uniform distribution. Note that the pulses' width is still bounded from above by OSwR^{-1}, in this case 10^{-1}.

5.3.3 Extra Switching in Multi-Level Pulse Width Modulation

Like in 2-PWM, extra switching may occur in N-PWM if the reference signal $x(t)$ intersects the carriers $c_i(t)$ more than once within each encoding interval (intrinsic slew rate constraint). In the multi-level case this condition becomes more restrictive since, as the number of levels N increases, the amplitude sweep of the carriers reduces thereby reducing the carrier's slew rate $\dot{c}_i(t)$, see figure 5.9.

An N-PWM is free of extra switching if the reference signal's slew rate $\dot{x}(t)$ is lower than the lowest slew rate of the carriers. In the case of an N-PWM using regularly-distributed levels (triangle carriers), the slew rate is the same for all carriers

$$|\dot{c}_i(t)| = \frac{2Z_{\text{pp}}}{(N-1)T_c} = \text{OSwR} f_0 \frac{2Z_{\text{pp}}}{N-1} \tag{5.14}$$

where the carrier's frequency is $f_c = 1/T_c = \text{OSwR} f_0$.

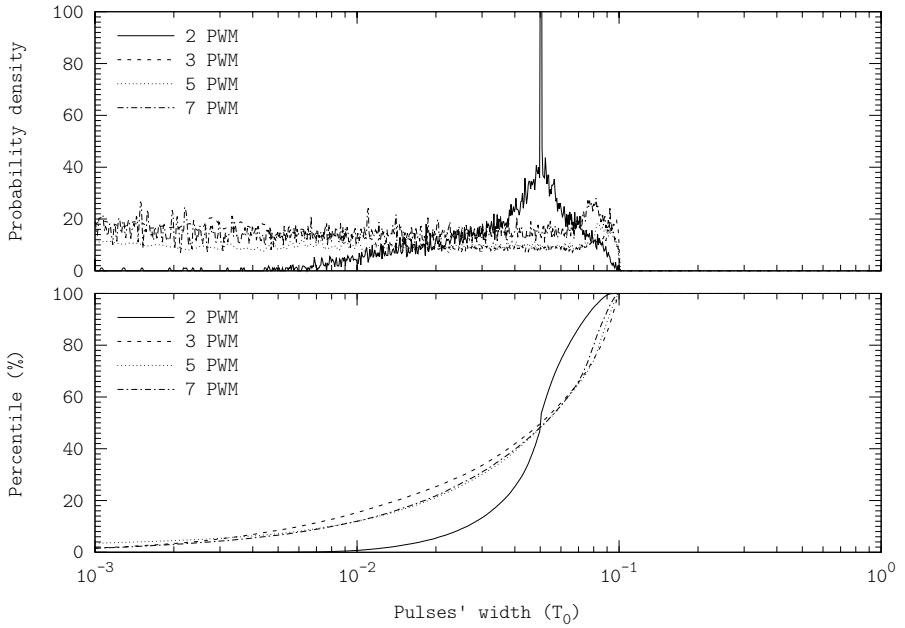

Figure 5.8: Histogram and percentile of pulses' width for different N-PWM, all of them tracking a f_0-bandlimited non-periodic signal at an OSwR of 10. Simulation performed using the configuration D.4.5.

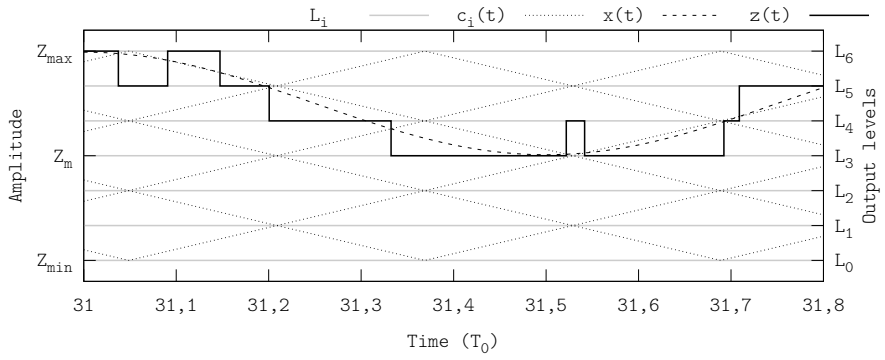

Figure 5.9: Extra switching in N-PWM. Example with seven levels (7-PWM) tracking a bandlimited signal at an OSwR of 3,2.

As discussed for 2-PWM, provided that the maximum slew rate of non-periodic f_0-bandlimited is difficult to estimate, a good approximation to estimate when extra switching may start being significant in bandlimited signal tracking is the analysis upon single tones. In the N-PWM case this threshold is (triangle carriers)

$$\mathrm{OSwR}_N \geq \frac{\pi c}{2}(N-1) \tag{5.15}$$

where c is the modulation depth. In the case of 100 % of modulation depth (the reference signal sweeps all the available dynamic range), extra switching may be significant at OSwRs below 3 in 3-PWM, below 6 in 5-PWM and below 9 in 7-PWM.

Despite the minimum OSwR to encode without extra switching increases proportionally to the number of levels N, common applications operate at high OSwRs and hence improper encoding is not the dominant inband error source. Nevertheless, in the context of this thesis of exploring low-OSwR operation, this intrinsic constraint may limit the amplifier's inband performance. Although extra switching can be avoided by including a latch, as in the 2-level case, it further degrades the tracking performance.

Related to this intrinsic constraint, note that N-PWM is not an incremental modulation. Even if N-PWM switching signal is free of extra switching, it may be necessary to switch between non-adjacent levels in order to properly track the reference signal $x(t)$ at a specified OSwR. N-PWM is unable of achieving that, since the switching signal $x(t)$ cannot evade the carriers $c_i(t)$ and hence it unavoidably intersects them when changing the encoding slot. However, the slew rate constraint is generally stronger than this one.

Furthermore, if one level is temporarily unavailable, this modulation cannot encode skipping that level. If the encoding levels L_i change, the carriers must be readjusted to the actual levels. This also applies in the case of non-constant voltage levels: the amplitude of the carriers should track the actual voltage levels.

5.3.4 Power Spectrum Analysis

The analytic expression of the power spectrum of N-PWM tracking an arbitrary bandlimited signal has not been derived. Nonetheless, the power spectrum can be simulated and, from this characterisation, conjecture the frequency content of N-PWM. Figure 5.10 shows the power spectrum and the cumulative-power frequency distribution of three different N-PWMs: 2 levels, 3 levels and 7 levels, all operating at an OSwR of 10 (further levels are not included because of the intrinsic slew rate limit, which would partially mask the N-PWM spectrum).

As the analysis of pulses' width shows (figure 5.8), when adding an intermediate level (from $N = 2$ to $N = 3$) the probability distribution of pulses' width shapes to a uniform-like distribution (approximately uniform between 0 and 1/OSwR); despite the switching frequency is constant, the pulses' width is much more variable. As a result, the power spectrum has no harmonics, although it still comprises replicas of the reference signal $X(f)$ scaled by Bessel-shaped functions centered at frequencies multiples of the PWM encoding frequency $f_{\mathrm{PWM}} = \mathrm{OSwR} f_0$.

These Bessel functions are scaled by a factor which depends upon the number of levels N, so that, as N increases, the maximum amplitude of these functions

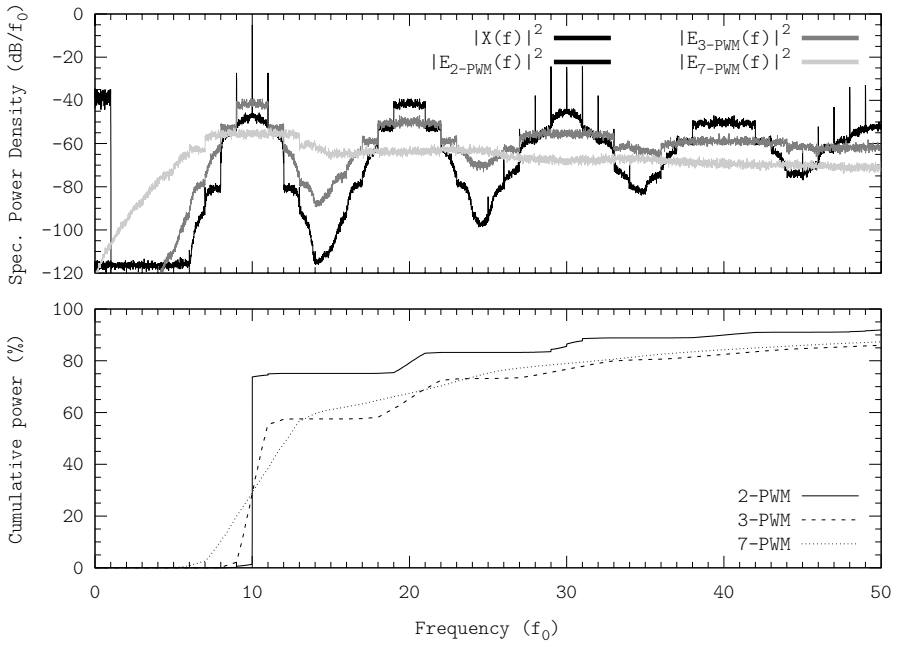

Figure 5.10: Power spectrum and cumulative-power frequency distribution of N-PWM. Displayed waveforms include 2 levels, 3 levels and 7 levels. Simulation performed using the configuration D.4.1.

decreases and their width increases. In a more practical standpoint, increasing the number of levels N yields a twofold effect: reducing the upperbound of the outband spectral power density (and also the outband power, as figure 5.2 already showed) and widening or spreading the power spectrum.

Further increasing the number of levels $N > 3$ yields a further reduction of the power density (the maximum level of the power spectrum decreases and the power $P_{e(t)}$ decreases as well) and a further spreading of the power spectrum, although the power spectrum still comprises replicas of the reference signal $X(f)$ scaled by Bessel functions. These replicas and the concentration around frequencies multiples of the switching frequency are hardly visible in figure 5.10 with seven levels because the OSwR is not high enough; the Bessel functions are wide and they overlap, yielding a smooth spread power density. If the OSwR would be high enough, the spectral power density of the N-PWM error signal would also concentrate around multiples of the switching frequency, although the replicas would not be as visible as in the other cases.

The differences in the power spectra are therefore related to the different distribution of pulses' width (figure 5.8). Consequently, spreading the power spectrum can also be seen in the cumulative-power frequency distribution, since a similar percentage of outband power is achieved at higher frequencies. Note that the scale is relative; for instance, 60 % of power in the 3-PWM case involves more power than 60 % of power in the 7-PWM case.

From the inband performance standpoint, the spreading of the power spectrum is a drawback, since it increases the inband error spectral content. It

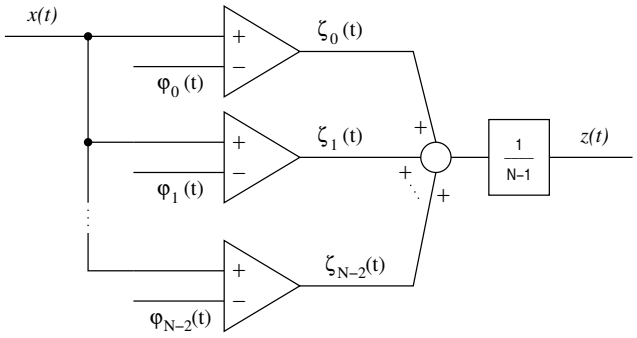

Figure 5.11: Block diagram of an N-level phase-shifted carrier pulse width modulator. The switching signal is scaled so that the input and output dynamic ranges are the same.

could seem a paradox that increasing the number of levels N degrades the inband tracking performance (i.e. the best tracking performance is achieved with two levels, additional levels only degrade it). Recalling the analysis of multi-level switching signals of section 5.2, the information conveyed by the reference signal $x(t)$ is encoded within the time edges of the switching signal $z(t)$. The amplitude of the pulses (i.e. the levels of the switching signal) only determines the outband power of the switching signal $P^{\mathrm{o}}_{z(t)}$, but it does not provide further tracking capabilities. Consequently, the inband tracking fidelity is only determined by the time edges t_k. Note that the minimum OSwR in multi-level encoding is also 1, regardless of the number of levels N.

5.3.5 Phase-Shifted Carrier Pulse Width Modulator

Implementing amplitude-shifted carriers $c_i(t)$ is challenging, especially at high frequencies. In the particular case of regularly-distributed voltage levels, it is possible to take advantage of the symmetry to generate the N-PWM switching signal $z(t)$ using an alternative (and simpler to implement) scheme based on phase-shifted carriers (Phase-Shifted Carrier Pulse Width Modulation, N-PSCPWM where the N denotes the number of levels) [46], [47].

The actual implementation details may vary depending on the application and the converter architecture, but the fundamental principle of operation is the same: combine several 2-PWM, using carriers of the same frequency but with different phases, to generate the N-PWM switching signal $z(t)$.

N-PSCPWM is an implementation of N-PWM but not a different modulation; the encoding algorithm is the same: multi-level pulse width modulation. An N-PSCPWM uses $N-1$ 2-PWMs to generate $N-1$ 2-level switching signals $\zeta_i(t)$; these switching signals are added (and scaled) thus generating an N-level switching signal $z(t)$, as figure 5.11 shows. $N-1$ comparators, an adder and $N-1$ phase-shifted carriers $\varphi_i(t)$ are therefore required to implement an N-PSCPWM.

The frequency of all carriers must be the same

$$f_{\varphi_i(t)} = f_\varphi, \qquad i = 0, \ldots, N-2,\ i \in \mathbb{N} \tag{5.16}$$

and therefore the frequency of each 2-level switching signal $\zeta_i(t)$, $i = 0, \ldots, N-2$,

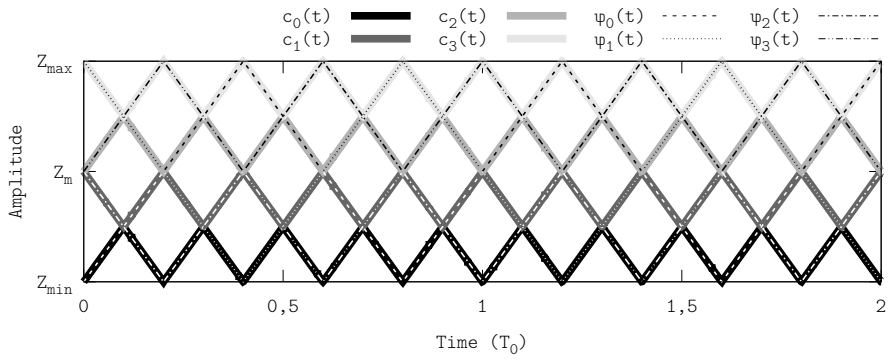

Figure 5.12: Equivalency between amplitude-shifted $c_i(t)$ and phase-shifted $\varphi_i(t)$ carriers in multi-level pulse width modulation. Example with 5-level modulators (four carriers).

$i \in \mathbb{N}$ is f_φ as well. The frequency of the resulting N-PWM switching signal $z(t)$, $f_{\text{PWM}} := f_{z(t)}$ is $N-1$ times higher than f_φ.

$$f_{\text{PWM}} = (N-1) f_\varphi \tag{5.17}$$

Using the first carrier $\varphi_0(t)$ as reference

$$\varphi_i(t) = \varphi_0(t + \phi_i), \quad i = 0, \ldots, N-2,\ i \in \mathbb{N} \tag{5.18}$$

the required phase-shift in each carrier is

$$\phi_i = i \frac{2\pi}{N-1}, \quad i = 0, \ldots, N-2,\ i \in \mathbb{N} \tag{5.19}$$

From a geometrical standpoint, it is easy to see the equivalency between the amplitude-shifted and the phase-shifted carrier schemes (see figures 5.12 and 5.13). Note, however, the different frequencies of the phase-shifted carriers $\varphi_i(t)$ and the amplitude-shifted carriers $c_i(t)$, necessary to achieve the same switching frequency f_{PWM} in the output multi-level switching signal $z(t)$. Also note that the 2-level switching signals $\zeta_i(t)$ in the PSCPWM scheme must be scaled in order to fit within the modulator's dynamic range.

The slew-rate constraint is not affected by the N-PWM implementation. Certainly, in the PSCPWM implementation, the carrier's slew rate is the same than that in a regular amplitude-shifted implementation. Whilst the amplitude of the phase-shifted carriers is scaled by factor $N-1$, their frequency is scaled by a factor $1/(N-1)$ thus yielding the same slew rate.

5.4 Multi-Level Asynchronous ΣΔ Modulation

Based on the waveforms of regular asynchronous Δ modulators [81], 2-level AΣΔM (2-AΣΔM) can be extended to N levels (N-AΣΔM) by replacing the hysteresis comparator by two symmetrical comparators, with thresholds $+\delta$ and $-\delta$, and a counter with analogue output (see figure 5.14).

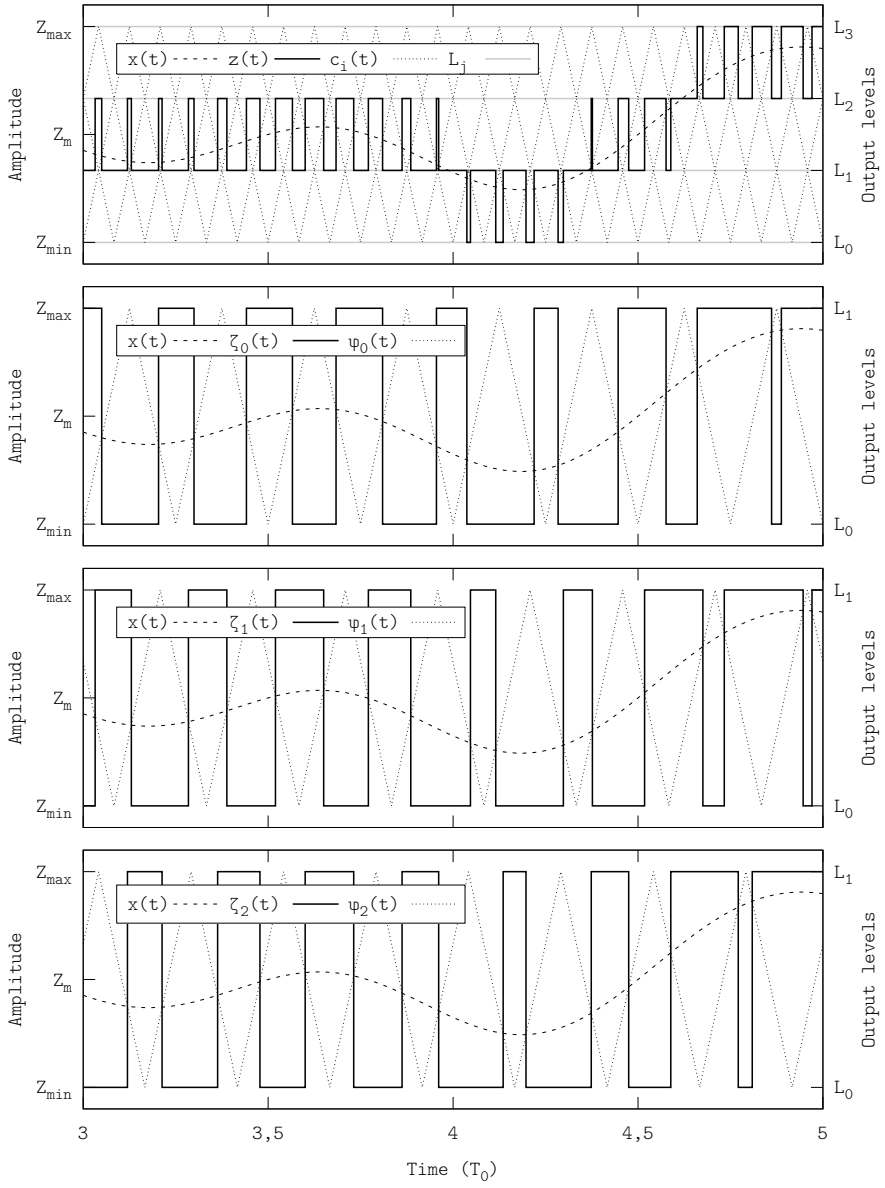

Figure 5.13: Equivalency between 4-PSCPWM and regular (amplitude-shifted) 4-PWM. The amplitude-shifted carrier's frequency f_{PWM} is 12, whereas the frequency of the phase-shifted carriers is $f_\varphi = f_{\mathrm{PWM}}/(N-1) = 12/3 = 4$.

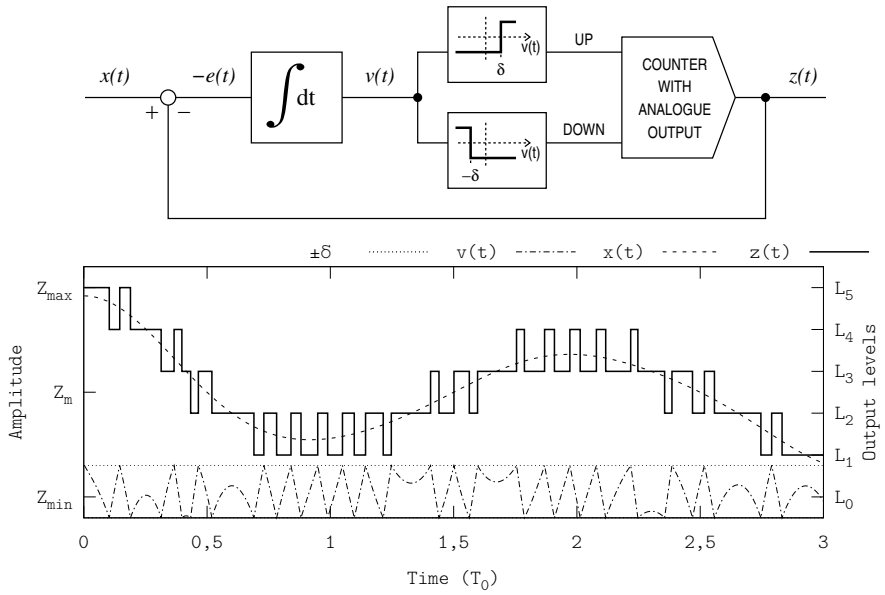

Figure 5.14: Block diagram and representative time waveforms of a multi-level asynchronous ΣΔ modulation. The time waveforms correspond to a 7-level example (7-AΣΔM); the integrator's output signal $v(t)$ and the comparators' threshold $\pm\delta$ have been shifted and scaled for better readability.

The comparator with positive threshold $+\delta$ (or positive comparator) triggers the counter up (i.e. to increase the magnitude of the switching signal $z(t)$), whereas the comparator with negative threshold $-\delta$ (or negative comparator) triggers the counter down (i.e. to decrease the magnitude of the switching signal $z(t)$). Together, the two comparators behave as a window comparator with polarity, since they trigger the comparator whenever the integrator's output signal $v(t)$ exceeds the window defined by $\pm\delta$. Figure 5.14 illustrates this operating performance with the representative time waveforms in a 7-AΣΔM.

5.4.1 Multi-Level Encoding Process

N-AΣΔM is an astable oscillator (asynchronous modulator) which generates a multi-level switching signal $z(t)$, whose amplitude and pulses' width are continuously adapted according to the reference signal $x(t)$. As discussed above, the information conveyed by the reference signal $x(t)$ is encoded within the time edges t_k or switching events of the switching signal $z(t)$. Like in the 2-level case (2-AΣΔM), the encoding process is still based in computing the integral of the error signal $e(t)$, i.e. the integral of the difference between the switching signal $z(t)$ and the reference signal $x(t)$, and triggering the comparator whenever the integrated error exceeds a certain value ($\pm\delta$ in this case).

Consequently, N-AΣΔM also encodes by equalling the integral (area) of the reference signal $x(t)$ and the switching signal $z(t)$, i.e. area-equalling encoding as in the 2-AΣΔM case, although not between whichever two pulses but between whichever two consecutive rising (or falling) edges. Certainly, area equalling is

achieved if

$$\int_{t_\mathrm{A}}^{t_\mathrm{B}} -e(u)\,\mathrm{d}u = v(t_\mathrm{B}) - v(t_\mathrm{A}) = 0 \rightarrow v(t_\mathrm{A}) = v(t_\mathrm{B}) \tag{5.20}$$

where t_A and t_B stand for the time instant of two switching events.

Provided that the switching events are triggered whenever the integrator's output signal $v(t)$ is $\pm\delta$, it follows that $v(t_\mathrm{A}) = v(t_\mathrm{B}) = \delta$ (or equal to $-\delta$) for the previous expression to hold. In N-AΣΔM, t_A and t_B can correspond to two consecutive switching events in the switching signal $z(t)$, either rising or falling, as figure 5.14 shows. Note that in 2-AΣΔM, a rising edge is always followed by a falling edge and vice versa, i.e. two consecutive edges in the two-level switching signal $z(t)$ cannot be both rising (or falling) and hence area-equalling is always achieved within one encoding interval (a pair of two consecutive pulses).

Like in 2-AΣΔM, area equalling is achieved regardless of the reference signal's waveform $x(t)$, even if underswitching, as long as it does not exceed the modulator's dynamic range $Z_\mathrm{min} \leq x(t) \leq Z_\mathrm{max}$. Besides, all the information conveyed by the reference signal $x(t)$ is used in the encoding process. No approximation nor implicit sampling is performed in N-AΣΔM either.

5.4.2 Operating Range

N-AΣΔM properly operates (astable operation) as long as the integrator's output signal $v(t)$ does not exceed the $\pm\delta$ window.

$$|v(t)| \leq \delta, \qquad \forall t \in \mathbb{R} \tag{5.21}$$

In order to fulfil this condition, the slope of the integrator's output signal $\dot{v}(t)$, i.e. the error signal $-e(t)$,

$$\dot{v}(t) = \frac{\mathrm{d}v(t)}{\mathrm{d}t} = \frac{\mathrm{d}}{\mathrm{d}t}\int_{-\infty}^{t} -e(u)\,\mathrm{d}u = -e(t) \tag{5.22}$$

must change its sign whenever the system switches. Let t_k be the time instant of a switching event; N-AΣΔM is astable if

$$\dot{v}(t_k^-)\dot{v}(t_k^+) < 0 \Leftrightarrow e(t_k^-)e(t_k^+) < 0 \tag{5.23}$$

Provided that the error signal $e(t)$ is defined as the difference between the switching signal $z(t)$ and the reference signal $x(t)$

$$e(t) = z(t) - x(t) \tag{5.24}$$

the switching signal $z(t)$ must cross over the reference signal $x(t)$ at every switching event for the modulator to operate as an astable oscillator. That is, the edges of the discrete-amplitude signal $z(t)$ must always intersect the reference signal $x(t)$, a necessary condition to guarantee signal tracking as discussed in subsection 5.2.1.

If the OSwR is low compared to the number of levels N, it may be necessary to switch between non-adjacent levels in order to fulfil the cross-over condition (5.23). The comparators trigger the counter either up or down whenever the switching signal $z(t)$ must increase or decrease its magnitude, but they do not

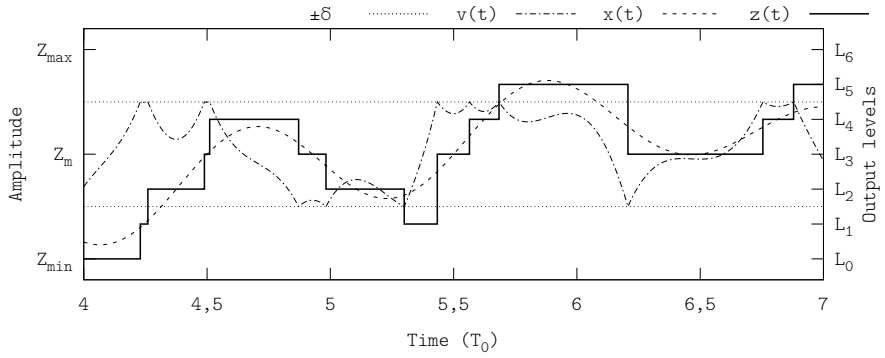

Figure 5.15: Switching between non-adjacent levels in N-AΣΔM. Example showing a 7-AΣΔM tracking a f_0-bandlimited signal at an OSwR of approximately 2. The switching policy determines the next level as the closest to the reference signal which fulfils the cross-over condition.

determine the next level (incremental modulation). The next level is determined by the counter, which must sense both the reference signal $x(t)$ and the actual output levels L_i, determine all valid next levels (not necessarily adjacent to the current level) so that the cross-over condition holds and, according to a switching policy, decide the level to switch to (see figure 5.15 for an example of non-adjacent level switching).

Note that more than one level may fulfil this condition (in a rising edge t_k, all levels L_i higher than $x(t_k)$ fulfil it), although the wider the distance between the reference signal $x(t)$ and the switching signal $z(t)$, the higher the error signal $e(t)$ (i.e. the higher the outband power of the switching signal $P^{\mathrm{o}}_{z(t)}$). Also note that, because of the incremental-encoding feature, N-AΣΔM can handle non-constant levels and/or skip some levels if they are temporarily unavailable. This requires a more complex counter and real-time sensing and comparing, but the counter is still ruled by the same principle of operation.

Despite the cross-over condition, the N-AΣΔM encoding process is not constrained by an intrinsic bandwidth limit (like the slew rate limit in N-PWM). N-AΣΔM can therefore take advantage of multi-level encoding, without compromising the inband tracking performance, even if underswitching.

The block diagram of N-AΣΔM is valid for any number of levels including two $N \geq 2$. Indeed, by constraining the counter to only use the two boundary levels $Z_{\min}$ and $Z_{\max}$, an N-AΣΔM behaves as a 2-AΣΔM implemented with a regular hysteresis comparator. However, whilst in 2-level operation the comparators alternatively trigger the counter (the same comparator never triggers the counter twice, see figure 4.6), when operating with N levels, each comparator can trigger the counter more than once before its counterpart triggers it. This is the feature which provides the multi-level capabilities.

5.4.3 Switching Signal's Time Waveform Analysis

N-AΣΔM continuously adapts the pulses' width according to the reference signal $x(t)$. If the modulator uses N regularly-distributed levels, by statically

sweeping all the input dynamic range with a DC constant-reference signal, the width of the pulses T_k of the switching signal $z(t)$ is bounded by

$$\frac{2\delta(N-1)}{Z_{\max}-Z_{\min}} \leq T_k \leq +\infty \tag{5.25}$$

These bounds can be found using a similar analysis than in the 2-level case. If the levels are irregularly distributed, the lowerbound becomes

$$\frac{2\delta}{\Delta L} \leq T_k \tag{5.26}$$

where ΔL is the widest distance between two consecutive levels

$$\Delta L = \max\left(L_{i+1}-L_i\right), \quad i=0,\ldots,N-2,\ i\in\mathbb{N} \tag{5.27}$$

However, when tracking a non-constant signal $x(t)$, the width of a pulse delimited by two consecutive rising (or falling) edges can be narrower than the lowerbound. Let us consider an example, the narrow pulse at $t = 4{,}5T_0$ in figure 5.15. When the integrator's output signal reaches the threshold δ, $v(t_0) = \delta$, the reference signal is lower (yet very close) than the level Z_{m}, $x(t_0) < Z_{\mathrm{m}}$. The modulator switches to the Z_{m} level and the integrator's output signal starts decreasing $v(t_0+\varepsilon) < \delta$, $\varepsilon > 0$, although since the reference signal quickly raises beyond Z_{m}, the threshold δ is reached again very quickly $v(t_1) = \delta$ and hence the modulator switches again. As a result, the width of the pulse defined by t_1 and t_0 is not bounded by (5.25).

Despite it is possible than an N-AΣΔM may generate narrow pulses, when tracking a non-periodic f_0-bandlimited signal, the probability of generating those narrow pulses is very low. Instead, the pulses' width T_k in N-AΣΔM is effectively bounded from below and from above. Figure 5.16 shows the histogram and percentile of pulses' width for different N-AΣΔMs tracking a non-periodic signal at an OSwR of approximately 10. In all multi-level cases ($N \geq 3$), the probability distribution is similar and the width of 90 % of pulses belongs to the range $[10^{-2}T_0, 10^{-1}T_0]$, yet it is more variable than in 2-AΣΔM (note the lower probability density of the maximum).

Whilst the probability out of the 90 %-range is not zero, it is very low. This quantifies the probability of generating narrow pulses when triggering twice the same comparator (as discussed above). Furthermore, the narrow pulses issue can be addressed with an appropriate switching policy, by constraining evaluation of the next level. For instance, as a first-order approach, the policy could constrain the distance between the next level and the reference signal to be higher than a certain value. A more advanced policy could also take into account the derivative (slope) of the reference signal.

5.4.4 Power Spectrum Analysis

The power spectrum of N-AΣΔM has not been analytically derived in the literature. Nonetheless, based on the expression of the power spectrum of 2-AΣΔM and simulations of power spectra of N-AΣΔM (figure 5.17), it can be conjectured that the power spectrum of N-AΣΔM is also defined by series of harmonic bands like 2-AΣΔM. However, the high-order bands are scaled by a factor which inversely depends upon N and hence the outband spectral content decreases as

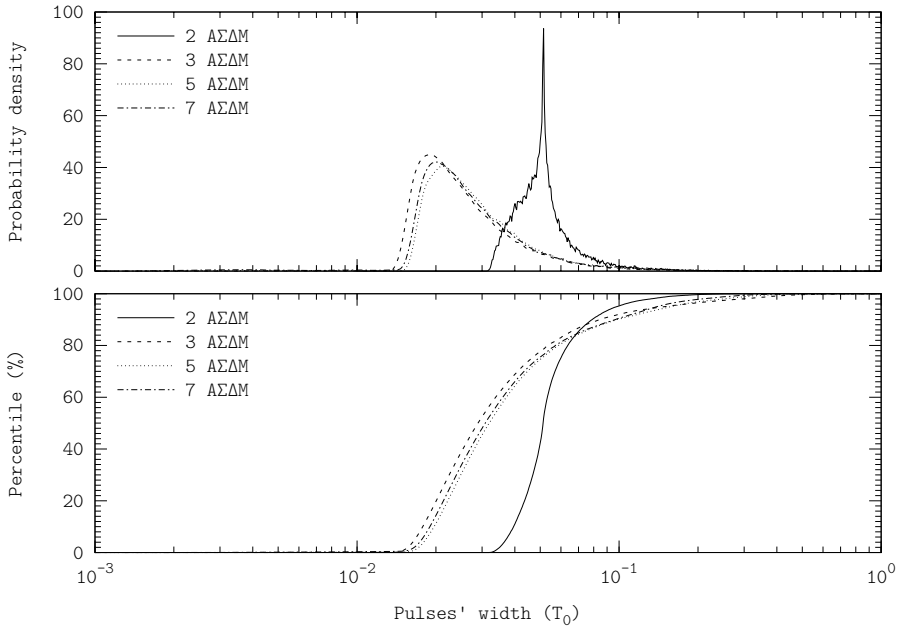

Figure 5.16: Histograms and percentile of pulses' width for different N-AΣΔMs tracking a non-periodic f_0-bandlimited signal at an OSwR of approximately 10. Simulation performed using the configuration D.4.5.

the number of levels N increases. Unlike in N-PWM, for $N \geq 3$ the high-frequency spectral content is not further spread.

Because of incremental encoding, the inband performance of N-AΣΔM is almost independent of the number of levels N, even for 2-level encoding $N = 2$ (in figure 5.17 the inband spectral power density of the 3-AΣΔM's error signal is higher than in the other cases because of the statistics of the reference signal). The inband content of the error signal $E(f)$ logarithmically increases from very low values up to a certain value which depends upon the OSwR, but not upon the number of levels N.

Note that the power spectrum is smooth (spread) for all number of levels N; there is neither discrete harmonics nor discrete replicas of the reference signal.

5.4.5 Encoding Limitations

The encoding limitations in 2-AΣΔM, the dependency of the encoding interval's length upon the instantaneous value of the reference signal $x(t)$, also apply to N-AΣΔM. Like in 2-AΣΔM, whenever the reference signal approaches to an output level L_i, the length of the encoding intervals increases thus resulting in a locally low switching frequency, which can be an issue in the decoding process.

Given that 2-AΣΔM only uses the two boundary levels $Z_{\min}$ and $Z_{\max}$ to encode, the local reduction of the switching frequency only occurs when the magnitude of the reference signal $x(t)$ is wide. Therefore the probability of generating wide pulses depends upon the modulation depth and the amplitude distribution of the reference signal $x(t)$.

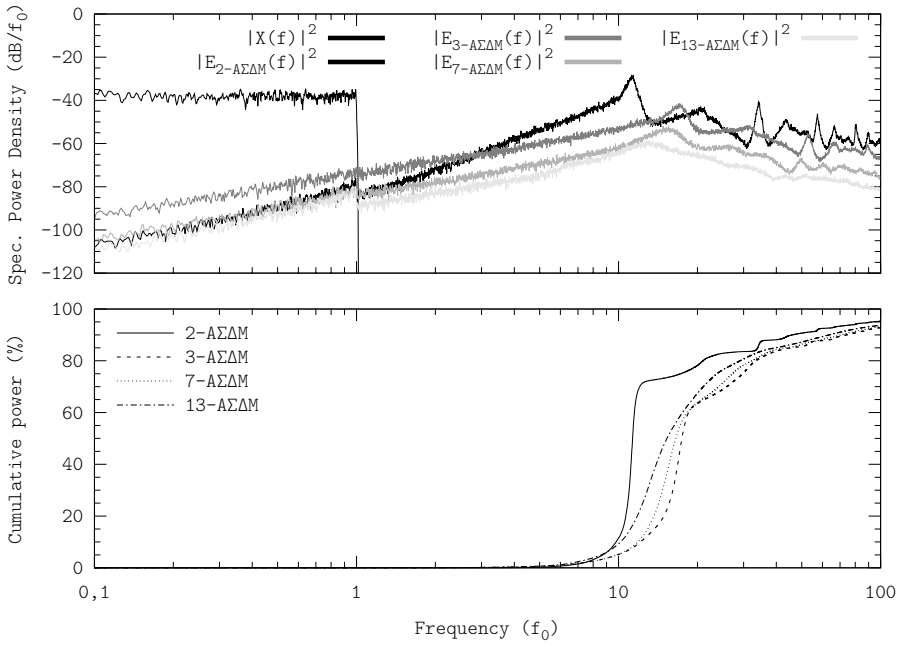

Figure 5.17: Power spectrum and cumulative-power frequency distribution of N-AΣΔM. The OSwR is approximately 10 in all cases. Simulation performed using the configuration D.4.1.

However, in N-AΣΔM, provided that there are intermediate levels, the local reduction of the switching frequency also occurs with intermediate values of the reference signal. For instance, in a 3-AΣΔM, the switching frequency locally reduces whenever the reference signal $x(t)$ approaches to Z_{m}, its mean value (very high probability).

This effect results in a reduction of the OSwR. When upgrading a 2-AΣΔM to N levels, the comparison threshold δ must be reduced (as the number of levels N increases) in order to maintain the OSwR constant. Consequently, narrower sweeps of the integrator's output signal $v(t)$ are required to trigger the comparator. That is, the minimum amplitude sweep (of the reference signal) around an output level L_i required to trigger the comparator, reduces as the number of levels N increases.

Figure 5.18 illustrates the encoding limitations in N-AΣΔM for an example, tracking a non-periodic f_0-bandlimited signal with a 7-AΣΔM at an average OSwR of approximately 11. Around $t = 8{,}5T_0$, the reference signal $x(t)$ remains locally close to Z_{m}, yielding an instantaneous OSwR of 1,65,

N-AΣΔM may stop switching whenever the reference signal $x(t)$ approaches any output level L_i, although even small variations around these values quickly trigger pulses. Together, both effects partially compensate; the probability of generating wide pulses (locally low OSwR) is not significantly higher than in 2-AΣΔM. Moreover, this probability is almost independent of the number of levels N in multi-level operation ($N \geq 3$, see figure 5.16).

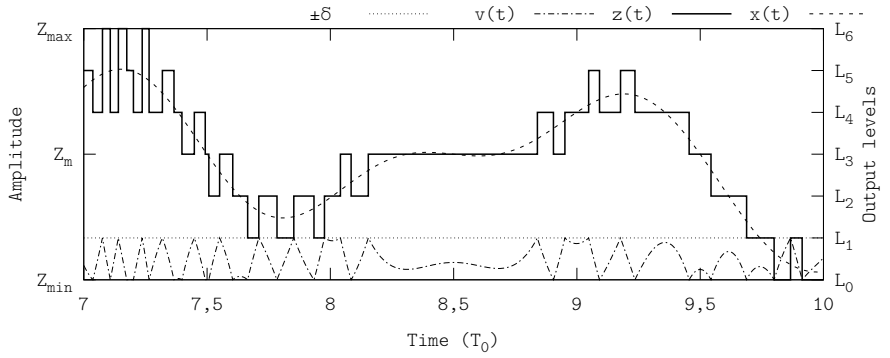

Figure 5.18: Encoding limitations in N-AΣΔM. Example showing a 7-AΣΔM tracking a f_0-bandlimited signal at an OSwR of 11. Around $t = 8{,}5T_0$, the instantaneous OSwR reduces to 1,65. The integrator's output signal $v(t)$ and the comparison threshold δ have been scaled and shifted for better readability.

5.5 Multi-Level Adaptive Asynchronous ΣΔ Modulation

The feedforward law used in 2-level AAΣΔM (2-AAΣΔM) to overcome the encoding limitations of 2-AΣΔM can also be extended to the N-level case (N-level multi-level Adaptive Asynchronous ΣΔ Modulation, N-AAΣΔM). The expression of the multi-level law can be derived using a similar analysis than in the 2-level case, but considering the local output levels $z_{\min}$ and $z_{\max}$ (the levels surrounding the reference signal $x(t_0)$).

$$z_{\min} < x(t_0) < z_{\max} \tag{5.28}$$

In this way, the required comparator thresholds become a time-dependent hysteresis-width function[2] $\delta(t)$ given by

$$\delta(t) = \frac{1}{2\alpha} \frac{1}{\dfrac{1}{z_{\max} - x(t)} - \dfrac{1}{z_{\min} - x(t)}} \tag{5.29}$$

where α is, again, a scaling parameter to set the switching frequency. Note that if $z_{\max} = Z_{\max}$ and $z_{\min} = Z_{\min}$, the absolute maximum and minimum bounds respectively, the previous expression (5.29) simplifies to the 2-level adaptive hysteresis law (4.14).

Figure 5.19 shows the block diagram of N-AAΣΔM and the representative time waveforms for an example, specifically, a 7-AAΣΔM tracking a non-periodic f_0-bandlimited signal. As this figure illustrates, the principle of operation is the same than in N-AΣΔM: integrating the error signal $e(t)$ and, once the magnitude of the integrated or accumulated error $v(t)$ exceeds the hysteresis-width function $\delta(t)$, the switching signal $z(t)$ is updated. This multi-level modulation is also incremental.

[2]Like in the 2-level case, strictly speaking, the hysteresis-width function depends upon the reference signal $x(t)$, which depends upon time $\delta(x(t))$. For the sake of notation simplicity, the hysteresis-width function is expressed as a time-dependent function $\delta(t)$.

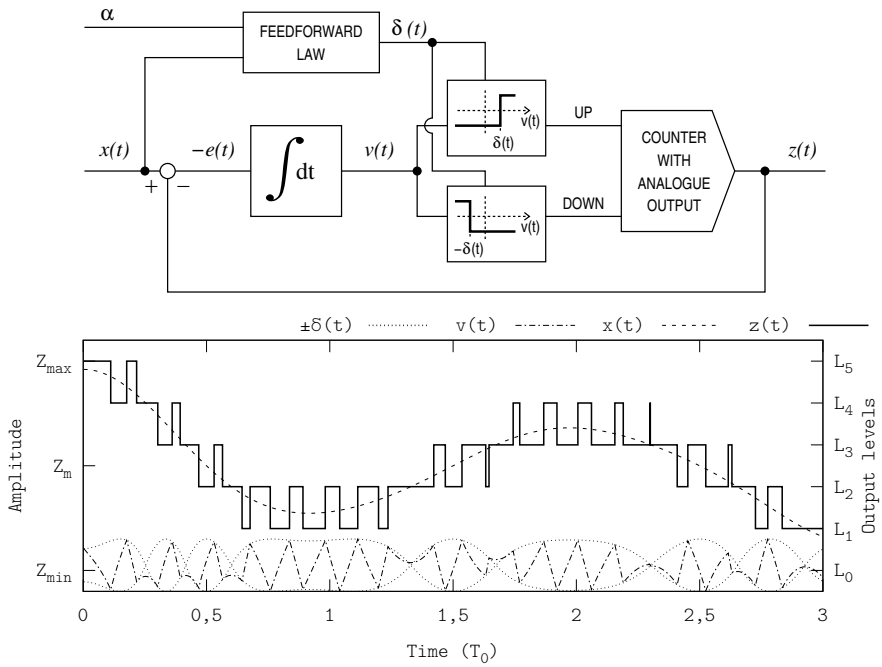

Figure 5.19: Block diagram and representative time waveforms in N-AAΣΔM. Example showing a 7-level case (7-AAΣΔM); the integrator's output signal $v(t)$ and the hysteresis-width function $\delta(t)$ have been scaled for better readability.

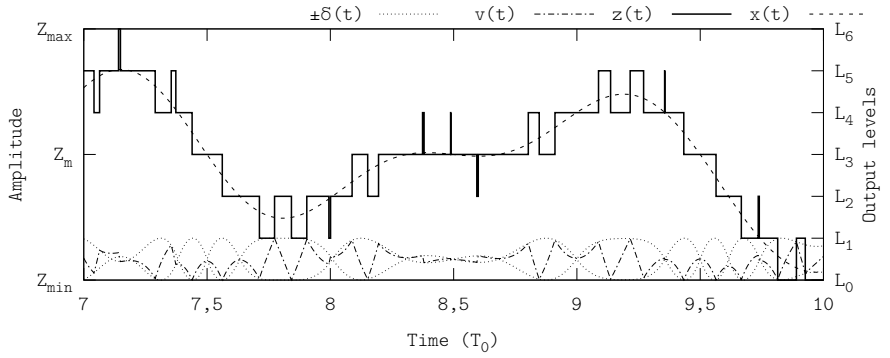

Figure 5.20: Overcoming the encoding limitations of N-AΣΔM with adaptive comparison window (N-AAΣΔM). Example showing a 7-AAΣΔM tracking a f_0-bandlimited signal at an OSwR of 11. The integrator's output signal $v(t)$ and the hysteresis-width function $\delta(t)$ have been scaled and shifted for better readability.

5.5.1 Switching Signal's Time Waveform Analysis

The aim of the feedforward law in the 2-level case, and so in the multi-level case, is to avoid wide pulses. As figure 5.20 shows (compare it to figure 5.18), this law overcomes this issue by locally reducing the width of the comparison window $\pm\delta(t)$ whenever the reference signal $x(t)$ approaches an output voltage level L_i.

The addition of the multi-level capabilities to AAΣΔM does not modify its encoding characteristics. Like in the 2-level case, in N-AAΣΔM, if sweeping the input dynamic range with a constant-reference signal, the modulator encodes all these constant-reference signals at the same OSwR, regardless of their amplitude. Nevertheless, N-AAΣΔM is still an asynchronous modulator (astable oscillator), since there is no external carrier nor synchronisation signal.

When tracking f_0-bandlimited reference signals, the non-dependency of the switching frequency upon the amplitude of the reference signal (when tracking constant-reference signals) results in narrow pulses in the switching signal $z(t)$ whenever the reference signal $x(t)$ approaches an output level L_i, including intermediate ones. Like in N-PWM, the probability of narrow pulses in N-AAΣΔM (with N $\geq$ 3) is very high as well, since the probability of the reference signal $x(t)$ crossing an intermediate level is high (e.g. in 3-AAΣΔM, the intermediate level is Z_m, the reference signal's mean value).

Formally, the upper and lowerbounds of the pulses' width in N-AAΣΔM can be obtained using a similar analysis than in the 2-level case, but considering the local levels z_max and z_min. Like in the 2-level case, the pulses' width is again bounded from above and not bounded from below (bounded by 0). Therefore, if an N-AAΣΔM is operating at OSwR, then

$$0 \leq \frac{T_k}{T_0} \leq \frac{1}{\mathrm{OSwR}} \tag{5.30}$$

Nonetheless, because of crossing intermediate levels, these bounds are more visible in the histograms in the multi-level case than in the 2-level case, see figure 5.21. Note the approximately uniform distribution from 0 to 1/OSwR.

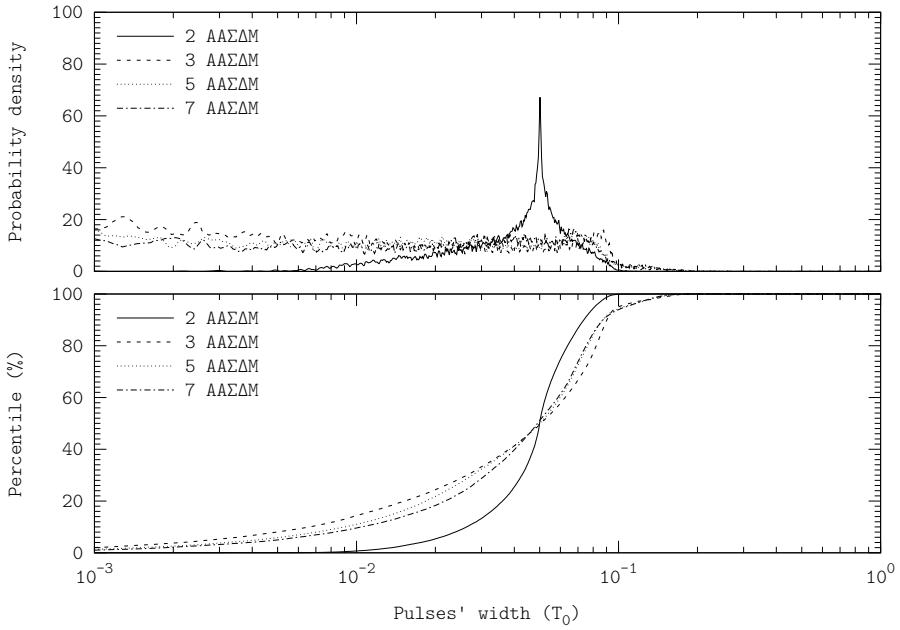

Figure 5.21: Histograms and percentile of pulses' width for different N-AAΣΔMs, tracking a f_0-bandlimited reference signal at an OSwR of approximately 10. Simulation performed using the configuration D.4.5.

Similarly to 2-AAΣΔM, because of the variable comparison threshold, N-AAΣΔM does not encode according to the area-equalling criterion either. Certainly, let t_A and t_B be the time instants of whichever two consecutive rising edges of the switching signal $z(t)$. The value of the hysteresis-width function at these time instants $\delta(t_\mathrm{A})$, $\delta(t_\mathrm{B})$ depends upon the reference signal $x(t)$, which, in general, may change its value $x(t_\mathrm{A}) \neq x(t_\mathrm{B})$; therefore

$$\int_{t_\mathrm{A}}^{t_\mathrm{B}} e(u)\,\mathrm{d}u = \delta(t_\mathrm{A}) - \delta(t_\mathrm{B}) \neq 0 \tag{5.31}$$

leading to

$$\int_{t_\mathrm{A}}^{t_\mathrm{B}} x(u)\,\mathrm{d}u \neq \int_{t_\mathrm{A}}^{t_\mathrm{B}} z(u)\,\mathrm{d}u \tag{5.32}$$

Regardless of the different areas, as long as the integrator's output signal $v(t)$ is inside the window $\pm\delta(t)$, the errors in the different encoding intervals compensate, so that the modulator operates as an astable oscillator and hence the multi-level switching signal $z(t)$ tracks the reference signal $x(t)$.

5.5.2 Operating Range

Like in N-AΣΔM, the error signal $e(t)$ must change its sign at every switching event, so that the integrator's output signal $v(t)$ changes its monotony (from increasing to decreasing or vice versa). If this condition is fulfilled (cross-over condition), all edges of the switching signal $z(t)$ intersect the reference signal

$x(t)$. However, in N-AA$\Sigma\Delta$M, the cross-over condition is not enough to guarantee that the modulator operates as an astable oscillator.

Right after a rising[3] switching event t_k, the hysteresis-width function $\delta(t_k)$ and the integrator's output signal $v(t_k)$ are the same.

$$\delta(t_k) = v(t_k) \tag{5.33}$$

If the cross-over condition holds, the integrator's output signal starts decreasing right after the switching event.

$$\dot{v}(t_k^-)\dot{v}(t_k^+) < 0 \tag{5.34}$$

However, the hysteresis-width function $\delta(t)$ can decrease at a faster rate than the integrator's output signal $v(t)$. Note that whenever the reference signal crosses over an output level, the hysteresis-width function becomes 0.

$$x(t_\mathrm{k}) = \begin{cases} z_\mathrm{max} \\ z_\mathrm{min} \end{cases} \rightarrow \delta(t_\mathrm{k}) = 0 \tag{5.35}$$

where $x(t_\mathrm{k}) = z_\mathrm{min}$ or $x(t_\mathrm{k}) = z_\mathrm{max}$ depending on the value of the switching signal at that time instant $z(t_\mathrm{k})$.

In such a case, $|\dot{\delta}(t_k^+)| > |\dot{v}(t_k^+)|$, the integrator's output signal $v(t)$ gets outside the window defined by $\pm\delta(t)$, $v(t_k^+) > \delta(t_k^+)$ and hence the modulator is no longer able to control this signal (the conditions for astable derived for A$\Sigma\Delta$M are not satisfied).

Depending on the waveform of the reference signal $x(t)$, the integrator's output signal $v(t)$ can get back inside the comparators' window (astable operation). However, if when being outside the comparators' window the integrator's output signal $v(t)$ changes again its monotony, it does not get back inside the comparators' window and therefore the switching signal $z(t)$ no longer tracks the reference signal $x(t)$, see figure 5.22.

A feasible way to address this issue is by continuously monitoring the distance $\gamma(t)$ between the integrator's output signal $v(t)$ and the hysteresis-width function $\delta(t)$.

$$\gamma(t) := |v(t)| - \delta(t) \tag{5.36}$$

Right after the reference signal crosses over an output level, $\gamma(t)$ is positive; in astable operation, $v(t)$ gets straight back inside the comparators' window ($\gamma(t)$ decreases until it becomes negative, i.e. inside the comparators' window). Instead, if $\gamma(t)$ starts increasing whilst it is still positive, then the modulator is to become unstable (non-astable operation). Forcing then the system to switch gets $v(t)$ inside the comparators' window again.

Figure 5.22 shows the operation of this control for astable operation. Around $t = 0{,}55T_0$, the modulator would become unstable (note that the distance function $\gamma(t)$ has a local minimum whose amplitude is larger than Z_m, i.e. a positive minimum) and the control forces then a switching event. The control for astable operation only forces the system to switch; the integrator's output signal $v(t)$ is not directly affected by this control and hence the encoding process continues normally.

[3] The derivation for falling edges is analogous, but with negative values instead of positive ones.

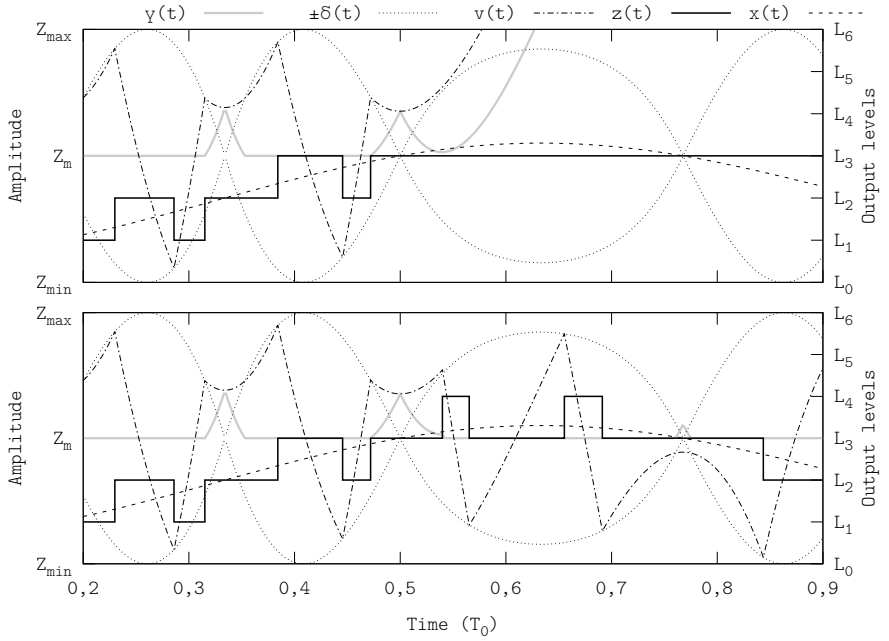

Figure 5.22: N-AAΣΔM without control for astable operation (upper plot) and with control for astable operation (lower plot). In the displayed example, the system is forced to switch when the integrator's output signal is outside the window $|v(t)| > \delta(t)$ and the distance signal $\gamma(t)$ starts increasing (the negative values have been omitted because they are not significant). These signals have been scaled for better readability.

5.5.3 Power Spectrum Analysis

The power spectrum of N-AAΣΔM has not been analytically derived, but it can be characterised (see figure 5.23). This characterisation has been carried out tracking a f_0-bandlimited signal at an OSwR of approximately 10.

An in-depth characterisation at different OSwRs and with different number of levels N reveals that, depending on the ratio of these two parameters, OSwR and N, the outband power spectrum is shaped to an N-AΣΔM-like spectrum or to an N-PWM-like spectrum. In this example, operating at an OSwR of approximately 10, the outband spectral content in the 2-level case is similar to that of 2-PWM; with three levels, replicas of the reference signal $X(f)$ can still be identified, as well as higher concentrations of spectral power density around multiples of the switching frequency. With higher number of levels (seven and thirteen), the spectrum is spread like in the N-AΣΔM case.

The inband performance is very similar to the N-AΣΔM, this is, the error signal's inband spectral power density logarithmically increases regardless of the number of levels N. The control for astable operation, whilst it ensures the proper operating performance of N-AAΣΔM, it may degrade the inband tracking performance if the number of levels N is high compared to the OSwR (i.e. if the number of edges triggered by the control for astable operation is comparable to the number of edges triggered by the modulation itself). This shortcoming is only significant if underswitching (even if the number of levels

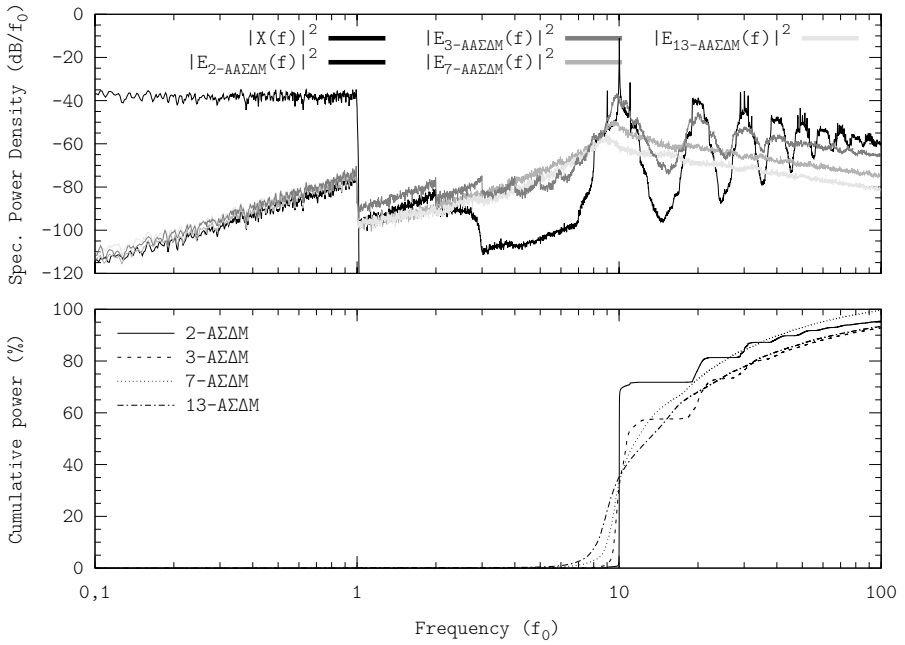

Figure 5.23: Power spectrum and cumulative-power frequency distribution of N-AAΣΔM. The OSwR is approximately 10 in all cases. Simulation performed using the configuration D.4.1.

N is high); besides, it can be partially overcome with an appropriate switching policy in the encoding process (similarly to that which would avoid narrow pulses in N-AΣΔM).

5.5.4 Hybrid Hysteresis-Width Functions

Whenever the reference signal $x(t)$ crosses over an intermediate level, the hysteresis-width function $\delta(t)$ becomes 0. Despite when evaluating the limit of the hysteresis-width function tending to zero the instantaneous switching frequency $f_{\mathrm{s}}(t)$ is bounded (assuming a constant-reference signal or a high OSwR),

$$\lim_{t \to t_k} \delta(t_k) = 0; \qquad \lim_{t \to t_k} f_{\mathrm{s\_}N-\mathrm{AA\Sigma\Delta M}}(t) < +\infty \tag{5.37}$$

there may be implementation issues due to the zero-width comparison window. Furthermore, very narrow comparison windows lead to very narrow pulses in the switching signal $z(t)$.

A feasible way to address both issues is by limiting the minimum value of the hysteresis-width function $\delta(t)$, i.e. a mixed mode between constant- and adaptive- comparison windows. Together with an appropriate switching policy (to avoid very narrow pulses if the next level is very similar to the reference signal, as discussed in section5.4.3), it is possible to bound the pulses width (from above and from below) regardless of the reference signal's time waveform $x(t)$. These bounds only depend upon design parameters, the minimum value of the hysteresis-width function and the α factor in the adaptive law).

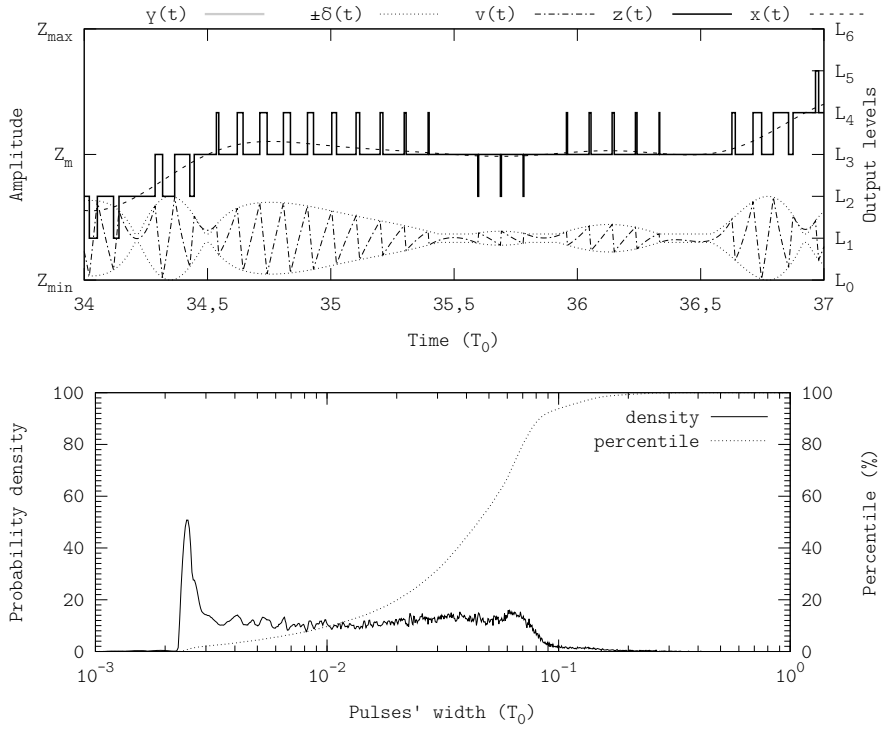

Figure 5.24: Hybrid hysteresis-width function in N-AΣΔM and histogram and percentile of pulses' width. Example with seven levels and limiting the minimum hysteresis-width function to $|\delta(t)| \geq Z_{\text{pp}}/20$ and operating at an OSwR of 10. Simulation performed using the configuration D.4.5.

Figure 5.24 shows the representative time waveforms in a N-AΣΔM using a hybrid hysteresis-width function $\delta(t)$. This hybrid approach avoids the very wide encoding intervals of N-AΣΔM and the narrow pulses of N-AAΣΔM (whenever the reference signal $x(t)$ is locally close to an output level L_i), i.e. the pulses' width is bounded from above and from below. This feature is clearly visible in the histogram of pulses' width, also included in figure 5.24.

The performance and the OSwR of this hybrid modulation depends upon the scaling factor of the hysteresis-width function and the minimum hysteresis-width function value. By properly tuning both parameters, it is feasible to achieve almost the same inband performance than N-AΣΔM whilst avoiding very wide encoding intervals.

5.6 Analysis Under the Fundamental Limit Perspective

The performance of N-PWM, N-AΣΔM and N-AAΣΔM has been characterised tracking a f_0-bandlimited reference signal, at different OSwRs. Consistently with the scope of this work, reducing the OSwR without degrading the tracking fidelity of switching amplifiers, this characterisation has been carried

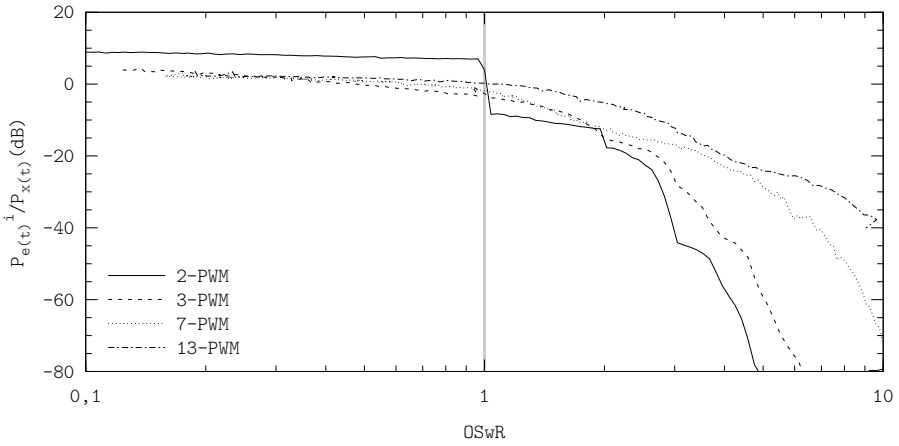

Figure 5.25: Characterisation of the error signal's inband power $P^{\mathrm{i}}_{e(t)}$, normalised to the reference signal's power $P_{x(t)}$, of N-PWM tracking a f_0-bandlimited signal. Simulation performed using the configuration D.4.4.

out at OSwRs below 10; even below 1 to explore the feasibility of underswitching.

5.6.1 Inband Performance

The inband performance of these three modulations in the cases of two, three, seven and thirteen levels is depicted in figures 5.25 (N-PWM), 5.26 (N-A$\Sigma\Delta$M) and 5.27 (N-AA$\Sigma\Delta$M).

Like in the 2-level case, at high OSwRs, the inband performance of N-PWM is better than that of N-A$\Sigma\Delta$M and N-AA$\Sigma\Delta$M, i.e. the PWM encoding algorithm better approximates inband-error-free encoding than the area-equalling encoding algorithm (A$\Sigma\Delta$M-based modulators). However, as the OSwR decreases, the inband performance of N-PWM quickly degrades, whereas the inband performance of N-A$\Sigma\Delta$M and N-AA$\Sigma\Delta$M degrades at a slower rate. These different rates become more visible as the number of levels N increases, since the degradation of the N-PWM inband performance is mainly because of the slew rate constraint (and, to a lesser extent, to adjacent level switching).

If N-PWM operates free of extra switching, the inband power of the error signal $P^{\mathrm{i}}_{e(t)}$ decreases at a similar rate in all N-PWMs. This is visible in figure 5.25, compare the performance of 2-PWM and 3-PWM below $-60\,\mathrm{dB}$ (both free of extra switching). 7-PWM also starts behaving in a similar way from OSwR ≈ 9, but 13-PWM still significantly suffers from extra switching at OSwR $= 10$.

As the OSwR decreases below the threshold given by (5.15), the error due to the slew-rate constraint becomes significant and hence the inband performance quickly degrades. Furthermore, the additional switching events[4]may

[4]A latch has been included in the characterisation of N-PWM. The latch only prevents extra switching by crossing the carrier(s) multiple times within one encoding interval. If the reference signal $x(t)$ sweeps more than two encoding slots within one encoding interval, additional switching events may be triggered regardless the latch. Because of this reason, the

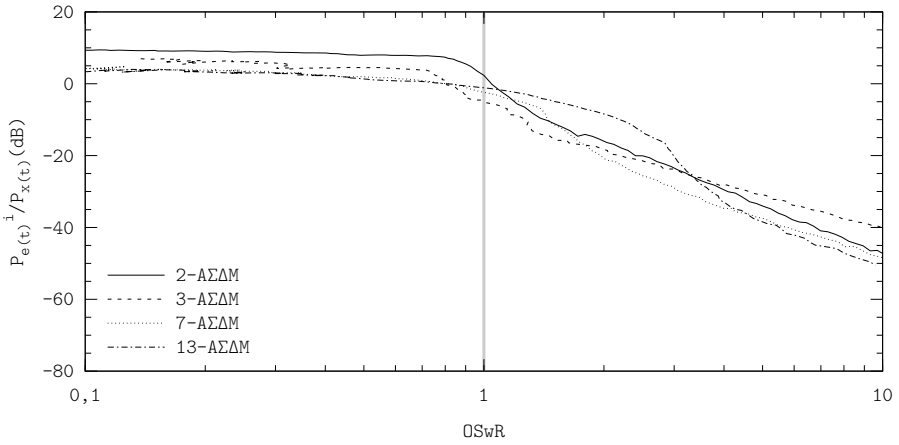

Figure 5.26: Characterisation of the error signal's inband power $P^{\mathrm{i}}_{e(t)}$, normalised to the reference signal's power $P_{x(t)}$, of N-AΣΔM tracking a f_0-bandlimited signal. Simulation performed using the configuration D.4.4.

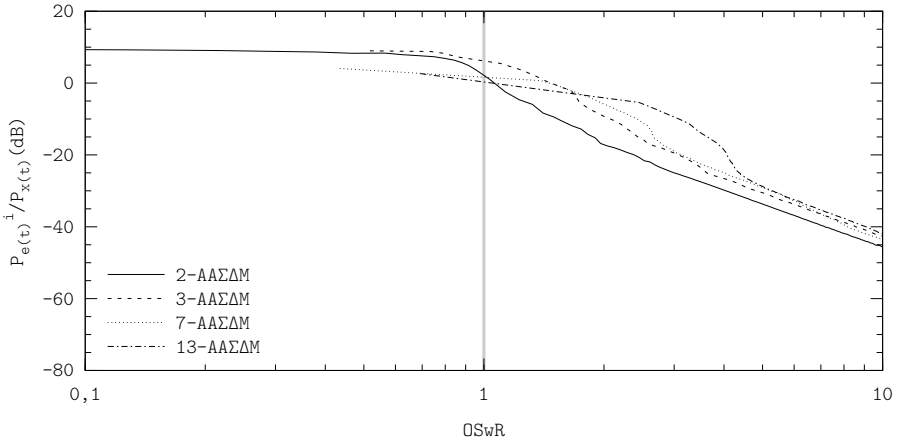

Figure 5.27: Characterisation of the error signal's inband power $P^{\mathrm{i}}_{e(t)}$, normalised to the reference signal's power $P_{x(t)}$, of N-AAΣΔM tracking a f_0-bandlimited signal. Simulation performed using the configuration D.4.4.

also increase the amplifier's switching losses. Note that the slew rate constraint becomes more restrictive as the number of levels N increases; consequently, a 7-PWM should not be used at OSwRs below 10 (the error due to improper encoding may become dominant).

On the other hand, the inband performance of N-A$\Sigma\Delta$M and N-AA$\Sigma\Delta$M hardly depends upon N at any OSwR (including close to 1). If the number of levels N is high compared to the OSwR (in the example of figures 5.27 and 5.26, thirteen levels), an advanced switching policy may be necessary to properly switch between levels and avoid narrow pulses (as discussed in section 5.4.3). In these simulations, the lack of an appropriate policy degrades the inband tracking performance (the policy used selects the first level to fulfil the cross-over condition). By upgrading the switching policy, a similar inband performance can be achieved regardless of the number of levels N.

Apart from this issue with the switching policy, the non-dependency of the inband performance respect to the number of levels N is due to the incremental multi-level modulation scheme. This feature, together with the absence of intrinsic bandwidth constraints, points out the suitability of A$\Sigma\Delta$M-based schemes to track non-constant signals, instead of PWM-based schemes, especially in multi-level systems.

5.6.2 Switching Signal's Time Waveform Comparison

Whilst the bounds of the pulses' width are the same if encoding with 2 levels or with N levels, the extension to multiple levels further emphasises the differences between modulations, as stated in section 5.2. Consequently, the probability of generating narrow pulses in N-PWM and N-AA$\Sigma\Delta$M is higher in the multi-level case $N \geq 3$ than in the 2-level case, because the intermediate level(s) are crossed over often (as described in section 5.3.2). On the other hand, despite the probability of generating wide pulses increases in N-A$\Sigma\Delta$M (when compared to the 2-level case), the pulses' width is still effectively bounded from above and from below (as discussed in section 5.4.3); N-A$\Sigma\Delta$M therefore is capable of tracking the reference signal without relying on narrow pulses.

Although it is not visible in the switching signals $z(t)$ nor in the histogram of pulses' width, N-PWM is a synchronous modulation (the frequency and the phase is set by the carriers $c_i(t)$, i.e. external signals), whereas N-A$\Sigma\Delta$M and N-AA$\Sigma\Delta$M are asynchronous modulators (astable oscillators).

5.6.3 Power Spectrum Comparison

Unlike in the time domain, the differences in the frequency domain become less significant as the number of levels N increases (if properly encoding), especially regarding the outband spectral content. Indeed, by increasing the number of levels N, the width of the pulses generated by N-PWM and N-AA$\Sigma\Delta$M becomes more variable, thereby spreading the spectral power density distribution. If increasing the OSwR as well, the spectral power density tends to concentrate around multiples of the switching frequency, but the differences between modulations would not become as visible as in the 2-level case. Still, the maximum in N-A$\Sigma\Delta$M is lower and shifted to higher frequencies than in the other two modulations (operating at the same OSwR).

minimum OSwR in the characterisation is not 0,1.

Like in the 2-level case, if the inband error due to improper encoding is much smaller than the level of the reference signal $|E(f)| \ll |X(f)|, |f| \leq f_0$, the outband power is independent of the modulation; the difference between modulations only concerns the distribution or shaping of the spectral power density. Given that, as the number of levels N increases, the outband power of the switching signal decreases and the spectral power density spreads, increasing the number of levels N mitigates the outband differences between modulations (the switching signal $z(t)$ tends to the reference signal $x(t)$ in all cases).

With regard to the inband error due to improper encoding, multi-level encoding yields no inband tracking improvements (note that inband-error-free encoding is already possible with two levels at an OSwR of 1); moreover, the extension to multiple levels even degrades the inband tracking performance in PWM. When operating at a certain OSwR, the most accurate inband tracking, i.e. the best approximation to inband-error-free encoding, is achieved by 2-PWM. In AΣΔM-based and AAΣΔM-based multi-level modulations, the inband error due to improper encoding is almost independent of the number of levels N.

5.6.4 Underswitching

The inband performance of these three modulations at OSwRs below 1 (underswitching) should be evaluated according to the inband spectral power density of the error signal $E(f)$ and not according to the error signal's inband power $P^{\mathrm{i}}_{e(t)}$, since the content around the switching frequency masks the baseband content.

Therefore, despite in figures 5.25 (N-PWM), 5.26 (N-AΣΔM) and 5.27 (N-AAΣΔM) the performance of these three modulations is similar in terms of the error signal's inband power $P^{\mathrm{i}}_{e(t)}$, the inband performance in terms of spectral power density of the error signal $E(f)$ of N-AΣΔM is better than that of N-PWM and N-AAΣΔM if underswitching. Similarly to the 2-level case, N-AΣΔM tracks the baseband content of the reference signal with small error (see figure 5.28), whereas in N-PWM the inband error spectral power density is almost constant (like in the 2-level case). The performance of N-AAΣΔM is strongly determined by the control for astable operation which, in this case, degrades the inband tracking performance.

In N-PWM (without latch) and N-AAΣΔM, the OSwR cannot be arbitrarily reduced. Certainly, because of extra switching in N-PWM, the reference signal intersects the carriers $c_i(t)$ more than once per encoding interval and hence the frequency of the N-PWM switching signal is not the same than the carrier's (in figure 5.25 a latch has been included so that extra switching is avoided, yet the inband tracking performance is degraded). Similarly, in N-AAΣΔM, despite the hysteresis-width function $\delta(t)$ can be scaled by a large factor, it locally tends to 0 whenever the reference signal $x(t)$ crosses over an output voltage level L_i. Provided that the reference signal $x(t)$ is not constant, this reduction yields a very high probability of triggering the comparator.

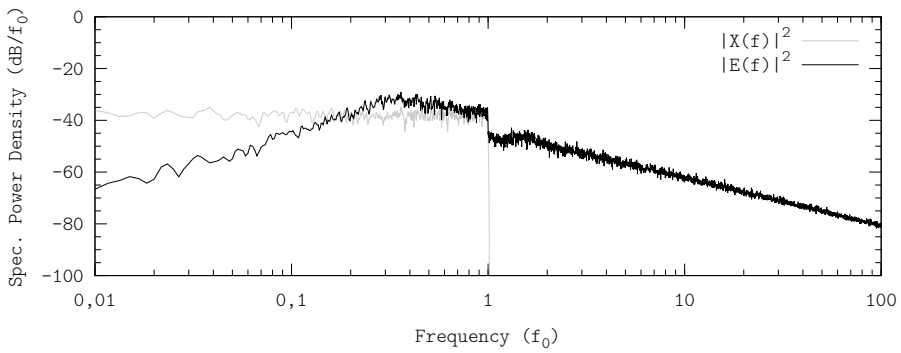

Figure 5.28: Underswitching in N-AΣΔM. Example showing a 7-AΣΔM tracking a bandlimited signal at an OSwR of 0,36. Simulation performed using the configuration D.4.1.

Chapter 6

Decoding Switching Signals

This chapter analyses the decoding process in switching amplifiers, i.e. the process of recovering a continuous-time continuous-amplitude signal from a switching signal. This process typically consists in filtering the baseband content of the power switching signal; different techniques to improve this process are analysed, including high-order filtering, cutoff frequency optimisation and pre-equalisation. Nevertheless, in accordance with the extended modelling of multi-level converters presented chapter 5, the decoding process in switching amplifiers also consists in translating the switching signal (i.e. the modulator's output signal) into a set of switch-driving signals; this chapter also explores the feasibility of improving the amplifier's decoding process by enhancing the logic translation of the switching signal.

6.1 Baseband Signal Recovering

According to the encoding-decoding interpretation of buck-based switching amplifiers presented in chapters 2 and 5, once the reference signal $x(t)$ is encoded into an N-level switching signal $z(t)$, it is power amplified by the switches of the switching power converter, thereby generating an N-level power switching signal $\tilde{z}(t)$ (with regard to time-domain waveforms, this power-amplification process is just a scaling factor G). The power switching signal $\tilde{z}(t)$ is subsequently filtered by a low-pass filter $H(s)$, also part of the switching power converter, thus recovering $\tilde{x}(t)$, a power-amplified distorted version of the reference signal $x(t)$.

The preferred converter topologies for switching amplifiers are the linear ones, i.e. those in which the control-to-output DC static characteristic is linear, typically buck-derived topologies (buck and full-bridge, either 2-level or multi-level). This section characterises the low-pass filtering process performed by linear switching power converters, i.e. the process of recovering the inband content of the power switching signal $\tilde{z}(t)$ by rejecting its outband content. The different techniques herein presented are hence intended for buck-based converters, although some of them are not limited to these particular topologies.

6.1.1 Ideal Low-Pass Filters

Ideally, in the context of buck-based switching amplifiers (band separation), the encoding process should consist in adding a f_0-high-pass error signal $e(t)$ to the

f_0-bandlimited signal $x(t)$ to shape it into the switching signal $z(t)$ (inband-error-free encoding); likewise, ideally, the decoding process should perform the opposite operation. Therefore, perfect decoding, i.e. the process performed by an ideal low-pass filter $H_{\mathrm{i}}(f)$, consists in completely rejecting the outband content of the power switching signal $\tilde{z}(t)$ whilst leaving its inband content unaltered.

Perfect decoding combined with inband-error-free encoding (and a non-distorting or G-scaling power-amplification process) yields perfect signal tracking and power amplification.

$$\tilde{x}(t) = Gx(t), \qquad \forall t \in \mathbb{R} \tag{6.1}$$

Certainly, let us assume a certain switching signal $z(t)$, either two-level or multi-level, inband-error-free tracking a f_0-bandlimited signal $x(t)$; if the power-amplification process is ideal (a linear scaling factor G), the power switching signal $\tilde{Z}(f)$ is

$$\tilde{Z}(f) = GZ(f) = \begin{cases} GX(f), & |f| \leq f_0 \\ GE(f), & |f| > f_0 \end{cases} \tag{6.2}$$

An ideal low-pass filter $H_{\mathrm{i}}(f)$ completely rejects the outband content, in this case the power error signal $GE(t)$, and leaves the inband content unaltered. The recovered signal $\tilde{X}(f)$ is hence a power-amplified version of the reference signal $X(f)$.

$$\tilde{X}(f) = H_{\mathrm{i}}(f)GZ(f) = \begin{cases} GX(f), & |f| \leq f_0 \\ 0, & |f| > f_0 \end{cases} \tag{6.3}$$

From the previous expressions, it follows that the frequency response of an ideal low-pass filter $H_{\mathrm{i}}(f)$ has unitary bandpass gain and infinite stopband rejection.

$$H_{\mathrm{i}}(f) = \begin{cases} 1, & |f| \leq f_0 \\ 0, & |f| > f_0 \end{cases} \tag{6.4}$$

Because of the high selectivity, this filter is often referred as "brick-wall filter" in the literature. Note that an ideal filter does not need to be necessarily lossless, e.g. the outband content could be dissipated $P_{\tilde{x}(t)} < P_{\tilde{z}(t)}$.

The concept of ideal filter can be generalised to other transfer functions such as high-pass or bandpass; all ideal filters have unitary bandpass gain and full rejection in the stopband. Unfortunately, ideal filters are not implementable.

In the context of power processing and switching amplifiers, filters should be implementable and lossless (except for stray resistances and other non-idealities). These constraints reduce the possible implementations of the low-pass filter to Linear Time Invariant (LTI) low-pass filters.

6.1.2 Lossless Linear Time Invariant Filters

Pure reactive or lossless Linear Time Invariant (LTI) filters consist of, exclusively, inductances and capacitances (non-resistive opposition to the passage of current). Different layouts of the reactive components yield different transfer functions, although the most common arrangement in switching amplifiers is the LC ladder layout for voltage-supplied filters (as figure 6.1 shows).

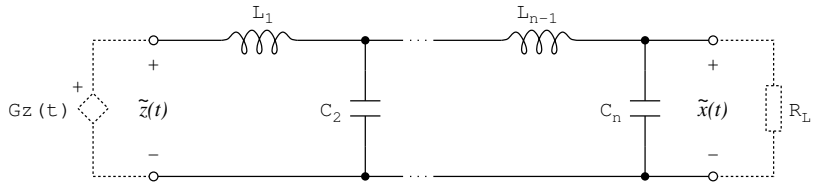

Figure 6.1: Lossless nth order low-pass LTI filter (LC ladder layout). In dotted lines, the load R_{L} and the supply $Gz(t)$, which models the power supply and the switches of the power converter.

The filter transfer function $H(s)$ depends upon all reactive components L_i, C_j, $i, j \in \mathbb{N}$, $i, j \leq n$ with i odd and j even, where n is the order of the filter, and upon the load R_{L}.

$$H(s) = f(L_i, C_j, R_{\mathrm{L}}), \quad i, j \in \mathbb{N},\ i, j \leq n,\ i \text{ even}, j \text{ odd} \tag{6.5}$$

Compared to ideal filters, neither the bandpass gain of LTI filters is constant nor their stopband rejection is infinite; these deficiencies result in a certain remaining error signal $\xi(t)$, extending both inband and outband, as discussed in section 2.3.2. On the other hand, due to the absence of passive components, pure reactive LTI filters are lossless and hence all power supplied by the power supply $P_{\tilde{z}(t)}$ is delivered to the load $P_{\tilde{x}(t)}$ (100 % of efficiency).

Unfortunately pure inductances and pure capacitances are ideal devices. Coils and actual capacitors are made of actual materials, whose conductivity is finite (effectively, it results in a series resistance); furthermore there are other effects which can also be modeled as a series resistance. As a first-order approach, each actual reactive component can be modeled as a pure reactive component with its corresponding ESR encompassing all losses mechanisms.

There are other effects which further modify the transfer function of the implemented LTI filters, such as the stray capacitance in soldering pads or the wiring between devices. These inductive and capacitive effects can also be added to the model, resulting in a more complex transfer function (yet still corresponding to a low-pass filter in the frequency range of interest).

Lossless LTI filters are hence not implementable, although, depending on the operating conditions, the effects due to these non-idealities are not significant and can be neglected. The most common low-pass filters in switching regulators, and also in switching amplifiers, are the second-order ones (one inductor and one capacitor) with maximally flat inband response (Butterworth-kind transfer functions). In general, the order of the low-pass filter can be higher and both the transfer function $H(s)$ and the cutoff frequency f_{c} (defined as the frequency in which the gain reduces by 3 dB) are design parameters.

6.1.3 High-Order Filter Extension in Buck-Based Converters

The stopband rejection of Butterworth filters is determined by their order n. Given that second-order filters are the most common, a feasible way to increase the stopband rejection of these converters, whilst keeping the linear control-to-output DC static characteristic, consists in increasing the order n of the filter (high-order filter converter topologies).

This high-order extension does not affect the operating performance of the switching power converter, i.e. the control-to-output DC static characteristic of high-order variants of the buck and the full-bridge topologies are linear as well. The only difference is that the converter's output signal is further filtered before being delivered to the load, with all its inband and outband consequences upon the output signal (as discussed in section 2.3.2).

Let us assume a buck-based topology (depicted in figure 6.1) with maximally flat inband response $H_{\mathrm{B}}(j\omega)$ (Butterworth filter, the most common configuration in switching amplifiers) with cutoff frequency ω_{c}; the specifications require minimising the power of the remaining error signal $P_{\xi(t)}$ in the recovered signal $\tilde{x}(t)$. By increasing the filter's order n, the module of the transfer function tends to that of an ideal filter: unitary bandpass gain and infinite stopband rejection.

$$\lim_{n\to+\infty} |H_{\mathrm{B}}(j\omega)| \to \begin{cases} 1 & |\omega| \leq \omega_{\mathrm{c}} \\ 0 & |\omega| > \omega_{\mathrm{c}} \end{cases} \tag{6.6}$$

Nevertheless, as the order n increases, the inband phase lag becomes less rectilinear, thus resulting in a wider non-constant group delay (increased inband error, see figure 6.2). In common applications using second-order filter converter topologies, amplitude errors dominate over phase errors; therefore, increasing the filter's order may yield tracking error improvements (a reduction of the amplitude error at the cost of increasing the inband phase error, i.e. balancing both errors). However, the filter's order n cannot be indefinitely increased, since beyond a certain filter's order, the inband phase errors dominate over amplitude errors and therefore further increasing the filter's order only degrades the recovering process.

Still, high-order filtering adds another degree of freedom in the decoding process and hence high-order converter topologies are candidates of interest to address the efficiency-distortion trade-off of switching amplifiers, especially if optimising the cutoff frequency (as described in section 6.1.4).

Transfer Function Analysis

The extension to high-order filter topologies unfolds a new design variable, shaping the filter's transfer function $H(s)$. With second-order filters it is already possible to shape the filter's transfer function, but as the filter's order n increases, the difference between different transfer functions becomes more significant.

Instead of shaping the filter with the typical maximally flat inband response (Butterworth filters), the filter can be shaped to alternative frequency responses (e.g. Chebyshev) to increase the filter's selectivity. The same stopband rejection may be achieved with a higher cutoff frequency f_{c} which, in the context of switching amplifiers for handheld and portable applications, may involve smaller and lighter reactive components.

A common requirement for the module of the filter's transfer function $H(s)$ is to asymptotically tend to zero at high frequency, so that spikes and other spread-frequency effects are attenuated.

$$\lim_{\omega\to+\infty} |H(j\omega)| \to 0 \tag{6.7}$$

This constraint reduces the transfer function candidates to Butterworth filters, Chebyshev (or type I Chebyshev) filters, Elliptic filters and Bessel filters.

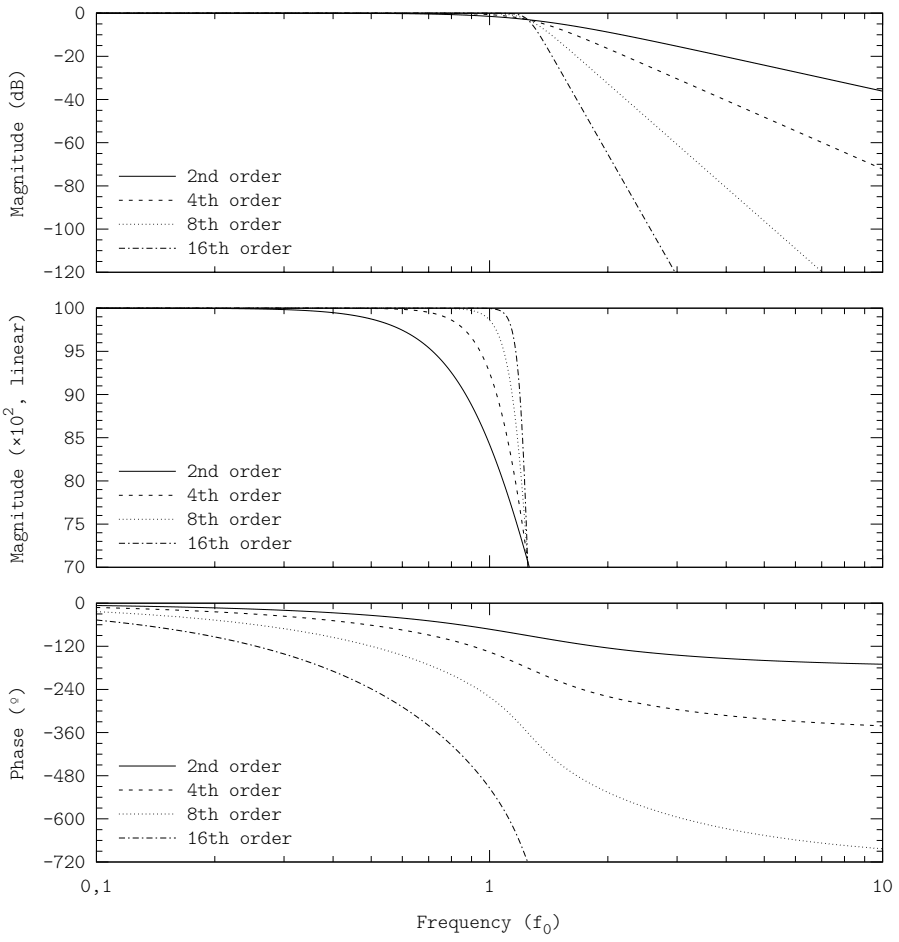

Figure 6.2: Bode plots of different Butterworth filters of different orders, all of them with the same cutoff frequency $f_c = 1{,}25 f_0$. Displayed plots show the module (upper plot), a detail of the inband magnitude in linear scale (middle plot) and the phase (lower plot).

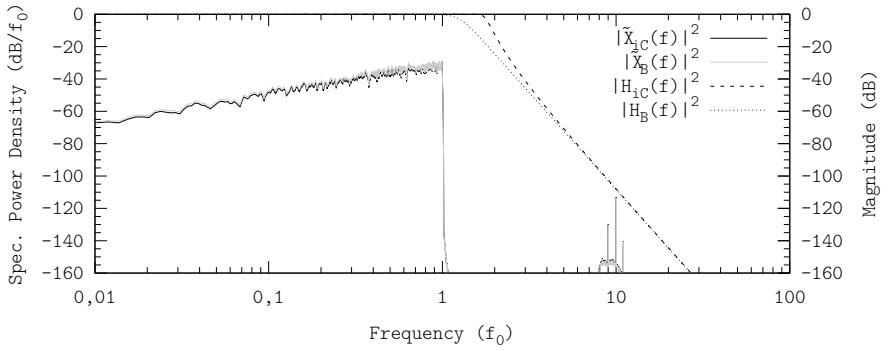

Figure 6.3: Bode plot of two sixth-order filters: Butterworth ($f_c = 1{,}25 f_0$, displayed with a B subscript) and inverse Chebyshev ($f_c = 1{,}63 f_0$ and inband ripple of 0,1 dB, displayed with a C subscript). Example showing a 2-PWM tracking a f_0-bandlimited signal at an OSwR of 10. Simulation performed using the configuration D.4.1.

The transfer function of odd-order inverse Chebyshev (or type II Chebyshev) filters also tends to zero as frequency increases, although at a slower rate and with non-monotonous stopband rejection.

Butterworth filters are generally used because of its maximally flat inband response, targeting to emulate the inband behaviour of ideal filters, as the fidelity in the decoding process is very sensitive to inband ripples. Despite the inband response of Bessel filters is also constant, Butterworth filters are generally preferred because of their higher selectivity.

However, if the order n is high enough, low inband ripples in Chebyshev filters may be feasible. For instance, consider the example of figure 6.3: a switching amplifier based on a 2-PWM tracking a f_0-bandlimited signal $x(t)$ at an OSwR of 10 and decoding with a sixth order filter. By replacing the classical Butterworth filter by a Chebyshev filter (0,1 dB of inband ripple[1], $f_c = 1{,}63 f_0$), the cutoff frequency f_c can be increased from $f_c = 1{,}25 f_0$ to $f_c = 1{,}65 f_0$ and still achieve a similar rejection around the switching frequency f_s ($10 f_0$ in this case). Moreover the power of the remaining error signal $P_{\xi(t)}$ decreases by 6 %, mostly because the better inband behaviour.

Nevertheless, the optimisation of the filter's order and transfer function is very specific for each application and specifications. Different filter transfer functions are not going to be characterised in this work. In what follows, all low-pass filters are going to be assumed Butterworth-kind unless otherwise stated.

High-Order Filter Extension in Other Converter Topologies

Any switching power converter topology can be extended to higher orders by adding an LC ladder filter before the load. For instance, figure 6.4 shows a fourth-order boost converter, consisting of a regular second-order boost converter with an additional second-order LC ladder before the load R_L.

In this case, the additional LC ladder is grounded because so is the converter topology; in floating-output topologies, such as full-bridge, the additional LC

[1] This value is just an example; the full design-space exploration should consider optimising the inband ripple as well.

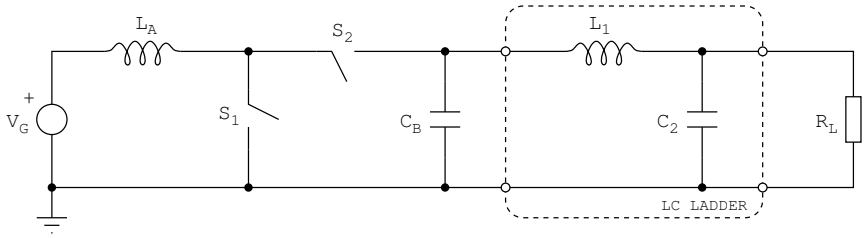

Figure 6.4: Fourth-order boost converter, consisting of a regular second-order boost converter with an additional second-order LC ladder before the filter.

filter floats (only the differential-mode voltage is filtered). Alternatively, in floating-output topologies, a grounded LC filter can be added at the input port of the floating load to filter both the differential- and the common-mode voltages (more precisely, two grounded LC filters must be added, one at each end of the input port; a further discussion about common-mode and differential-mode voltages and filters is included in section 7.5.5).

In non-linear converter topologies such as boost, the additional LC ladder also further filters the output signal before being delivered to the load, thereby yielding a high-order low-pass control-to-output transfer function (non-linear as so is the control-to-output DC static characteristic of the converter without the LC ladder). If properly designed, it is feasible to model the resulting high-order transfer function.

6.1.4 Filter's Cutoff Frequency Optimisation

Actual switching amplifiers consist of an actual modulator and a buck-based switching converter (i.e. a LTI filter). Generally, actual modulators do not perform inband-error-free encoding; likewise, LTI filters suffer from inband attenuation and finite stopband rejection. Therefore, even if the OSwR (modulator) and the filter's order n are set, due to the smooth transition between bandpass and stopband of the filter's transfer function $H(s)$, the filter's cutoff frequency f_c must be tuned so that the amplifier's performance is optimised.

Let us consider an example, an amplifier which must be optimised to minimise the remaining error signal's power $P_{\xi(t)}$, i.e. the power of the error signal after filtering (this example corresponds to minimising the power provided by the linear amplifier in a linear-assisted power amplifier). The design is based on an ideal modulator, inband-error-free tracking the reference signal $x(t)$ at an OSwR of 2.

In order to reject the outband spectral content of the power switching signal $\tilde{Z}(f)$, i.e. the modulation harmonics, the filter's cutoff frequency f_c should be set to a low value; in this way, the outband power of the remaining error signal $\Xi(f)$ is reduced. However, if the filter's cutoff frequency f_c is too low, the inband content of the power switching signal $\tilde{Z}(f)$, i.e. the information to track and power amplify, will be partially rejected by the filter, thereby increasing the inband power of the remaining error signal $\Xi(f)$. In this case, the recovered signal $\tilde{x}(t)$ only tracks the baseband content of the reference signal $x(t)$ (baseband-tracking approximation).

On the other hand, in order to preserve the original information as much as

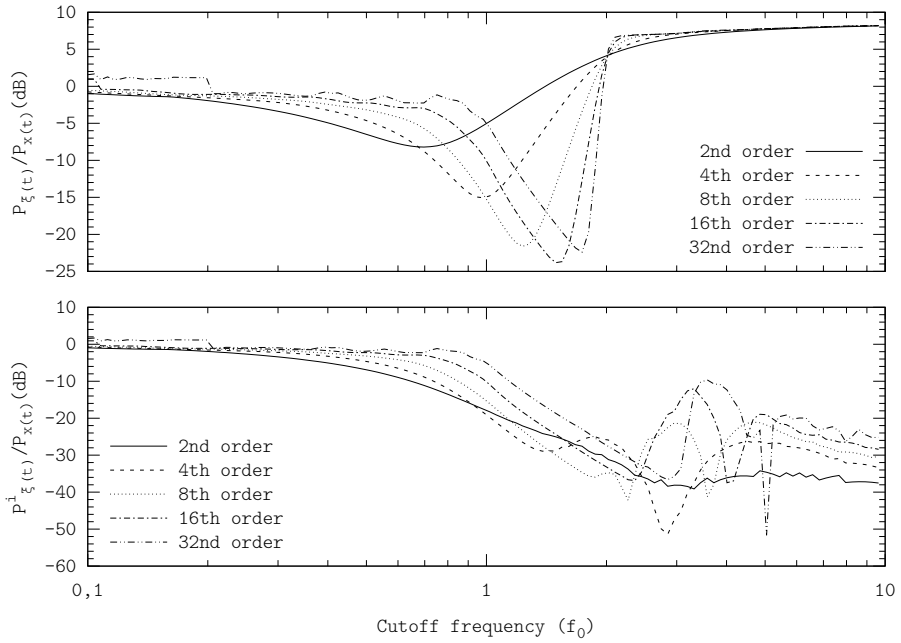

Figure 6.5: Filter's cutoff frequency optimisation for minimum remaining error signal's power $P_{\xi(t)}$ (upper plot); the lower plot shows the remaining error signal's inband power $P^{\mathrm{i}}_{\xi(t)}$. Example optimising Butterworth filters for a f_0-bandlimited reference signal inband-error-free encoded at an OSwR of 2. Simulation performed using the configuration D.4.6.

possible, the filter's cutoff frequency f_c should be set to a high value, to avoid attenuating the inband content of the power switching signal $\tilde{Z}(f)$. However, if the filter's cutoff frequency f_c is too high, the high frequency spectral content of the power switching signal $\tilde{Z}(f)$ will not be rejected by the filter, thereby increasing the outband power of the remaining error signal $\Xi(f)$. In this case the recovered signal $\tilde{x}(t)$ contains modulation outband harmonics.

Therefore, there exists a trade-off in the design of the filter's cutoff frequency f_c. The optimum solution depends upon the operating conditions, the specifications and the FoM to minimise or maximise. This trade-off can be characterised by sweeping different filter's cutoff frequencies f_c, from very low frequencies up to frequencies beyond the switching frequency; the optimum cutoff frequency corresponds to an intermediate frequency.

In the conditions of this example, figure 6.5 shows the full design-space characterisation of the filter's cutoff frequency for filters of different order n (the delay due to the LTI filter has been equalised by cross-correlating the reference signal $x(t)$ and the recovered signal $\tilde{x}(t)$ before evaluating the power of the remaining error signal). Both opposite trends, baseband-tracking approximation and partially recovering the modulation outband content, become more evident as the filter's order n increases (the transition between trends sharpens).

Figure 6.5 also splits the inband power of the remaining error signal $P^{\mathrm{i}}_{\xi(t)}$. If the cutoff frequency f_c is much lower than the reference signal's bandwidth

f_0, the inband error power $P^{\mathrm{i}}_{\xi(t)}$ dominates over the outband error power $P^{\mathrm{o}}_{\xi(t)}$ (baseband-tracking approximation).

$$P^{\mathrm{o}}_{\xi(t)} \ll P^{\mathrm{i}}_{\xi(t)} \approx P_{\xi(t)}, \qquad f_{\mathrm{c}} \ll f_0 \tag{6.8}$$

On the other hand, if the filter's cutoff frequency f_{c} is much higher than the modulator's switching frequency $f_{\mathrm{s}} = \mathrm{OSwR} f_0$, the outband error power dominates over the inband error power (recovering modulation outband harmonics).

$$P^{\mathrm{i}}_{\xi(t)} \ll P^{\mathrm{o}}_{\xi(t)} \approx P_{\xi(t)}, \qquad f_{\mathrm{c}} \gg f_{\mathrm{s}} = \mathrm{OSwR} f_0 \tag{6.9}$$

Beyond the optimum cutoff frequency, the inband error power no longer monotonously decreases because the correlator minimises the total power of the remaining error signal $P_{\xi(t)}$, which, with high cutoff frequencies, is mainly determined by the outband power $P^{\mathrm{o}}_{\xi(\mathrm{t})}$ (beyond the optimum cutoff frequency, the outband power monotonously increases).

Figure 6.5 also illustrates the issues due to high-order filters (the inband performance of very-high order filters do not tend to that of an ideal filter). Indeed, as the filter's order n increases, so does the optimum filter's cutoff frequency f_{c}. This is a consequence of the increased inband error due to the non-rectilinear the phase lag; by shifting the cutoff frequency to higher frequencies, the non-rectilinear phase lag is partially avoided. However, whilst the (non-rectilinear) phase lag increases proportionally to the filter's order, the filter's optimum cutoff frequency asymptotically tends to the switching frequency f_{s}, $2f_0$ in this example (the filter's cutoff frequency f_{c} should no be increased beyond the switching frequency f_{s}, otherwise modulation harmonics would be recovered as well). After a certain filter's order n, if further increasing the filter's order, the increased inband error due to the non-rectilinear phase lag cannot be compensated by shifting the filter's cutoff frequency f_{c} to higher frequencies and hence the remaining signal's error power $P_{\xi(t)}$ starts increasing. Therefore, if optimising the filter's cutoff frequency f_{c} for each filter's order n, a finite optimum filter's order will be found.

6.1.5 Equalisation of Linear Time Invariant Filters

The inband error due to LTI filters can be equalised by pre-emphasising or pre-equalising the amplifier's input signal $x_{\mathrm{i}}(t)$, as figure 6.6 shows. Certainly, if the reference signal $x(t)$ is generated as

$$x(t) = x_{\mathrm{i}}(t) * h^{-1}(t) \tag{6.10}$$

where $h^{-1}(t)$ denotes the LTI filter's inverted impulse response, then the recovered signal $\tilde{x}(t)$ becomes

$$\tilde{x}(t) = \tilde{z}(t) * h(t) = Gx(t) * h(t) + \xi(t) \tag{6.11}$$

and hence

$$\tilde{x}(t) = G(x_{\mathrm{i}}(t) * h^{-1}(t) * h(t)) + \xi_{\mathrm{i}}(t) = Gx_{\mathrm{i}}(t) + \xi_{\mathrm{i}}(t) \tag{6.12}$$

where $\xi_{\mathrm{i}}(t)$ stands for the remaining error signal when tracking the amplifier's input signal $x_{\mathrm{i}}(t)$.

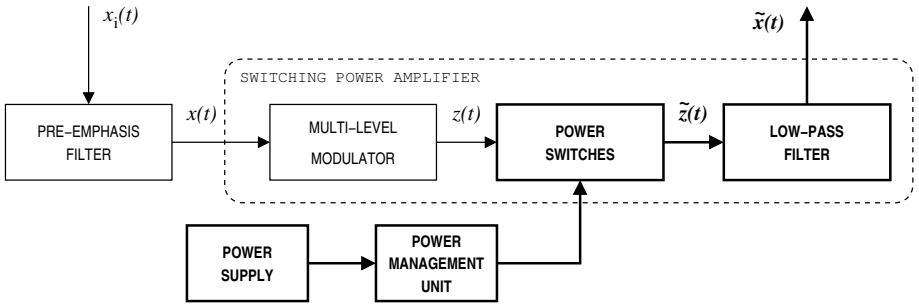

Figure 6.6: Block diagram of a switching amplifier with pre-equalisation. The power path is highlighted in bold.

In the particular case of inband-error-free encoding, the inband content of the remaining error signal $\Xi(f)$ is zero and therefore the inband content of the recovered signal $\tilde{X}(f)$ tracks the amplifier's input signal $X_\mathrm{i}(f)$ with no error despite the non-constant filter's inband response.

Nevertheless, perfect pre-emphasis of LTI filters is not possible. Certainly, an implementable low-pass transfer function $H(s)$ has more poles than zeros.

$$H(s) = \frac{\sum_{i=0}^{n} a_i s^i}{\sum_{i=0}^{m} b_i s^i}, \qquad n < m, m, n \in \mathbb{N} \tag{6.13}$$

Ideal or perfect pre-equalisation consists in inverting the transfer function

$$H^{-1}(s) = \frac{\sum_{i=0}^{m} b_i s^i}{\sum_{i=0}^{n} a_i s^i}, \qquad n < m,\ m, n \in \mathbb{N} \tag{6.14}$$

leading to an improper transfer function (more zeroes than poles, i.e. the out-band gain tends to infinite as the frequency increases).

This non-implementable high-pass transfer function can be approximated by an implementable low-pass transfer function $H_\mathrm{PRE}(s)$, by adding, at least, $n-m$ far-apart poles p_i. Due to practical and implementation limitations, these poles are typically one decade above the filter's cutoff frequency f_c.

$$H_\mathrm{PRE}(s) = \frac{\sum_{i=0}^{m} b_i s^i}{\sum_{i=0}^{n} a_i s^i} \frac{1}{\prod_{j=n-m}^{k} 1 + \frac{s}{p_j}}, \quad n < m,\ k \geq n-m,\ k, m, n \in \mathbb{N} \tag{6.15}$$

Therefore, even with pre-equalisation, the reference signal is affected by an equivalent low-pass transfer function $H_\mathrm{e}(s)$. Note that its order is independent

of the low-pass filter's order n.

$$H_{\mathrm{e}}(s) := H_{\mathrm{PRE}}(s)H(s) = \frac{1}{\prod_{i=n-m}^{k} 1 + \frac{s}{p_i}}, \qquad k \in \mathbb{N} \tag{6.16}$$

Despite the poles p_i are outband, this equivalent low-pass transfer function results in a certain inband error, as discussed in section 2.3.2. Even assuming that amplitude and phase errors are not significant, the recovered signal $\tilde{x}(t)$ is delayed with respect to the input signal $x_{\mathrm{i}}(t)$.

$$\tilde{x}(t) = Gx_{\mathrm{i}}(t) * h_{\mathrm{inv}}(t) * h(t) + \xi(t) \approx Gx_{\mathrm{i}}(t - \sigma) \tag{6.17}$$

This time delay σ is smaller than the time delay of the amplifier's output filter τ, since the cutoff frequency of the equivalent filter $H_{\mathrm{e}}(s)$ is higher than that of the amplifier's output filter $H(s)$. Furthermore, the order n of the amplifier's output filter may be high (and hence the time delay τ may be high as well), but the order of the equivalent filter is only determined by the far-apart poles p_i.

Let us consider an example of pre-equalisation, a second-order Butterworth filter with cutoff frequency $f_{\mathrm{c}} = 1{,}25 f_0$ (a typical filter in audio applications). The pre-emphasis filter includes two far-apart poles $p_{1,2}$, one decade beyond the filter's cutoff frequency. To emphasise the inband effects upon the amplifier's input signal $x_{\mathrm{i}}(t)$, let us consider inbnad-error-free encoding or, equivalently in terms of inband behaviour, no modulation (the amplifier's input signal $x_{\mathrm{i}}(t)$ is pre-emphasised, yielding the reference signal $x(t)$, and subsequently low-pass filtered thus recovering $\tilde{x}(t)$). The input signal $x_{\mathrm{i}}(t)$ is f_0-bandlimited.

As figure 6.7 shows, the inband attenuation of the equivalent transfer function corresponding to this example is below 0,1 dB. The inband group delay is not constant either; its variation with respect to the group delay at low frequencies $-\mathrm{d}\angle H_{\mathrm{PRE}}(jw)/\mathrm{d}\omega$ is wider than 0,6 %. Even if equalising the phase delay (cross-correlation between the amplifier's input signal $x_{\mathrm{i}}(t)$ and the recovered signal $\tilde{x}(t)$), the inband content of the remaining error signal $\Xi(f)$ is only 40 dB below the input signal's level.

Actual filters are made with coils and actual capacitors, with their respective ESR; furthermore, all components have some tolerance and not all values are available. Therefore, the actual transfer function to equalise is not shaped to any of these variants and is more complex than a pure LC ladder. Nonetheless, pre-equalisation can still be used to reduce the tracking error, by experimentally tuning the pre-emphasis filter until the error (or the corresponding FoM) is minimised. This technique has successfully been applied to wireless transmitters [7].

6.2 Enhanced Decoding Logic and Switching Policy

The modulator's output signal $z(t)$, a low-power multi-level switching signal, must be translated into a set of switch-driving signals $s_i(t)$ in order to drive the switching power converter, one for each switch, as discussed in section 5.1;

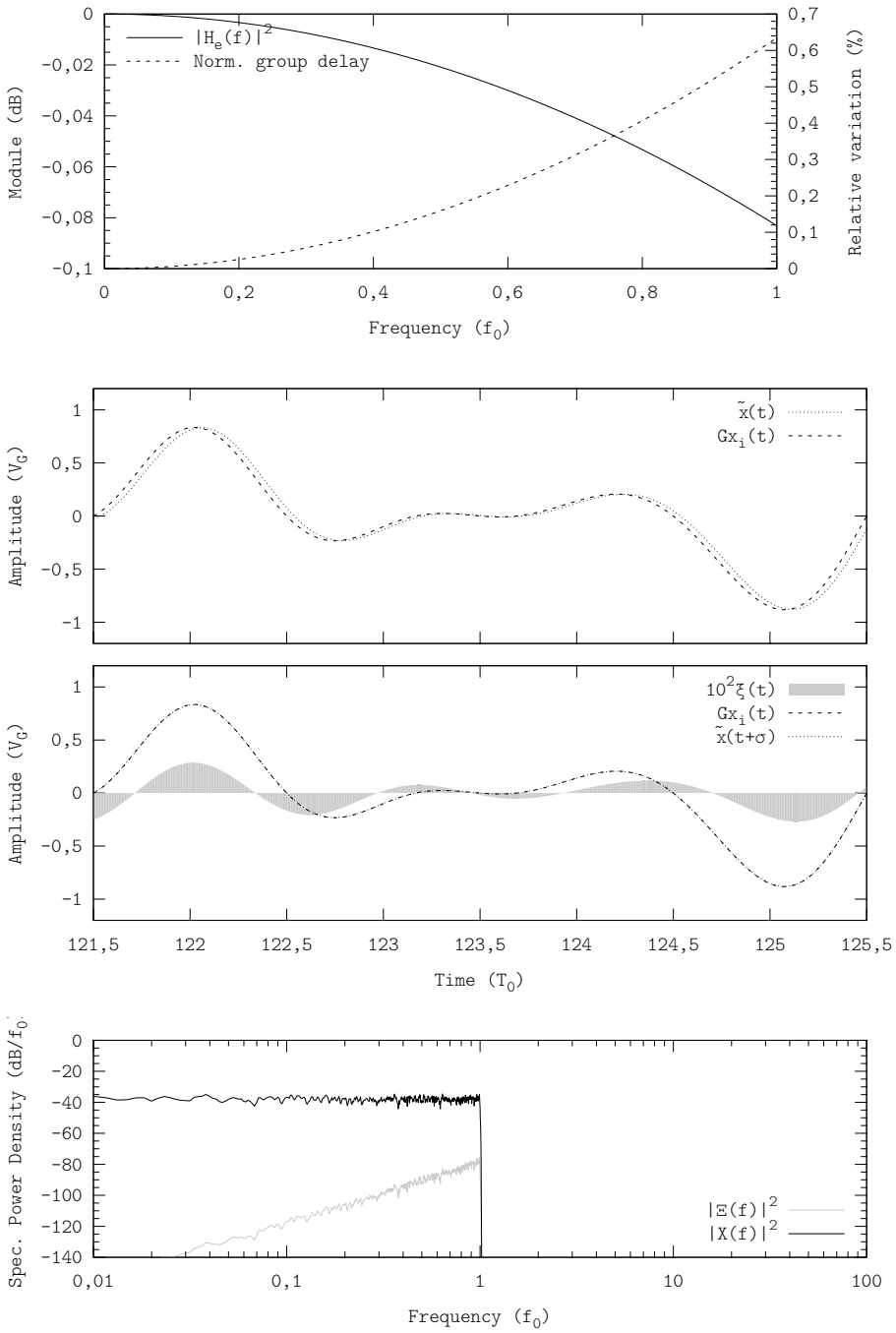

Figure 6.7: Pre-equalisation of a second-order Butterworth filter (cutoff frequency $1{,}25 f_0$). Showing a detail of the equivalent transfer function (the group delay is displayed as relative variation with respect to the group delay at very low frequencies, upper plot), the time-domain waveforms (without equalising and equalising the filter's delay σ, the two middle plots respectively) and the frequency-domain waveforms of the cross-correlated signals (lower plot). Simulation performed using the configuration D.4.1.

this translation can be constrained by a switching policy. Both the decoding logic and the switching policy can be upgraded to achieve additional features in switching amplifiers. Enhanced decoding logics and enhanced switching policies are commonly used together, since usually one requires the other one to take advantage of any them.

This section proposes an enhanced switching policy for multi-level full-bridge switching power converters, which incorporates the voltage difference between supply voltages (assuming voltage-input converters) in order to maximise the number of output voltage levels L_i for a given set of supply voltages and connection switches.

This section also proposes an enhanced decoding logic for 3-level full-bridge converters. This logic allows shaping the common-mode of the converter's output without adding power resources nor affecting the operation of the modulator (i.e. the 3-level modulation and the OSwR).

6.2.1 Output Levels Maximisation

The purpose of this policy is to maximise the number of available distinct output levels L_i for the generation of the power switching signal $\tilde{z}(t)$, targeting switching amplifiers based on multi-level full-bridge converters.

Most consumer-electronic devices include a power-management unit which provides several supply voltages V_i. It is possible to take advantage of these voltages to generate a multi-level power switching signal $\tilde{z}(t)$; by incorporating this policy, it is possible to take further advantage of all the already available power resources by generating a multi-level power switching signal $\tilde{z}(t)$ comprising more levels than the number of available supply voltages. Inversely, this policy can also be used to minimise the amount of power resources (supply voltages and connection switches) required to generate a power switching signal $\tilde{z}(t)$ with a specified number of levels.

Conventional Switching Policy

Let us consider a multi-level full-bridge converter supplied by $N + 2$ supply voltages, GND and V_i with $i = 0, \ldots, N$ and $i \in \mathbb{N}$ (see figure 6.8). The multi-level power switching signal $\tilde{z}(t)$ is typically generated by driving one end of the output filter's input port to GND and the other of the available supply voltages V_i or GND (conventional switching policy).

Using this conventional switching policy, the multi-level power switching signal $\tilde{z}(t)$ comprises twice the number of available voltage levels V_i plus three. The first power supply provides two supply voltages GND and V_0, which allow generating the levels of value $\pm V_0$ and 0; each additional power supply provides one additional supply voltage V_i, which allows generating two additional voltage levels of value $\pm V_i$. Therefore, by using this conventional policy and given an $N + 2$ supply voltages, the maximum number of distinct levels N_{conv} in the power switching signal $\tilde{z}(t)$ is

$$N_{\text{conv}} = 2N + 3 \tag{6.18}$$

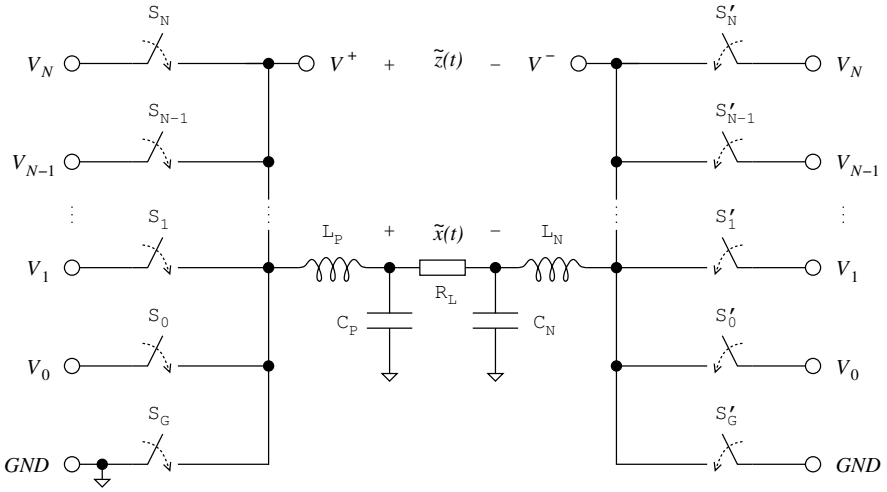

Figure 6.8: Multi-level full-bridge converter. Example with $N+2$ supply voltages (a power supply providing GND, V_0 plus N additional supply voltages V_i).

Enhanced Switching Policy

Because of the two subsets of switches, it is possible to apply any available supply voltage $GND, V_0, \ldots, V_N$ at each end V^+, V^- of the output filter's input port. By driving both input ends V^+, V^- to an active voltage V_i, it is possible to generate the levels corresponding to the voltage difference between supply voltages, $V_j - V_i$, $i = j$, $i, j \in \mathbb{N}$.

Let us consider an example, a system with four different supply voltages ($N = 2$): V_0, V_1, V_2 and GND. By driving the negative input end V^- of the output filter to GND, the positive input end V^+ can be supplied with GND, V_0, V_1 or V_2, yielding four distinct output voltage levels: $L_6 = GND$, $L_7 = V_0$, $L_{10} = V_1$ and $L_{12} = V_2$. By reversing the polarity (i.e. driving the filter's positive input end V^+ to GND and the negative input end V^- to an active voltage V_i), three additional levels are generated: $L_5 = -V_0$ and $L_2 = -V_1$ and $L_0 = -V_2$ (these levels are generated according to the conventional switching policy).

By employing the proposed policy it is possible to generate six additional levels. Certainly, by driving each input end V^+, V^- of the output filter to an active voltage V_i, it is possible to generate the levels $L_{4,8} = \mp(V_2 - V_1)$, $L_{3,9} = \mp(V_1 - V_0)$ and $L_{1,11} = \mp(V_2 - V_0)$ (enhanced switching policy). If these additional levels are all distinct and if $|V_i - V_j| \neq V_k$ with $i \neq j$ and $i, j, k \in \{0, 1, 2\}$, then the number of distinct output voltage levels in the power switching signal $\tilde{z}(t)$ becomes thirteen (instead of seven with the conventional policy). Table 6.1 summarises the output voltage levels and the active switches in this example, and figure 6.9 illustrates it with time-domain waveforms.

In general, in a multi-level full-bridge topology supplied by $N+2$ supply voltages, the maximum number of distinct output voltage levels N_{enh} in the power switching signal $\tilde{z}(t)$ is

$$N_{\text{enh}} = 1 + \frac{(N+2)!}{N!} \tag{6.19}$$

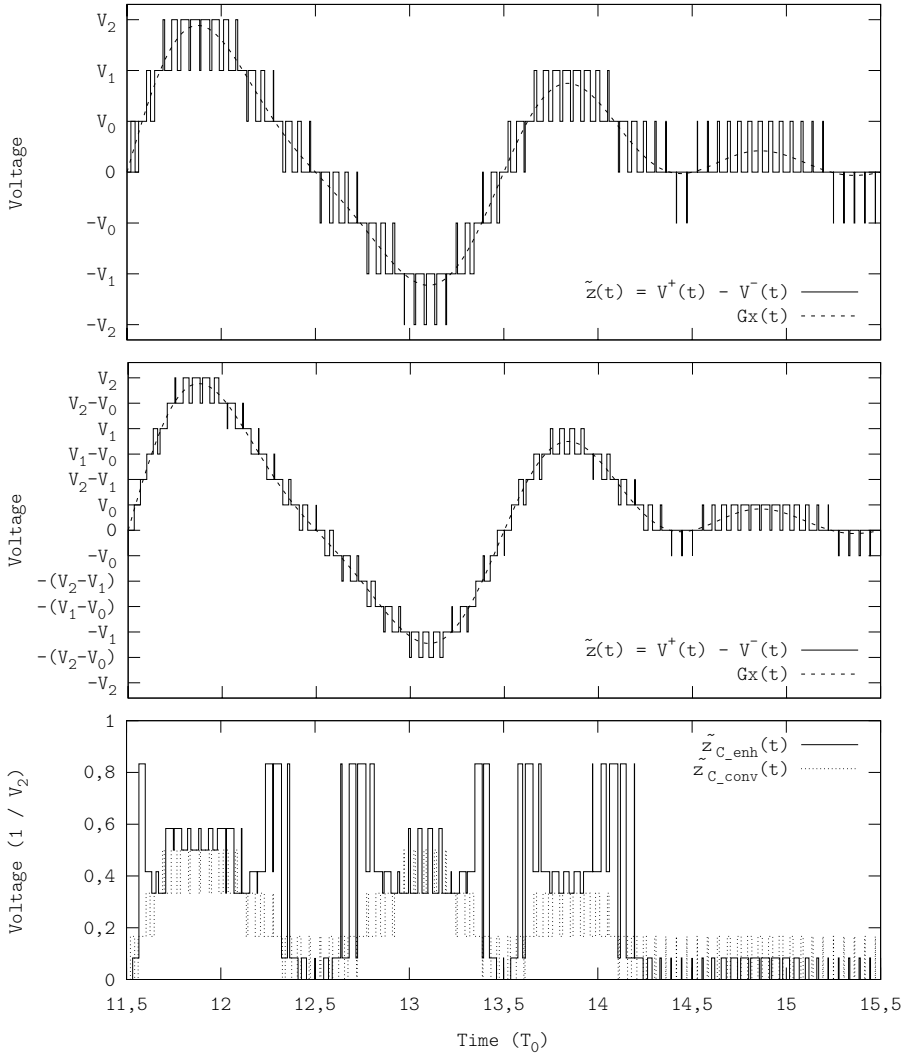

Figure 6.9: Time waveforms comparison between a conventional switching policy (7 levels obtained from 4 supply voltages, upper plot) and an enhanced switching policy (13 levels obtained from 4 supply voltages, middle plot). The voltages V_0 and V_1 are adjusted for each policy so that the output levels L_i are regularly distributed in each case. The lower plot shows the common-mode voltage signals in both cases.

Level	*Active switches*	*Level*	*Active switches*
$L_0 = -V_2$	$S_\mathrm{G}\ S'_2$	$L_{12} = V_2$	$S_2\ S'_\mathrm{G}$
$L_1 = -(V_2 - V_0)$	$S_0\ S'_2$	$L_{11} = V_2 - V_0$	$S_2\ S'_0$
$L_2 = -V_1$	$S_\mathrm{G}\ S'_1$	$L_{10} = V_1$	$S_1\ S'_\mathrm{G}$
$L_3 = -(V_1 - V_0)$	$S_0\ S'_1$	$L_9 = V_1 - V_0$	$S_1\ S'_0$
$L_4 = -(V_2 - V_1)$	$S_1\ S'_2$	$L_8 = V_2 - V_1$	$S_2\ S'_1$
$L_5 = -V_0$	$S_\mathrm{G}\ S'_0$	$L_7 = V_0$	$S_0\ S'_\mathrm{G}$
$L_6 = 0$	$S_\mathrm{G}\ S'_\mathrm{G}$		

Table 6.1: Summary of levels and switches with the enhanced switching policy; example showing a multi-level full-bridge converter supplied from 4 supply voltages. L_6 can also be generated by enabling the switches S_i, S'_i with $i = 0, \ldots, 2$.

Additional supply voltages	$N = 0$	$N = 1$	$N = 2$
Conventional policy	3 (1,0)	5 (0,5 1,0)	7 (0,$\bar{3}$ 0,$\bar{6}$ 1,0)
Proposed policy	3 (1,0)	7 {(0,$\bar{3}$ 1,0) (0,$\bar{6}$ 1,0)	13 (0,1$\bar{6}$ 0,$\bar{6}$ 1,0)

Table 6.2: Maximum number of distinct output voltage levels in a multi-level full-bridge converter using different policies; between brackets, the supply voltages which yield equally distributed output voltage levels (normalised to V_N).

Nevertheless, N_enh will only be achieved if the value of each supply voltage and the value of each voltage difference between any two of the supply voltages are distinct.

$$\begin{cases} V_i > 0 \\ V_i \neq V_j, & i \neq j \\ |V_i - V_j| \neq V_k \end{cases} \tag{6.20}$$

where $i, j, k \in \{0, \ldots, N\} \subset \mathbb{N}$. If the previous set of conditions is not satisfied, the number of effective output voltage levels becomes lower.

Supply Voltages

There are some values of the supply voltages V_i which are particularly interesting, those which yield equally or regularly distributed output voltage levels (the difference between whichever two adjacent levels is the same).

$$L_i - L_{i-1} = L_1 - L_0, \qquad i = \{1, \ldots, N\} \subset \mathbb{N} \tag{6.21}$$

Equally distributed output levels allow simpler modulation schemes. However, it is not possible to satisfy (6.21) for any number of levels. Table 6.2 compares the maximum number of distinct output voltage levels that can be generated with two supply voltages ($N = 0$), with three supply voltages ($N = 1$) and with four supply voltages ($N = 2$), using a conventional policy and the proposed policy (and also the supply voltages that yield equally distributed output levels in the proposed policy).

Drawbacks

The maximisation of the number of voltage levels is achieved at a twofold cost, increasing switching losses and increasing the common-mode output voltage signal $\tilde{z}_{\mathrm{C}}(t)$, defined as

$$\tilde{z}_{\mathrm{C}}(t) := \frac{V^{+}(t) + V^{-}(t)}{2} \tag{6.22}$$

Let us consider again the example of a multi-level full-bridge converter supplied by four different supply voltages $N = 2$. Using a conventional switching policy (seven levels), when switching between adjacent levels (from L_i to either L_{i+1} or L_{i-1}) only one input end of the output filter changes its voltage (i.e. only two switches switch in each switching event).

If using the enhanced switching policy, when switching between certain adjacent levels, e.g. between $L_7 = V_0$ and $L_8 = V_2 - V_1$, both input ends of the output filter V^{+}, V^{-} change its voltage. Four switches switch in those switching events, thereby increasing switching losses.

Also related to the switching losses increase, the voltages at each input end of the input filter V^{+}, V^{-} become more variable; precisely, instead of grounding one end, both are set to an active voltage V_i.

Certainly, if using N additional supply voltages and a conventional switching policy, the maximum common-mode voltage is

$$V_{\mathrm{CM\_1}} = \frac{V_N}{2} \tag{6.23}$$

If normalising to the highest supply voltage, V_N, the maximum becomes 0,5. If using the enhanced policy, the maximum becomes

$$V_{\mathrm{CM\_2}} = \frac{V_N + V_{N-1}}{2} = \frac{1}{2} + \frac{V_{N-1}}{2V_N} \tag{6.24}$$

As the number of additional levels N increases, the relative distance between supply voltages V_i decreases and hence the maximum common-mode voltage tends to 1, double than that with a conventional policy. With one additional supply voltage $N = 1$ and regularly distributed levels (table 6.2), the maximum common-mode increases up to $0{,}\bar{6}$ (33 % of increase) or up to $0{,}8\bar{3}$ (67 % of increase), depending on the supply voltages; with two additional supply voltages and regularly distributed levels (table 6.2), it increases up to $0{,}8\bar{3}$ (67 % of increase). A further discussion about common-mode and differential-mode signals is included in section 7.5.5.

6.2.2 Common-Mode Control in 3-Level Full-Bridge Converters

In multi-level full-bridge converters, more than one converter state may yield the same output voltage level L_i in the power switching signal $\tilde{z}(t)$. By using the proper decoding logic and switching policy, it is feasible to take advantage of this redundancy to shape the spectral power density of the common-mode voltage $\tilde{Z}_{\mathrm{C}}(f)$. Note that this enhanced decoding process affects neither the encoding process nor the amplifier's tracking capabilities; the modulator generates the

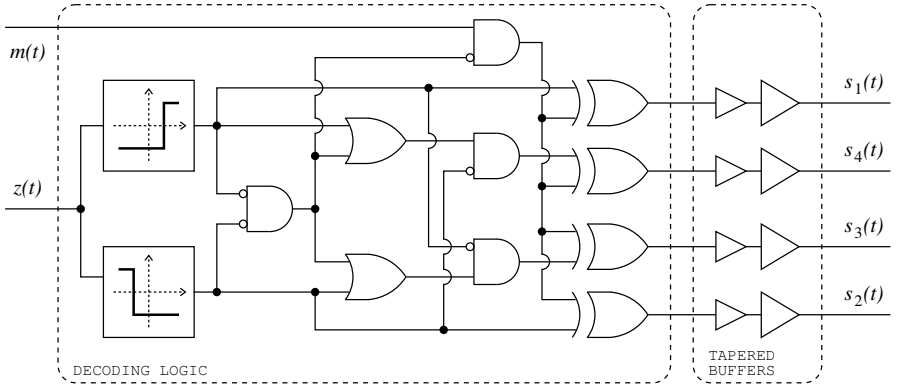

Figure 6.10: Enhanced decoding logic for full-bridge converters driven by 3-level modulations. The signal $m(t)$ can be used to shape the common-mode voltage.

switching signal $z(t)$ regardless of the decoding process and the time waveform of the differential-mode output voltage, i.e. the power switching signal $\tilde{z}(t)$, tracks the switching signal $z(t)$ whatsoever.

Let us consider a simple example, a 3-level full-bridge converter driven by a 3-level switching signal $z(t)$; the levels of this low-power signal are $L'_0 = Z_{\min}$, $L'_1 = Z_{\mathrm{m}}$ and $L'_2 = Z_{\max}$. After the power amplification, these levels are respectively mapped to the voltage levels $L_0 = -V_0$, $L_1 = 0$ and $L_2 = V_0$ in the power switching signal $\tilde{z}(t)$. The generation of the levels $L'_{0,1} = \mp V_0$ is unique; however, the level $L_1 = 0$ can be generated by setting both input ends V^+, V^- of the output filter to GND or to V_0. In order to use this redundancy to shape the common-mode voltage $\tilde{z}_{\mathrm{C}}(t)$, the decoding logic must decode the level L'_1 according to an external signal, namely $m(t)$, which determines how this level is generated (either from GND or from V_0). Figure 6.10 shows a possible circuit to perform this operation. In this case $m(t)$ is a binary signal: a high level decodes L'_1 into V_0 and V_0, whereas a low level decodes L'_1 into GND and GND.

The common-mode voltage signal $\tilde{z}_{\mathrm{C}}(t)$ can be now considered an output variable, which can be partially controlled by the binary control signal $m(t)$. This control signal $m(t)$ should only change its value when the converter is generating either V_0 or $-V_0$, i.e. when the operation of $m(t)$ is disabled. Otherwise the converter would switch between both 0 states when generating the level L_1 (this could be deliberated to further shaping the common-mode signal $z_{\mathrm{C}}(t)$, at the cost of increasing switching losses). The control circuit to drive the signal $m(t)$ can be designed using common control and/or modulation techniques, such as an AΣΔM-based loop.

In order to show indeed that common-mode shaping is feasible, let us consider two representative decoding strategies: always-low (the level L_1 is always generated by driving both input ends V^+, V^- of the output filter to GND) and alternate (L_1 is alternatively generated from GND and from V_0). Figure 6.11 shows the operation in the time domain of both strategies (the switching signal $z(t)$ is generated from a 3-PWM tracking a f_0-bandlimited signal at an OSwR of 10): alternate $\tilde{z}_{\mathrm{C1}}(t)$ and always-low $\tilde{z}_{\mathrm{C2}}(t)$.

The always-low strategy, compared to the alternate strategy, reduces the dynamic range of the common-mode signal $\tilde{z}_{\mathrm{C}}(t)$ to half; consequently, the power

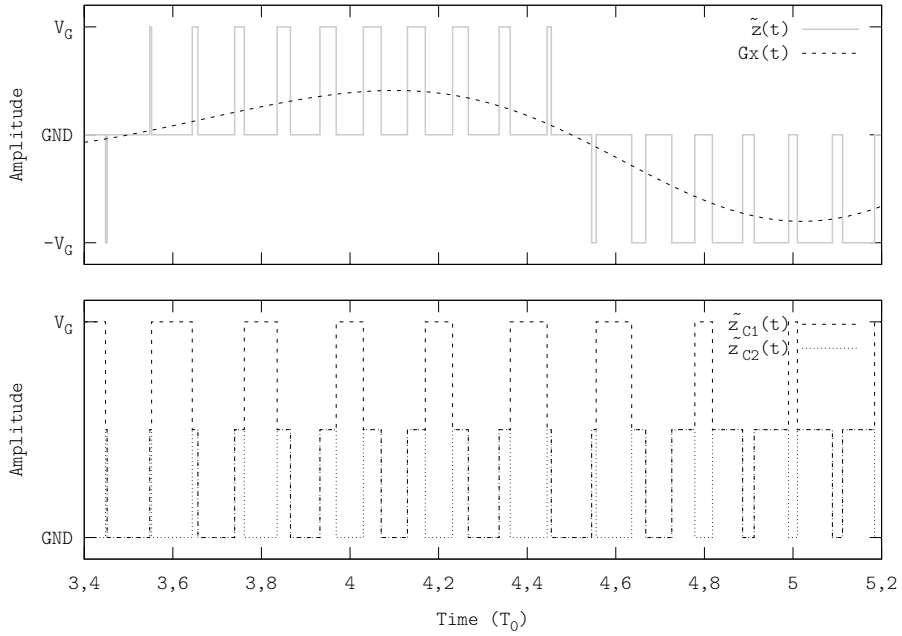

Figure 6.11: Different decoding strategies of a 3-level switching signal in a full-bridge converter (operating at an OSwR of 5 and tracking a f_0-bandlimited signal). $\tilde{z}_{\mathrm{C1}}(t)$ corresponds to the common-mode voltage with alternate decoding and $\tilde{z}_{\mathrm{C2}}(t)$ to always-low decoding. $\tilde{z}(t)$ shows the differential-mode voltage (in both decoding strategies is the same) and the reference signal $Gx(t)$.

of the common-mode signal $P_{\tilde{z}_{\mathrm{C}}(t)}$ reduces by 54 %. By analysing in more detail the spectral power density of the common-mode signals $\tilde{Z}_{\mathrm{C1}}(f)$, $\tilde{Z}_{\mathrm{C2}}(f)$, not only the power is reduced but the spectral power density is reshaped as well (see figure 6.12). The always-low strategy shifts 95 % of the power to DC and the main harmonic is shifted to the switching frequency $f_{\mathrm{s}} = \mathrm{OSwR} f_0$; the DC level is $-7{,}3\,\mathrm{dB}$. However, the inband content of the common-mode signal $\tilde{Z}_{\mathrm{C2}}(t)$ is less than 20 dB below the recovered signal $\tilde{X}(f)$, which could be an issue if the modulator's input Common Mode Rejection Ratio (CMRR) is low.

On the other hand, in the alternate strategy, the inband content of the common-mode signal $\tilde{Z}_{\mathrm{C1(f)}}$ is much smaller than the recovered signal $\tilde{X}(f)$, but the main harmonic is shifted to half the switching frequency. Furthermore, only 60 % of the power is shifted to DC; almost the entire remaining 40 % is shifted at half the switching frequency. In this case, the DC level increases up to $-6{,}0\,\mathrm{dB}$. Note that driving a full-bridge converter as two independent 2-level buck converters tracking the reference signal and its inverted version $\pm x(t)$ (3-level audio switching amplifiers) results in the alternate decoding strategy.

Each decoding strategy has its own advantages and drawbacks; their advisability depends upon the specifications. In either case, this technique based on enhanced decoding logic and switching policy allows controlling the common-mode voltage regardless of the modulation; furthermore, it does not require any additional power resources and neither the efficiency nor the tracking fidelity

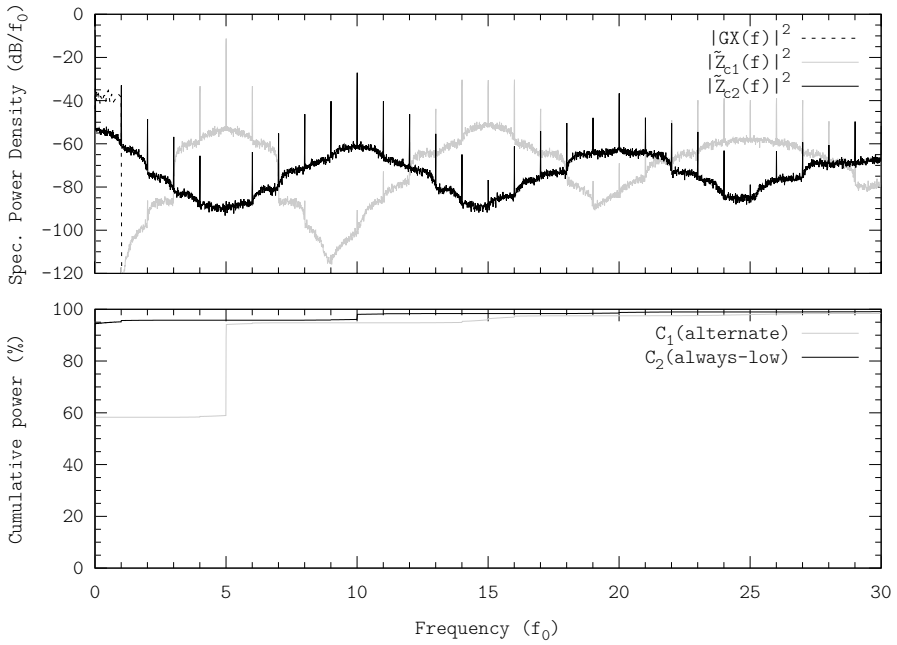

Figure 6.12: Common-mode shaping in a 3-level full-bridge converter (the displayed waveforms show the power spectrum of the time-domain signals displayed in figure 6.11). Simulation performed using the configuration D.4.1.

is affected. Similar approaches have also been reported in the literature [52], but constrained to a specific modulator and implementation; other approaches reported in the literature require additional power resources (described in section 1.5.3).

Without adding power resources, the common-mode signal $\tilde{z}_{\mathrm{C}}(t)$ can be further shaped if constraining the encoding process as well, especially if more levels are available, although this kind of strategies require an incremental modulation. Moreover, note that the power spectrum of the common-mode signal $\tilde{Z}_{\mathrm{C}}(f)$ depends upon the modulation; a spread-spectrum modulation such as AΣΔM, yields a spread-spectrum common-mode voltage signal $\tilde{Z}_{\mathrm{C}}(f)$ (a more detail analysis of the common-mode signal is included in section 7.5.5).

6.3 Preliminary Extension to Non-Linear Converter Topologies

All analyses and characterisations presented so far are intended and for amplifiers based on buck-derived switching power converters, the most common amplifiers in state-of-the-art applications and the main subject of research in high-efficiency power amplifiers. The linear control-to-output DC static characteristic of buck-based converters results in direct low-pass filtering (or band separation) of the modulator's output signal $z(t)$; therefore, this kind of converters are suitable to decode switching signals generated by modulators whose

input-output DC ratio is linear (such as PWM and AΣΔM).

If properly designed, the combination of an input-output DC linear modulator and a linear converter topology results in a power amplifier with linear input-output DC ratio and approximately constant inband gain. Even though switching amplifiers often include a control loop to guarantee good inband tracking fidelity, using this design strategy, the control loop only needs to compensate performance deviations due non-idealities and external factors (typically supply and load variations).

Nonetheless, the switching signal $z(t)$ can be power amplified and decoded with any converter topology, in particular with those in which the control-to-output DC static characteristic is not linear (such as buck-boost). In such a case, the modulator and/or the control loop must compensate the converter's non-linearity.

The control loop can compensate the non-linearity, but at the cost of a higher OSwR. Note that now the control loop is devoted to a twofold operation: compensating external variations and the converter's non-linearity. Whilst non-linear converters further constraint the OSwR, additional features can be achieved with them.

6.3.1 Motivation for Amplifiers Based on Non-Linear Converter Topologies

The power requirements of switching amplifiers for battery-powered devices often make advisable (sometimes even mandatory) to deliver signals exceeding the battery voltage V_{G}. In such a case, since it is not possible to boost the supply voltage with a linear converter topology, the power-amplification process must be split in two stages: a voltage-boosting stage, which steps up the battery voltage, and an inversion stage (a regular switching amplifier typically based on a linear converter topology, either buck or full-bridge), which modulates the amplifier's output signal.

Two-stage amplifiers require two switching converters (i.e. at least two power inductors and two power capacitors), which may compromise the size, weight and cost of the overall system; this is especially critical in portable and handheld devices. Furthermore, in applications which require delivering bipolar voltage signals, the full-bridge topology is widely used in the inversion stage; whilst this topology doubles the output dynamic range by reversing the output voltage polarity, the load is no longer grounded (floating output) thus resulting in eventual common-mode radiation. This can be an issue in EMI-sensitive applications such as car-audio, in which long cables distribute the power audio signals inside the car; a dedicated common-mode EMI-filter is generally necessary in such cases which, again, increases the system's size, weight and cost.

Switching amplifiers are generally based on linear converter topologies because they are simpler to design and implement. However, with more advanced control systems and/or modulators, it should be possible to take advantage of non-linear converters to design switching amplifiers with enhanced features (e.g. voltage boosting and signal tracking in a single stage). Even with conventional modulations and control techniques, it should be possible to take advantage of non-linear converters in high-OSwR applications such as audio.

Pursuing alternative power-amplification architectures for switching amplifiers, non-linear converter topologies are also candidates of interest for switching

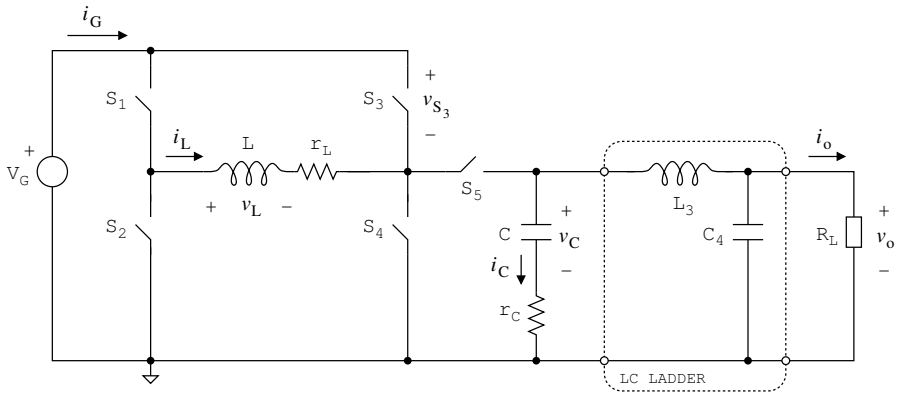

Figure 6.13: 5-switch converter topology with a second-order additional LC ladder (r_L and r_C are the ESR of the inductor and the capacitor respectively). Displayed currents and voltages show the polarity which is considered positive.

amplifiers. Next, a switching converter topology is presented, which can step up and step down the supply voltage and deliver both positive and negative voltages to a grounded load (bipolar converter topology with non-floating output).

6.3.2 Five-Switch Topology

The size, weight and cost of switching amplifiers based on two stages (a boosting stage followed by an inversion stage) can be improved by performing both voltage amplification (gain) and signal tracking in a single stage (non-linear converter topology).

Whilst a non-inverting buck-boost can be used in unipolar applications (supplied form a single voltage source V_G, it can deliver voltages from GND up to several times V_G), there is no converter topology capable of both stepping up and stepping down the magnitude of the supply voltage V_G and delivering a bipolar output signal (e.g. in audio applications, to supply a speaker with a voltage up to $\pm 3V_G$ from a single supply V_G).

Nonetheless, the inverting and the non-inverting buck-boost topologies can be merged into a single converter topology (5-switch topology), consisting of five switches, one inductor and one capacitor (additionally, as in any other converter topology, an LC ladder filter can be added before the load), as figure 6.13 shows. Note that by removing the switches S_1 and S_4 and grounding S_2 (permanently ON), the 5-switch topology simplifies to the regular inverting buck-boost topology, whereas by removing the switch S_3 the 5-switch topology simplifies to the non-inverting buck-boost topology.

The operating principle of the 5-switch topology is the same than that of the buck-boost topology: the converter drains power in DC constant voltage form, stores it as current in the inductor and delivers it to the load as a voltage supply by charging the output capacitor (or the output LC filter).

The switches $S_1, \ldots, S_4$ control the inductor charging process (energy storing), whereas the switch S_5 controls the inductor discharging process (energy delivering). Like in most switching power converter topologies, not all the possible states in the 5-switch topology are allowed, since the inductor cannot be

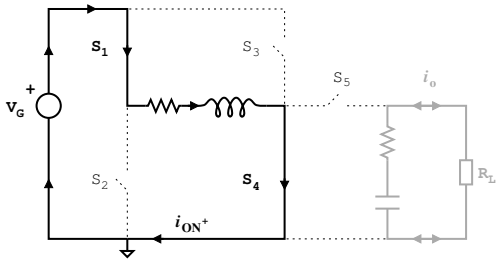

Figure 6.14: 5-switch topology driven in the positives ON-state. The load current is positive or negative depending on the converter's previous state.

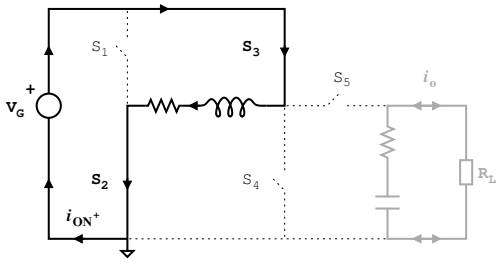

Figure 6.15: 5-switch topology driven in the negative ON-state. The load current is positive or negative depending on the converter's previous state.

in open-circuit and the capacitor cannot be short-circuited.

Allowed States for Symmetrical Output

The switches S_1 and S_2 must be operated as a commutator switch, thus connecting the inductor positive end to either V_G or GND (only one of these can be ON at a time). Likewise, the switches S_3, S_4 and S_5 must be operated as another commutator switch.

The main interest of this topology is for bipolar applications (mostly symmetrical, see section 6.3.2), therefore, despite it can also be driven as a buck or boost converter, only the four allowed states which yield symmetrical bipolar behaviour (inverting and non-inverting buck-boost) are analysed next.

Positive ON-State (ON^+) This state is achieved by switching ON switches S_1 and S_4 and OFF the remaining ones (see figure 6.14). In this state, the inductor is subdued to a positive voltage and hence it is charged with positive current (the converter drains power from the source). The load is supplied from the output capacitor, which discharges through the load.

Negative ON-State (ON^-) This state is achieved by switching ON switches S_2 and S_3 and OFF the remaining ones (see figure 6.15). It is analogous to ON^+, the only difference concerns the inductor charging current (and voltage), which is negative instead of positive.

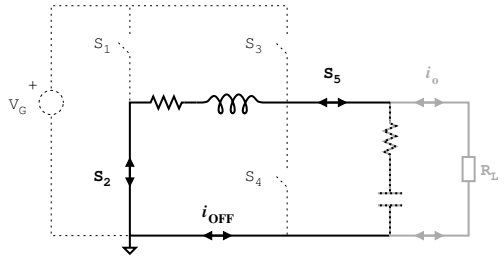

Figure 6.16: 5-switch topology driven in the OFF-state. The currents are positive or negative depending on the converter previous state.

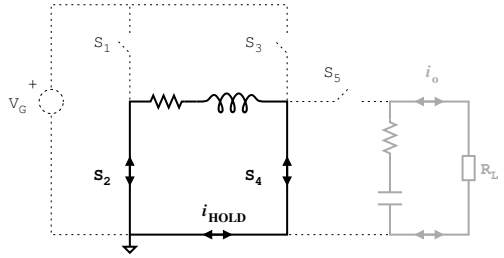

Figure 6.17: 5-switch topology driven in the HOLD-state. This state can also be achieved by switching ON switches S_1 and S_3. The load current is positive or negative depending on the converter's previous state.

OFF-State (*OFF*) This state is achieved by switching ON switches S_2 and S_5 and OFF the remaining ones (see figure 6.16). In this state, the inductor discharges its current (either positive or negative) to the output capacitor, which is charged (or quickly discharged depending on the converter state). The converter drains no energy from the source.

HOLD-State (*HOLD*) This state can be achieved by connecting both inductor ends to the same voltage (either V_{G} or GND), and switching OFF the remaining switches (see figure 6.17). The inductor voltage v_{L} is zero, thus the inductor current remains approximately constant (the converter drains no energy from the voltage supply); the load is supplied from the output capacitor, which discharges through the load as in the ON-states.

Topology Analysis

Despite this topology comprises four valid states, $HOLD$ may only be necessary under light-load conditions (as discussed in section 6.3.2); usually, in regular operation, only three states are used: ON^+, ON^- and OFF. The converter state is determined by the switching signal $z(t)$. Although there is no constraint regarding how the states are encoded within $z(t)$, for the sake of notation simplicity, it has been assumed that $z = 1$ maps to ON^+, $z = -1$ maps to ON^- and $z = 0$ maps to OFF.

Let $\underline{x}$ be the state vector, defined as

$$\underline{x} = \begin{pmatrix} v_{\mathrm{C}}(t) \\ i_{\mathrm{L}}(t) \end{pmatrix} \tag{6.25}$$

The state equations during ON^+ and ON^- are very similar; they can be grouped and written together using $z(t)$

$$\underline{\dot{x}}_{\mathrm{ON}} = \underline{\underline{A_1}}\,\underline{x} + \underline{b} V_{\mathrm{G}} \mathrm{sgn}(z) \tag{6.26}$$

where

$$\underline{\underline{A_1}} = \begin{pmatrix} \dfrac{-1}{C\,(R_{\mathrm{L}} + r_{\mathrm{C}})} & 0 \\ 0 & -\dfrac{r_{\mathrm{L}}\mathrm{sgn}(z)}{L} \end{pmatrix} \quad \underline{b} = \begin{pmatrix} 0 \\ \dfrac{1}{L} \end{pmatrix} \tag{6.27}$$

During OFF, the state equations become

$$\underline{\dot{x}}_{\mathrm{OFF}} = \begin{pmatrix} \dfrac{-1}{C\,(R_{\mathrm{L}} + r_{\mathrm{C}})} & \dfrac{R_{\mathrm{L}}}{C\,(R_{\mathrm{L}} + r_{\mathrm{C}})} \\ \dfrac{-R_{\mathrm{L}}}{L\,(R_{\mathrm{L}} + r_{\mathrm{C}})} & \dfrac{-\,(R_{\mathrm{L}} \| r_{\mathrm{C}}) - r_{\mathrm{L}}}{L} \end{pmatrix} \underline{x} \tag{6.28}$$

Equations (6.26) and (6.28) can be combined in a single state equation, yielding

$$\underline{\dot{x}} = \underline{\dot{x}}_{\mathrm{ON}} |z| + \underline{\dot{x}}_{\mathrm{OFF}} (1 - |z|) \tag{6.29}$$

By simplifying the previous expression, the state equation (6.30) is obtained, which characterises the converter dynamics.

$$\underline{\dot{x}} = \begin{pmatrix} \dfrac{-1}{C\,(R_{\mathrm{L}} + r_{\mathrm{C}})} & \dfrac{1 - |z|}{C} \dfrac{R_{\mathrm{L}}}{R_{\mathrm{L}} + r_{\mathrm{C}}} \\ \dfrac{|z| - 1}{L} \dfrac{R_{\mathrm{L}}}{R_{\mathrm{L}} + r_{\mathrm{C}}} & (1 + |z|) \dfrac{-R_{\mathrm{L}}(r_{\mathrm{C}} + r_{\mathrm{L}}) - r_{\mathrm{L}} r_{\mathrm{C}}}{L(R_{\mathrm{L}} + r_{\mathrm{C}})} - |z| \dfrac{r_{\mathrm{L}}\mathrm{sgn}(z)}{L} \end{pmatrix} \underline{x} + \\ + \begin{pmatrix} 0 \\ \dfrac{1}{L} \end{pmatrix} V_{\mathrm{G}} z \tag{6.30}$$

Averaged Steady-State Analysis From (6.30) it is possible to derive the averaged Steady-State (SS) expressions. In average modeling, the switching signal $z(t)$ or, control variable $u(t)$ if using the usual notation of control theory, becomes a continuous variable, whose range extends from -1 to 1; in steady-state, the amount of energy stored within each reactive component remains constant over a switching period, hence $\underline{\dot{x}} = 0$. In the ideal case ($r_{\mathrm{L}} = r_{\mathrm{C}} = 0$), this topology fulfils

$$\underline{x_{\mathrm{SS}}} = \begin{pmatrix} 1 \\ \dfrac{-1}{R_{\mathrm{L}}(1 - |z|)} \end{pmatrix} V_{\mathrm{G}} \frac{z}{1 - |z|} \tag{6.31}$$

Note that this expression simplifies to that of the inverting buck-boost topology if $z < 0$ and to that of the non-inverting buck-boost topology if $z > 0$ (see figure 6.18).

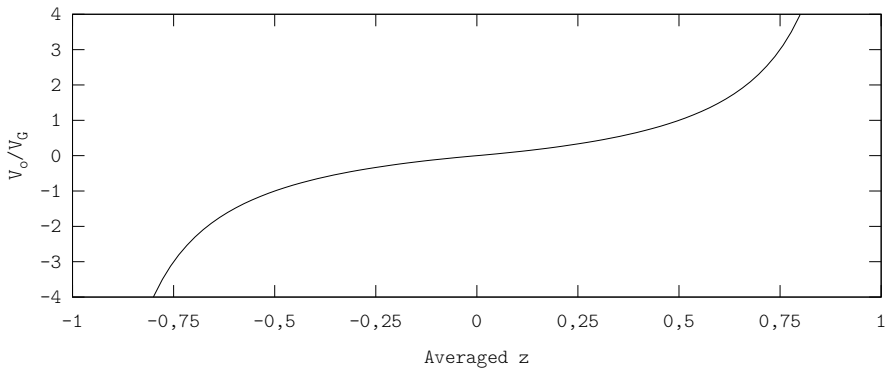

Figure 6.18: Ideal ($r_{\mathrm{L}} = r_{\mathrm{C}} = 0$) steady-state DC transfer characteristic (output voltage V_{o} to the supply voltage V_{G}) of the proposed topology, as a function of the averaged switching signal $z(t)$.

Topology Characteristics

The 5-switch topology is mainly intended for bipolar signal tracking targeting high-efficiency bipolar power amplifiers. The characteristics of this topology are analysed considering this specific application.

The 5-switch topology can be interpreted as merging a regular buck-boost and a non-inverting buck-boost converters [61]; indeed most of the features of the 5-switch topology are similar to the features of the buck-boost converter, including the non-linear static control-to-output ratio (see figure 6.18). Whilst it is possible to operate this topology in a different way (e.g. as a boost or as a buck converter), it is not possible to achieve symmetrical behaviour and hence they are not analysed in this work.

One of the main features of this topology is its capability of both reversing the output polarity and stepping up and stepping down the supply voltage V_{G}, even in its second-order variant. As in common buck-boost designs, the maximum boost ratio is limited by the switches ON-resistance the the ESR of the reactive components (mainly the inductor L). If implementing this topology with regular reactive components, it is feasible to supply a grounded load with bipolar signals whose magnitude extends up to several times the magnitude of the supply voltage V_{G}.

The other main feature of this topology is the grounded output (see figure 6.13): both the positive and the negative output voltages are applied to a non-floating output; this feature is especially important in EMI-sensitive applications, since common-mode radiation is often an issue in these applications. On the other hand, as in the buck-boost topology, both the input and the output currents are discontinuous. Note that this is the only converter topology capable of stepping up and stepping down the supply voltage and delivering bipolar voltages to a grounded load (from a single supply V_{G}); typical bipolar converter topologies (e.g. full-bridge) and even higher-order ones (such as Ćuk) use a floating output to achieve bipolarity [11], [57].

The HOLD-state may be useful in light-load conditions, to improve the converter dynamics [82]. In the proposed topology, no additional resources are necessary to achieve this state.

Operating Example

Figure 6.19 shows the representative waveforms of the 5-switch topology voltage-amplifying a single-tone sinusoid by a factor 2 ($G = 2$). The output voltage $v_{\mathrm{C}} = \tilde{x}(t)$ tracks the waveform of the reference signal $x(t)$. This figure also includes a detail of the topology delivering high power (middle plot) and changing the polarity (from negative voltage to positive voltage in this example) of the output signal (lower plot).

Note that since the load R_{L} is resistive, the power consumption depends upon the magnitude of the output voltage. When reversing the polarity, the magnitude of the output voltage is very low, and so is the power consumption; therefore, when the converter is in an ON state (also in $HOLD$), the capacitor voltage remains approximately constant. In order to quickly charge the output capacitor so that its voltage tracks the reference signal waveform $x(t)$, the inductor current i_{L} discharges the capacitor. This situation is captured in the lower plot of figure 6.19, when the output voltage is approaching to GND but still negative and the inductor current is positive.

The performance in terms of tracking fidelity and OSwR that can be achieved with a switching amplifier based on this topology mostly depends the modulator and the control strategy (in this example, the control is proportional and the modulation is 3-PWM). Figure 6.19 is only intended as proof-of-concept, to show indeed the amplification and bipolar capabilities of the 5-switch topology.

When designing a modulator for this topology it is mandatory to include a switching policy. This converter supplies the load during OFF; during both ON states, ON^{+} and ON^{-}, the load is supplied from the capacitor C and the inductor is charged with positive or negative current. An OFF period must always follow an ON state and vice versa; otherwise, if switching between the two ON states, the inductor would be charged with positive current and subsequently charged with negative current (or vice versa). Current would flow through the inductor without being released to the load, thereby dissipating power due to the switches' ON resistance r_{S_i} and the ESR of the inductor r_{L}.

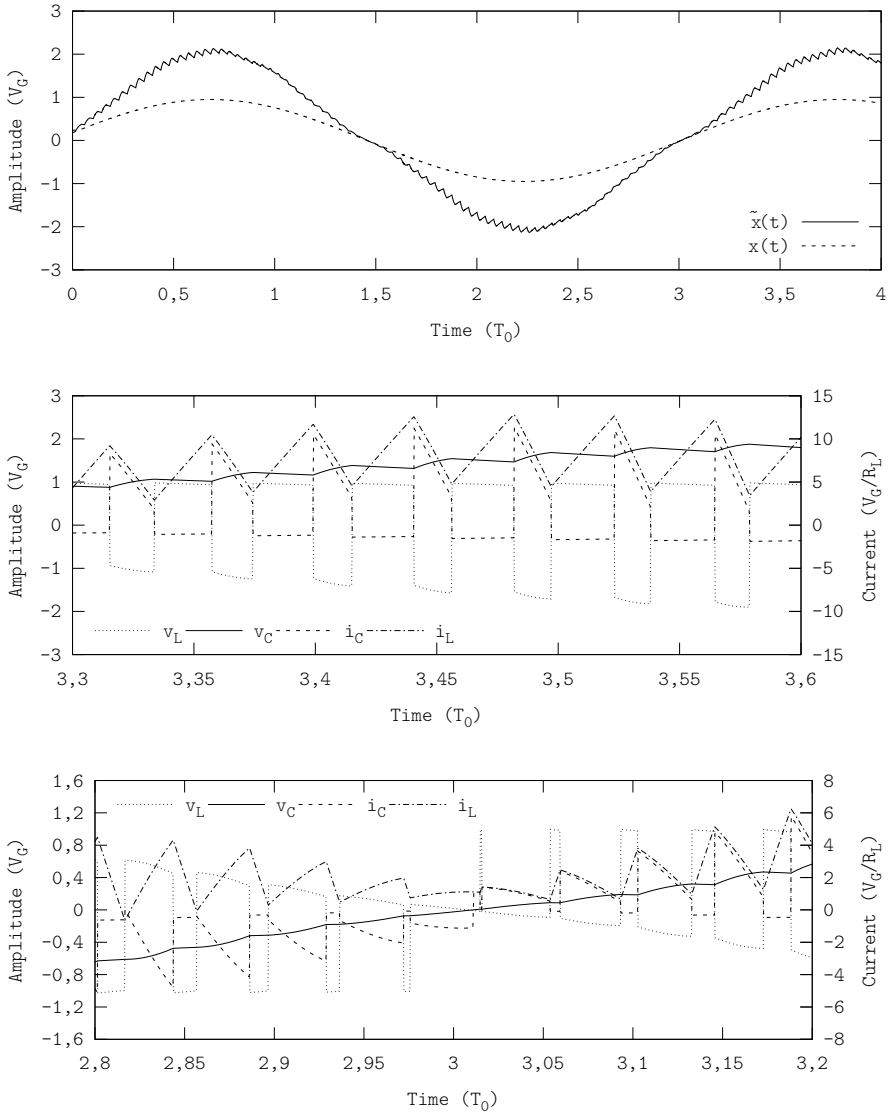

Figure 6.19: Representative time waveforms in the 5-switch converter topology. Example showing a second-order variant, providing a voltage gain of 2, using switches with on resistance $r_{S_i} = 3 \cdot 10^{-3} R_\mathrm{L}$, $r_\mathrm{C} = r_\mathrm{L} = 0$.

Chapter 7

Performance of Switching Amplifiers

The previous chapters, by in-depth analysing the power-amplification process performed by switching amplifiers and splitting it into sub-processes (encoding, translating, power amplifying and decoding), have presented different techniques to improve the performance of each individual sub-process. The present chapter explores the advantages of combining these techniques in a single amplifier, targeting to extend the relative bandwidth of switching amplifiers when tracking a general f_0-bandlimited reference signal.

7.1 Comparison Framework

The scope of this thesis is to extend the relative bandwidth of switching amplifiers when tracking a general f_0-bandlimited reference signal. The advantages of this extension can be interpreted from two complementary standpoints: either reducing the OSwR required for satisfactory tracking (i.e. reducing switching losses thereby increasing the efficiency of the amplifier) or reducing the outband power when operating at a certain OSwR (effectively increasing the amplifier's tracking bandwidth).

There exists no unique universal or optimum design of switching amplifiers suitable for all applications; instead each design must be specifically tuned and optimised according to the particular specifications of each application. Nevertheless, there exist three main trends in common specifications: minimising the total error power, minimising the inband error power and reducing the upper-bound of the outband spectral power density.

The performance of all candidates herein considered is first characterised from these three different standpoints, aiming to encompass a wide variety of applications. Besides these characterisations based on tracking error and switching frequency, a more implementation-oriented analysis is also included, to evaluate the suitability of these candidates in more realistic operating conditions (mostly robustness against non-idealities).

Depending on the specifications and the available technology and/or resources, only a few among all candidates may be feasible for some applications. Therefore, the candidates have been grouped depending on the number of levels

N: 2-level amplifiers and multi-level amplifiers. Appendix B includes a summary of the definition of different signals in switching amplifiers, including the definitions of the error signal $e(t)$ and the filtered or remaining error signal $\xi(t)$.

7.1.1 Optimisation Strategies

The most generic application or optimisation approach consists in minimising the remaining error signal's power $P_{\xi(t)}$, targeting to recover a signal $\tilde{x}(t)$ with minimum error. Both inband and outband contents weight the same and hence, because of the low-pass filter, the inband and the outband power of the remaining error signal $\xi(t)$ are generally balanced $P^{\mathrm{i}}_{\xi(t)} \approx P^{\mathrm{o}}_{\xi(t)}$ or, at least, in the same range. Amongst the common applications comprising a switching power amplifier, this approach minimises the power supplied by the linear amplifier in linear-assisted power amplifiers.

In some applications the inband performance is more important than the outband content (e.g. in audio, wherein the outband content mostly concerns efficiency and ElectroMagnetic Compatibility, EMC). These applications should be optimised mainly according to the inband error power $P^{\mathrm{i}}_{\xi(t)}$, similarly to the analysis under the fundamental limit perspective described in sections 4.5.1 and 5.6 but considering the output filter as well. This kind of optimisation generally leads to an unbounded (and hence unfeasible) solution, e.g. the higher the filter's cutoff frequency f_{c}, the better the amplifier's performance. In actual applications, other constraints such as switching losses finally determine the design; still, this approach can be used to compare the inband performance of a certain candidate with the inband performance of a conventional reference design.

A third comparison framework or optimisation strategy consists in evaluating the upperbound of the outband spectral power density of the remaining error signal $\Xi(f)$, instead of evaluating the power itself. This strategy can be used to evaluate the compliance with communication spectral masks, typically in broadband communication systems.

7.1.2 Conventional Design

Conventional designs of switching amplifiers are based on second-order linear converter topologies, either buck or full-bridge, driven by a 2-PWM (even in the 3-level audio amplifier case). The filter's cutoff frequency is generally not optimised (a common value in that application field is used); the OSwR is high, typically 10 and beyond.

However, in order to establish a general comparison framework, the second-order 2-PWM amplifier is considered the conventional or reference design, regardless of the OSwR and cutoff frequency f_{c}. Low-OSwR and/or optimised cutoff frequency f_{c} designs are indeed not conventional, but they are the direct candidates from state of the art.

7.1.3 Design Space

The performance characterisation of all candidates must sweep all the range of interest of OSwR. Consistently with the scope of this work of extending the relative bandwidth of switching amplifiers, the design space considered in

these characterisations extends from 1 to 10 (underswitching or OSwRs below 1 is separately analysed because of its specificity). Besides the OSwR and the modulation (a design choice), the other design parameters are the number of levels N, the filter's order n and the filter's cutoff frequency f_c.

Neither shaping the filter's transfer function nor pre-emphasising the reference signal $x(t)$ is included in these characterisations. These two techniques have not been included because their performance improvements depend upon the implementation (e.g. pre-equalisation depends upon the actual transfer function to pre-equalise and upon the computation capacity in digital implementations); moreover, both techniques can be applied to any candidate, regardless of the OSwR.

The main goal is to extend the relative bandwidth of switching amplifiers (mostly tracking error and switching frequency). Nonetheless, since any design must be implemented to be used, the performance evaluation also comprises other implementation-related effects, such as required power resources (decoding logic and switching policy), variable operating conditions, robustness against non-idealities and EMC (including crosstalk).

7.2 Two-Level Switching Amplifiers

The first set of candidates are based on 2-level modulations, for systems which do not support multi-level power amplification. In such cases, the performance improvements must be achieved by using alternative modulations, increasing the filter's order n and optimising the filter's cutoff frequency f_c.

Starting with a conventional second-order 2-PWM amplifier, alternative modulations can be used to extend its relative bandwidth. Figure 7.1 shows the performance characterisation (in terms of power of the remaining error signal $P_{\xi(t)}$) of second-order amplifiers based on the modulations described in chapter 4: 2-PWM, 2-A$\Sigma\Delta$M and 2-AA$\Sigma\Delta$M. The filter's cutoff frequency f_c has been optimised to minimise the power of the remaining error signal $P_{\xi(t)}$ for each candidate (i.e. for each combination of modulation, OSwR and filter's order).

At low OSwRs (between 1 and 3), the performance of A$\Sigma\Delta$M-based amplifiers is better than that of the PWM-based amplifier. Recalling the inband characterisation of 2-level modulations (section 4.5.1), the inband error due to improper encoding of 2-PWM is significantly lower than that of 2-A$\Sigma\Delta$M and 2-AA$\Sigma\Delta$M for OSwRs beyond 2. This opposite behaviour is due to the output filter $H(s)$ and the trade-off involving its cutoff frequency f_c.

Certainly, because of the high power around the switching frequency f_s in 2-level time encoding, the filter's cutoff frequency f_c is set to a low value to guarantee enough rejection around the switching frequency f_s. However, this low frequency results in a significant inband error (attenuation and phase lag), which dominates over all other inband error sources (i.e. the different inband error due to improper encoding of the three modulations).

As discussed in chapter 4, the power of the 2-level power switching signal $P_{\tilde{z}(t)}$ is independent of the modulation, as long as the DC component is properly tracked. Therefore, provided that the filter's optimisation leads to similar designs in all three cases, the performance difference is mainly due to the different spectral distribution. A$\Sigma\Delta$M yields spread-spectrum error signals $E(f)$ whose spectral power density slowly decreases from the switching frequency f_s

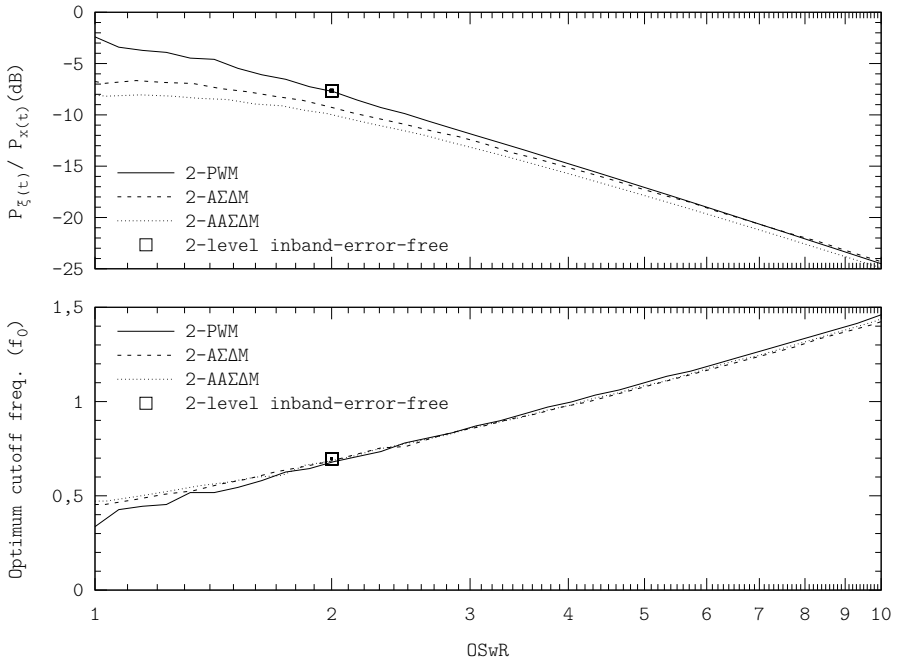

Figure 7.1: Performance of optimised 2nd order 2-level amplifiers. Simulation performed using the configuration D.4.4.

away (including inband, i.e. error due to improper encoding). Nevertheless, in the characterisation of AΣΔM-based amplifiers of figure 7.1, the inband error due to improper encoding is masked by the error due to the output filter $H(s)$, even at OSwRs close to 10, which finally determines the inband power of the remaining error signal $P^{\mathrm{i}}_{\xi(t)}$ (the power of the remaining error signal is similar in the three modulations, i.e. it is not determined by the modulation).

On the other hand, comparing PWM and AΣΔM, the AΣΔM error signal's outband power $P^{\mathrm{o}}_{e(t)}$ is lower (it has been partially shifted inband) and spread. The combination of both contributions, similar inband error and lower outband error in AΣΔM, accounts for the slightly better performance in the AΣΔM-based amplifier than in the PWM-based amplifier at low OSwRs.

Consistently with the high inband error due to the filter, if an amplifier would be based on inband-error-free encoding (the harmonic-matching process described in chapter 3), its performance in terms of power of the remaining error signal $P_{\xi(t)}$ would be worse than that of AΣΔM-based amplifiers, since the inband error due to the filter would mask the modulation's inband-error-free feature (similarly to the PWM-based case). Figure 7.1 includes one specific example, inband-error-free encoding at an OSwR of 2; like in the 2-PWM case (also at an OSwR of 2), the power of the remaining error signal $P_{\xi(t)}$ is higher than in the AΣΔM-based case. Note that the filter's optimised cutoff frequency f_{c} is the same in all modulations, which corroborates again that the power of the remaining error signal is not determined by the modulation but by the filter. The filter is also responsible of the different performance of both AΣΔM-based amplifiers, as the more constant encoding dynamics of AAΣΔM better adapts

to the constant dynamics of the output filter $H(s)$.

As the OSwR increases, so does the optimum cutoff frequency f_c; the inband error added by the output filter becomes less significant and hence the inband error due to improper encoding may become visible. Although the power of the remaining error signal $P_{\xi(t)}$ decreases at a faster rate in the PWM-based amplifier than in the AΣΔM-based amplifiers, at an OSwR of 10, the difference between these three amplifiers is below 1 dB and the performance of the AAΣΔM-based amplifier is still better than that of PWM-based amplifier. Still, if the OSwR (and thus the filter's cutoff frequency f_c) would be high enough, the best performance would be achieved with a 2-PWM amplifier. A very accurate pre-equalisation may also aid in reducing the remaining error signal's inband power $P^{\mathrm{i}}_{\xi(t)}$, although pre-equalisation usually limits the amplifier's dynamic range.

These characterisations corroborate that by only changing the modulation, no significant performance improvements can be achieved in terms of the remaining error signal's power $P_{\xi(t)}$, as already pointed out at the end of chapter 4. However, with regard to the upperbound of the outband spectral power density, the 2-AΣΔM amplifier significantly reduces it when compared to the 2-PWM amplifier (operating at the same OSwR and filtering with the same filter). This reduction is because of the spread-spectrum modulation, whose peak is typically more than 20 dB below the peak in the 2-PWM case (as figure 4.18 showed). Figure 7.2 illustrates this reduction, by showing the power spectrum of a 2-PWM and a 2-AΣΔM amplifiers, both operating at an OSwR of approximately 4 and using a filter's cutoff frequency of $f_c = f_0$ (note that the peak reduction is almost independent of the OSwR and the filter's cutoff frequency f_c, as long as they are the same in both amplifiers). In this particular example, with regard to the remaining error signal $\Xi(f)$, the inband power is similar and the total power reduces by 1,5 dB.

7.2.1 High-Order Filter Amplifiers

By upgrading a second-order amplifier to higher orders, it is feasible to improve its performance targeting any of the three optimisation strategies herein considered. The higher stopband rejection allows shifting the filter's cutoff frequency f_c to higher frequencies whilst achieving the same rejection around the switching frequency f_s; consequently the inband attenuation and phase lag decreases, thereby reducing the inband content of the remaining error signal $\xi(t)$.

For instance, still with the example of figure 7.2, by upgrading the second-order 2-AΣΔM to fourth order and optimising again its cutoff frequency f_c to minimise the remaining error signal's power $P_{\xi(t)}$, the inband error power by reduces 7 dB and the total power reduces by 9 dB (compared to the second-order 2-PWM amplifier, see figure 7.3). Furthermore, the upperbound of the outband power spectrum is now 42 dB lower than that of the reference second-order 2-PWM amplifier, instead of 23 dB in the second-order case. In this case, the high-order upgrade improves the performance according to the three optimisation strategies.

The full design-space characterisation of optimised fourth-order amplifiers reveals that this performance-improvement trend is general, and more noticeable at high OSwRs (see figure 7.4). Moreover, the high-order filter further heightens the differences between amplifiers (i.e. modulations).

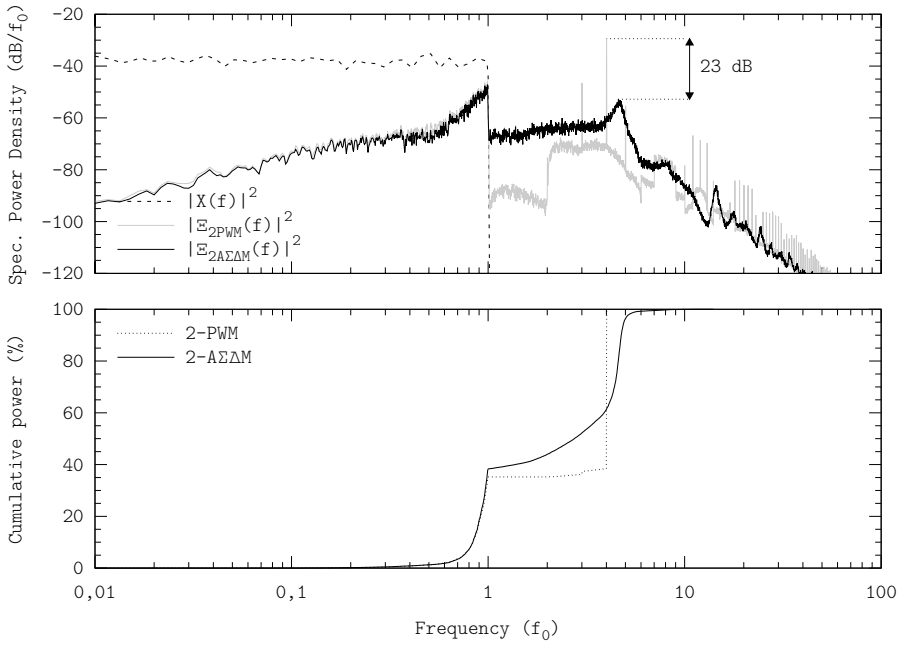

Figure 7.2: Power spectra of 2-PWM and 2-AΣΔM amplifiers (OSwR ≈ 4, $f_c = f_0$ the optimum cutoff frequency to minimise the power of the remaining error signal in both cases). Simulation performed using the configuration D.4.1.

Certainly, the OSwR range in which the filter's cutoff frequency is set to an inband value $f_c < f_0$ is narrower than in the second-order case (within this range, the performance of AΣΔM-based amplifiers is better than that of the PWM-based amplifier). Once the OSwR is high enough to shift the optimum cutoff frequency outband (already at OSwRs below 3 with fourth-order filters), the different rates of decrease (of the remaining signal's error power $P_{\xi(t)}$ as the OSwR increases) become visible; so much, so that at OSwRs beyond 4, the performance of the PWM-based amplifier is better than that of the AΣΔM-based amplifiers.

Note that the optimum cutoff frequency in all fourth-order designs is higher than that in second-order designs, operating at the same OSwR. Provided that the filter's inband attenuation decreases as the filter order n increases, the inband error is mainly due to the non-rectilinear phase lag, in fourth-order filters with cutoff frequency higher than f_0.

Also note that the optimum cutoff frequency in AΣΔM increases at a slower rate than in the other cases. This is a consequence of the spread spectrum; the inband error due to improper encoding is now masking the inband error due to the filter. In the AAΣΔM case, the cutoff frequency optimisation sets a higher cutoff frequency f_c because the outband spectral power density concentrates within a narrower band.

With a fourth-order filter, the optimisation of a hypothetical amplifier performing inband-error-free encoding (based on harmonics' matching, as described in chapter 3 and operating at an OSwR of 2), results in a higher cutoff frequency

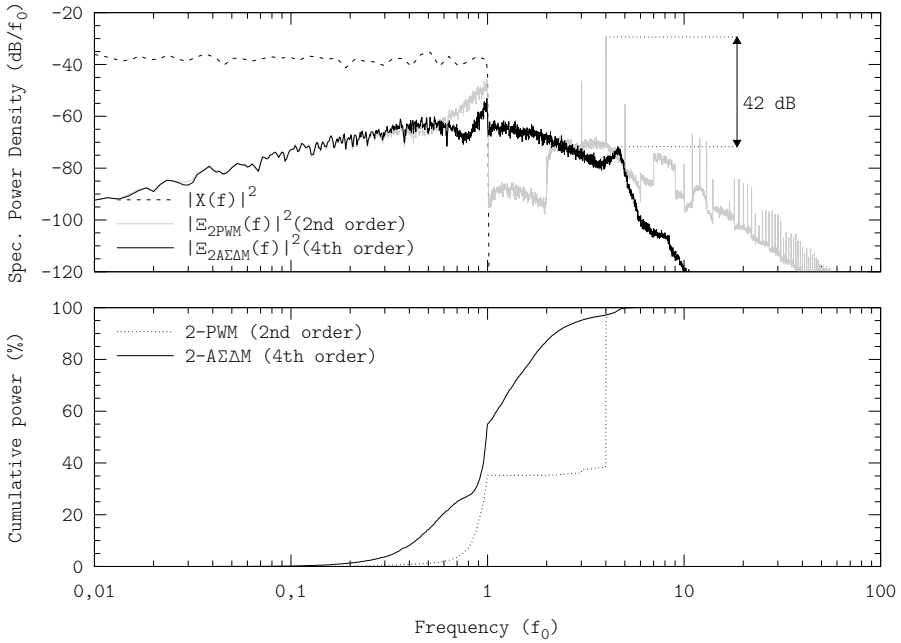

Figure 7.3: Power spectra of second-order 2-PWM and fourth-order 2-AΣΔM amplifiers (OSwR ≈ 4 in both cases, $f_c = f_0$ and $f_c = 1{,}24 f_0$ respectively, the optimum cutoff frequency to minimise the power of the remaining error signal in each case). Simulation performed using the configuration D.4.1.

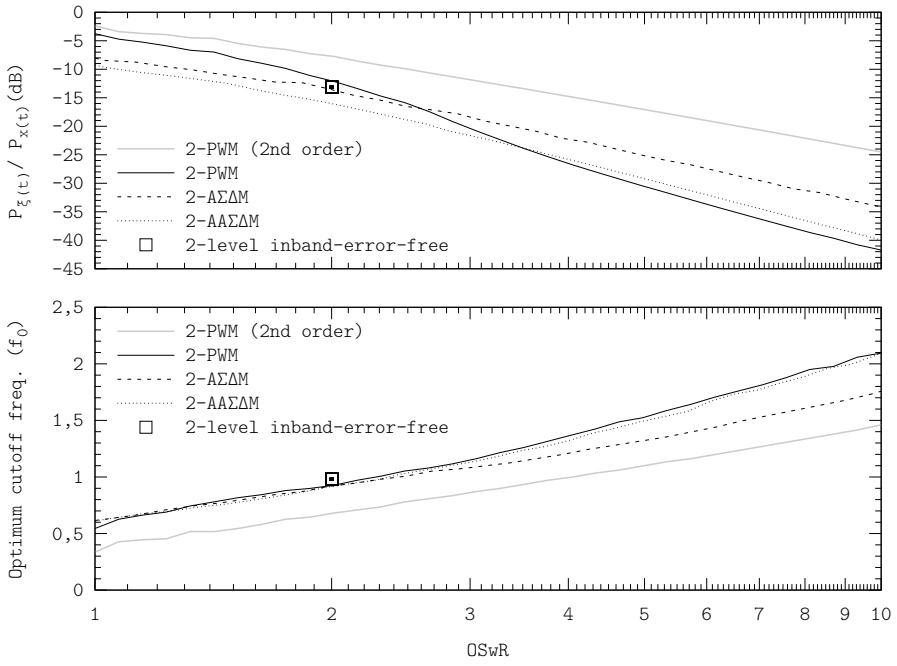

Figure 7.4: Performance of optimised 4th order 2-level amplifiers. Simulation performed using the configuration D.4.4.

f_c than in any other 2-level fourth-order candidate, which corroborates that the inband error due to the filter is lower than that of AΣΔMs and even PWM at this OSwR (see figure 7.4).

Comparing with a second-order amplifier, upgrading to fourth order and optimising the filter's cutoff frequency f_c may also reduce the inband power of the remaining error signal $P^{i}_{\xi(t)}$, as well as the upperbound of the power spectrum of the remaining error signal $\Xi(f)$ with any of the three modulations. For instance, in the example depicted in figure 7.5 (two 2-PWM-based amplifiers operating at an OSwR of 4 with optimised second-order and fourth-order filters), the inband power $P^{i}_{\xi(t)}$ reduces by 11 dB, the total power $P_{\xi(t)}$ by 12 dB and the peak by 13 dB. Optimised high-order filters therefore extend the relative bandwidth of switching amplifiers.

By further increasing the filter's order n, e.g. to eighth order (figure 7.6), the different trends and behaviours are further heightened. The minimum cutoff frequency f_c so that the filter is not dominant inband error source increases (general trend for all modulations and OSwRs), because of the higher filter's phase lag. Note that high-order filters with low cutoff frequencies f_c (yet outband $f_c > f_0$), result in a higher inband error due to non-rectilinear phase lag.

Beyond this range (in this example based on eighth-order filters, beyond OSwR 3), the performance of the overall amplifier tends to that of the modulations. The high stopband rejection plays down the importance of shaping the outband content. Indeed, in the example of inband-error-free encoding at an OSwR of 2, the upperbound of the outband power spectrum is higher than

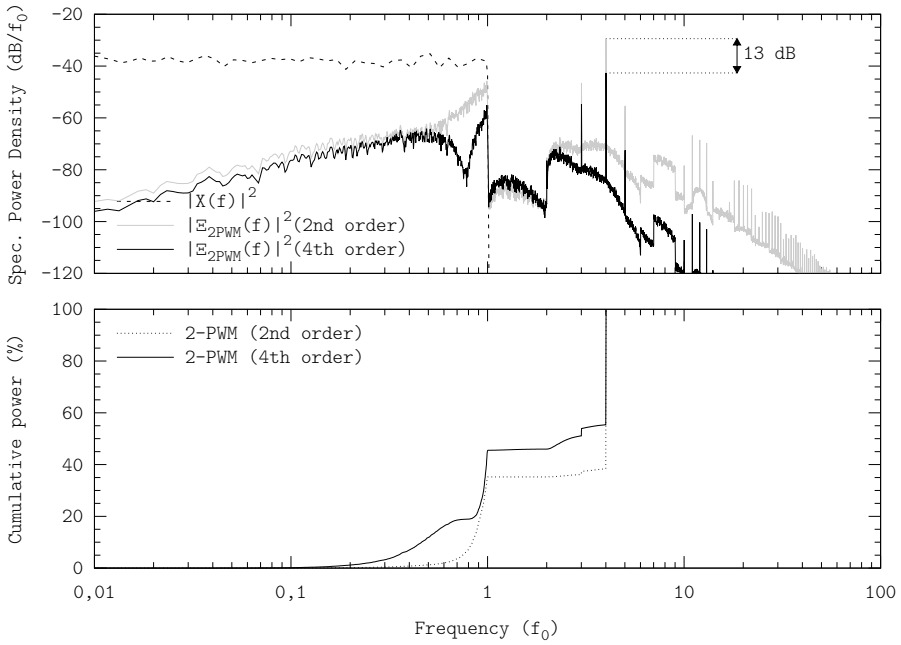

Figure 7.5: Power spectra of optimised second-order and fourth-order 2-PWM amplifiers (OSwR ≈ 4 in both cases, $f_c = f_0$ and $f_c = 1{,}37 f_0$ respectively, the optimum cutoff frequency to minimise the power of the remaining error signal in each case). Simulation performed using the configuration D.4.1.

that of PWM- and AΣΔM-based amplifiers and at a lower frequency; however, comparing with the three candidates, the filter's cutoff frequency optimisation sets a higher cutoff frequency f_c and yet the power of the remaining error signal $P_{\xi(t)}$ is lower.

7.3 Multi-Level Switching Amplifiers

If the application supports generating more than 2 levels in the power switching signal $\tilde{z}(t)$, multi-level power amplification becomes another feasible technique to extend the relative bandwidth of switching amplifiers. The main advantage of multi-level modulations is the reduction of the outband power (and also the upperbound of the outband content, as discussed in chapter 5), i.e. a simplification of the decoding or recovery process.

The power switching signal $\tilde{z}(t)$ is the power image of the switching signal $z(t)$. Because of multi-level time encoding, provided that the power switching signal's outband power $P^{o}_{\tilde{z}(t)}$ is already lower than in the 2-level case, the filter's cutoff frequency f_c can be increased and still achieve the same outband performance at the same OSwR. The inband error due to the filter accordingly reduces, thereby reducing the total power of the remaining error signal $P_{\xi(t)}$ without increasing the switching frequency f_s (i.e. extending the switching amplifier's relative bandwidth). This reasoning can be applied to the other optimisation strategies, inband power and upperbound of the outband spectral

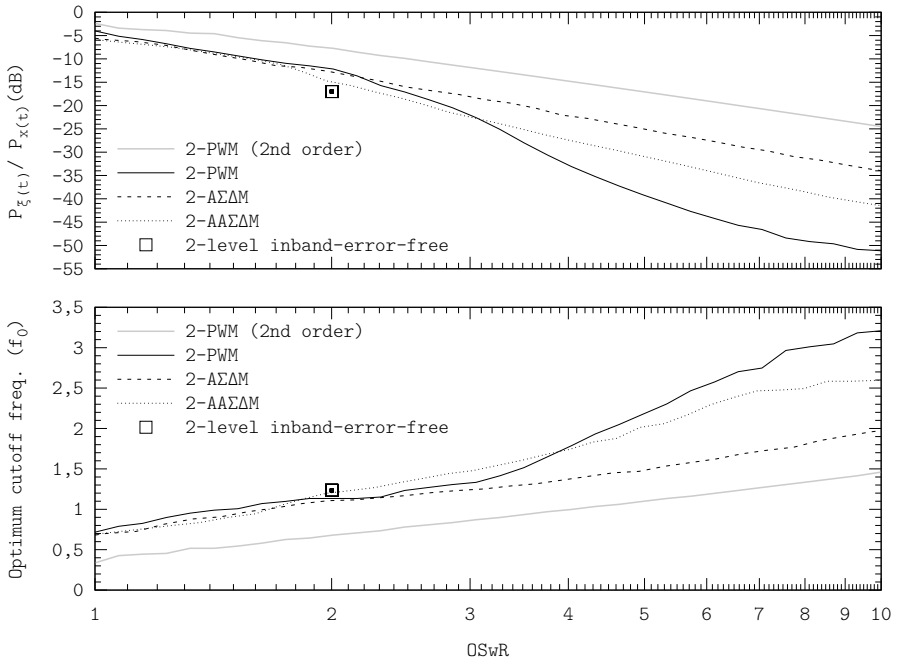

Figure 7.6: Performance of optimised eighth order 2-level amplifiers (values below −50 dB are masked by simulation errors). Simulation performed using the configuration D.4.4.

content.

Note that inband-error-free encoding is already possible with 2 levels at an OSwR of 1; assuming that the inband error due to improper encoding of 2-level modulations is small (which is generally true if the OSwR is higher than 2), the extension to multiple levels improves the amplifier's inband performance by reducing the inband error due to the filter.

The performance characterisation, in terms of power of the remaining error signal $P_{\xi(t)}$ of 3-level and 7-level amplifiers is shown in figures 7.7 and 7.8 respectively (the filter's cutoff frequency f_c has been optimised for each specific amplifier). As discussed above, as the number of levels N increases, the outband power $P^o_{\xi(t)}$ reduces and, consequently, the filter's optimisation leads to a higher cutoff frequency f_c, thereby resulting in a lower power of the remaining error signal $P_{\xi(t)}$. If properly encoding (i.e. encoding at an OSwR high enough to take advantage of all levels, without suffering from bandwidth constraints), the higher the number of levels N, the lower the remaining error signal's power $P_{\xi(t)}$.

Like in the 2-level case, if the OSwR is high enough, the best performance is achieved with N-PWM. Nevertheless, the intrinsic slew-rate constraint of PWM results in a high error at low OSwRs; this range of improperly encoding widens as the number of levels N increases, since the extra-switching condition depends upon the number of levels (as discussed in section 5.3.3). Similarly, the control for astable operation of N-AAΣΔM also constraints its inband performance at low OSwRs.

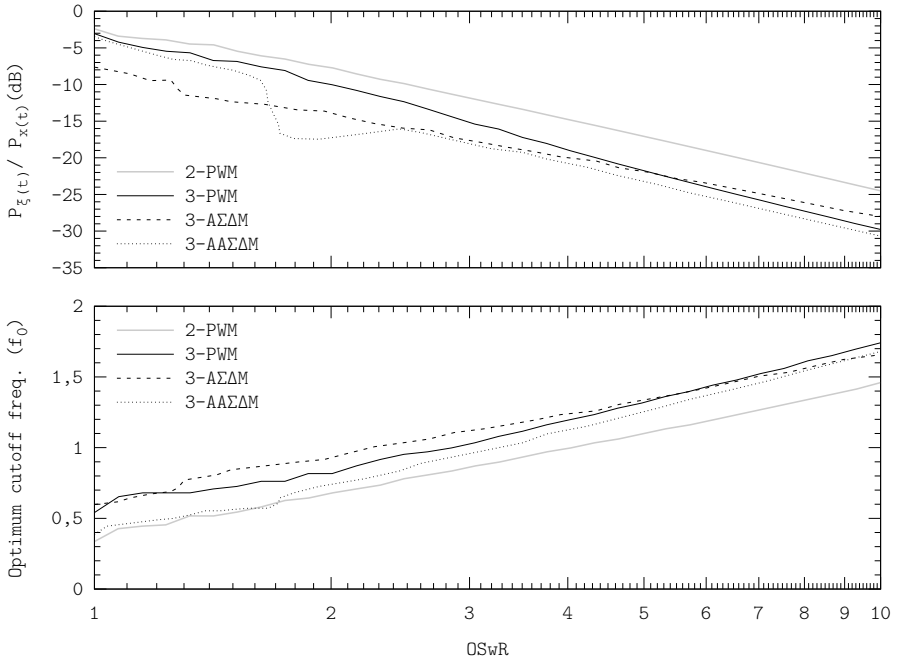

Figure 7.7: Performance of optimised 2nd order 3-level amplifiers. Simulation performed using the configuration D.4.4.

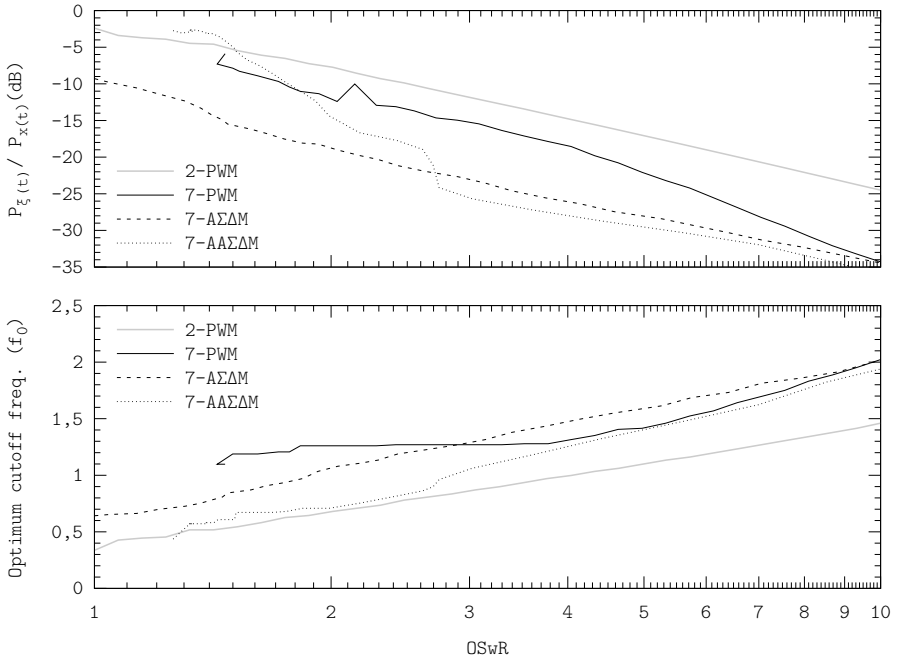

Figure 7.8: Performance of optimised 2nd order 7-level amplifiers. Simulation performed using the configuration D.4.4.

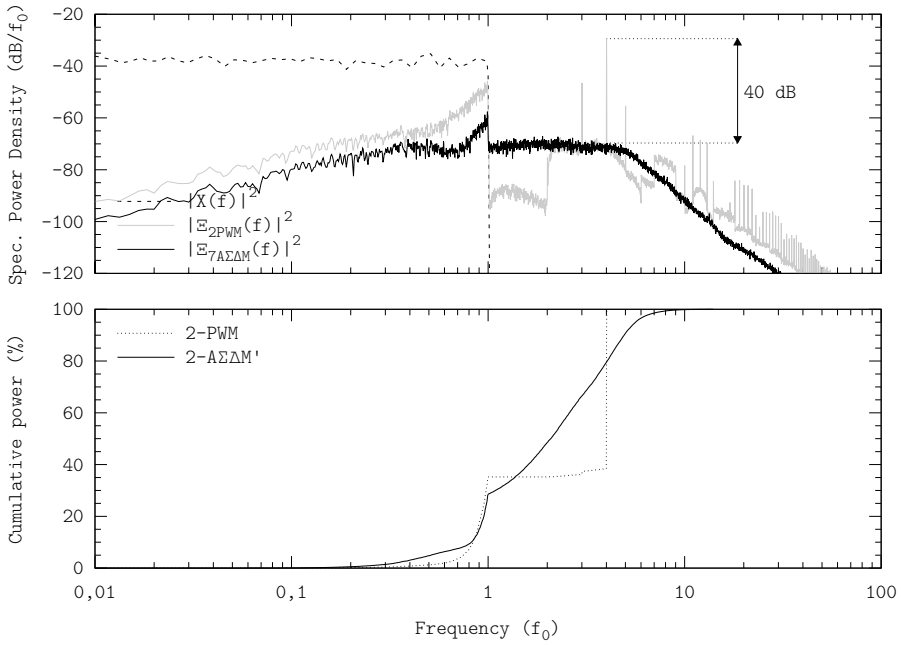

Figure 7.9: Power spectra of optimised second-order 2-PWM and 7-AΣΔM amplifiers (OSwR ≈ 4 in both cases, $f_c = f_0$ and $f_c = 1{,}48 f_0$ respectively, the optimum cutoff frequency to minimise the power of the remaining error signal in each case). Simulation performed using the configuration D.4.1.

If properly encoding, multi-level power amplification is also a feasible technique to extend the relative bandwidth of switching amplifiers. Figure 7.9 illustrates the benefits of multi-level power amplification with an example in the frequency domain, showing the power spectrum of the remaining error signal $\Xi(f)$ in the 2-PWM and 7-AΣΔM cases, both operating at an OSwR of 4 and with an optimised second-order filter (cutoff frequencies of $f_c = f_0$ and $f_c = 1{,}48 f_0$ respectively). Compared to the second-order 2-PWM case, also operating at an OSwR of 4, the power of the remaining error signal $P_{\xi(t)}$ decreases by 12 dB despite the higher cutoff frequency f_c. Besides, the inband power reduces by 13 dB (mainly because of the higher cutoff frequency, since the inband performance at OSwR = 4 of 2-PWM is about 25 dB better than that of 7-AΣΔM, see section 5.6) and the upperbound of the outband power spectrum reduces by 40 dB.

7.3.1 High-Order Filter Multi-Level Switching Amplifiers

The combination of multi-level power amplification and high-order filtering does not result in a clear performance improvement, since both techniques reduce the outband power of the remaining error signal $P^{\mathrm{o}}_{\xi(t)}$ at the cost of increasing the inband power $P^{\mathrm{i}}_{\xi(t)}$ (especially if the OSwR is not very high). Figures 7.10 and 7.11 show the performance of 3-level and 7-level fourth-order amplifiers respectively, whereas figures 7.12 and 7.13 show the performance of 3-level and 7-level

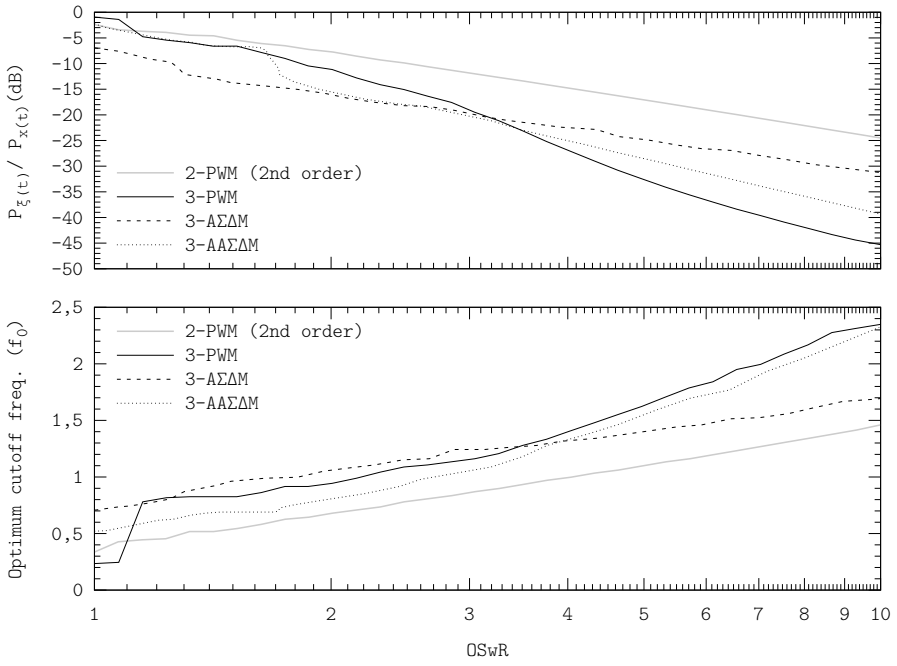

Figure 7.10: Performance of optimised 4th order 3-level amplifiers. Simulation performed using the configuration D.4.4.

eighth-order amplifiers respectively (the cutoff frequency f_c of each candidate has been optimised to minimise the power of the remaining error signal $P_{\xi(t)}$).

In all these characterisations the trend is the same: once the OSwR is high enough to avoid the slew-rate constraint, the best performance at low OSwRs is achieved with a PWM-based amplifier. At lower OSwRs, the performance of AΣΔM-based designs is better. Comparing the performance of AΣΔM-based and AAΣΔM-based amplifiers, the adaptive version is constrained by the stability control (discussed in section 5.5.2), which degrades its performance at low OSwRs (depending on the number of levels N). The different filter's optimum cutoff frequencies f_c also illustrate these trends.

However, the differences between each group of candidates (amplifiers using the same number of levels N and the same filter's order n) are not wider than in the previous cases, i.e. 2-level high-order candidates or multi-level second-order candidates. Furthermore, the combination of high-order filtering and multi-level power amplification do not improve the amplifier's performance within the considered range of OSwRs.

Indeed, by individually comparing the performance of each kind of amplifier (PWM-based, AΣΔM-based and AAΣΔ-based, figures 7.14, 7.15 and 7.16 respectively), it turns out that, depending on the modulation, either the filter's order n or the number of levels N mostly determine their performance.

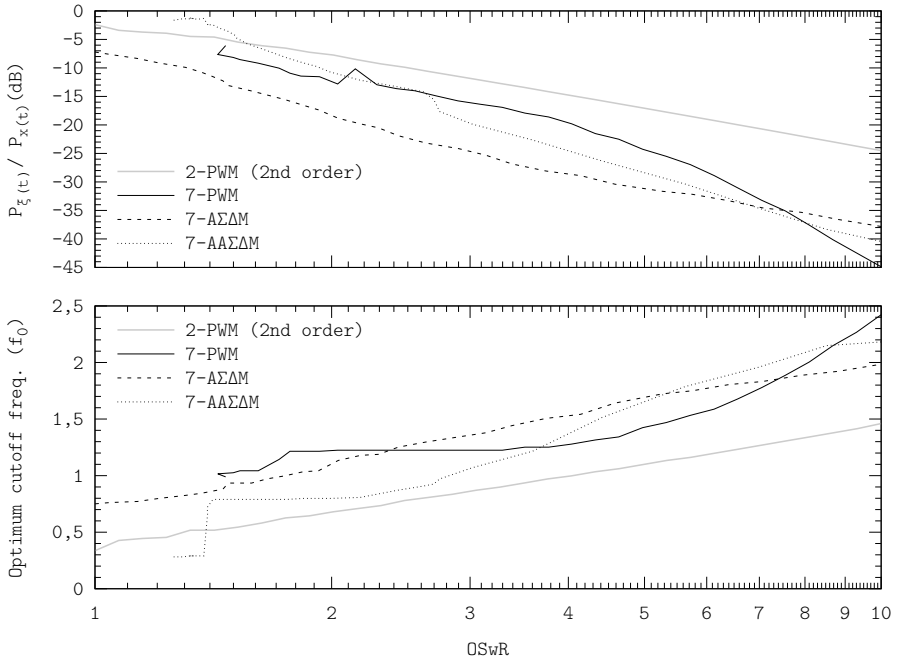

Figure 7.11: Performance of optimised 4th order 7-level amplifiers. Simulation performed using the configuration D.4.4.

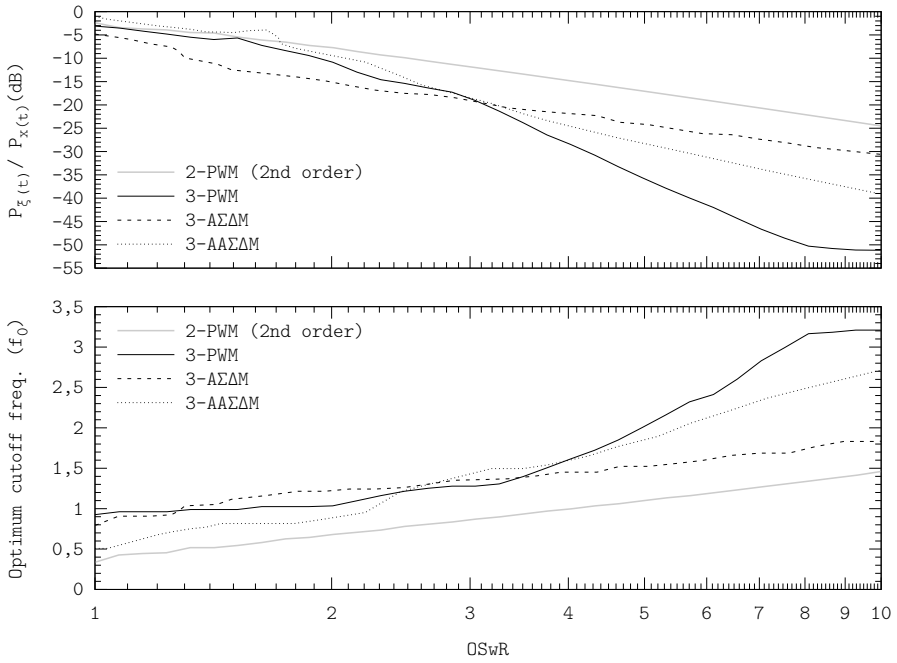

Figure 7.12: Performance of optimised eighth order 3-level amplifiers (values below −50 dB are masked by simulation errors). Simulation performed using the configuration D.4.4.

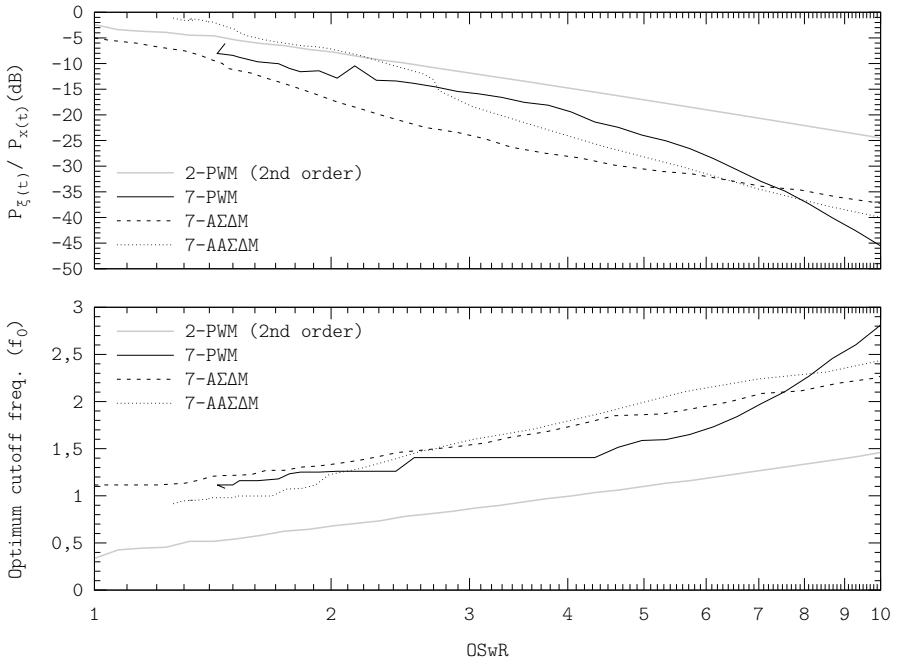

Figure 7.13: Performance of optimised eighth order 7-level amplifiers. Simulation performed using the configuration D.4.4.

Performance Summary of PWM-Based Amplifiers

In PWM-based amplifiers, as long as the slew-rate constraint is avoided, the performance is mostly determined by the filter's order n (see figure 7.14). The eighth-order 2-PWM and 3-PWM amplifiers clearly illustrate this issue, since the remaining error signal's power $P_{\xi(t)}$ in the 2-level amplifier is lower than in the 3-level amplifier, even if operating beyond the OSwR range constrained by the intrinsic slew-rate limitation. Despite the filter's cutoff frequency f_c is set to a higher value in the 3-PWM amplifier than in the 2-PWM amplifier, the stopband rejection of the eighth-order filter is high enough to reveal the inband error due to improper encoding in 3-PWM. Likewise, at an OSwR of 10, the remaining error signal's power $P_{\xi(t)}$ of the second-order 7-PWM amplifier is more than 5 dB higher than that of the fourth-order 2-PWM amplifier.

At lower OSwRs, the performance of multi-level PWM-based amplifiers is strongly constrained by the slew-rate limit. The encoding process do not correspond to PWM, and hence no conclusions can be drawn from their performance.

Performance Summary of AΣΔM-Based Amplifiers

In AΣΔM-based amplifiers the trend is opposite; provided that N-AΣΔM is an incremental multi-level modulation (i.e. no constraints regarding the number of levels N and the OSwR), the performance is mainly determined by the number of levels N (see figure 7.15). For instance, at an OSwR of 7, the error power $P_{\xi(t)}$ in the second-order 7-AΣΔM amplifier is lower than the error power $P_{\xi(t)}$ in the eighth-order 2-AΣΔM amplifier.

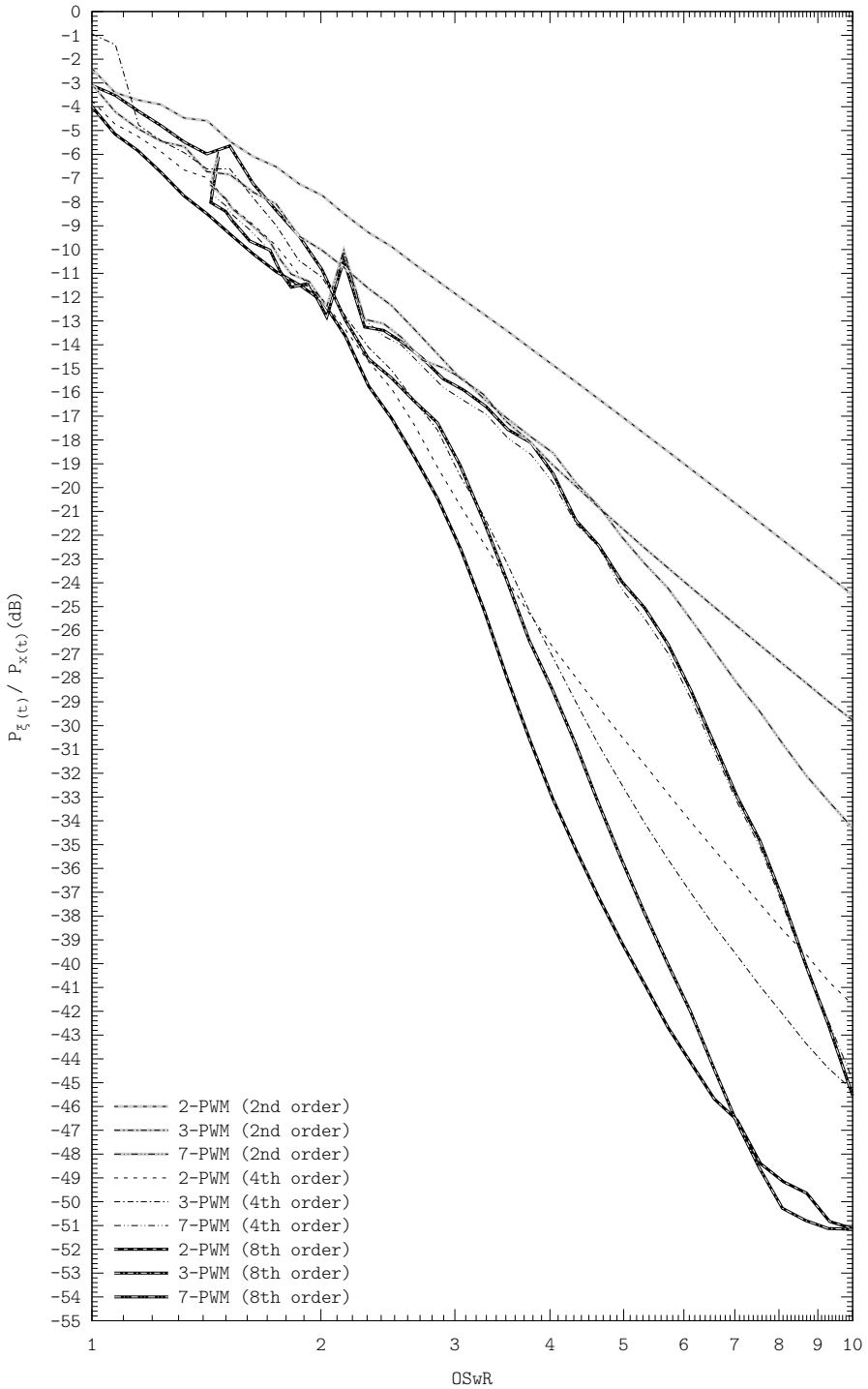

Figure 7.14: Performance summary of different PWM-based amplifiers (values below −50 dB are masked by simulation errors). Simulation performed using the configuration D.4.6.

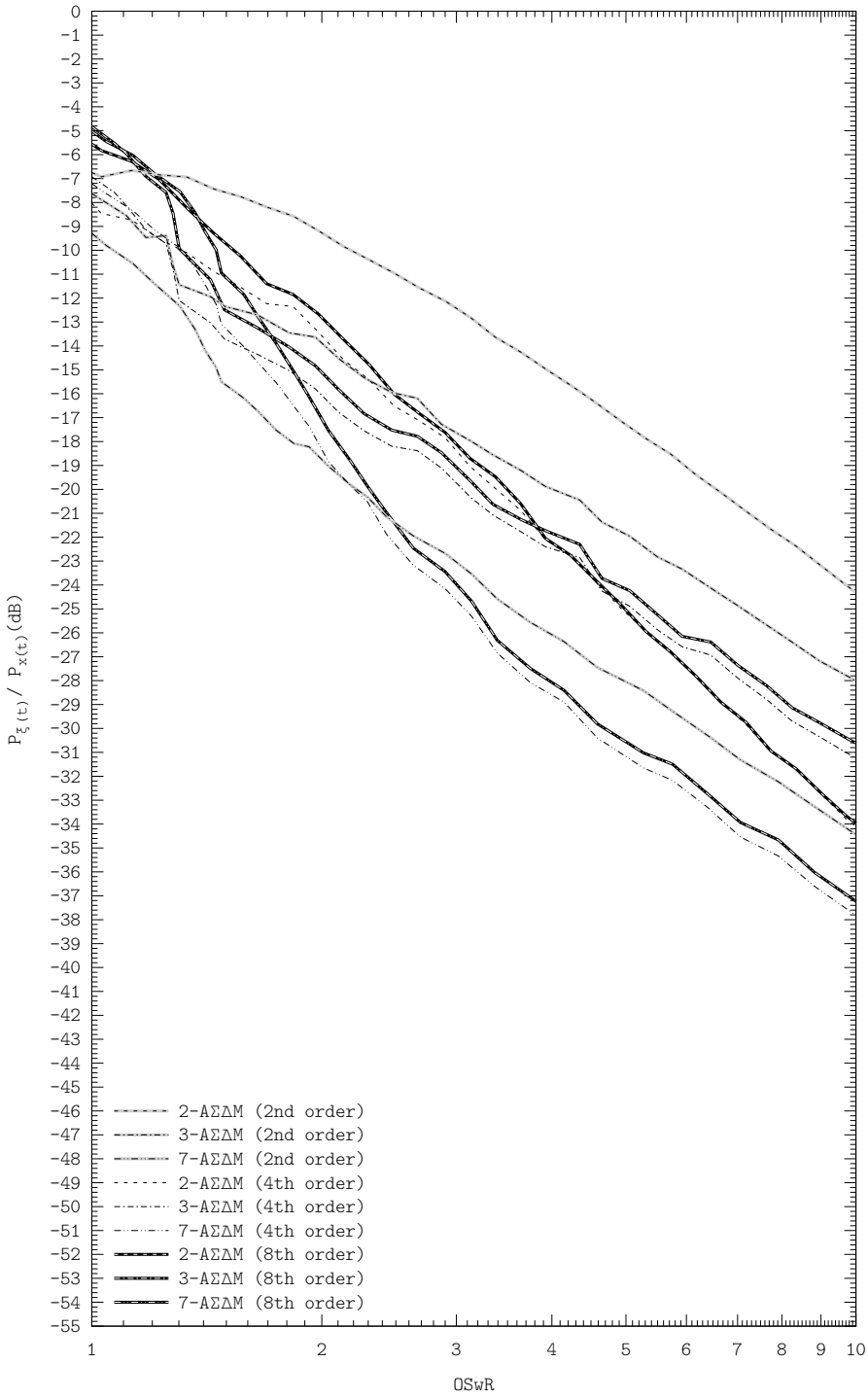

Figure 7.15: Performance summary of different AΣΔM-based amplifiers. Simulation performed using the configuration D.4.6.

This trend becomes more visible at low OSwRs. The filter's cutoff frequency f_c is always set to a lower value than the switching frequency $f_c < f_s$; to avoid high inband errors due to the filter's inband attenuation and phase lag, the ratio of the switching frequency $f_s = \mathrm{OSwR} f_0$ to the filter's cutoff frequency f_c is low. Consequently, the outband spectral content is only partially rejected by the filter. Note that, depending on the OSwR and the operating conditions, increasing the filter's order n may even degrade the amplifier's performance (despite optimising the cutoff frequency f_c).

On the other hand, increasing the number of levels N becomes a very effective technique to reduce the remaining error signal's outband power $P^{\mathrm{o}}_{\xi(t)}$, and hence reduce the total power of the remaining error signal $P_{\xi(t)}$, as it hardly degrades the inband performance.

These issues become especially visible if comparing different high-order amplifiers, such as a fourth-order and an eighth-order 7-AΣΔM amplifiers (at any OSwR, the trend is general). Because of the spread-spectrum, when increasing the filter's cutoff frequency f_c, part of the modulation's outband spectral content passes through the filter's bandpass (i.e. is not rejected). The further rejection of the remaining outband spectral content does not compensate this error increase and hence the remaining error signal's power $P_{\xi(t)}$ increases. Whilst AΣΔM-based amplifiers are suitable to operate at low OSwRs, their performance at high OSwRs is significantly worse than that of PWM-based designs; mainly because the higher inband error due to improper encoding.

Nevertheless, N-AAΣΔM has all the advantages and benefits of multi-level incremental modulations, like N-AΣΔM, but it achieves better performance at high OSwRs.

Performance Summary of AAΣΔM-Based Amplifiers

AAΣΔM-based amplifiers go by a similar trend than PWM-based amplifiers (see figure 7.16). At high OSwRs, the outband power spectrum accumulates within bands around frequencies multiples of the switching frequency. This behaviour is suitable to be decoded by high-order filters. Nevertheless, because of the higher inband error (compared to PWM-based amplifiers), AAΣΔM-based amplifiers achieve worse performance than PWM-based amplifiers.

Like in the PWM case, the best performance is achieved with an eight-order 2-AAΣΔM design; however, similar performances are achieved using more levels or using a fourth-order filter (and different number of levels). With a second-order filter, the amplifier's performance is worse and more dependent upon the number of levels N.

At low OSwRs, because of the control for astable operation of multi-level AAΣΔM, the performance significantly degrades.

7.4 Robustness Against Non-Idealities

When designing a switching amplifier for an actual application, the theoretical or ideal behaviour may not be achieved by actual amplifiers because of non-idealities and other implementation issues. This non-ideal behaviour is generally compensated with feedback (closed-loop operation), which can be applied regardless of the modulation.

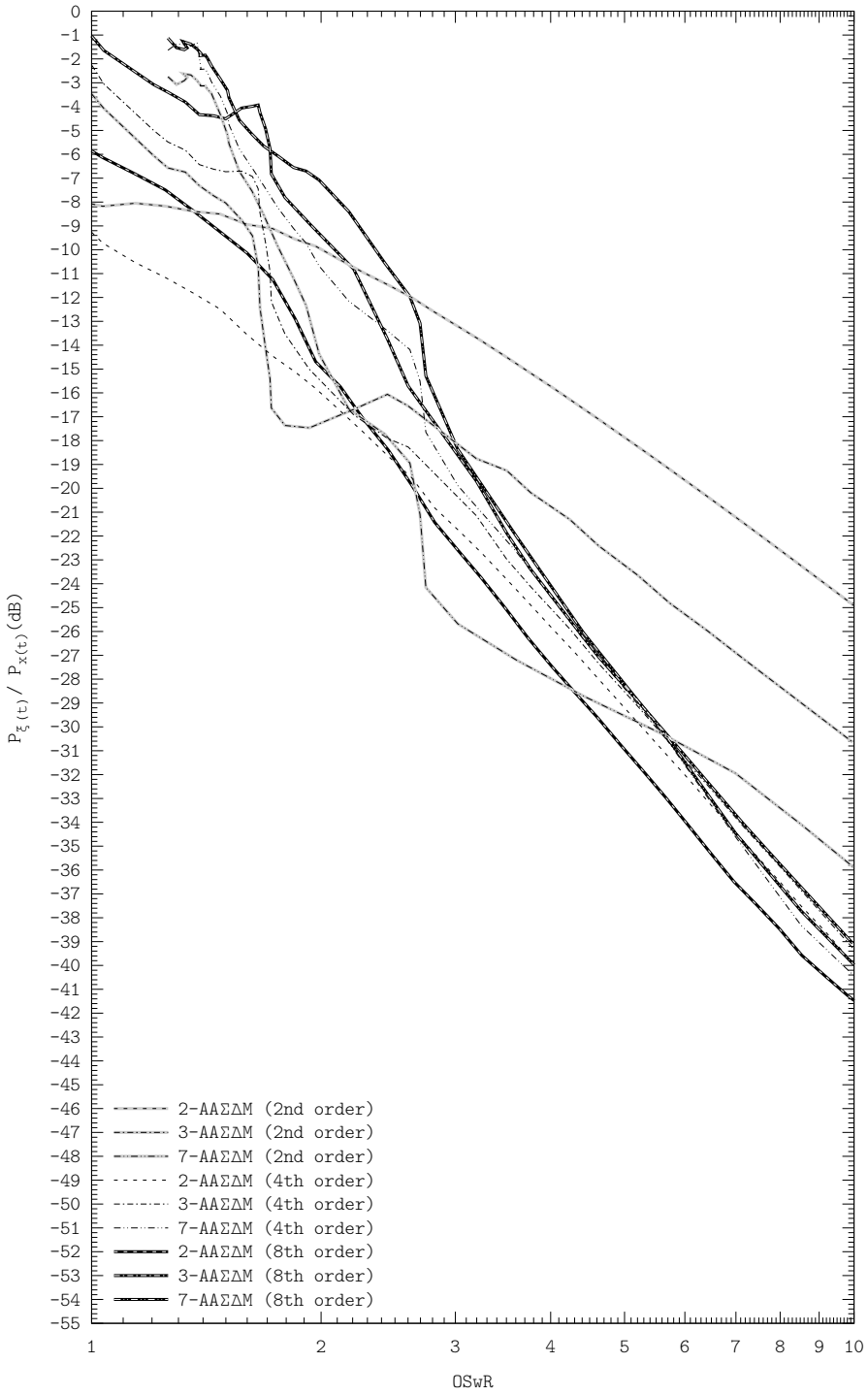

Figure 7.16: Performance summary of different AAΣΔM-based amplifiers. Simulation performed using the configuration D.4.6.

However, AΣΔM-based amplifiers can be implemented aiming enhanced robustness against non-idealities. Instead of sensing and feeding back the switching signal $z(t)$, the actual power switching signal $\tilde{z}(t)$ can be sensed, scaled by a factor G^{-1} and fed back into the modulator (see figure 7.17). This alternative implementation requires a wideband adder, a wideband integrator and is sensitive to the buffer delay t_{b}, but it provides the modulator with enhanced robustness against waveform distortion in the power switching signal $\tilde{z}(t)$, i.e. variations in the levels, slow edges, dead time, etc. Hereinafter, all AΣΔM-based designs sense the power switching signal $\tilde{z}(t)$, unless otherwise stated.

7.4.1 Power Supply Rejection Ratio and Switches' ON Resistance

The supply voltage V_{G} provided by an actual power supply is not constant. Because of the non-zero output impedance Z_{G}, the actual voltage $\tilde{V}_{\mathrm{G}}$ depends upon the supplied current i_{G}. Furthermore, parasitic or remaining signals $v_{\mathrm{G}}(t)$ may be present in the supply voltage as well, resulting in a non-constant and current-dependent voltage.

$$\tilde{V}_{\mathrm{G}}(t, i_{\mathrm{G}}) \approx (1 - Z_{\mathrm{G}} i_{\mathrm{G}}) \, (V_{\mathrm{G}} + v_{\mathrm{G}}(t)) \tag{7.1}$$

Additionally, the ON resistance R_{S_i} of actual switches is not zero and its OFF resistance is finite. Both non-idealities result in a similar effect, non-constant voltage levels in the power switching signal $\tilde{z}(t)$. The variations in the voltage levels can be uncorrelated with the recovered signal $\tilde{x}(t)$ –e.g. a remaining sine-like signal added to the supply voltage– or correlated with the recovered signal $\tilde{x}(t)$ –switches' ON resistance R_{S_i} and power supply's output impedance Z_{G}, whose voltage drop depends upon the generator current i_{G} which is finally determined by the load R_{L}–.

In an N-AΣΔM (or N-AAΣΔM) sensing the actual power switching signal $\tilde{z}(t)$, the voltage variations $\tilde{V}_{\mathrm{G}} - V_{\mathrm{G}}$ are also fed back to the modulator thus becoming part of the encoding process. Therefore, the modulator threats (and rejects) them in the same way as it encodes the reference signal $x(t)$. For instance let a parasitic sine wave add to the supply voltage V_0.

$$\tilde{V}_0(t) = V_0 + A \sin(2\pi f_{\mathrm{A}} t) \tag{7.2}$$

Let a modulator tracking a f_0-bandlimited reference signal $x(t)$ generate the power switching signal $\tilde{z}(t)$ from this supply voltage $\tilde{V}_0(t)$ during $t_0 \in [t_k, t_{k+1}]$.

$$\tilde{z}(t_0) = V_0 + A \sin(2\pi f_{\mathrm{A}} t_0) \tag{7.3}$$

The integrator's input signal $-e(t)$ is then

$$-e(t_0) = x(t_0) - \frac{V_0}{G} - \frac{A}{G} \sin(2\pi f_{\mathrm{A}} t_0) \tag{7.4}$$

From the encoding process standpoint, encoding these signals is equivalent to encode a different reference signal $y(t) = x(t) - \frac{A}{G} \sin(2\pi f_{\mathrm{A}} t)$, still f_0-bandlimited assuming $f_{\mathrm{A}} < f_0$[1], with an ideal voltage supply V_0 and an ideal

[1] A common case, since the switching frequency of switching voltage regulators is generally lower than the switching frequency of switching amplifiers.

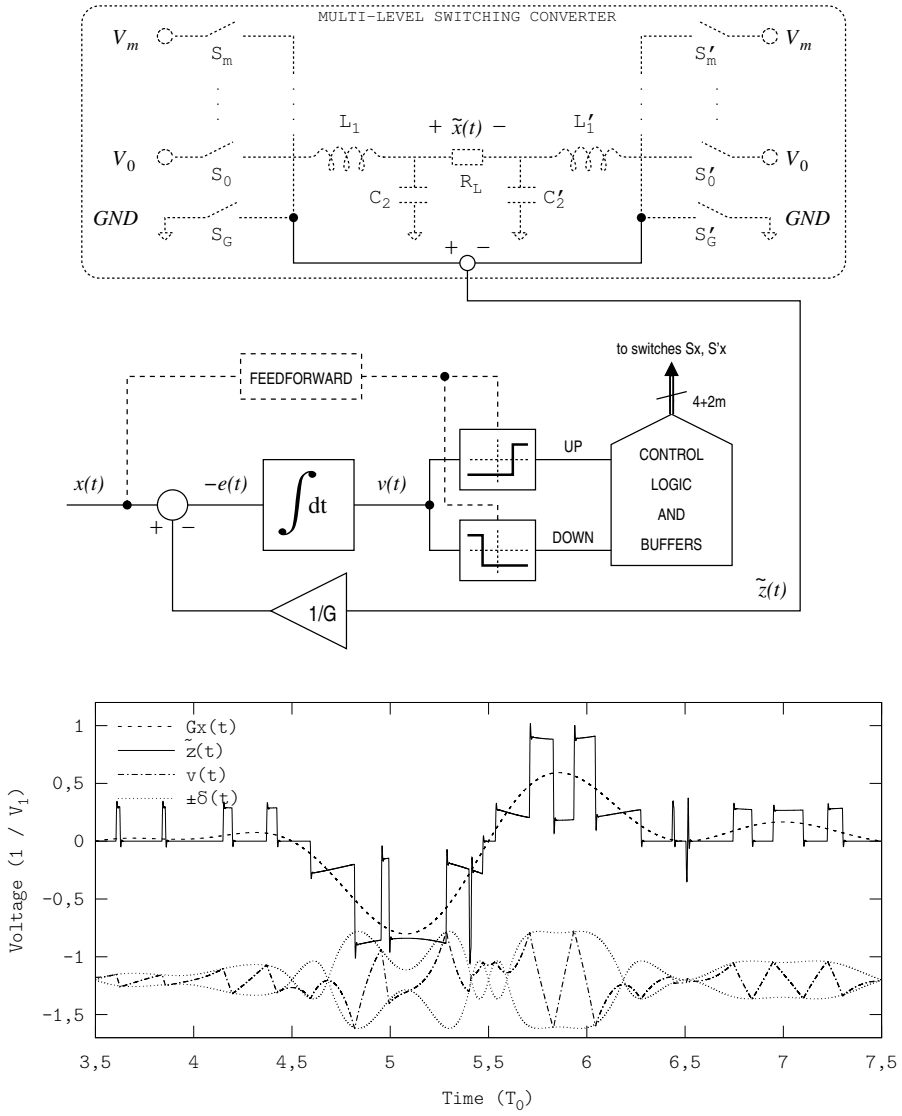

Figure 7.17: Block diagram of an N-AΣΔM sensing the power switching signal $\tilde{z}(t)$, in this example driving a multi-level full-bridge converter supplied by $m+2$ supply voltages, and representative time waveforms for a 5-AAΣΔM (non-regularly distributed levels) generated from power supplies with output impedance $Z_G/R_L = 20\,\%$. The integrator's output signal $v(t)$ and the hysteresis-width function $\delta(t)$ have been shifted and scaled for better readability.

power converter.

$$-e(t_0) = y(t_0) - \frac{V_0}{G} \tag{7.5}$$

A similar analysis can be carried out for the switches' ON resistance R_{S_i} and the power supply's output impedance Z_{G}. In all cases the encoding process is equivalent to encoding a different (yet still f_0-bandlimited) reference signal $y(t)$ with an ideal voltage supply V_0 and an ideal power converter, as long as the recovered signal $\tilde{x}(t)$ does not saturate the actual supply voltages $\tilde{V}_i$.

Therefore, the performance of AΣΔM-based modulators should be very robust against this kind of non-idealities. To illustrate this robustness, figure 7.18 shows the representative time waveforms and the power spectrum of the power error signal $\tilde{Z}(f) - GX(f)$ in a 7-AΣΔM amplifier, whose active supply voltages have an added parasitic tone, as in (7.2). The amplitude A is $Z_{\mathrm{pp}}/20$ and the frequency f_{A} is f_0. At the tone's frequency f_{A}, the spectral power density of the error signal $\tilde{Z}(f) - GX(f)$ is about 30 dB below the reference signal $GX(f)$. This remaining harmonic is partially due to the modulator's saturation (the added tone eventually decreases the maximum supply voltage below the reference signal $Gx(t)$). Furthermore, the rejection depends upon the ratio of the switching frequency $f_{\mathrm{s}} = \mathrm{OSwR} f_0$ to the tone's frequency f_{A}; the higher the ratio is, the higher the rejection becomes.

Figure 7.18 also includes the power spectrum corresponding to a 7-AΣΔM modulator operating under the same conditions, but sensing the switching signal $z(t)$ instead of the power switching signal $\tilde{z}(t)$, i.e. without the enhanced robustness against non-idealities. In this case, the power spectrum not only has a main harmonic at the tone's frequency f_{A} (whose amplitude exceeds the reference signal's level), but its inband error is very high as well.

N-PWM encodes without sensing the power part. All the differences between the actual $\tilde{z}(t)$ and $Gz(t)$ directly result in error in the recovered signal $\tilde{x}(t)$, similarly to the N-AΣΔM case shown in figure 7.18. On the other hand, N-PWM is not sensitive to the buffer delay t_{b}.

N-PWM can also be improved to increase the robustness against these non-idealities by adapting the carriers' amplitude to the actual output voltage levels L_i (see figure 7.19). However, implementing such carriers is not feasible and therefore these non-idealities must be compensated by an external slower control loop (closed-loop operation).

7.4.2 Time Delays and Bandwidth Limitations

The implementation of an AΣΔM-based modulator sensing the power switching signal $\tilde{z}(t)$ requires a wideband adder and a wideband integrator (see figure 7.17). According to the power spectrum of N-AΣΔM (see figure 5.17), most of the power concentrates around the switching frequency $f_{\mathrm{s}} = \mathrm{OSwR} f_0$. Therefore, in order to properly sense the power switching signal $\tilde{z}(t)$, the bandwidth of both the adder and the integrator must be wider than this value; otherwise, the signal sensed and fed back would be a bandlimited approximation to the power switching signal $\tilde{z}(t)$.

The bandwidth issue of both the adder and the integrator can be merged and modeled as an ideal adder and a bandlimited integrator $H_{\mathrm{i}}(s)$ (i.e. an integrator with a main pole at frequency f_{i} and a non-dominant pole at frequency f_{p}). Moreover, the DC gain of implementable integrators is finite, yet typical values

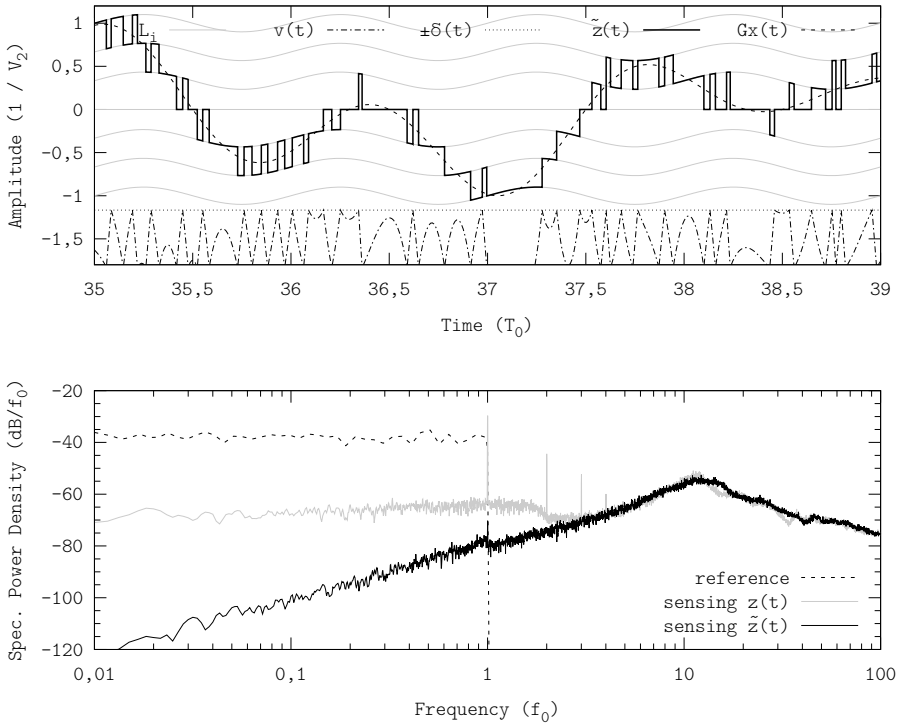

Figure 7.18: Enhanced PSRR in N-AΣΔM (sensing the actual power switching signal $\tilde{z}(t)$). 7-AΣΔM example operating at OSwR $\approx$ 8,4, showing the time waveforms (upper plot) and the power spectrum (sensing the power switching signal $\tilde{z}(t)$ and sensing the switching signal $z(t)$, i.e. without enhanced robustness against non-idealities, lower plot). Power spectra computed using the configuration D.4.1.

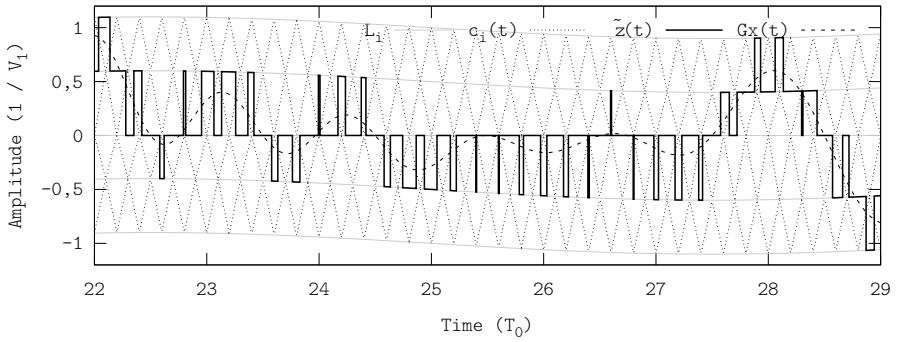

Figure 7.19: Amplitude-shifted 5-PWM with adaptive carriers for enhanced PSRR.

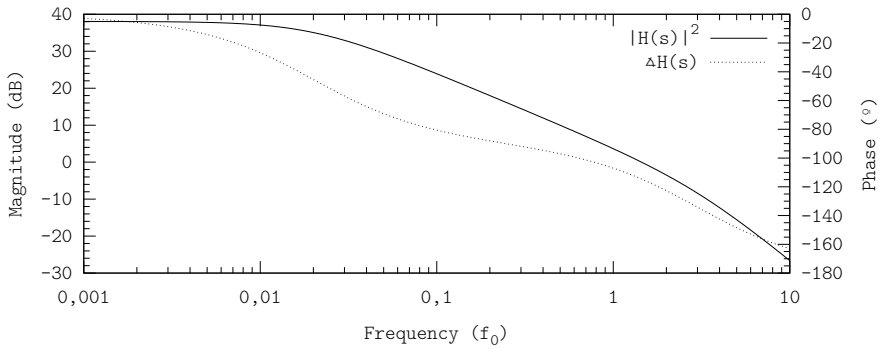

Figure 7.20: Bode plot of a bandlimited integrator (example with $f_\mathrm{p} \approx 3f_0$ and $f_\mathrm{i} \approx 2 \cdot 10^{-2} f_0$).

do not lead to a significant error ($f_\mathrm{i} \ll f_0$, where f_i stands for the frequency of the main pole and f_0 stands for the bandwidth of the reference signal $x(t)$, see figure 7.20).

$$H_\mathrm{i}(s) = \frac{A_0}{(p_\mathrm{i} + s)(p_\mathrm{p} + s)} \tag{7.6}$$

In regular operating conditions, i.e. a N-AΣΔM tracking a f_0-bandlimited signal at a certain OSwR, the effect of the non-dominant pole can be characterised by sweeping its frequency from very high frequencies $f_\mathrm{p} \gg f_\mathrm{s} = \mathrm{OSwR} f_0$ to f_0 (see figure 7.21). As the frequency of the non-dominant pole f_p approaches to the switching frequency f_s, the second-order transient response becomes visible. Instead of instantaneously changing the slope whenever the system switches, the transitions become smooth and slow; the integrator's output signal $v(t)$ exceeds the comparator's window $\pm\delta$ during the transition (see figure 7.22).

The effect is twofold, the quality of the encoding process is degraded and the OSwR decreases. If the OSwR is increased (by increasing the integrator's gain or reducing the hysteresis width), the system would not behave as an ideal AΣΔM operating at the same OSwR, since overshooting limits the minimum width of a pulse (see figure 7.21, if the OSwR reduces because of a non-ideality, the error power increases at a faster rate than if the OSwR is reduced by widening the hysteresis width δ). The amplitude of overshooting depends upon the integrator's output waveform $v(t)$.

A time delay between triggering the comparator and triggering the power part, typically the buffer delay t_b, also results in a similar effect (see figures 7.21 and 7.22). The integrator's output signal $v(t)$ still changes the slope instantaneously, but it exceeds the comparator's window $\pm\delta$. Overshooting depends upon the waveform of the integrator's output signal $v(t)$ around every switching event, since the time delay is constant t_b and hence its slope $\dot{v}(t)$ determines the overshooting.

Both issues result in an effective delay between triggering the comparator and reversing the slope of the integrator's output signal $v(t)$; alternatively, this effect can also be interpreted as a random-variable hysteresis width $\delta(t)$. Note

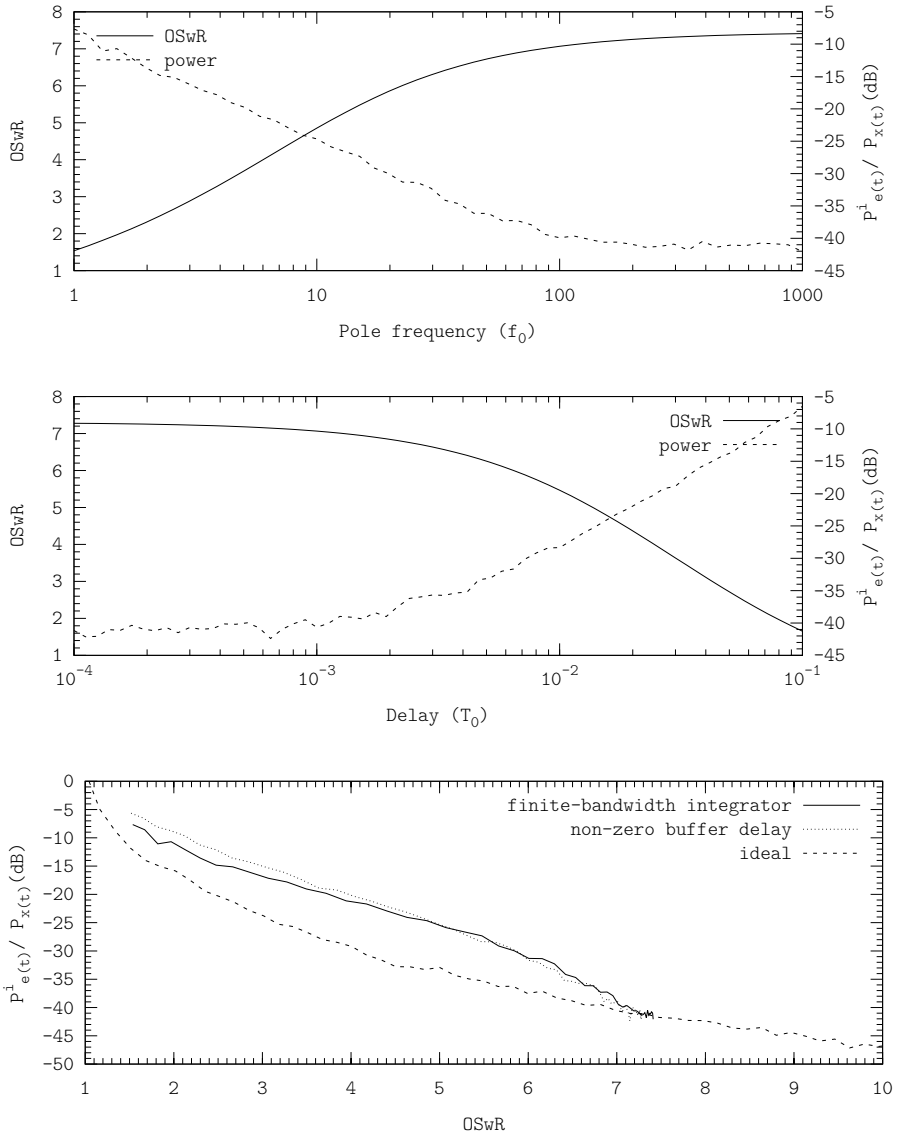

Figure 7.21: Performance characterisations of a 2-AΣΔM with a finite-bandwidth integrator (sweeping the frequency of the non-dominant pole f_{p}, upper plot), with non-zero buffer delay t_{b} (middle plot) and comparison with the ideal case (comparing the performance degradation due to the non-idealities with the ideal case, lower plot). Simulation performed using the configuration D.4.6

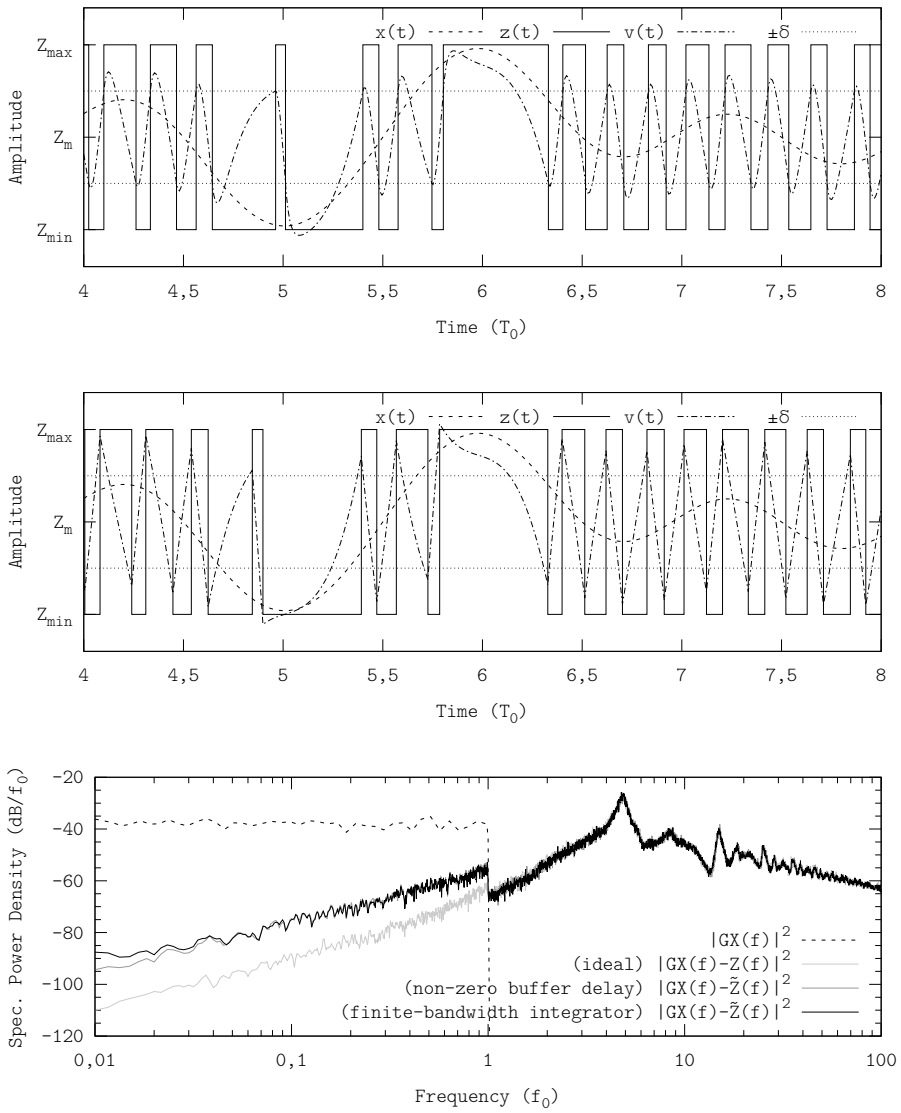

Figure 7.22: Performance example of 2-AΣΔM with a finite-bandwidth integrator (in the time domain, $f_\mathrm{p} \approx 7{,}6 f_0$ and OSwR $\approx 4{,}4$, upper plot), with non-zero buffer delay t_b (time domain, $t_\mathrm{b} \approx 2 \cdot 10^{-2} T_0$ and OSwR $\approx 4{,}5 f_0$, middle plot) and comparison with the ideal case (frequency domain, lower plot). Simulation performed using the configuration D.4.1.

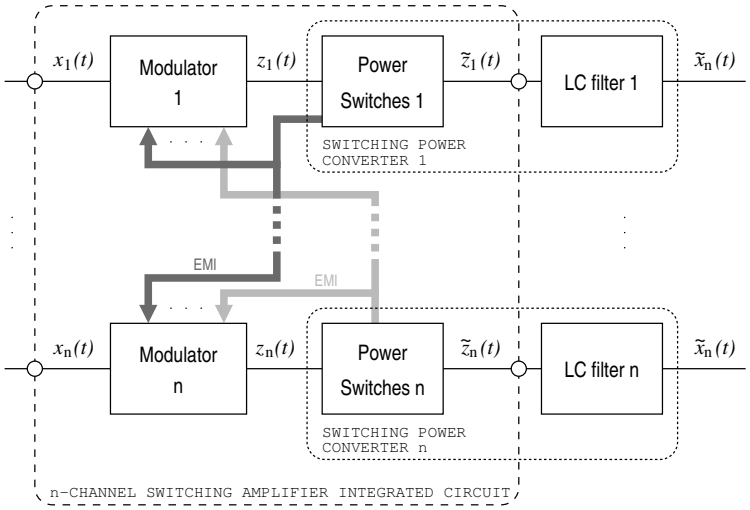

Figure 7.23: Crosstalk in multi-channel integrated switching amplifiers; example showing an n-channel integrated amplifier, each channel suffers crosstalk from all the channels, including itself. Displayed waveforms correspond to channel 1 (upper plot) and channel 2 (lower plot).

that, according to this latter interpretation, an N-AA$\Sigma\Delta$M suffering a significant delay tends to behave as an N-A$\Sigma\Delta$M, since the variations in the effective hysteresis-width function $\delta(t)$ mask the desired reference signal-dependent hysteresis-width function. Still, with state-of-the-art technology, it is feasible to design wideband integrators with moderate power consumption; besides, this issue may be addressed by adapting the hysteresis width according to the slope of the integrator's output signal, i.e. the error signal $-e(t)$, thereby compensating wide overshoots with earlier switching.

7.4.3 ElectroMagnetic Interferences and Crosstalk

A multi-channel integrated switching amplifier consists of n switching amplifiers, each one with its corresponding modulator and switching power converter. Every switching event in the power part, in any channel, involves high currents, resulting in EMI which may couple to any modulator in the integrated circuit (i.e. to any of the n channels, see figure 7.23). The coupled EMIs may modify the circuit conditions, thereby degrading the quality of the encoding process (crosstalk). Similarly, EMIs can also be external (causing a similar effect), yet they can be mitigated by shielding the chip.

EMI Modeling

Both the modulator and the power switches have been modeled as ideal devices. The buffers are ideal as well, but with a time delay t_b; therefore

$$\tilde{z}(t) = Gz(t - t_\mathrm{b}) \tag{7.7}$$

The EMI generated by each power switching event (the power switching signal $\tilde{z}(t)$ changes its value) has been modeled as an instantaneous glitch (ca-

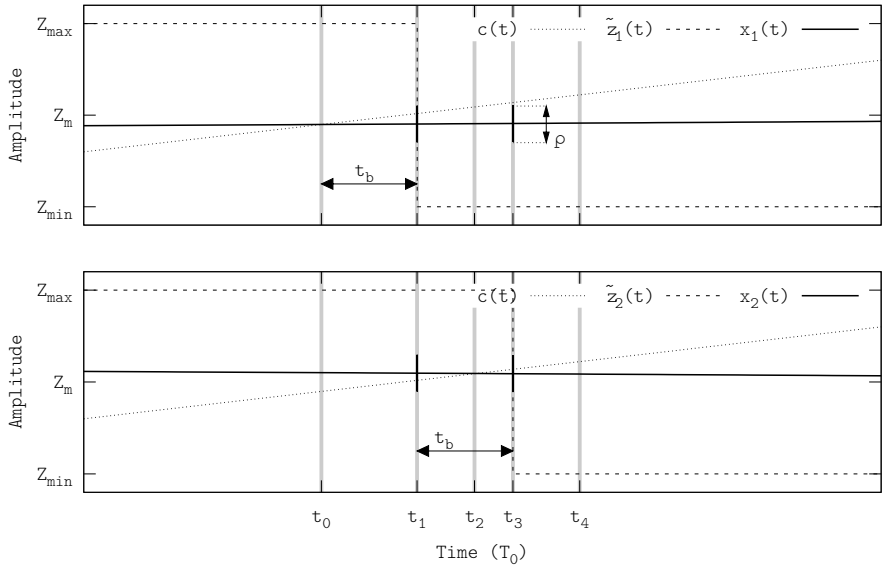

Figure 7.24: EMI modeling for crosstalk analysis. Example with 2-PWM, $\varrho = 20\,\%$ and a buffer delay t_b. Displayed waveforms correspond to channel 1 (upper plot) and channel 2 (lower plot).

pacitive coupling), which couples into the low-power circuitry (modulator). The peak-to-peak amplitude of this glitch is defined as the coupling factor ϱ and is expressed relative to the modulator's dynamic range.

The most EMI-sensitive nodes in the modulator's circuitry are the comparators' inputs, because of their high impedance. The glitches are added to the input signals of the comparators, so that they may prematurely trigger the comparators thus shifting forward the edges of the comparators' output signals (i.e. 2-level switching signals).

Figure 7.24 summarises the crosstalk EMI modeling with a 2-channel example ($\varrho = 20\,\%$); the modulation is 2-PWM in both cases. Channel 1 triggers a switching event at t_0, which triggers the power switches at $t_1 = t_0 + t_\mathrm{b}$. The glitch resulting of this power switching event couples into both channel 1 and channel 2; because of the latch (see below), channel 1 does not switch despite the comparator is triggered again. On the other hand, the glitch causes channel 2 to prematurely trigger at t_1, instead of at t_2, thereby triggering the power switches at $t_3 = t_1 + t_\mathrm{b}$ instead of at $t_3 = t_2 + t_\mathrm{b}$. The second glitch couples again to both channels, but none of them can switch again within this encoding interval.

Crosstalk in Multi-Level Pulse Width Modulators

Crosstalk effects upon N-PWM depend upon its implementation. Both phase-shifted an amplitude-shifted variants use $N - 1$ comparators per channel and therefore are prone to suffer from crosstalk, although the actual effects depend upon the specific variant. Since phase-shifted implementations of multi-level

PWM are more common than amplitude-shifted implementations, the phase-shifted variant is analysed.

In an n-channel integrated amplifier, each channel based on N-PWM, there are $n(N-1)$ comparators. Each switching event in the power part (any channel) yields a glitch which couples to all comparators' inputs, regardless of the channel. Therefore, in multi-level PWM, two comparators belonging to the same channel could crosstalk to each other (in-channel crosstalk).

All PWMs used in these simulations include a latch (one for each comparator), which is reset whenever the carrier inverts its slope. Latches are very common in PWM implementations to prevent extra switching, mainly because of EMI.

In-Channel Crosstalk A single-channel multi-level PWM amplifier uses more than one comparator, so it is prone to suffer from in-channel crosstalk.

Let us consider a simple example, 3-PWM. Whenever the reference signal approaches the intermediate level, the glitch produced by one comparator may also trigger the other comparator (the reference signal $x(t)$ is close to both carriers $\varphi_{1,2}(t)$, see figure 7.25), resulting in narrow pulses which convey no information of the reference signal (phoney pulses).

Certainly, when the first comparator is triggered, the power part is triggered with a delay of t_b. The glitch due to the EMI generated by this power switching event couples into the reference signal $x(t)$ and triggers the other comparator; after another delay of t_b, the power part is triggered again. This results in a phoney pulse, whose width is t_b, independent of the reference signal $x(t)$.

In general, when encoding with N levels, phoney pulses may appear whenever the reference signal approaches any intermediate level, thus there are ranges of very low tracking fidelity or rough encoding. Assuming that $t_\mathrm{b} \ll 1/f_\mathrm{s}$ (f_s stands for the switching frequency), the rough encoding ranges can be identified by encoding constant signals. The width of the rough encoding ranges corresponds to the coupling factor ϱ (see figure 7.26).

Note that 2-PWM is free of in-channel crosstalk, as it only uses one comparator.

Crosstalk Between n Channels When a single integrated amplifier includes n channels, each channel may suffer its own in-channel crosstalk and also crosstalk between the other channels. Let us assume that all channels encode with the same scheme (the same modulation and the same number of levels), a very common design strategy.

If at the time instant t_0 the value of the reference signals of two different channels, $x_i(t_0)$ and $x_j(t_0)$, are close to a carrier (not necessarily the same carrier in the two channels), then the glitch produced by one channel may prematurely trigger the other channel, thereby resulting in a phoney pulse. Figure 7.27 shows an example of this situation. Note that, unlike in-channel crosstalk, the crosstalk between channels may occur at value of the reference signal.

Crosstalk in Multi-Level Asynchronous ΣΔ Modulators

There exist two main variants of N-AΣΔM, sensing the switching signal $z(t)$ or the power switching signal $\tilde{z}(t)$. Whilst the former is not sensitive to the buffer delay t_b, the latter has better tracking performance (mainly because it is able

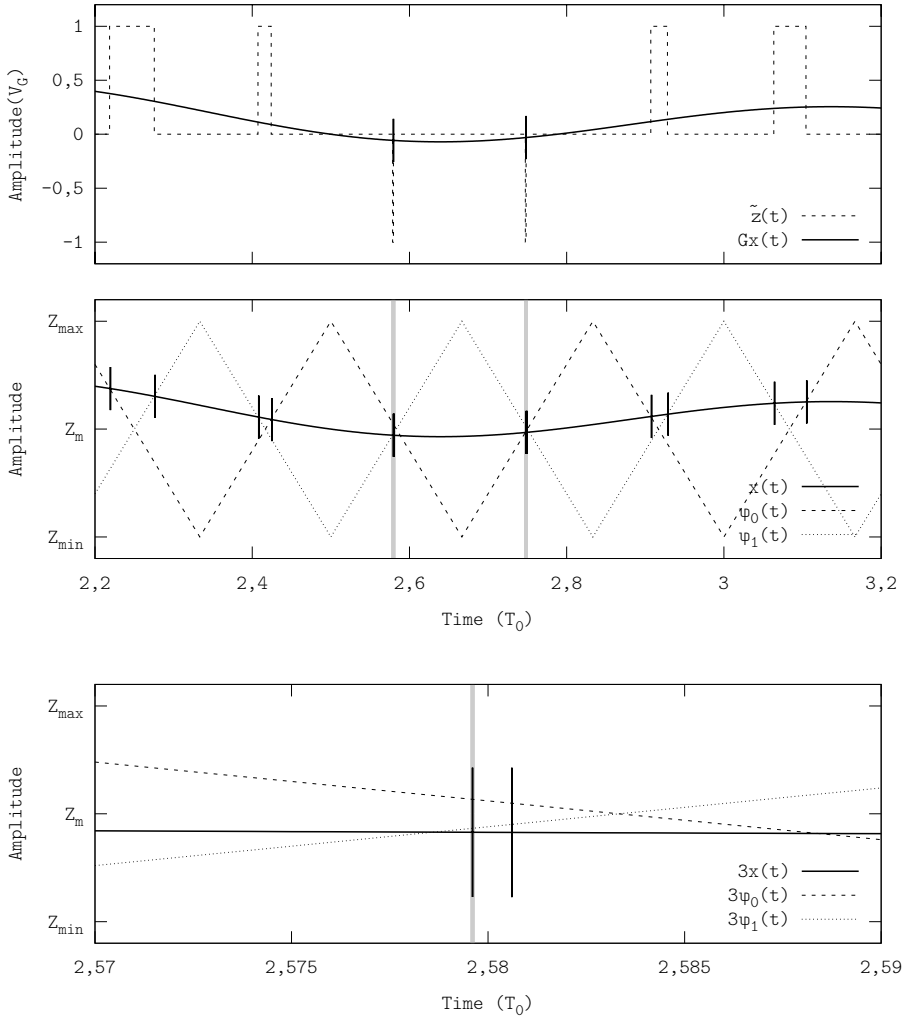

Figure 7.25: In-channel crosstalk in a single-channel 3-PWM amplifier ($\varrho = 20\,\%$ and $t_\mathrm{b} = 10^{-3}T_0$), displaying the power switching signal $\tilde{z}(t)$ and the scaled reference signal $Gx(t)$ with the glitches that cause in-channel crosstalk (upper plot), the carriers $\varphi_i(t)$ and the reference signal $x(t)$ (with the glitches that cause crosstalk highlighted in grey, middle plot) and a detail of in-channel crosstalk (lower plot).

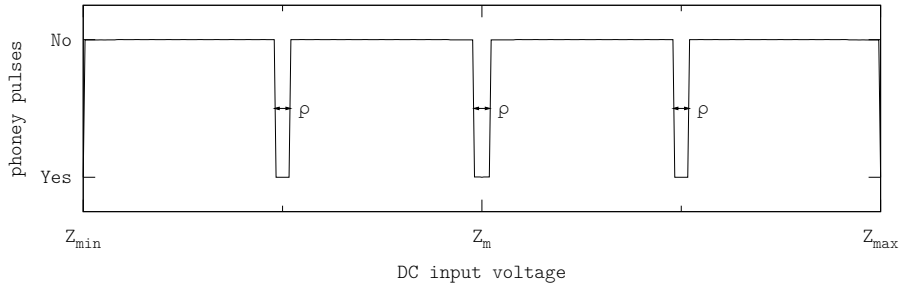

Figure 7.26: Rough encoding ranges in a 5-PWM ($\varrho = 2\,\%$). Simulation performed by setting the buffer delay to zero $t_\mathrm{b} = 0$ and measuring the switching frequency (tracking and sweeping the amplitude of the DC constant-reference signal); in such a case, crosstalk results in zero-width phoney pulses (pulse skipping).

to partially compensate variations in the supply voltages) and hence it is used in this analysis.

In N-AΣΔMs, the glitches are added to the integrator's output signal $v(t)$, which directly triggers the comparators (highest impedance node). The comparators use all the available dynamic range, i.e. from Z_min to Z_max, and therefore the coupling factor ϱ is the same in both PWM and AΣΔM (they can be directly compared).

In-Channel Crosstalk Unlike N-PWM, N-AΣΔM does not suffer from in-channel crosstalk because each N-AΣΔM only uses two comparators whose thresholds are set to the opposite bounds of the dynamic range (they cannot be triggered at the same time). There are no phoney pulses in the N-AΣΔM encoding process.

Crosstalk Between n Channels Two (or more) N-AΣΔM channels may crosstalk each other at any time, regardless of the value of the input signals $x_i(t)$ (see figure 7.28). Given the asynchronous nature of this modulator, it is difficult to beforehand foresee crosstalk, as it can happen at any time, any channel and with any value of the reference signals.

Figure 7.28 illustrates crosstalk in two N-AΣΔMs ($\varrho = 20\,\%$ and $t_\mathrm{b} = 10^{-3}T_0$). As this figure shows, there is no direct relation between the value of the reference signals $x_1(t)$ and $x_2(t)$ and crosstalk.

Adding more levels in the encoding process does not directly affect the crosstalk performance, as N-AΣΔMs use two comparators, whose thresholds are set to the bounds of the dynamic range, regardless of the number of levels N.

Crosstalk in Multi-Level Adaptive Asynchronous ΣΔ Modulators

Crosstalk in N-AAΣΔM is similar to the N-AΣΔM case. A single-channel N-AAΣΔM does not suffer from in-channel crosstalk, as it only uses two comparators which cannot be triggered at the same time. Like in N-AΣΔM, in a multi-channel system, two (or more) N-AAΣΔM channels may crosstalk each

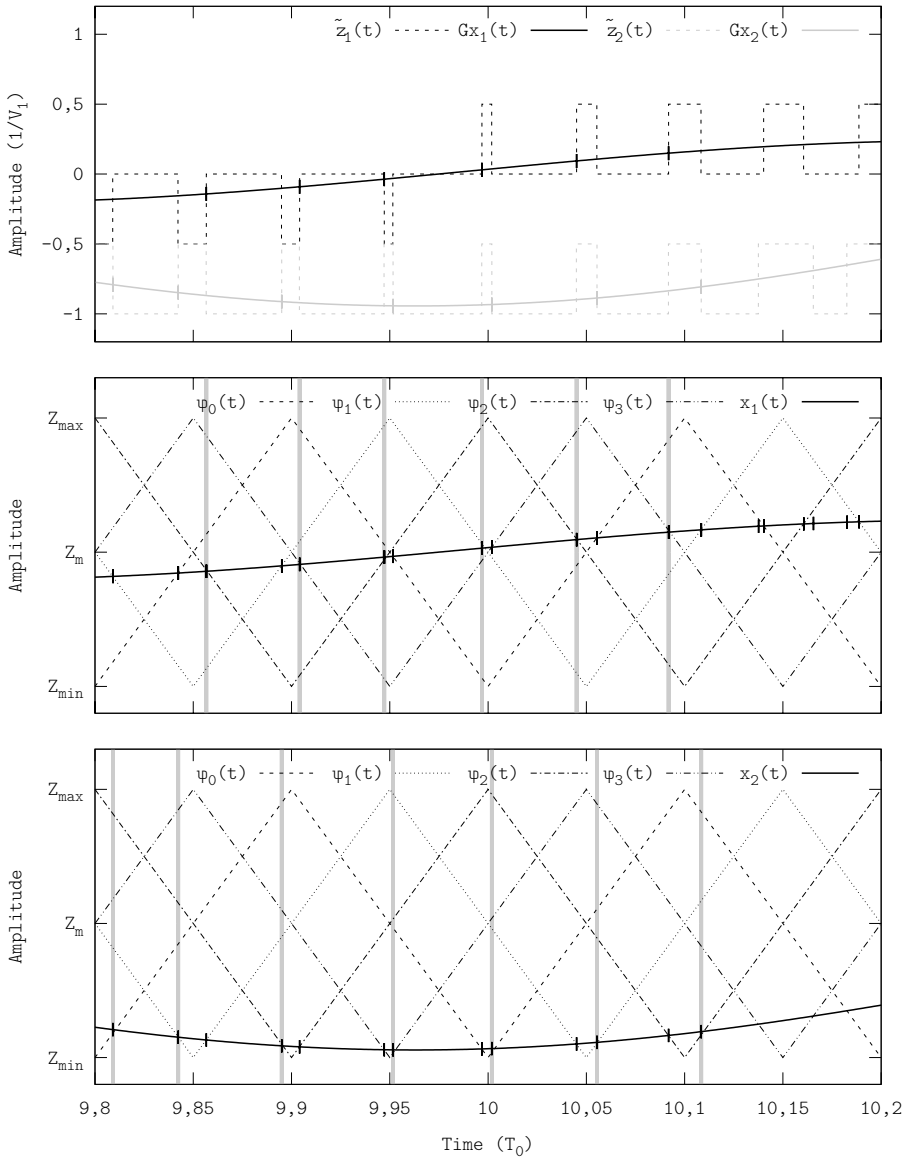

Figure 7.27: Crosstalk between two 5-PWM channels ($\rho = 5\,\%$ and $t_\mathrm{b} = 10^{-4}T_0$). Displayed waveforms show both 5-PWM signals and both reference signals, each one with the glitches that affect its encoding process (upper plot); the detailed generation of $\zeta_1(t)$ with the glitches that affect the encoding process highlighted in grey (middle plot); the detailed generation of $\zeta_2(t)$ with the glitches that affect the encoding process highlighted in grey (lower plot).

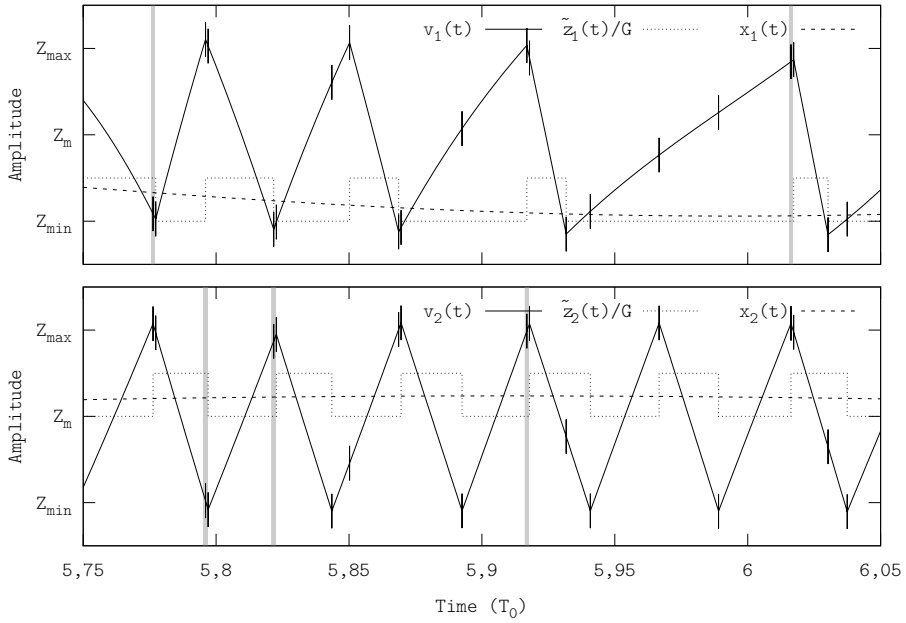

Figure 7.28: Crosstalk between two 5-AΣΔM channels ($\varrho = 20\,\%$ and $t_\mathrm{b} = 10^{-3}T_0$). Displayed waveforms correspond to channel 1 (upper plot) and channel 2 (lower plot). The glitches that affect the encoding process are highlighted in grey in each channel.

other at any time, regardless of the value of the input signals $x_i(t)$ (see figure 7.29).

Since the hysteresis-width function $\delta(t)$ can reduce its magnitude to very low values, N-AAΣΔM is more sensitive to crosstalk than N-AΣΔM. Nevertheless, the sensitiveness depends upon the implementation. For instance, if instead of implementing the hysteresis-width function $\delta(t)$ as variable thresholds in the comparators it is implemented as a variable gain in the integrator, the robustness against crosstalk would be similar than in the N-AΣΔM case.

Besides, crosstalk in N-AAΣΔM results in variations in the effective comparison threshold (defined by the value of the integrator's output signal $v(t)$ at the time instants in which the power switching signal $\tilde{z}(t)$ switches); i.e. N-AAΣΔM is not ruled by the hysteresis-width function $\delta(t)$. As pointed out in the inband performance characterisation of chapter 5 (in particular, figures 5.26 and 5.27), the adaptive-hysteresis upgrade does not significantly modifies the inband tracking performance. In the case of crosstalk, a similar behaviour is to be expected.

The robustness against crosstalk of 5-PWM and 5-AΣΔM is characterised and compared next, both operating at an OSwR of 10, with a coupling factor of $\varrho = 10\,\%$ and a buffer delay t_b of $10^{-3}T_0$.

The purpose of these characterisations is to evaluate the suitability of each family of modulators (constant switching frequency or asynchronous operation) for multi-channel integration. These characterisations have been performed in the representative case of 5 levels, although the results can be generalised to

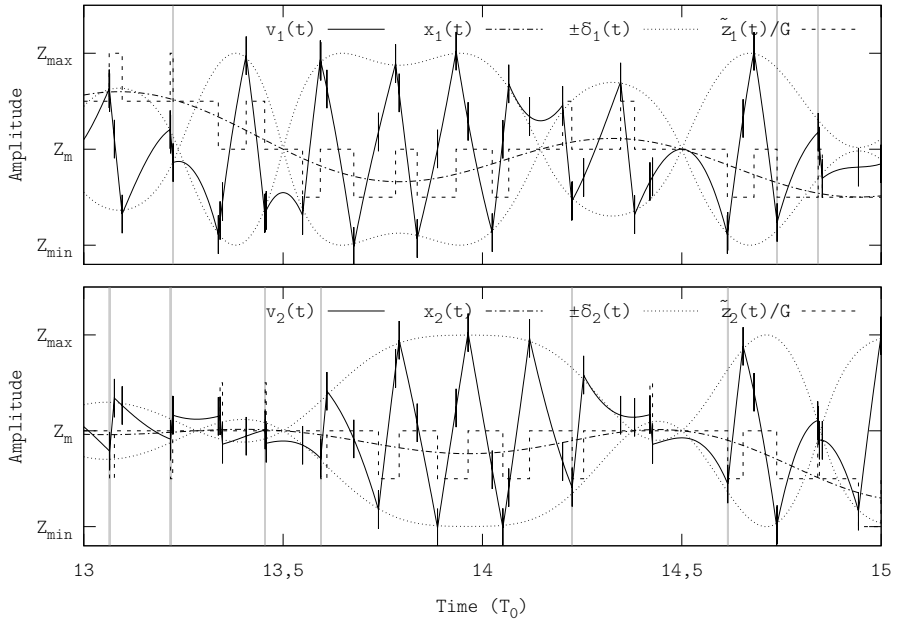

Figure 7.29: Crosstalk between two 5-AAΣΔM channels ($\varrho = 20\,\%$ and $t_\mathrm{b} = 10^{-3}T_0$). Displayed waveforms correspond to channel 1 (upper plot) and channel 2 (lower plot). The glitches that affect the encoding process are highlighted in grey in each channel.

any number of levels.

As discussed above, the low-power circuitry (i.e. the modulator) uses the same dynamic range in PWM- and AΣΔM-based amplifiers. The coupling factor ϱ is hence the same for all modulations (the peak-to-peak amplitude of the glitches).

In either modulation, crosstalk may increase the inband error due to improper encoding. According to the additive model of time encoding presented in chapter 2, crosstalk results in additional content (in principle up to the switching frequency f_s, i.e. both inband and outband) in the error signal. In periodic signals this additional content may be more visible, since the power switching signal $\tilde{Z}(f)$ generated under crosstalk conditions may have harmonics at frequencies which had no content otherwise (i.e. without crosstalk).

Performance Evaluation (Constant Signal)

This test is intended to determine whether multiple channels could lock each other, i.e. generate a power switching signal $\tilde{z}(t)$ locally independent of the reference signal $x(t)$; formally, small variations of the reference signal $x(t)$ yield the same power switching signal.

In the case of PWM, the value of the constant-reference signals (of any channel) cannot be similar to an output voltage level. Indeed, the distance between the reference signal and any output voltage level must be greater than $\varrho/2$ to avoid in-channel crosstalk. Furthermore, because of the same reason,

the relative distance[2] between whichever to reference signals, namely $x_i(t)$ and $x_j(t)$, must be greater than $\varrho/2$; otherwise they would crosstalk to each other.

Figure 7.30 illustrates the latter situation with an example, specifically a dual-channel 5-PWM amplifier tracking two constant-reference signals of value $x_1(t) = -0{,}3012$ and $x_2(t) = 0{,}3996$ (using the normalisation $Z_{\max} = 1$ and $Z_{\min} = -1$). The output voltage levels are equally distributed, which maps to the values ± 1, $\pm 0{,}5$ and 0 in the normalised modulator range. These reference signals are too close for this coupling factor. Certainly, ϱ determines a minimum normalised distance $\Delta x_{\min}$ of

$$\Delta x_{\min} = \frac{\varrho}{2} Z_{\text{pp}} = 0{,}1 \tag{7.8}$$

The reference signals belong to different encoding slots.

$$\begin{aligned} -0{,}5 \leq \quad & x_1(t) \quad \leq 0 \\ 0 \leq \quad & x_2(t) \quad \leq 0{,}5 \end{aligned} \tag{7.9}$$

Since the slots are adjacent; therefore, the projection of $x_2(t)$ to the slot of $x_1(t)$ flips the signal (i.e. $x_2(t) = -0{,}3012$ maps to the value 0,3012 in the encoding slot of $x_1(t)$), yielding a relative distance of $\Delta x_{\text{PWM}} = 0{,}0984 < 0{,}1 = \varrho$. The glitch produced by one channel will prematurely trigger the other channel. Note that this effect is static, i.e. it does not depend upon the switching frequency.

In this example, 50 % of the switching events in each channel are affected by EMI. The inband content in both channels is empty, i.e. crosstalk adds no harmonics in this case; however the constant signal is hence not properly tracked, since the spectral power density at DC (channel 1) is $|\tilde{Z}_1(0) - GX_1(0)|^2 \approx -27\,\text{dB}$.

In the 5-AΣΔM case, it becomes harder to beforehand know the average switching frequency, since it depends upon the reference signal's waveform and amplitude (variable frequency). In the particular case of constant-reference signal tracking, each channel oscillates at a certain switching frequency (namely free frequency). If the free frequency of two channels are very similar, the coupled glitches may lock both modulators; both channels will then oscillate at the same frequency (in particular, the slowest will lock at the fastest's) resulting in very low tracking fidelity (a similar effect than in PWM). However, in the AΣΔM case, the signals can be closer than in PWM (also considering the relative distance within encoding slots).

For instance, consider a worse case than the previous one, $x_1(t) = 0{,}35$ and $x_2(t) = 0{,}3$ (both reference signals already belong to the same encoding slot, see figure 7.31). Despite the relative distance between these two signals is $\Delta x_{\text{A}\Sigma\Delta\text{M}} = 0{,}05 < \Delta x_{\text{PWM}}$, smaller than in the PWM case, both reference signals are properly tracked. In the worst case (channel 2 under these specific conditions), the value of the spectral power density at DC is $|\tilde{Z}_2(0) - GX_2(0)|^2 \approx -104\,\text{dB}$ and approximately 8 % of the switching events are affected by EMI. The inband content of the power switching signal $\tilde{Z}_2(f)$ has content at all frequencies; nonetheless, the power of this content is very small, about $-68\,\text{dB}$.

[2]The relative distance is measured within the encoding slot defined by the two output

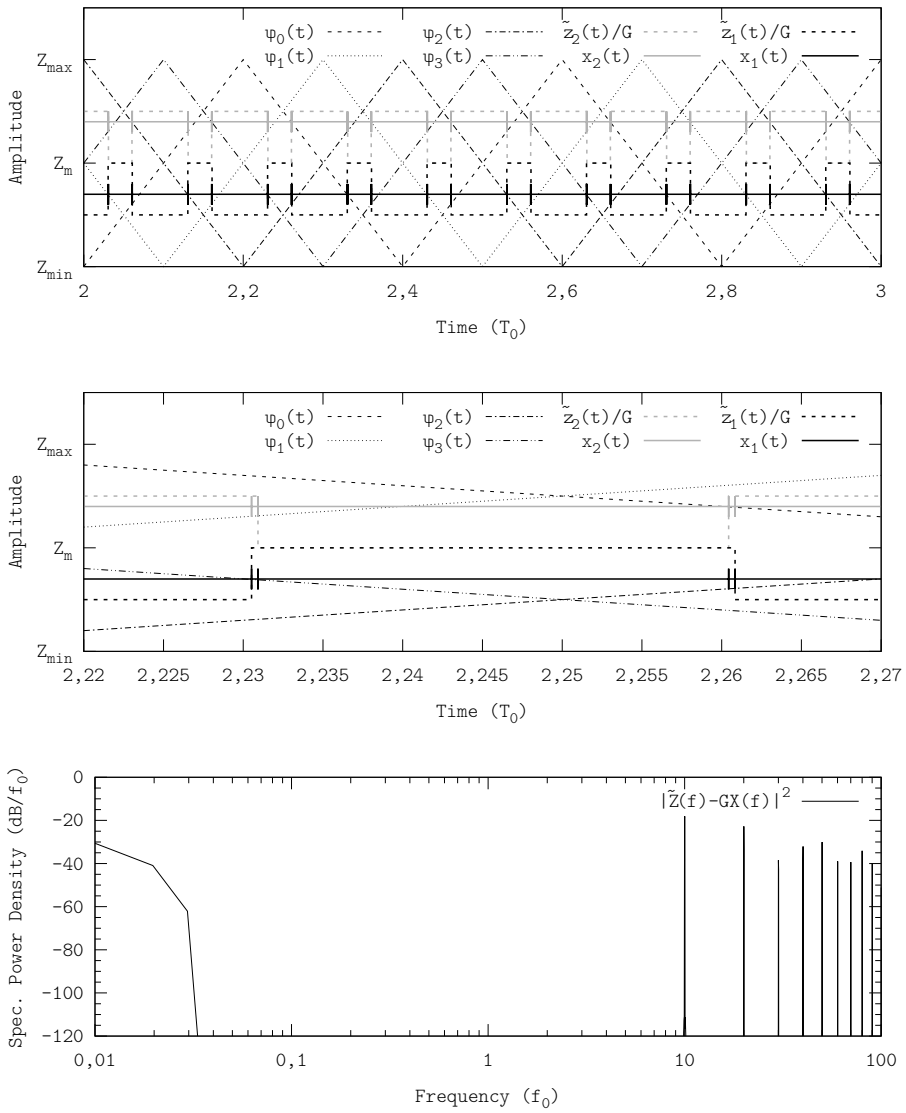

Figure 7.30: Crosstalk in dual-channel 5-PWM tracking constant-reference signals at an OSwR of 10. Displayed waveforms show the encoding process in the time domain (upper and middle plots, with all coupled glitches) and the power spectrum of the error signal $\tilde{Z}_1(f) - GX_1(f)$ of channel 1 (lower plot). Simulation performed using the configuration D.4.1.

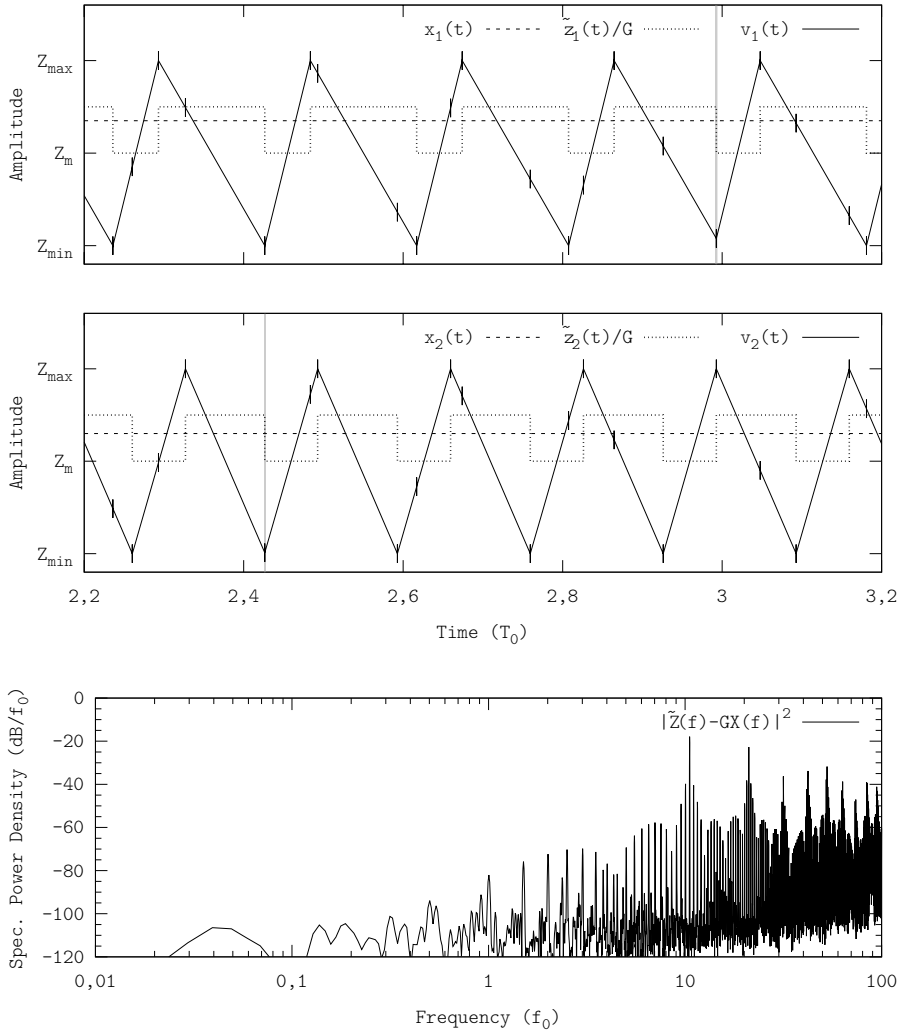

Figure 7.31: Crosstalk in dual-channel 5-AΣΔM tracking constant-reference signals at an OSwR of 10. Displayed waveforms show the encoding process in the time domain of channels 1 and 2 (upper and middle plots respectively, with the switching events affected by EMI highlighted in grey) and the power spectrum of the error signal $\tilde{Z}_1(f) - GX_1(f)$ of channel 1 (lower plot). Simulation performed using the configuration D.4.1.

Note that, unlike in the PWM case, this effect is not static in AΣΔM-based amplifiers, i.e. it does not directly depend upon the value of the reference signal $x(t)$, but indirectly, through the integrator's output signal $v(t)$ which changes its value even if the reference signal is constant. If two channels do not lock, the robustness against crosstalk depends upon the switching frequency f_s (or, more generic, upon the OSwR).

Performance Evaluation (Single-Tone Sinusoid)

The purpose of this test is to characterise crosstalk when encoding locally (in time) correlated signals (dual-channel test). When the correlation between both reference signals is high, both channels may significantly suffer from crosstalk (even locking each other); on the other hand, when the correlation between reference signals is low, both channels may be able to properly track the corresponding reference signal.

This behaviour can be simulated with two tones of similar frequencies, in this case

$$\begin{aligned} x_1(t) &= \cos(2\pi f_0 t) \\ x_2(t) &= \cos(2\pi 0{,}99 f_0 t) \end{aligned} \tag{7.10}$$

Using these signals, both channels will periodically lock and subsequently release, thereby resulting in a variable-frequency signal. The more sensitivity to locking, the worse tracking fidelity. Both modulators are set to operate at an OSwR of 10.

Figure 7.32 shows the result of this test in the frequency domain. As pointed out by the constant-reference signal tracking test, the higher sensitivity to crosstalk of PWM results in an increased error. Certainly, in the PWM case approximately 23 % of the switching events are affected by EMI, leading to an inband error of $-17\,\mathrm{dB}$. The outband distribution of the spectral power density (specifically, the concentration in harmonics) shows the lock-and-release behaviour.

In the case of the AΣΔM-based amplifier, the inband content is significantly lower (with a main harmonic at the frequency of the reference signal of that channel), leading to an inband error of $-47\,\mathrm{dB}$. Approximately 8 % of switching events is affected by EMI, although the outband spectral power density also shows harmonics revealing the lock-and-release behaviour.

Whilst increasing the OSwR improves the robustness against crosstalk in both cases, the improvement is more significant in the AΣΔM-based case, since crosstalk effects are not static.

Performance Evaluation (Uncorrelated Signals)

The purpose of these tests is to evaluate the robustness against crosstalk when tracking uncorrelated reference signals, i.e. crosstalk may happen at any time (no periodic behaviour). In these set of tests (single-channel, dual-channel and quad-channel), the OSwR is 10 in all cases. All reference signals have the same statistics: flat-spectrum and f_0-bandlimited.

---

voltage levels (normalised by the gain factor G) surrounding the reference signal. When comparing signals belonging to different slots, they should be all projected to the same slot (flipping them if necessary, as adjacent encoding slots have vertical symmetry).

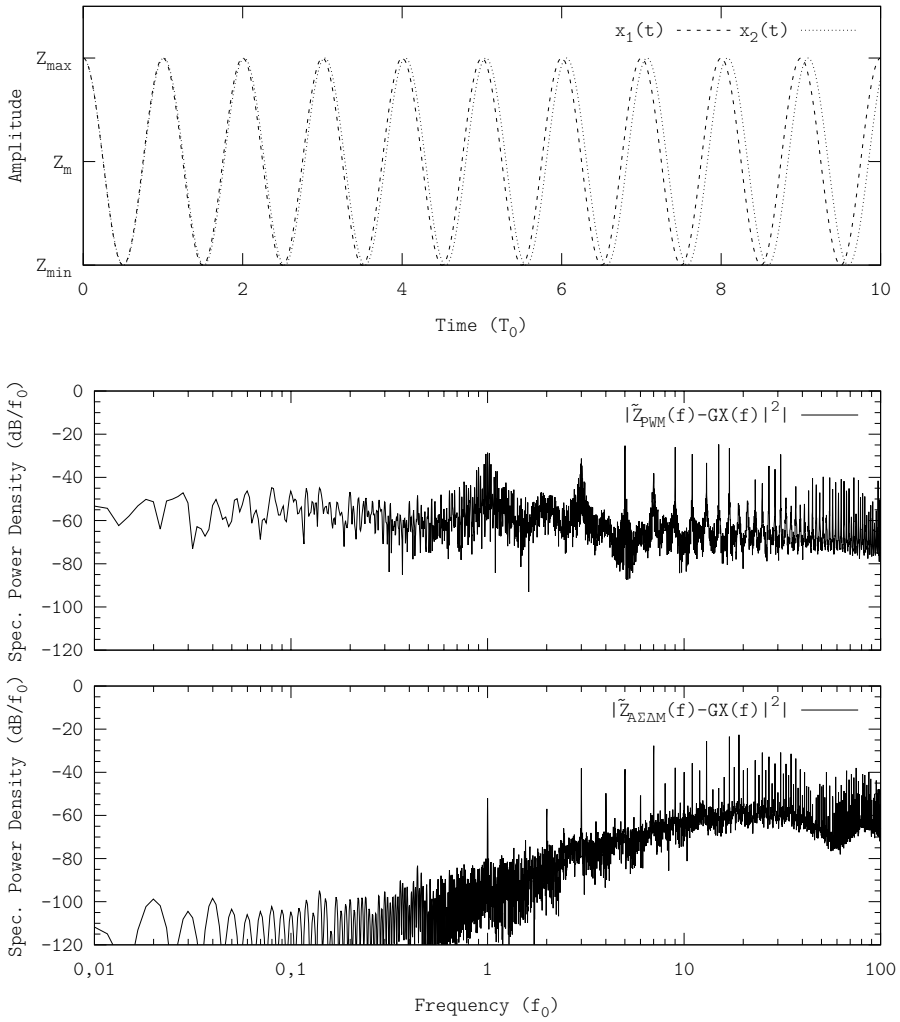

Figure 7.32: Correlated signal tracking crosstalk test. Displayed waveforms show the reference signals of each channel (upper plot), the power error signal in the PWM case (channel 1, middle plot) and the power error signal in the AΣΔM case (channel 1, lower plot). Simulation performed using the configuration D.4.1.

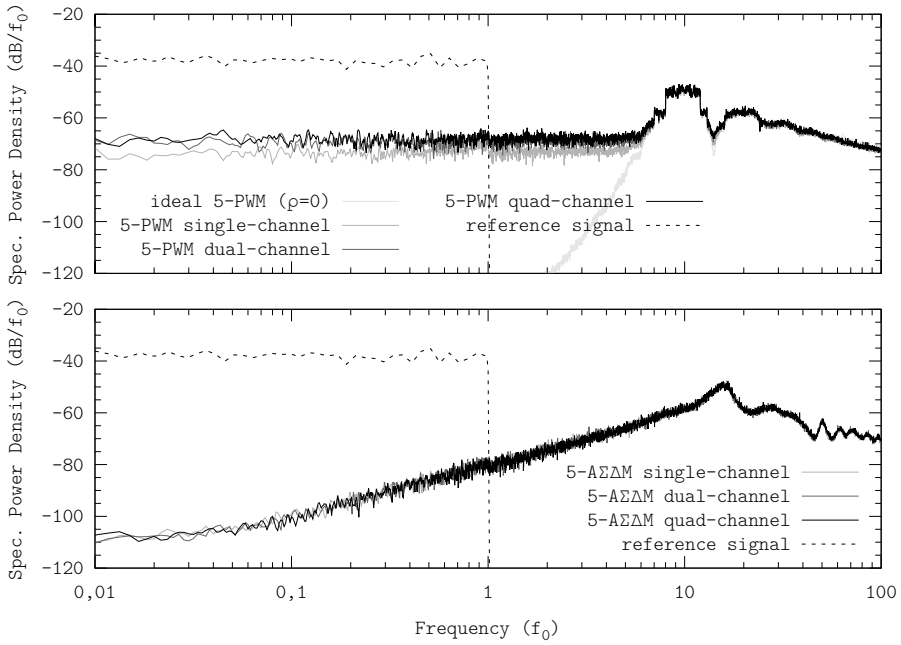

Figure 7.33: Uncorrelated signal tracking crosstalk test. Displayed waveforms show the reference signal (channel 1) and the error signal (channel 1) in the frequency domain, for PWM-based amplifiers (upper plot) and AΣΔM-based amplifiers (lower plot). Simulation performed using the configuration D.4.1.

Figure 7.33 summarises the results of these tests, in the frequency domain. Similarly to the previous tests, PWM is more sensitive to crosstalk than AΣΔM. In particular, by comparing with the ideal case (no crosstalk, $\varrho = 0$) even in single-channel mode the performance degradation is significant (in-channel crosstalk). Adding more channels further degrades the tracking fidelity, although the differences are very small.

In the case of AΣΔM, this simulation corroborates the previous conjectures, i.e. a random effective hysteresis width does not degrade the inband tracking performance. Note that in the constant-reference signal tracking test the effective hysteresis-width function is not random but shifted, which results in biased signal tracking. By extension, in the correlated signal test, the hysteresis-width function alternates between random and shifted, depending on the reference signals. This also applies to the AAΣΔM case. A summary of switching events affected by EMI and error power is included in table 7.1.

7.5 Other Implementation Issues

When designing a switching amplifier, besides the ideal tracking error-OSwR performance and the robustness against non-idealities, there are other issues which may also determine the suitability of a certain candidate for each particular application, such as the common-mode voltage or generating the supply voltages V_i in multi-level applications. This section briefly describes how the

Modulator	*Inband error power in the power switching signal*	*EMI-affected switching events (%)*
Ideal ($\varrho = 0$) 5-PWM	$< -70\,\text{dB}^*$	0
Single-channel 5-PWM	$-38\,\text{dB}$	10
Dual-channel 5-PWM	$-34\,\text{dB}$	24
Quad-channel 5-PWM	$-33\,\text{dB}$	42
Single-channel 5-AΣΔM	$-54\,\text{dB}$	0
Dual-channel 5-AΣΔM	$-55\,\text{dB}$	8
Quad-channel 5-AΣΔM	$-55\,\text{dB}$	22

Table 7.1: Summary of the error power $\tilde{Z}_1(f) - GX_1(f)$ and the number of switching events affected by EMI (channel 1) in the uncorrelated signal tracking crosstalk test. *Note: this value is determined by simulation errors (see figure 7.33).

different candidates are affected by these issues.

7.5.1 Minimum Pulses' Width

Both N-PWM and N-AAΣΔM rely on narrow pulses to achieve very good tracking fidelity, as discussed in chapters 4 and 5. However, when implementing amplifiers based on these modulations, the actual performance may be worse because generating accurate narrow pulses in the power switching signal $\tilde{z}(t)$ is challenging (mostly because of dead time and the transitions of actual power transistors).

Therefore, not only the average switching frequency f_s is significant, but also the instantaneous switching frequency (or pulses' width). This is especially important in wideband applications, wherein the relative effect of these non-idealities is higher. N-AΣΔM does not generates narrow pulses, regardless of the number of levels N (as analysed in chapter 5), and hence it is suitable to track reference signals $x(t)$ even if the available technology constraints the maximum instantaneous switching frequency to ten times the average switching frequency f_s.

7.5.2 Quiescent Losses

Quiescent losses are defined as power consumption when the system is idle, i.e. when the amplifier tracks the constant-reference signal $x(t) = Z_\text{m}$ in bipolar systems and the constant-reference signal $x(t) = Z_\text{min}$ in unipolar systems. Quiescent losses comprise the modulator's power consumption and switching converter's power consumption, although the latters are generally much higher than the formers.

In PWM-based designs, the constant switching frequency forces the system to switch even if it is idle (very narrow pulses). The current through the load R_L is small and hence so are the switching losses, yet they are still significant. Similarly, in AAΣΔM-based designs, the situation is similar, as the hysteresis reduces to very small values whenever the reference signal $x(t)$ approaches to an output voltage level.

On the other hand, in AΣΔM-based designs, the system stops switching whenever the reference signal $x(t)$ approaches to an output level (self-oscillating

behaviour); particularly, if the system is idle, the power part stops switching. This reduces quiescent losses to minimum, i.e. to the modulator's power consumption.

7.5.3 Underswitching

In the context of linear-assisted power amplifiers, the switching amplifier may operate at OSwRs below 1 (underswitching). As discussed in chapters 4 and 5, the modulation harmonics are shifted inband, thereby masking the amplifier's performance in terms of power of the remaining error signal $P_{\xi(t)}$, both inband and outband. The performance must be then evaluated in the frequency domain, by analysing the baseband tracking fidelity.

This analysis from the modulation's standpoint also applies to switching amplifiers. The filtering process does not modify this behaviour. Therefore, analysing the suitability of a certain candidate for underswitching is worth analysing whether the high-frequency content of the reference signal $x(t)$ constrains the encoding process of the baseband content.

This has already been analysed in sections 4.5.2 and 5.6.4, and N-A$\Sigma\Delta$M is more suitable for underswitching than N-PWM and N-AA$\Sigma\Delta$M, regardless of the number of levels N.

7.5.4 Filterless Amplifiers

Multi-level power amplification makes filterless amplifiers feasible. Without the LC reactive low-pass filter, both the inband and the outband contents are supplied to the load. The receiver only interprets the inband content; the outband content can be considered losses (power supplied to the load but not interpreted by the receiver). Whilst the unfiltered outband power $P^{\mathrm{o}}_{\tilde{z}(t)}$ is much higher than the filtered outband power $P^{\mathrm{o}}_{\xi(t)}$ (increased losses), the absence of filter saves all power dissipated in it (mainly due to the ESRs) and the inband error due to the filter's attenuation and phase lag. Furthermore, the size, weight and cost of the LC filter is saved as well.

As the number of levels N increases, the ratio of inband power to total power in the power switching signal increases $P^{\mathrm{i}}_{\tilde{z}(t)}/P_{\tilde{z}(t)}$ (as long as the OSwR is high enough to properly use all levels). This is illustrated in figure 7.34, with an example based on N-PWM operating at an OSwR of 20. With 2 levels almost 90 % of power would be lost because of filterless operation; however, already with 5 levels more than 75 % of power would be interpreted by the receiver and more than 85 % in with 7 levels (in order to properly evaluate the efficiency degradation due to filterless, the percentage of inband power $P^{\mathrm{i}}_{\tilde{z}(t)}/P_{\tilde{z}(t)}$ should be compared with the efficiency of the LTI filter).

If the reference signal is properly tracked, the power loss due to filterless operation is independent of the modulation (only the number of levels N determine the amount of outband power). However, given a certain number of levels N, the minimum OSwR required to achieve proper signal tracking is higher in the PWM and AA$\Sigma\Delta$M cases than in the A$\Sigma\Delta$M case.

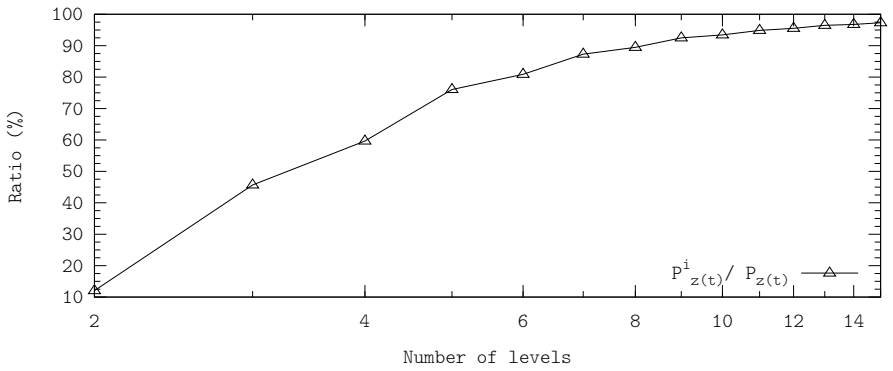

Figure 7.34: Efficiency because of filterless in multi-level amplifiers. Example showing N-PWM operating at an OSwR of 20. Simulation performed using the configuration D.4.4.

7.5.5 Common-Mode and Differential-Mode Voltages

In floating-output converters, basically full-bridge converters, the power switching signal $\tilde{z}(t)$ is generated as the voltage difference between two active ends, V^+ and V^- (differential-mode voltage). The output filter's input port is connected between these two ends; therefore, the modulator and the decoding logic drive the power converter so that the waveform of the differential-mode voltage signal is the power switching signal $\tilde{z}(t)$. The common-mode voltage is usually not considered.

Nevertheless, depending on the application, the common-mode voltage signal $\tilde{z}_{\mathrm{C}}(t)$ can be an issue. For instance, in EMI-sensitive applications, the common-mode voltage signal $\tilde{z}_{\mathrm{C}}(t)$ may be radiated; in such a case, common-mode radiation is generally addressed with a dedicated common-mode filter (the most usual and widespread technique to address common-mode signal issues). Indeed, the layout of the converter's LC low-pass filter determines whether the common-mode voltage signal $\tilde{z}_{\mathrm{C}}(t)$ is filtered before being supplied to the load R_{L}. If the filter floats (i.e. no reactive components are grounded, see figure 7.35), only the differential-mode voltage signal $\tilde{z}(t)$ is filtered; the common-mode voltage signal $\tilde{z}_{\mathrm{C}}(t)$ supplied at the filter's input port is directly supplied by the filter's output port, i.e. to the load R_{L} (e.g. if the load is an antenna, the common-mode voltage signal $\tilde{z}_{\mathrm{C}}(t)$ may be radiated). On the other hand, if the filter is grounded (typically the capacitors, see figure 7.35), the common-mode voltage signal $\tilde{z}_{\mathrm{C}}(t)$ is filtered and therefore the common-mode voltage signal supplied to the load R_{L} is much smaller than the common-mode voltage signal $\tilde{z}_{\mathrm{C}}(t)$ supplied to the filter.

All bandwidth extension techniques herein presented (high-order filtering, multi-level power amplification, etc.) are aimed to shape and/or reduce the differential-mode voltage signal $\tilde{z}(t)$. However, some of these techniques have also an impact upon the common-mode voltage signal $\tilde{z}_{\mathrm{C}}(t)$, which may shape, reduce or even increase it.

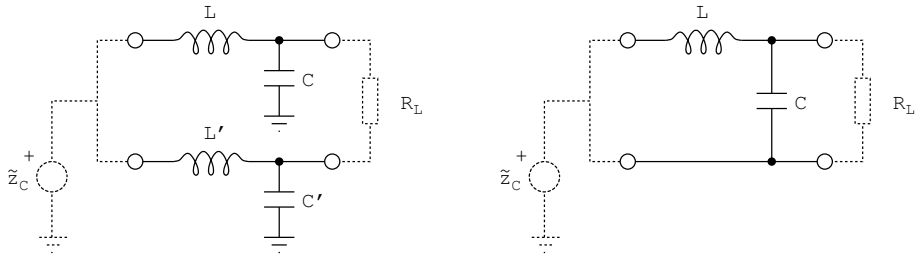

Figure 7.35: Common-mode (left) and differential-mode (right) filters. The common-mode filter filters both common- and differential-mode voltages.

Common-Mode Voltage in Multi-Level Full-Bridge Amplifiers

The common-mode voltage signal $\tilde{z}_{\mathrm{C}}(t)$ is mostly determined by the modulation and the switching policy. In general, if using N levels and a conventional switching policy (and the 0 level is always generated by driving the both ends of the filter's input port to GND, i.e. always-low decoding strategy), the common-mode signal $\tilde{z}_{\mathrm{C}}(t)$ tracks the rectified reference signal $x(t)$ according to the modulation used to generate the differential-mode voltage signal $\tilde{z}(t)$. Figure 7.36 illustrates this equivalence with an example (7-PWM operating at an OSwR of 10 and using a conventional switching policy).

The outband power spectrum of both the differential-mode and the common-mode signals, $\tilde{Z}(f)$ and $\tilde{Z}_{\mathrm{C}}(f)$ respectively, is therefore shaped similarly, although the spectrum of the common-mode signal $\tilde{Z}_{\mathrm{C}}(f)$ has more harmonics than that of the differential-mode signal $\tilde{Z}(f)$ due to the rectification. The in-band content is different and the common-mode signal $\tilde{z}_{\mathrm{C}}(t)$ has a higher DC component. Still regarding the example of figure 7.36, figure 7.37 shows the power spectrum of these signals, which illustrates the harmonic increase. Note that the outband spectral content is shaped similarly.

Therefore, like in the differential-mode voltage signals case, the upperbound of the outband power spectrum of the common-mode voltage signal $\tilde{Z}_{\mathrm{C}}(f)$ can be reduced by using a spread-spectrum modulation such as AΣΔM, when compared to conventional PWM-based amplifiers. The harmonics at multiples of the reference signal's bandwidth are independent of the modulation, but the other outband content can be reshaped (figure 7.38 shows an example, the common-mode voltage signals of 3-PWM and 3-AΣΔM). This feature can especially important in EMI-sensitive applications in which the common-mode signal may be radiated (e.g. in power audio applications in which the speakers are supplied by long cables, the content around the switching frequency may be radiated).

Common-Mode Voltage with Other Switching Policies

This equivalency between the common-mode (tracking the rectified reference signal) and the differential-mode voltage signals only applies with a conventional switching policy. For instance, if using an enhanced switching policy to maximise the number of distinct differential-mode output voltage levels, the common-mode signal no longer tracks the rectified reference signal. Nevertheless, from the frequency-domain standpoint, the outband spectral power density is not significantly reshaped; the common-mode voltage signal $\tilde{Z}_{\mathrm{C}}(f)$ still

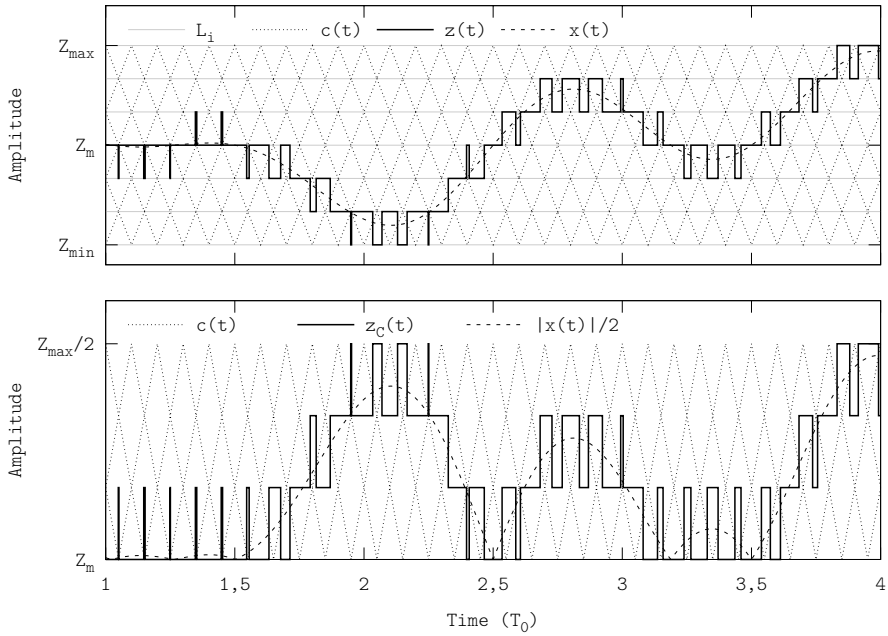

Figure 7.36: Example of time-domain common-mode voltage signals in 7-PWM (conventional switching policy). Showing the differential-mode waveforms (upper plot) and the common-mode of the switching signal (lower plot). This plot also includes the rectified reference signal and a set of carriers to illustrate the tracking equivalence.

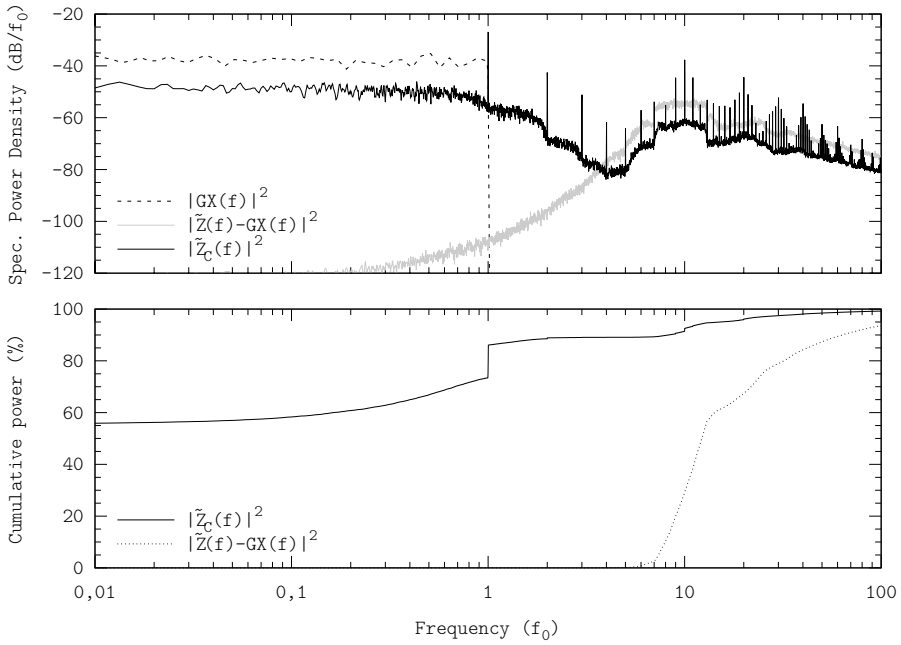

Figure 7.37: Power spectrum (upper plot) and cumulative-power frequency distribution (lower plot) of 7-PWM operating at an OSwR of 10 and using a conventional switching policy. Displayed waveforms correspond to the common-mode and the differential-mode voltage signals. Simulation performed using the configuration D.4.1.

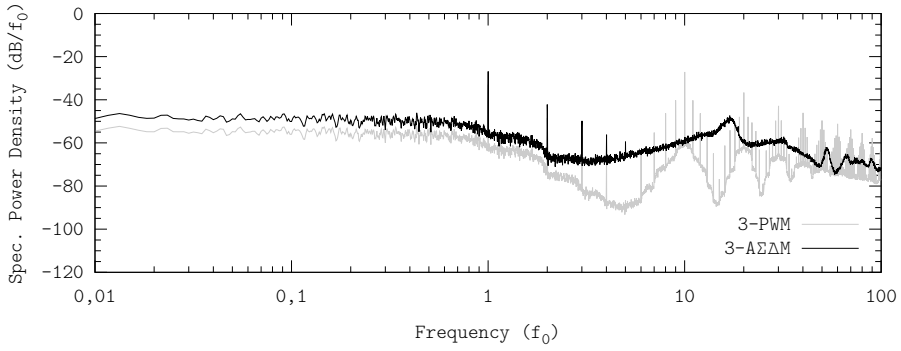

Figure 7.38: Comparison between the common-mode voltage signals of 3-PWM and 3-AΣΔM, both operating at an OSwR of 10 and using the always-low decoding strategy. Simulation performed using the configuration D.4.1.

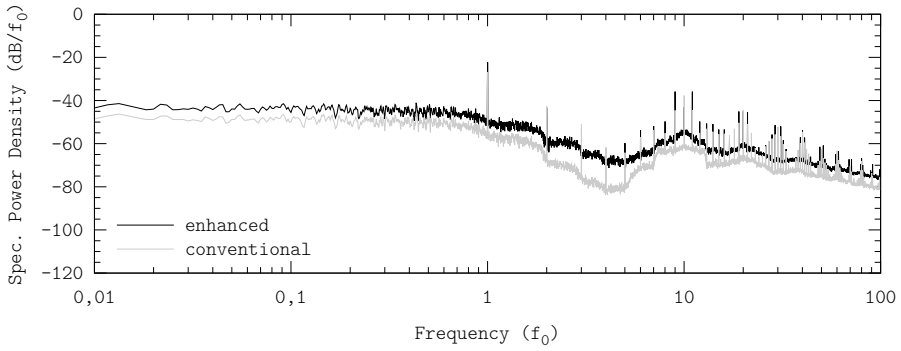

Figure 7.39: Common-mode signals of 7-PWM generated with an enhanced switching policy (three supply voltages) and a conventional switching policy (four supply voltages). The OSwR is 10 in both cases. Simulation performed using the configuration D.4.1.

comprises harmonics at the same frequencies, but with different amplitude distribution (see figure 7.39).

In the example of figure 6.9 of chapter 6, by upgrading system with the enhanced switching policy (with four supply voltages, from generating seven distinct levels with a conventional policy to generating thirteen distinct output levels with the enhanced policy), the power of the common-mode voltage signal $P_{\tilde{z}_C(t)}$ increases by 133 %.

Note that combining an enhanced switching policy and a spread-spectrum modulation may still reduce the upperbound of the outband power spectrum (e.g. comparing a 7-AΣΔM amplifier using an enhanced switching policy and a conventional 5-PWM). Also note that it is feasible to partially shape the common-mode voltage signal $\tilde{z}_C(t)$ by using an enhanced decoding logic (as described in section 6.2).

7.5.6 Filters with Equivalent Series Inductance

When increasing the filter's order n, the number of (series) inductors increases. If the filter's cutoff frequency f_c is the same, the total series inductance increases, even though each single inductor is smaller than in the second-order case. When comparing inductors of similar inductance and technology, the ESR is approximately proportional to the inductance; higher series inductances lead to higher ESRs, thereby increasing the filter's conduction losses.

Nevertheless, taking advantage of the higher stopband rejection, the cutoff frequency f_c of high-order filter may be higher than that of second-order filters, and still fulfil the specifications. If the cutoff frequency is high enough, the total series inductance in high-order filters may be lower than the inductance in a second-order filter, and therefore switching losses would be lower as well.

Table 7.2 summarises the total series inductance in different Butterworth filters, normalised to the inductance in the second-order case (the required inductance scales proportionally to the filter's cutoff frequency f_c). For instance, if replacing a second-order filter with cutoff frequency $f_c = 1{,}5f_0$ by a fourth-order filter with cutoff frequency $f_c = 3{,}0f_0$, the filter's conduction losses would

Filter's order	*Norm. total inductance*
2	1
4	1,848
6	2,732
8	3,586

Table 7.2: Filters with equivalent series inductance for Butterworth transfer functions, with normalised load resistance $R_{\mathrm{L}} = 1\,\Omega$ in all cases. The cutoff frequency f_{c} proportionally scales these values.

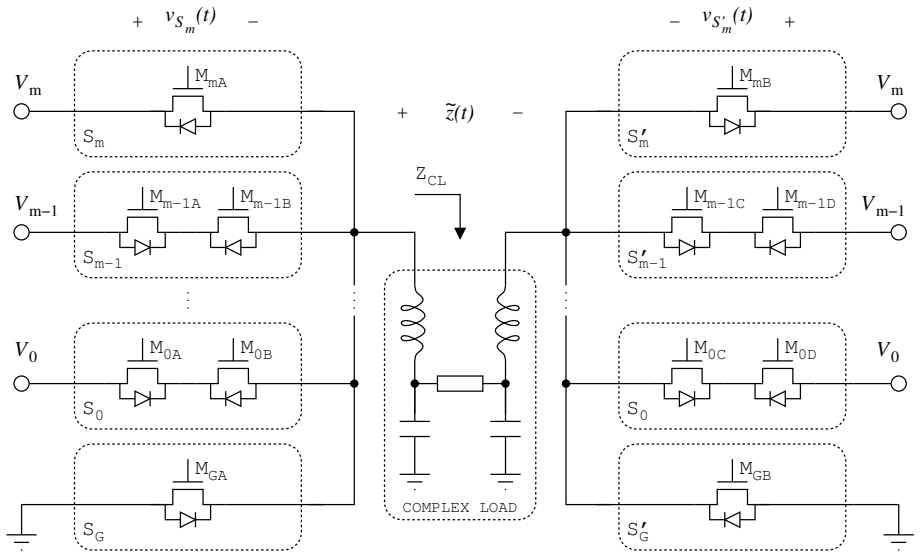

Figure 7.40: Multi-level full-bridge converter ($m + 2$ supply voltages). The switches S_i, S'_i have been synthesised with power MOSFETs.

be reduced[3]. Furthermore, still with this example, the inband error power would reduce by 4 dB (because of the lower filter's inband attenuation and the more rectilinear phase lag); the stopband rejection in the fourth-order filter ($f_{\mathrm{c}} = 3{,}0 f_0$) is higher than that of the second-order filter ($f_{\mathrm{c}} = 1{,}5 f_0$) from $6 f_0$ on.

7.5.7 Switch Synthesis with Power MOSFETs

In multi-level converter topologies and in the 5-switch converter topology presented in section 6.3.2, some switches must withstand bipolar voltages. Specifically, in the multi-level buck and the multi-level full-bridge topologies, all switches connected to intermediate voltages withstand a bipolar voltage (figure 7.40 shows a multi-level full-bridge converter).

Certainly, if the converter uses $m + 2$ supply voltages $(GND, V_0, \ldots, V_m)$ and $GND < V_0 < \cdots < V_m$, the switches S_i with $i = 0 \ldots, m - 1$ withstand negative voltage when the switch S_m is ON, whereas they withstand positive

[3]The actual reduction depends upon the actual components; usually only commercial values are available, especially inductors, which may constrain the implementation of these filters.

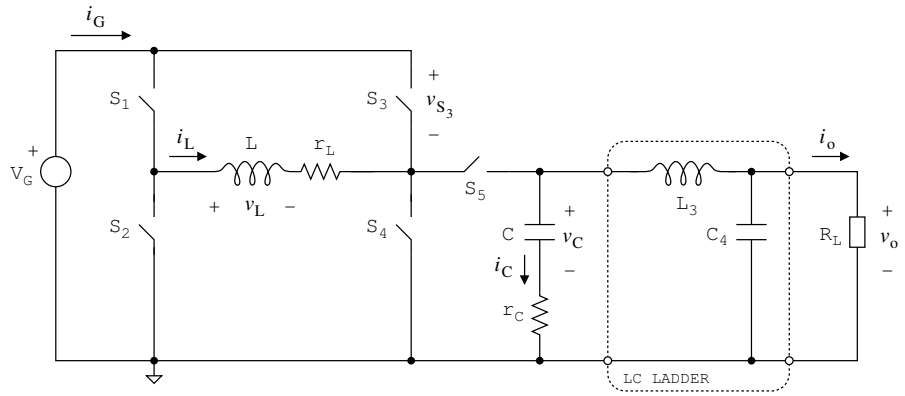

Figure 7.41: 5-switch converter topology with a second-order additional LC ladder (r_L and r_C are the ESR of the inductor and the capacitor respectively). Displayed currents and voltages show the polarity which is considered positive.

voltage when the switch S_G is ON (and analogously for the other set of switches, see figure 7.40).

In the 5-switch topology, included again in figure 7.41, the output voltage $v_o(t)$ is bipolar. When the switch S_5 is ON, switches S_3 and S_4 are connected to a bipolar voltage, whose magnitude can be higher than the supply voltage V_G.

$$V_o \in [-kV_G, kV_G], \quad |k| > 1,\ k \in \mathbb{R} \tag{7.11}$$

Therefore, in the 5-switch topology, switches S_3[4], S_4 and S_5 block bipolar voltages.

When synthesising a switch which must withstand bipolar voltages with power MOSFETs (a very common technique in integrated power applications), the built-in body diode should never conduct. Each of these switches must be then synthesised with two back-to-back MOSFETs to avoid body-diode conduction (see figure 7.40).

The ON resistance of a switch must not depend on how it is synthesised. Therefore, if the ON resistance of a bipolar switch must be R, the ON resistance of each back-to-back power MOSFET must be $R/2$, half of that of the switch that they implement, so that the total ON resistance of the back-to-back synthesis is R.

Assuming that the ON resistance of a power MOSFET is proportional to their area, the area occupied by a bipolar switch (back-to-back synthesis) is four times the area occupied by a unipolar switch (both synthesised with power MOSFETs and with the same ON resistance).

7.5.8 Switch Dimensioning for Equalised Conduction Losses

In multi-level converter topologies, not all switches handle the same current (also in other topologies comprising more than two switches, such as the 5-

[4]If the converter tracks a certain reference signal $x(t)$ but does not power amplifies it, i.e. $|k| < 1$ in (7.11), the switch S_3 only withstands positive voltages. Despite the output dynamic range is the same than in the full-bridge case, this is still a case of interest, as the load is grounded in the 5-switch topology.

switch topology). This feature can be used to optimise the ON resistance of each switch, thereby minimising the occupied area in integrated implementations (or allowing simpler devices in discrete-components implementations).

A possible, yet not the only one, design criterion to dimension the switches is their static DC power consumption (similar DC conduction losses in all switches). Another possible criterion consists in dimensioning the switches according to their average usage in regular operation. To illustrate the advantages of optimisation, each of these criteria has been applied to an example.

Design Example (Multi-Level Full-Bridge Converter)

Let us consider a multi-level full-bridge converter supplied from $m+2$ supply voltages $GND, V_0, \ldots, V_m$ (see figure 7.41). Switches must be dimensioned so that in static DC operation, the power dissipated in the is the same. For the sake of notation simplicity, let us merge the output filter $H(s)$ and the load R_L into a complex load $Z_\mathrm{CL}(j\omega)$. Let us also assume that the ON resistance R_{S_i} of any switch is always much lower than the complex load impedance at any frequency (i.e. the filter's transfer function has no gain peaks)

$$R_{S_i,S_i'} \ll Z_\mathrm{L}, \quad i = \{G, 0, 1, \ldots, n\} \tag{7.12}$$

where Z_L is the complex load's minimum impedance at any frequency

$$Z_\mathrm{L} \leq |Z_\mathrm{CL}(j\omega)|, \quad \forall\omega \in \mathbb{R} \tag{7.13}$$

Statically (i.e. DC operation) the highest current flows through switches S_m and S_G' when generating the highest level V_m (analogously for the negative case). The power loss in these switches is (example with S_m)

$$P_{S_m} = R_{S_m} I_{S_m}^2 = R_{S_m} \left(\frac{V_m}{Z_\mathrm{L}}\right)^2 \tag{7.14}$$

If using this value as design reference, the power loss in the other switches S_i should not be higher.

$$P_{S_i} \leq P_{S_m}, \quad i = \{0, \ldots, m-1\} \tag{7.15}$$

Let V_j be the voltage yielding the highest current through the switch S_i (static DC operation). Then the maximum power loss in S_i is given by

$$P_{S_i} = R_{S_i} I_{S_i}^2 = R_{S_i} \left(\frac{V_j}{Z_\mathrm{L}}\right)^2 \tag{7.16}$$

By joining the three previous expressions, it follows that

$$R_{S_i} \leq R_{S_m} \left(\frac{V_m}{V_j}\right)^2 \tag{7.17}$$

The switches handling the highest current ($S_\mathrm{G}, S_\mathrm{G}', S_m, S_m'$) must therefore have the lowest ON resistance R_{S_m}. However, if these switches are to be synthesised with power MOSFETs, because of the back-to-back synthesis, the area occupied by the intermediate switches S_i, S_i' with $i = 0 \ldots, m-1$ increases by

	S_1	S_2	S_3	S_4	S_5
ON^+	$\|u\|/2$	0	0	$\|u\|/2$	0
ON^-	0	$\|u\|/2$	$\|u\|/2$	0	0
OFF	0	$1-\|u\|$	0	0	$1-\|u\|$
av. usage	$\|u\|/2$	$1-\|u\|/2$	$\|u\|/2$	$\|u\|/2$	$1-\|u\|$

Table 7.3: Switch usage (%) in the 5-switch topology when supplying bipolar symmetrical signals (average 0).

a factor 4 (two MOSFETs in series, each of them with half the ON resistance of the switch that they implement).

For instance, if using three supply voltages (GND, 1 V and 3 V) to generate seven levels (0 V, ±1 V, ±2 V and ±3 V, using the enhanced switching policy), the ON resistance of the intermediate switches S_0, S_0' can be $2{,}25R_{S_1}$ (the ON resistance of all other switches, $S_\mathrm{G}, S_\mathrm{G}', S_1, S_1'$, is the same). Nevertheless, because of the back-to-back synthesis, the ON resistance of each back-to-back MOSFET must be $1{,}13R_{S_1}$. Considering that the size of a power MOSFET is inversely proportional to its ON resistance, the are required by each switch consisting of two back-to-back power MOSFETs (S_0 and S_0') is 1,78 times the area of a single power MOSFET switch ($S_\mathrm{G}, S_\mathrm{G}', S_1, S_1'$). Note that if the ON resistance would not be optimised, the area required by S_0 and S_0' would have been four time the area of a single power MOSFET switch.

Design Example (5-Switch Topology)

Let us consider a 5-switch converter, supplied by a voltage source V_G. The converter must be dimensioned so that the power loss in all switches is, in average, the same when voltage amplifying a single-tone sinusoid by a factor 4. The RMS value of the tone is $1/\sqrt{2}V_\mathrm{G}$ and its average value is zero. Therefore, the RMS value of the output signal must be $4/\sqrt{2}V_\mathrm{G} \approx 2{,}8V_\mathrm{G}$. According to the steady-state DC transfer characteristic of this converter (depicted in figure 6.18), the required average duty cycle is $|u| \approx 0{,}74$.

Provided that the average of the reference signal is 0, the average usage of ON^+ and ON^- is the same. Furthermore, if the hold-state is not used, the converter operates at OFF during $1-|u|$ (%) of time and at ON^+ and ON^- during $|u|/2$ (%) of time each. From this estimation, the average usage of each switch can be estimated. Table 7.3 summarises the switches' usage under these conditions.

In the case of this example $|u| \approx 0{,}74$, the switches S_1, S_3 and S_4 are used during 37 % of time, whereas the switch S_2 is used during 63 % of time and the switch S_5 during 26 % of time. The switch S_2 must therefore have the lowest ON resistance.

Nonetheless, if synthesising the switches with power MOSFETs, because of the back-to-back synthesis, the switches requiring more area are S_3 and S_4, instead of S_2. Assuming ON resistances inversely proportional to the MOSFET's silicon area and being A_{S_1} the area of the smallest switch (regular unipolar switch), the switches area are $A_{S_2} = 1{,}7A_{S_1}$, $A_{S_5} = 2{,}8A_{S_1}$ and $A_{S_3,S_4} = 4A_{S_1}$.

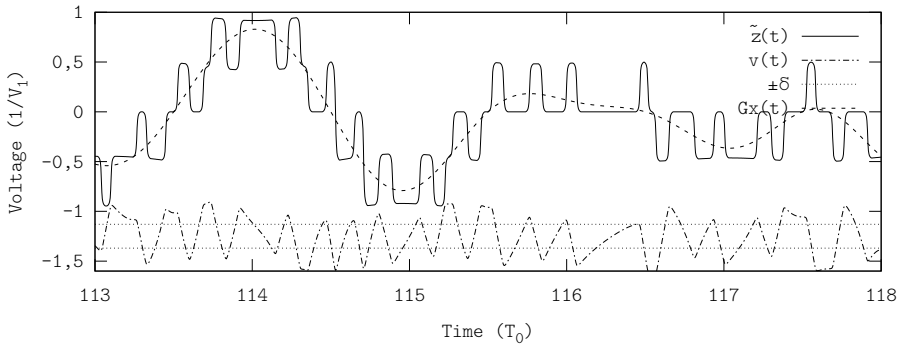

Figure 7.42: 5-level AΣΔM amplifier with soft switching. The integrator's output signal $v(t)$ and the comparators' threshold $\pm\delta$ have been shifted and scaled for better readability.

7.5.9 Soft-Switching

A feasible technique to reduce switching losses consists in upgrading the switching power converter with soft-switching. Soft-switching techniques use additional reactive components next to the power switches to switch when the voltage or the current across them is very low (zero-voltage switching, zero-current switching). Whilst these kind of techniques minimise switching losses, they are not popular in switching amplifiers because they smooth and delay the transitions, which generally degrades the inband tracking fidelity.

However, since AΣΔM-based amplifiers sense and encode according to the actual power switching signal $\tilde{z}(t)$, it may be feasible to use soft-switching techniques in AΣΔM-based amplifiers. As figure 7.42 shows, the smoothing effects upon the time edges cause similar consequences upon the integrator's output signal $v(t)$ than the time delays or the bandwidth limitations of the integrator and the adder.

Soft-switching techniques, combined with AΣΔM-based amplifiers, are hence candidates of interest to improve the efficiency (in particular to reduce switching losses) of switching amplifiers without increasing the switching frequency.

7.6 Implementation-Oriented Comparison

When designing a switching amplifier for a particular application, the specifications (including the overall cost) determine how the amplifier is finally designed and tuned. In commercial applications cost is generally the main constraint (more precisely, the Bill of Materials, BoM); a cost increase must be compensated with value added, e.g. lighter and smaller devices or better EMC.

Inband-error-free encoding is possible even if encoding with two levels at an OSwR of 1. Therefore, the scope of all bandwidth extension techniques for switching amplifiers is to reduce the switching modulation's outband spectral content (either by rejecting or by partially avoiding its generation), without compromising the inband content; i.e. to reduce the power of the remaining error signal $\xi(t)$, within a specific band or globally. Note that adding a cer-

tain outband spectral content is mandatory in all power-amplification processes based on switching converters.

The characterisation in terms of power of the remaining error signal $P_{\xi(t)}$ and OSwR, earlier presented in this chapter, has identified two opposite strategies or bandwidth extension techniques: 2-level PWM encoding combined with high-order filtering and multi-level AΣΔM-based encoding combined low-order decoding (typically second-order or even filterless). Depending on the application and the specifications, one or the other may be preferred.

7.6.1 High-OSwR Applications

If the application allows high OSwRs, the best performance in terms of power of the remaining error signal (either inband or total) is achieved with a 2-PWM and a high-order filter. Broadly speaking, 2-PWM performs the most accurate inband tracking (if the OSwR is higher than 3) but at the cost of a high spectral content around the switching frequency f_s; to properly reject this content without affecting the inband content, both the filter's order n and the filter's cutoff frequency f_c must be high, to achieve high stopband rejection whilst avoiding the non-rectilinear inband phase lag (the OSwR must be then high). Compared to a conventional design, this bandwidth extension technique is therefore based on further rejecting the outband spectral content.

In bipolar applications (full-bridge topology), the 3-PWM may be more suitable than 2-PWM, since upgrading from 2-PWM to 3-PWM in a regular full-bridge topology is straightforward and, what makes this upgrade more interesting, the switching frequency can be doubled without increasing switching losses (if driving a full-bridge converter as a 2-level converter four switches must switch in every switching event, whereas if driving it as a 3-level converter only two switches switch in every switching event). Therefore, 2-PWM may be the most suitable design for unipolar applications (buck topology) and 3-PWM may be the most suitable design for bipolar applications (full-bridge topology).

Amplifiers based on this design strategy, high OSwR operation combined with 2-level or 3-level PWM and high-order filtering, are very sensitive to variations in the supply voltages, dead time, interferences and other non-idealities in general. The performance of an actual 2-level high-order amplifier would be constrained and determined by these non-idealities, leading to a significantly worse performance. Nevertheless, at high OSwRs, it may feasible to compensate the inband effects of these non-idealities and implementation-induced effects with feedback, i.e. an external slower loop typically based on conventional control techniques. If the closed-loop design is not robust enough and the performance of the actual amplifier still does not fulfil the specifications, the PWM-based design should be deprecated in favour of an AΣΔM-based or an AAΣΔM-based one, less accurate in terms of signal tracking but more robust against non-idealities (the amplifier should be then optimised according to the criteria for low-OSwR applications, see next subsection, 7.6.2). AΣΔM-based designs also reduce the upperbound of the outband power spectrum, which may be necessary in EMI-sensitive applications.

From an economical standpoint, upgrading a second-order filter to higher orders generally results in a BoM increase. Even if the high-order filter has the same series inductance than the second-order one (reference BoM), the total BoM would be higher, as the cost of each coil is not proportional to its induc-

tance. For instance, the cost of two coils of inductance $L/2$ is generally higher than the cost of a single coil of inductance L, assuming the same technology and ESR per inductance unit in all coils. Furthermore, often only commercial values are available and hence the inband response of high-order filters may not be maximally flat (if designing a Butterworth filter), although the higher filter's cutoff frequency f_c may mitigate the inband consequences upon the recovered signal.

From the ergonomics standpoint (pursuing value added to compensate an eventual cost increase), the cost-scaling coil issue also applies to its size. Note that increasing the filter's order does not modify the amplifier's efficiency (assuming filters with similar ESR).

7.6.2 Low-OSwR Applications

Whilst high-OSwR applications are state of the art, the main challenge is to address low-OSwR applications. According to the characterisations, the best performance is achieved by second-order and fourth-order (depending on the OSwR) amplifiers based on a 7-AΣΔM. The strategy is now the opposite than in high-OSwR applications: instead of further rejecting the outband spectral content, its generation is partially avoided (multi-level time encoding). Indeed, at low OSwRs, the filter's cutoff frequency f_c is low as well; high-order filters would then result in a high inband error due to the non-rectilinear phase lag.

Provided that increasing the number of levels N mitigates the outband differences between modulations (regarding the error signal $e(t)$), in multi-level amplifiers, the amplifier's performance in terms of power of the remaining error signal $P_{\xi(t)}$ is mostly determined by the inband tracking capabilities of the modulation with a certain number of levels N and at the specified OSwR. The suitability of AΣΔM for multi-level time encoding (the modulation is incremental and, given the OSwR, the inband error due to improper encoding hardly depends upon the number of levels N) combined with its spread-spectrum feature, makes it the most feasible candidate to address low-OSwR power amplification. Based on the characterisation, a fourth-order filter may be used at OSwRs beyond 2; if the cost and ergonomics issues prevail, the performance achieved with a second-order filter is less than 5 dB worse.

Nonetheless, AΣΔM is especially interesting and suitable for low-OSwR because of implementation issues: its intrinsic high robustness against non-idealities and the incremental multi-level modulation feature. The classical solutions to address non-idealities and implementation-induced effects in switching amplifiers mostly rely on feedback and high OSwRs; these techniques are not feasible in low-OSwR designs. AΣΔM bases on alternative techniques to achieve similar performance, at the cost of a more complex (yet feasible) implementation compared to a regular PWM.

Robustness Against Non-Idealities

The built-in feedback loop of AΣΔM operates at the switching frequency f_s, i.e. at the fastest frequency possible; all the information sensed and fed back to the modulator is hence processed at the switching frequency f_s. By sensing the power switching signal $\tilde{z}(t)$, the encompassed effects include any variation

in the levels of the power switching signal $\tilde{z}(t)$, typically due to stray resistances, crosstalk and dead time. All these effects are partially compensated in a frequency-dependent ratio.

Other effects such as the inband error due to the LTI filter's non-ideal inband response, are not compensated. However, these uncompensated effects are usually stationary (i.e. they are not time dependent, or they vary at a very slow rate); therefore it is feasible to compensate them with feedback, operating at a very slow frequency, and pre-emphasising the amplifier's input signal $x_{\mathrm{i}}(t)$ accordingly.

Voltage Levels and Filterless Amplifiers

From the power resources standpoint, with AΣΔM-based amplifiers it is feasible to use any supply voltage already available in the system, since the modulation is incremental; even non-constant voltages can be used (as long as their variation is slower than the switching frequency f_{s}). Furthermore, if some voltage levels become unavailable during a certain time period, AΣΔM is still capable of tracking the reference signal $x(t)$, without changing the layout of power switches nor degrading the inband tracking performance.

The incremental multi-level modulation feature of N-AΣΔM-based amplifiers makes these kind of amplifiers compatible with any kind of supply voltages. In particular, if the specificity of the supply voltages constrain their usage (e.g. recharging time in charge pump-based systems), the incremental multi-level modulation can adapt the encoding process to the instantaneously available supply voltages and still track the reference signal.

Despite both the filter's order n and the ratio of the switching frequency f_{s} to the filter's cutoff frequency f_{c} would be low, the upperbound of the outband spectral content would not be very high because of the spread-spectrum feature and multi-level power amplification. Therefore, multi-level AΣΔM-based designs are also suitable from the standpoint of EMI.

Multi-level amplifiers also make filterless amplifiers feasible, especially if using an enhanced switching policy to maximise the number of distinct output voltage levels (even though the power of the common-mode voltage signal may increase because of the enhanced switching policy, the spectral power density would spread because of AΣΔM, thereby leading to a lower upperbound of the common-mode signal's outband power spectrum). The maximisation of the number of distinct output voltage levels minimises the losses due to filterless operation (i.e. the recovered signal's outband power, power delivered to the load but not interpreted by the receiver) at the cost of increasing switching losses (more transistors switching in each switching event), thereby unfolding a new trade-off. Even if this trade-off does not yield an efficiency improvement with state-of-the-art technology, it is still a candidate of interest, especially considering the upcoming low-switching losses technologies such as silicon carbide. Note that increasing the switching frequency does not yield efficiency improvements in filterless amplifiers.

Chapter 8

Experimental Verification

This chapter briefly describes an integrated circuit implementation of a 2-level AΣΔM / AAΣΔM switching amplifier for low-OSwR signal tracking applications; this amplifier has been used to experimentally validate the analyses and the results obtained in the previous chapters.

8.1 Brief Description of the Integrated Circuit

Within the framework of this thesis, an Integrated Circuit (IC) implementing an AΣΔM-based switching power amplifier (buck topology) for low-OSwR signal tracking applications was designed by Dr. Daniel Fernández [83]. The modulator implements 2-level AΣΔM, with the possibility of adding feedforward according to the quadratic law presented in chapter 4 (AAΣΔM).

The performance characterisation of non-idealities (mostly the linearity and bandwidth limitations of the integrator and the comparator) determined the modulator's implementation. The modulator was finally based on a programmable operational amplifier, to implement an opamp-R-C integrator, which allows selecting three different ranges of switching frequencies: tens of kHz, hundreds of kHz and MHz.

The power switches are implemented with synchronous rectifiers dimensioned to balance the loss breakdown; the NMOS' ON resistance is $119\,\mathrm{m\Omega}$ ($W = 12\,000\,\mu\mathrm{m}$) and the PMOS' ON resistance is $205\,\mathrm{m\Omega}$ ($W = 22\,000\,\mu\mathrm{m}$). The amplifier was designed to deliver 500 mW when supplied by $V_\mathrm{G} = 3,3\,\mathrm{V}$. The technology is AMIS 0.35µm C035U 5M and the die size is $1\,000\,\mu\mathrm{m} \times 640\,\mu\mathrm{m}$ (excluding pads). Operating at 400 kHz and delivering 480 mW, the efficiency of the IC is beyond 89 %. Figure 8.1 shows the IC layout.

8.2 Performance Validation

The performance of this amplifier has been used to experimentally validate the analyses and the results obtained in the previous chapters. Figures 8.2 and 8.3 show the time waveforms corresponding to the IC operating as AΣΔM[1]; in par-

[1]The signals are labeled as in the previous chapters, i.e. the reference signal $x(t)$, the recovered or filtered signal $\tilde{x}(t)$, the power switching signal $\tilde{z}(t)$ and the integrator's output signal $v(t)$.

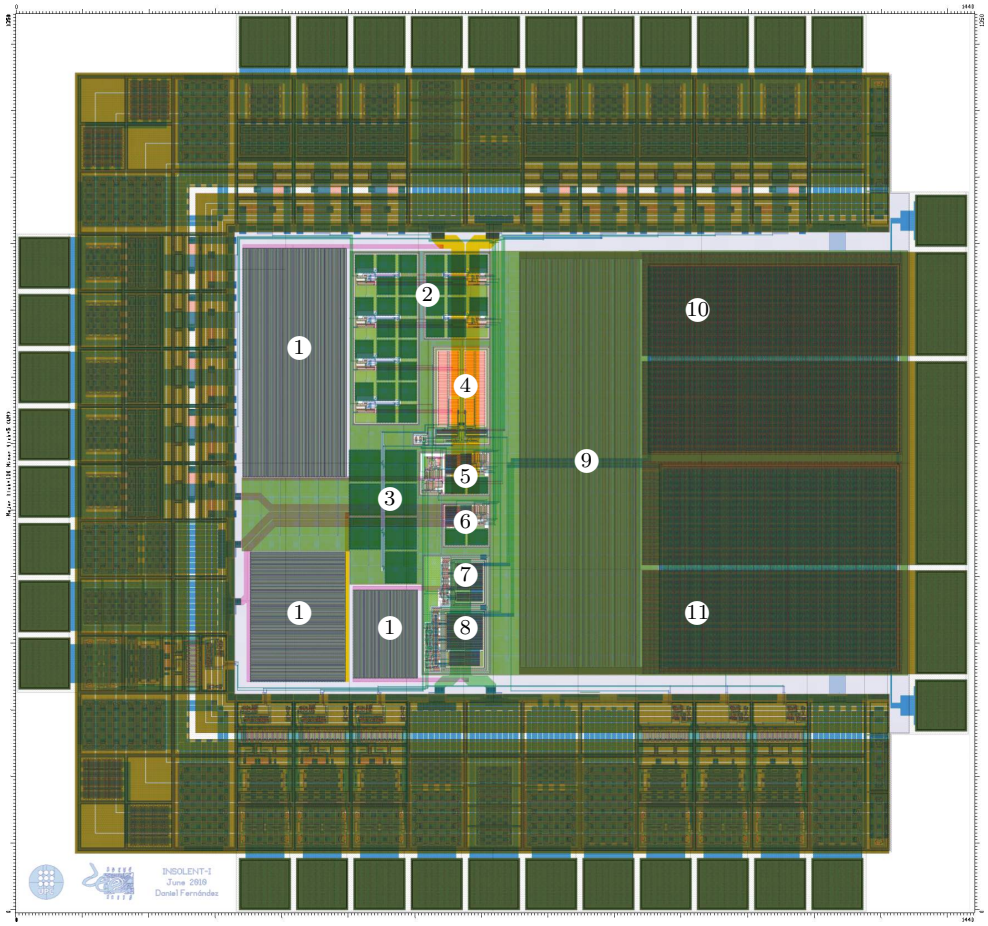

Figure 8.1: Integrated circuit layout view (IC designed by Dr. Daniel Fernández). The blocks are: decoupling capacitors (1), biasing (2), integrator capacitor (3), digitally programmable resistor (4), integrator operational amplifier and comparator (5), I/O voltage follower for debugging (6), NMOS driver (7), PMOS driver (8), deep-trench isolation and power-transistor supply decoupling-capacitor (9), PMOS power transistor (10) and NMOS power transistor (11).

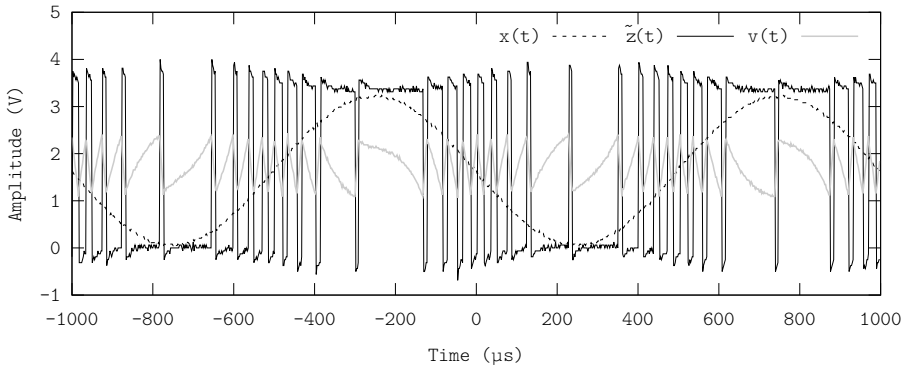

Figure 8.2: Experimental validation of AΣΔM tracking a 1 kHz single-tone sinusoid. The switching frequency is 17 kHz.

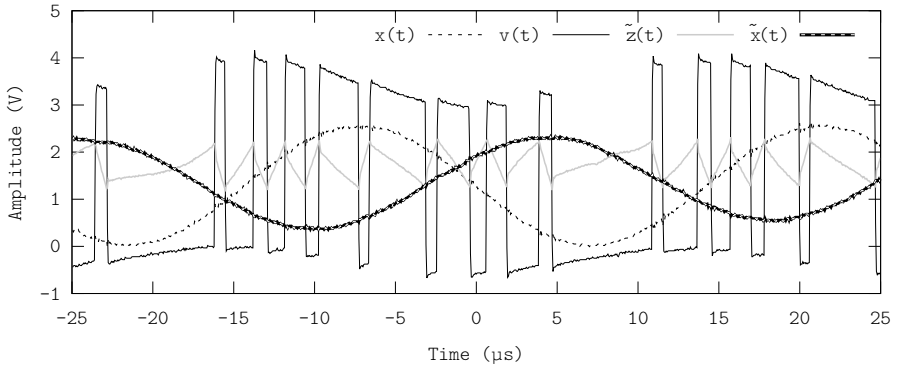

Figure 8.3: Experimental validation of AΣΔM tracking a 35 kHz single-tone sinusoid. The switching frequency is 533 kHz and the filter's cutoff frequency is 28 kHz.

ticular, in the former a 1 kHz single-tone sinusoid is tracked at 17 kHz (an OSwR of 17, operating at the minimum f_s programmable in this implementation) and in the latter a 35 kHz single-tone sinusoid is tracked at 533 kHz (yielding an OSwR of 15) and filtered with a second-order Butterworth low-pass filter with cutoff frequency of 28 kHz.

The effect of the switches' ON resistance and the supply voltage's output impedance is captured in these figures, as the two levels of the power switching signal $\tilde{z}(t)$ are not constant. The voltage of the low level sweeps below GND because the filter's coil drains current from GND during OFF. Note that in figure 8.2, the filter's cutoff frequency f_c is higher than the switching frequency f_s and thus the filter's input current (i.e. the current through the inductor) widely varies, almost tracking the power switching signal. Consequently, the variation of the levels of the power switching signal $\tilde{z}(t)$ approximately tracks the reference signal $x(t)$ with no delay.

On the other hand, in figure 8.3, the filter properly rejects the outband content of the power switching signal $\tilde{z}(t)$; the variations of the levels of the power switching signal $\tilde{z}(t)$ are hence delayed with respect to the reference signal $x(t)$. Also note that the recovered signal $\tilde{x}(t)$ is further delayed, since it

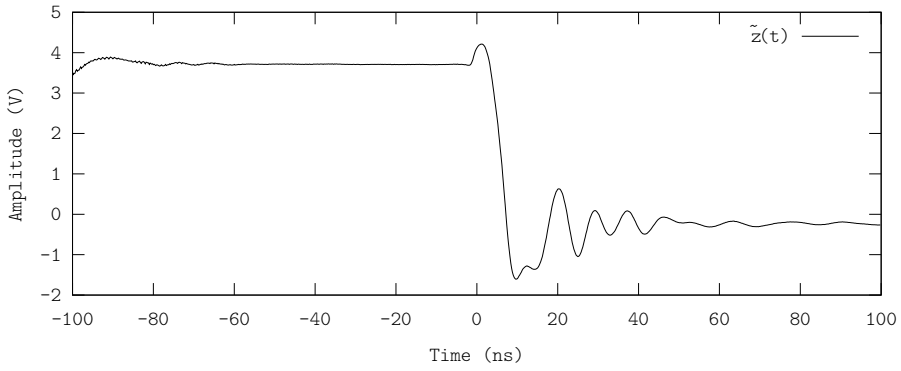

Figure 8.4: Detail of the power switching signal.

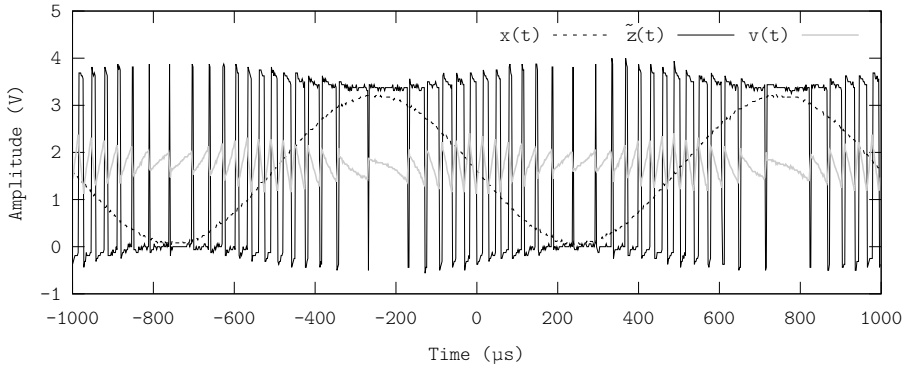

Figure 8.5: Experimental validation of AAΣΔM tracking a single-tone sinusoid.

is determined by the filter's output current.

Figure 8.4 shows a detail of the settling of the power switching signal $\tilde{z}(t)$. Because of parasitic and stray capacitances and inductances, the power switching signal suffers from ringing and overshooting. This capture shows the width of each switching event, in the range of 40 ns in this case.

Figure 8.5 shows the amplifier operating in AAΣΔM mode, at a switching frequency of 25 kHz. As can be seen, the hysteresis width (defined by the peaks of the integrator's output signal $v(t)$) is reduced according to the reference signal, which leads to an approximately constant switching frequency regardless of the reference signal's instantaneous value.

Figure 8.6 shows the time waveforms of AΣΔM operating at the maximum switching frequency, more than 7 MHz (beyond the system's specifications), tracking a 1 MHz single-tone sinusoid.

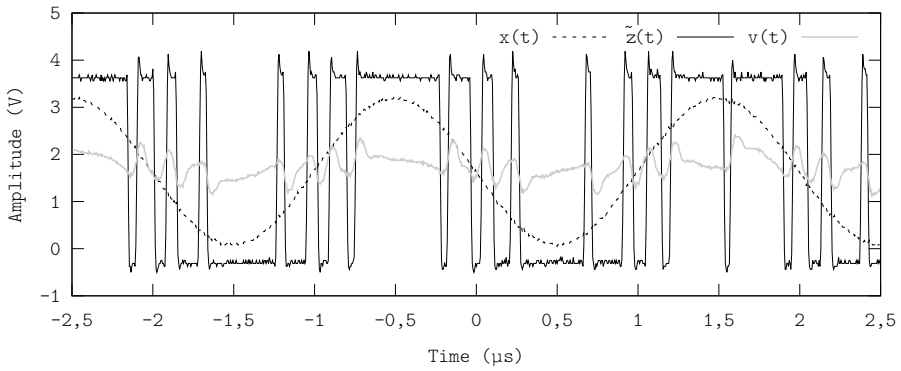

Figure 8.6: Testing the IC at maximum switching frequency (more than 7 MHz).

Chapter 9

Conclusions

This final chapter draws conclusions by summarising and recapitulating, one by one, the contributions of this research. A quick summary of the main outcomes of this thesis is also included, as well as a short list of topics and issues to consider in future research.

9.1 Thesis' Contributions

In the context of high-efficiency power processing for signal tracking (typically, switching power amplifiers for audio applications and wired and wireless transceivers) and motivated by the necessity of improving the efficiency of switching amplifiers using state-of-the-art technology (to fulfil the market demands of smaller, lighter and faster electronic devices), this work has researched different techniques to extend the bandwidth of switching amplifiers without increasing the switching frequency.

Due to the wide diversity of signals and systems encompassed by the different signal tracking applications, this work has first identified the funcionalities in the power-amplification process performed by switching amplifiers, which has led to define performance metrics to quantify and compare their behaviour. From this identification, the research has been focused in analysing different aspects of switching amplifiers; specifically, in determining their fundamental bandwidth limits, in analysing their signal processing (time encoding) and proposing alternatives to conventional techniques, in analysing the power processing and adapting it to the proposed time encoding techniques and, finally, in characterising and comparing their performance in different application frameworks.

More precisely, regarding the identification of funcionalities and the definition of performance metrics (chapters 1 and 2),

- The signals involved by the different applications have been characterised in both time and frequency domains. Due to heterogeneity of these signals
  - a flat-spectrum bandlimited signal has been proposed as a general reference signal
  - a parameter to measure the switching frequency, valid for both synchronous and asynchronous and/or both 2-level and multi-level switch-

ing signals and systems, has been defined (OverSwitching Ratio, OSwR).

- Conventional switching amplifiers have been interpreted as an encoding-reconstruction process, thereby identifying three sub-processes
  - encoding the reference signal into a 2-level switching signal (low-power signal processing, operation performed by the modulator).
  - power amplifying the switching signal, thereby generating a 2-level power switching signal (operation performed by the switches of the switching power converter).
  - low-pass filtering the power switching signal, thereby recovering a power-amplified distorted approximation to the reference signal (power signal processing, operation performed by the reactive components of the switching power converter).
- This interpretation has revealed that neither the control loop nor the assisting linear amplifier, very common in state-of-the-art switching amplifiers, modify the operating performance of the modulator nor the power converter (and hence they are not included in these analyses).
- Two error signals have been defined in order to aid in evaluating the amplifier's performance, being
  - the difference between the reference signal and the (low-power) switching signal (error signal)
  - the difference between the (scaled) reference signal and the recovered signal (remaining error signal)
- The three different sub-processes have been separately analysed (in conventional switching amplifiers under regular operating conditions), targeting to identify the different mechanisms which degrade the amplifier's tracking fidelity. Besides the error added by the modulator (encoding process), the effects of non-idealities upon the recovered signal have also been characterised, including
  - error due to the supply voltage's output impedance and due to the switches' ON resistance
  - error due to dead time
  - error due to LTI filters
- According to the results of these characterisations, it has been proposed to quantify the tracking fidelity of switching amplifiers according to the power of the different error signals; to compare low-power and power signals, a voltage-gain scaling factor has to be applied and the time delay due to the low-pass filter must be equalised. In order to supplement this performance metrics, the cumulative-power frequency distribution is also quantified (mainly to split inband and outband power).

Arising from the encoding-reconstruction interpretation of switching amplifiers, the fundamental bandwidth limits in 2-level time encoding have been explored (chapter 3).

- The concept of inband-error-free encoding in switching amplifiers has been defined.
- A 2-level switching signal inband-error-free tracking a single tone at an OSwR of 2 has been synthesised.
- A 2-level switching signal inband-error-free tracking a bandlimited periodic signal (consisting of N tones) at an OSwR of $1 + 1/N$ has been synthesised.
- Based on the previous synthesised switching signal, the minimum OSwR required to inband-error-free track a periodic bandlimited signal has been derived.
- The minimum OSwR required to inband-error-free track a non-periodic bandlimited signal has been derived by generalising the previous result.
- Inband-error-free encoding has been applied to common cases in switching amplifiers: signal tracking at non-minimum OSwR (i.e. OSwR > 1) and underswitching (tracking signals whose bandwidth exceeds the amplifier's switching frequency, i.e. OSwR < 1, typically infinite-band signals).
- Starting from minimum OSwR inband-error-free encoding, the OSwR has been increased to partially shape the outband spectral content whilst keeping the inband-error-free tracking feature.
- The time waveforms of inband-error-free encoding have been analysed, targeting to evaluate whether actual modulators approximate inband-error-free encoding under some operating conditions.

Once the bandwidth limits of two-level time encoding have been determined, different 2-level modulations have been characterised, to evaluate the room for improvement of these modulations (in terms of switching frequency) compared to the fundamental limit previously derived (chapter 4).

- Pulse Width Modulation (PWM), the most common modulation in switching amplifiers, has been in-depth characterised under non-conventional operating conditions.
  - The encoding algorithm of PWM tracking constant-reference signals has been analysed, including different modulation variants (leading and trailing sawtooth, triangle and non-linear carriers).
  - Two different strategies to generalise PWM to non-constant signal tracking, uniform sampling and natural sampling, have been considered.
  - The histogram of pulses' width of PWM tracking a non-constant reference signal has been characterised.
  - The power spectrum of the PWM error signal has been characterised, including the analysis of the cumulative-power frequency distribution.
- Asynchronous $\Sigma\Delta$ Modulation (A$\Sigma\Delta$M), a well-known modulation yet not widely used in switching amplifiers, has been proposed as alternative to PWM for enhanced signal tracking in switching amplifiers.

  - The encoding algorithm of AΣΔM and its suitability for signal tracking in switching amplifiers have been analysed.
  - The time-domain waveforms of AΣΔM have been characterised, including the characterisation of the pulses' width when tracking a non-periodic bandlimited signal.
  - The power spectrum of the error signal of AΣΔM tracking a non-periodic bandlimited signal has been characterised, including the identification of harmonic bands and analysing the cumulative-power frequency distribution.
  - Encoding limitations in AΣΔM have been identified.

- Pursuing to overcome the encoding limitations of AΣΔM, an upgrade to this modulator has been proposed (Adaptive Asynchronous ΣΔ Modulator, AAΣΔM).
  - A feedforward quadratic law (from the reference signal to the hysteresis width) has been proposed.
  - The conditions for astable operation of AAΣΔM tracking constant and non-constant reference signals has been discussed.
  - The time-domain waveforms of AAΣΔM have been characterised, including the characterisation of the pulses' width when tracking a non-periodic bandlimited signal.
  - The power spectrum of the error signal of AAΣΔM tracking a non-constant reference signal has been characterised, at different OSwRs, analysing the cumulative-power frequency distribution.

- The feasibility of using other common modulations in switching amplifiers has been discussed, like click modulation and minimum time.

- The inband performance (error signal's inband power) of PWM, AΣΔM and AAΣΔM has been characterised according to the fundamental limit derived in this work.
  - The inband performance of these two conventional modulations and the proposed one has been characterised under non-conventional operating conditions (OSwR from 1 to 10, consistently with the scope of this thesis and the fundamental limit earlier derived).
  - The performance of these three modulations has been characterised when tracking reference signals wider than the switching frequency (OSwRs below 1, underswitching), a common situation in envelope-tracking applications.
  - The encoding bandwidth limits of each modulation, more restrictive than the fundamental modulation limit of 2-level switching signals, have been analysed.
  - Targeting to reduce the power of the remaining error signal in switching amplifiers, the outband power of the error signal has been analysed (for any modulation properly tracking the reference signal).

According to the analysis of 2-level modulations, the outband power of the error signal cannot be reduced by only changing the modulation. Targeting to reduce the power of the remaining error signal in switching amplifiers, multi-level time encoding and power amplification is proposed (chapter 5).

- In the power-amplification process performed by multi-level switching power amplifiers, a new sub-process has been identified (translating the switching signal into a set of switch-driving signals, operation performed by the decoding logic).
- The concept of switching policy, applied to the modulator and to the decoding logic, has been defined.
- The advantages and benefits of multi-level time encoding for switching amplifiers have been discussed.
- The fundamental bandwidth limit of multi-level time encoding has been explored.
- Multi-level PWM, the extension of 2-level PWM to multiple levels, has been in-depth analysed.
  - The PWM encoding algorithm has been generalised to N levels (amplitude-shifted carriers).
  - The performance of different carrier alignments has been analysed.
  - The histogram of pulses' width of N-level PWM tracking a non-constant reference signal has been characterised, for different number of levels N.
  - The encoding bandwidth limit of 2-level PWM (intrinsic slew-rate constraint) has been generalised to the N-level case.
  - The power spectrum of the error signal of N-level PWM tracking a non-constant reference signal has been characterised, for different number of levels N, and the cumulative-power frequency distribution has been analysed for all of them.
  - Targeting a simpler implementation, the equivalency between amplitude-shifted and phase-shifted N-level PWM has been discussed.
- The extension of 2-level AΣΔM to multiple levels has been proposed.
  - An AΣΔM modulator capable of handling multiple levels has been proposed.
  - The AΣΔM encoding algorithm has been generalised to N levels.
  - The conditions for astable operation of N-level AΣΔM have been derived.
  - The time-domain waveforms of N-level AΣΔM have been characterised for different number of levels N, including the characterisation of the pulses' width, when tracking a non-periodic bandlimited signal.

  - The power spectrum of the error signal of N-level A$\Sigma\Delta$M tracking a non-periodic bandlimited signal has been characterised, for different number of levels N, including the analysis of the cumulative-power frequency distribution.
  - Encoding limitations in N-level A$\Sigma\Delta$M have been identified.

- The extension of 2-level AA$\Sigma\Delta$M to multiple levels has been proposed.
  - The feedforward quadratic law of 2-level AA$\Sigma\Delta$M has been generalised to N levels.
  - The time-domain waveforms of N-level AA$\Sigma\Delta$M have been characterised for different number of levels N, including the characterisation of the pulses' width, when tracking a non-periodic bandlimited signal.
  - The conditions for astable operation of N-level AA$\Sigma\Delta$M tracking constant and non-constant reference signals have been analysed.
  - The power spectrum of the error signal of N-level AA$\Sigma\Delta$M tracking a non-periodic reference signal has been characterised, for different number of levels N, including the analysis of the cumulative-power frequency distribution.

- The inband performance of these three modulations, N-level PWM, N-level A$\Sigma\Delta$M and N-level AA$\Sigma\Delta$M has been characterised in the non-conventional framework of this research.
  - The inband performance of N-level PWM, N-level A$\Sigma\Delta$M and N-level AA$\Sigma\Delta$M has been characterised and compared from OSwRs below 1 (underswitching) to OSwRs up to 10.
  - The performance degradation due to the bandwidth limits of each multi-level modulation has been analysed.

Once the low-power switching signal is generated, either two-level or multi-level, it must be power-amplified and filtered by the switching power converter in order to recover a power-amplified distorted version of the reference signal (chapter 6).

- The switching power converter itself generates a power switching signal and filters it out, thus recovering the baseband information conveyed by the switching signal.
  - The concept of ideal low-pass filter for switching amplifiers and lossless LTI low-pass filters have been reviewed.
  - The high-order filter extension of switching converters has been reviewed.
  - Different transfer functions for the low-pass filter have been considered.
  - A method for optimising the filter's cutoff frequency has been proposed.
  - The feasibility of pre-equalising the reference signal according to the filter's inband response to improve the tracking fidelity has been discussed.

- In the context of multi-level switching amplifiers, improving the translation of the modulator's output signal into the set of switch-driving signals has been proposed as a method for achieving additional features.
  - A switching policy to maximise the number of distinct output voltage levels for a given number of supply voltages has been presented.
  - An enhanced decoding logic to partially shape the common-mode voltage signal in 3-level full-bridge converters has been proposed.
- A preliminary extension of switching amplifiers to non-linear converter topologies has been presented.
  - The advantages of non-linear converters and some of the additional features that can be achieved with them are introduced.
  - A grounded-output 5-switch bipolar buck-boost converter topology for switching amplifiers has been presented.
    - The four valid states have been described.
    - The converter's dynamic equations have been derived.
    - The averaged steady-state expressions have been derived.
    - The topology characteristics have been described.
    - An operating example has been included.

All these individual contributions for each sub-process have been merged into a single amplifier, to evaluate the aggregate performance improvement in different scenarios (chapter 7).

- The comparison framework has been defined, including a description of the three different optimisation strategies considered (regarding the remaining error signal, minimising its power, minimising its inband power or reducing the upperbound of the outband spectral content), the description of the conventional design used as comparison reference and the definition of the design space.
- 2-level, 3-level, 5-level and 7-level switching amplifiers based on PWM, AΣΔM and AAΣΔM have been in-depth characterised in the OSwR range extending from 0,1 to 10 (including underswitching and a low-OSwR range). Each modulator has been combined with a second-order optimised filter, a fourth-order optimised filter and an eighth-order optimised filter.
- Based on the previous characterisations, a summary of all amplifiers based on the same kind of modulation has been provided.
- The performance degradation and the robustness against non-idealities of these amplifiers has been analysed.
  - An upgrade to improve the robustness against non-idealities for AΣΔM-based and AAΣΔM-based amplifiers has been presented.
  - The robustness against variations in the levels of the power switching signal (typically due to non-idealities in the supply voltages and the power switches) has been characterised.

  - The impact of time delays and bandwidth limitations in the modulator's components (comparators, adders and integrators) upon the encoding process (error signal) and also its consequences upon remaining error signal have been characterised.
  - The effects of electromagnetic interferences and crosstalk upon PWM-based and AΣΔM-based amplifiers have been evaluated.
    * A capacitive-coupling model for EMI has been introduced.
    * Crosstalk in phase-shifted multi-level PWM has been analysed (including in-channel crosstalk and crosstalk between n channels).
    * Crosstalk in multi-level AΣΔM has been analysed (including in-channel crosstalk and crosstalk between n channels).
    * The performance degradation due to crosstalk when tracking constant-reference signals has been evaluated for PWM-based and AΣΔM-based multi-level amplifiers.
    * The performance degradation due to crosstalk when tracking single tones of similar frequency has been evaluated for PWM-based and AΣΔM-based multi-level amplifiers.
    * The performance degradation due to crosstalk when tracking uncorrelated bandlimited signals has been evaluated for PWM-based and AΣΔM-based multi-level amplifiers.

- Other implementation-induced effects and issues have also been considered.
  - The minimum pulses' width required for each kind of modulator when operating at the same OSwR has been compared.
  - Switching losses when the system is idle for each kind of modulator has been compared.
  - The suitability of each kind of amplifier for underswitching has been analysed.
  - The feasibility of filterless amplifiers has been discussed.
  - Common-mode and differential-mode voltage signals and filters have been analysed.
    * The common-mode voltage in multi-level full-bridge amplifiers has been analysed.
    * The consequences upon the common-mode signal's power spectrum of using different modulation schemes have been characterised.
    * The consequences upon the common-mode signal's power spectrum of using different switching policies have been characterised.
  - Filters of different orders but with equivalent series inductance have been described.
  - The synthesis of bipolar switches with power MOSFETs has been described.

  - An switch optimisation criterion for equalised conduction losses has been presented and applied to two examples (multi-level full-bridge converter and 5-switch converter topology).
  - The feasibility of upgrading the amplifiers with soft-switching has been briefly discussed.

- Based on the in-depth characterisations of ideal amplifiers (different modulations, number of levels and filters' order), the robustness against non-idealities and other implementation issues, the different possible amplifiers are finally compared to select the most suitable candidates for different scenarios (high-OSwR or low-OSwR applications).

Some of the bandwidth extension techniques for switching amplifiers herein proposed have been applied to the design of an integrated switching amplifier for low-OSwR applications.

- The 2-level AAΣΔM modulator has been implemented for a buck switching power amplifier.
- The bandwidth limitations characterisations of the integrator and the adder have been considered as design guidelines in the design of the integrated switching amplifier.
- The performance of 2-level AΣΔM and 2-level AAΣΔM has been experimentally validated.
- The effects of the switches' ON resistance and the supply voltage's output impedance upon the power switching signal have been experimentally validated.

9.2 Thesis' Outcomes

According to the characterisations and the comparison between the conventional and the proposed designs, if the OSwR is high enough (typically beyond 5), the most effective technique to reduce the power of the remaining error signal (both inband and outband), as well as minimising the upperbound of its outband spectral content, is improving the decoding process; i.e. upgrading a conventional second-order 2-level switching amplifier based on PWM to high-order filtering and optimising the filter's cutoff frequency. Broadly speaking, this technique takes advantage of the very accurate inband tracking of 2-level PWM (at high OSwRs) to reduce the inband error; the filter's order is then increased to widely reject the modulation's outband content, mostly concentrated around the switching frequency.

Nonetheless, there are applications wherein high OSwRs are not feasible. As the bandwidth limits exploration of time encoding has shown, it is possible to inband-error-free track a bandlimited signal at an OSwR of 1 (in both 2-level and multi-level time encoding). Given that it is not possible to reject the switching signal's outband content without affecting its inband content, if operating at low OSwRs and filtering with a LTI low-pass filter, the outband content of the switching signal must be partially avoided (i.e generated with lower power) instead of generated and subsequently rejected.

Accordingly, the characterisations and comparisons between candidates reveal that, in this low-OSwR framework (typically between 1 and 5), the most effective technique to improve the performance of a conventional amplifier is upgrading it to multiple levels; in particular, the conventional 2-level PWM-based amplifier should be upgraded to a 7-level AΣΔM-based amplifier (the modulator must be changed to an incremental multi-level modulation, such as N-level AΣΔM, to properly track the reference signal with multiple levels at a low OSwR). Provided that the switching signal's outband power is lower, very high stopband rejection is no longer necessary and hence low-order filters are suitable for these multi-level amplifiers; even filterless amplifiers become feasible.

From a more implementation-oriented standpoint, AΣΔM-based amplifiers are more robust to non-idealities than PWM-based amplifiers. The built-in feedback loop of AΣΔM (either 2-level or multi-level) provides the amplifier with enhanced robustness against variations in the levels of the power switching signal (typically due to the power supplies' output impedance and the switches' ON resistance), dead time and EMI in general (including crosstalk); furthermore, the ratio of the maximum instantaneous switching frequency to the average switching frequency is much lower in AΣΔM than in PWM, especially in multi-level amplifiers, and the upperbound of the outband spectral content is lower in AΣΔM (spread-spectrum modulation) than in PWM. AΣΔM can be easily upgraded to an incremental multi-level modulation, whereas multi-level PWM is not incremental; consequently, N-level AΣΔM can be used at any OSwR.

Therefore, considering all these implementation issues, upgrading from 2-level PWM to N-level AΣΔM may also be a feasible option to improve the performance of switching amplifiers in high-OSwR applications. Additionally, feedforward from the reference signal to the comparison threshold (2-level and multi-level AAΣΔM) can be added to achieve better tracking performance.

9.3 Future Research

This thesis has explored different techniques to extend the bandwidth of switching amplifiers. Some topics for future research, to further extend the bandwidth of switching amplifiers and/or achieve additional features, are listed next.

The performance of all candidates has been evaluated based on a generic bandlimited signal. The performance improvements achieved by the techniques herein proposed should be evaluated for particular applications, i.e. when tracking the actual signals of each specific application.

The feedforward law of AAΣΔM should be improved or a modulator based on a different structure should be proposed, pursuing to better approximate inband-error-free encoding at low OSwRs.

The preliminary extension to non-linear converters should be further explored. Related to this extension, the control loop should be included in the analysis, to evaluate which candidates simplify the design and implementation of the control loop. Consistently with this analysis, dynamic models of switching amplifiers should be proposed.

Appendix A

List of Acronyms and Abbreviations

AC	Alternate Current
ADC	Analog to Digital Converter
AET	Average Envelope Tracking
AAΣΔM	Adaptive Asynchronous ΣΔ Modulation
	Adaptive Asynchronous ΣΔ Modulator
AΣΔM	Asynchronous ΣΔ Modulation
	Asynchronous ΣΔ Modulator
BER	Bit Error Rate
BJT	Bipolar Junction Transistor
BPSK	Binary Phase Shift Keying
BoM	Bill of Materials
CCFL	Cold Cathode Fluorescent Lamp
CD	Compact Disc
CD-DA	Compact Disc Digital Audio
CDMA	Code Division Multiple Access
CMOS	Complementary Metal Oxide Semiconductor
CMRR	Common-Mode Rejection Ratio
DC	Direct Current
DFT	Discrete Fourier Transform
DFT^{-1}	Inverse Discrete Fourier Transform

DSP	Digital Signal Processor
EER	Envelope Elimination and Restoration
EMC	ElectroMagnetic Compatibility
EMI	ElectroMagnetic Interferences
EPP	End of Point Prediction
ESR	Equivalent Series Resistor
ET	Envelope Tracking
EVM	Error Vector Magnitude
FCC	Federal Communications Commission
FDM	Frequency Division Multiplexing
FDMA	Frequency Division Multiple Access
FFT	Fast Fourier Transform
FFTW	Fastest Fourier Transform in the West
FoM	Figure of Merit
FPGA	Field Programmable Gate Array
GMSK	Gaussian Minimum Shift Keying
GPRS	General Packet Radio Service
GSM	Global System for Mobile communications (former *Groupe Spécial Mobile*)
HDVC	High-Voltage Direct Current
HiFi	High-Fidelity
IEEE	Institute of Electrical and Electronics Engineers
LASER	Light Amplification by Stimulated Emission of Radiation
LED	Light Emission Diode
LTI	Linear Time Invariant
MOSFET	Metal Oxide Semiconductor Field-Effect Transistor
OSwR	OverSwitching Ratio
PCM	Pulse-Code Modulation
PID	Proportional–Integral–Derivative
PFC	Power Factor Correction
PFM	Pulse Frequency Modulation

PLC	Power Line Communications
PSCPWM	Parallel phase-Shifted Carrier Pulse Width Modulation / Parallel phase-Shifted Carrier Pulse Width Modulator
PSK	Phase Shift Keying
PSRR	Power Supply Rejection Ratio
PWM	Pulse Width Modulation / Pulse Width Modulator
QAM	Quadrature Amplitude Modulation
QPSK	Quadrature Phase Shift Keying
RMS	Root Mean Square
RF	Radio Frequency
RFPA	Radio Frequency Power Amplifier
SEPIC	Single-Ended Primary Inductor Converter
SPDT	Single-Pole Double-Throw
THD	Total Harmonic Distortion
THD+N	Total Harmonic Distortion plus Noise
UMTS	Universal Mobile Telecommunications System
VRM	Voltage Regulator Module
WBET	Wide-Bandwidth Envelope Tracking
WiFi	Wireless Fidelity
WiMAX	Worldwide Interoperability for Microwave Access
WCDMA	Wideband Code Division Multiple Access
WLAN	Wireless Local Area Network
xDSL	Digital Subscriber Line
ZAD	Zero Averaged Dynamics
ZOH	Zero Order Hold

Appendix B

Parameters and Definitions

This appendix defines the most relevant parameters and figures of merit used throughout this work, as well as the signals' amplitude and the power normalisation. Given the heterogeneous nature of the signals and systems analysed in this work, all parameters are defined so that they can be applied to synchronous and asynchronous signals and systems, as well as to 2-level and multi-level switching signals and systems.

B.1 Notation

In all this document, time-domain waveforms are typeset in italics lower-case letters and frequency-domain waveforms are typeset in italics upper-case letters. To further emphasise the notation, the independent variable is expressed between brackets (also typeset in italics). In chapter 1, upper-case letters are also used to denote the averaged value of state variables. To avoid notation abuse, the independent variable is not explicit in the state variables. Table B.1 includes the list of lower-case and upper-case letters used to denote time-domain and frequency-domain waveforms respectively.

The impulse response of a Linear Time Invariant (LTI) system is denoted with $h(t)$ and its transfer function, defined as the Laplace transform of the

signal	*time domain*	*frequency domain*
error	$e(t)$	$E(f)$
remaining error	$\xi(t)$	$\Xi(f)$
input	$x_{\mathrm{i}}(t)$	(not used)
reference	$x(t)$	$X(f)$
recovered	$\tilde{x}(t)$	$\tilde{X}(f)$
switching	$z(t)$	$Z(f)$
power switching	$\tilde{z}(t)$	$\tilde{Z}(f)$
integrator's output	$v(t)$	(not used)

Table B.1: Lower-case and upper-case letters used to denote signals in time and frequency domains. The signals (and their respective letters) which only appear in the introduction are not included in this table.

impulse response, is denoted $H(s)$.

$$H(s) := \mathcal{L}[h(t)] := \int_{-\infty}^{+\infty} h(t)e^{-st}\,\mathrm{d}t \tag{B.1}$$

The Root Mean Square (RMS) value of a certain signal $x(t)$ is denoted as $x(t)_{\mathrm{RMS}}$, which is zero or a positive real number as well.

$$x(t)_{\mathrm{RMS}} := \lim_{T\to+\infty} \sqrt{\frac{1}{2T}\int_{-T}^{T} x^2(u)\,\mathrm{d}u} \in \mathbb{R}, \quad x(t)_{\mathrm{RMS}} \geq 0 \tag{B.2}$$

B.2 Summary of Signals in Switching Amplifiers

This section summarises the representative signals in switching amplifiers. According to figure B.1,

- Input signal $x_{\mathrm{i}}(t)$: the signal to track and power amplify in amplifiers using pre-emphasis (low-power signal).
- Reference signal $x(t)$: pre-emphasised input signal. Pre-emphasis is considered an external operation (not part of the switching amplifier itself); the reference signal is hence the signal to track and power amplify.
- Switching signal $z(t)$: the modulator's output signal, a N-level switching signal (low-power signal).
- Error signal $e(t)$: difference between the switching signal and the reference signal $e(t) := z(t) - x(t)$ (low-power signal).
- Switch-driving signals $s_i(t)$: a set of binary signals to drive the switches of the switching power converters through a chain of tapered buffers (one signal for each switch of the switching power converter).
- Power switching signal $\tilde{z}(t)$: the signal supplied to the filter's input port, generated by the switches of the switching power converter and the supply voltages V_j (power signal).
- Recovered signal $\tilde{x}(t)$: low-pass filtered version of the power switching signal $\tilde{z}(t)$; it is the switching amplifier's output signal (power signal).
- Remaining error signal $\xi(t)$: the content of the recovered signal $\tilde{x}(t)$, properly compensating the filter's delay τ, differing from the (scaled) reference signal $x(t)$; $\xi(t) := \tilde{x}(t-\tau) - Gx(t)$ (power signal).
- Common-mode output signal $\tilde{z}_{\mathrm{C}}(t)$: the arithmetic mean of the two voltage signals applied to two ends of the output filter's input port (power signal, only valid for floating-output converter topologies).

The switching signal $z(t)$ is a continuous-time N-level discrete-amplitude signal bounded by $Z_{\min}$ and $Z_{\max}$ (the modulator's output dynamic range).

$$Z_{\min} \leq z(t) \leq Z_{\max}, \quad \forall t \in \mathbb{R} \tag{B.3}$$

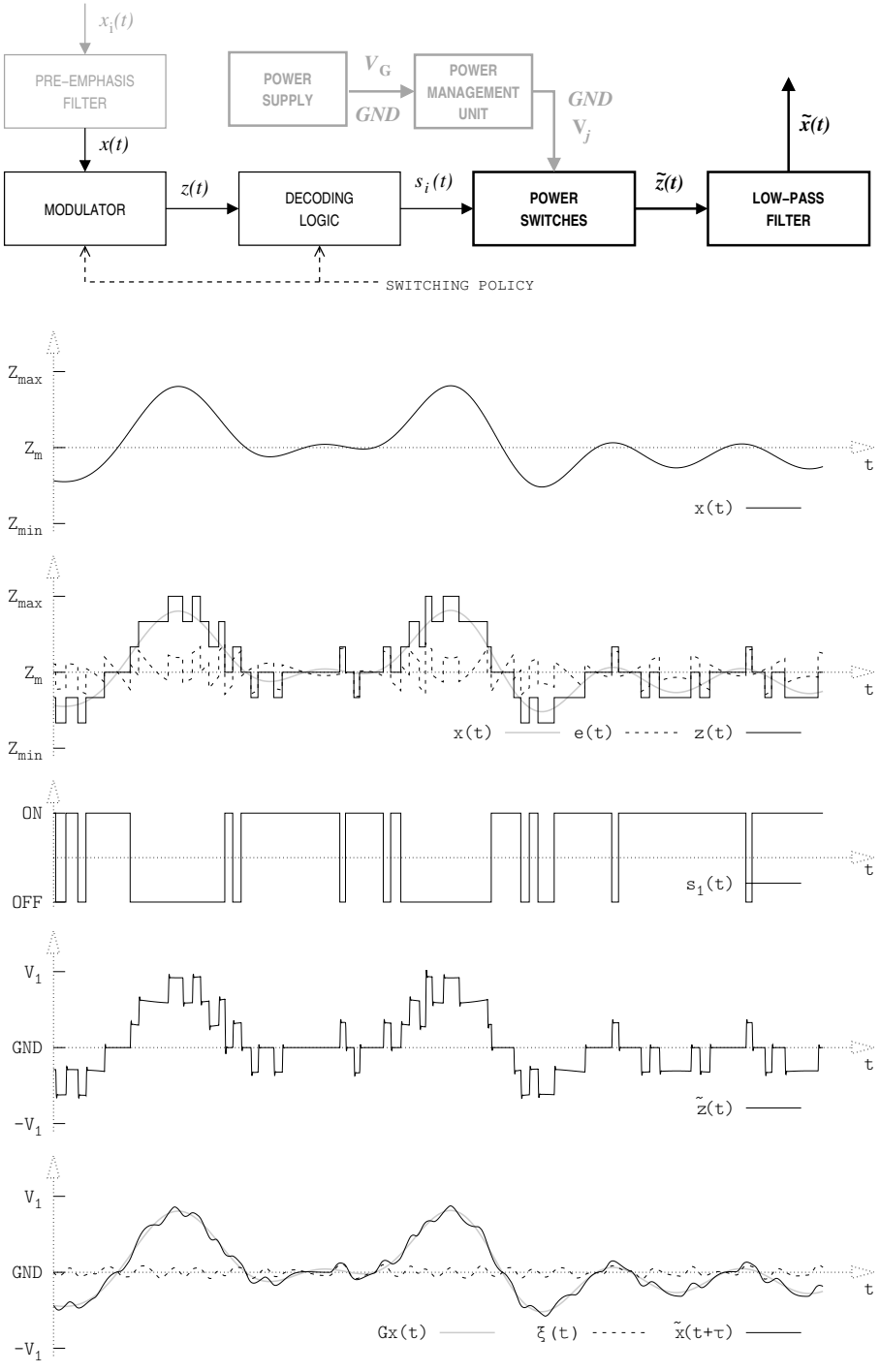

Figure B.1: Block diagram and time-domain waveforms of a switching amplifier (example based on 7-AΣΔM, using the enhanced policy and a second-order Butterworth filter; only one of the six switch-driving signals is displayed). The power path is highlighted in bold and the external elements to the amplifier are displayed in grey.

The reference signal $x(t)$ is a continuous-time continuous-amplitude bandlimited flat-spectrum signal bounded by $X_{\min}$ and $X_{\max}$ (modulator's input dynamic range). Both the input and the output dynamic ranges of the modulator are assumed to belong to the same range. Therefore

$$Z_{\min} \leq X_{\min} \leq x(t) \leq X_{\max} \leq Z_{\max}, \quad \forall t \in \mathbb{R} \tag{B.4}$$

The ratio of the reference signal's amplitude sweep (or dynamic range) to the modulator's input dynamic range is defined as the modulation depth c. 100 % is modulation depth is assumed in all this work, unless otherwise stated.

$$c := \frac{X_{\max} - X_{\min}}{Z_{\max} - Z_{\min}} \tag{B.5}$$

For the sake of notation simplicity, it is often convenient to express these signals according to the mean value Z_{m} and to the peak-to-peak Z_{pp} value of the modulator's dynamic range, defined as

$$Z_{\mathrm{m}} := \frac{Z_{\max} + Z_{\min}}{2} \tag{B.6}$$

$$Z_{\mathrm{pp}} := Z_{\max} - Z_{\min} \tag{B.7}$$

The power switching signal $\tilde{z}(t)$ is bounded by the highest supply voltage V_n and GND or $-V_n$ (in full-bridge converters). The recovered signal $\tilde{x}(t)$ is also bounded by these values, as the filter do not provide voltage gain. In order to compare power signals and low-power signals, it is necessary to scale them by the level-shifting factor G defined as

$$G := \frac{V_{\mathrm{n}}}{Z_{\mathrm{pp}}} \tag{B.8}$$

assuming a buck-based amplifier (in full-bridge-based amplifiers $G := 2V_{\mathrm{o}}/Z_{\mathrm{pp}}$).

B.3 Switching Frequency

This work deals with synchronous and asynchronous systems, as well as with 2-level and multi-level switching signals and systems. In order to compare the performance of signals and systems of such heterogeneous natures, it is necessary to define a unified switching frequency. In the literature, when dealing with multi-level systems and signals, different definitions of switching frequency have been used.

Since both synchronous and asynchronous systems are to be compared, the switching frequency of a switching signal $z(t)$ must be evaluated on average. The average switching frequency $\bar{f}_{\mathrm{s}}$ is then defined as

$$\bar{f}_{\mathrm{s}} := \lim_{T \to +\infty} \frac{N_{\mathrm{sw}}}{2T} \tag{B.9}$$

where N_{sw} is the number of time that the switching signal $z(t)$ changes its value within the observation time T.

If the reference signal is stationary, which is generally the case in the context of switching amplifiers, the average switching frequency $\bar{f}_{\mathrm{s}}$ can be approximated

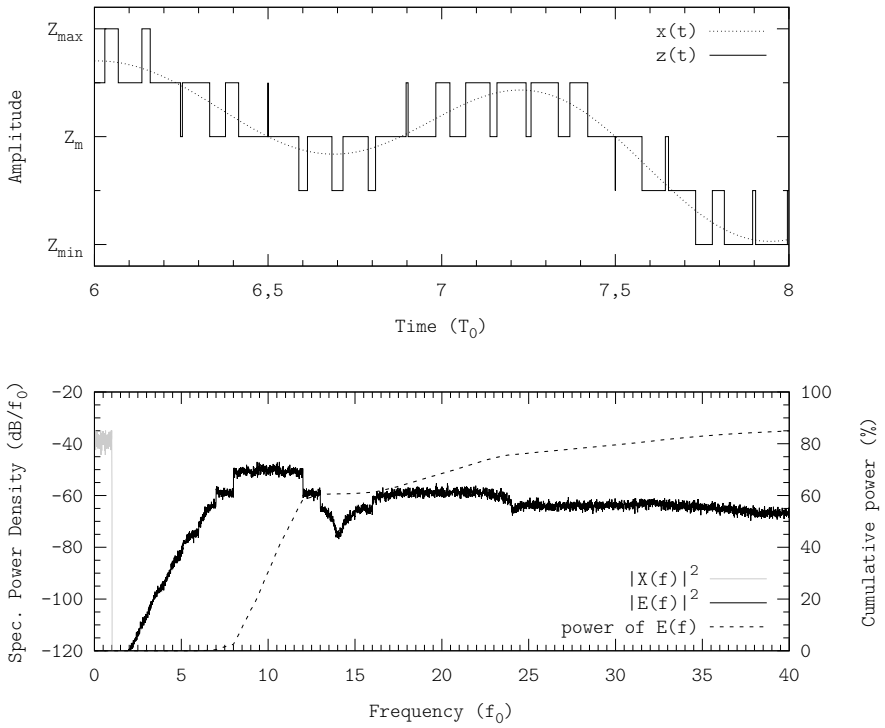

Figure B.2: Average switching frequency in a multi-level switching signal, showing the time waveform (upper plot) and the power spectrum (lower plot). The definition of switching frequency ($10f_0$, 40 edges within $2T_0$) is consistent with the power spectrum.

by evaluating it within a time interval[1] Δt. The average switching frequency $\bar{f}_\mathrm{s}$ can be then obtained as

$$\bar{f}_\mathrm{s} \approx \frac{N_\mathrm{sw}}{2\Delta t} \tag{B.10}$$

Note that this definition can also be applied to synchronous systems, as it leads to the switching frequency f_s. For the sake of notation simplicity and given that the average definition is valid for both synchronous and asynchronous systems, the average switching frequency is denoted by f_s in this work.

Also note that this definition is consistent with the power spectra of multi-level switching signals. For instance, consider the 5-level example shown in figure B.2. According to (B.10), the switching frequency of this signal is $10f_0$, regardless of how it was generated[2]. The Fourier transform corroborates this definition, since more than 60 % of the error signal's power concentrates around $10f_0$.

[1] This time interval must be long enough so that the difference between evaluating the average switching frequency within different time intervals is not significant.

[2] In the literature different definitions of the switching frequency of switching signals have been used, especially in the context of multi-level PSCPWM. These other definitions were discarded because they are not consistent with the power spectrum.

B.4 OverSwitching Ratio

In the context of switching amplifiers, is often necessary to compare the switching frequency f_s of a switching signal $z(t)$ with the bandwidth of the baseband reference signal $x(t)$ that it is tracking (i.e. the frequency of the highest non-zero spectral content of $X(f)$).

Aiming to aid in this comparison, as well as to provide a unified general comparison framework, all frequencies (times) are expressed relative to $f_0 = 1/T_0$, an arbitrary frequency (time). f_0 is only intended to set a reference frequency and has no physical interpretation, although, usually, the reference signal $x(t)$ is normalised so that its bandwidth is f_0; similarly, regarding the modulator, the switching frequency f_s is set so that its tracking bandwidth is f_0 as well (note that, because of encoding limitations, $f_\mathrm{s} > f_0$).

The ratio between the average switching frequency f_s to f_0 is defined as the OverSwitching Ratio (OSwR)

$$\mathrm{OSwR} := \frac{f_\mathrm{s}}{f_0} = \frac{N_\mathrm{sw}}{2\Delta t f_0} = \frac{N_\mathrm{sw}}{2N_{T_0}} \tag{B.11}$$

where N_{T_0} denotes the number of T_0 periods within Δt.

This parameter expresses how fast the switching signal is, relative or compared to the reference frequency f_0 (how many switching events occur, in average, within one T_0-cycle).

Note that the OSwR can also be used to quantify the relative bandwidth of switching amplifiers, i.e. the ratio of the amplifier's switching frequency f_s to the amplifier's tracking bandwidth, as long as the amplifier's tracking bandwidth is f_0 (the switching frequency of the switching signal $z(t)$ determines the amplifier's switching frequency).

B.5 Power Normalisation

Given an arbitrary time-dependent finite-power signal $x(t)$, its average power or simply power $P_{x(t)}$[3] is given by

$$P_{x(t)} := \lim_{T\to+\infty} \frac{1}{2T} \int_{-T}^{T} \frac{x^2(u)}{R_\mathrm{L}}\,\mathrm{d}u, \qquad R_\mathrm{L} \in \mathbb{R}^+ \tag{B.12}$$

where R_L is a normalisation factor. The physical interpretation of this factor depends on the nature of the magnitude of the signal $x(t)$. In voltage signals, R_L can be interpreted as the impedance of the load supplied by the signal $x(t)$, whereas in current signals this parameter should be interpreted as the admittance of the load. Since voltage signals are more common and the loads are mainly resistive, this parameter is denoted as R_L, which expresses a resistor.

Therefore, the power conveyed by an arbitrary signal $X_\mathrm{min} \leq x(t) \leq X_\mathrm{max}$, $\forall t \in \mathbb{R}$, $X_\mathrm{min}, X_\mathrm{max} \in \mathbb{R}$ depends upon its dynamic range (X_min and X_max), the load R_L and the time waveform itself. Note that, depending on the time waveform, the power of the switching signal may be infinite (finite-energy signals, in contrast to finite-power signals).

[3] Power is expressed with a number, not a function; the time-dependency in the subscript refers to the signal and not to the power itself.

Despite power is generally expressed in relative scales throughout this work, all signals have been normalised to $X_{\min} = -1$ and $X_{\max} = 1$ before evaluating their power, both low-power and power signals, and the normalisation factor has been set to $R_{\mathrm{L}} = 1$. This normalisation only involves a multiplicative factor; the relative differences between signals are not affected by the power normalisation.

If the reference signal $x(t)$ is stationary, the power can be approximated with small error by evaluating it within an appropriate time interval (i.e. the time interval Δt). In the context of switching amplifiers, signals are usually stationary and their power is finite.

$$P_{x(t)} \approx \frac{1}{\Delta t} \int_{\Delta t} \frac{x^2(u)}{R_{\mathrm{L}}} \, \mathrm{d}u \tag{B.13}$$

B.6 Signal Representation in the Frequency Domain

A time-dependent signal $x(t)$, i.e. a real function, can be represented in the frequency domain $X(f)$ by computing its Fourier transform, defined as

$$X(f) := \mathcal{F}[x(t)] := \int_{-\infty}^{+\infty} x(t) e^{-j2\pi ft} \, \mathrm{d}t \tag{B.14}$$

where j is the complex variable.

The frequency-domain representation $X(f)$ of a real signal $x(t)$ is, in general, a complex function $X(f) \in \mathbb{C}$. Two dependent variables are therefore associated to the frequency-domain representation, the module $|X(f)|$, measured in the same units than the time-domain signal $x(t)$ per frequency unit (typically V/Hz, since it is a spectral power density), and the phase $\measuredangle X(f)$. The module is used to analyse the frequency distribution of the energy conveyed by a signal.

The spectral amplitude density $|X(f)|$ can be represented as spectral power density by squaring the magnitude $|X(f)|^2$ and applying the proper normalisation factor ${R_{\mathrm{L}}}^4$. The spectral power density is hence measured in power units per frequency (typically W/Hz).

The dynamic range of the spectral power density of common signals in switching amplifiers is wide. To prevent the high-power content masking the low-power content, the spectral power density is generally expressed in logarithmic scale (decibels). Because of the power normalisation, the spectral power density is all this work is expressed in relative units dB/Hz (note that, in logarithmic scale, the power normalisation involves a power shift). Anyway the spectral power density is only used to quantify relative values (e.g. differences between two normalised signals), not to quantify absolute values.

For the sake of readability, the term "Normalised Spectral Power Density (dB/Hz)" has been abbreviated as "Spec. Power Density (dB/Hz)" in all frequency-domain plots.

[4] In the literature of signal processing, the spectral power density of a finite-average power signal $x(t)$ is denoted by $S_x(f)$ and defined as the Fourier transform of the signal's autocorrelation $S_x(f) := \mathcal{F}[R_x(\tau)] = \mathcal{F}[x(\tau) * x(-\tau)] = |X(f)|^2$, where $*$ denotes the convolution integral, without normalisation factor. In this work, the term spectral power density refers to power per frequency unit, including the normalisation factor, so that power is obtained by directly integrating the spectral power density.

In the context of switching amplifiers, it is often convenient to split the spectral power density in bands, to separately analyse the inband and the outband contents. If the threshold between inband and outband is set by f_0, then "inband", denoted by an "i" superscript, refers to the frequency range below f_0, $|f| \leq f_0$, whereas "outband", denoted by an "o" superscript, refers to the frequency range beyond f_0, $|f| > f_0$.

$$P^{\mathrm{i}}_{x(t)} := \int_{-f_0}^{f_0} \frac{X^2(u)}{R_{\mathrm{L}}}\,\mathrm{d}u, \quad R_{\mathrm{L}} \in \mathbb{R}^+ \tag{B.15}$$

$$P^{\mathrm{o}}_{x(t)} := P_{x(t)} - P^{\mathrm{i}}_{x(t)} \tag{B.16}$$

Appendix C

Fourier Series of a Two-Level Switching Signal

This appendix derives the expression of the Fourier series decomposition of a generic two-level switching signal, as well as it discusses the frequency normalisation herein used and in chapter 3.

C.1 Frequency Normalisation

In signal processing, the Fourier series decomposition of a periodic signal is generally expressed according to the frequency of its slowest harmonic. Nevertheless, for the sake of notation simplicity, the Fourier series decomposition of periodic signals is expressed according to the frequency of their fastest harmonic in this work.

For instance, let us consider a T_{L}-periodic signal $x(t)$ consisting of N harmonics

$$x(t) = x(t + T_{\mathrm{L}}) \qquad \forall t \in \mathbb{R} \tag{C.1}$$

According to the common frequency normalisation, the harmonics' frequencies are kf_{L}, with $0 \leq k \leq N$, $k \in \mathbb{N}$ and $f_{\mathrm{L}} = 1/T_{\mathrm{L}}$. The signal is therefore expressed as

$$x(t) = \frac{a_0}{2} + \sum_{k=1}^{N} a_k \cos\left(\frac{2\pi kt}{T_{\mathrm{L}}}\right) + b_k \sin\left(\frac{2\pi kt}{T_{\mathrm{L}}}\right) \tag{C.2}$$

Using this frequency normalisation, the period is independent of the signal's complexity (i.e. the number of harmonics N), although its bandwidth does depend upon the signal's complexity N (DC to $Nf\mathrm{L}$).

In this work, the signal is expressed according to the frequency of the fastest harmonic (normalised to f_0), hence

$$f_0 = Nf_{\mathrm{L}} \tag{C.3}$$

The harmonics' frequencies become kf_0/N, using the same k. Consistently,

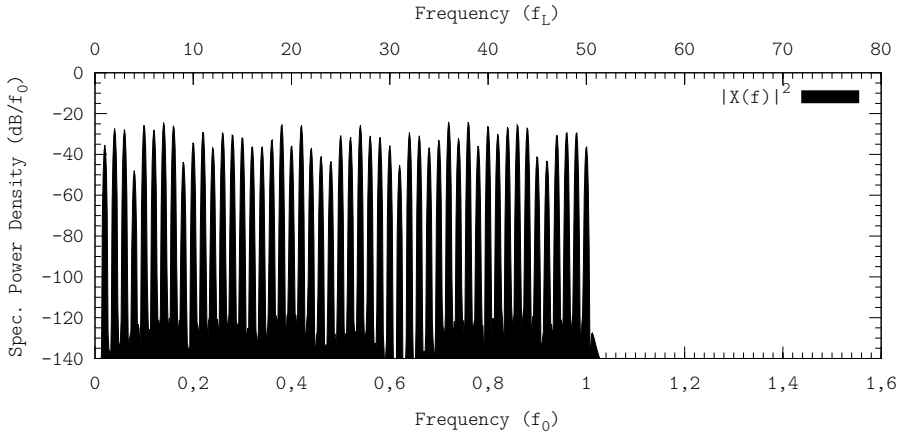

Figure C.1: 50-tone reference signal displayed with two different frequency normalisations: according to the frequency of the slowest harmonic f_{L} (common normalisation) and according to the frequency of the fastest harmonic f_0 (normalisation used in this work).

the signal can be expressed as

$$x(t) = \frac{a_0}{2} + \sum_{k=1}^{N} a_k \cos\left(\frac{2\pi kt}{NT_0}\right) + b_k \sin\left(\frac{2\pi kt}{NT_0}\right) \tag{C.4}$$

Signal's period becomes NT_0, with $T_0 = 1/f_0$, hence it depends upon the signal's complexity N.

$$x(t) = x(t + NT_0) \qquad \forall t \in \mathbb{R} \tag{C.5}$$

On the other hand, its bandwidth is f_0, independent of N. With the approach used in this work, based on bandlimited signals, it is more convenient dealing with f_0-bandlimited signals. Indeed, as N tends to infinite, the f_{L} normalisation leads to an infinite-band non-periodic signal, whereas the f_0 normalisation leads to a f_0-low-pass non-periodic signal (the distance between harmonics tends to zero). As a representative example, figure C.1 shows a 50-tone reference signal using both normalisations, f_{L} and f_0.

C.2 Fourier Series Derivation

A generic periodic two-level switching signal $z(t)$ is a continuous-time discrete-amplitude NT_0-periodic signal (with $N \in \mathbb{N}$ and $T_0 \in \mathbb{R}^+$) whose instantaneous value can only be either $Z_{\max}$ or $Z_{\min}$. Within one NT_0 period, the switching signal changes its value $2M$ times (with $M \in \mathbb{N}$), i.e. there are $2M$ switching events per NT_0 period (defined in this way, the OSwR of this signal is M/N).

Let us label, in order, the switching events using the normalised coefficients t_i, $i = 1, \ldots, 2M$, as Figure C.2 shows. The switching events therefore occur at the time instants NT_0t_i. For the sake of notation simplicity, let us define two

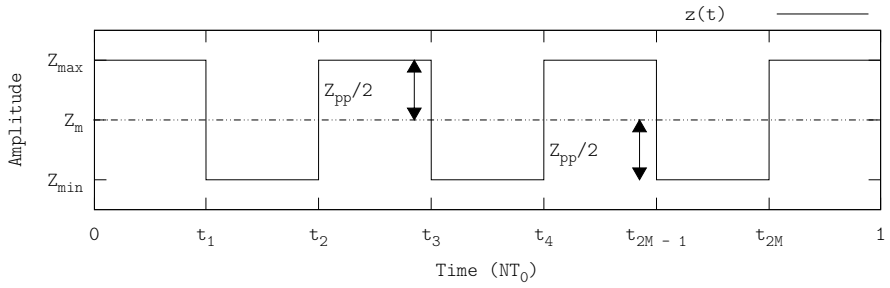

Figure C.2: Two-level switching signal with OSwR $= M/N$.

additional normalised time instants, the beginning t_0 and the end t_{2M+1} of the NT_0 time interval.

$$0 =: t_0 < t_1 < t_2 < \ldots < t_{2M} < t_{2M+1} := 1 \tag{C.6}$$

Using these normalised time instants, the two-level switching signal $z(t)$ can be expressed as

$$z(t) = Z_{\mathrm{m}} + (-1)^{s+1}\frac{Z_{\mathrm{pp}}}{2}\left(1 + \sum_{i=1}^{2M}(-1)^i \mathrm{u}(t - T_0 t_i)\right) \tag{C.7}$$

where $\mathrm{u}(t)$ denotes the Heaviside function, $0 < t_i < 1$ with $i = 1, \ldots, 2M$ and s is either 1 or 0 depending on the switching signal initial value (high or low respectively).

According to the Fourier Series decomposition, this switching signal can also be expressed as

$$z(t) = \frac{a_0^*}{2} + \sum_{k=1}^{+\infty} a_k^* \cos\left(\frac{2\pi k t}{NT_0}\right) + b_k^* \sin\left(\frac{2\pi k t}{NT_0}\right) \tag{C.8}$$

The a_0^* coefficient is given by

$$a_0^*(t_1, \ldots, t_{2M}) = \frac{2}{NT_0}\int_0^{NT_0} z(t)\,\mathrm{d}t \tag{C.9}$$

Since the switching signal can only be either $Z_{\max}$ or $Z_{\min}$, it is possible to simplify the integral into a compact expression by using the normalised times, the mean Z_{m} and the peak-to-peak Z_{pp} values, namely

$$a_0^*(t_1, \ldots, t_{2M}) = 2\sum_{i=0}^{2M}\left(Z_{\mathrm{m}} - (-1)^{s+i}\frac{Z_{\mathrm{pp}}}{2}\right)(t_{i+1} - t_i) \tag{C.10}$$

where s is either 1 or 0 depending on the switching signal initial value (high or low respectively). This expression can be rewritten with only one summation

$$a_0^*(t_1, \ldots, t_{2M}) = 2Z_{\mathrm{m}} - (-1)^s Z_{\mathrm{pp}}\left(1 - 2\sum_{i=1}^{2M}(-1)^i t_i\right) \tag{C.11}$$

This expression, as expected, does not depend upon the switching signal's period NT_0, since this coefficient expresses the DC component.

The other a_k^* coefficients are given by

$$a_k^*(t_1,\ldots,t_{2M}) = \frac{2}{NT_0}\int_0^{NT_0} z(t)\cos\left(\frac{\omega_0 kt}{N}\right)\mathrm{d}t =$$

$$= \frac{2}{NT_0}\sum_{i=0}^{2M}\left(Z_\mathrm{m} - (-1)^{s+i}\frac{Z_\mathrm{pp}}{2}\right)\int_{t_i NT_0}^{t_{i+1}NT_0}\cos\left(\frac{\omega_0 kt}{N}\right)\mathrm{d}t \tag{C.12}$$

This expression can be written as

$$a_k^*(t_1,\ldots,t_{2M}) = (-1)^s\frac{Z_\mathrm{pp}}{k\pi}\sum_{i=1}^{2M}(-1)^i\sin(2k\pi t_i) \tag{C.13}$$

Similarly, the analysis for the b_k^* yields

$$b_k^*(t_1,\ldots,t_{2M}) = \frac{2}{NT_0}\int_0^{NT_0} z(t)\sin\left(\frac{\omega_0 kt}{N}\right)\mathrm{d}t =$$

$$= (-1)^{s+1}\frac{Z_\mathrm{pp}}{k\pi}\sum_{i=1}^{2M}(-1)^i\cos(2k\pi t_i) \tag{C.14}$$

Note that the value of all Fourier coefficients, including a_k^* and b_k^*, only depend upon the normalised coefficients t_i, with $i = 1,\ldots,2M$. The levels Z_m and Z_pp are set by the application and are not design parameters; similarly the harmonics frequency is set by NT_0, the switching signal's period.

Therefore, in a two-level switching signal $z(t)$ comprising $2M$ switching events within one period (NT_0), there are $2M$ variables or degrees of freedom to set the value of all Fourier coefficients. Each pair of additional switching events add two additional variables or degrees of freedom. Note that, despite the Fourier coefficients only depend upon $2M$ variables, the Fourier series of the switching signal $z(t)$ has infinite harmonics (C.8).

C.2.1 Odd Number of Time Edges

The number of switching events within a NT_0 period has been constrained to be even, otherwise the switching signal would not be NT_0-periodic. Certainly, with an odd number $2M-1$ of switching events within NT_0

$$t(kNT_0^+) \neq t(kNT_0^-) \qquad \forall k, k \in \mathbb{Z} \tag{C.15}$$

At time instants kNT_0, the Fourier series of the switching signal $z(t)$ based on NT_0 harmonics would converge to Z_m (the half-sum of the left- and right-limit of $z(t)$ at $t = kNT_0$); effectively, this is equivalent to adding a switching event (i.e. $2M$ switching events within NT_0). Note that this case is also considered in the general case depicted in Figure C.2, since t_1 can tend to 0 or t_{2M} can tend to 1.

Appendix D

Numerical Simulations

This appendix briefly describes the hardware and the programs used to compute the simulations presented in this work, as well as it provides specific information about the parameters used in each simulation (simulated data, points per cycle, etc.).

D.1 Hardware

All simulations have run on a desktop computer, powered by an AMD Athlon™ 64 X2 Dual Core Processor 6000+ (maximum clock frequency of 2 GHz). The computer has 4 GB of memory (RAM), specifically four DIMMs of 1 024 kB DDR2 at 800 MHz, plus 40 GB of swap partition. The swap partition has a dedicated hard-drive and bus, so that it is possible to write the swap partition and the main hard-drive at the same time.

Using this hardware, each individual simulation (including time-domain processing and power spectrum computation) needs CPU time in the region of minutes.

D.2 Simulation Software

The simulations shown in this work have been computed using custom C programs, *Maxima* version 5.22.1 and *GNU Octave* version 3.2.4. The C programs have bee compiled with the *GNU Compiler Collection* (GCC) version 4.4.5 and linked against the *GNU C Library* version 2.12.1 and the *GNU Scientific Library* (GSL) version 1.14. The Fourier transforms have been computed using the *Fastest Fourier transform in the West* (FFTW) library, version 3.2.2.

All these programs, including the non-custom ones, have been optimised for the specific architecture by compiling them with the options `-march=native -O2`. The `native` option selects the 64-bit architecture `k8-sse3`, which enables the SSE3 instruction set support.

Both *Maxima* and *GNU Octave* have been used to perform beforehand calculations (e.g. computing the coefficients of a Butterworth filter); the simulations themselves have been computed by the custom C programs. This custom environment has been chosen to get the most of the available computation hardware and to have full control of all simulation parameters, to guarantee that simulation errors are not significant.

D.2.1 Precision and Simulation Accuracy

All programs used in this work employ double precision variables: *double* (64 bits) or *complex* (2×64 bits)[1]. In double precision variables, the total precision is 53 bits, approximately 16 decimal digits $\log_{10} 2^{53} \approx 15{,}95$. This quantisation error results in a noise level of $-300\,\mathrm{dB}$ in Fourier transforms (with respect to the maximum displayed); furthermore, the precision in time simulations is also limited (e.g. 1 s of simulated data can be represented with a precision up to 10 fs).

In most simulations, the quantisation error due to double precision variables is not significant, as the simulation accuracy is generally limited by other parameters such as the sampling frequency N_{PPC} or the window function's dynamic range. Note that with single precision variables (*float*, 32 bits, total precision of 24 bits) the dynamic range in Fourier transforms is limited to about $-140\,\mathrm{dB}$, therefore the quantisation error noise would partially mask the power spectra shown in some figures (e.g. figures 1.5 and 1.6).

Since most simulations involve switching systems, variable step size has been used in time-domain simulations. When a switching event is detected at a certain time instant, the last simulated point is discarded and the step size is reduced. This process is repeated until the step size cannot be further reduced (minimum step size); the system then switches and the step size is increased to the maximum. In this way, all switching events are simulated using the minimum step size (high precision in all switching events).

Analogue Signals and Discrete Sequences

All simulations have been performed in the discrete domain, using discrete sequences $x[n]$. The values of a sequence $x[n]$ are sampled values of a continuous-time signal $x(t)$, i.e. $x[n] = x(t_i)$.

When reducing the step size, interpolations between samples may be performed. Because of computation time, these interpolations are linear. The sampling frequency N_{PPC} (i.e. the number of points per cycle) must be adjusted so that the error due to the linear interpolation is not significant, generally well beyond Nyquist's sampling criterion.

For instance, let $x[n+1] = x(t_{n+1})$, $x[n] = x(t_n)$; if the sampling frequency is high enough

$$x(t_i) \approx \frac{x[n+1] - x[n]}{t_{n+1} - t_n} (t_i - t_n) + x[n], \quad t_n < t_i < t_{n+1} \tag{D.1}$$

Despite discrete sequences have been simulated, in all this work (including this appendix), the simulated data is referred as continuous signals $x(t)$, unless otherwise stated to emphasise the difference.

D.2.2 Generation of Bandlimited Flat-Spectrum Signals

The process of generating a f_0-bandlimited signal consists in filtering an impulse train with an ideal low-pass filter (often referred as "brickwall" in the literature).

[1] The *complex* variable type defines an array of two *double* variables to store the real and the imaginary part of a complex number. The precision of *complex* variables is therefore the same than *double*'s.

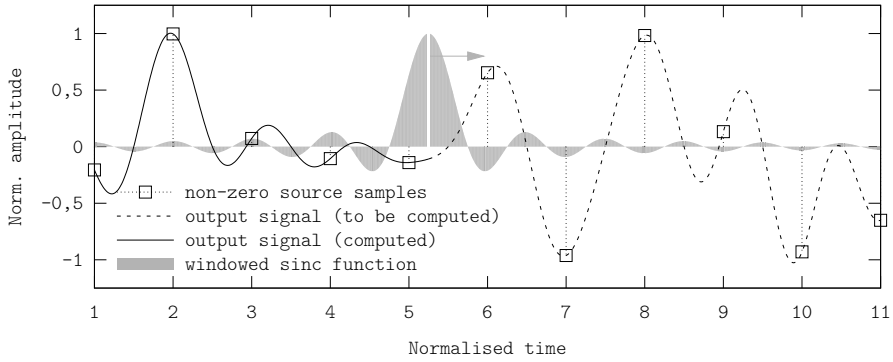

Figure D.1: Generating a bandlimited flat-spectrum signal. In this example, the signal has been generated up to 5,25 (normalised time).

In the time domain, this process can be performed by convolutioning the impulse train with the impulse response of an ideal low-pass filter $h_{\mathrm{iLPF}}(t)$ (see figure D.1)

$$h_{\mathrm{iLPF}}(t) = \frac{\sin\left(\dfrac{\pi t}{T_{\mathrm{w}}}\right)}{\dfrac{\pi t}{T_{\mathrm{w}}}} =: \operatorname{sinc}\left(\frac{t}{T_{\mathrm{w}}}\right), \quad \forall t \in \mathbb{R} \tag{D.2}$$

where $f_{\mathrm{w}} = 1/T_{\mathrm{w}}$ is the filter's cutoff frequency (T_{w} also expresses half the width of the sinc function). Note that this impulse response is infinite.

When generating a f_0-bandlimited signal $x[n]$ with a simulation program (discrete time), a finite impulse response filter $h_1[n]$ must be convoluted with an impulse train $s[n]$. Let N_{PPC} be the number of points per T_0 cycle, i.e. the sampling frequency.

The finite impulse response window $h_1[n]$ can be generated by simply windowing the ideal filter's impulse response (infinite sinc) with a window function $h_{\mathrm{w}}[n]$. Therefore

$$h_1[n] = \begin{cases} \operatorname{sinc}\left[\dfrac{1}{T_0}\left(n - \dfrac{A}{2}\right)\right] h_{\mathrm{w}}[n, A], & n \in [0, A] \\ 0, & n \notin [0, A] \end{cases} \tag{D.3}$$

where the parameter A expresses the window function's length and $n \in \mathbb{Z}$.

In the custom C programs, the sinc function has been windowed with the Nuttall's 4-Term with Continuous First Derivative window function [84], yielding a finite impulse response window $h_1[n]$ comprising $M = 250$ sinc lobes per side. The width of the sinc function (measured, in samples, as the distance between the two nulls of the main lobe) is $A = N_{\mathrm{PPC}}M + 1$.

The (finite) impulse train $s[n]$ can be generated by padding with zeros a set of random values r_i, where $i = 0, \ldots, N-1$, $i \in \mathbb{N}$. The total length of $s[n]$, including the padding zeros, determines the final length of the signal generated $x[n]$.

In the custom C programs, the random values r_i have been computed using the `random` function, which uses a nonlinear additive feedback random number generator to return successive pseudo-random numbers in the range from 0

to `RAND_MAX` (2 147 483 647). The period of this random number generator is approximately $16(2^{31} - 1)$.

In the impulse train $s[n]$, each value r_i has been padded with $N_{\mathrm{PPC}}L$ zeros, with $L = 2$ (i.e. two sinc lobes fit within two non-zero samples of the impulse train $s[n]$).

The distribution of the random values r_i determines the distribution of the bandlimited signal (e.g. r_i values generated with a uniform probability distribution yield a bandlimited flat-spectrum signal). The parameter L modifies the generated signal's parameters, such as peak-to-average or RMS. Note that L does not need to be an integer.

Generation of Other Signals

Besides bandlimited flat-spectrum signals, other signals have also been generated and used in this work. Some signals are simple to generate, such as constant signals, single tones or multi-tone signals.

The signals generated by multibit modulations (such as QPSK or 8-PSK) can also be easily generated with C programs as well, since the IQ scheme (see figure 1.3) involve no special operations but convolution (to apply pulse-shaping), which is not challenging to implement either. The afterwards processing to split the signals into envelope and phase is simple as well.

D.3 Computation of Power Spectra

The results obtained with time-domain simulations are often analysed in the frequency domain. During the time-frequency transformation (Fourier transform), some information conveyed by the time-domain signals may be lost or may appear masked in the frequency-domain signals. It is therefore necessary to properly set the computation parameters of Fourier transforms, to preserve the time-domain information.

D.3.1 Window Function

In all Fourier transforms, the time-domain signals have been windowed using the Nuttall's 4-Term with Continuous First Derivative window [84]. This window function has the highest dynamic range (the sidelobe peak is about $-93{,}28\,\mathrm{dB}$ and asymptotic decay is $20\,\mathrm{dB/dec}$), although the frequency resolution is low (wide main lobe). The resolution issue can be addressed by transforming more data, which, in off-line simulations like these ones, is only limited by hardware capacity and simulation time. Note that the dynamic range cannot be addressed otherwise.

More than 90 dB of dynamic range is generally enough to display the Fourier transforms; the sidelobes are either not visible because they are masked by the signal itself (as in figure 1.21) or because their amplitude is much lower than that of the signal (as in figure 2.7). Nevertheless, the accuracy of Fourier transforms is also constrained by the sampling frequency, especially in switching signals.

D.3.2 Fourier Transforms of Switching Signals

The Fast Fourier Transform (FFT) algorithm can only be applied to transform signals sampled at constant frequency, hence all time-domain signals must be resampled at a constant frequency $f_1 = 1/T_1$ before being transformed. As a result, regardless of the high accuracy achieved in time-domain simulations by variable step size, the accuracy achieved in the frequency domain is finally limited by f_1.

This issue is especially visible when transforming switching signals, since time edges convey a significant amount of information. Indeed the accuracy degradation due to the resampling process is twofold: the edges are smoothed and they are shifted with a variable delay (see figure D.2). This latter effect can be modeled as jitter in the time domain, which results in noise in the frequency domain. The actual effect is rounding.

The resampling issue and its consequences in the frequency domain are illustrated in figure D.2. This figure shows the waveforms resulting of encoding a constant signal (normalised amplitude 0,8) with a triangle PWM operating at $f_\mathrm{s} \approx 10{,}02$ (normalised frequency) and subsequently filtering it with a second-order Butterworth filter (normalised cutoff frequency 1). Ideally, the discrete-amplitude signal should be a two-level signal (with constant switching frequency f_s and constant duty cycle) and its power spectrum should only contain harmonics at frequencies kf_s, $k \in \mathbb{N}$.

The time-domain simulation comprises 10^3 cycles (normalised time), the sampling frequency is 10^3 (samples per cycle) and the step size can be reduced five orders of magnitude. The power spectra have been computed resampling at 10^3 points per cycle. Since the sampling frequency is not a multiple of the switching frequency, neither the frequency nor the duty cycle of the switching signal $z(t)$ are constant (there may be a deviation of one sample). This jitter results in a noise level whose peaks are only 28 dB below the main harmonic of the PWM signal.

On the other hand, the filtering process in time domain does take advantage of the variable step size, thus the recovered signal $\tilde{x}(t)$ preserves the high accuracy. Since the recovered signal $\tilde{x}(t)$ is continuous, the error due to resampling is much lower (see middle plot of figure D.2). The noise level is set by the variable step size (in this simulation it is about five orders of magnitude lower), yielding a noise level whose power is approximately $20\log_{10}(10^{-5}) = -100\,\mathrm{dB}$ lower than before (compare the amplitudes of the peaks at normalised frequency 2,1 in figure D.2).

Note that the noise level is independent of the simulated circuit, i.e. it is not affected or attenuated by the filtering process. Therefore in figure D.2, the high-frequency harmonics of the recovered signal $\tilde{x}(t)$ are attenuated because of filtering (the attenuation obeys the 40 dB/dec decay of a second-order filter), whereas the noise level is reduced because of the higher accuracy.

Even though the jitter could be avoided by simply using a sampling frequency multiple of the switching frequency, when simulating non-periodic signals the switching signal would not be periodic. The noise level would appear whatsoever.

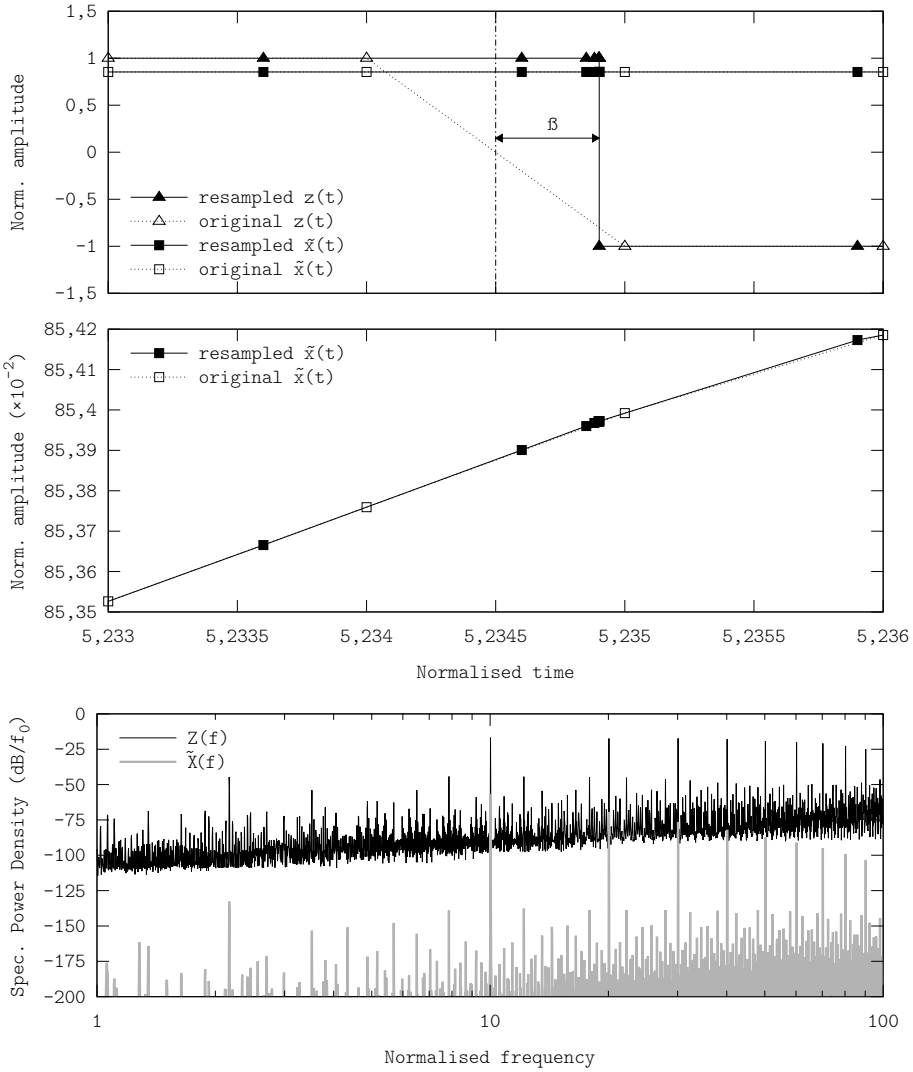

Figure D.2: Effects of constant-frequency resampling in the computation of Fourier transforms. The upper plot shows the time-domain waveforms, the middle plot shows a detail of the recovered signals $\tilde{x}(t)$ and the lower plot shows the power spectra. The simulation parameters are described in the text. ß shows the jitter error due to resampling.

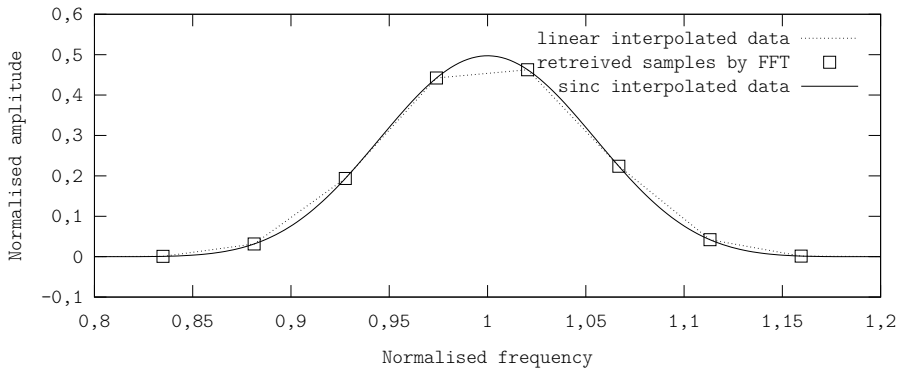

Figure D.3: Sinc interpolation. Example showing the Fourier transform of a single tone of normalised frequency 1 and normalised amplitude 1.

D.3.3 Sinc Interpolation and Decimation

The Discrete Fourier Transform (DFT), including the FFT variant, of a time signal $x[n]$ retrieves data sampled at constant frequency $X[k]$. Let (the complex function of continuous variable ω) $X\left(\mathrm{e}^{j\omega}\right)$ be the Fourier transform of the signal $x[n]$. If $x[n] = 0$ for $n < 0$ and for $n > N-1$ (i.e. $x[n]$ is windowed) then

$$X[k] := \sum_{n=0}^{N-1} x[n]\mathrm{e}^{-j\frac{2\pi}{N}kn} = X\left(\mathrm{e}^{j\omega}\right)\Big|_{\omega\,=\,\frac{2\pi}{N}k}, \quad k = 0, \ldots, N-1 \tag{D.4}$$

If transforming a sufficiently large amount of data (N big), $X(e^{j\omega})$ can be approximated with small error by linearly interpolating the samples of $X[k]$. Nonetheless, in some cases it is necessary to interpolate with more precision, e.g. when evaluating the amplitude at a specific frequency (see figure D.3) or when displaying very low frequency components (as in figure 1.22).

Ideal interpolation can be achieved with sinc interpolation, similarly as the as in the generation of a f_0-bandlimited signal (also with an infinite-bandwidth impulse response). The sinc interpolation performed in this simulation programs has been approximated by convolutioning the transformed data $X[h]$ with a windowed sinc function h_2

$$h_2[n] = \mathrm{sinc}\left[\frac{n}{T_\mathrm{w}}\right] \cos\left[B\frac{\pi n}{T_\mathrm{w}}\left(1 - \left(\frac{2Bn}{T_\mathrm{w}}\right)^2\right)\right] \tag{D.5}$$

where T_w is $2\pi/N$ and $B = 0{,}22$. The windowed function $h_2[n]$ comprise 240 zero-crossings (lobes) per side.

Whilst this interpolation is still not perfect, the interpolation error is significantly reduced. In the example of figure D.3, the Fourier transform of a single tone of normalised frequency 1 and normalised amplitude 1, the sinc-interpolated peak is 0,497 (amplitude error of $2{,}77 \cdot 10^{-3}$, lower than 0,6 %) whereas the linear-interpolated peak is 0,453 (amplitude error of $47 \cdot 10^{-3}$, higher than 9 %). The theoretical analogue value is 0,5.

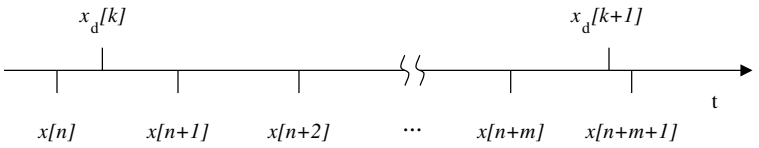

Figure D.4: Peak decimation. $x[n]$ stands for the source samples and $x_{\mathrm{d}}[n]$ stands for the peak-decimated data. The decimation factor does not need to be an integer (as this example shows).

D.3.4 Peak Decimation

All Fourier transforms have been computed using millions of points, to achieve high spectral resolution and to ensure that simulation errors are not significant. However, when displaying the Fourier transforms, not all simulated data points should be included in the plots, since this would significantly increase the file size of this document and, more important, rendering each figure would require high computational effort, which is very uncomfortable. Furthermore, there is no clear benefit in including figures with more data points than a regular computer screen or printer are able to display.

Because of these reasons all power spectra have been decimated. Fourier transforms often have peaks at high frequency (as in figure 2.7); to avoid loosing this information in the decimation process, a peak-detection algorithm has been used.

According to this algorithm, the value of a decimated sample $x_{\mathrm{d}}[k]$ is the maximum value of the source samples $x[n]$ comprised from the previous decimated sample $x_{\mathrm{d}}[k-1]$ to the decimated sample itself $x_{\mathrm{d}}[k]$. Referring to figure D.4, the decimated sample $x_{\mathrm{d}}[k+1]$ is obtained as

$$x_{\mathrm{d}}[k+1] = \max\left(x[n+1], x[n+2], \ldots, x[n+m]\right) \tag{D.6}$$

The data retrieved by DFTs is sampled at constant frequency (regularly separated samples). Nevertheless, the decimation process can be either linear (constant decimation factor) or logarithmic (variable decimation factor), depending on the plot scale. Figure D.5 shows an example of logarithmic peak decimation, corresponding to the power spectrum shown in figure 1.21.

D.3.5 Approximating an Ideal Low-Pass Filter

The Fourier transform $X[k]$ of a certain sequence $x[n]$, being $x[n] = 0$ if $n < 0$ or $n > N-1$, can be inverted through the Inverse Discrete Fourier Transform (DFT$^-$1), defined as

$$\tilde{x}[n] := \frac{1}{N} \sum_{k=0}^{N-1} X[k] e^{-j\frac{2\pi}{N}kn}, \quad n = 0, \ldots, N-1 \tag{D.7}$$

The retrieved samples $\tilde{x}[n]$ fulfil

$$\tilde{x}[n] = \sum_{r=-\infty}^{\infty} x[n + rN] \tag{D.8}$$

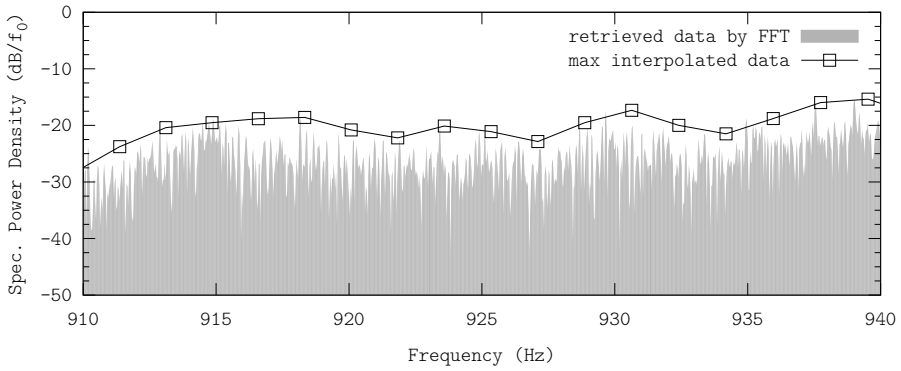

Figure D.5: Example of peak decimation. The interpolated data correspond to the industrial metal power spectrum shown in figure 1.21. The FFT raw data has a frequency resolution of 30,3 mHz, and the peak interpolation yields an approximated frequency resolution of 2 Hz at these frequencies (1 211 points per decade).

hence $\tilde{x}[n] = x[n]$ for $n = 0, \ldots, N-1$.

Therefore, the sequence $x[n]$ can be transformed to the frequency domain $X[n]$, operated in that domain $\tilde{X}[n]$ and transformed back to the time domain $\tilde{x}[n]$. In particular, it is possible to apply an ideal filter in the frequency domain by properly modifying the samples $X[n]$

$$\tilde{X}[n] = X[n]H[n] \tag{D.9}$$

where $H[n]$ is the discrete transfer function of the desired ideal filter.

Nevertheless, due to the windowing effect of DFT, applying an ideal filter in the frequency domain is not straightforward. For instance, let the sequence $x[n]$ be a f_0-bandlimited signal, generated as described in section D.2.2. Its DFT is a sequence $X[k]$ whose outband samples are not 0 (their value depend upon the window function used, but they are not zero, see figure D.6).

Similarly, the frequency-domain operation of an ideal filter does not set the rejected samples to 0 (i.e. the samples of the sequence $X[k]$ belonging to the filter's stopband); instead it sets them to a (very low) value according to the window function.

The operation of an ideal filter can be approximated in the frequency domain by setting the rejected samples to 0. Around the bandpass-stopband and stopband-bandpass transitions the error will be high, although the power of this error and its frequency range depend upon the simulation parameters (window function, sampling frequency and simulated time). Ideal filters can also be approximated in the time domain, by convolutioning the sequence $x[n]$ with a windowed impulse response. However, the frequency-domain operation provides more flexibility to implement band-pass and band-stop filters.

Figure D.6 shows the error due to the approximation of an ideal f_0-low-pass filter in the frequency domain (the x axes have been scaled to time and frequency, for better readability). The sequence $x[n]$, a f_0-bandlimited signal, is filtered with an (approximately) ideal f_0-low-pass filter. Ideally, the sequence $x[n]$ should not be altered by this filter but, because of the approximation, the retrieved sequence $\tilde{x}[n]$ has some error $\xi[n]$.

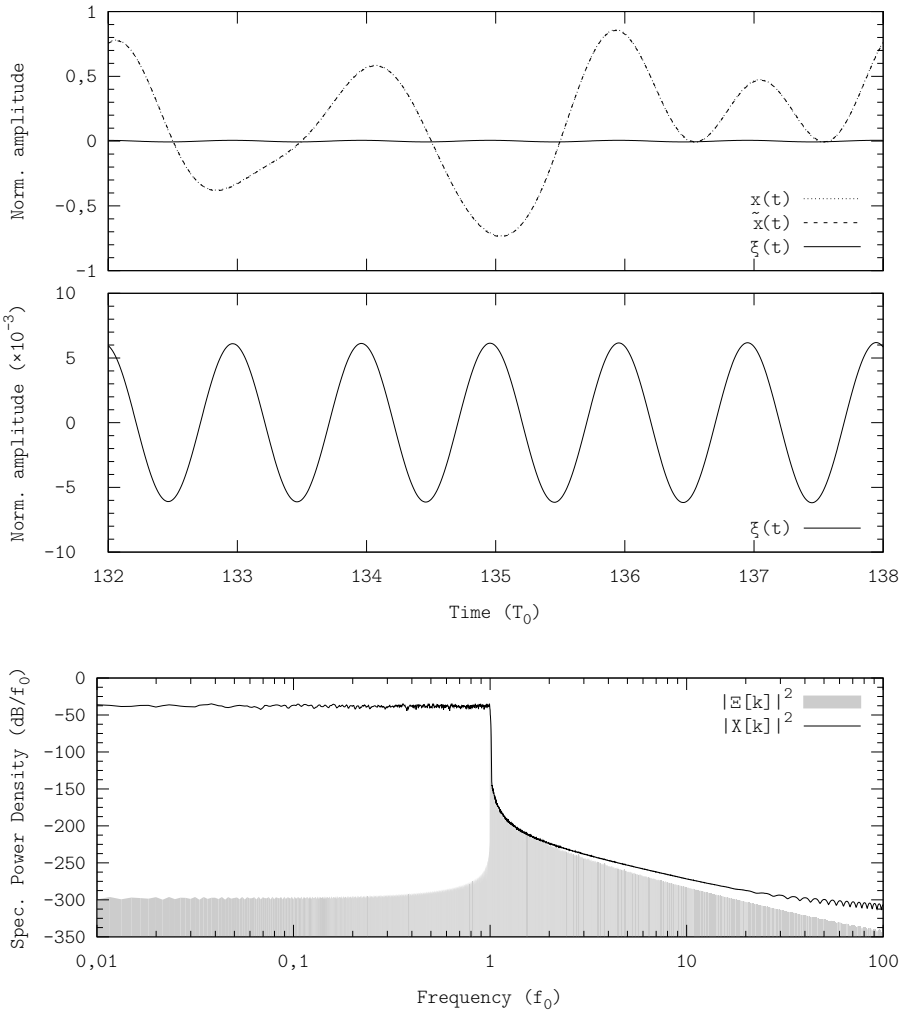

Figure D.6: Approximating an ideal f_0-low-pass filter. A f_0-bandlimited signal is filtered with an ideal f_0-low-pass filter. The filtered signal is defined as $\tilde{x}(t) := x(t) + \xi(t)$, where $\xi(t)$ is the error signal due to the frequency-domain approximation.

The power spectrum shows an error peak around the filter's cutoff frequency f_0; consistently, the time-domain waveform of the error signal $\xi[n]$ shows a sine-like waveform, whose frequency is f_0 and whose normalised amplitude is $6 \cdot 10^{-3}$. Quantifying, the ratio of the inband error power $P^{\mathrm{i}}_{\xi[n]}$ to the reference sequence power $P_{x[n]}$ is $-47\,\mathrm{dB}$ (lower than 21 ppm) and the ratio of the error power $P_{\xi[n]}$ to the reference sequence power $P_{x[n]}$ is $-37\,\mathrm{dB}$ (lower than 0,2 ‰).

D.4 Simulation Parameters

This section summarises the different configurations used to perform all simulations. The simulation parameters of each configuration are summarised in table D.1 and a brief summary of hardware usage is included in table D.2.

In all configurations, the time-domain simulations use variable step size. The minimum step size is adjusted for each configuration, so that the 53 bits of precision are used. When computing the Fourier transforms, the time-domain signals have been resampled. All signals have been resampled at the sampling frequency N_{PPC} (the value *Points per* T_0 *cycle* shown in table D.1) but switching signals (not necessarily discrete-amplitude ones, such as the error signal $e(t)$), which have been resampled at higher frequency (the value between brackets in the column *Points per* T_0 *cycle* in table D.1).

D.4.1 Averaged Power Spectra

This configuration is intended for noise minimisation when displaying power spectra with high frequency-resolution. Even in (locally) flat-spectrum signals, the data retrieved by the Fourier transform may not be constant (flat), as the number of input samples is finite. Similarly, each realisation (i.e. simulation) results in a different amplitude at each frequency sample.

Therefore, it is feasible to reduce the noise in the Fourier transforms by averaging several different realisations (it requires stationary reference signals). The averaged power spectrum is subsequently interpolated and decimated to reduce the amount of data to be stored and displayed. In this configuration, ten different realisations have been averaged.

Figure D.7 illustrates the averaging effects; it shows the power spectra of a f_0-bandlimited reference signal computed using a single realisation and averaging ten different realisation. The noise in the frequency domain reduces from more than 20 dB in the single realisation to 5 dB in the averaged realisations. The averaged spectrum tracks the upper content of the single-realisation spectrum because of the peak decimation.

The signals have been resampled 10^5 points per T_0 cycle before transforming, to reduce the noise level in the transformed signal. This is especially important when transforming switching signals, not necessarily discrete-amplitudes ones, as discussed in section D.3.2.

D.4.2 Power Spectra of Audio Signals

The computation of power spectra of audio signals is determined by the audio samples (external data files). The available audio samples are encoded using the CD-DA standard (see section 1.4.1), thus the sampling frequency has been

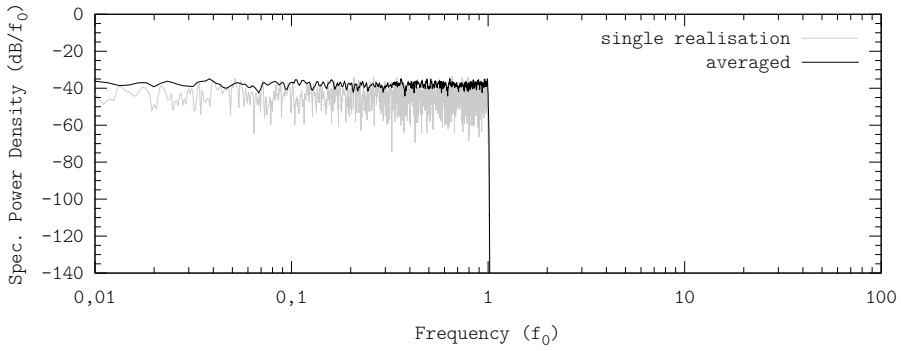

Figure D.7: Power spectrum averaging example. Displayed waveforms show the power spectrum of a f_0-bandlimited signal: a single realisation (grey) and 10 averaged realisations (D.4.1 configuration, black).

Configuration	*Simulated time (T_0)*	*Points per T_0 cycle*	*Decimation*
averaged	600	10^4 (10^5)	sinc, peak (1 211)
audio signals	variable	44 100	peak (1 211)
high accuracy	600	$2 \cdot 10^5$	no
inband error	600	10^4 (10^5)	no
parameters sweep	1 000	1 000	no

Table D.1: Summary of simulation parameters. In the *Points per T_0 cycle*, the value between brackets expresses the resampling frequency when computing the DFT of discrete-amplitude signals; in the *Decimation* column, the number between brackets expresses the decimation in output samples per decade.

set to 44 100 points per T_0 cycle. The whole audio sample has been transformed (the number of transformed T_0 cycles is set by the audio sample); the power spectrum is subsequently decimated using the peak algorithm.

D.4.3 High-Accuracy Power Spectra

This configuration is intended to display the power spectrum of switching signals with very high accuracy. Each simulation has been computed using $1{,}2 \cdot 10^8$ points (600 T_0 cycles, with $2 \cdot 10^5$ points per T_0 cycle), with variable step size (the minimum step size is approximately $10^{-12} T_0$).

The high sampling frequency ensures that constant-frequency resampling errors (jitter-kind) do not compromise the actual plot. This configuration is mostly used in chapter 3, to illustrate inband-error-free encoding (e.g. in figure 3.4). The inband content is not 0 ($-\infty$ dB) because of errors due to constant-frequency resampling; nevertheless the accuracy is high enough to illustrate inband-error-free encoding.

Configuration	*Real time*	*Maximum virtual memory (MB)*
averaged	2 min 56,467 s	2 781
audio signals	8,327 s	121
high accuracy	5 min 42,691 s	2 853

Table D.2: Summary of hardware usage in the computation Fourier transforms (data corresponding to a single realisation); the computer was performing no other operations but computing the Fourier transforms (the computer was idle). *Real time* shows the elapsed real time between the invocation and the termination of the program and *Maximum virtual memory* shows the maximum total amount of memory used by the program (it includes all code, data and shared libraries plus pages that have been swapped out).

D.4.4 Inband Error Characterisation

This configuration is intended to split the power of switching signals (not necessarily discrete-amplitude ones) into inband and outband. Simulation parameters are the same than in D.4.1 (averaged configuration), to keep the error due to constant-frequency resampling low (see section D.3.2). Since these power spectra are not to be displayed, no decimation is applied.

D.4.5 Histograms and Percentile of Pulses' Width

This configuration is intended to evaluate the histograms and percentile of pulses' width. Each simulation has been computed using 10^4 points per T_0 cycle, and $2 \cdot 10^3$ T_0 cycles have been simulated. Since no Fourier transform needs to be performed, this configuration takes advantage of the variable step size (the minimum step size is $10^{-10}T_0$).

D.4.6 Recovered Signal Characterisation

This configuration is intended to quantify the power of the remaining error signal. The computation of the recovered signal $\tilde{x}(t)$ takes advantage of variable step size; the simulation accuracy of the recovered signal $\tilde{x}(t)$ is therefore determined by the minimum step size.

The time delay due to the filter must be equalised to compute the remaining error signal $\xi(t)$; this equalisation is performed in the time domain, by cross-correlating the reference signal $x(t)$ and the recovered signal $\tilde{x}(t)$ until the RMS value (i.e. power) of the resulting remaining error signal $\xi(t)$ is minimised. In order to guarantee high accuracy in the cross-correlation process, 10^4 points per T_0 cycle are used in this configuration (600 T_0 cycles are simulated in this configuration).

Appendix E

Thesis' General Information

This appendix provides general information about this document and the list of thesis-derived publications and patents. The list of other author's publications, not directly related to this thesis, is also included at the end of this appendix.

E.1 About This Document

This document is the full report of Albert Garcia i Tormo's PhD thesis to apply for the degree of Doctor in Electronic Engineering. This research has been carried out during approximately four years and five months, from October 2006 to March 2011, with the support of a FI grant from AGAUR, the Department of Innovation, Universities and Companies of the Catalan Government (Generalitat de Catalunya). This work has included a four-months research internship, from July 2009 to October 2009, at the company NXP Semiconductors (High Tech Campus Eindhoven, The Netherlands), with the support of a BE grant from AGAUR, the Department of Innovation, Universities and Companies of the Catalan Government (Generalitat de Catalunya).

This document is going to be available online at TDX (Tesis Doctorals en Xarxa), http://www.tesisenxarxa.net/, under the Creative Commons license Attribution-NonCommercial-NoDerivs (at the time of writing this document, version 2.5 Spain, CC BY-NC-ND 2.5).

E.2 Thesis-Derived Publications

The publications derived from this thesis are listed next. They have been sorted according to the kind of publication; amongst the same kind of publications, they have been chronologically sorted.

E.2.1 Publications in Scientific Conferences

- A. Garcia i Tormo, E. Alarcón, A. Poveda, and F. Guinjoan, "Low-OSR Asynchronous Σ-Δ Modulation High-Order Buck Converter for Efficient Wideband Switching Amplification", in *Proc. IEEE International Symposium on Circuits and Systems ISCAS 2008*, May 18–21, 2008, pp. 2198—2201. Seattle, WA, United States of America. Poster.

- A. Garcia i Tormo, A. Poveda, E. Alarcón, and F. Guinjoan, "Design-Oriented Characterisation of Adaptive Asynchronous ΣΔ Modulation Switching Power Amplifiers for Bandlimited Signals", in *Proc. IEEE International Symposium on Circuits and Systems ISCAS 2009*, May 24–27, 2009, pp. 2882–2885. Taipei, Taiwan. Oral presentation.

- A. Garcia i Tormo, A. Poveda, E. Alarcón, H. J. Bergveld, B. Buter, and R. Karadi, "An Enhanced Switching Policy for Buck-Derived Multi-Level Switching Power Amplifiers", in *Proc. IEEE Int. Symp. Circuits and Systems ISCAS 2010*, may 2010, pp. 3196–3199. Paris, France. Oral presentation.

- A. Garcia i Tormo, A. Poveda, E. Alarcón, F. Guinjoan. "Multi-Level Asynchronous ΣΔ Modulators for Wideband Switching Power Amplifiers", in *Proc. IEEE Control and Modeling for Power Electronics COMPEL 2010*, june 2010. Boulder, CO, United States of America. Poster.

- A. Garcia i Tormo, A. Poveda, E. Alarcón, and F. Guinjoan, "A Grounded-Output 5-Switch Bipolar Buck-Boost Converter Topology for Switching Power Amplifiers", in *Proc. IEEE International Symposium on Circuits and Systems ISCAS 2011*, May 15–18, 2011, Rio de Janerio, Brazil. Poster.

- E. Alarcón, D. Fernández, A. Garcia i Tormo, A. Poveda and J. Madrenas, "Continuous-time CMOS adaptive asynchronous sigma-delta modulator approximating low-fs low-inband-error on-chip wideband power amplifier", in *Proc. IEEE International Symposium on Circuits and Systems ISCAS 2011*, May 15–18, 2011, Rio de Janerio, Brazil. Special session.

E.2.2 Publications in Journals

- A. Garcia i Tormo, A. Poveda, E. Alarcón, F. Guinjoan. "Fundamental Modulation Limits for Minimum Switching Frequency Inband-Error-Free High-Efficiency Power Amplifiers", in *Transactions on Circuits and Systems I.* (accepted February 5, 2011).

E.2.3 Publications in Books

- H.Casier, M. Steyaert, A. H. M. Van Roermund. Analog Circuit Design: High-speed clock and data recovery, High-performance amplifiers, power management. Chapter "Wideband efficient amplifiers for on-chip adaptive power management applications". Chapter's authors L. Marco, V. Yousefzadeh, A. Garcia i Tormo, A. Poveda, D. Maksimović, E. Alarcón. Springer 2009.

E.2.4 Patents

- A. Garcia i Tormo, A. Poveda, E. Alarcón, H. J. Bergveld, B. Buter, R. Karadi. "Multi-level switching power converter". Filed October 9, 2009 by NXP Semiconductors. Europe region. Application number 09252395.0 (pending).

E.3 Other Author's Publications

- A. Garcia i Tormo, A. Poveda, F. Guinjoan, Ll. Prat, "Sistema de adquisición de banda ancha para prácticas remotas con convertidores conmutados DC-DC", in *Proc. Seminario Anual de Automática, Electrónica Industrial e Instrumentación SAAEI 2007*, Sep 10-12, 2007. Puebla de Zaragoza, México. Oral presentation.

- L. Marco, A. Garcia i Tormo, F. Guinjoan, A. Poveda, E. Alarcón. "Sliding-mode controlled buck converter ripple and switching frequency design-oriented characterization", in *Proc. Seminario Anual de Automática, Electrónica Industrial e Instrumentación SAAEI 2007*, Sep 10-12, 2007. Puebla de Zaragoza, México. Poster.

- E. Rodríguez, A. Garcia i Tormo, F. Guinjoan, A. Poveda, A. El-Aroudi, E. Alarcón, "Extensión de la detección de inestabilidades de periodo-2 basada en el rizado de los convertidores conmutados de potencia", in *Proc. Seminario Anual de Automática, Electrónica Industrial e Instrumentación SAAEI 2007*, Sep 10-12, 2007. Puebla de Zaragoza, México. Poster.

- E. Alarcón, D. Fernández, A. Garcia i Tormo, J. Madrenas, A. Poveda. "Continuous-time CMOS adaptive asynchronous $\Sigma\Delta$ modulator for on-chip wideband power amplifiers targeting adaptive supply of RF Transmitters", in *Europractice Annual Activity Report 2010*, Europtractice IC service, 2010. [Online]. Available: http://www.europractice-ic.com/documents_annual_reports.php

Bibliography

[1] Comisión del Mercado de las Telecomunicaciones. (2009, September) La telefonía móvil supera los 52 millones de líneas en España. [Online]. Available: http://www.cmt.es/cmt_ptl_ext/SelectOption.do?nav=comunicados_prensa

[2] P. Ross, "Top 11 technologies of the decade," *Spectrum, IEEE*, vol. 48, no. 1, pp. 27 –63, 2011.

[3] IEEE Computer Society. (2007, June) IEEE standard for information technology – telecommunicationsand information exchange between systems – local and metropolitanarea networks-specific requirements – part 11: Wireless LAN mediumaccess control (MAC) and physical layer (PHY) specifications. [Online]. Available: http://standards.ieee.org/getieee802/802.11.html

[4] J. G. Proakis and M. Salehi, *Communication Systems Engineering*, 2nd ed. Upper Saddle River, New Jersey: Prentice Hall, 2002.

[5] L. R. Kahn, "Single-sideband transmission by envelope elimination and restoration," *Proceedings of the IRE*, vol. 40, no. 7, pp. 803–806, 1952.

[6] G. Hanington, P.-F. Chen, P. M. Asbeck, and L. Larson, "High-efficiency power amplifier using dynamic power-supply voltage for cdma applications," *IEEE Transactions on Microwave Theory and Techniques*, vol. 47, no. 8, pp. 1471–1476, 1999.

[7] J. Jeong, D. F. Kimball, M. Kwak, P. Chin Hsiaand Draxler, and P. M. Asbeck, "Wideband envelope tracking power amplifiers with reduced bandwidth power supply waveforms and adaptive digital predistortion techniques," *IEEE Transactions on Microwave Theory and Techniques*, vol. 57, no. 12, pp. 3307–3314, 2009.

[8] R. D. Middlebrook and S. Ćuk, "A general unified approach to modelling switching-converter power stages," in *Proc. IEEE Power Electronics Specialists Conf. PESC '76*, 1976, pp. 18–34.

[9] T. López, "Prospects of voltage regulators for next generation computer microprocessors," Ph.D. dissertation, Electronic Engineerig Department (DEE) in Universitat Politècnica de Catalunya (UPC), Barcelona, Spain, June 2010.

[10] T. H. Lee, *The Design of CMOS Radio-Frequency Integrated Circuits*, 2nd ed. Cambridge University Press, 2003.

[11] R. W. Erickson and D. Maksimović, *Fundamentals of Power Electronics*, 2nd ed. Kluwer Academic Publishers, 2001.

[12] I. D. Mosely, P. H. Mellor, and C. M. Bingham, "Effect of dead time on harmonic distortion in class-d audio power amplifiers," *Electronics Letters*, vol. 35, no. 12, pp. 950–952, 1999.

[13] M. Berkhout, "A class D output stage with zero dead time," in *Proc. Digest of Technical Papers Solid-State Circuits Conf. ISSCC.2003 IEEE Int*, 2003, pp. 134–135.

[14] V. Yousefzadeh, E. Alarcón, and D. Maksimović, "Band separation and efficiency optimization in linear-assisted switching power amplifiers," in *Proc. 37th IEEE Power Electronics Specialists Conf. PESC '06*, 2006, pp. 1–7.

[15] D. Rudolph, "Out-of-band emissions of digital transmissions using kahn eer technique," *IEEE Transactions on Microwave Theory and Techniques*, vol. 50, no. 8, pp. 1979–1983, 2002.

[16] M. Berkhout and L. Dooper, "Class-d audio amplifiers in mobile applications," *IEEE Transactions on Circuits and Systems—Part I: Regular Papers*, vol. 57, no. 5, pp. 992–1002, 2010.

[17] T. Piessens and M. Steyaert, "Highly efficient xDSL line drivers in 0.35-μm CMOS using a self-oscillating power amplifier," *IEEE Journal of Solid-State Circuits*, vol. 38, no. 1, pp. 22 – 29, jan 2003.

[18] K. Ogata, *Modern control engineering*, 5th ed. Prentice Hall, 2010.

[19] A. Huffenus, G. Pillonnet, N. Abouchi, F. Goutti, V. Rabary, and C. Specq, "A phase-shift self-oscillating stereo class-d amplifier for battery-powered applications," in *Proc. IEEE Int Circuits and Systems (ISCAS) Symp*, 2010, pp. 769–772.

[20] J. Das and P. D. Sharma, "Some asynchronous pulse-modulation systems," *Electronics Letters*, vol. 3, no. 6, pp. 284–286, 1967.

[21] A. Lazar and L. Tóth, "Perfect recovery and sensitivity analysis of time encoded bandlimited signals," *IEEE Transactions on Circuits and Systems—Part I: Regular Papers*, vol. 51, no. 10, pp. 2060–2073, Oct. 2004.

[22] P. van der Hulst, A. Veltman, and R. Groenenberg, "An asynchronous switching high-end power amplifier," in *Audio Engineering Society Convention 112*, no. 5503, May 2002.

[23] S. Poulsen and M. A. E. Andersen, "Simple pwm modulator topology with excellent dynamic behavior," in *Proc. Nineteenth Annual IEEE Applied Power Electronics Conf. and Exposition APEC '04*, vol. 1, 2004, pp. 486–492.

[24] S. Poulsen and M. A. E. Andersen, "Hysteresis controller with constant switching frequency," *IEEE Transactions on Consumer Electronics*, vol. 51, no. 2, pp. 688–693, 2005.

[25] B. Logan, "Click modulation," *AT&T Bell Lab. Tech. J.*, vol. 63, no. 3, pp. 401–422, March 1984.

[26] N. E. Rüger, O. Schnick, W. Mathis, and A. Mertens, "New modulation strategy with low switching frequency and minimum baseband distortion," in *Proc. 13th Power Electronics and Motion Control Conf. EPE-PEMC 2008*, 2008, pp. 132–138.

[27] M. Streitenberger, H. Bresch, and L. Mathis, "Theory and implementation of a new type of digital power amplifier for audio applications," in *Proc. ISCAS 2000 Geneva Circuits and Systems The 2000 IEEE Int. Symp*, vol. 1, 2000, pp. 511–514.

[28] M. Streitenberger, F. Felgenhauer, H. Bresch, and W. Mathis, "Zero-position coding with separated baseband in low-power class-D audio amplifiers for mobile communications," in *Proc. 5th Int. Conf. Telecommunications in Modern Satellite, Cableand Broadcasting Service TELSIKS 2001*, vol. 2, 2001, pp. 567–570.

[29] M. Streitenberger, F. Felgenhauer, H. Bresch, and W. Mathis, "Class-d audio amplifiers with separated baseband for low-power mobile applications," in *Proc. 1st IEEE Int. Conf. Circuits and Systems for Communications ICCSC '02*, 2002, pp. 186–189.

[30] W. W. Burns and T. G. Wilson, "A state-trajectory control law for dc-to-dc converters," *IEEE Transactions on Aerospace and Electronic Systems*, no. 1, pp. 2–20, 1978.

[31] L. Y. Pao and G. F. Franklin, "Proximate time-optimal control of third-order servomechanisms," *IEEE Transactions on Automatic Control*, vol. 38, no. 4, pp. 560–580, 1993.

[32] D. Biel, L. Martínez, J. Tenor, B. Jammes, and J. C. Marpinard, "Optimum dynamic performance of a buck converter," in *Proc. IEEE Int Circuits and Systems ISCAS '96., 'Connecting the World'. Symp*, vol. 1, 1996, pp. 589–592.

[33] V. Yousefzadeh, A. Babazadeh, B. Ramachandran, E. Alarcón, L. Pao, and D. Maksimović, "Proximate time-optimal digital control for synchronous buck DC–DC converters," *IEEE Transactions on Power Electronics*, vol. 23, no. 4, pp. 2018–2026, 2008.

[34] M. Carpita, M. Marchesoni, M. Oberti, and L. Puglisi, "Power conditioning system using sliding model control," in *Proc. 19th Annual IEEE Power Electronics Specialists Conf. PESC '88 Record*, 1988, pp. 626–633.

[35] M. Carpita and M. Marchesoni, "Experimental study of a power conditioning system using sliding mode control," *IEEE Transactions on Power Electronics*, vol. 11, no. 5, pp. 731–742, 1996.

[36] D. Biel, E. Fossas, F. Guinjoan, E. Alarcon, and A. Poveda, "Application of sliding-mode control to the design of a buck-based sinusoidal generator," *IEEE Transactions on Industrial Electronics*, vol. 48, no. 3, pp. 563–571, 2001.

[37] V. M. Nguyen and C. Q. Lee, "Tracking control of buck converter using sliding-mode with adaptive hysteresis," in *Proc. 26th Annual IEEE Power Electronics Specialists Conf. PESC '95 Record*, vol. 2, 1995, pp. 1086–1093.

[38] A. Kawamura and R. Hoft, "Instantaneous feedback controlled pwm inverter with adaptive hysteresis," *IEEE Transactions on Industry Applications*, no. 4, pp. 769–775, 1984.

[39] J. M. Ruiz, S. Lorenzo, I. Lobo, and J. Amigo, "Minimal ups structure with sliding mode control and adaptive hysteresis band," in *Proc. th Annual Conf Industrial Electronics Society IECON '90. of IEEE*, 1990, pp. 1063–1067.

[40] J. F. Silva and S. S. Paulo, "Fixed frequency sliding mode modulator for current mode pwm inverters," in *Proc. 24th Annual IEEE Power Electronics Specialists Conf. PESC '93 Record*, 1993, pp. 623–629.

[41] H. Sira-Ramírez, "A geometric approach to pulse-width modulated control in nonlinear dynamical systems," *IEEE Transactions on Automatic Control*, vol. 34, no. 2, pp. 184–187, 1989.

[42] R. R. Ramos, D. Biel, E. Fossas, and F. Guinjoan, "A fixed-frequency quasi-sliding control algorithm: application to power inverters design by means of fpga implementation," *IEEE Transactions on Power Electronics*, vol. 18, no. 1, pp. 344–355, 2003.

[43] P. F. Miaja, M. Rodríguez, A. Rodríguez, and J. Sebastián, "Approximation of envelopes of telecommunication signals to be used in envelope tracking techniques," in *Proc. IEEE 12th Workshop Control and Modeling for Power Electronics (COMPEL)*, 2010, pp. 1–8.

[44] M. Siu, P. K. T. Mok, K. N. Leung, Y.-H. Lam, and W.-H. Ki, "A voltage-mode pwm buck regulator with end-point prediction," *IEEE Transactions on Circuits and Systems—Part II: Express Briefs*, vol. 53, no. 4, pp. 294–298, 2006.

[45] R. Giral, L. Martinez-Salamero, and S. Singer, "Interleaved converters operation based on cmc," *IEEE Transactions on Power Electronics*, vol. 14, no. 4, pp. 643–652, 1999.

[46] K. Nielsen, "Paralleled phase shifted carrier pulse width modulation (PSCPWM)- a novel approach to switching power amplifier design," in *Audio Engineering Society Convention 102*, no. 4447, May 1997.

[47] F. S. Christensen, T. M. Frederiksen, and K. Nielsen, "Paralleled phase shifted carrier pulse width modulation (PSCPWM) schemes - a fundamental analysis," in *Audio Engineering Society Convention 106*, no. 4917, May 1999.

[48] M. Vasić, O. García, J. A. Oliver, P. Alou, D. Díaz, and J. A. Cobos, "Multilevel power supply for high-efficiency rf amplifiers," *IEEE Transactions on Power Electronics*, vol. 25, no. 4, pp. 1078–1089, 2010.

[49] G. R. Walker, "Modulation and control of multilevel converters," Ph.D. dissertation, Department of Computer Science and Electrical Engineering, University of Queensland, Queensland, Australia, November 1999.

[50] G. Carrara, S. Gardella, M. Marchesoni, R. Salutari, and G. Sciutto, "A new multilevel pwm method: a theoretical analysis," *IEEE Transactions on Power Electronics*, vol. 7, no. 3, pp. 497–505, 1992.

[51] L. M. Tolbert and T. G. Habetler, "Novel multilevel inverter carrier-based pwm methods," in *Proc. Thirty-Third IAS Annual Meeting Industry Applications Conf. The 1998 IEEE*, vol. 2, 1998, pp. 1424–1431.

[52] A. Matamura, N. Nishimura, and B. Y. Liu, "Filterless multi-level delta-sigma class-d amplifier for portable applications," in *Proc. IEEE Int. Symp. Circuits and Systems ISCAS 2009*, 2009, pp. 1177–1180.

[53] E. Gaalaas, B. Y. Liu, N. Nishimura, R. Adams, and K. Sweetland, "Integrated stereo $\Delta\Sigma$ class D amplifier," *IEEE Journal of Solid-State Circuits*, vol. 40, no. 12, pp. 2388–2397, 2005.

[54] G. Walker and G. Ledwich, "Bandwidth considerations for multilevel converters," *IEEE Transactions on Power Electronics*, vol. 14, no. 1, pp. 74–81, 1999.

[55] T. A. Meynard and H. Foch, "Multi-level conversion: high voltage choppers and voltage-source inverters," in *Proc. 23rd Annual IEEE Power Electronics Specialists Conf. PESC '92 Record*, 1992, pp. 397–403.

[56] V. Yousefzadeh, E. Alarcón, and D. Maksimović, "Three-level buck converter for envelope tracking applications," *IEEE Transactions on Power Electronics*, vol. 21, no. 2, pp. 549–552, 2006.

[57] S. Ćuk and R. W. Erickson, "A conceptually new high-frequency switched-mode power amplifier technique eliminates current ripple," in *Proc. 5th National Solid-State Power Conversion Conf. Powercon 5*, 1978.

[58] J. Neely, R. DeCarlo, and S. Pekarek, "Real-time model predictive control of the Ćuk converter," in *Proc. IEEE 12th Workshop Control and Modeling for Power Electronics (COMPEL)*, 2010, pp. 1–8.

[59] P. Midya, K. Haddad, and M. Miller, "Buck or boost tracking power converter," *IEEE Power Electronics Letters*, vol. 2, no. 4, pp. 131–134, 2004.

[60] R. Paul and D. Maksimović, "Smooth transition and ripple reduction in 4-switch non-inverting buck-boost power converter for wcdma rf power amplifier," in *Proc. IEEE Int. Symp. Circuits and Systems ISCAS 2008*, 2008, pp. 3266–3269.

[61] B. Sahu and G. A. Rincón-Mora, "A low voltage, dynamic, noninverting, synchronous buck-boost converter for portable applications," *IEEE Transactions on Power Electronics*, vol. 19, no. 2, pp. 443–452, 2004.

[62] P. P. Siniscalchi and R. K. Hester, "A 20 w/channel class-d amplifier with near-zero common-mode radiated emissions," *IEEE Journal of Solid-State Circuits*, vol. 44, no. 12, pp. 3264–3271, 2009.

[63] F. Wang, A. Yang, D. Kimball, L. Larson, and P. Asbeck, "Design of wide-bandwidth envelope-tracking power amplifiers for OFDM applications," *IEEE Transactions on Microwave Theory and Techniques*, vol. 53, no. 4, pp. 1244 – 1255, april 2005.

[64] J. Staudinger, B. Gilsdorf, D. Newman, G. Norris, G. Sadowniczak, R. Sherman, and T. Quach, "High efficiency cdma rf power amplifier using dynamic envelope tracking technique," in *Proc. IEEE MTT-S Int. Microwave Symp. Digest*, vol. 2, 2000, pp. 873–876.

[65] B. Sahu and G. A. Rincón-Mora, "A high-efficiency linear rf power amplifier with a power-tracking dynamically adaptive buck-boost supply," *IEEE Transactions on Microwave Theory and Techniques*, vol. 52, no. 1, pp. 112–120, 2004.

[66] L. Marco, E. Alarcón, and D. Maksimović, "Effects of switching power converter nonidealities in envelope elimination and restoration technique," in *Proc. IEEE Int. Symp. Circuits and Systems ISCAS 2006*, 2006.

[67] D. F. Kimball, J. Jeong, C. Hsia, P. Draxler, S. Lanfranco, W. Nagy, K. Linthicum, and P. M. Larson, L. E. andAsbeck, "High-efficiency envelope-tracking w-cdma base-station amplifier using gan hfets," *IEEE Transactions on Microwave Theory and Techniques*, vol. 54, no. 11, pp. 3848–3856, 2006.

[68] F. Wang, D. Kimball, J. Popp, A. Yang, D. Y. Lie, P. Asbeck, and L. Larson, "Wideband envelope elimination and restoration power amplifier with high efficiency wideband envelope amplifier for wlan 802.11g applications," in *Proc. IEEE MTT-S Int. Microwave Symp. Digest*, 2005.

[69] S.-C. Choi, J.-W. Lee, W.-K. Jin, J.-H. So, and S. Kim, "A design of a 10-w single-chip class d audio amplifier with very high efficiency using cmos technology," *IEEE Transactions on Consumer Electronics*, vol. 45, no. 3, pp. 465–473, 1999.

[70] Y. Li and D. Maksimović, "High efficiency wide bandwidth power supplies for gsm and edge rf power amplifiers," in *Proc. IEEE Int. Symp. Circuits and Systems ISCAS 2005*, 2005, pp. 1314–1317.

[71] M. Helfenstein, E. Baykal, K. Müller, and A. Lampe, "Error vector magnitude (EVM) measurements for GSM/EDGE applications revised under production conditions," in *Proc. IEEE Int. Symp. Circuits and Systems ISCAS 2005*, 2005, pp. 5003–5006.

[72] L. Noël and P. Brousse, "Low-cost EVM test methodology for wireless transmitters applied to W-CDMA," *IEEE Transactions on Instrumentation and Measurement*, vol. 60, no. 1, pp. 170–175, 2011.

[73] S. Ouzounov, "On the characterization of limit cycle modes in oversampled data converters," in *Proc. IEEE Int Circuits and Systems (ISCAS) Symp*, 2010, pp. 1073–1076.

[74] A. van Roermund, F. A. Malekzadeh, M. Sarkeshi, and R. Mahmoudi, "Extended modelling for time-encoding converters," in *Proc. IEEE Int Circuits and Systems (ISCAS) Symp*, 2010, pp. 1077–1080.

[75] I. Daubechies and R. DeVore, "Approximating a bandlimited function using very coarsely quantized data: A family of stable sigma-delta modulators of arbitrary order," *Annals of Mathematics*, vol. 158, no. 2, pp. 679–710, 2003.

[76] A. Lazar, E. Simonyi, and L. Tóth, "Fast recovery algorithms for time encoded bandlimited signals," in *Proc. IEEE Int. Conf. on Acoustics, Speech, and Signal Processing ICASSP 2005*, vol. 4, 18-23 2005, pp. iv/237 – iv/240 Vol. 4.

[77] A. Lazar, E. Simonyi, and L. Tóth, "An overcomplete stitching algorithm for time decoding machines," *IEEE Transactions on Circuits and Systems—Part I: Regular Papers*, vol. 55, no. 9, pp. 2619 –2630, oct. 2008.

[78] Z. Song and D. Sarwate, "The frequency spectrum of pulsewidth modulated signals," *Signal Processing*, vol. 83, pp. 2227–2258, 2003.

[79] E. Roza, "Analog-to-digital conversion via duty-cycle modulation," *IEEE Transactions on Circuits and Systems—Part II: Analog and Digital Signal Processing*, vol. 44, no. 11, pp. 907–914, 1997.

[80] M. C. W. Høyerby and M. A. E. Andersen, "Carrier distortion in hysteretic self-oscillating class-d audio power amplifiers: Analysis and optimization," *IEEE Transactions on Power Electronics*, vol. 24, no. 3, pp. 714–729, 2009.

[81] H. Inose, T. Aoki, and K. Watanabe, "Asynchronous delta-modulation system," *Electronics Letters*, vol. 2, no. 3, pp. 95–96, 1966.

[82] R. Mahadevan, S. El-Hamamsy, W. M. Polivka, and S. Ćuk, "A converter with three switched-networks improves regulation, dynamics and control," in *Advances in Switched-Mode Power Conversion Vol. III by R. D. Middlebrook and S. Ćuk*, 1984, pp. 219–237.

[83] E. Alarcón, D. Fernández, A. Garcia i Tormo, J. Madrenas, and A. Poveda, "Continuous-time CMOS adaptive asynchronous $\Sigma\Delta$ modulator approximating low-fs low-inband-error on-chip wideband power amplifier," in *Proc. IEEE Int Circuits and Systems (ISCAS) Symp*, 2011.

[84] A. Nuttall, "Some windows with very good sidelobe behavior," *IEEE Transactions on Acoustics, Speech, and Signal Processing*, vol. 29, no. 1, pp. 84–91, 1981.

[85] A. Hasan and S. Gregori, "Design of a step-up dc-dc converter with on-chip coupled inductors," in *Proc. IEEE Int Circuits and Systems (ISCAS) Symp*, 2010, pp. 2730–2733.

[86] A. Jerri, "The shannon sampling theorem–Its various extensions and applications: A tutorial review," *Proceedings of the IEEE*, vol. 65, no. 11, pp. 1565 – 1596, nov. 1977.

[87] A. A. Lazar, "Time encoding machines with multiplicative coupling, feedforward, and feedback," *IEEE Transactions on Circuits and Systems—Part II: Express Briefs*, vol. 53, no. 8, pp. 672–676, 2006.

[88] L. Marco, A. Poveda, E. Alarcón, and D. Maksimović, "Bandwidth limits in PWM switching amplifiers," in *Proc. IEEE Int. Symp. Circuits and Systems ISCAS 2006*, 2006.

[89] J. Márkus and G. C. Temes, "An efficient $\Delta\Sigma$ ADC architecture for low oversampling ratios," *IEEE Transactions on Circuits and Systems—Part I: Regular Papers*, vol. 51, no. 1, pp. 63–71, 2004.

[90] A. Papoulis, "Error analysis in sampling theory," *Proceedings of the IEEE*, vol. 54, no. 7, pp. 947 – 955, july 1966.

[91] J. F. Silva, "Pwm audio power amplifiers: sigma delta versus sliding mode control," in *Proc. IEEE Int Electronics, Circuits and Systems Conf*, vol. 1, 1998, pp. 359–362.

[92] P. M. Aziz, H. V. Sorensen, and J. van der Spiegel, "An overview of sigma-delta converters," *IEEE Signal Processing Magazine*, vol. 13, no. 1, pp. 61–84, 1996.

[93] S.-H. Yu, "Analysis and design of single-bit sigma-delta modulators using the theory of sliding modes," *IEEE Transactions on Control Systems Technology*, vol. 14, no. 2, pp. 336–345, 2006.

[94] B. Pilloud and W. H. Groeneweg, "A 650mw filterless class-d audio power amplifier for mobile applications in 65-nm technology," in *Proc. IEEE Int. Symp. Circuits and Systems ISCAS 2009*, 2009, pp. 1173–1176.

[95] G. Villar and E. Alarcón, "Monolithic integration of a 3-level DCM-operated low-floating-capacitor buck converter for DC-DC step-down conversion in standard CMOS," in *Proc. IEEE Power Electronics Specialists Conf. PESC 2008*, 2008, pp. 4229–4235.

[96] T. López and E. Alarcón, "Design and roadmap methodology for integrated power modules in high switching frequency synchronous buck voltage regulators," in *Proc. Twenty-Fourth Annual IEEE Applied Power Electronics Conf. and Exposition APEC 2009*, 2009, pp. 90–96.

[97] J. Marchán, E. Barba, L. Marco, D. Maksimović, and E. Alarcón, "Circuit/system design space characterization of EER-based transmitter for 802.11a WLAN standard," in *Proc. IEEE Int Circuits and Systems (ISCAS) Symp*, 2010, pp. 881–884.

[98] A. Garcia i Tormo, E. Alarcón, A. Poveda, and F. Guinjoan, "Low-OSR asynchronous Σ-Δ modulation high-order buck converter for efficient wideband switching amplification," in *Proc. IEEE Int. Symp. Circuits and Systems ISCAS 2008*, may 2008, pp. 2198 –2201.

[99] A. Garcia i Tormo, A. Poveda, E. Alarcón, and F. Guinjoan, "Design-oriented characterisation of adaptive asynchronous ΣΔ modulation switching power amplifiers for bandlimited signals," in *Proc. IEEE Int. Symp. Circuits and Systems ISCAS 2009*, may 2009, pp. 2882 –2885.

[100] A. Garcia i Tormo, A. Poveda, E. Alarcón, H. Bergveld, B. Buter, and R. Karadi, "An enhanced switching policy for buck-derived multi-level switching power amplifiers," in *Proc. IEEE Int. Symp. Circuits and Systems ISCAS 2010*, may 2010, pp. 3196 –3199.

[101] A. Garcia i Tormo, A. Poveda, E. Alarcón, and F. Guinjoan, "Multilevel asynchronous ΣΔ modulators for wideband switching power amplifiers," in *Proc. IEEE 12th Workshop Control and Modeling for Power Electronics (COMPEL)*, 2010, pp. 1–8.